SEISMIC PERFORMANCE OF SEMI-ACTIVE CONTROL SYSTEMS

A thesis

submitted in partial fulfilment

of the requirements for the degree of

Doctor of Philosophy

in

Civil Engineering

by

Roberto Franco Anaya

at the

University of Canterbury

Christchurch, New Zealand

April 2008

To my mother

ABSTRACT

The main purpose of this research is to investigate the effectiveness and feasibility of semi-active control systems for structural protection during severe earthquake loading. However, the research reported herein also involves analytical studies on the effect of adding viscous damping to the second and fourth quadrants of the force-displacement curve, and laboratory and field testing of a fibre-optic gyroscope (FOG) for measuring rotations in civil engineering structures.

The concept of the 2-4 viscous damping is introduced to reduce the response of single-degree-of-freedom (SDOF) systems subjected to harmonic and earthquake excitations. This concept involves the addition of structural viscous damping to the second and fourth quadrants of the force-displacement graph. Time-history analyses and response spectra for various SDOF systems are carried out to assess the effect of adding 2-4 viscous damping. The analytical results indicate that the addition of 2-4 viscous damping is beneficial for reducing the harmonic and seismic response of a wide range of SDOF systems.

A newly developed semi-active resettable device is proposed to reduce the seismic response of a one-fifth scale structure. The device is investigated as part of a resettable tendon system installed in the structure. Nonlinear dynamic analyses are performed to determine the optimal configuration of the resettable tendon in the structure. Several shake table tests are performed on the structure equipped with two resettable devices. The dynamic characteristics of the structure and the devices are described. Various earthquake records at different levels of intensity are used during the seismic testing. Different control laws are employed to manipulate the hysteretic behaviour of the devices. The results of the shake table tests validate the effectiveness of the resettable devices to reduce the seismic response of structures.

Analytical studies are performed to determine the optimal utilization of the resettable devices in a twelve-storey reinforced concrete building. The seismic performance of the

structure is discussed in relation to the number and distribution of the devices. Inelastic time-history analyses are carried out to assess the effectiveness of the devices to reduce the seismic response of the building. The impact of various tendon arrangements and different control laws on the earthquake response is investigated. Relevant issues for the implementation of the resettable devices in actual building systems are identified.

Finally, a new measurement concept based on the use of the fibre-optic gyroscope is proposed to measure rotation rates, rotations, displacements and inter-storey drifts of civil engineering structures. FOGs are compact, easy to install and, unlike conventional linear potentiometers, do not require a fixed reference frame to operate. Measurements recorded during the seismic testing of the one-fifth scale structure and displacement measurements at the Sky Tower in Auckland validate the suitability of the FOGs for applications in civil engineering.

ACKNOWLEDGEMENTS

I have no doubt that I could not have completed this project without the support, advice and encouragement of many people.

I would like to thank Prof. Athol J. Carr for having shared his immense knowledge and expertise with me throughout the research process. His encouragement, guidance and support during difficult times are deeply appreciated.

I wish to express my sincere appreciation to Prof. J. Geoffrey Chase for his invaluable suggestions and significant contributions to the project. Without his cooperation and help this project would not have been possible.

I am very grateful to Prof. John B. Mander for his advice and support during the early stages of the research work.

Very special thanks go to Dr. Stefano Pampanin for his encouragement and continuous interest in my research.

I am indebted to my colleagues Kerry J. Mulligan, Geoffrey W. Rodgers and Min Ho Chey for offering assistance in every aspect of the project. Their support and readiness to help are greatly appreciated.

I wish to acknowledge the helpful assistance of Mr. John Maley during the experimental part of the research.

I want to express my profound gratitude to Dr. Piotr Omenzetter for his comprehensive and detailed review of the thesis. His insightful comments and invaluable suggestions have significantly strengthened the contents of the thesis.

My sincere thanks are extended to Prof. K. Ulrich Schreiber for his intellectual support and encouragement over the past few years.

I am very appreciative of the encouragement and academic advice received from Prof. Andrew H. Buchanan, Dr. Rajesh P. Dhakal, Assoc. Prof. Gregory A. MacRae and Dr. Bruce L. Deam.

The generous financial support provided by the Foundation for Research, Science and Technology, and the University of Canterbury is very much appreciated.

I owe a special debt of gratitude to my wife Tomoe for her understanding and never-ending love, and to my son Kai for brightening up my life.

I wish to express my heartfelt thanks and gratitude to my family and friends for their continuing support and encouragement throughout my postgraduate studies.

This thesis is dedicated to my mother María de los Angeles for her unstinting love and support that have been beyond anything I could have hoped for.

CONTENTS

Abstract v

Acknowledgements vii

List of Figures xv

List of Tables xxi

List of Symbols xxiii

1 Introduction 1

1.1 Limitations of the conventional design 1

1.2 Structural control concept 3

1.3 Semi-active control systems 6

1.4 Resettable devices 8

1.5 Objectives and scope of the research 9

1.6 Organization of the thesis 11

1.7 Original contributions of the thesis 12

1.8 Summary 13

2 Effect of adding 2-4 viscous damping 15

2.1 Introduction 15

2.2 Energy dissipated by viscous damping 16

2.3 Concept of 2-4 viscous damping 21

2.3.1 Response to harmonic excitation 21

2.3.2 Response to seismic excitation 26

2.3.3 Earthquake response spectra 32

2.4 Summary 37

3 Semi-active resettable devices 39

3.1 Introduction 39

3.2 Definition and brief history 39

3.3 Two-chambered design 40

3.4 Design characteristics 42

3.5 Control laws 44

3.5.1 1-2-3-4 control law 45

3.5.2 1-3 control law 46

3.5.3 2-4 control law 48

3.6 Resettable device 49

3.6.1 Description of the device 50

3.6.2 Dynamic characteristics of the device 52

3.7 Summary 55

4 Analytical studies on resettable devices 57

4.1 Introduction 57

4.2 Effect of adding energy dissipation devices 57

4.2.1 Effect of the additional damping 58

4.2.2 Effect of the additional stiffness 58

4.2.3 Optimal placement and distribution 59

4.3 One-fifth scale structure 60

4.3.1 Description of the structure 61

4.3.2 Analytical modelling of the structure 65

4.4 Ideal resettable tendon 68

4.4.1 Computational model of the resettable tendon 68

4.4.2 Tendon systems and earthquake ground motions 70

4.4.3 Interpretation of the analytical results 74

4.4.4 Complementary tendon systems 80

4.4.5 Seismic response using a resettable spring member 88

4.5 Summary 91

5 Experimental validation of resettable devices 93

5.1 Introduction 93

5.2 The need for experimental testing 93

5.3 Implementation of the control system 95

5.4 Measurement instrumentation 97

5.5 Free vibration testing 99

5.6 Seismic testing 102

5.6.1 Control configurations 103

5.6.2 Earthquake ground motions 105

5.6.3 Interpretation of the experimental results 109

5.7 Summary 118

6 Analytical predictions of the shake table test results 121

6.1 Introduction 121

6.2 Numerical model of the resettable tendon 121

6.2.1 Analytical modelling of the resettable device 122

6.2.2 Analytical modelling of the steel tendon 124

6.2.3 Analytical modelling of the restraint element 125

6.3 Numerical model of the stiff and flexible bracing systems 126

6.4 Comparison of the analytical predictions with the experimental results 127

6.4.1 Comparison of displacement time-histories 127

6.4.2 Comparison of the device response 138

6.4.3 Contribution of a passive tendon to seismic response reduction 144

6.5 Additional comments on the analytical predictions 147

6.6 Summary 148

7 Implementation of resettable devices in structural building systems 149

7.1 Introduction 149

7.2 Characteristics of the twelve-storey building 149

7.3 Characteristics of the control system 155

7.3.1 Description of the resettable device 156

7.3.2 Description of the rigid rod 158

7.3.3 Description of the pre-stressed tendon 158
7.4 Earthquake record and control law 160
7.5 Impact of the distribution and number of devices 160
7.6 Impact of the tendon configuration 165
7.6.1 Seismic response of the tendon configurations 165
7.6.2 Contribution of the pre-stressed tendons and bracing systems to the seismic response reduction of system A2_3 171
7.6.3 Response of system A1_2 under different earthquakes 175
7.7 Impact of the control law 185
7.8 Improving the performance of resettable devices 191
7.8.1 Lever system 191
7.8.2 High-pressure air source 192
7.8.3 Simulation results 193
7.9 Recommendations for device implementation 197
7.10 Summary 198

8 Fibre-optic gyroscopes for civil engineering applications 201
8.1 Introduction 201
8.2 Measurement of rotations in civil engineering 202
8.3 Optical gyroscopes 204
8.3.1 Ring laser gyroscopes 204
8.3.2 Fibre-optic gyroscopes 205
8.4 Operation and verification 206
8.4.1 Operation principle of the FOG 207
8.4.2 Shake table measurements 208
8.4.3 Measurements at the Sky Tower 219
8.5 Summary 221

9 Conclusions and contributions of the research 223
9.1 Executive summary 223
9.2 Conclusions of the research 226
9.3 Contributions of the research 229

10 Future research **231**

References **235**

A Comparison of response spectra **245**

B Response of the A-Systems and B-Systems under different earthquakes **251**

C Measurement of displacements and record modification **265**

C.1 Verification of the displacement measurements 266

C.2 Modification of the earthquake records 269

D Experimental results **279**

D.1 Maximum response envelopes for El Centro earthquake 280

D.2 Maximum response envelopes for Taft earthquake 301

D.3 Maximum response envelopes for Sylmar earthquake 310

D.4 Maximum response envelopes for Kobe earthquake 323

LIST OF FIGURES

CHAPTER 2

Figure 2.1 SDOF system subjected to dynamic force. 17

Figure 2.2 Force-displacement diagrams. 19

Figure 2.3 Response to harmonic loading (β = 0.25). 23

Figure 2.4 Response to harmonic loading (β = 1). 24

Figure 2.5 Response to harmonic loading (β = 1.5). 25

Figure 2.6 SDOF system subjected to ground motion. 26

Figure 2.7 Seismic response under El Centro ground motion. 28

Figure 2.8 Seismic response under Taft ground motion. 29

Figure 2.9 Seismic response under Sylmar ground motion. 30

Figure 2.10 Seismic response under Kobe ground motion. 31

Figure 2.11 Response spectra for El Centro ground motion. 33

Figure 2.12 Response spectra for Taft ground motion. 34

Figure 2.13 Response spectra for Sylmar ground motion. 35

Figure 2.14 Response spectra for Kobe ground motion. 36

CHAPTER 3

Figure 3.1 Two-chambered design of the device. 41

Figure 3.2 1-2-3-4 control law. 46

Figure 3.3 1-3 control law. 47

Figure 3.4 2-4 control law. 49

Figure 3.5 Resettable device. 50

Figure 3.6 Schematic of the resettable device. 51

CHAPTER 4

Figure 4.1 One-fifth scale structure. 61

Figure 4.2 Isometric view of the structure (Rodriguez et al. 2006). 62

Figure 4.3 Location and dimensions of the fuses (Rodriguez et al. 2006). 64

Figure 4.4 Tendon member (Carr 2006). 69

Figure 4.5 Linear resettable hysteresis. 69
Figure 4.6 System A. 70
Figure 4.7 A-Systems. 72
Figure 4.8 B-Systems. 73
Figure 4.9 Maximum response envelopes of A-Systems under El Centro earthquake. 76
Figure 4.10 Maximum response envelopes of B-Systems under El Centro earthquake. 78
Figure 4.11 Complementary tendon systems. 80
Figure 4.12 Maximum response envelopes of the complementary systems. 82
Figure 4.13 Maximum response envelopes of the best tendon systems. 84
Figure 4.14 Comparison of the seismic response for the B1-3 and A1-3_S systems. 86
Figure 4.15 Spring member (Carr 2006). 88
Figure 4.16 Comparison of the seismic response for the tendon and spring members. 89

CHAPTER 5

Figure 5.1 Implementation of the control system. 96
Figure 5.2 Measurement instrumentation of the test structure. 97
Figure 5.3 Test set-up for free vibration. 99
Figure 5.4 Comparison of displacement time-history for free vibration testing. 100
Figure 5.5 Power spectrum of the acceleration at level 4. 101
Figure 5.6 Free vibration response with the device valves closed. 102

CHAPTER 6

Figure 6.1 Analytical model of the resettable tendon. 122
Figure 6.2 Elasto-plastic hysteresis. 123
Figure 6.3 Bi-linear with slackness hysteresis. 124
Figure 6.4 Linear elastic hysteresis. 125
Figure 6.5 Comparison of the displacement time-history for the 1-2-3-4 control law. 128

Figure 6.6 Comparison of the displacement time-history for the 1-3 control law. 130
Figure 6.7 Comparison of the displacement time-history for the 2-4 control law. 132
Figure 6.8 Comparison of the displacement time-history for the valves closed case. 134
Figure 6.9 Comparison of the displacement time-history for the valves open case. 136
Figure 6.10 Comparison of device response for the 1-2-3-4 control law. 139
Figure 6.11 Comparison of device response for the 1-3 control law. 140
Figure 6.12 Comparison of device response for the 2-4 control law. 141
Figure 6.13 Comparison of device response for the valves closed case. 142
Figure 6.14 Comparison of device response for the valves open case. 143
Figure 6.15 Contribution of the passive tendon to the seismic response reduction. 145

CHAPTER 7

Figure 7.1 Twelve-storey reinforced concrete building. 150
Figure 7.2 Schematic of the system implementation. 156
Figure 7.3 Control laws. 157
Figure 7.4 Distribution of the resettable devices. 162
Figure 7.5 Effect of the distribution and number of devices. 163
Figure 7.6 Tendon systems for the twelve-storey building. 167
Figure 7.7 Effect of the tendon configuration. 169
Figure 7.8 System A2_B. 172
Figure 7.9 Contribution of system A2_B to the seismic response reduction. 173
Figure 7.10 Maximum response envelopes for El Centro earthquake. 176
Figure 7.11 Maximum response envelopes for Taft earthquake. 178
Figure 7.12 Maximum response envelopes for Sylmar 70% earthquake. 180
Figure 7.13 Maximum response envelopes for Kobe earthquake. 182
Figure 7.14 Effect of the control law. 186
Figure 7.15 Effect of combining the control laws. 189
Figure 7.16 Lever system attached to the resettable device. 191
Figure 7.17 Resettable device connected to a high-pressure air source. 193
Figure 7.18 Effect of improving the device force. 195

CHAPTER 8

Figure 8.1	Ring laser gyroscope (Britannica).	205
Figure 8.2	Fibre-optic gyroscope.	206
Figure 8.3	Opreration principle of the FOG.	207
Figure 8.4	One-fifth scale structure with fixed reference frame.	208
Figure 8.5	FOG attached to the centre column.	209
Figure 8.6	Measurements for El Centro 30% earthquake.	211
Figure 8.7	Measurements for Taft 40% earthquake.	212
Figure 8.8	Measurements for Sylmar 10% earthquake.	213
Figure 8.9	Measurements for Kobe 10% earthquake.	214
Figure 8.10	Measurements at the third floor for El Centro 30% earthquake.	215
Figure 8.11	Measurements at the third floor for Taft 40% earthquake.	216
Figure 8.12	Measurements at the third floor for Sylmar 10% earthquake.	217
Figure 8.13	Measurements at the third floor for Kobe 10% earthquake.	218
Figure 8.14	FOG attached to the window of the Sky Tower.	219
Figure 8.15	Measurements at level 54 of the Sky Tower.	220

APPENDIX A

Figure A.1	Comparison of response spectra for El Centro earthquake.	246
Figure A.2	Comparison of response spectra for Taft earthquake.	247
Figure A.3	Comparison of response spectra for Sylmar earthquake.	248
Figure A.4	Comparison of response spectra for Kobe earthquake.	249

APPENDIX B

Figure B.1	Maximum response envelopes of A-Systems for Taft 90% earthquake.	252
Figure B.2	Maximum response envelopes of B-Systems for Taft 90% earthquake.	254
Figure B.3	Maximum response envelopes of A-Systems for Sylmar 20% earthquake.	256
Figure B.4	Maximum response envelopes of B-Systems for Sylmar 20% earthquake.	258

Figure B.5 Maximum response envelopes of A-Systems for Kobe 20% earthquake (System A2 collapses under this earthquake ground motion). 260
Figure B.6 Maximum response envelopes of B-Systems for Kobe 20% earthquake. 262

APPENDIX C

Figure C.1.1 Displacement comparison at third floor for the uncontrolled case. 267
Figure C.2.1 Comparison of ground motion components for El Centro earthquake. 270
Figure C.2.2 Comparison of response spectra for El Centro earthquake (ξ = 5%). 271
Figure C.2.3 Comparison of ground motion components for Sylmar earthquake. 272
Figure C.2.4 Comparison of response spectra for Sylmar earthquake (ξ = 5%). 273
Figure C.2.5 Comparison of ground motion components for Kobe earthquake. 274
Figure C.2.6 Comparison of response spectra for Kobe earthquake (ξ = 5%). 275
Figure C.2.7 Ground motion components of Taft earthquake. 276
Figure C.2.8 Response spectra for Taft earthquake (ξ = 5%). 277

APPENDIX D

Figure D.1.1 Maximum response envelopes for El Centro 10% earthquake. 281
Figure D.1.2 Maximum response envelopes for El Centro 20% earthquake. 283
Figure D.1.3 Maximum response envelopes for El Centro 30% earthquake. 285
Figure D.1.4 Maximum response envelopes for El Centro 40% earthquake. 287
Figure D.1.5 Maximum response envelopes for El Centro 50% earthquake. 289
Figure D.1.6 Maximum response envelopes for El Centro 60% earthquake. 291
Figure D.1.7 Maximum response envelopes for El Centro 70% Modified earthquake. 293
Figure D.1.8 Maximum response envelopes for El Centro 80% Modified earthquake. 295
Figure D.1.9 Maximum response envelopes for El Centro 90% Modified earthquake. 297

Figure D.1.10 Maximum response envelopes for El Centro 100% Modified earthquake. 299
Figure D.2.1 Maximum response envelopes for Taft 20% earthquake. 302
Figure D.2.2 Maximum response envelopes for Taft 40% earthquake. 304
Figure D.2.3 Maximum response envelopes for Taft 60% earthquake. 306
Figure D.2.4 Maximum response envelopes for Taft 80% earthquake. 308
Figure D.3.1 Maximum response envelopes for Sylmar 5% earthquake. 311
Figure D.3.2 Maximum response envelopes for Sylmar 10% earthquake. 313
Figure D.3.3 Maximum response envelopes for Sylmar 15% earthquake. 315
Figure D.3.4 Maximum response envelopes for Sylmar 20% earthquake. 317
Figure D.3.5 Maximum response envelopes for Sylmar 25% Modified earthquake. 319
Figure D.3.6 Maximum response envelopes for Sylmar 30% Modified earthquake. 321
Figure D.4.1 Maximum response envelopes for Kobe 5% earthquake. 324
Figure D.4.2 Maximum response envelopes for Kobe 10% earthquake. 326
Figure D.4.3 Maximum response envelopes for Kobe 15% earthquake. 328
Figure D.4.4 Maximum response envelopes for Kobe 20% earthquake. 330
Figure D.4.5 Maximum response envelopes for Kobe 25% earthquake. 332
Figure D.4.6 Maximum response envelopes for Kobe 30% Modified earthquake. 334
Figure D.4.7 Maximum response envelopes for Kobe 35% Modified earthquake. 336

LIST OF TABLES

CHAPTER 5

Table 5.1 Description of the measurement instrumentation (refer to Figure 5.2). 98

Table 5.2 Peak values of the El Centro ground motion. 108

Table 5.3 Peak values of the Taft ground motion. 108

Table 5.4 Peak values of the Sylmar ground motion. 108

Table 5.5 Peak values of the Kobe ground motion. 108

Table 5.6 Summary of the maximum response for the El Centro earthquake. 110

Table 5.7 Summary of the maximum response for the Taft earthquake. 112

Table 5.8 Summary of the maximum response for the Sylmar earthquake. 113

Table 5.9 Summary of the maximum response for the Kobe earthquake. 114

CHAPTER 7

Table 7.1 Section properties of the column and beam members (refer to Figure 7.1). 151

Table 7.2 Fixed-end moments and shear forces (refer to Figure 7.1). 152

Table 7.3 Positive and negative yield moments (refer to Figure 7.1). 152

Table 7.4 Distribution of the seismic weight. 154

LIST OF SYMBOLS

A	area of the piston
c	damping coefficient; constant
D	diameter of the piston
E	elastic modulus
E_D	energy dissipated per cycle in viscous damping
EI	flexural rigidity
$(EI)_{eff}$	effective flexural rigidity
F	device force
f	natural frequency
f_D	damping force
FOG	fibre-optic gyroscope
G	shear modulus
g	gravity acceleration
H_1	amplitude of dynamic load factor
I	moment of inertia
k	stiffness coefficient
k_R	stiffness of the resettable device
L	length
L_0	chamber length
MDOF	multi-degree-of-freedom
m	mass
PGA	peak ground acceleration
PGD	peak ground displacement
PGV	peak ground velocity
PSA	pseudo-spectral acceleration
PSV	pseudo-spectral velocity
p	dynamic force

p_0	amplitude of the applied force; initial or atmospheric pressure
p_1	chamber pressure before piston displacement
p_2	chamber pressure after piston displacement
SA	spectral acceleration
SD	spectral displacement
SDOF	single-degree-of-freedom
SV	spectral velocity
T	natural period
t	time
u	displacement
$\dot{u}$	velocity
$\ddot{u}$	acceleration
u_0	amplitude of motion
u_g	ground acceleration
V_0	initial volume
V_1	chamber volume before piston displacement
V_2	chamber volume after piston displacement
x	piston displacement
$\dot{x}$	piston velocity
β	frequency ratio
γ	ratio of specific heats
δ	maximum piston displacement
ξ	damping ratio
ξ_{2-4}	2-4 viscous damping
ρ	density
ϕ	phase angle
Ω	frequency of the exciting force
ω	natural circular frequency

Chapter 1
INTRODUCTION

1.1 LIMITATIONS OF THE CONVENTIONAL DESIGN

Conventional structural design procedures are generally based on two requirements, safety and serviceability. Safety relates to extreme loadings which are likely to occur no more than once during the lifetime of the structure. The concerns here are the collapse of the structure, major damage to the structure and its contents, and loss of life. Serviceability refers to moderate loadings which may occur several times during the lifetime of the structure. For service loadings, the structure should remain operational, i.e. the structure should suffer minimal damage and, furthermore, the motion experienced by the structure should not exceed specified comfort limits for humans and motion sensitive equipment mounted on the structure (Connor and Klink 1996).

The safety concerns are satisfied by requiring the resistance (i.e. strength) of the individual structural elements to be greater than the demand associated with the extreme loading. Once the structure is proportioned, the stiffness properties are derived and used to check the various serviceability constraints such as elastic behaviour. Iteration is usually necessary to converge to an acceptable structural design. This approach is referred to as strength based design since the elements are proportioned according to strength requirements.

Applying a strength based approach for preliminary design is appropriate when strength is the dominant design requirement. In the past, most structural design problems have fallen in this category. However, a number of developments have occurred recently which have limited the effectiveness of the strength based approach. They include the following (Connor and Klink 1996):

1. The trend towards more flexible structures such as tall slender buildings and longer span horizontal structures has resulted in more structural motion under service

loading, thus shifting the emphasis from safety towards serviceability. Under service loading, limiting the damage that non-structural components can experience restricts the magnitude and distribution of the displacements, while human and equipment comfort limits the peak acceleration. The controlling criterion for wind dominant design tends to be the peak acceleration. Humans begin to feel uncomfortable when the acceleration reaches about 0.02g. Displacement is the controlling criterion for earthquake dominant designs. Some design codes limit the inter-storey displacement measured between two successive floors to 0.01 of the inter-storey height.

2. New types of facilities such as space platforms and semi-conductor manufacturing centres have more severe design constraints on motion than the typical civil structure. The design strategy for these motion sensitive structures is to design the members based on the stiffness needed to satisfy the motion constraints, and then check if the strength requirements are satisfied.

3. Recent advances in material science and engineering have resulted in significant increases in the strength of traditional civil engineering materials such as steel and concrete, as well as a new generation of composite materials. However, the material stiffness has not increased at the same rate. For instance, the strength of structural steel has recently doubled, however its elastic modulus has remained constant. There has also been some increase in the modulus of elasticity for concrete, but this improvement is still small in comparison to the increment in strength. This lag in material stiffness versus material strength has led to a problem with satisfying the serviceability requirements on the various motion parameters. Indeed, for very high strength materials, it is possible for the serviceability requirements to be dominant.

4. Under extreme loading, structural performance and stability requirements constrain the magnitude and distribution of damage that structural components can experience. Structural damage is the key measure for earthquake dominant design. Although design codes allow a structure to experience substantial damage under an extreme earthquake, experience with recent earthquakes has shown that the cost of repairing the structural damage due to inelastic deformation was considerably greater than

anticipated (Horwich 2000). This finding has resulted in a trend towards decreasing the reliance on inelastic deformation and controlling the structural response with other types of energy dissipation and absorption mechanisms.

Conventional structural design was originally developed for static loading conditions and evolved through the assignment of a proper level of ductility reserve for the structural members. Under ordinary loads, the structure remains elastic for the major part of its lifetime but it will enter the plastic state under exceptional lateral loads, such that the input energy should be dissipated in this way. Even if there might be permanent damage to the structural members, the structure is designed in such a way that it should not collapse and no loss of life should result. However, the structure should be retrofitted after each strong event in which damage occurs in the structure, and this can be very expensive and time consuming.

Another limitation of the conventional approach is that it is not capable of mitigating vibrations that do not induce damage in the structure (e.g. the swaying of tall buildings caused by low intensity winds). This means that comfort aspects cannot be considered with this approach. It is important to note that, for very flexible structures such as long bridges or tall buildings, the comfort requirements can be more stringent than those related to the resistance (Casciati et al. 2006).

1.2 STRUCTURAL CONTROL CONCEPT

As a result of the limitations presented by the conventional design approach, the engineering community has moved towards the concept of structural control. The earliest attempts in this direction can be attributed to T. Kobori, who as early as 1956 proposed the idea of incorporating the automatic control philosophy into the seismic-resistant design of structures for enhancing safety against severe earthquakes. In those days, however, control engineering was not ready in terms of either theoretical or practical development to accomplish automatic control of buildings during a seismic event (Nishitani and Inoue 2001). Systematic research on structural control did not

begin until the early 1970s, when J. T. P. Yao (Yao 1972) laid down a rigorous control-theory based concept of structural control as an alternative approach to address the safety problem in structural engineering (Soong 1990). An overview of the structural control concepts and applications can be found in Housner et al. (1997).

Structural control means that the structure is regarded as a dynamic system in which some properties, typically the stiffness or the damping, can be adjusted in such a way that the dynamic effect of the load on the structure decreases to an acceptable level. The natural frequency of the structure, its mode shapes and the corresponding damping values are changed in such a way that the dynamic forces from the environmental loads are reduced (Casciati et al. 2006). Three major structural control strategies can be identified:

1. *Passive control systems*. A passive control system does not require an external power source to operate and utilises the motion of the structure to develop control forces. The control forces are developed as a function of the response of the structure at the location of the passive control system (Symans and Constantinou 1999). Once installed, passive systems cannot be modified instantaneously. A reliable estimate of the design loading and an accurate numerical model of the physical system are needed for any control strategy to be effective. A passive control system also lacks the ability to fine tune the response in a local region. Passive control systems prevail in engineering practice due to their simplicity and the low cost of installing and maintaining them.

2. *Active control systems*. An active control system requires a large power source to operate electro-hydraulic or electromechanical actuators which supply control forces to the structure. The control forces are developed based on feedback from sensors that measure the excitation and/or the response of the structure. The feedback from the structural response may be measured at locations remote from the location of the active control system (Symans and Constantinou 1999). Since active control systems require an external energy source for their operation, it is imperative that the power supply remains uninterrupted throughout a severe seismic disturbance to maintain

structural integrity and performance (Soong 1990). Besides, active control systems have the potential to destabilise the structural system by injecting mechanical energy into the structure and the control device. Therefore, active control will be primarily used as a supplement to passive control in civil engineering applications.

3. *Semi-active control systems*. A semi-active control system requires a small external power source to operate and utilises the motion of the structure to develop the control forces, the magnitude of which can be adjusted by the external power source. The control forces are developed based on feedback from sensors that measure the excitation and/or the response of the structure. The feedback from the structural response may be measured at locations remote from the location of the semi-active control system (Symans and Constantinou 1999). Semi-active control systems provide the reliability and low power requirements of passive control systems while maintaining the versatility and adaptability of fully active control systems. Preliminary studies indicate that appropriately implemented semi-active systems perform significantly better than passive systems and have the potential to achieve the majority of the performance of fully active systems, thus allowing for the possibility of effective response reduction during a wide array of dynamic loading conditions (Spencer and Sain 1997).

The three major classes of control systems are sometimes combined to form so-called *hybrid control systems*. Typically, a hybrid control system employs a combination of passive and active devices however a combination of passive and semi-active devices has also been described in the literature (Symans and Constantinou 1999). A hybrid control system may use active control to supplement and improve the performance of a passive control scheme. Alternatively, passive control may be added to an active control scheme to decrease its energy requirements. Hybrid control systems can alleviate some of the restrictions and limitations that exist for either a passive or an active control system acting alone. Thus, higher levels of performance may be achievable. Moreover, in the case of a power failure, the passive component of a hybrid control system still offers some degree of protection, unlike an active control system (Casciati et al. 2006).

It is important to note that the control system and the structure do not behave as independent dynamic systems but rather interact with each other. In addition, interaction effects also occur between the excitation and structure (i.e. soil-structure interaction) and between the sensors and structure (Symans and Constantinou 1999).

1.3 SEMI-ACTIVE CONTROL SYSTEMS

Semi-active control techniques have been extensively studied from the theoretical, numerical and, more recently, experimental point of view. A state-of-the-art review of semi-active control systems is provided by Symans and Constantinou (1999) and several papers on the subject are also available (e.g. Spencer and Sain 1997, Soong and Spencer 2002, Spencer and Nagarajaiah 2003).

A semi-active control system generally originates from a passive control system which has been subsequently modified to allow for adjustment of mechanical properties. Consequently, semi-active control devices are often viewed as controllable passive devices. The mechanical properties of these systems may be adjusted based on feedback from the excitation and/or from the measured response. In a semi-active control scheme, a controller (a computer) monitors the feedback measurements and, based on a pre-determined control algorithm, generates an appropriate command signal for operation of the semi-active devices. The control forces are developed as a result of the motion of the structure itself and appropriate adjustment of the mechanical properties of the semi-active control system. Furthermore, the control forces in many semi-active control systems primarily act to oppose the motion of the structural system and therefore promote the global stability of the structure. Semi-active control systems generally require a small amount of external power to operate (Symans and Constantinou 1999).

Semi-active control systems are typically nonlinear in nature and have many of the advantages of active control systems, but without requiring the input of a large amount of energy. Some semi-active control systems are completely decentralised using local measurements so that they are robust with respect to the uncertainty of the structural

system. Semi-active control devices do not add mechanical energy to the structural system and require a minimum amount of energy to turn the mechanical component devoted to change the behaviour of the system (for example, an electrically controlled valve). In addition, the control force generated by a semi-active device is always related to the relative velocity and displacement of the device.

A large amount of research on semi-active control has been carried out in the mechanical and aeronautical engineering fields for applications to automotive vibration control and vibration isolation. The concept of semi-active control was introduced by Karnopp et al. (1974) for applications to vehicle vibration isolation. The authors proposed to modify the force of a fluid damper by controlling the opening of a pair of poppet valves. The first proposal for semi-active control of civil engineering structures can be found in Hrovat et al. (1983). The authors examined a tuned mass damper (TMD) equipped with a semi-active variable-orifice fluid damper for control of wind induced vibrations in tall buildings. They demonstrated through numerical simulations the superior performance of the semi-active TMD compared to a passive TMD and a response reduction comparable to that obtained with an active TMD. Since then, several semi-active control systems suited for civil engineering applications have been developed and some of them are now at the stage where large-scale experimentation is underway and actual semi-active control devices have been designed and installed in full-scale structures. Examples of such devices include variable-orifice fluid dampers, variable-stiffness devices, controllable friction devices, smart tuned mass dampers and tuned liquid dampers, controllable-fluid dampers and controllable impact dampers (Spencer and Sain 1997, Spencer and Nagarajaiah 2003).

Because of the intrinsically nonlinear nature of semi-active control devices, the development of control algorithms that are practically implementable and can fully utilise the capabilities of these unique devices is an important and challenging task. A number of nonlinear control algorithms have been developed to take advantage of the particular characteristics of semi-active devices, including bang-bang control, clipped optimal control, bi-state control, fuzzy control methods and adaptive nonlinear control. System integration is another important area of research. Structural systems are complex

combinations of individual structural components. Integration of semi-active control strategies directly into the basic design of these complex systems can offer the optimal combination of performance enhancement versus construction costs and long term effects (Housner et al. 1997).

1.4 RESETTABLE DEVICES

Semi-active resettable devices are essentially hydraulic or pneumatic spring elements in which the un-stretched spring length can be reset to obtain maximum energy dissipation from the structural system. These novel devices are particularly suited for earthquake engineering applications because of their reliability and ability to effectively reduce the structural response. Resettable devices manipulate the stiffness characteristics of the structure and are capable of producing large resisting forces. The lack of dependence on velocity also contributes to beneficial response in shock-type disturbances, because the force transmitted through the device is considerably smaller than those in traditional devices (Bobrow et al. 2000). The basic design of the device is feasible for pneumatic and hydraulic implementations and employs relatively simple mechanisms and control logic. The device offers great reliability due to its reliance on standard hydraulic or pneumatic concepts, particularly when compared to semi-active devices that employ more mechanically and dynamically complicated smart materials such as electro-rheological and magneto-rheological fluids. Like other semi-active devices, resettable devices rely on very low power consumption and are subjected to a set of decentralised control logic (Jabbari and Bobrow 2002).

Resettable devices were introduced by Bobrow et al. (1995) for vibration suppression. The device is essentially a cylinder, a double acting piston and a valve. The valve connects the two chambers of the cylinder and controls the hysteretic response of the device by holding or releasing the pressure between chambers. The valve is activated on the peak displacement of every cycle of motion by equilibrating the pressure in each chamber (Mulligan 2007). This conventional design of the device assumes that the stored energy and working fluid can switch chambers relatively instantly, compared to

the structural motion input to the device, otherwise significant supplemental damping and device performance will be lost (Chase et al. 2006).

In contrast, the resettable device examined in this research has a two-chambered design that utilises each side of the piston independently. This approach eliminates the need to rapidly dissipate energy from one side of the device to the other by treating each side of the piston as an independent chamber with its own valve and control. The two-chambered design allows a wider variety of control laws to be imposed, as each valve can be operated independently, allowing independent control of the pressure on each side of the piston. Air is utilised as the working fluid of the device for simplicity and to make use of the surrounding atmosphere as the fluid reservoir (Chase et al. 2005a).

This novel device also offers the opportunity to sculpt or re-shape the structural hysteretic behaviour due to the possibility to control the device valve and the reset times actively. The ability to semi-actively sculpt the hysteretic behaviour to meet different design needs suggests the potential use of the device in a wider range of structural and civil engineering applications.

1.5 OBJECTIVES AND SCOPE OF THE RESEARCH

The main purpose of this research is to investigate the effectiveness and feasibility of semi-active resettable devices as a means of adding supplemental damping and stiffness in structures subjected to severe earthquake ground motions. The principal objectives of this research include the following:

a. Analytical studies to evaluate the effects of adding viscous damping on the harmonic and seismic response of single-degree-of-freedom systems. This topic is an aside to the main direction of the thesis. However, it introduces important concepts that will appear in subsequent chapters of the thesis.

b. Development of analytical models to describe the dynamic behaviour of a newly developed semi-active resettable device.

c. Development of analytical models to describe the seismic behaviour of a four-storey model structure equipped with two semi-active resettable devices.

d. Seismic testing of the four-storey model structure with and without resettable devices using different earthquake ground motions.

e. Assessment of the seismic response of the model structure with and without semi-active resettable devices based on the experimental results.

f. Analytical investigations to evaluate the effectiveness of semi-active resettable devices to reduce the seismic response of full-scale civil engineering structures.

g. Assessment of the performance of a fibre-optic gyroscope utilised to measure the rotation rates of structural components during the seismic testing. Although this objective is not related to the research topic covered in the thesis, it is included herein because of the significance of the FOG as a new measurement concept in civil engineering. Besides, the investigation on the FOG was conducted simultaneously with the seismic testing of the model structure.

It is intended that this research will provide insights into the seismic performance of civil engineering structures controlled by semi-active resettable devices. The thesis will present analytical and experimental studies that evaluate the potential of the resettable devices in reducing the seismic response of structures. Results obtained from numerical simulations and shake table tests will be evaluated and interpreted. Conclusions will be drawn based on the analytical and experimental results and recommendations for future research will be made.

1.6 ORGANIZATION OF THE THESIS

This thesis investigates the application of semi-active control schemes to reduce the response of civil engineering structures subjected to large earthquake ground motions. The research focuses on the seismic performance of newly developed semi-active resettable devices. The material of this research study flows from analytical modelling to experimental testing to implementation issues. A brief description of the individual chapters is provided below.

Chapter 2 examines the effect of adding structural viscous damping for single-degree-of-freedom systems subjected to harmonic and seismic excitations. The concept of 2-4 viscous damping is introduced. The concept involves the addition of viscous damping to the second and fourth quadrants of the force-displacement curve. Numerical simulations evaluate the effectiveness of the concept to reduce the structural response.

Chapter 3 describes a semi-active resettable device with a novel two-chambered design. The device design utilises each chamber independently that allows a wider variety of control laws to be imposed. The prototype device employs air as the working fluid. The resettable device also offers the opportunity to manipulate hysteretic behaviour via innovative control laws.

Analytical studies of an ideal semi-active resettable tendon are presented in Chapter 4. The optimal configuration of the resettable tendon in a four-storey model structure is investigated to reduce the earthquake response. Computer simulations are performed to evaluate the seismic performance of the resettable tendon. The effects resulting from the addition of the resettable tendon to the model structure are examined.

Chapter 5 describes the seismic testing of a four-storey one-fifth scale structure equipped with two semi-active resettable devices. The model structure is subjected to different earthquake ground motion and controlled by the resettable devices. The seismic response of the model structure with and without resettable devices is examined. Results of the shake table tests are presented and interpreted.

Chapter 6 focuses on the development of a numerical model to predict the behaviour of the semi-active model structure during the shake table tests. The assumptions adopted for the analytical modelling of the resettable tendon are described. Comparisons of the analytical predictions with the experimental results are used to evaluate the performance of the numerical model.

The application of the semi-active resettable devices to reduce the seismic response of structural building systems is investigated in Chapter 7. Analytical studies examine the performance of a twelve-storey reinforced concrete building subject to earthquake loads and controlled by resettable devices. Several arrangements and control configurations for the resettable devices are investigated.

Chapter 8 explores the feasibility of the use of a newly developed fibre-optic gyroscope to measure the rotation rates, rotations, displacements and inter-storey drifts of civil engineering structures. Fibre optic gyroscopes are devices that use the interference of light to detect mechanical rotations. They are very compact, easy to install and, unlike conventional displacement measuring devices, do not require a fixed reference frame to operate.

Finally, overall conclusions of this research and recommendations for future research on semi-active structural control are presented in Chapters 9 and 10, respectively.

1.7 ORIGINAL CONTRIBUTIONS OF THE THESIS

The principal research contribution of this thesis is the experimental validation of the resettable devices for seismic protection of civil engineering structures. The shake table tests described herein are the first large-scale structural application of the resettable devices proposed in this research. The experiments also validate the capability of the devices to sculpt or re-shape structural hysteretic behaviour for the first time. The findings of this research represent an important step for the design and implementation of the resettable devices in full-scale structures.

The thesis also introduces the concept of 2-4 viscous damping to reduce harmonic and seismic vibrations. Numerical simulations are conducted to assess the effect of adding viscous damping to the second and fourth quadrants of the force-displacement curve. The initial results reported herein demonstrate the validity of this concept for a range of SDOF systems subjected to harmonic and seismic excitations.

Finally, the thesis proposes the use of a fibre-optic gyroscope to measure rotation rates, rotations, displacements and inter-storey drifts of structures. The shake table tests and the in-situ testing described herein represent the first applications of the FOG in civil engineering. The experimental results validate the accuracy and the dynamic range of the FOG. The in-situ measurements confirm the suitability of the FOG for applications in actual structures.

The general conclusions and a more detailed description of the research contributions of this doctoral thesis are given in Chapter 9.

1.8 SUMMARY

This chapter has introduced the concept of structural control and described the limitations of the conventional approach to design earthquake-resistant structures. The main structural control techniques were presented and their benefits and limitations were discussed. The advantages of semi-active control systems to reduce earthquake-induced vibrations were described. Semi-active resettable devices can be defined as hydraulic or pneumatic spring elements that possess the ability to release the stored spring energy at any time. Resettable devices can manipulate the stiffness properties of the structure and are capable of producing large resisting forces. The potential of the resettable devices for earthquake engineering applications was highlighted. The objectives and scope of the research were presented. The chapter ended by describing the organization of the material presented in the thesis.

Chapter 2
EFFECT OF ADDING 2-4 VISCOUS DAMPING

2.1 INTRODUCTION

Damping is the process by which physical systems, such as civil engineering structures, dissipate and absorb the energy input from external excitations. Damping prevents energy build-up and reduces the system response, especially near resonance conditions where it governs the response (Connor and Klink 1996). The dissipation or absorption of energy is caused by several external and internal mechanisms. They include the following:

a. Energy dissipation due to the viscosity of the material.

b. Energy dissipation and absorption caused by the material undergoing cyclic inelastic deformation and ending up with some residual deformation.

c. Energy dissipation associated with overcoming the friction between moving bodies in contact, such as flexible connections.

d. Energy dissipation resulting from the interaction of the structure with its surrounding environment.

e. Damping devices installed at discrete locations in the structures to supplement their natural energy dissipation and/or absorption capabilities.

The presence of some damping in conventional structures has long been recognized. Although the nature of inherent energy dissipation in civil structures has not been explicitly identified, inherent equivalent viscous damping of about 2% to 5% of critical damping has become accepted in practice for linear response analyses of typical

buildings. In fact, most of the design spectra developed assume 5% of critical viscous damping in the system (Hanson and Soong 2001).

It is important to note that this chapter is an aside to the principal direction of the thesis. However, it covers significant concepts studied in subsequent chapters of the thesis. The chapter is mainly concerned with the fundamental principles of adding viscous damping to certain quadrants of the force-displacement curve and does not intend to be complete. The basic concept is introduced and preliminary results are presented. It is hoped that this brief exploration will lead to more serious studies into this fascinating subject.

In this chapter, the effect of adding structural viscous damping is examined for a single-degree-of-freedom (SDOF) system. The concept of 2-4 viscous damping is introduced. Numerical simulations are used to demonstrate the validity of this concept for linear SDOF systems subjected to harmonic and seismic excitations. Linear time-history analyses and response spectra for SDOF systems are presented to assess the effect of adding 2-4 viscous damping.

Finally, the approach presented herein can be generalised to examine the effects of adding viscous damping to all quadrants (1-2-3-4 viscous damping) and to the first and third quadrants (1-3 viscous damping) of the force-displacement diagram. The 2-4 viscous damping is chosen because it may reduce the structural response without increasing the loads on the foundation of the structure.

2.2 ENERGY DISSIPATED BY VISCOUS DAMPING

The actual damping in a SDOF system can be idealised satisfactorily by a linear viscous damper or dashpot. The damping coefficient is selected in such a way that the vibratory energy it dissipates is equivalent to the energy dissipated in all of the combined damping mechanisms present in the actual system. This idealisation is therefore called equivalent viscous damping (Chopra 2001, Clough and Penzien 1993).

Consider the lateral motion of the basic SDOF system shown in Figure 2.1, consisting of a mass *m*, connected to a firm support by two elements in parallel, a spring with linear elastic stiffness *k*, and a damper with linear viscosity *c*. The system is subjected to an externally applied dynamic force *p* that varies with time *t*. Under the influence of such a force, the mass of the system displaces in the lateral direction by an amount *u*.

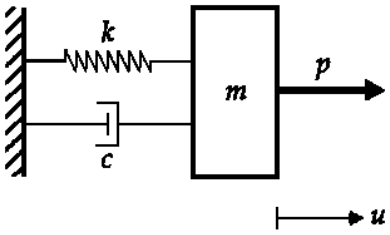

Figure 2.1 SDOF system subjected to dynamic force.

The equation of motion governing the displacement $u(t)$ of the SDOF system shown in Figure 2.1 is

$$m\ddot{u} + c\dot{u} + ku = p(t) \tag{2.1}$$

Now consider the case when the external force is varying harmonically with time:

$$p(t) = p_0 \sin \Omega t \tag{2.2}$$

where p_0 is the amplitude or maximum value of the load and Ω is the excitation or forcing frequency. The equation of motion becomes

$$m\ddot{u} + c\dot{u} + ku = p_0 \sin \Omega t \tag{2.3}$$

Equation (2.3) can be solved by the standard procedures to obtain the system response. The steady-state response of the system due to harmonic force can be written as

$$u(t) = u_0 \sin(\Omega t - \phi) \tag{2.4}$$

where

$$u_0 = \frac{p_0}{k} H_1 \tag{2.5}$$

$$H_1 = \frac{1}{\sqrt{(1-\beta^2)^2 + (2\xi\beta)^2}} \tag{2.6}$$

$$\tan\phi = \frac{2\xi\beta}{1-\beta^2} \tag{2.7}$$

$$\beta = \frac{\Omega}{\omega} \tag{2.8}$$

$$\omega = \sqrt{\frac{k}{m}} \tag{2.9}$$

$$\xi = \frac{c}{2\omega m} \tag{2.10}$$

In these equations, u_0 represents the amplitude of motion, ω is the natural circular frequency of vibration and ξ represents the damping ratio or fraction of critical damping. The term $\frac{p_0}{k}$ is the displacement response that would occur if the load were applied statically, β is the frequency ratio and H_1 represents the effect of the time-varying nature of the response (Humar 2002).

The damping force f_D is related to the velocity $\dot{u}$ across the linear viscous damper by

$$f_D = c\dot{u} \tag{2.11}$$

where the viscous damping coefficient, c, is a property of the system or the damping device used. It is not possible to identify all the mechanisms that dissipate vibratory energy of actual structures. Therefore, free and force vibration experiments on actual structures provide the data to evaluate the equivalent damping coefficient.

The equivalent viscous damper is intended to model the energy dissipation at deformation amplitudes within the linear elastic limit of the overall structure. Over this range of deformation, the damping coefficient c determined from experiments may vary with the deformation amplitude. This nonlinearity of the damping property is usually not considered explicitly in dynamic analyses. It may be handled indirectly by selecting a value for the damping coefficient that is appropriate for the expected deformation amplitude, usually taken as the deformation associated with the linearly elastic limit of the structure (Chopra 2001).

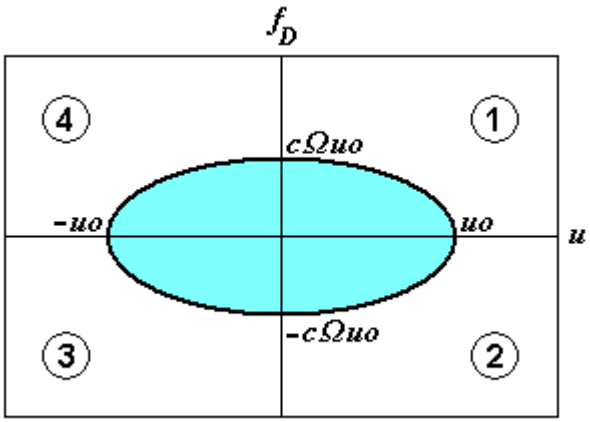

(a) Normal viscous damping

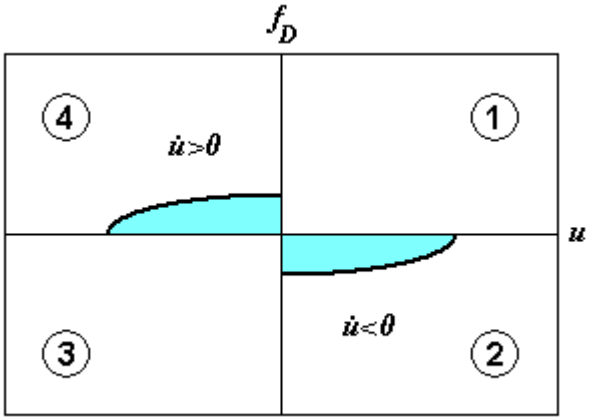

(b) 2-4 viscous damping

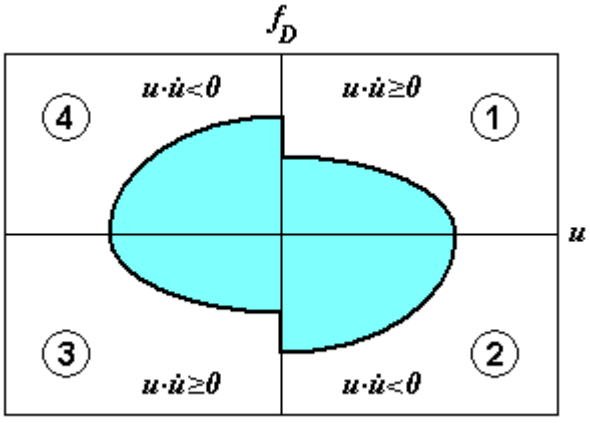

(c) Added viscous damping

Figure 2.2 Force-displacement diagrams.

The energy dissipated by viscous damping can be calculated by using the Equations (2.4) and (2.11) as follows:

$$f_D = c\dot{u}(t) = c\Omega u_0 \cos(\Omega t - \phi)$$

$$f_D = c\Omega\sqrt{u_0^2 - u_0^2 \sin^2(\Omega t - \phi)}$$

$$f_D = c\Omega\sqrt{u_0^2 - [u(t)]^2}$$

This equation can be rewritten as

$$\left(\frac{f_D}{c\Omega u_0}\right)^2 + \left(\frac{u}{u_0}\right)^2 = 1 \tag{2.12}$$

Equation (2.12) represents the equation of the ellipse shown in Figure 2.2a. The area enclosed by the ellipse gives the energy dissipated by viscous damping in one cycle of harmonic vibration:

$$E_D = \pi(c\Omega u_0)(u_0)$$

$$E_D = \pi c \Omega u_0^2 \tag{2.13}$$

The energy dissipated is proportional to the square of the amplitude of motion. It is not a constant value for any given amount of damping and amplitude since the energy dissipated increases linearly with excitation frequency. The hysteresis loop associated with the viscous damping is the result of dynamic hysteresis since it is related to the dynamic nature of the loading. The loop area is proportional to the excitation frequency; this implies that the force-deformation curve becomes a single-valued curve if the cyclic load is applied slowly enough ($\Omega = 0$). A distinguishing characteristic of the dynamic hysteresis is that the hysteresis loops tend to be elliptical in shape rather than pointed shape, which is associated with plastic deformations. In the latter case, the hysteresis loops develop even under static cyclic loads; this phenomenon is therefore known as static hysteresis because the force-deformation curve is insensitive to the deformation rate (Chopra 2001).

2.3 CONCEPT OF 2-4 VISCOUS DAMPING

Supplemental damping devices can be used to add damping to the structure and improve its natural energy dissipation capacity. Research has shown that supplemental dampers have a significant effect on the response of the structure under earthquake excitations (Pekcan 1998, Soong and Spencer 2002). Structural displacements, inter-storey drifts and accelerations are markedly reduced. The ductility demand of the structure under the design earthquake is also greatly reduced (Lin 1999). In general, when incorporated into a structure, supplemental dampers dissipate earthquake-induced energy and may add stiffness and strength to the structure (Hanson and Soong 2001).

The response of the SDOF system will now be examined by adding viscous damping to the second and fourth quadrants of the force-displacement curve as shown in Figure 2.2b. This represents the addition of damping to the system when it is moving from its displaced position to its equilibrium position. The added damping will be denoted as the 2-4 viscous damping.

2.3.1 Response to harmonic excitation

Dividing Equation (2.3) by the mass *m* and utilising Equations (2.9) and (2.10) leads to

$$\ddot{u} + 2\xi\omega\ \dot{u} + \omega^2 u = \frac{p_0}{m}\sin\Omega t \tag{2.14}$$

This is the equation of motion of the SDOF system with normal or conventional viscous damping as shown in Figure 2.2a. Consider now the case when viscous damping is added to the second and fourth quadrants of the force-displacement curve (Fig. 2.2c). The equation of motion of the SDOF system subjected to harmonic load becomes

$$\ddot{u} + 2(\xi + \xi_{2-4})\omega\ \dot{u} + \omega^2 u = \frac{p_0}{m}\sin\Omega t \tag{2.15}$$

where $\xi_{2-4} = 0$ (when $u\dot{u} \geq 0$)

$\xi_{2\text{-}4}$ represents the amount of viscous damping added to the second and fourth quadrants of the dynamic hysteresis loop and ξ is the damping ratio or fraction of critical damping coefficient.

The response of the SDOF system with added 2-4 viscous damping was analysed using MATLAB [Version 7.0.0.19920 (R14)]. The linear second-order differential equation of motion of the system was solved by using the in-built ordinary differential equation solver, ode45. The ode45 solver is based on the Runge-Kutta algorithm (Rosser 1967) to solve a differential equation numerically.

Figures 2.3, 2.4 and 2.5 show the dynamic response of the SDOF system described by Equations (2.14) and (2.15) for different values of β (0.25, 1 and 1.5) and m, k and p_0 equal to 0.125 kg, 2 N/m and 1 N, respectively. Three values of $\xi_{2\text{-}4}$ were used in the analyses, namely 0.05, 0.10 and 0.15. The damping ratio ξ was considered to be equal to 5% of critical damping for all cases studied.

The response of the SDOF system will now be examined for the three regions of the excitation-frequency scale shown in Figures 2.3, 2.4 and 2.5:

a. If the force is slowly varying (β = 0.25), the displacements decrease with the addition of 2-4 viscous damping very slightly. Figure 2.3 shows that the displacements appear to be unaffected by the addition of 2-4 viscous damping. Effect of the added damping starts to be apparent when $\xi_{2\text{-}4}$ = 0.15 (Fig. 2.3c).

b. If the forcing frequency is equal to the natural frequency of the system (β = 1), the displacements are greatly reduced by the addition of 2-4 viscous damping as shown in Figure 2.4.

c. If the force is rapidly varying (β = 1.5), the displacements markedly decrease with the addition of 2-4 viscous damping as shown in Figure 2.5.

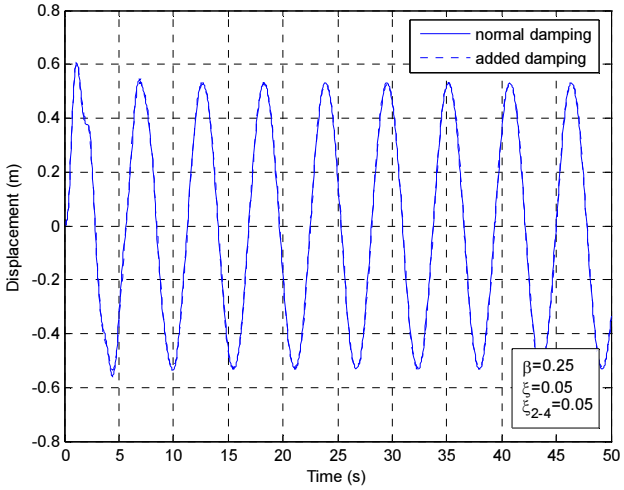

(a) Comparison of displacements ($\xi_{2\text{-}4}$ = 0.05)

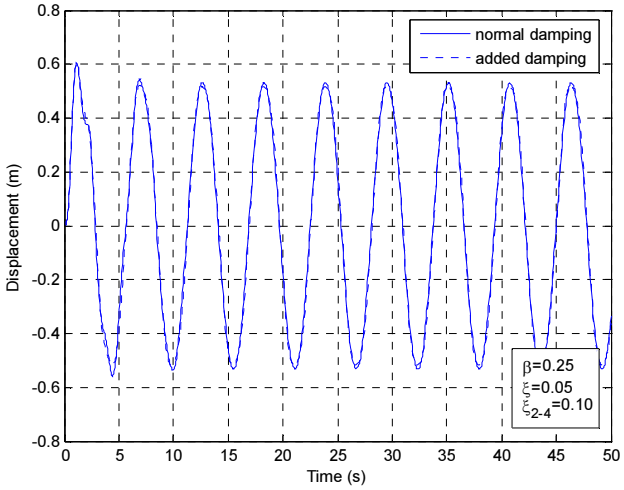

(b) Comparison of displacements ($\xi_{2\text{-}4}$ = 0.10)

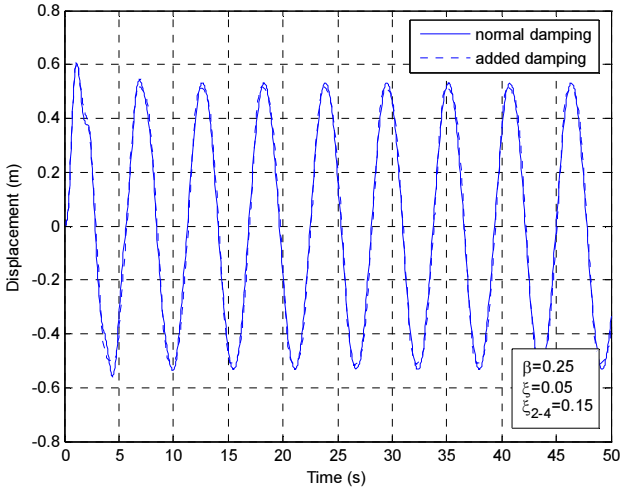

(c) Comparison of displacements ($\xi_{2\text{-}4}$ = 0.15)

Figure 2.3 Response to harmonic loading (β = 0.25).

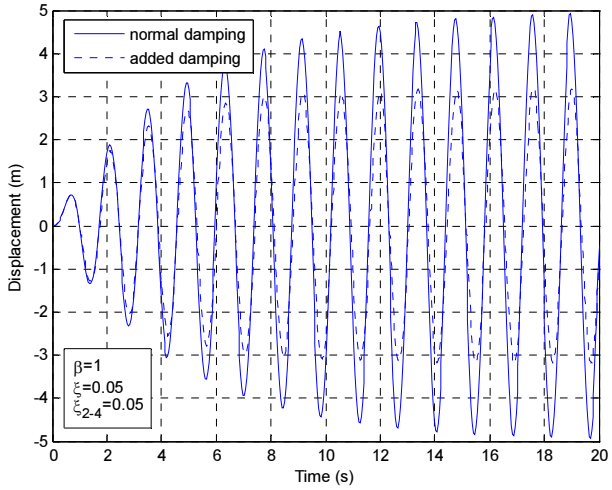

(a) Comparison of displacements ($\xi_{2\text{-}4}$ = 0.05)

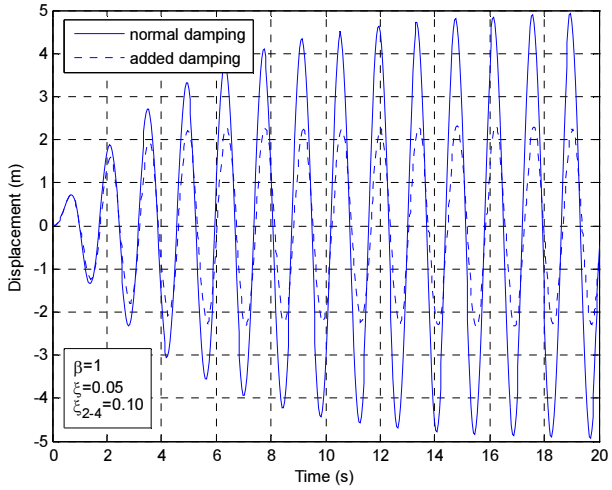

(b) Comparison of displacements ($\xi_{2\text{-}4}$ = 0.10)

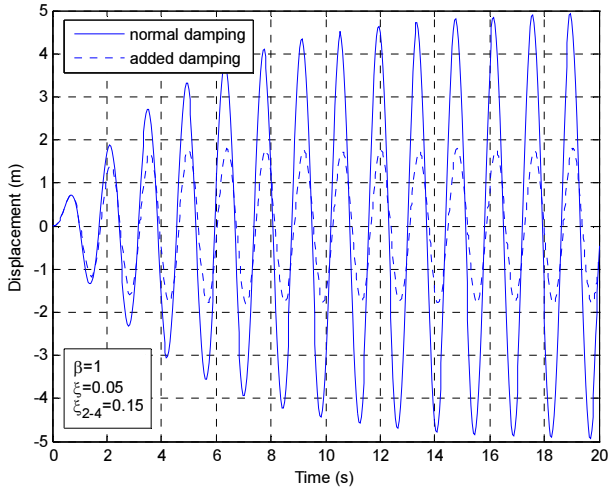

(c) Comparison of displacements ($\xi_{2\text{-}4}$ = 0.15)

Figure 2.4 Response to harmonic loading (β = 1).

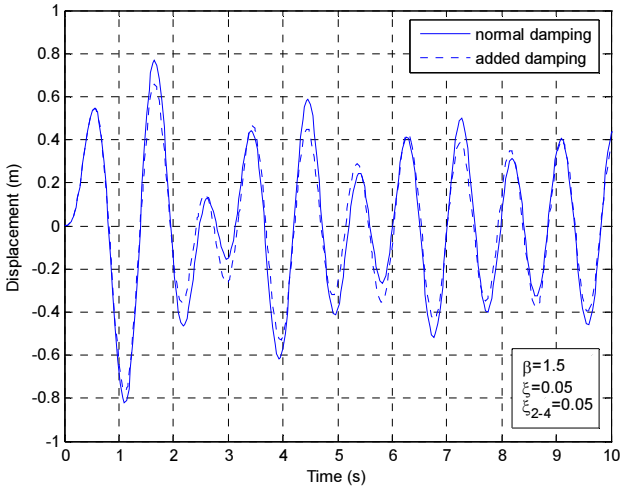

(a) Comparison of displacements ($\xi_{2\text{-}4}$ = 0.05)

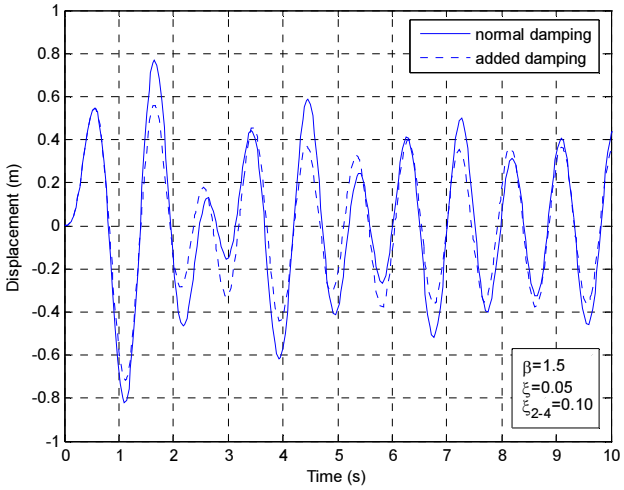

(b) Comparison of displacements ($\xi_{2\text{-}4}$ = 0.10)

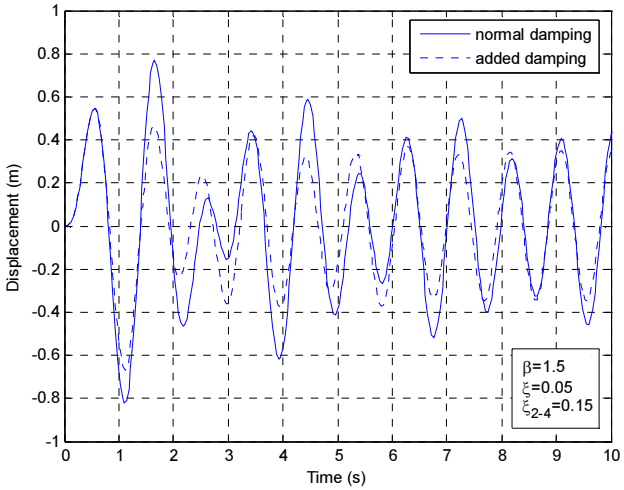

(c) Comparison of displacements ($\xi_{2\text{-}4}$ = 0.15)

Figure 2.5 Response to harmonic loading (β = 1.5).

These results show that the response reduction of SDOF systems with added 2-4 viscous damping is dependent on the excitation frequency and that the addition of 2-4 viscous damping is more effective in reducing the dynamic response when the forcing frequency is very close or equal to the natural frequency (resonance case). Although these findings can also be true for any dynamic system with or without 2-4 damping added, the results confirm that adding viscous damping to only one half of the vibration cycle is beneficial for a wide range of SDOF systems under harmonic excitation.

2.3.2 Response to seismic excitation

The equation of motion for the SDOF system subjected to seismic excitation (Fig. 2.6) has the form

$$m\ddot{u} + c\dot{u} + ku = -m\ddot{u}_g \tag{2.16}$$

where m, c and k are the mass, damping and stiffness parameters of the SDOF system, u is the displacement relative to the ground and $\ddot{u}_g$ is the ground acceleration.

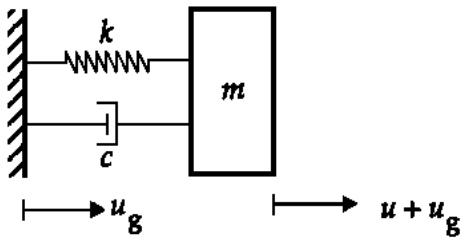

Figure 2.6 SDOF system subjected to ground motion.

Dividing by m and utilising Equation (2.9) for the natural circular frequency ω and Equation (2.10) for the damping ratio ξ, Equation (2.16) can be rewritten as

$$\ddot{u} + 2\xi\omega\,\dot{u} + \omega^2 u = -\ddot{u}_g \tag{2.17}$$

For the case of viscous damping added to the second and fourth quadrants of the force-displacement curve, Equation (2.17) takes the form

$$\ddot{u} + 2(\xi + \xi_{2-4})\omega\,\dot{u} + \omega^2 u = -\ddot{u}_g \qquad (2.18)$$

where $\xi_{2-4} = 0$ (when $u\dot{u} \geq 0$)

A MATLAB-based code was written to examine the response of the SDOF system with added 2-4 viscous damping under earthquake excitation. The equation of motion of the system was solved using the Newmark-Beta method (Newmark 1959) with the constant average acceleration solution for earthquake ground motion. The following earthquake ground motions were chosen for this study:

a. Imperial Valley, 18 May 1940 – El Centro north-south (NS) component
b. Kern County, 21 July 1952 – Taft S21W component
c. Northridge, 17 January 1994 – Sylmar County Hospital (Chan 9: 0 deg)
d. Kobe, 17 January 1995 – JMA Observatory N00E component.

Linear time-history analyses were carried out for three natural periods (T = 0.5 s, 1 s and 1.5 s), ξ = 0.05 of critical damping and $\xi_{2\text{-}4}$ = 0.05. Figures 2.7 to 2.10 show the response of the SDOF system with normal and added viscous damping to the different earthquake ground motions.

In general, it is seen that the added 2-4 viscous damping reduces the earthquake-induced displacements of linear SDOF systems. The amount of reduction varies depending on the inherent mass, stiffness and damping characteristics of the system, on the amplitude, frequency content and duration characteristics of the earthquake ground motion that the system is expected to experience, and on the amount of supplemental viscous damping added.

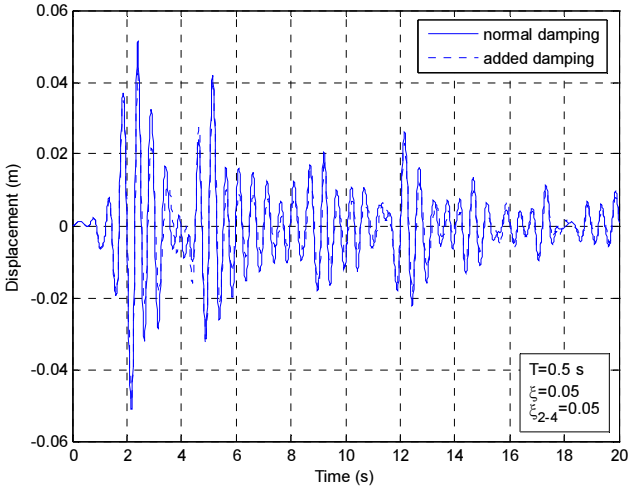

(a) Displacement time-history for $T = 0.5$ s

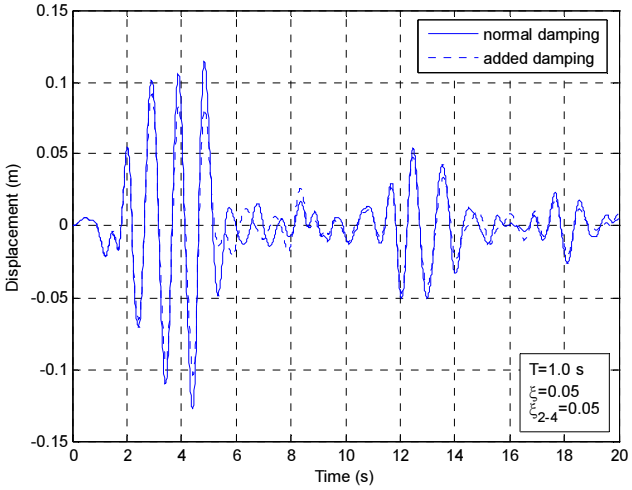

(b) Displacement time-history for $T = 1$ s

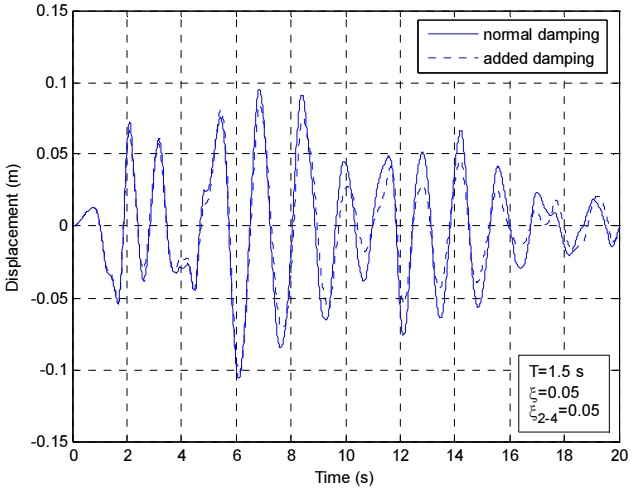

(c) Displacement time-history for $T = 1.5$ s

Figure 2.7 Seismic response under El Centro ground motion.

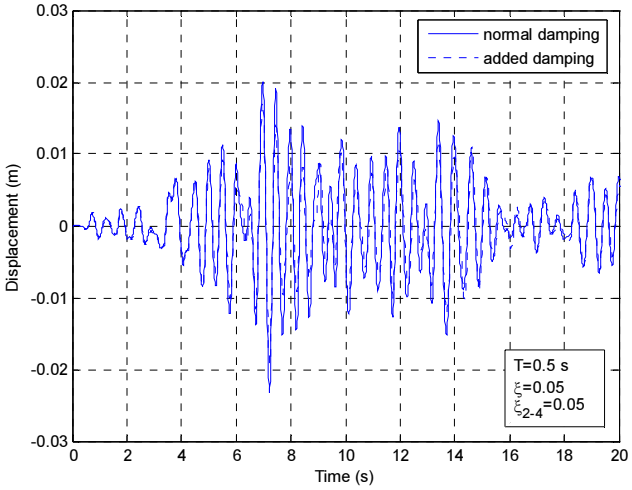

(a) Displacement time-history for $T = 0.5$ s

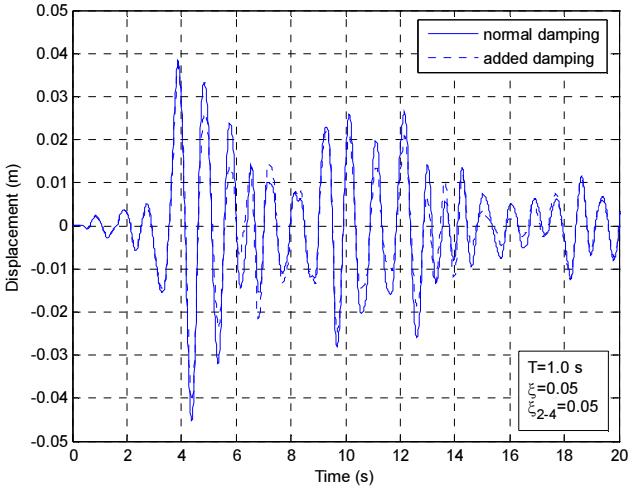

(b) Displacement time-history for $T = 1$ s

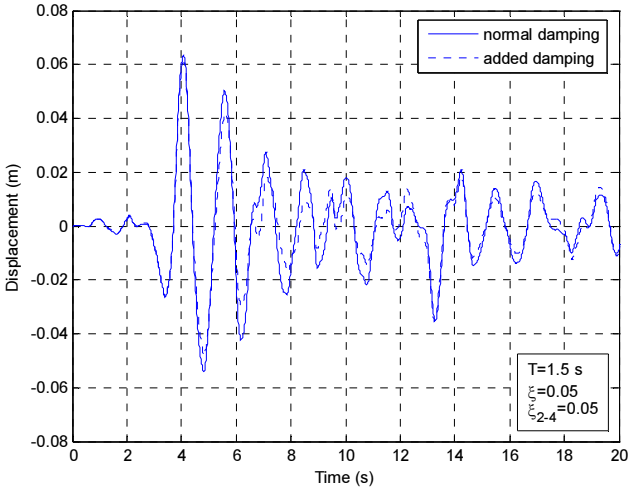

(c) Displacement time-history for $T = 1.5$ s

Figure 2.8 Seismic response under Taft ground motion.

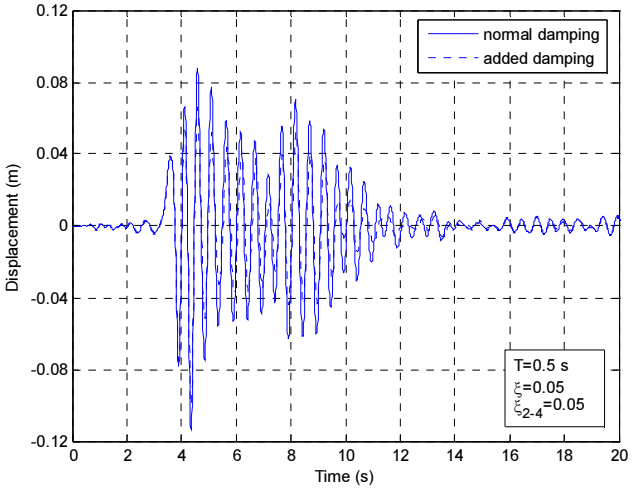

(a) Displacement time-history for $T = 0.5$ s

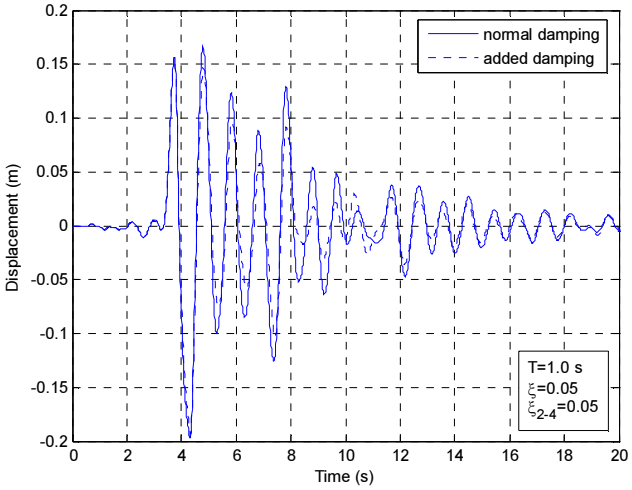

(b) Displacement time-history for $T = 1$ s

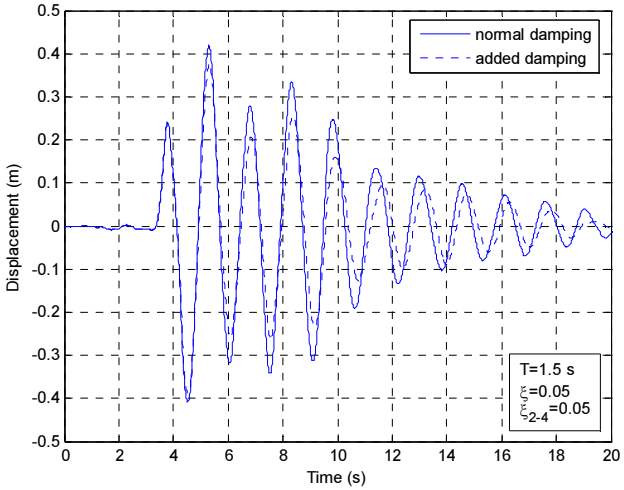

(c) Displacement time-history for $T = 1.5$ s

Figure 2.9 Seismic response under Sylmar ground motion

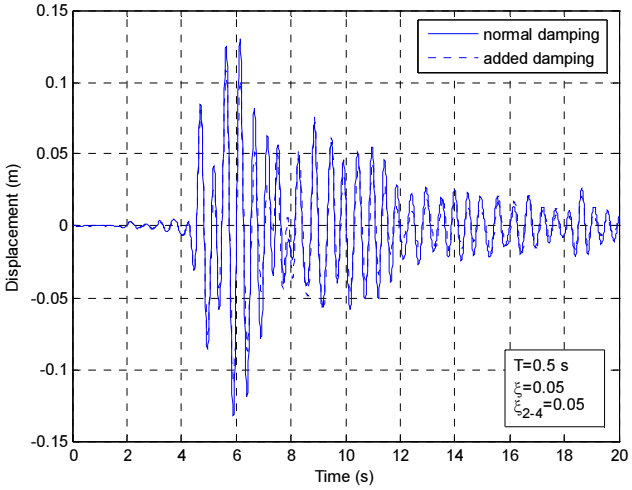

(a) Displacement time-history for $T = 0.5$ s

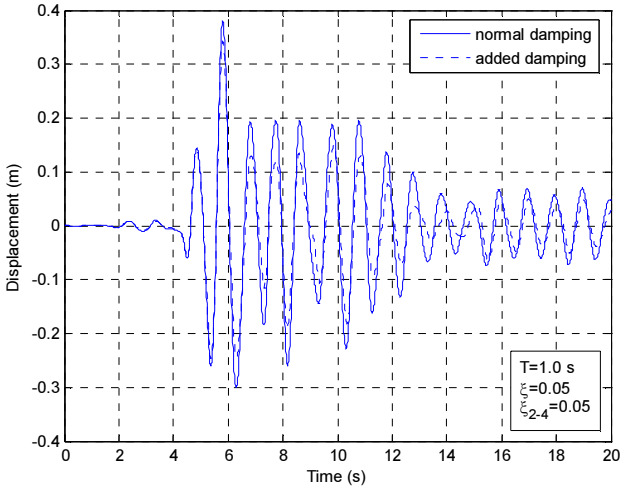

(b) Displacement time-history for $T = 1$ s

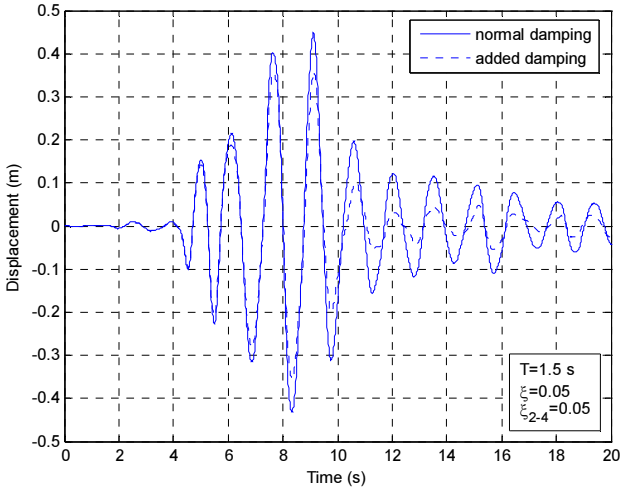

(c) Displacement time-history for $T = 1.5$ s

Figure 2.10 Seismic response under Kobe ground motion.

2.3.3 Earthquake Response Spectra

The acceleration response spectrum (SA), the velocity response spectrum (SV) and the displacement response spectrum (SD) provide a convenient means to summarize the maximum response of all possible linear SDOF systems to a particular component of ground motion (Chopra 2001). These spectra are defined, respectively, as the maximum absolute acceleration of the mass, the maximum relative velocity and maximum relative displacement of the mass with respect to the ground, as a function of the natural period of the system. Typically, the maximum relative displacement between the mass and its base is computed from a ground motion acceleration record for different structural periods to obtain the spectral displacement, SD. The corresponding pseudo-spectral acceleration (PSA) and pseudo-spectral velocity (PSV) values are then calculated from SD by using period factors. Research has shown that the PSA value is reasonably close to the actual SA value when the damping is small (less than 10%). For larger damping, this simple mathematical relationship does not work so well, and the actual SA value will always equal or exceed the PSA value (Hanson and Soong 2001).

In order to determine the impact of the addition of viscous damping in a wide range of systems, response spectra for SDOF systems with and without added 2-4 damping were created using a MATLAB-based code. Relative displacements are recognized as a key parameter for estimating building damage. Therefore, the spectral displacement, SD, is used here to illustrate the effect of adding viscous damping. Nevertheless, the pseudo-spectral velocity, PSV, and the pseudo-spectral acceleration, PSA, are also included because they are useful in studying characteristics of response spectra, constructing design spectra, and relating structural dynamics results to building codes (Chopra 2001).

Figures 2.11 to 2.14 show the response spectra for the four earthquake ground motions considered. Equations (2.17) and (2.18) are utilised to calculate the seismic response of the SDOF systems. The natural periods of vibration vary from 0 to 5 s. For clarity in the presentation, only the response spectra for SDOF systems with $\xi = 0.05$ and $\xi_{2\text{-}4} = 0.05$ are shown.

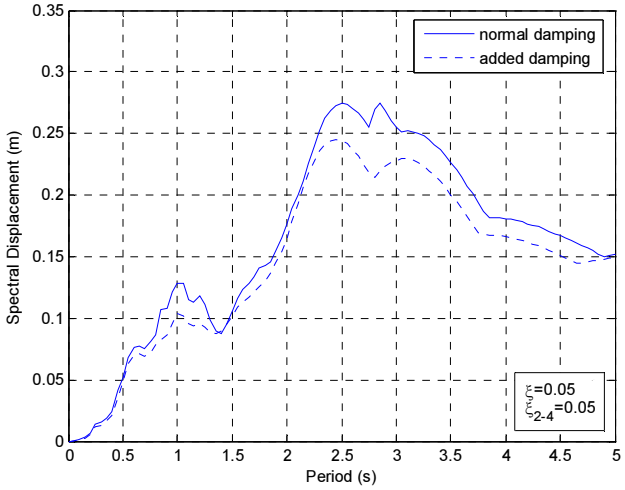

(a) Displacement response spectrum

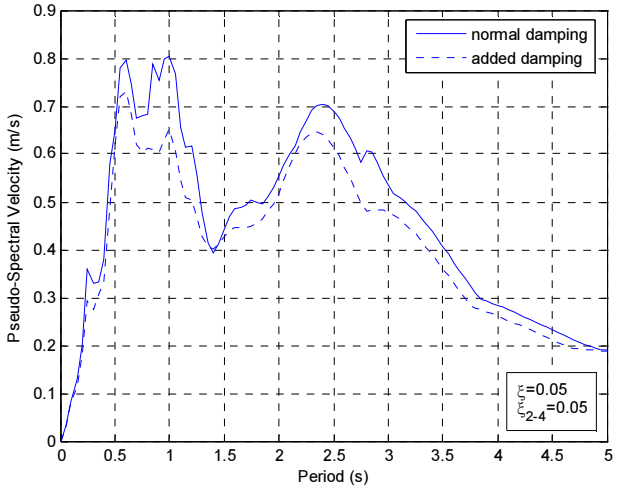

(b) Pseudo-velocity response spectrum

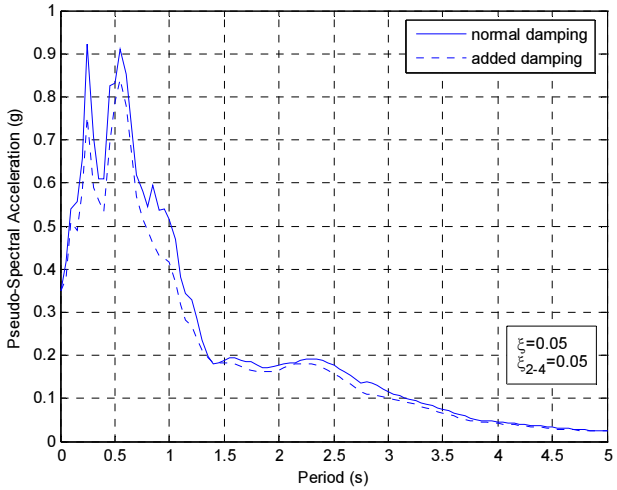

(c) Pseudo-acceleration response spectrum

Figure 2.11 Response spectra for El Centro ground motion.

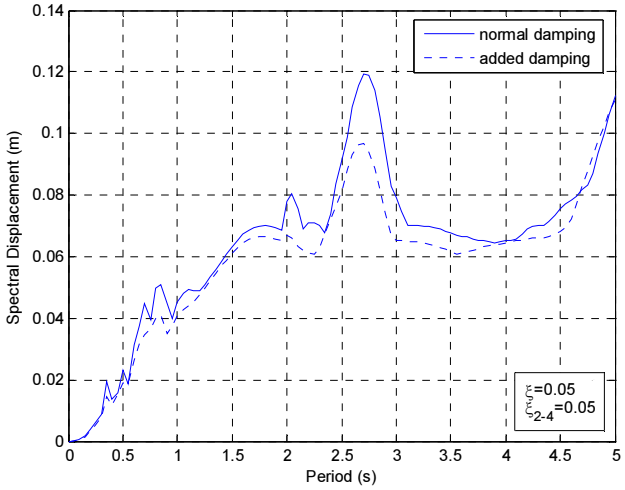

(a) Displacement response spectrum

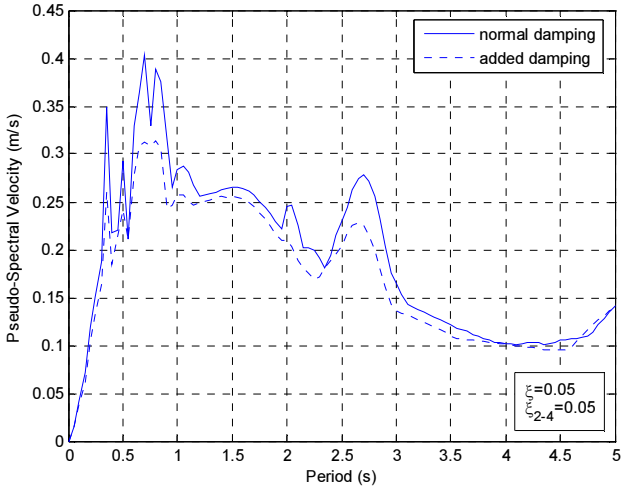

(b) Pseudo-velocity response spectrum

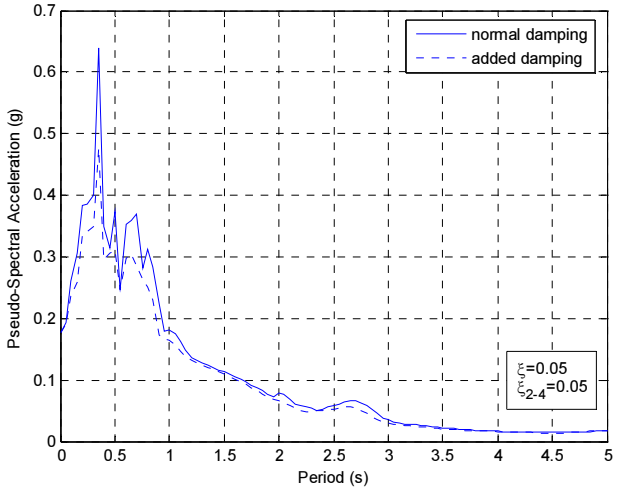

(c) Pseudo-acceleration response spectrum

Figure 2.12 Response spectra for Taft ground motion.

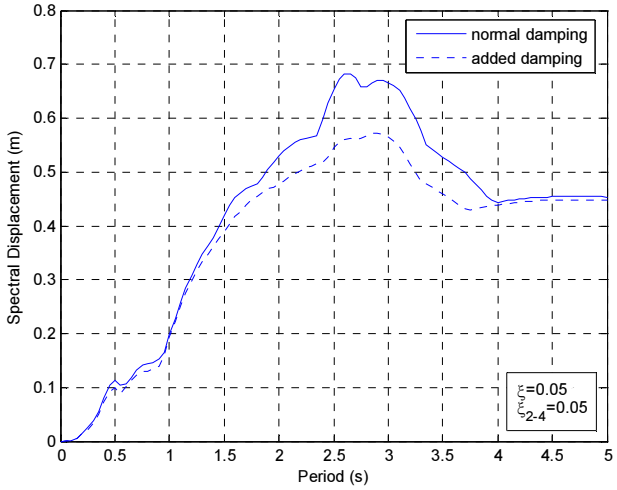

(a) Displacement response spectrum

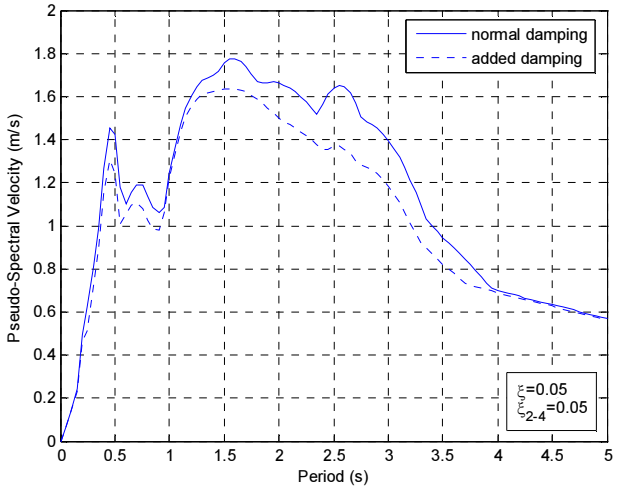

(b) Pseudo-velocity response spectrum

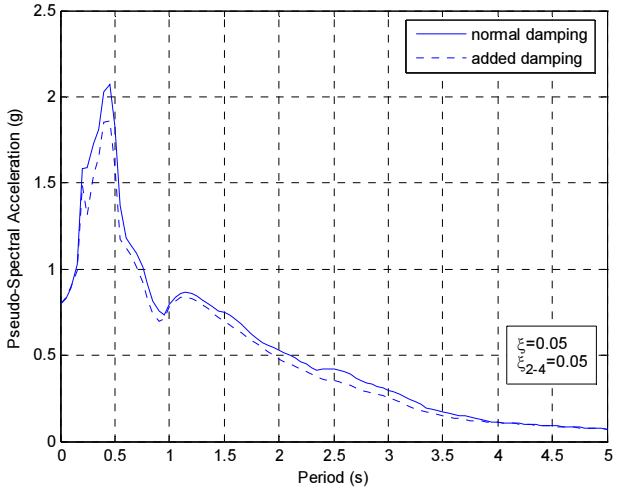

(c) Pseudo-acceleration response spectrum

Figure 2.13 Response spectra for Sylmar ground motion.

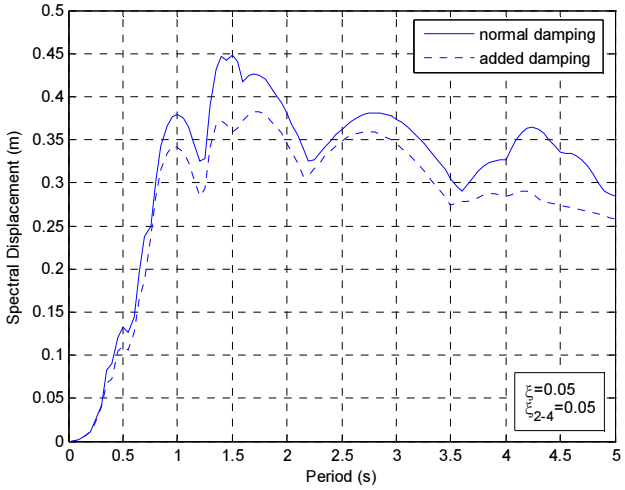

(a) Displacement response spectrum

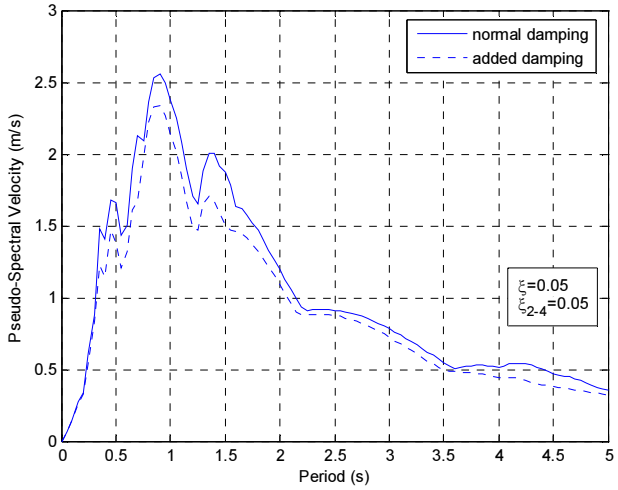

(b) Pseudo-velocity response spectrum

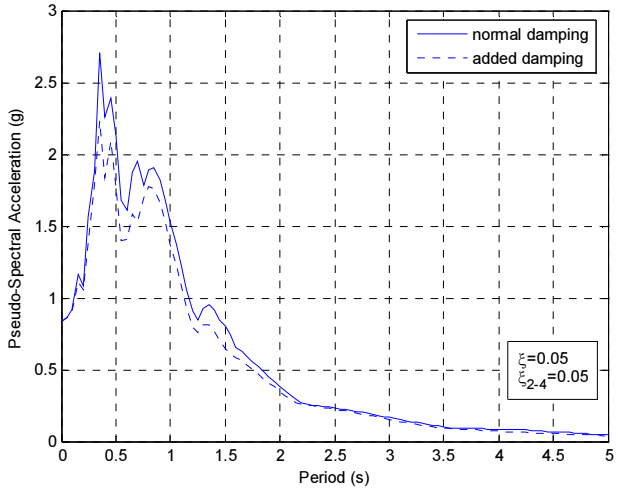

(c) Pseudo-acceleration response spectrum

Figure 2.14 Response spectra for Kobe ground motion.

It can be observed that the addition of 2-4 viscous damping significantly reduces the spectral displacement of SDOF systems with longer periods and the pseudo-spectral acceleration of SDOF systems with shorter periods of vibration.

Overall, the addition of viscous damping to the second and fourth quadrants of the force-displacement relationship is shown to be beneficial for a wide range of SDOF systems subjected to different earthquake ground motions.

Appendix A compares the response spectra obtained with the MATLAB-based code developed here with the response spectra provided by the sub-program SPECTRA of the RUAUMOKO computer program.

2.4 SUMMARY

The primary purpose of this chapter was to examine the effect of adding structural viscous damping for SDOF systems subjected to harmonic and seismic excitations. The concept of 2-4 viscous damping was introduced. This concept involves the addition of viscous damping to the second and fourth quadrants of the force-displacement curve. The validity of the concept was demonstrated by performing a large number of numerical simulations using different MATLAB-based codes. The response of SDOF systems with conventional and added 2-4 viscous damping was analysed and interpreted. Linear time-history analyses and response spectra were presented to assess the effect of adding viscous damping. Simulation results showed that the addition of 2-4 viscous damping is beneficial for reducing the harmonic and seismic response of a wide range of SDOF systems.

Chapter 3
SEMI-ACTIVE RESETTABLE DEVICES

3.1 INTRODUCTION

Semi-active resettable devices have recently been considered to reduce the seismic response of civil engineering structures (Jabbari and Bobrow 2002, Hunt 2002, Barroso et al. 2003, Chase et al. 2006, Mulligan 2007). Resettable energy dissipation devices are fundamentally hydraulic or pneumatic spring elements that possess the ability to release the stored spring energy at any time. These devices manipulate the stiffness properties of the structure and are capable of producing large resisting forces. The basic design of the device is feasible for both pneumatic and hydraulic implementation and employs relatively simple mechanisms and control logic. Resettable devices also offer the opportunity to sculpt or re-shape hysteretic behaviour enabled by the possibility to control the device valve and reset times actively. This chapter will describe a newly developed semi-active resettable device used to control the response of civil engineering structures subjected to large earthquake ground motions.

3.2 DEFINITION AND BRIEF HISTORY

Resettable devices are described as nonlinear hydraulic or pneumatic spring elements in which the un-stretched length of the spring can be reset to obtain maximum energy dissipation from the structural system (Bobrow et al. 2000). Instead of altering the damping directly, resettable devices nonlinearly alter the stiffness, with the stored energy being released rather than returned to the structure as the compressed fluid is allowed to revert to its initial pressure (Chase et al. 2005a). In contrast to more complicated semi-active devices such as electro-rheological and magneto-rheological devices, resettable devices utilise well-understood fluids (e.g. air) and can be constructed with ease. In addition, semi-active resettable devices do not require a large external power source to operate.

Resettable devices were first proposed by Bobrow et al. (1995) who investigated the basic analytical and experimental techniques needed to characterise structural systems that utilise resettable devices for vibration suppression. Hunt (2002) and Barroso et al. (2003) presented a deeper investigation on resettable devices to mitigate the structural response in the presence of hysteretic, geometric and yielding nonlinearities under several seismic hazard suites of different levels of intensity. Chey et al. (2006) investigated the incorporation of resettable devices in multi-storey structures divided into two segments to reduce earthquake-induced vibrations. Chase et al. (2006) and Rodgers et al. (2007) examined the potential of resettable devices to re-shape structural hysteretic behaviour and presented the results as cumulative hazard distributions based on responses to probabilistically scaled suites of earthquake ground motions. More recently, Mulligan (2007) presented an exhaustive study of semi-active and passive structural control of buildings with emphasis on the use of resettable devices for mitigating damage during seismic events.

3.3 TWO-CHAMBERED DESIGN

The resettable device described in this research was first proposed by Chase et al. (2005a) for seismic hazard mitigation of structures. Unlike conventional devices, this device has a novel two-chambered design that eliminates the need to rapidly dissipate energy between the two chambers. The two-chambered design shown in Figure 3.1 uses each side of the device piston independently. This approach treats each piston side as an independent chamber with its own valve and control. The independent chamber design allows a wider variety of control laws to be imposed, as each valve can be operated independently, allowing independent control of the pressure on each side of the piston (Chase et al. 2005a, Mulligan et al. 2005).

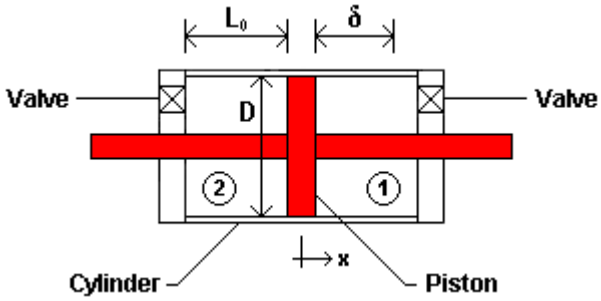

Figure 3.1 Two-chambered design of the device.

The resettable device utilises air as the working fluid thus eliminating the need for complex external plumbing systems. The compressed air of the chamber is vented to the surrounding atmosphere in order to release the stored energy. In combination with independent valves, this approach allows much more time for the chamber pressures to equalise. Therefore, while the opposite chamber is under compression, the previously reset chamber can release pressure over a longer period of time by having its valve open (Chase et al. 2006, Mulligan 2007).

Independent control of each chamber also allows a wider range of hysteretic behaviour of the device to be implemented. This ability to semi-actively sculpt the hysteretic behaviour and allow for long reset times leads to the potential use of resettable devices in a wider range of civil engineering applications. Moreover, the resisting forces developed by the device can be modified by using a different working fluid or pre-pressurising the device chambers. However, regardless of any additional working fluid or plumbing system used, the overall independent chamber approach can be generalised with all its potential advantages (Mulligan 2007). In summary, for the resettable device presented in this research, the novel two-chambered design possess the advantage of allowing significant amounts of energy to be stored and dissipated.

3.4 DESIGN CHARACTERISTICS

The size of the device and the nominal stiffness required from the device are the two principal considerations for the design of the resettable device. Size restrictions may be present during the implementation of the device in structural applications. The stiffness in turn determines the magnitude of the resisting forces delivered by the device. Additionally, the development of particular forces at specified piston displacements also takes into consideration the size parameters and the stiffness (Mulligan 2007). The primary design parameters of the device are the individual chamber length L_0, the maximum piston displacement δ, where $\delta \leq L_0$, and the piston diameter D. These design parameters are shown schematically in Figure 3.1.

The modelling of the force-displacement characteristics of the device utilises fundamental thermodynamic laws. Each chamber volume can be directly related to the piston displacement of the device, which causes a change in pressure and generates the resisting force in the device. Resetting the device, by opening the valve of the compressed chamber, dissipates the stored energy as the chamber pressure equalises with the fluid reservoir (i.e. the atmosphere) (Chase et al. 2006, Rodgers et al. 2007).

Consider the device with the two-chambered design shown in Figure 3.1. The resisting force, defined as a function of the displacement x, is equal to:

$$F(x) = (p_2 - p_1)A \tag{3.1}$$

where p_1 and p_2 are the chamber pressures on the right-hand and left-hand sides of the device, respectively, and A is the area of the piston.

Assuming that air is an ideal gas with no heat transfer through the walls of the cylinder, the pressures on both sides of the cylinder are governed by isentropic compression

$$p_i V_i^{\gamma} = c \quad i = 1, 2 \tag{3.2}$$

where γ is the ratio of specific heats ($\gamma = 1.4$ for air), V_i are the volumes on the two sides of the cylinder, and c is a constant.

Assuming that the piston starts moving from the centre position so that the initial pressure p_0 and volume V_0 are equal on both sides of the cylinder

$$p_0 V_0^{\gamma} = c \tag{3.3}$$

Equation 3.1 then takes the form

$$F(x) = [(V_0 + Ax)^{-\gamma} - (V_0 - Ax)^{-\gamma}]Ac \tag{3.4}$$

where Ax is the change in volume of the chambers as the piston moves. Equation (3.4) can also be written as

$$F(x) = \left[\left(1 + \frac{Ax}{V_0}\right)^{-\gamma} - \left(1 - \frac{Ax}{V_0}\right)^{-\gamma}\right] A p_0 \tag{3.5}$$

This equation can be linearised for small motions of x and an approximate resisting force can be defined. By applying Maclaurin's series, the following expressions can be obtained

$$\left(1 + \frac{Ax}{V_0}\right)^{-\gamma} = 1 - \gamma \frac{Ax}{V_0} \tag{3.6}$$

and

$$\left(1 - \frac{Ax}{V_0}\right)^{-\gamma} = 1 + \gamma \frac{Ax}{V_0} \tag{3.7}$$

Substituting Equations (3.6) and (3.7) into Equation (3.5) leads to

$$F(x) = -\frac{2A^2 \gamma p_0}{V_0} x \tag{3.8}$$

From Equation (3.8), the effective stiffness of the device is found to be

$$k_R = \frac{2A^2 \gamma p_0}{V_0} \tag{3.9}$$

Equations 3.8 and 3.9 can be used to determine an approximate stiffness and a simple model of the device for design purposes (Mulligan 2007).

The initial volume of the device V_0 and the area of the piston A can be calculated as follows

$$V_0 = L_0 A \tag{3.10}$$

and

$$A = \frac{\pi D^2}{4} \tag{3.11}$$

Substituting Equations (3.10) and (3.11) into Equation (3.9) and rearranging for the device diameter D lead to

$$D = \sqrt{\frac{2 k_R L_0}{\gamma p_0 \pi}} \tag{3.12}$$

Equation 3.12 relates the device diameter D to the required device stiffness k_R. The chamber length L_0 is typically constrained by the minimum device diameter and practical limitations on the size of the device. The maximum piston displacement required during large structural responses determines the value of L_0. The initial pressure of the chamber p_0 is the atmospheric pressure. This equation can be used to design a resettable device for a set of resisting forces at a given displacement or for a set of additional stiffness. Since the equation relates the primary design parameters of the device as a function of the required stiffness, it can be utilised to parameterise the design space to determine the appropriate device architecture (Chase et al. 2006, Mulligan 2007).

3.5 CONTROL LAWS

Since the device valves and reset times can be controlled actively, the resettable device offers the unique opportunity to sculpt or re-shape structural hysteretic behaviour to meet different design needs. The hysteretic response of the device can be determined by the control system managing each valve of the device chambers. A robust control system relies on systematically and accurately detecting specific points or events over a

sine-wave motion cycle. The piston motion is known in advance by using a sine-wave motion. Thus, the control law for a simple sinusoidal test can be based on specific displacements rather than specific characteristics of an unknown displacement. For generic motion, there is no way to determine the amplitude of the motion prior to each cycle. Thus, for a completely generic control law the only systematically detectable points are the maximum displacements, as they occur in each cycle before reversal, and the zero crossing points. These two generalised points can be found in the response to any input motion by using displacement sensors on the device or inferring them via other sensors (Mulligan 2007).

The maximum piston displacement during a cycle of motion coincides with a change in sign of the velocity. The piston velocity can be determined from the displacement signal. Because of the noise associated with the displacement signal, filtering is required to avoid repeated valve actuation. A zero crossing is detected when the sign of the displacement changes. Thus, a typical sine-wave cycle can be divided into the four quadrants shown in Figures 3.2, 3.3 and 3.4. Different control laws based on these four quadrants can easily be implemented.

3.5.1 1-2-3-4 Control Law

For a sine-wave input, energy is stored in the device by compressing the air as the piston is displaced from its centre or zero position. When the piston reaches its maximum displaced position, the stored energy is also at a maximum. At this point, the stored energy is released by discharging the compressed air to the atmosphere, thus resetting the un-stretched spring length. As the piston begins moving in the other direction, the device resists that motion until the next change of direction (Fig. 3.2a). Therefore, the device releases the stored energy at the maximum and minimum peaks of each sine-wave cycle (i.e. when the velocity is zero), and resists the motion between the peaks (Chase et al. 2006, Rodgers et al. 2007). This hysteretic behaviour is shown in Figure 3.2b. It is termed the 1-2-3-4 control law because the device provides resisting forces in all quadrants of the force-displacement curve.

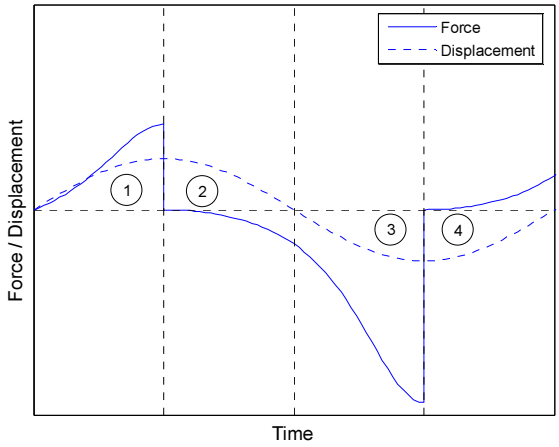

(a) Device response

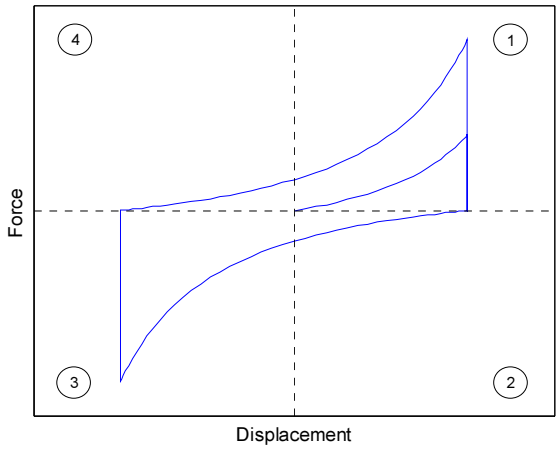

(b) Hysteresis loop

Figure 3.2 1-2-3-4 control law.

3.5.2 1-3 Control Law

Figure 3.3a shows the response of a device that resists the motion only away from the centre position of the piston during sine-wave excitation. In this control law, the valve of the active chamber (i.e. the chamber under compression) is closed when the piston is moving from its centre position to its maximum displaced position, while the valve of the opposite chamber is held open. At the peak displacement of the piston, or zero

velocity point, the valve of the active device chamber is opened and the stored energy is released. As the device piston passes the centre position, while moving in the opposite direction, the valve of the opposite chamber is closed and that specific motion is resisted. As shown in Figure 3.3a, the device does not provide resisting forces in the second and fourth quadrants of the sine-wave cycle.

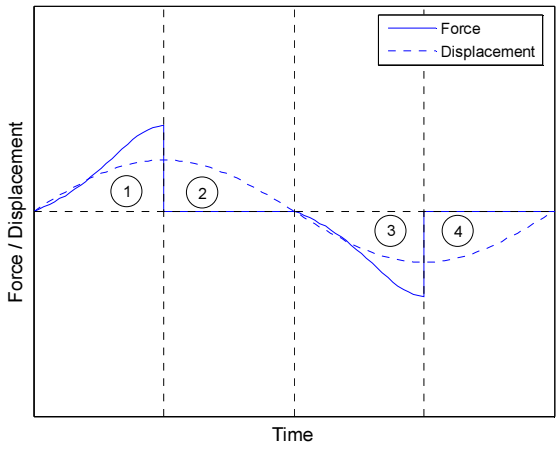

(a) Device response

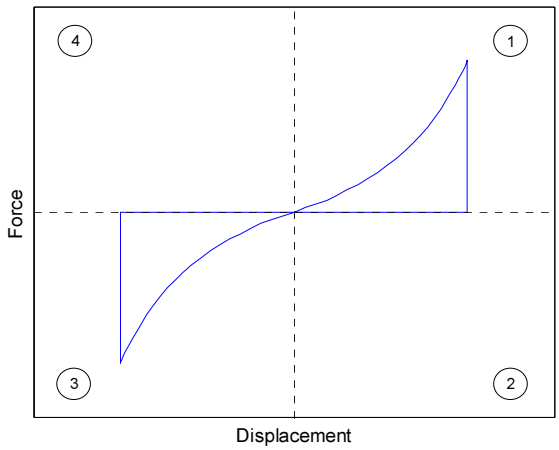

(b) Hysteresis loop

Figure 3.3 1-3 control law.

Figure 3.3b shows the hysteretic behaviour given by this control law. The law is denoted as the 1-3 control law because the resisting forces are provided only in the first and the third quadrants. Typical peak forces delivered by the device under the 1-3 control law are smaller than those under the 1-2-3-4 control law for the same piston displacement (Figs. 3.2b and 3.3b). This reduction in the peak force is expected as only half the amount of the motion input is resisted by the device (Mulligan 2007).

3.5.3 2-4 Control Law

The response of a device that resists the sine-wave motion from the peak displacements towards the centre position of the piston is shown in Figure 3.4a. In this control law, the valve of the active chamber is closed at the peak displacement of the piston and the stored energy is released when the piston crosses the centre position. The motion from the centre position to the maximum displaced position of the piston is not resisted by the device, as shown in Figure 3.4a.

This hysteretic behaviour is shown in Figure 3.4b. The law is denoted as the 2-4 control law because the resisting forces are provided only in the second and fourth quadrants of the force-displacement relationship. The peak forces developed by the device under the 2-4 control law are smaller than those under the 1-2-3-4 control law for the same displacement of the piston. Furthermore, the peak forces under the 2-4 control law are also smaller than those under the 1-3 control law because the volume of the active chamber is relatively large (Mulligan 2007).

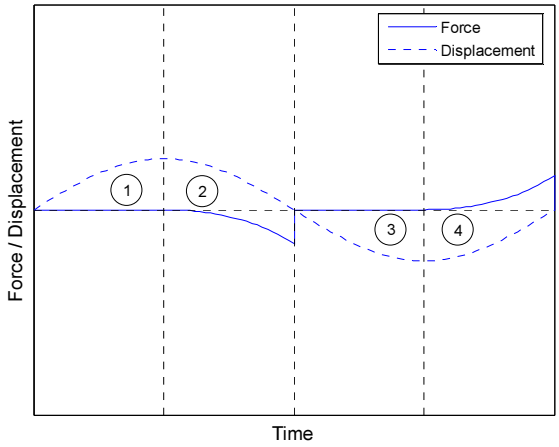

(a) Device response

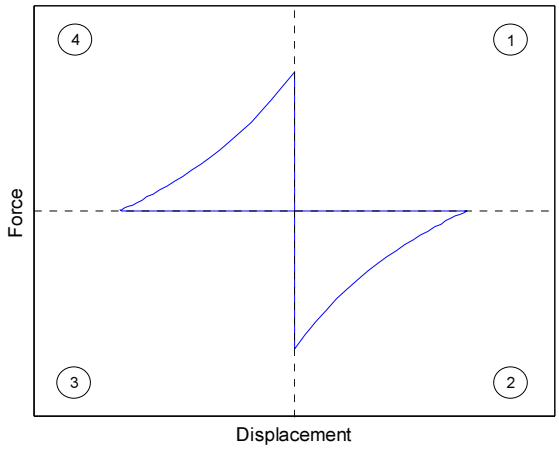

(b) Hysteresis loop

Figure 3.4 2-4 control law.

3.6 RESETTABLE DEVICE

This section provides a brief description of the semi-active resettable device used during the shake table testing of the one-fifth scale structure described in Section 4.3. A more detailed description of the design and characterisation tests of the resettable device can be found in Mulligan (2007).

3.6.1 Description of the Device

As described in Section 3.3, the resettable device used in this research dissipates energy by using a two-chambered design that treats each side of the piston as an independent chamber with its own valve and control. Air is used as the working fluid of the device, because of its simplicity and the possibility to use the surrounding atmosphere as the fluid reservoir. This novel semi-active resettable device allows significant amounts of energy to be stored and dissipated. A photograph of the resettable device is shown in Figure 3.5.

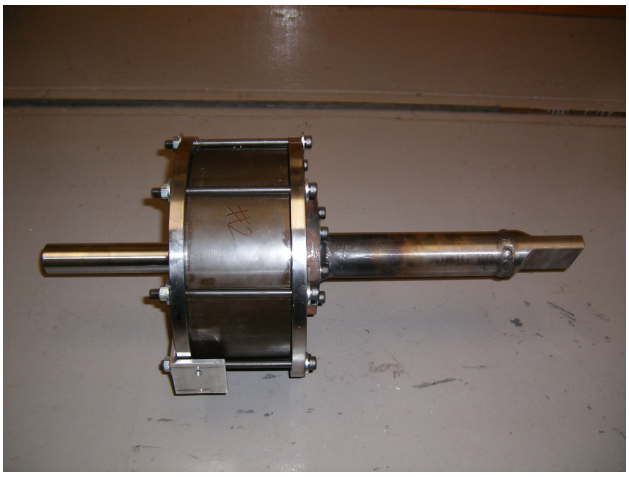

Figure 3.5 Resettable device.

The piston located inside the cylinder has various seals to ensure minimal air movement between the two chambers, each of the seals is located in a groove. It is important to notice that such air movement would reduce the effective stiffness and energy dissipated by the device. The end caps are press fitted into the cylinder and held in place by eight clamping rods. An O-ring located between the end caps and the cylinder further ensures no leakage of air. Where the piston shaft passes through the end caps, air is prevented from escaping by seals located in the end caps. Figure 3.6 shows a schematic of the resettable device.

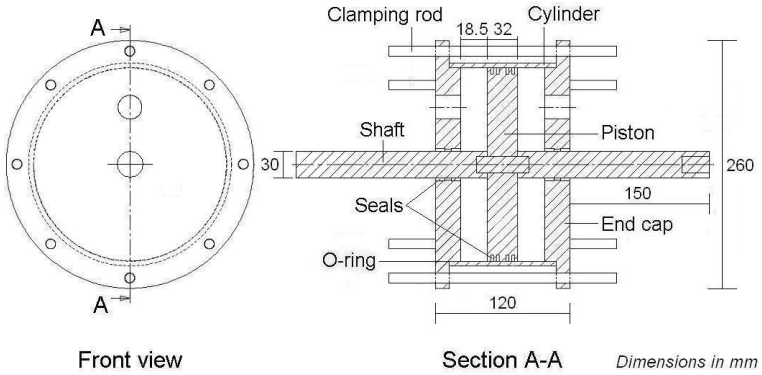

Figure 3.6 Schematic of the resettable device.

The dimensions of the device are dependent on the device stiffness, the maximum stroke expected and the maximum force required. However, the dimensions of each component of the device are further defined by material and hardware availability, and the manufacturing process. The components of the device must also have adequate strength and avoid material failure (Mulligan 2007). Approximate dimensions of the device are shown in Figure 3.6. The device has a wide flat piston with a thickness of 32 mm and the length of the device chamber is 18.5 mm. The primary design parameters of the device are the diameter, the individual chamber length and the maximum piston displacement. These parameters can be used to control the stiffness of the device (Chase et al. 2006, Mulligan 2007).

The valve of the resettable device is two-way operating so that air can flow in both ways. This is an important characteristic because the device valve not only holds and releases the chamber pressure, but it is also required to let the air into the chamber from the atmosphere to recharge the inactive device chamber. The valve utilised in this research is a Buschjost solenoid actuated diaphragm valve with a maximum operating pressure of 10 bar. The valve of the device remains closed when it is not in operation or switched off. This is the normal state of the valve. If power is lost to the valve solenoids or control system, the device is still able to provide supplemental reaction forces by resisting structural motion as an air spring with additional friction damping (Mulligan 2007).

3.6.2 Dynamic Characteristics of the Device

The dynamic characteristics of the device depend on a number of parameters. The most influential parameters include: the diameter and length of the device chamber, the maximum displacement of the device piston, and the effective opening size of the valve. The first and second parameters influence the forces generated by the device, and the third parameter affects the time required to equalise and reset the chamber pressure after valve opening.

The system characteristics of particular interest for the device performance include the maximum force, energy release rate and time, piston offset, response delay and friction. These characteristics were quantified by experimental tests exploring the response of the device to various input signals. The resettable device was first tested to ensure that it had been manufactured to the specifications and all the components, including seals and valves, behaved as expected. This included a series of quasi-static tests with a cycle frequency of less than 0.1 Hz. Dynamic tests with frequencies above 0.1 Hz and valves uncontrolled were then used to examine the device characteristics, such as the peak force and the device stiffness. Finally, controlled tests, where the valves were either controlled manually or by the control system, examined parameters such as the maximum force generated, friction, valve lag, the effect of initial piston offset, and the importance of energy release time. The controlled tests were also used to investigate the impact and efficacy of different device control laws in adding supplemental damping. Particular focus was given to the amount of time required to dissipate large amounts of stored energy and its impact on performance, as well as the impact of different control laws on the resulting hysteresis loop. Once the device was characterised, a detailed model was created and validated experimentally (Chase et al. 2006, Rodgers et al. 2007, Mulligan 2007).

1. **Maximum Force**. The maximum response force delivered by the device during the uncontrolled tests was approximately 6 kN at a 10 mm piston displacement, resulting in a nominal stiffness of 600 kN/m. However, this nominal stiffness does not give a full representation of the device response because of the nonlinear response of the

device. The maximum response force of the device during the controlled tests was dependent on the control law used. Maximum response forces at 10 mm piston displacement are approximately 8, 4.5 and 3 kN for the 1-2-3-4, 1-3 and 2-4 control laws, respectively (Mulligan 2007).

2. **Energy Release Rate and Time**. The hysteretic response of the device is highly influenced by the energy release rate. This rate is a function of the valve orifice size and can be altered depending on the size and number of valves available. There is a maximum rate at which air can flow through the valve orifice thus the energy release time is finite and not negligible, in particular for large piston motion. The effect of the energy release rate on the response of the device is more evident at relatively high frequency motion and large displacements of the device piston. In these cases, a large amount of stored energy is required to be released, that results in a significant period of time needed to release all the stored energy.

   When the device valve is open, air begins to flow out of the active chamber. This flow continues until the pressure inside the chamber equalises the atmospheric pressure. The equalisation of the pressures is not an instantaneous event. A certain amount of time is required to release the stored energy and return the response force to a zero value. Therefore, the release or reset time is an important factor affecting the response of the device, particularly for control laws that require equilibration of the active chambers before resisting further motion (Mulligan 2007).

   The longer the release time the greater the effect on the performance of the device. In particular, at high frequency piston motion the stored energy may not be released from the device before the valves are closed. To mitigate the impact of long release times, additional valves or valves that enable greater exit flow rates can be utilised. The independent chamber design employed in this research reduces the potentially adverse effects of long release times by allowing one chamber to store energy while the opposite chamber is still releasing energy.

3. **Piston Offset**. Exact zero positioning of the device piston is important to avoid undesired piston offset and asymmetric device response. Piston offset is the difference between where the control system considerers the zero position to be and the actual centre position of the piston. Piston offset may occur due to either incorrect centring during installation or a prior event in which the piston fails to return to its exact centre position. Moreover, a structure may have a permanent deflection after a strong event so that the centre position of the piston would require to be adjusted to the new zero position of the structure (Mulligan 2007).

   Direct consequence of the piston offset is a volume difference between the two cambers that results in a difference in the response forces delivered by the device. Specifically, for the same displacement in each direction, the resulting force response will be greater in one direction than the other. The difference in response is particularly marked if the piston approaches the end of the chamber in the short chamber direction.

   In normal working conditions, there is no guarantee that the piston will be exactly at the centre every time the device is utilised. Therefore, allowances for initial piston offset need to be incorporated into the design of semi-active control systems. Furthermore, the zero position needs to be defined correctly in the control system. In structures where a permanent offset is expected, zero tracking should be used to align the device response with the dynamics of the new deformed structure to avoid instabilities in the control action (Mulligan 2007).

4. **Response Delay**. Response delay or lag is an important aspect in the design of the control system. Any time delay between a specific valve activation point and the actual valve operation will reduce the efficiency of the resettable device. Among the factors that contribute to the response delay of the device are (Mulligan 2007):

   a. Time delays due to data filtering
   b. Number of time steps required to determine the change of sign in displacement or velocity that is needed for implementation of the control laws

c. Valve operation which is independent of the control system.

The total delay is measured in terms of cumulative number of time steps between the specific point occurring and the valves operating. The main task is to reduce the first two factors to a minimum value based on the system design and sensors utilised. These two factors are functions of the noise environment, filtering and electronics in the specific implementation. The operation delay can be reduced by the selection of specialised valve and valve solenoid. The optimisation of the filtering and a smart design of the control system can minimise the detrimental effects of delays in the control system dynamics.

5. **Friction**. A large amount of the force generated by the device is attributed to friction between two Teflon seals around the device piston and the internal wall of the cylinder. Additionally, close tolerances between the device piston and the cylinder wall increase the static friction. The contribution of the friction is approximately 0.5 kN. This value represents the friction force that needs to be overcome before the device piston can be displaced. The friction value was determined experimentally by testing the device with both valves open under a sine wave input with amplitude of 10 mm and over a range of frequencies. The friction force constitutes the amount of the response force that cannot be dissipated by the resettable device. However, the friction force is still a reaction force that resists structural motion and dissipates energy. Therefore, some friction force does not degrade the ability of the device to dissipate energy (Mulligan 2007).

3.7 SUMMARY

This chapter has described a newly developed semi-active resettable device. Fundamental concepts and a brief review of previous research on resettable devices were presented. The resettable device has a novel two-chambered design that utilises each side of the piston independently. This approach treats each piston side as an independent chamber with its own valve and control. The independent chamber design

allows a wider variety of control laws to be imposed. The resettable device also offers the opportunity to manipulate the structural hysteretic behaviour via innovative control laws. For a sine-wave motion, the 1-2-3-4 control law represents the behaviour of a device that releases stored energy at the peaks of each sine-wave cycle and resists the motion between those peaks. The 1-3 control law designates the behaviour of a device that resists motion only away from the centre position of the piston. Finally, the 2-4 control law represents the behaviour of a device that resists the motion from the peaks of the sine-wave motion towards the centre position of the device piston.

Chapter 4
ANALYTICAL STUDIES ON RESETTABLE DEVICES

4.1 INTRODUCTION

Energy dissipation has long been recognized as an effective means to control excessive vibration of mechanical and structural systems under dynamic loads. The main purpose of adding energy dissipation devices to a structure is to increase its capacity to dissipate energy. Supplemental devices dissipate the energy that must otherwise be dissipated by the structure's lateral displacement resisting systems, thus eliminating or reducing potential damage to the structural elements or connections. In this chapter, an ideal (linear) semi-active resettable tendon is considered as the energy dissipation device. The optimal configuration of the resettable tendon in a four-storey one-fifth scale structure is investigated to improve the structural response under earthquake loading. The seismic performance of the model structure is evaluated in terms of reductions in relative displacements, absolute accelerations, inter-storey drift ratios and total base shear.

4.2 EFFECT OF ADDING ENERGY DISSIPATION DEVICES

Different devices provide different means by which energy is dissipated. The addition of energy dissipation devices to a structure results in a reduction of the inter-storey drift and therefore a reduction of damage. Supplemental energy dissipation devices may also add structural strength and stiffness. An increase in strength or stiffness reduces the effective structural period, thus further reducing the maximum displacement. However, such an increase may also increase the total lateral force exerted on the structure and the acceleration experienced during the earthquake excitation.

Another important issue is whether the structure behaves linearly or nonlinearly under a given loading condition. In general, a structure equipped with supplemental damping devices exhibits nonlinear behaviour, because the device dynamics are generally

nonlinear in local displacements and velocities. This fact complicates exact structural analysis procedures considerably (Hanson and Soong 2001).

4.2.1 Effect of the Additional Damping

Structures equipped with added damping devices exhibit significantly higher modal damping ratios than those associated with conventional structures (Hanson and Soong 2001). This is particularly true for the higher modes, where damping ratios can reach values close to or even exceed their critical values. Therefore, the damping term in the equation of motion of a structure with added dampers becomes important to determine the modal properties of the structure. Moreover, the addition of damping devices to a structure represents not only a significant increase in equivalent damping but also a redistribution of modal damping. Some modal response components that have minor contributions to the total response of the structure may become important after the damping devices are added.

The traditional assumption of proportional damping used in the analysis of conventional structures is generally not valid for structures with added dampers, because it may not be practical to try to match the characteristics of added dampers to the variations in the stiffness and mass of the structure. In fact, in some cases it may be desirable to add dampers only at specific floors in the structure. Thus, the distribution of the damping properties within the structure will not be proportional. In this case, modifications of the traditional model analysis must be considered (Hanson and Soong 2001).

4.2.2 Effect of the Additional Stiffness

Irrespective of the type of energy dissipation device used, adding supplemental devices to a structure involves an increase in the lateral stiffness of the structure. Lateral forces may increase or decrease in the structure, depending on the effect of the devices and connections on the dynamic characteristics of the structure, and on the characteristics of

the ground motion. Moreover, the magnitude of the increased lateral stiffness in a typical structure varies depending on the type of device used. In all cases, however, the intensity of the lateral forces induced by the ground motion is a function of the overall lateral stiffness of the structure. Therefore, these forces must be resisted by the energy dissipation devices (Pekcan 1998).

The stiffness added by supplemental devices leads to the following interrelated effects: the natural frequencies of vibration of the system are increased, leading to changes in the dynamic amplification factors associated with the modal responses; the modes of vibration are changed; the static response of the structure is decreased; and the modal damping ratios are modified. Because of the multitude of parameters that are changed by the stiffness increase, it is difficult to make generalizations about its effects (Hahn and Sathiavageeswaran 1992).

4.2.3 Optimal Placement and Distribution

As mentioned earlier, the installation of an energy dissipation device will cause a reduction in the seismic response of a structure. However, some response quantities will be reduced more than others. The damping capacity of a device and where and how many devices are placed on a structure will have a significant effect on the ability to reduce the seismic response (Singh and Moreschi 2002).

It is recommended to place the supplemental devices at the locations that will maximize the damping ratio of the fundamental mode, as this mode is often the most dominant mode in the deflection of multi-storey structures. The distribution of the devices is typically based on the level of the maximum device forces and on the requirements as to how these forces are transferred within the structural system. Hence, the devices should be distributed throughout the structure to ensure stiffness regularity and redundancy (Pekcan 1998). However, it is not essential that supplemental devices should be distributed over the entire height of the structure, because such a distribution may not be the most effective arrangement (Hunt et al. 2002, Barroso et al. 2003, Chase et al.

2005c). There may be cases in which supplemental devices can be installed only in the lower storeys for a more economical design. Moreover, research has shown that the earthquake response of tall buildings may be effectively reduced by adding damping devices only to the lower half of the building (Hahn and Sathiavageeswaran 1992).

Lateral resisting forces increase cumulatively from the top level to the lower levels and finally to the foundation. Therefore, it implies that supplemental devices, that resist and transfer the lateral seismic forces to the ground level, should have capacities in proportion to the storey shears at which they are installed. In fact, one of the most commonly used design methods is based on the inter-storey deformations along the height of the building. Damping devices are sized to achieve the required damping ratio at the design inter-storey deformations. Since a constant inter-storey drift is generally the design objective for a regular building which has a first-mode dominant response, a uniform one-size damper would be dictated by this approach. However, if the total damper size is distributed in proportion to the design storey shears, a desired moment frame-truss action can be achieved. The lateral seismic forces are transferred by the damping devices installed on the gravity load-carrying interior frames in all directions, thus reducing the demand on the moment frames (Pekcan 1998).

4.3 ONE-FIFTH SCALE STRUCTURE

To assess the effectiveness of a semi-active resettable tendon to reduce the seismic response of civil structures, a series of computer simulations were performed using a two-dimensional numerical model of the structure shown in Figure 4.1. The four-storey one-fifth scale structure was designed and tested by Kao (1998) and is widely used for seismic testing in the Department of Civil and Natural Resources Engineering at the University of Canterbury. This section will present a brief description of the one-fifth scale structure. A more detailed description of the computational model, material properties and design procedure of the structure can be found in Kao (1998).

Figure 4.1 One-fifth scale structure.

4.3.1 Description of the Structure

The model building is a 2.1 m high three-dimensional four-storey frame structure. The frames are built using 50 mm square by 4mm thick hollow steel sections for beam and column members. These members were designed using capacity design principles to ensure that they remain elastic during the seismic testing. They are connected to special joint elements or fuses designed to develop plastic hinges in critical regions of the structure. The fuses, beam-column joints and other connecting components are made of steel flat bars. The model structure has two frames in the longitudinal direction that provide the lateral load resistance. Each frame has two bays with 0.7 m and 1.4 m long spans, respectively. In the transverse direction, three one-bay frames limit the torsional and transversal response of the structure. The transverse frames have a 1.2 m long span and carry most of the gravity load. Figure 4.2 shows an isometric view of the one-fifth scale structure.

The mass at each floor on the model structure is provided by a number of steel ingots. The ingots are simply supported on the beams of the transversal frames and on the intermediate beam supported by the long span beams of the longitudinal frames. The floor system is designed to model a one-way floor slab and is connected to a rigid steel topping plate to ensure that the inertia forces are transferred to the frames by diaphragm

action. The floor masses that contribute to the inertia forces are 9730 N for level 1, 8757 N for levels 2 and 3, and 8062 N for level 4 (Kao 1998).

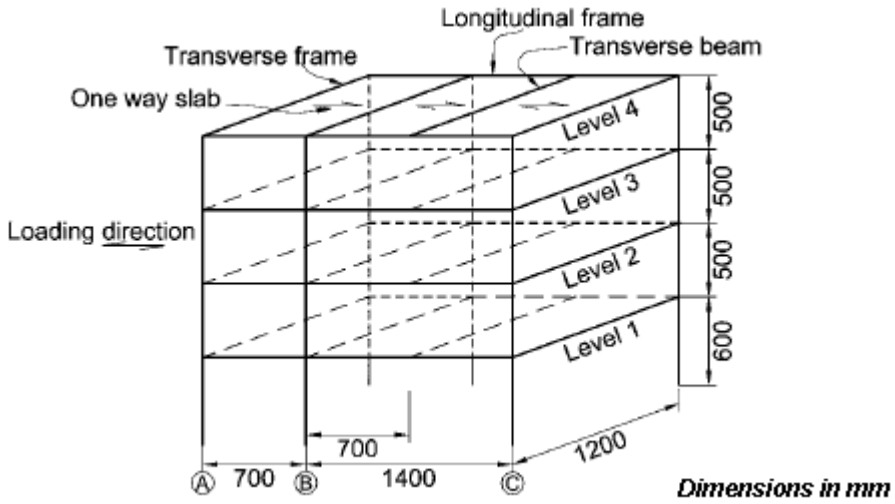

Figure 4.2 Isometric view of the structure (Rodriguez et al. 2006).

Due to the distribution of the steel ingots, the short span beams of the longitudinal frames are loaded with their own weight, whereas the long span beams have an extra point load induced by a transverse beam at the mid-span at each level in addition to their own weight. The intention of such gravity load distribution is to show the difference in behaviour between beams with earthquake and gravity dominated responses within the frames (Rodriguez et al. 2000).

In beams with earthquake dominated response, such as the short span beams of the longitudinal frames, positive and negative plastic hinges form at the same location at the column faces. In contrast, in beams with gravity dominated response, such as the long span beams of the longitudinal frames, positive and negative plastic hinges form at different locations. In such beams, negative plastic hinges typically form at the column faces while positive hinges form within the beam span. This leads to shakedown of the beams and, as a result, the ductility demands in the plastic hinge regions are expected to be greater than those derived from kinematics of the collapse mechanism (Kao 1998, Rodriguez et al. 2000).

The joint elements or fuses are designed to show the effects of inelastic structural performance under seismic loading. These fuses can be replaced with minimum effort and at low cost. The location and dimensions of the fuses are shown in Figure 4.3. The fuses located in the beam members were machined from 100 mm wide by 20 mm thick steel flat bars. The bars were cut and then milled down to form 7 mm thick by 5 mm long grooves. The reduced section in a groove acts as a weak element or fuse. Similar elements of 12 mm and 14 mm in thickness and 5 mm in length were provided by machining 100 mm cube steel blocks for fuses located at the column bases. The width of the fuses was determined from flexural strength requirements (Kao 1998, Rodriguez et al. 2000, Bishay-Girges 2004).

The four-storey model building was designed as a one-fifth scale structure. It was intended to model the structure as a typical four-storey reinforced concrete frame building, therefore, the natural period of the model was required to be within 0.4 s to 0.6 s to obtain similar response under earthquake excitation (Kao 1998). The equivalent static method, outlined in the New Zealand Loadings Standard NZS 4203: 1992, was employed to calculate the earthquake forces. The seismic weight of the one-fifth scale structure is 35.3 kN. A structural ductility factor of 6 was adopted for the structural design. Thus, the model structure was designed for a base shear force of 8.7% of its seismic weight.

Steel sections are used throughout the moment-resisting frame structure. The following steel properties were adopted in the design:

a. Elastic modulus: E = 200 GPa
b. Shear modulus: G = 80 GPa
c. Density: ρ = 7850 kg/m^3.

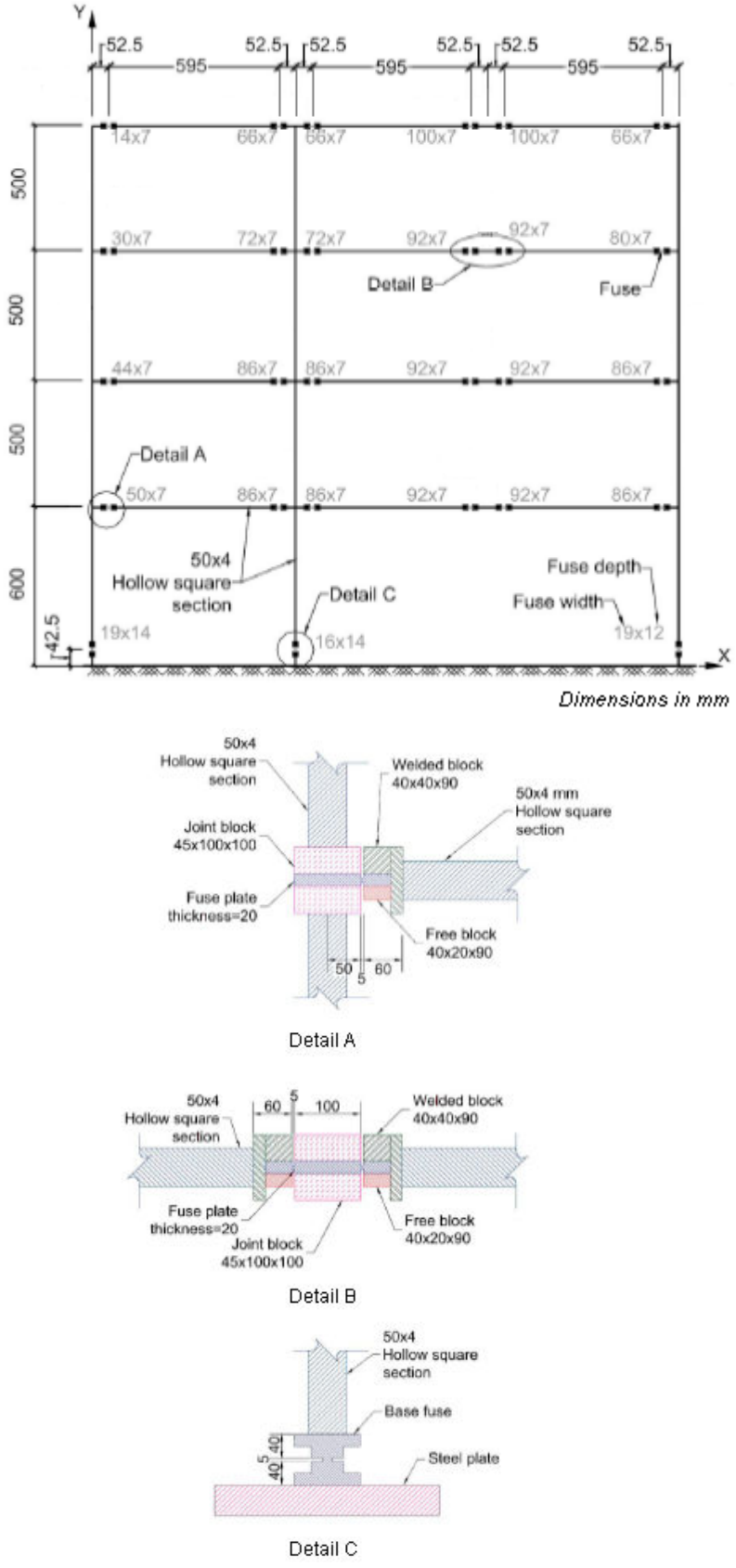

Figure 4.3 Location and dimensions of the fuses (Rodriguez et al. 2006).

Apart from the square hollow sections, all of the sections of the frame are made of Grade 250 standard mild steel with yield strength of 250 MPa. The square hollow sections of all beam and column members are made of Grade 350 standard mild steel. For the welds, nominal electrode strength of 410 MPa was specified. All the cap-screws required for the connections are made of high tensile strength steel (Kao 1998).

4.3.2 Analytical Modelling of the Structure

A two-dimensional computer model of the one-fifth scale structure was developed by Kao (1998) for use in the RUAUMOKO computer program (Carr 2006). The model was later on modified by Rodriguez et al. (2000) to investigate the floor accelerations in buildings. A two-dimensional instead of a three-dimensional analysis was chosen because the response of the transversal frames and the out-of-plane behaviour of the members were considered to be insignificant and a two-dimensional analysis would give sufficient required information. The model has 121 nodes and each node has 3 degrees of freedom. All the degrees of freedom of the base nodes are restrained for fully fixed boundary condition, while the nodes of the horizontal elements are slaved to the external nodes at each level to couple the degree of freedom of the horizontal displacement (Kao 1998).

As mentioned above, a one-way floor slab provides a significant proportion of the model mass that contributes to the horizontal inertial forces. The mass applied to the frame model is approximately 1.6 tonnes that corresponds to one half of the entire mass of the model structure. This is because of the structure's symmetry in the longitudinal direction. The concentration of structural mass at every level enables the use of a lumped mass model for the modelling of the structure.

The RUAUMOKO program offers the opportunity to model a structural member using four nodal points. This four-node element consists of two outer nodes and two inner nodes that define rigid links connecting the flexible part of the member to the outer nodes. The two outer nodes are the usual nodes where the stiffness and the member

forces act and the two inner nodes define the length of the rigid links. Displacements and rotations of the inner nodes are rigidly linked to the displacements and rotations of the outer nodes (Carr 2006). Four-node elements are used to model the rotational fuses connecting the beam and column members. To model the column members, four-node elements are used with the rigid links modelling the joint blocks at the top and bottom of the columns. Two-node elements with no rigid links are used to model the beam members of the structure. Shear deformations in the fuses and in the beam and column members are considered to be non-critical and are neglected in the analyses (Kao 1998, Rodriguez et al. 2006).

A frame type member is adopted for all the elastic members of the model structure (i.e. beams and columns members). The behaviour of the frame type members follows the concept of the Giberson's one-component model (Giberson 1969) which can have a plastic hinge at one or both ends of the elastic central length of the member. In the analysis, all frame type members are assumed to remain elastic. A rotational spring type member is selected to model all the fuses. The spring type member can model the fuse more appropriately than a frame type member since the fuse is designed to form a plastic hinge over its entire length, instead of just at the two ends. A modified version of the Dodd-Restrepo hysteretic model for reinforcing steel (Dodd and Restrepo-Posada 1995) is used to model the nonlinear moment-rotation response of the fuses. The stiffness of the spring in the longitudinal direction is assumed to be infinite, while in the transversal direction is equal to GA/L, where G is the shear modulus, A is the area and L is the length of the section. The rotational stiffness of the spring is equal to EI/L, where E is the elastic modulus and I is the moment of inertia of the section. An effective flexural rigidity $(EI)_{eff}$ is used for the beam fuses to take into account an excess of flexibility found by quasi-static tests on a number of joint specimens. The normal flexural rigidity EI is used for the column base fuses due to their rigid design. For both member types, no initial loads are applied, and strength degradation and damage indices are not computed (Kao 1998).

A major difficulty in the development of analytical models is the selection of the structural damping properties. Unlike the mass and stiffness, the damping mechanisms

of a structure are not well understood. Energy dissipation mechanisms that result in structural damping may be of viscous or non-viscous type (e.g. Coulomb friction, stick-slip friction, etc.). Traditionally, the structural damping is assumed to be viscous. Furthermore, because of its simplicity and computational economy, the structural damping matrix is computed as a linear combination of the stiffness matrix and the mass matrix in what is known as Rayleigh damping. Rayleigh damping is chosen mainly for convenience, although it does not have any physical meaning (Rodriguez et al. 2006). A main disadvantage of the Rayleigh damping model is that the damping ratios become very large for high frequency modes and this has a marked effect on the response of inelastic structures where the high frequency mode response is more critical to the overall response of the structure (Carr 1997).

To prevent the over-damping of the higher modes, a model that utilises the linear variation of damping with elastic natural frequencies is adopted in this research. The model follows the concept of the Wilson-Penzien damping model (Wilson and Penzien 1972) and is based on the frequencies and modes of free vibration at the beginning of the time-history analysis. The damping levels associated with each mode vary linearly with the frequency. The computed damping matrix is constant throughout the time-history analysis. The tangent, secant and elastic damping matrices are identical. This means that as the structure softens (e.g. by yielding), the effective damping will increase. However, as the damping in the higher modes of free vibration is much less than that implied in the Rayleigh damping model, this does not appear to have significant consequences (Carr 2006). The damping ratio ξ is considered to be 1.21% of critical damping, according to the experimental results presented in Chapter 5.

The P-Delta effects are considered in the analysis by using the P-Delta option available in the RUAUMOKO program. The displacements are assumed to be small and the coordinates are unchanged but the stiffness of the beam and column members are adjusted for the axial forces from the static analysis. This allows for the lateral softening of the columns due to the gravity loads. The P-Delta effect is assumed to be constant as the increase in stiffness on one side of the structure due to overturning moments is compensated by the decrease in stiffness on the other side of the structure (Carr 2006).

The Newmark's constant average acceleration method (Newmark 1959) is utilised to integrate the equation of dynamic equilibrium. As with any numerical-integration procedure, the accuracy of this step-by-step method depends on the length of the time step. The time step should be equal to or less than 0.1 of the period of the highest mode of free vibration that contributes significantly to the structural response. Experience has shown that a time step of 0.01 seconds is satisfactory for multi-storey framed buildings but for most digitized earthquake accelerograms the time step should never exceed 0.02 seconds (Carr 2006). A time step of 0.001 seconds is chosen in this research. This value was obtained by using a trial-and error procedure in which absolute accelerations and relative displacements at each floor level were evaluated by decreasing the size of the time step until the results from the last and previous analysis were considered to be similar (Rodriguez et al. 2006).

4.4 IDEAL RESETTABLE TENDON

During a large earthquake, the maximum displacement of a structure will likely exceed its yield displacement. It may even do so when energy dissipation devices are added to the structure. The behaviour of a device is generally nonlinear in local displacement or local velocity as well as in displacement at the device (Hanson and Soong 2001). Therefore, a dynamic analysis, in which nonlinearities in structural members as well as in devices are accounted for, provides the most rigorous and complete design approach.

4.4.1 Computational Model of the Resettable Tendon

The computer model of the one-fifth scale structure was modified to include a tendon type member available in the RUAUMOKO program (Fig. 4.4). Tendon members have no stiffness properties but are used to apply forces to the structure. The forces acting on the joints at each end of the member are a function of the displacements between the joints and the direction of the change in the member deformation. The tendon type member is like a truss member in that it carries only an axial force (Carr 2006).

The hysteretic behaviour of the tendon member follows the hysteresis rule shown schematically in Figure 4.5. This hysteresis represents the behaviour of a semi-active damper member. The hysteresis rule allows the force to be proportional to the displacement until a saturation force is attained, +FPP or −FPP, when the system appears to show a perfectly plastic response. On any reversal of displacement, the force is automatically reset to zero and the origin is moved to the existing displacement, the system will then behave as an elastic member until either the saturation force is achieved or the displacement changes sign (Carr 2006). This behaviour matches an ideal (linear) resettable device (Jabbari and Bobrow 2002, Hunt 2002, Mulligan et al. 2005).

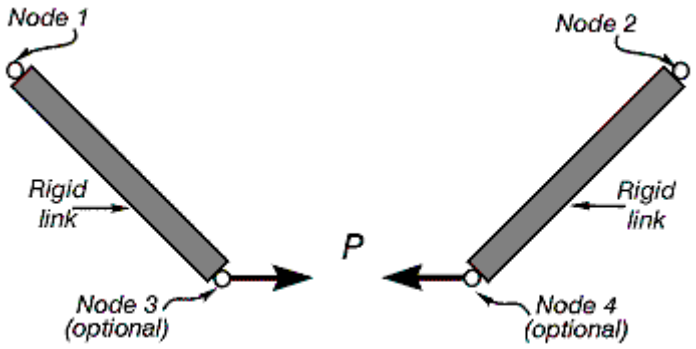

Figure 4.4 Tendon member (Carr 2006).

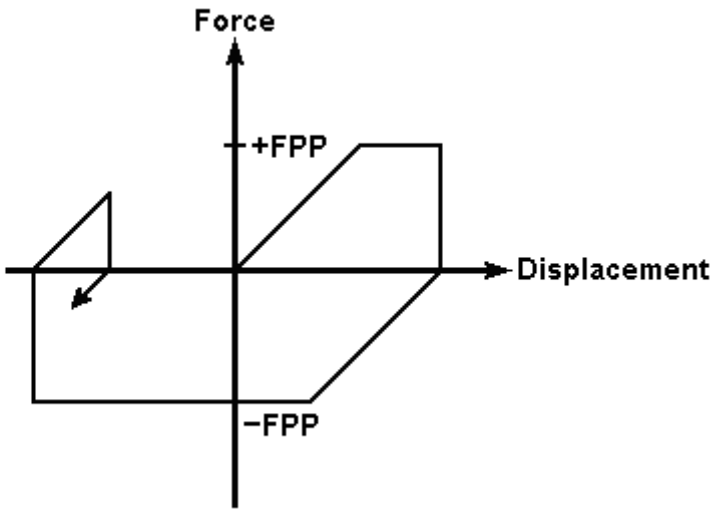

Figure 4.5 Linear resettable hysteresis.

All input parameters of the semi-active tendon member are based on the demands of the one-fifth scale structure. The structural weight of the four-storey model structure is approximately 35.3 kN (Kao 1998). Previous studies have shown that a saturation force of between 10% and 15% of the total structural weight is needed for effective structural control (Hunt 2002). Therefore, a saturation force of 5.295 kN is used in the computer analyses. This force represents the 15% of the seismic weight of the structure. Since it is planned to install two resettable devices (one at each side of the structure), a maximum force of approximately 2.5 kN per tendon member is needed. According to preliminary studies, the model structure is required to develop this maximum force at a 10-milimeter floor displacement when subjected to a large earthquake loading. This requirement results in a nominal stiffness of 250 kN/m for the semi-active tendon member.

4.4.2 Tendon Systems and Earthquake Ground Motions

Energy dissipation devices for the seismic protection of civil structures are most commonly implemented in the form of bracing elements or tendon systems (Yang et al 2000). The response of the structure can be reduced by carefully selecting the tendon layout. In this research, a number of tendon configurations are investigated to assess the effects of the semi-active tendon member on the seismic response of the one-fifth scale structure. The system A shown in Figure 4.6 represents the original structure without any added resettable tendon member. Figures 4.7 and 4.8 show the other systems considered.

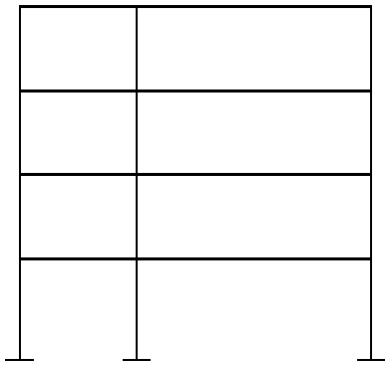

Figure 4.6 System A.

In the A-Systems shown in Figure 4.7, the semi-active tendon is installed within the short bay of the structure and spans through one floor only. In the B-Systems shown in Figure 4.8, the semi-active tendon is installed along the two bays and diagonally spans between one or more floors of the one-fifth scale structure. The systems A1 and B1 represent the well known first-storey damped case, which only involves the installation of a one-storey tendon (Figs 4.7a and 4.8a). This case is important because of its practicality and potential as an efficient retrofitting solution. Additionally, for largely linear first mode dominant structures it presents a very efficient solution (Barroso et al. 2003, Bishay-Girges 2004).

The straight tendon configuration of the B-Systems is an approximate solution of the draped tendon configuration based on the load-balancing concept. This concept was introduced by Lin (1963) for the design of prestressed concrete elements. Pekcan et al. (2000) applied the concept to the seismic design of structures. A load-balancing system is a geometrically feasible system used to apply forces of equal magnitude and opposite direction to the lateral seismic forces acting on a structure. The load-balancing system, when properly designed, reduces the overturning moment demand as well as the storey shear demand on the structural elements. In most cases, it is economically more feasible because of the reduced number of devices needed in the supplemental damping system. Moreover, it provides optimal forces for the assumed vertical distribution of the inertial loads at each floor level. This approach can be applied to relatively stiff as well as flexible structures (Pekcan et al. 2000).

Earthquake ground motions are time-dependent and create inertia or lateral forces by shaking the structure back and forth. The deformation of the structure at any instant of time is a function of the characteristics of the ground motion and of the stiffness and damping of the structure. However, the maximum response quantities observed during the ground motion are the main concern in seismic design (Pekcan et al. 2000). Four earthquake ground motions at different levels of peak ground acceleration are used to evaluate the response of the tendon systems described above. These ground motions include:

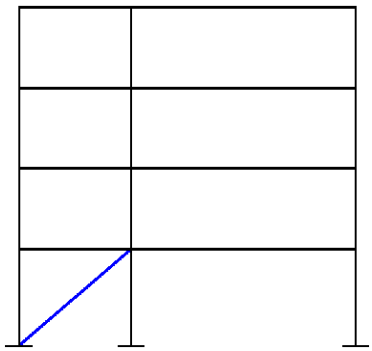

(a) System A1

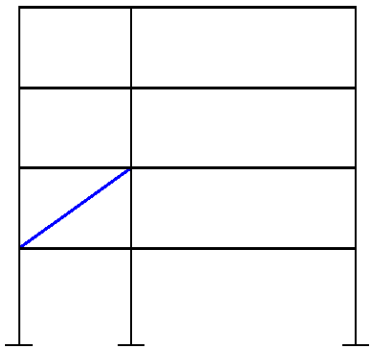

(b) System A2

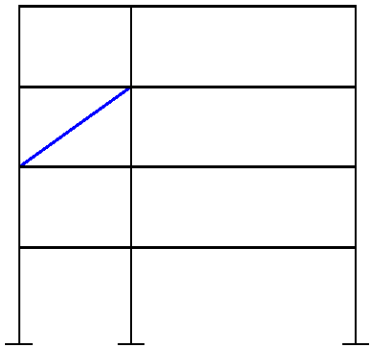

(c) System A3

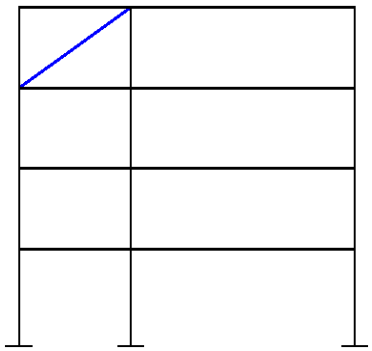

(d) System A4

Figure 4.7 A-Systems.

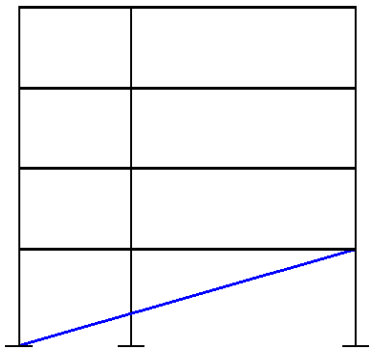

(a) System B1

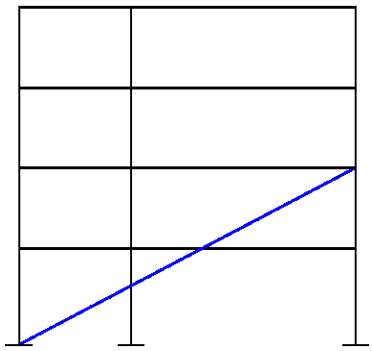

(b) System B1-2

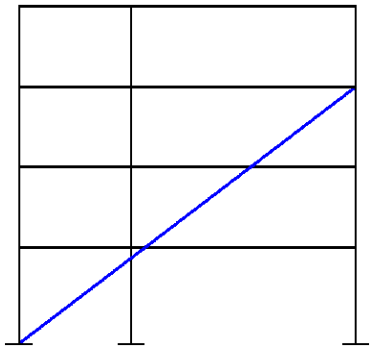

(c) System B1-3

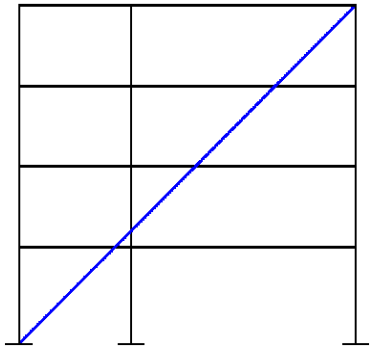

(d) System B1-4

Figure 4.8 B-Systems.

a. Imperial Valley, 18 May 1940 – El Centro north-south (NS) component
b. Kern County, 21 July 1952 – Taft S21W component
c. Northridge, 17 January 1994 – Sylmar County Hospital (Chan 9: 0 deg)
d. Kobe, 17 January 1995 – JMA Observatory N00E component.

Apart from the El Centro record (0.3483g), the amplitude of the earthquake records was scaled in order to excite the one-fifth scale structure with ground motions of different intensity. The scaled records are Taft 90% (0.1602g), Sylmar 20% (0.1595g) and Kobe 20% (0.1673g).

4.4.3 Interpretation of the Analytical Results

Nonlinear dynamic analyses using the RUAUMOKO computer program are performed to evaluate the effectiveness of the different tendon configurations. The responses of the systems shown in Figures 4.7 and 4.8 are examined for the first nineteen seconds of the north-south component of the 1940 El Centro earthquake. The results are presented for comparison to the uncontrolled case (system A) shown in Figure 4.6. The seismic performance of the model structure is evaluated in terms of reductions in relative displacements, absolute accelerations, inter-storey drift ratios and total base shear, i.e. including the contribution of the tendon member (Franco-Anaya et al. 2006).

Maximum response profiles shown in Figures 4.9 and 4.10 present the overall benefits of the semi-active resettable tendon in reducing the earthquake response of the one-fifth scale structure. In particular, the structural response is significantly improved by the B-Systems. This indicates that the seismic response of the structure is effectively reduced by the tendon configurations based on the load-balancing concept.

Figure 4.10 shows that considerable response reductions are achieved by the system B1-3 (Fig. 4.8c). The reductions in floor displacements and inter-storey drifts achieved by the system B1-3 are slightly more significant than the reductions obtained by the system B1-4 (Fig. 4.8d). However, the reductions in floor accelerations and base shear achieved

by the system B1-3 are much more significant than the reductions obtained by the system B1-4. This is because of the steeper angle of the tendon used by system B1-4.

The response profiles shown in Figure 4.9 suggest that system A1 (Fig. 4.7a), the first-storey damped case, might also be effectively used to reduce the seismic response of the structure. However, a close comparison of Figures 4.9 and 4.10 reveals that system A1 is less effective in reducing the overall seismic response than system B1 (Fig. 4.8a), the first-storey damped case of the B-Systems. This last result is due to the steeper angles of the tendon and the reduced resisting forces offered by the A-Systems.

The effectiveness of the system B1-3 in reducing the seismic response under the El Centro ground motion can be clearly seen in Figure 4.10. A reduction of up to 77% in the maximum relative displacement at the fourth floor is observed (Fig. 4.10a). The maximum absolute acceleration at the fourth floor is reduced by up to 5% (Fig. 4.10b). However, the absolute accelerations in other levels of the structure increased slightly, which represents a common trade-off with resettable stiffness-based devices (Hunt 2002, Barroso et al. 2003). A 74% reduction in the maximum inter-storey drift ratio at the second floor is achieved (Fig. 4.10c). The maximum total base shear is reduced by up to 36% (Fig. 4.10d). These results demonstrate the significant potential of semi-active resettable devices in reducing the seismic response of structures.

Although no significant reduction in absolute floor accelerations is obtained by using system B1-3, the reductions in floor displacements and inter-storey drifts achieved by the system are still very significant. It is important to note that, increased accelerations may damage contents and/or disturb occupants. However, this trade-off depends on the building use and any other isolation or protection systems employed.

Similar results are achieved by the B-System for the other earthquake records used in this investigation. Maximum response envelopes can be found in Appendix B. It is shown, that the effectiveness of the semi-active resettable tendon depends on the properties of the model structure, the characteristics of the earthquake ground motion, and the configuration of the semi-active resettable tendon.

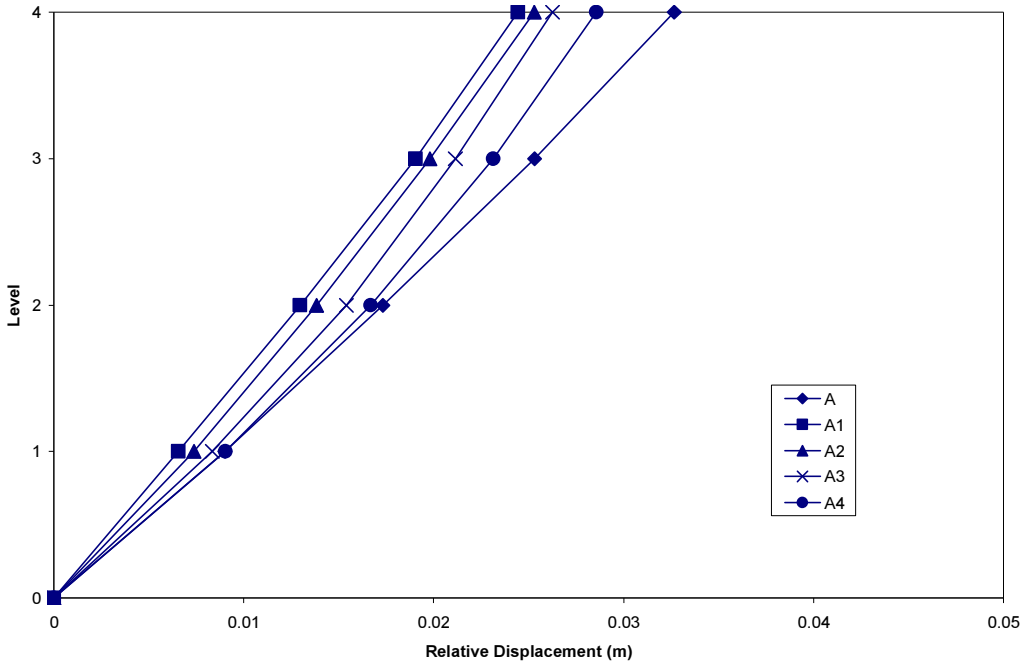

(a) Maximum relative displacements

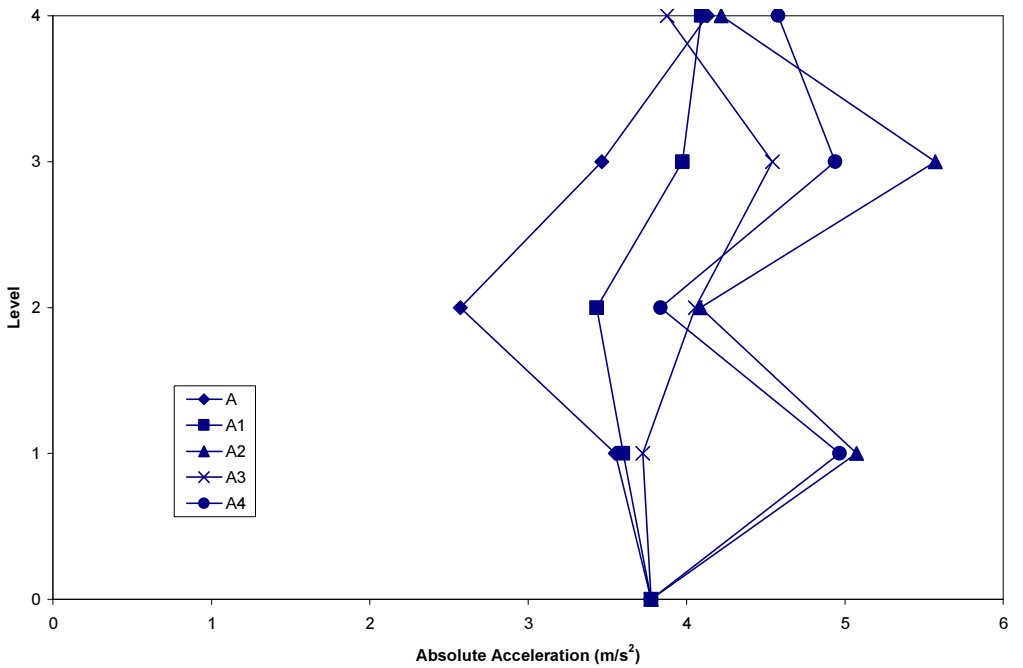

(b) Maximum absolute accelerations

Figure 4.9 Maximum response envelopes of A-Systems under El Centro earthquake.

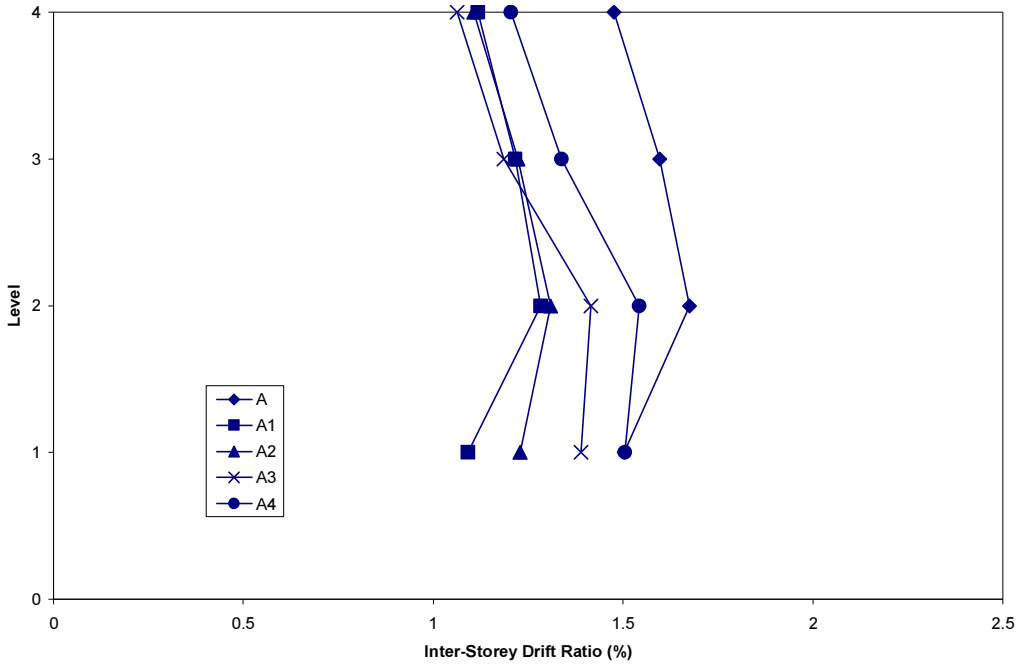

(c) Maximum inter-storey drift ratios

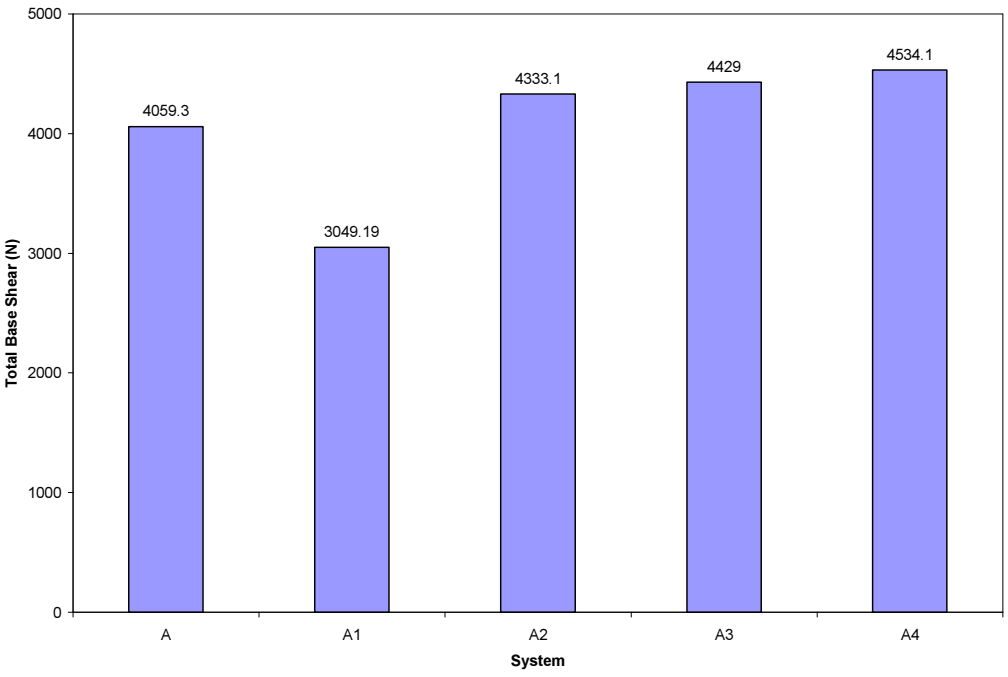

(d) Maximum total base shear

Figure 4.9 (Continued).

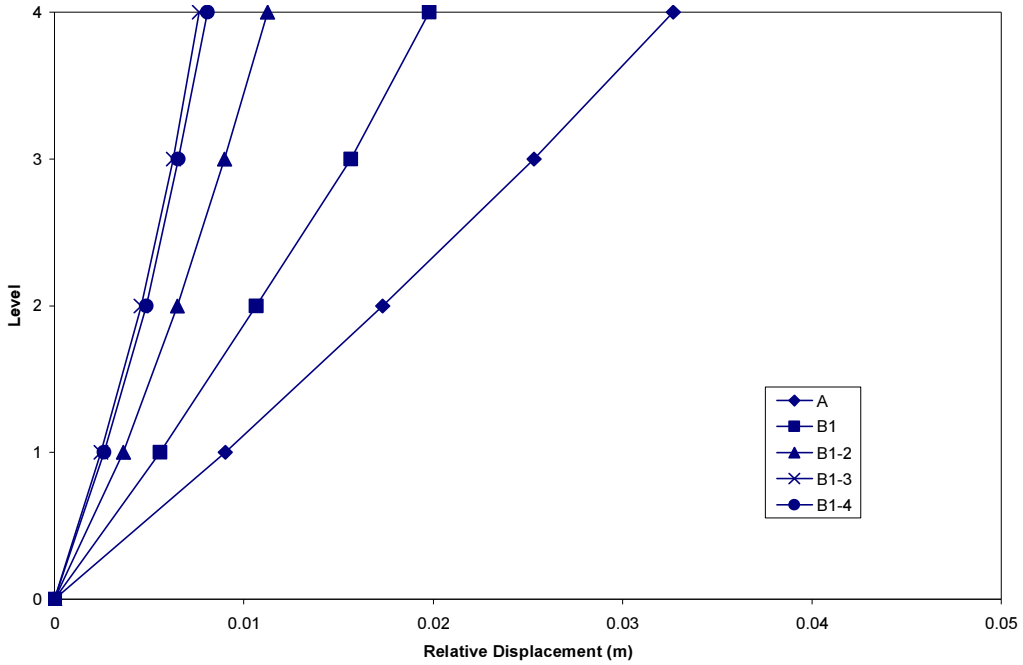

(a) Maximum relative displacements

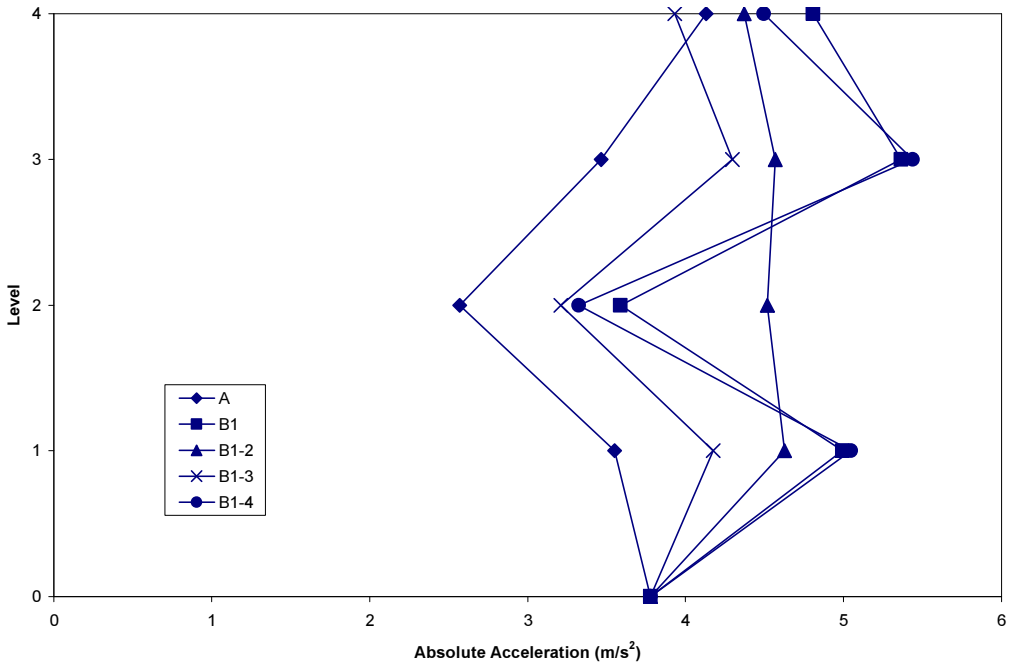

(b) Maximum absolute accelerations

Figure 4.10 Maximum response envelopes of B-Systems under El Centro earthquake.

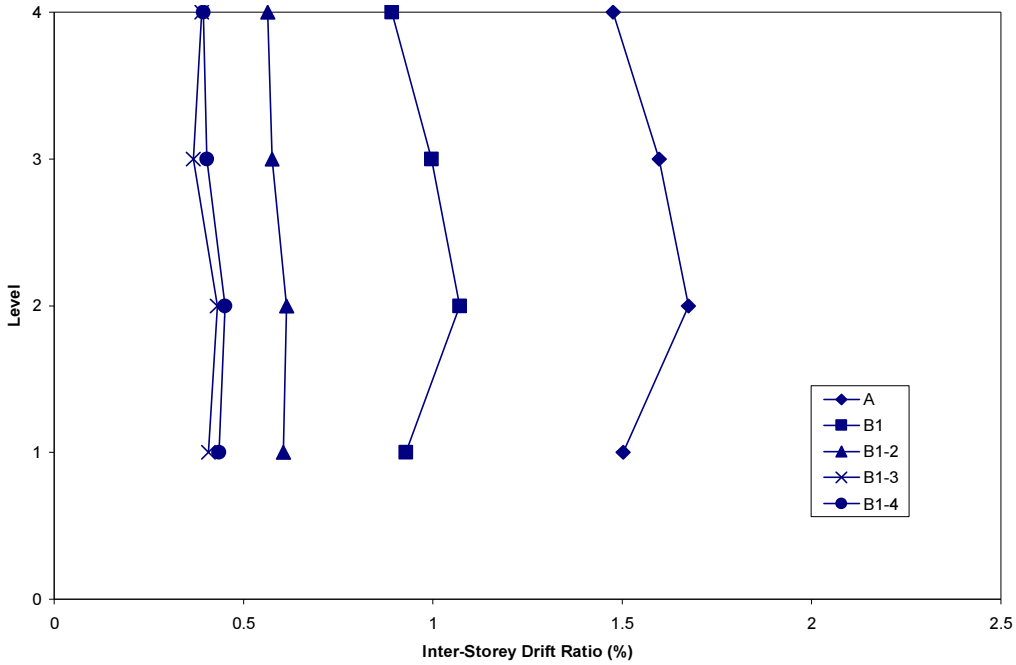

(c) Maximum inter-storey drift ratios

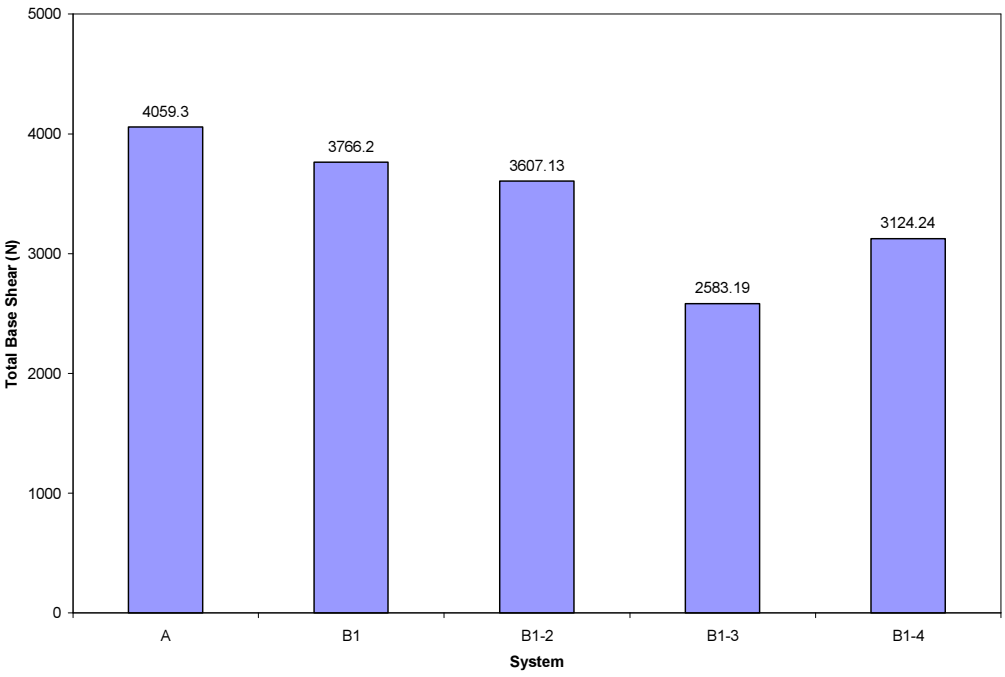

(d) Maximum total base shear

Figure 4.10 (Continued).

4.4.4 Complementary Tendon Systems

It is of interest to investigate the seismic performance of the systems shown in Figure 4.11. In these systems, the resettable tendon member is installed within the short bay and diagonally spans between two or more floors of the structure.

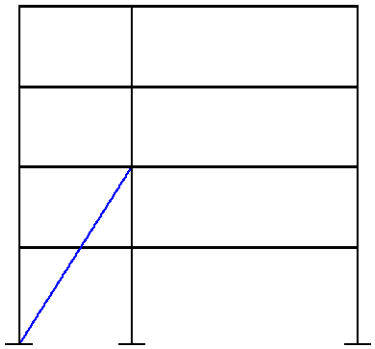

(a) System A1-2

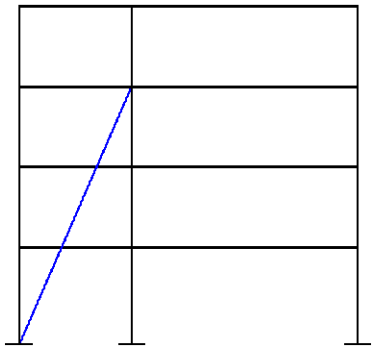

(b) System A1-3

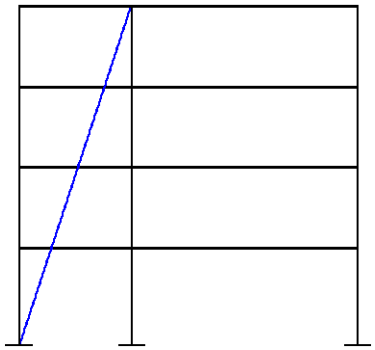

(c) System A1-4

Figure 4.11 Complementary tendon systems.

Figure 4.12 shows maximum response envelopes for the complementary systems under the north-south component of the 1940 El Centro earthquake. System A represents the original structure without any added semi-active resettable tendon (Fig. 4.6). System A1 is the first-storey damped case shown in Figure 4.7a. It can be seen that the system A1-3 (Fig. 4.11b) shows the best performance in reducing the relative displacements and inter-storey drift ratios of the one-fifth scale structure.

Based on these results, system A1-3 appears to be very suitable to reduce the seismic response of the model structure. However, a comparison of the maximum response profiles shows that the reductions achieved by the system B1-3 (Fig. 4.8c) are still more significant than those provided by the system A1-3, as shown in Figure 4.13. It is also shown that the first-storey damped case (system A1) is not particularly effective in reducing the seismic response of the model structure.

From the architectonical point of view, the system A1-3 may be more attractive than the system B1-3, whose tendon configuration is based on the load balancing concept. This is because the system A1-3 has a less intrusive effect on the architectonical view of the structure. However, an analytical investigation reveals that the tendon stiffness of the system A1-3 needs to be increased by up to 261% in order to achieve similar response reductions as those provided by the system B1-3. Figure 4.14 shows a comparison of response time-history for both systems under the El Centro ground motion. The original system A1-3 with the increase in tendon stiffness is denoted as system A1-3_S.

The response time-history is compared in terms of relative displacements, absolute accelerations and inter-storey drift ratios at the third floor of the model structure, as shown in Figures 4.14a, 4.14b and 4.14c. The time-history of the total base shear is shown in Figure 4.14d and includes the contribution of the resettable tendon to the base shear. For clarity in the presentation, the results are shown for the strong part of the earthquake record only.

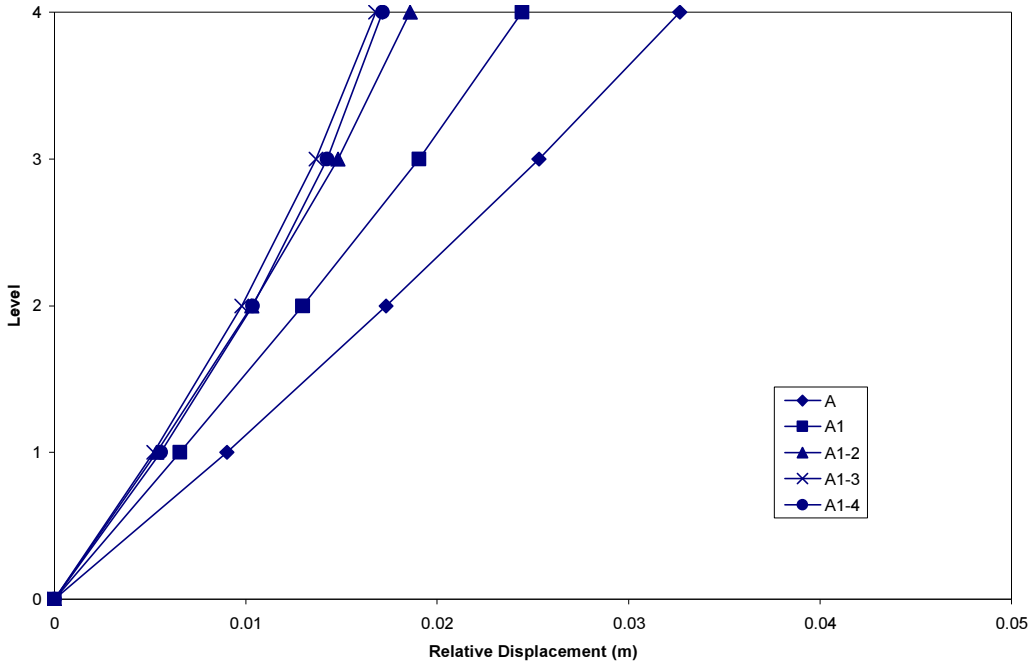

(a) Maximum relative displacements

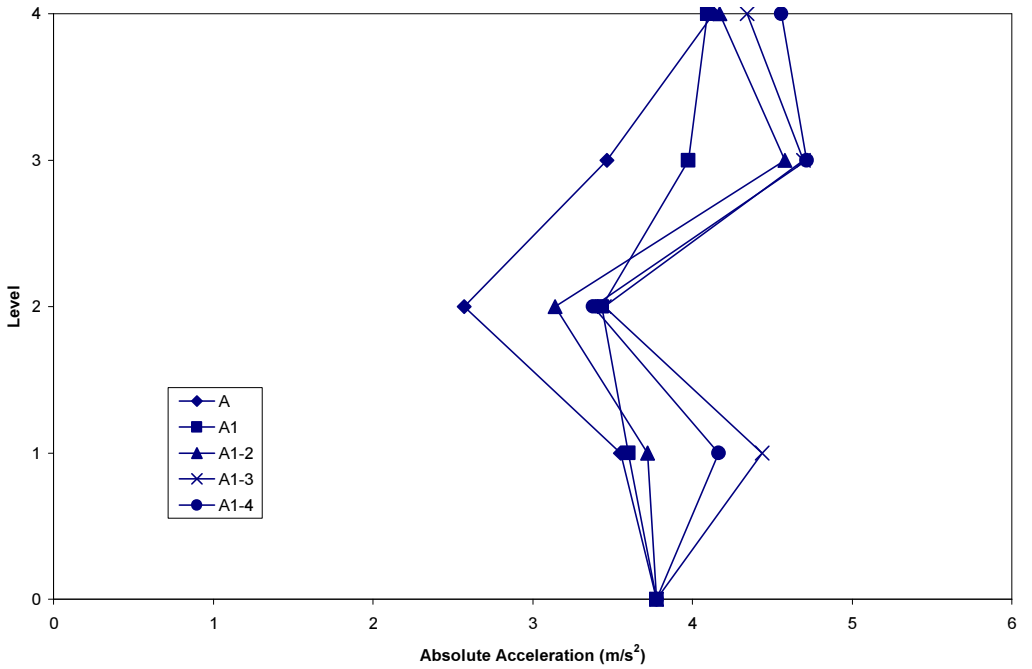

(b) Maximum absolute accelerations

Figure 4.12 Maximum response envelopes of the complementary systems.

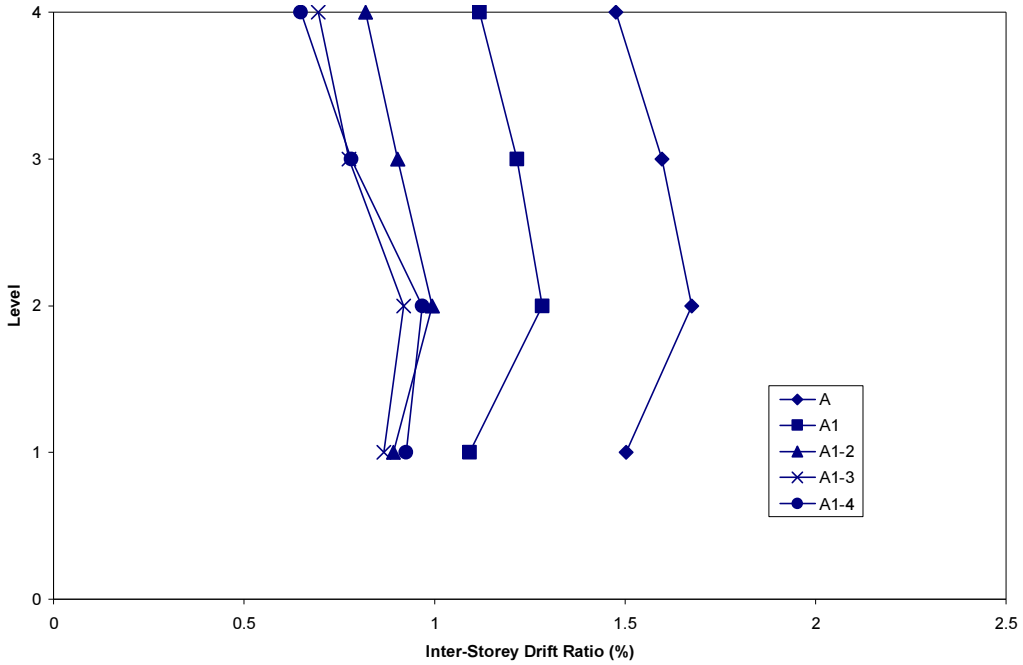

(c) Maximum inter-storey drift ratios

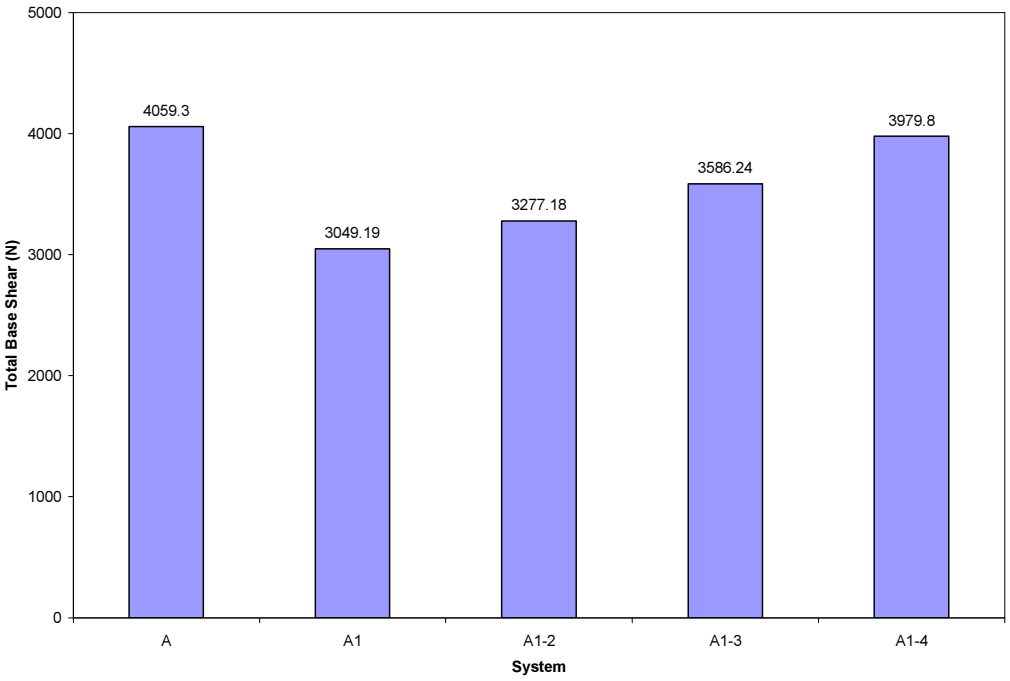

(d) Maximum total base shear

Figure 4.12 (Continued).

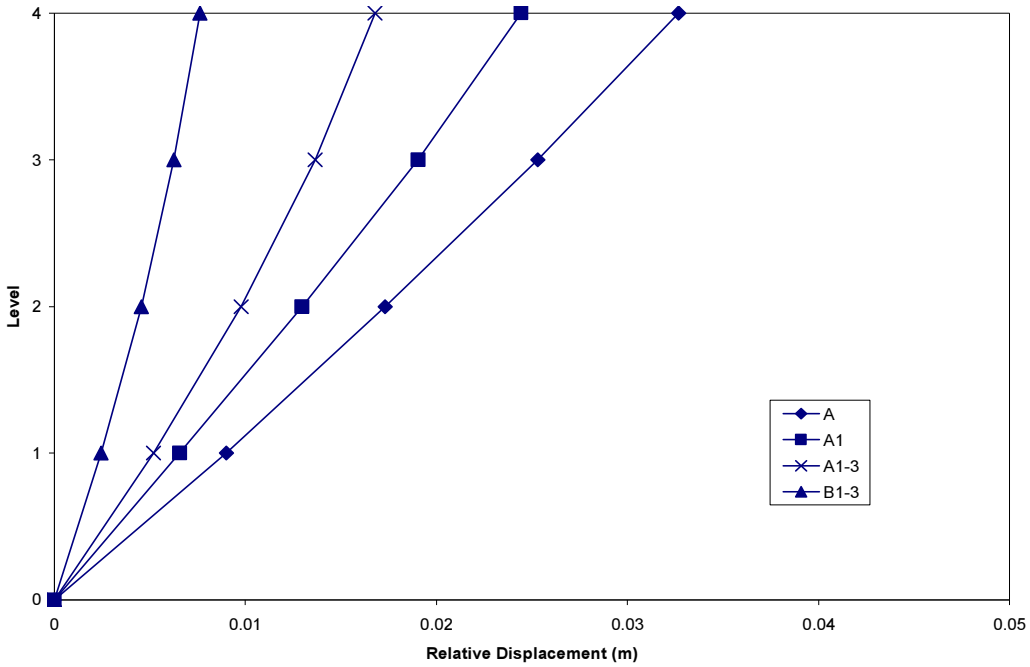

(a) Maximum relative displacements

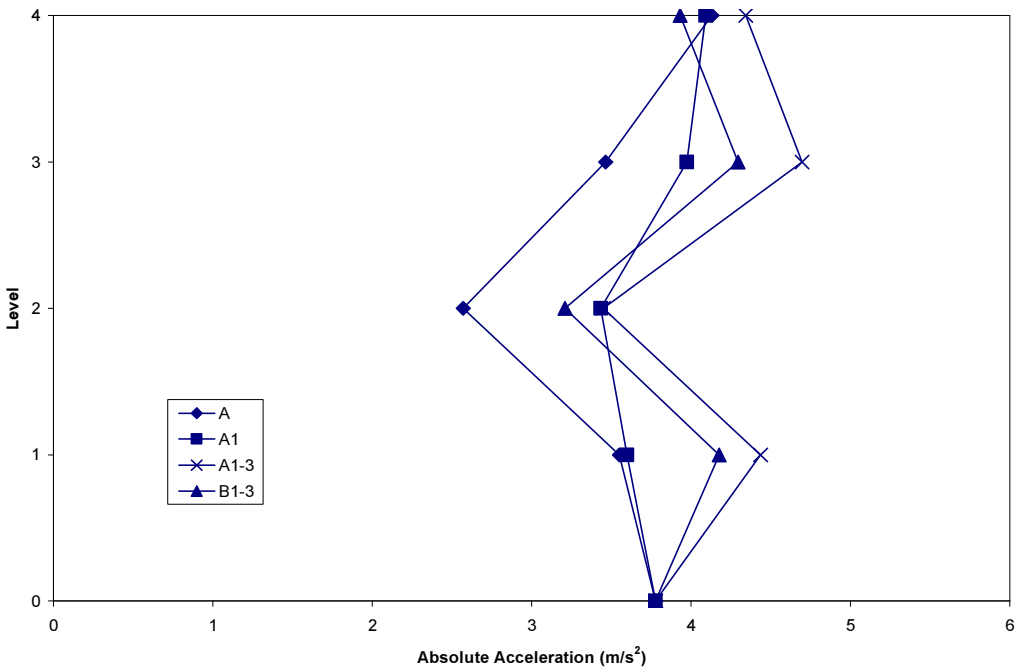

(b) Maximum absolute accelerations

Figure 4.13 Maximum response envelopes of the best tendon systems.

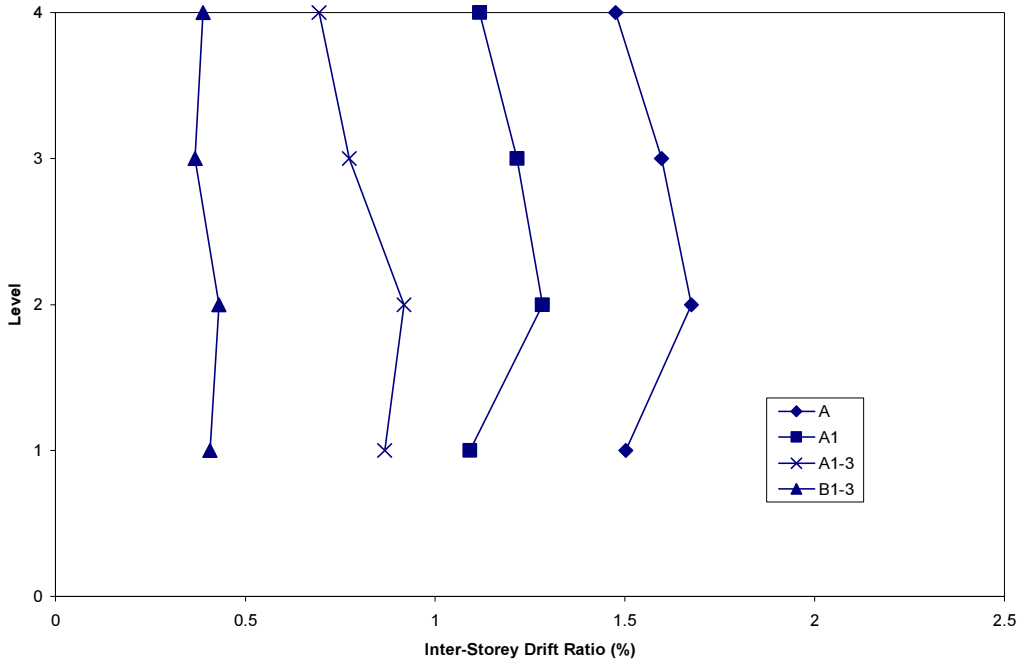

(c) Maximum inter-storey drift ratios

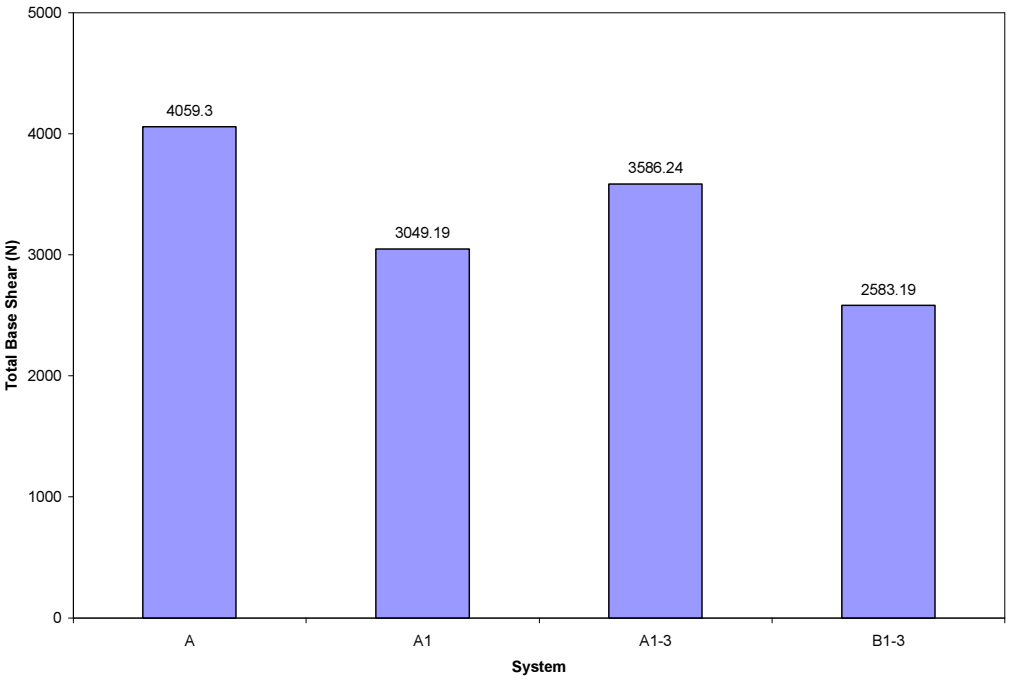

(d) Maximum total base shear

Figure 4.13 (Continued).

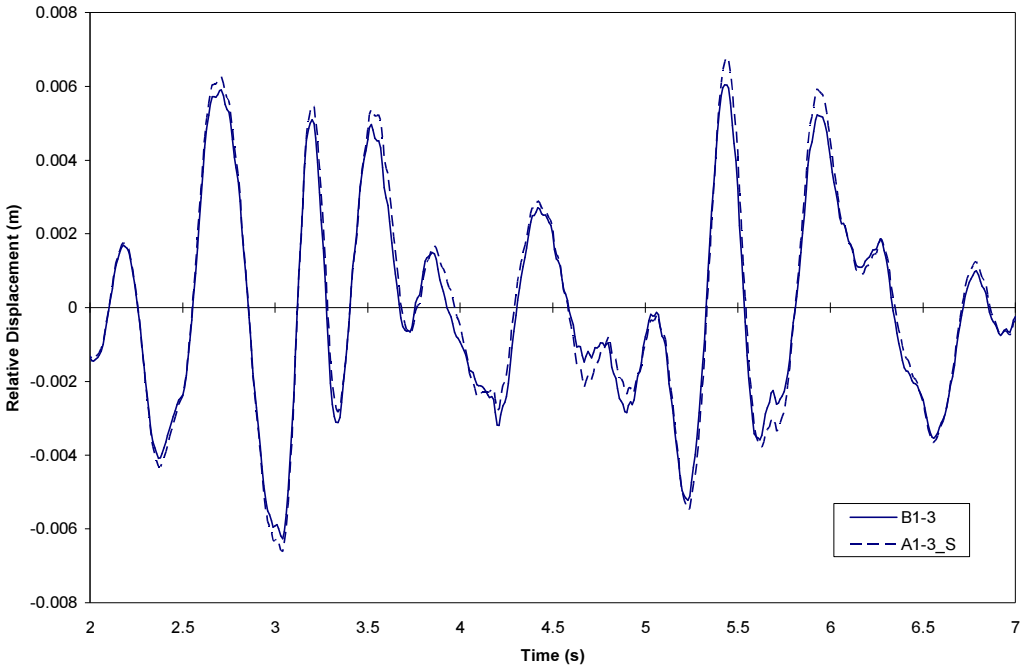

(a) Relative displacement at third floor

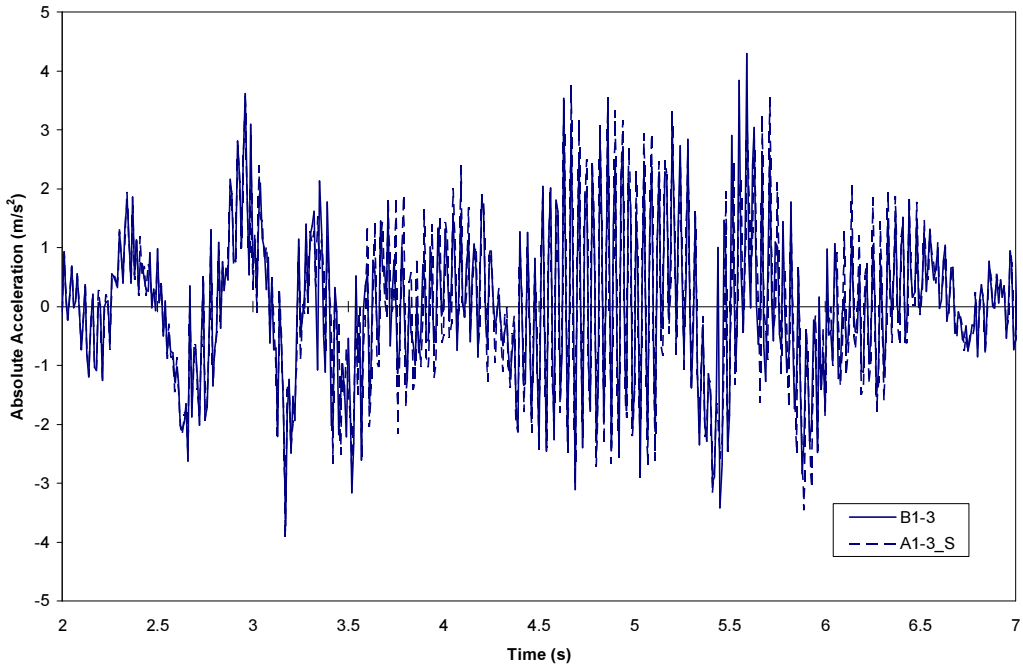

(b) Absolute acceleration at third floor

Figure 4.14 Comparison of the seismic response for the B1-3 and A1-3_S systems.

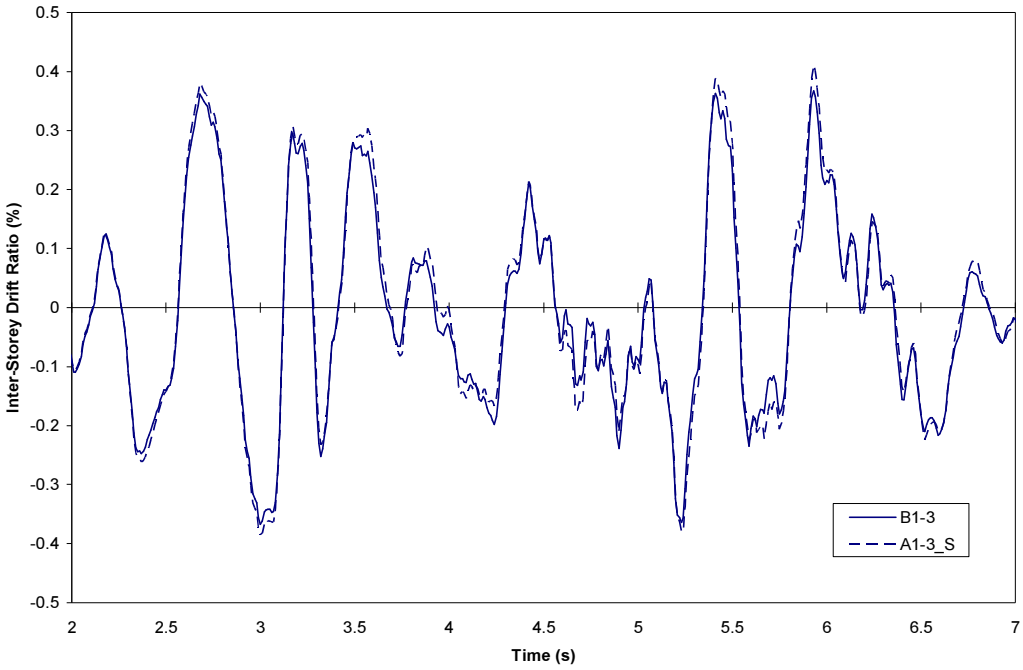

(c) Inter-storey drift ratio at third floor

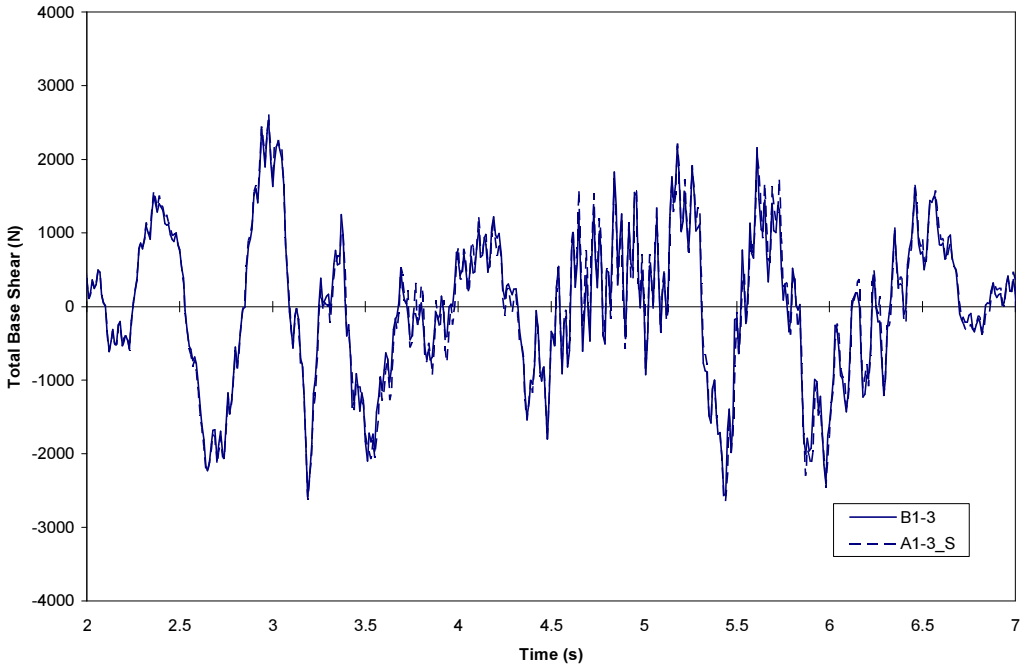

(d) Total base shear

Figure 4.14 (Continued).

4.4.5 Seismic Response Using a Resettable Spring Member

In the previous sections, a tendon member with an ideal (linear) resettable hysteresis rule was utilised to reduce the response of the one-fifth scale structure. For comparison purposes, the seismic response of the structure is now investigated by using the spring member shown schematically in Figure 4.15. The spring member also follows the ideal resettable hysteresis rule shown in Figure 4.5.

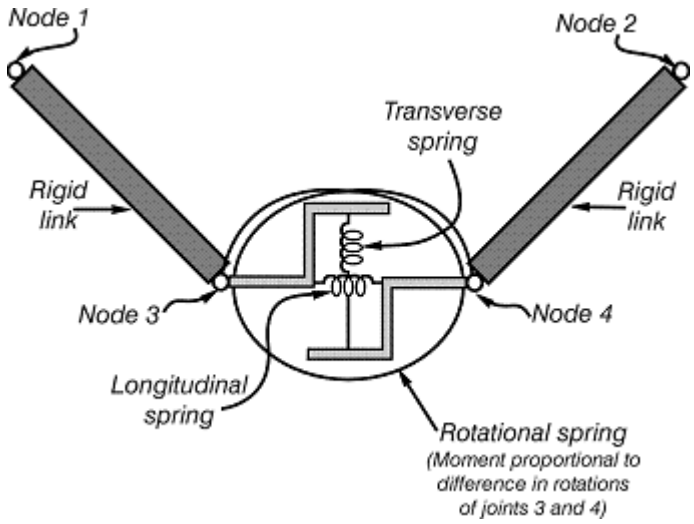

Figure 4.15 Spring member (Carr 2006).

Spring members are used to model special effects in the structure. In two-dimensional structural analyses, they are utilised to represent members acting out of the plane of a frame but representing forces that act in the plane of the frame. The spring member may have a longitudinal, a transversal and a rotational spring component. The forces in the spring components are proportional to the differences in the longitudinal and transversal displacements of the two ends of the spring member. The rotational spring moments are only proportional to the differences in the rotations at each end of the member. Spring member may be thought of as a generalised truss member, which may follow any of the hysteresis rules available in the RUAUMOKO program (Carr 2006).

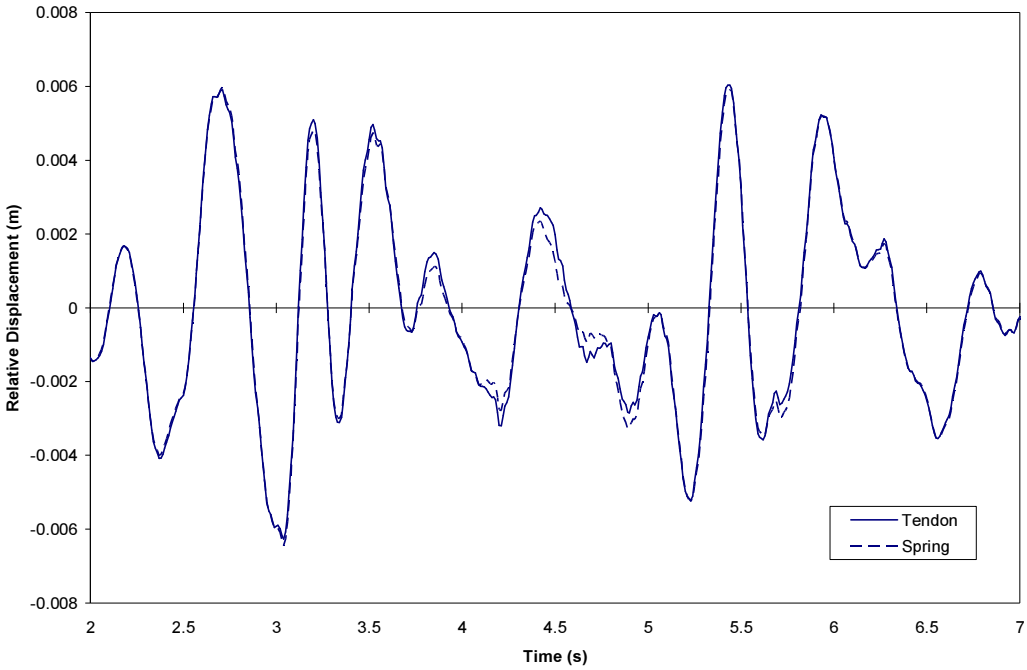

(a) Relative displacement at third floor

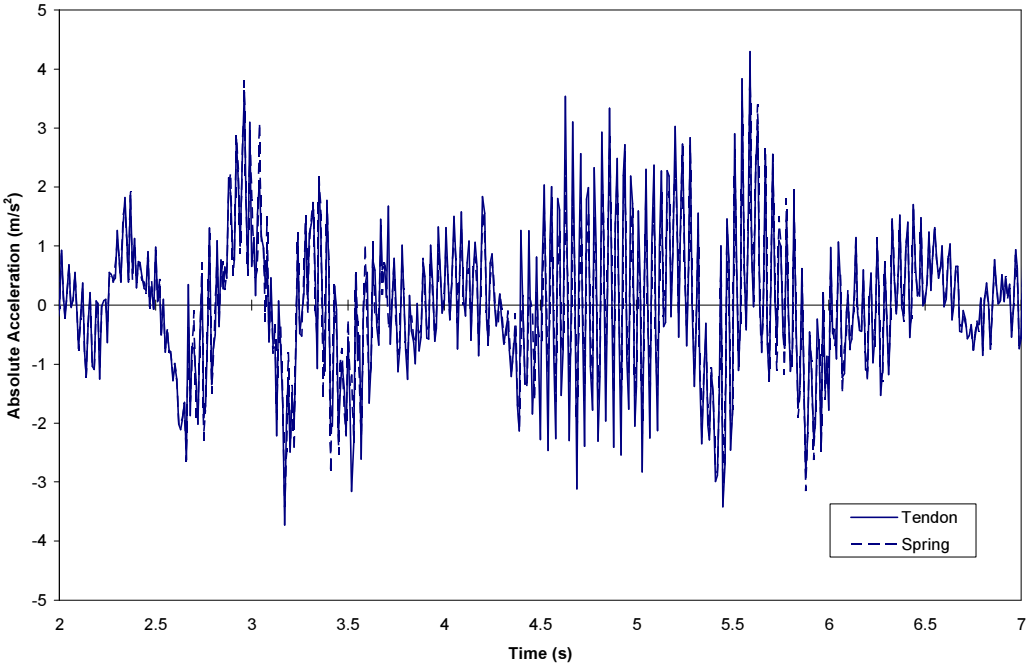

(b) Absolute acceleration at third floor

Figure 4.16 Comparison of the seismic response for the tendon and spring members.

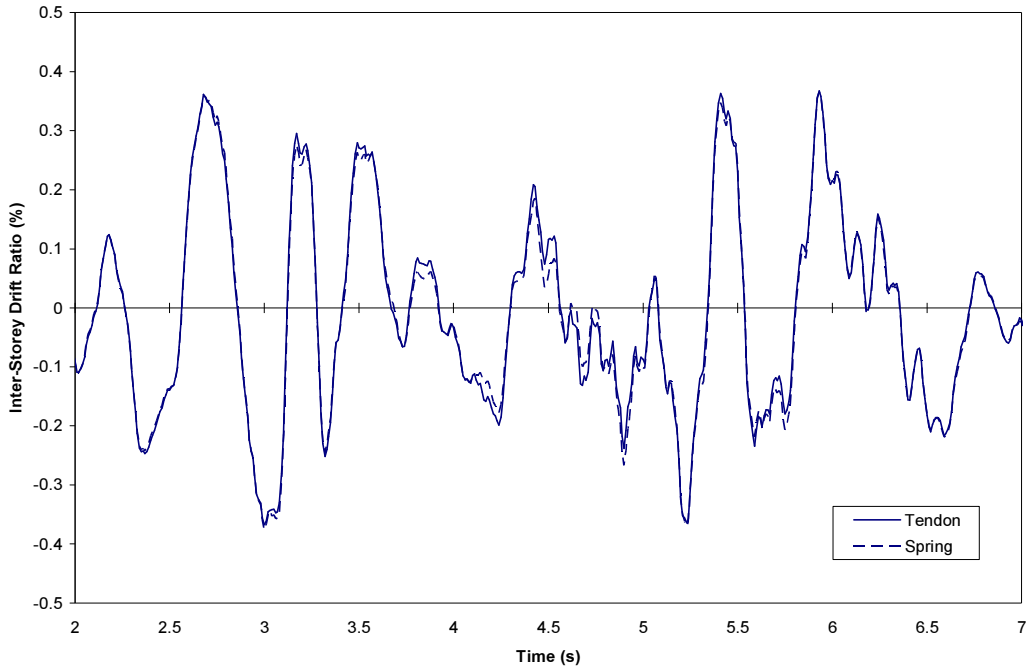

(c) Inter-storey drift ratio at third floor

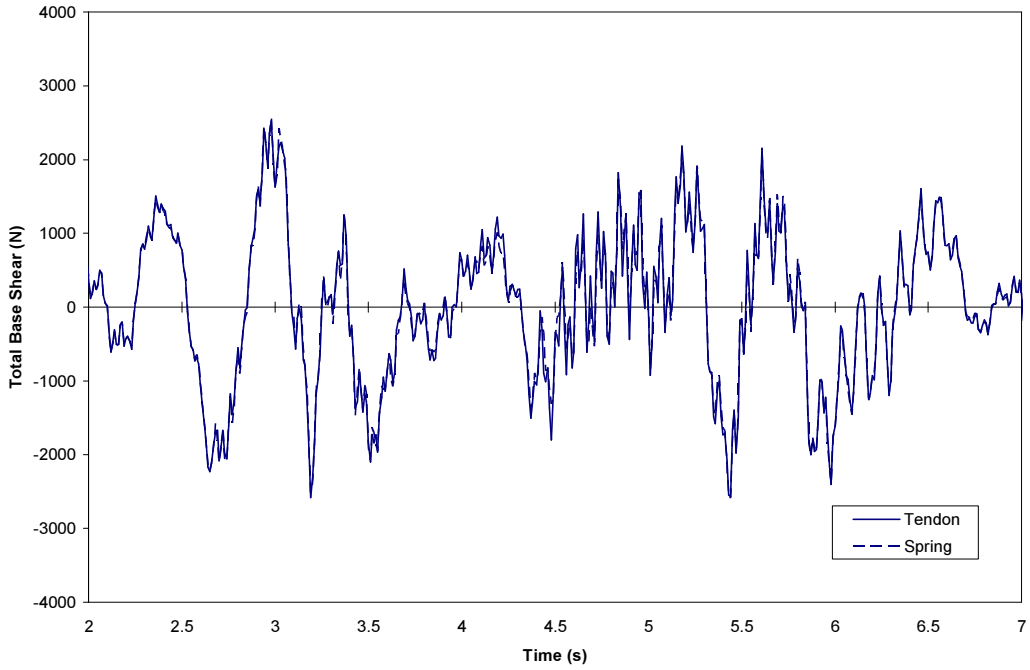

(d) Total base shear

Figure 4.16 (Continued).

A nonlinear dynamic analysis using the RUAUMOKO computer program is performed to evaluate the effectiveness of the resettable spring member under the 1940 El Centro earthquake. A spring stiffness of 250 kN/m and a saturation force of 5.295 kN are used in the computer analyses (i.e. the same properties previously utilised in the computer analyses of the resettable tendon member).

The system B1-3 (Fig. 4.8c) is used to examine the seismic response of the one-fifth scale structure equipped with the semi-active resettable spring. Figure 4.16 shows a comparison of the response time-history for the two computational members. A very good agreement can be observed between the earthquake response achieved by the resettable spring member and the response provided by the resettable tendon member.

As shown in Figures 4.16a, 4.16b and 4.16c, the response time-history is compared in terms of relative displacements, absolute accelerations and inter-storey drift ratios at the third floor of the one-fifth scale structure (i.e. the floor which the semi-active resettable members are attached to). The time-history of the total base shear shown in Figure 4.16d includes the contribution of the resettable member to the base shear. Results are shown only for the strong part of the earthquake ground motion for clarity purposes.

4.5 SUMMARY

This chapter has presented an analytical investigation into the earthquake performance of structures equipped with resettable energy dissipation devices. The effects on the seismic response induced by damping and stiffness increases resulting from the addition of energy dissipation devices were described. The optimal placement and distribution of these devices were also discussed. The effects of changing the location and configuration of a semi-active resettable tendon on the seismic response of a four-storey model structure were investigated. Nonlinear dynamic analyses using the RUAUMOKO computer program were performed to determine the optimal configuration of the resettable tendon in the model structure. Several tendon configurations under different earthquake ground motions were used to evaluate the effectiveness of the semi-active

resettable tendon. Maximum response envelopes for the 1940 El Centro earthquake were presented and interpreted. The optimal configuration of the tendon was found to be based on the load-balancing concept widely used in the design of prestressed concrete elements. An examination of the seismic response of the structure showed that the addition of the semi-active resettable tendon to the structure leads to significant reductions in relative displacements and inter-storey drift ratios. Notable reductions in total base shear and absolute accelerations were also achieved.

Chapter 5
EXPERIMENTAL VALIDATION OF RESETTABLE DEVICES

5.1 INTRODUCTION

Semi-active control systems have only recently been considered for applications to full-scale civil engineering structures. Therefore, most of the research in this area has been devoted to analytical and numerical studies in which a number of idealized assumptions are made. The validity of such assumptions must be evaluated through experimental research (Symans and Constantinou 1997, Serino et al. 2001). Large-scale experimental testing of semi-active control systems can be helpful to identify important aspects of eventual actual implementations, including nonlinear structural effects, control-structure interaction, actuator and sensor dynamics, actuator-actuator interaction effects, system integration, etc. In addition, experimental testing can be important to detect potential obstacles and limitations for the implementation of semi-active control systems in actual civil engineering structures.

5.2 THE NEED FOR EXPERIMENTAL TESTING

Despite significant progress being achieved in the dynamic analysis of structures in recent years, there is still a strong necessity for experimental evaluation of structural performance. Experimental testing of structures is currently undergoing deep changes motivated by a variety of reasons, including the following:

1. A widespread consensus about the necessity for developing design methods based on performance objectives rather than strict practical rules. A performance-based design defines the performance required for a structure. This approach is concerned with what a structure is required to provide, rather than prescribing how it should be

designed, detailed and constructed. Performance-based design requires that engineers have a comprehensive knowledge of the structural performance and, notably gain access to complete data on material behaviour in the nonlinear range and energy dissipation mechanisms. The approach considers a shift towards a more scientifically oriented design process with emphasis on more accurate characterizations and predictions, often based on a higher level than that of the technology used in the past.

2. A rapid advancement of technologies related to earthquake and wind engineering. New approaches to hazard mitigation based on novel equipment are in progress and need to be endorsed. They include: smart materials and intelligent structures, advanced sensors, remote sensing technology, supercomputing power, wireless communication, and control of structures. These new approaches provide not only an unprecedented opportunity to improve vibration risk control, but also new means to better understand damage that cannot be solved by traditional approaches (Casciati et al. 2006).

3. The introduction of semi-active devices has stimulated the development of advanced on-line testing techniques with sub-structuring able to validate their dynamic properties as well as to verify the overall performance of their control laws applied to a realistic structure. The on-line testing can be utilised to test any sub-structure within a structural system, be it a new control device or a structural connection (Mulligan 2007).

As a result, many research programmes have been extended to support the development of new technologies to prevent adverse vibration effects and more generally to control the movements of large structures such as buildings and bridges. Relevant contributions are currently made in full-scale and large-scale testing of structures effectively protected by base isolation or energy dissipation devices (Casciati et al. 2006).

5.3 IMPLEMENTATION OF THE CONTROL SYSTEM

The one-fifth scale structure was tested on a shake table facility in the Structures Laboratory at the University of Canterbury. The shaking table is a unidirectional table with an unloaded mass of 5000 kg supported by two sets of linear Teflon bearings. The system is driven by a 280 kN double-acting hydraulic actuator powered by a 224 kW motor operating at 276 bar. The hydraulic actuator is controlled by a set of two Moog E072-054 servo-valves capable of supplying up to 3.87 l/s each. The servo-valves are controlled by a TestStar control system from MTS Systems Corporation that includes a controller and signal conditioners to drive the current based servo-valves and decode sensor signals. The table displacement is measured by a Linear Variable Differential Transducer (LVDT) and displacement input reference signals are produced from an external computer (Chase et al. 2005b).

The model structure was bolted to the shake table in such a way that the longitudinal frames of the model were parallel to the motion of the table. The model structure was tested without resettable devices and with two resettable devices. Each of the devices was installed at the lower end of a steel tendon element. The steel tendon element was placed along the two bays and was connected to the model structure at the third floor to transfer the control forces. This arrangement of the steel tendon follows the same tendon layout of the highly effective System B1-3 studied in Chapter 4. The tendon is made of a 40 × 40 × 2 mm steel hollow section. The diagonal steel tendons were connected to the structure by using a horizontal transverse beam of 100 × 100 × 4 mm square hollow section (SHS). The steel hollow section was fixed to the beam-column connections at the third floor of the test structure. The hollow section was required to have negligible deflection during the testing to ensure the adequate transfer of the control forces to the structure. An assemblage of steel plates fixed to the shake table was built to support and keep the test device in the right position. The assemblage of plates acts as a restraint element of the tendon system. Figure 5.1 shows a photograph of the control system implementation on the structure.

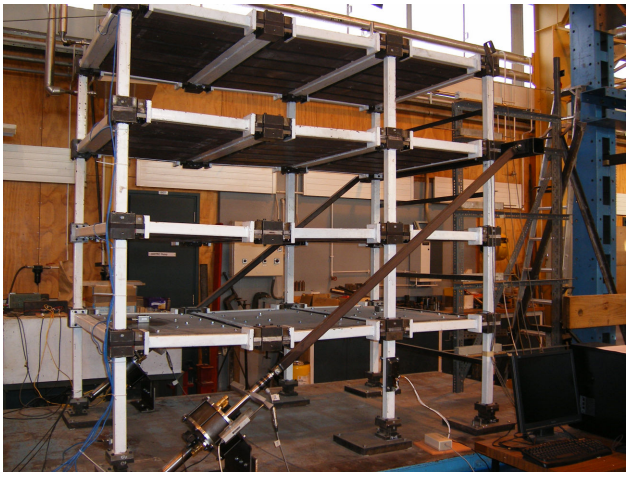

Figure 5.1 Implementation of the control system.

The control system consists of the resettable device, including the valves, sensors and a control computer. The sensors measure the responses of the model structure and the control computer controls the operation of the device. During the experimental testing, the responses of the model structure are measured by the sensors and then sent to the control computer. The control computer processes the structural responses according to a predetermined control algorithm and sends an appropriate command signal to the valves of the resettable device.

The control logic command for the device valves depends on the current and previous position of the piston, which is determined by a displacement potentiometer attached to the device. The resulting signal of the potentiometer is converted to a displacement signal with high resolution. The raw data of the sensor is processed to determine the piston position and direction of the motion. The potentiometer data is filtered in order to obtain a clean signal to eliminate erroneous or erratic valve commands. The valve commands are determined from this filtered feedback signal and the specific control law logic utilised (Mulligan 2007).

5.4 MEASUREMENT INSTRUMENTATION

Various linear potentiometers and accelerometers are used to measure the response of the model structure and the motion of the shaking table. A schematic of the model structure indicating the location of the transducers is shown in Figure 5.2. Five linear potentiometers installed along the height of the model structure measure the absolute displacement at the mid-height of each storey and the roof. The absolute displacement of the shaking table is also measured by a linear potentiometer. The measurements from the potentiometers are interpolated to obtain the absolute floor displacements at the first, second and third floor of the model structure. Appendix C shows that these calculated displacements represent the floor displacements accurately. The absolute displacement at the fourth floor is directly measured by one of the potentiometers. The absolute floor displacements are then converted into relative displacements by subtracting the absolute displacement of the shaking table.

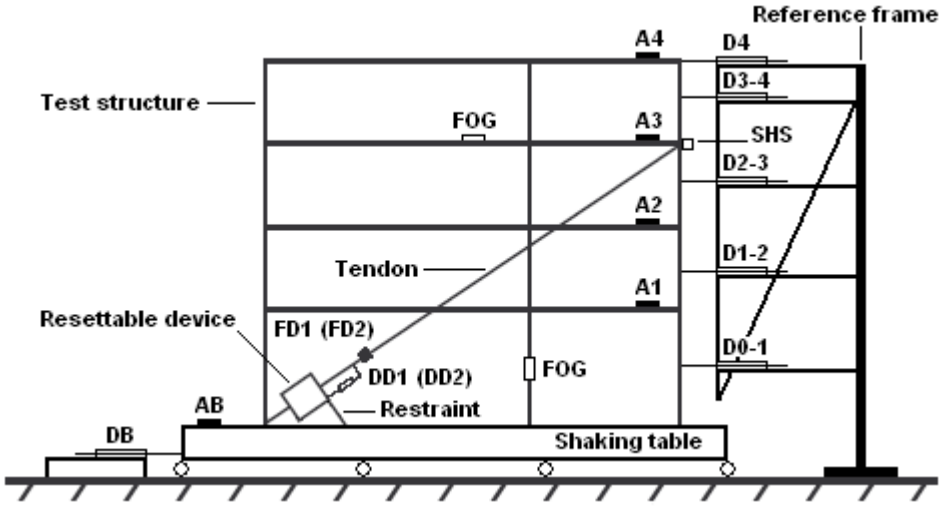

Figure 5.2 Measurement instrumentation of the test structure.

Another linear potentiometer located along the axis of each resettable device is used to measure the displacement of the piston shaft with respect to the device housing. The force in each device is measured by a load cell placed between the device and the steel tendon element. Five unidirectional accelerometers are used to measure the absolute acceleration of each floor of the model structure and the shaking table. The fibre-optic

gyroscope (FOG) described in Chapter 8 is utilised to measure the rotation rates of structural elements. The FOG is first attached to the centre-column at level 1 and then to the floor system at level 3. Experimental data recorded by the transducers is sampled at 1 kHz. A list of the acquisition channels and a description of the response measured is given in Table 5.1.

Table 5.1 Description of the measurement instrumentation (refer to Figure 5.2).

Channel	Transducer	Notation	Response Measured
0	Accelerometer	AB	Horizontal acceleration of shake table
1	Accelerometer	A1	Horizontal acceleration at level 1
2	Accelerometer	A2	Horizontal acceleration at level 2
3	Accelerometer	A3	Horizontal acceleration at level 3
4	Accelerometer	A4	Horizontal acceleration at level 4
5	Potentiometer	D0-1	Horizontal displacement at level 0-1
6	Potentiometer	D1-2	Horizontal displacement at level 1-2
7	Potentiometer	D2-3	Horizontal displacement at level 2-3
8	Potentiometer	D3-4	Horizontal displacement at level 3-4
9	Potentiometer	D4	Horizontal displacement at level 4
10	Load cell	FD1	Axial force of device 1
11	Load cell	FD2	Axial force of device 2
12	Potentiometer	DB	Horizontal displacement of shake table
13	Potentiometer	DD1	Axial displacement of device 1
14	Potentiometer	DD2	Axial displacement of device 2
--	Fibre-optic gyroscope	FOG	Rotation rates of centre-column at level 1 and floor system at level 3

All linear potentiometers, unidirectional accelerometers and load cells are connected to a high-speed data logger and a dSpace rapid prototyping system. The data logger is a device with the capability of taking an analogue input signal, converting it to a string of digital data and storing it for retrieval at later time. dSpace is the software and real-time integration system that controls the operation of the resettable device. It is also utilised for collection and processing of experimental data. The FOG is connected to a personal computer and a power supply.

5.5 FREE VIBRATION TESTING

The dynamic properties of the model structure with and without resettable devices were identified by using free vibration tests. Free vibration tests were carried out by pulling the model structure to one side using a steel wire. After achieving a target displacement at level 4, the steel wire was cut to allow the structure to vibrate freely. The target floor displacement was controlled by a dial-gauge attached to the potentiometer located at the top level of the model structure. Figure 5.3 shows a photograph of the experimental set-up for the free vibration testing of the model structure.

Figure 5.3 Test set-up for free vibration.

Before attaching the resettable devices to the model structure, free vibration testing was carried out with a maximum 2.5 mm displacement at the top floor to ensure that the structure remained elastic. The experimental and analytical displacement time-histories at level 4 during the free vibration testing are compared in Figure 5.4. A very good agreement is observed between the experimental response and the response predicted by the two-dimensional computer model of the one-fifth scale structure that is described in Section 4.3.

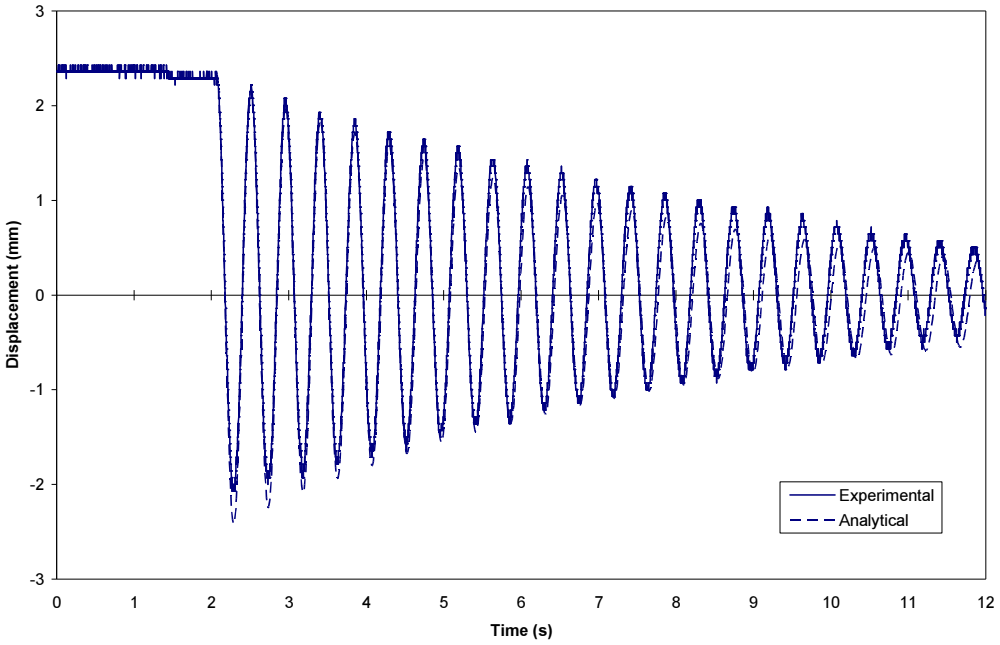

Figure 5.4 Comparison of displacement time-history for free vibration testing.

Fourier transforms of the recorded floor accelerations were utilised to determine the frequencies of the structure. The half-power or band-width method (Clough and Penzien 1993) was applied as the damping ratio of the *k*th mode was determined from the frequencies for which the response at the frequency of the *k*th mode is reduced by $1/\sqrt{2}$. The power spectrum of the acceleration recorded at level 4 of the one-fifth scale structure is shown in Figure 5.5.

The natural frequencies of free vibration were found to be 2.268 (2.231), 9.763 (9.611) and 25.447 Hz (26.274 Hz) with corresponding equivalent viscous damping ratios of 1.211 (1.210), 0.374 (0.305) and 0.182% (0.172%) for the first, second and third modes of vibration, respectively. Analytical results obtained with the computational model are given in parentheses. The analytical results compare very well to those derived from the analysis of the data captured during the free vibration testing of the model structure.

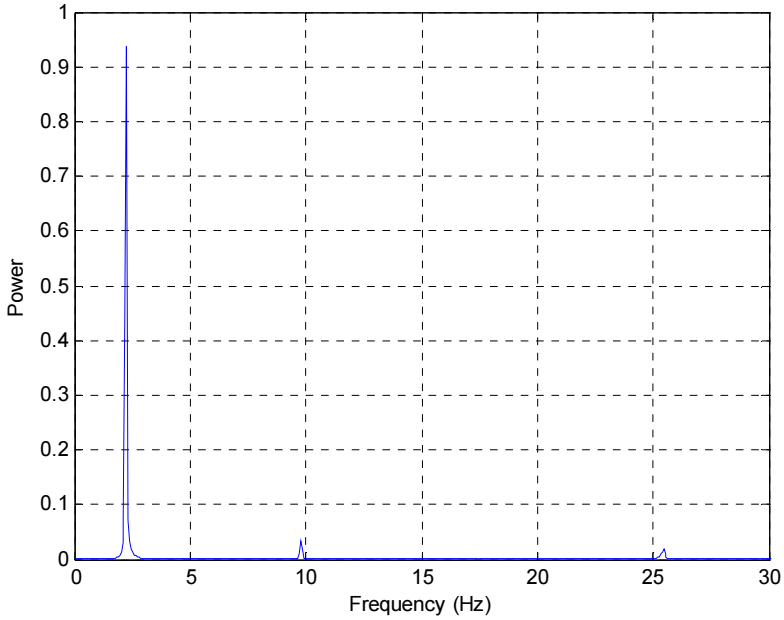

Figure 5.5 Power spectrum of the acceleration at level 4.

Free vibration testing was also performed on the model structure equipped with two resettable devices. The semi-active model structure was tested with the valves of each device closed. When the device valve is closed, the bracing system (device and steel tendon) serves as a stiffness element. The structure was pulled laterally by using a steel wire until a specific displacement at level 4 was reached. The steel wire was the cut and the structure oscillated freely.

The test structure was first pulled by up to 2.5 mm and then by up to 4 mm. It was not possible to clearly identify the dynamic properties of the test structure, as the response decays very quickly after the initial displacement. This can be seen in Figures 5.6a and b. However, it appears that the natural period ranges between 0.24 s and 0.28 s and the corresponding damping ratio between 9.61% and 17.71%. It can be inferred that closing the device valves adds a significant amount of stiffness to the structure. For the one-fifth scale structure, the bracing system is able to provide large resisting forces. Therefore, the bracing can be considered as a stiff bracing system that can be passively controlled.

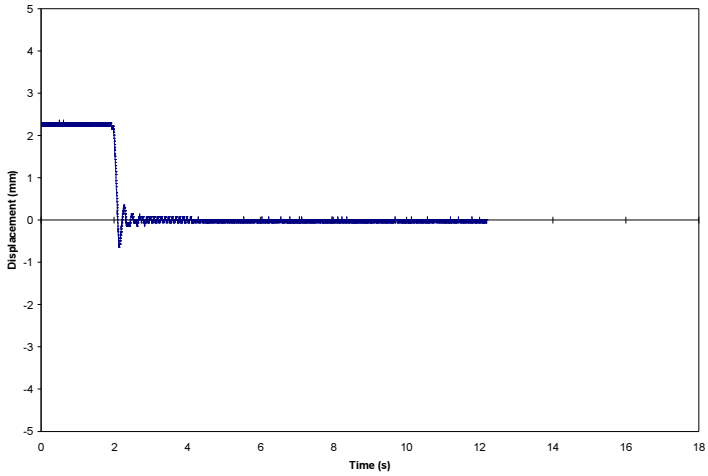

(a) 2.5 mm top displacement

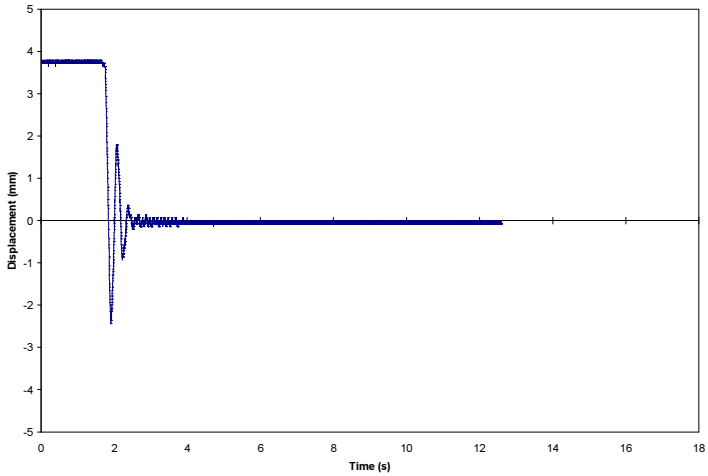

(b) 4 mm top displacement

Figure 5.6 Free vibration response with the device valves closed.

5.6 SEISMIC TESTING

This section describes an experimental investigation of the four-storey model structure subjected to seismic excitation and controlled by two semi-active resettable devices. Shaking table tests are performed on the model structure both with and without the resettable devices. The devices are installed in the lateral bracing of the moment-resisting steel frame structure. The mechanical properties of the devices are modified

according to a control algorithm that takes into account the measured response of the model structure. The one-fifth scale structure is subjected to four different simulated earthquake ground motions at various peak ground accelerations. Reductions in relative floor displacements, absolute floor accelerations, inter-storey drift ratios and total base shear are used to evaluate the seismic performance of the model structure.

5.6.1 Control Configurations

As described in Chapter 3, the independent control of the device valves enables semi-active re-shaping of the structural hysteretic behaviour by using different control laws. The control laws are based on the four quadrants defined by a sine-wave motion cycle and they are termed according to the quadrant of the force-displacement graph in which the device provides resisting forces. Although earthquake records are random signals and vary significantly from the sine-wave responses studied in Chapter 3, the control implementation does not change. The relative displacement data across the device is utilised as the control law input. This is the only feedback measurement required to determine the displacement and velocity needed to define the current quadrant of the displacement-velocity graph and consequently the valve position required.

The one-fifth scale structure was tested on the shaking table using the following control configurations for the semi-active resettable tendon which includes the device and steel tendon:

1. **Valves closed**. When the valves of the device are closed, the resettable tendon serves as a stiff bracing system in which the stiffness is provided by the bulk modulus of the air in the device cylinder and the steel tendon. Closing the device valves corresponds to adding stiffness to the system. This is termed the fail-safe mode because it is the state of the device that occurs if power is lost to the control system (Mulligan 2007, Chase et al. 2007).

2. **1-2-3-4 control law**. This control law provides resisting forces in all four quadrants of the force-displacement curve, as shown in Figure 3.2. The control law defines the behaviour of the resettable device that releases the stored energy at the maximum piston displacement and resists all motion of the piston out of the maximum displacement.

3. **1-3 control law**. As shown in Figure 3.3, the 1-3 control law provides resisting forces only in the first and third quadrants of the force-displacement graph. For this control law, the resettable device resists the motion only away from the equilibrium position of the piston.

4. **2-4 control law**. The 2-4 control law provides resisting forces only in the second and fourth quadrants of the force-displacement plot, as shown in Figure 3.4. This control law describes the behaviour of the device that resists the motion only towards the equilibrium position of the piston.

5. **1-2-3-4 to 2-4 control law**. Switching between two control laws depending on the input ground motion and resulting structural dynamics can offer the benefits of both of these control laws. For this particular case, the control configuration is switched from the 1-2-3-4 to the 2-4 control law when the relative displacement across the resettable device exceeds 7 mm in both directions. This value represents a large displacement for the model structure when subjected to strong seismic excitations. For a large earthquake record, the initial large structural motion is resisted with the 1-2-3-4 control law while the remainder of the record is resisted with the 2-4 control law (Mulligan 2007).

   It should be noted that the 1-2-3-4 to 2-4 control law was implemented only later on during the shake table testing of the model structure. Therefore, no investigations on this control law have been reported in previous chapters of the thesis.

6. **Valves open**. When the valves of the device are open, the piston is free to move and the air in the cylinder provides only a small amount of damping due to leakage and

heat loss. The friction between the moving parts inside the cylinder also contributes to the damping provided by the device. Opening the device valves corresponds to removing stiffness and there is no potential energy stored in the device. It is assumed that the orifice size of the valves is large enough so that no force is generated from the device as the piston moves. By opening the valves of the device, the resettable tendon serves as a flexible bracing system.

7. **Uncontrolled case**. The uncontrolled case describes the seismic response of the test structure without any resettable tendons attached. For this case, very few earthquake intensities were chosen in order to prevent inelastic deformations in the model structure during the seismic testing (Franco-Anaya et al. 2007a, 2007b).

As mentioned earlier, the independent control of the pressure and energy dissipation on each side of the piston for each portion of the response motion allows greater flexibility in designing the overall device behaviour. Since each device valve can be operated independently, the device design also enables a much broader range of control laws with significant potential for structural engineering applications.

5.6.2 Earthquake Ground Motions

The selection of the earthquake ground motions and the load and deformation effects associated are an essential part in the design of earthquake-resistant structures. Hence, one of the most important steps in the seismic analysis and design of structures is the appropriate evaluation and selection of the design earthquakes. However, because of the highly random nature of the parameters involved, ground motions for which the design is to be carried out are inherently probabilistic. Furthermore, the design of structures must be based on realistic earthquake loading for a satisfactory performance under the expected seismic conditions (Pekcan 1998).

Earthquake loading for design earthquakes can be established by studying seismological and geophysical data recorded at a specific active region. Parameters considered in such

process include: the earthquake size in terms of its peak ground acceleration (PGA), peak ground velocity (PGV) and peak ground displacement (PGD); the type of faulting; the distance from the fault; the duration of shaking; and the soil conditions. Earthquake records contain random combinations of all of these parameters and therefore must be studied carefully.

In recent years, much attention has been given to the near-source ground motions and their effects on the seismic response of various types of structures. Near-source ground motions have a large long-period pulse, because of the effect of the first wave passage of the rupture propagation coupled with other rupture propagation (directivity) effects, which is generally observed at locations near to the fault in the direction normal to the fault. Large displacement responses are observed in the long-period range of response spectra due to such long-period pulses. However, similar observations are still valid at soft-soil sites for a large distant earthquake because of the amplification of long-period harmonics. Therefore, since the actual characteristics of the ground motions producing similar responses are different, they should be properly considered in the design.

It is important to note that current design methods may not be appropriate for sites adjacent to the active faults since such pulse-type ground motions cannot be represented adequately by design response spectra. The characteristics of near-source acceleration time-histories are greatly dependent on the point of rupture initiation and direction of rupture propagation. Furthermore, when response time-histories are selected for design of relatively flexible structures, pulse characteristics should be carefully studied in terms of PGA, PGV, PGD and the duration of the ground motion.

Near-source ground motions result in a sudden burst of energy into the structure which must be dissipated at once. This is usually characterised by one large yield excursion with a few reversals. It should be noted that this type of sudden absorption of energy cannot be achieved by most of the currently deployed energy dissipation devices. This is because these devices require at least one full response cycle in order to become fully effective. Moreover, inelastic behaviour is usually concentrated in the lower floors of a

building subjected to a long-period pulse, since the upper floors do not have enough time to respond because of the short duration of the pulse (Pekcan 1998).

In this research, four earthquake ground motions at a different intensity levels were used as input to the shaking table:

a. Imperial Valley, 18 May 1940 – El Centro north-south (NS) component
b. Kern County, 21 July 1952 – Taft S21W component
c. Northridge, 17 January 1994 – Sylmar County Hospital (Chan 9: 0 deg)
d. Kobe, 17 January 1995 – JMA Observatory N00E component.

The El Centro and Taft ground motions are historical earthquake records of vibratory nature, while the Sylmar and the Kobe earthquakes are recent earthquake records with pulse type characteristics. A total of 27 input ground motions were used to test the one-fifth scale structure. Tables 5.2 through 5.5 show peak values of ground acceleration, ground velocity and ground displacement for the input ground motions utilised during the seismic testing. The accelerograms and response spectra of the selected earthquake records can be found in Appendix C.

The amplitude of the earthquake records was scaled in order to excite the test structure with earthquake ground motions of different intensity levels. The records were scaled according to the pseudo spectral acceleration (PSA) of a single-degree-of-freedom (SDOF) system with a given natural period and damping ratio. The scale of the record was chosen such that the percentages for each of the four records had similar spectral response. For example, the value of the PSA for a SDOF system with natural period of 0.24 s and damping ratio of 7.5% is 0.0737g for the El Centro 10% record, 0.0749g for the Taft 20% record, 0.0747g for the Sylmar 5% record and 0.0699g for the Kobe 5% record, respectively.

Table 5.2 Peak values of the El Centro ground motion.

Ground Motion	PGA (g)	PGV (m/s)	PGD (m)	Remarks
El Centro 10%	0.0348	0.0335	0.0143	
El Centro 20%	0.0697	0.0671	0.0287	
El Centro 30%	0.1045	0.1006	0.0430	
El Centro 40%	0.1393	0.1342	0.0573	
El Centro 50%	0.1742	0.1677	0.0716	
El Centro 60%	0.2091	0.2014	0.0860	
El Centro 70%	0.2451	0.1584	0.1187	Modified
El Centro 80%	0.2800	0.1809	0.1356	Modified
El Centro 90%	0.3150	0.2036	0.1526	Modified
El Centro 100%	0.3500	0.2262	0.1696	Modified

Table 5.3 Peak values of the Taft ground motion.

Ground Motion	PGA (g)	PGV (m/s)	PGD (m)	Remarks
Taft 20%	0.0356	0.0280	0.0600	
Taft 40%	0.0712	0.0560	0.1201	
Taft 60%	0.1068	0.0840	0.1802	
Taft 80%	0.1424	0.1119	0.2401	

Table 5.4 Peak values of the Sylmar ground motion.

Ground Motion	PGA (g)	PGV (m/s)	PGD (m)	Remarks
Sylmar 5%	0.0399	0.0568	0.0123	
Sylmar 10%	0.0798	0.1135	0.0246	
Sylmar 15%	0.1196	0.1703	0.0369	
Sylmar 20%	0.1595	0.2271	0.0492	
Sylmar 25%	0.1369	0.0626	0.0608	Modified
Sylmar 30%	0.1643	0.0751	0.0730	Modified

Table 5.5 Peak values of the Kobe ground motion.

Ground Motion	PGA (g)	PGV (m/s)	PGD (m)	Remarks
Kobe 5%	0.0418	0.0458	0.0106	
Kobe 10%	0.0836	0.0916	0.0213	
Kobe 15%	0.1255	0.1374	0.0319	
Kobe 20%	0.1673	0.1833	0.0426	
Kobe 25%	0.2091	0.2291	0.0532	
Kobe 30%	0.1583	0.0738	0.0248	Modified
Kobe 35%	0.1847	0.0861	0.0290	Modified

The maximum velocity that the shaking table can achieve is 0.24 m/s before a saturation of the servo-valve occurs. This restricts the capability of the shaking table to accurately track the desired displacement input motion. Therefore, some of the earthquake records were modified to ensure that they could be tracked accurately by the control system of the shaking table. The approach adopted was to modify the acceleration record in order to obtain a similar peak ground acceleration (PGA) such that the velocity saturation was avoided. Displacement information for a given earthquake record was differentiated into velocity, which was then limited to the maximum allowable velocity magnitude. The new velocity profile was then integrated back into modified displacement input data (Chase et al. 2005b, Mulligan 2007).

The maximum travel displacement that the double-acting hydraulic actuator of the shaking table can deliver is approximately 130 mm, therefore, care was taken to avoid using earthquake records whose displacement would exceed this displacement limit. The ground motion characteristics and response spectra for the original and modified earthquake records are compared in Appendix C.

5.6.3 Interpretation of the Experimental Results

An assessment of the effectiveness of the semi-active resettable devices in reducing the seismic response is made by comparing the response of the model structure with and without devices for the same earthquake ground motion. In presenting the shaking table tests results major emphasis is given to the overall response of the model structure. Effects of adding the resettable devices to the structure are identified from the shaking table tests in terms of relative displacements, absolute accelerations, inter-storey drift ratios and total base shear which includes the contribution of the resettable tendon. Tables 5.6 through 5.9 summarise the maximum response of the model structure for all of the input ground motions. The results of the shaking table tests are also presented in graphical form in Appendix D. Comparisons of the experimental results across the different earthquake ground motions can be found in Mulligan (2007).

Table 5.6 Summary of the maximum response for the El Centro earthquake.

Ground Motion	Control Configuration	Relative Displacement (mm)				Absolute Acceleration (g)				Inter-Storey Drift Ratio (%)				Total Base Shear (kN)
		1st Fl.	2nd Fl.	3rd Fl.	4th Fl.	1st Fl.	2nd Fl.	3rd Fl.	4th Fl.	1st Fl.	2nd Fl.	3rd Fl.	4th Fl.	
El Centro 10%	Closed	0.533	0.681	0.854	1.199	0.115	0.125	0.063	0.142	0.089	0.057	0.079	0.120	2.412
	1-2-3-4	0.535	0.750	0.855	1.330	0.127	0.143	0.057	0.144	0.089	0.068	0.104	0.121	2.399
	2-4	0.568	0.818	1.062	1.339	0.124	0.134	0.058	0.157	0.095	0.064	0.089	0.130	2.353
	Open	0.567	0.780	1.033	1.553	0.125	0.126	0.055	0.142	0.094	0.072	0.089	0.134	2.303
	Uncontrolled	2.736	4.785	6.422	7.772	0.083	0.101	0.112	0.143	0.456	0.424	0.346	0.311	3.285
El Centro 20%	Closed	1.018	1.893	2.654	3.300	0.123	0.132	0.099	0.137	0.170	0.189	0.159	0.151	3.213
	1-2-3-4	1.092	1.919	2.485	2.900	0.178	0.202	0.102	0.210	0.182	0.181	0.145	0.174	3.481
	2-4	1.190	2.063	2.740	3.331	0.189	0.207	0.084	0.210	0.198	0.181	0.169	0.180	3.207
	Open	2.217	3.936	5.329	6.466	0.155	0.174	0.111	0.180	0.369	0.358	0.289	0.273	3.622
	Uncontrolled	5.455	9.959	13.829	17.266	0.170	0.212	0.186	0.278	0.909	0.908	0.774	0.694	5.922
El Centro 30%	Closed	1.935	3.405	4.655	5.915	0.187	0.203	0.175	0.231	0.323	0.301	0.257	0.259	5.342
	1-2-3-4	1.545	2.803	3.944	5.129	0.199	0.212	0.154	0.227	0.257	0.266	0.235	0.251	4.750
	2-4	2.089	3.813	5.355	6.820	0.235	0.251	0.139	0.278	0.348	0.359	0.323	0.302	4.164
	Open	3.827	6.927	9.378	11.453	0.185	0.201	0.173	0.217	0.638	0.620	0.497	0.449	5.544
	Uncontrolled	8.180	14.825	20.392	25.410	0.164	0.203	0.226	0.287	1.363	1.338	1.127	1.011	6.600
El Centro 40%	Closed	2.497	4.418	6.227	7.814	0.232	0.253	0.218	0.300	0.416	0.413	0.362	0.331	6.908
	1-2-3-4	2.192	3.919	5.266	6.883	0.248	0.274	0.217	0.312	0.365	0.371	0.312	0.338	6.884
	2-4	3.170	5.570	7.535	9.383	0.203	0.223	0.193	0.259	0.528	0.487	0.438	0.397	6.126
	Open	5.404	9.720	13.182	16.229	0.193	0.211	0.225	0.274	0.901	0.870	0.713	0.615	7.019
	Uncontrolled	10.389	19.161	26.688	33.561	0.212	0.252	0.241	0.353	1.731	1.761	1.522	1.382	7.474
El Centro 50%	Closed	3.267	5.925	8.012	10.071	0.248	0.298	0.302	0.366	0.544	0.539	0.452	0.432	9.793
	1-2-3-4	2.983	5.394	7.408	9.426	0.214	0.248	0.285	0.358	0.497	0.489	0.410	0.418	9.136
	2-4	4.175	7.376	10.092	12.512	0.226	0.250	0.236	0.307	0.696	0.666	0.569	0.510	7.660
	Open	6.923	12.656	17.381	21.378	0.237	0.278	0.255	0.314	1.154	1.154	0.959	0.845	7.971

Table 5.6 (Continued).

Ground Motion	Control Configuration	Relative Displacement (mm)				Absolute Acceleration (g)				Inter-Storey Drift Ratio (%)				Total Base Shear (kN)
		1st Fl.	2nd Fl.	3rd Fl.	4th Fl.	1st Fl.	2nd Fl.	3rd Fl.	4th Fl.	1st Fl.	2nd Fl.	3rd Fl.	4th Fl.	
El Centro 60%	Closed	4.364	7.794	10.656	13.400	0.316	0.347	0.360	0.495	0.727	0.693	0.572	0.563	11.403
	1-2-3-4	3.618	6.343	8.595	10.898	0.305	0.330	0.351	0.431	0.603	0.556	0.507	0.494	10.895
	2-4	4.513	8.087	11.011	13.861	0.254	0.283	0.265	0.336	0.752	0.731	0.636	0.599	9.420
	Open	8.112	14.829	20.636	25.806	0.220	0.280	0.307	0.358	1.352	1.355	1.181	1.073	9.327
El Centro 70% Modified	Closed	4.915	8.919	12.361	15.937	0.341	0.334	0.429	0.625	0.819	0.809	0.697	0.744	12.874
	1-2-3-4	4.158	7.559	10.612	13.931	0.333	0.359	0.369	0.609	0.693	0.687	0.625	0.679	11.171
	2-4	5.821	10.261	13.878	17.202	0.332	0.340	0.284	0.362	0.970	0.896	0.746	0.695	10.619
	1-3	5.202	9.147	12.232	15.301	0.342	0.372	0.400	0.518	0.867	0.796	0.674	0.694	12.788
	1-2-3-4 to 2-4	4.550	8.226	11.430	14.827	0.302	0.298	0.373	0.572	0.758	0.737	0.667	0.694	11.032
	Open	7.773	14.191	19.781	24.925	0.310	0.298	0.359	0.529	1.296	1.285	1.118	1.055	11.582
El Centro 80% Modified	Closed	5.594	10.177	14.314	18.422	0.315	0.341	0.455	0.676	0.932	0.930	0.835	0.836	13.644
	1-2-3-4	4.516	8.205	11.561	14.983	0.327	0.425	0.452	0.665	0.753	0.739	0.704	0.749	14.254
	2-4	6.035	10.847	14.827	18.482	0.368	0.372	0.340	0.368	1.006	0.965	0.811	0.749	12.577
	1-3	5.327	9.469	12.665	15.785	0.330	0.374	0.389	0.482	0.888	0.835	0.705	0.681	12.324
	1-2-3-4 to 2-4	4.769	8.770	12.223	15.532	0.320	0.327	0.392	0.518	0.795	0.811	0.705	0.724	12.009
	Open	9.513	17.320	24.260	30.660	0.341	0.366	0.343	0.462	1.586	1.576	1.390	1.290	11.217
El Centro 90% Modified	Closed	6.239	11.316	15.838	20.260	0.364	0.375	0.509	0.701	1.040	1.024	0.911	0.906	15.636
	1-2-3-4	5.594	9.954	13.760	17.609	0.370	0.405	0.511	0.737	0.932	0.879	0.796	0.826	15.934
	2-4	7.568	13.674	18.948	23.563	0.413	0.400	0.350	0.446	1.261	1.232	1.069	0.936	13.031
El Centro 100% Modified	Closed	7.509	13.710	19.017	24.325	0.390	0.412	0.524	0.700	1.251	1.248	1.078	1.069	15.971
	1-2-3-4	6.371	11.361	15.749	20.234	0.357	0.438	0.556	0.748	1.062	1.017	0.913	0.904	16.932
	2-4	11.204	20.606	29.018	36.670	0.362	0.397	0.436	0.668	1.867	1.889	1.691	1.543	14.016

Table 5.7 Summary of the maximum response for the Taft earthquake.

Ground Motion	Control Configuration	Relative Displacement (mm)				Absolute Acceleration (g)				Inter-Storey Drift Ratio (%)				Total Base Shear (kN)
		1st Fl.	2nd Fl.	3rd Fl.	4th Fl.	1st Fl.	2nd Fl.	3rd Fl.	4th Fl.	1st Fl.	2nd Fl.	3rd Fl.	4th Fl.	
Taft 20%	Closed	0.598	0.921	1.161	1.601	0.071	0.086	0.058	0.098	0.100	0.078	0.079	0.103	1.893
	1-2-3-4	0.604	1.027	1.173	1.530	0.086	0.103	0.067	0.116	0.101	0.085	0.083	0.104	2.035
	2-4	0.633	0.958	1.197	1.531	0.142	0.149	0.055	0.162	0.106	0.079	0.086	0.123	2.141
	Open	0.747	1.133	1.445	1.744	0.104	0.119	0.056	0.130	0.124	0.091	0.100	0.108	2.060
	Uncontrolled	3.213	5.801	7.896	9.547	0.096	0.123	0.129	0.182	0.535	0.525	0.419	0.373	3.867
Taft 40%	Closed	1.316	2.333	3.125	3.789	0.150	0.172	0.118	0.177	0.219	0.211	0.180	0.183	3.740
	1-2-3-4	1.422	2.412	3.201	3.930	0.179	0.200	0.123	0.210	0.237	0.212	0.180	0.224	4.048
	2-4	1.315	2.258	3.120	3.611	0.150	0.157	0.096	0.172	0.219	0.203	0.193	0.196	3.178
	Open	1.969	3.510	4.751	5.964	0.179	0.186	0.118	0.209	0.328	0.324	0.274	0.284	3.931
	Uncontrolled	5.148	9.304	12.702	15.664	0.109	0.151	0.176	0.230	0.858	0.845	0.694	0.607	5.131
Taft 60%	Closed	3.016	5.378	7.357	9.224	0.182	0.246	0.273	0.305	0.503	0.480	0.402	0.415	8.360
	1-2-3-4	2.307	4.171	5.612	7.006	0.181	0.235	0.230	0.296	0.385	0.373	0.323	0.328	7.322
	2-4	2.096	3.591	4.817	6.228	0.220	0.240	0.144	0.250	0.349	0.325	0.308	0.310	4.773
	Open	3.242	5.771	7.840	9.697	0.166	0.183	0.149	0.205	0.540	0.514	0.433	0.399	4.781
	Uncontrolled	6.018	10.963	15.095	18.795	0.126	0.178	0.193	0.269	1.003	0.991	0.827	0.748	5.826
Taft 80%	Closed	4.292	7.781	10.842	13.728	0.225	0.295	0.364	0.503	0.715	0.705	0.625	0.612	10.981
	1-2-3-4	3.472	6.397	8.882	11.438	0.213	0.273	0.308	0.420	0.579	0.592	0.518	0.546	9.480
	2-4	2.662	4.770	6.678	8.576	0.174	0.205	0.157	0.298	0.444	0.440	0.420	0.394	5.329
	Open	4.551	7.888	10.468	13.078	0.202	0.233	0.195	0.304	0.759	0.683	0.590	0.561	6.443

Table 5.8 Summary of the maximum response for the Sylmar earthquake.

Ground Motion	Control Configuration	Relative Displacement (mm)				Absolute Acceleration (g)				Inter-Storey Drift Ratio (%)				Total Base Shear (kN)
		1st Fl.	2nd Fl.	3rd Fl.	4th Fl.	1st Fl.	2nd Fl.	3rd Fl.	4th Fl.	1st Fl.	2nd Fl.	3rd Fl.	4th Fl.	
Sylmar 5%	Closed	0.642	1.071	1.255	1.718	0.125	0.140	0.066	0.152	0.107	0.100	0.101	0.135	2.483
	1-2-3-4	0.671	1.170	1.463	1.886	0.092	0.116	0.063	0.131	0.112	0.109	0.108	0.121	2.166
	2-4	0.622	1.099	1.590	2.033	0.071	0.080	0.051	0.108	0.104	0.116	0.107	0.118	1.664
	Open	1.057	2.005	2.726	3.442	0.086	0.086	0.063	0.111	0.176	0.197	0.167	0.166	2.217
	Uncontrolled	3.329	6.010	8.317	10.385	0.117	0.148	0.136	0.223	0.555	0.558	0.475	0.442	4.205
Sylmar 10%	Closed	2.041	3.478	4.516	5.436	0.169	0.206	0.189	0.244	0.340	0.302	0.242	0.268	6.113
	1-2-3-4	1.578	2.840	3.734	4.720	0.147	0.168	0.160	0.212	0.263	0.260	0.223	0.239	5.284
	2-4	1.764	3.075	4.377	5.739	0.165	0.175	0.109	0.232	0.294	0.301	0.283	0.287	3.942
	Open	2.997	5.455	7.543	9.531	0.166	0.184	0.138	0.257	0.500	0.519	0.434	0.433	4.568
	Uncontrolled	5.604	10.121	13.899	17.267	0.086	0.149	0.190	0.267	0.934	0.910	0.770	0.687	5.395
Sylmar 15%	Closed	2.903	5.276	7.009	8.796	0.193	0.261	0.280	0.327	0.484	0.482	0.361	0.378	8.973
	1-2-3-4	2.548	4.497	6.050	7.724	0.182	0.220	0.261	0.333	0.425	0.404	0.339	0.349	8.215
	2-4	2.843	5.234	7.271	9.108	0.178	0.196	0.164	0.247	0.474	0.503	0.414	0.396	5.767
	Open	4.513	8.199	11.341	14.264	0.158	0.174	0.192	0.273	0.752	0.758	0.636	0.598	5.924
Sylmar 20%	Closed	3.769	6.617	8.723	11.016	0.278	0.338	0.355	0.437	0.628	0.577	0.449	0.508	11.529
	1-2-3-4	3.200	5.660	7.653	9.564	0.287	0.346	0.331	0.394	0.533	0.499	0.447	0.413	11.122
	2-4	4.213	7.607	10.295	12.557	0.210	0.216	0.209	0.279	0.702	0.686	0.538	0.527	7.140
	Open	5.894	10.499	14.191	17.720	0.179	0.240	0.248	0.298	0.982	0.928	0.771	0.732	7.535
Sylmar 25% Modified	Closed	4.848	8.918	12.378	15.997	0.340	0.449	0.416	0.586	0.808	0.815	0.714	0.747	13.623
	1-2-3-4	5.342	9.700	13.513	17.426	0.290	0.383	0.364	0.551	0.890	0.885	0.779	0.791	11.730
	2-4	2.994	5.612	7.833	9.712	0.221	0.259	0.225	0.372	0.499	0.524	0.466	0.426	6.958
Sylmar 30% Modified	Closed	5.456	9.903	13.725	17.500	0.311	0.420	0.454	0.616	0.909	0.892	0.772	0.770	13.863
	1-2-3-4	6.054	11.105	15.466	19.786	0.278	0.389	0.458	0.642	1.009	1.019	0.873	0.872	13.518
	2-4	3.901	7.063	9.707	11.870	0.234	0.270	0.235	0.417	0.650	0.639	0.550	0.496	7.212
	1-3	5.252	9.474	13.505	17.520	0.329	0.433	0.401	0.647	0.875	0.868	0.826	0.828	12.771
	1-2-3-4 to 2-4	5.638	10.099	13.800	17.500	0.330	0.395	0.385	0.634	0.940	0.906	0.772	0.799	11.518

Table 5.9 Summary of the maximum response for the Kobe earthquake.

Ground Motion	Control Configuration	Relative Displacement (mm)				Absolute Acceleration (g)				Inter-Storey Drift Ratio (%)				Total Base Shear (kN)
		1st Fl.	2nd Fl.	3rd Fl.	4th Fl.	1st Fl.	2nd Fl.	3rd Fl.	4th Fl.	1st Fl.	2nd Fl.	3rd Fl.	4th Fl.	
Kobe 5%	Closed	0.634	1.018	1.080	1.621	0.094	0.110	0.059	0.134	0.106	0.084	0.103	0.127	2.170
	1-2-3-4	0.722	1.118	1.332	1.680	0.111	0.114	0.060	0.145	0.120	0.089	0.098	0.123	2.334
	2-4	0.763	1.234	1.427	1.842	0.112	0.127	0.058	0.131	0.127	0.095	0.100	0.139	2.356
	Open	0.919	1.551	1.826	2.335	0.127	0.135	0.070	0.142	0.153	0.134	0.126	0.151	2.483
	Uncontrolled	4.054	7.127	9.607	11.802	0.135	0.177	0.155	0.237	0.676	0.629	0.536	0.474	4.975
Kobe 10%	Closed	1.798	3.298	4.567	5.799	0.161	0.178	0.170	0.275	0.300	0.308	0.268	0.275	5.040
	1-2-3-4	1.616	3.020	4.248	5.370	0.163	0.180	0.161	0.215	0.269	0.288	0.246	0.232	4.984
	2-4	2.225	3.895	5.389	6.642	0.166	0.179	0.119	0.188	0.371	0.353	0.306	0.285	4.088
	Open	3.108	5.463	7.271	8.857	0.143	0.175	0.145	0.201	0.518	0.492	0.392	0.372	4.826
	Uncontrolled	6.367	11.445	15.727	19.454	0.146	0.174	0.189	0.260	1.061	1.028	0.865	0.782	5.622
Kobe 15%	Closed	3.347	6.078	8.233	10.270	0.191	0.271	0.321	0.411	0.558	0.547	0.438	0.450	9.949
	1-2-3-4	3.276	5.904	7.805	9.696	0.253	0.328	0.312	0.439	0.546	0.533	0.424	0.457	9.921
	2-4	3.870	6.854	9.280	11.254	0.230	0.238	0.180	0.310	0.645	0.618	0.519	0.483	6.187
	Open	5.466	9.669	12.977	15.957	0.218	0.242	0.210	0.289	0.911	0.856	0.679	0.628	6.906
Kobe 20%	Closed	4.722	8.434	11.510	14.526	0.271	0.390	0.456	0.561	0.787	0.750	0.622	0.625	14.137
	1-2-3-4	4.724	8.401	11.435	14.311	0.291	0.407	0.443	0.539	0.787	0.743	0.616	0.618	13.889
	2-4	5.621	9.967	13.394	16.350	0.251	0.267	0.228	0.393	0.937	0.889	0.703	0.631	7.469
	Open	7.304	13.323	18.366	22.713	0.265	0.281	0.244	0.326	1.217	1.206	1.009	0.914	8.292
Kobe 25%	Closed	5.955	10.797	14.976	19.290	0.294	0.431	0.548	0.677	0.992	0.982	0.849	0.869	16.724
	1-2-3-4	5.742	10.293	14.182	17.998	0.280	0.407	0.522	0.669	0.957	0.911	0.778	0.784	16.190
	2-4	7.002	12.740	17.527	21.672	0.244	0.290	0.308	0.460	1.167	1.155	0.970	0.856	9.340
	Open	8.603	15.715	21.783	27.807	0.296	0.389	0.438	0.585	1.434	1.437	1.251	1.212	14.653
Kobe 30% Modified	Closed	7.049	12.784	17.896	23.011	0.309	0.383	0.551	0.763	1.175	1.154	1.029	1.030	16.258
	1-2-3-4	6.049	10.966	15.434	20.005	0.347	0.435	0.550	0.815	1.008	0.990	0.907	0.935	16.395
	2-4	6.442	11.607	16.146	20.792	0.331	0.423	0.539	0.811	1.074	1.040	0.921	0.957	16.013
	1-3	6.957	12.592	17.301	21.801	0.284	0.421	0.501	0.655	1.160	1.128	0.950	0.914	15.174
	1-2-3-4 to 2-4	6.886	12.555	17.512	22.014	0.317	0.338	0.418	0.603	1.148	1.141	1.000	0.951	13.139
Kobe 35% Modified	Closed	7.653	14.058	19.885	25.657	0.354	0.446	0.580	0.807	1.276	1.281	1.166	1.175	17.267
	1-2-3-4	7.217	13.187	18.557	24.149	0.409	0.479	0.605	0.875	1.203	1.202	1.080	1.132	18.118
	2-4	6.776	12.341	17.192	21.698	0.334	0.323	0.354	0.605	1.129	1.128	0.982	0.922	11.068

The results of the shaking table tests show that the effect of the 1-2-3-4 and 2-4 control laws is almost negligible for earthquake ground motions of low intensity. The primary source of energy dissipation appears to be through friction between the moving parts of the device, mainly the piston rings and the internal wall of the cylinder. The friction force needs to be overcome before the piston of the device can be displaced. Once the friction force is overcome, the effect of the different control laws on the reduction of the seismic response becomes apparent.

In general, the seismic response of the one-fifth scale structure is significantly reduced by the 1-2-3-4 control law. The 1-2-3-4 control law shows significant reductions in relative floor displacements and inter-storey drift ratios compared to the uncontrolled case for a given earthquake record (Franco-Anaya et al. 2007a, 2007b). The response reductions achieved by the 1-2-3-4 control law for selected earthquake records are now examined and compared to the uncontrolled case. The level of intensity of the selected earthquakes was aimed to prevent inelastic deformations in the uncontrolled structure during the seismic testing:

1. For the El Centro 40% earthquake record (0.1393g): A reduction of up to 79% in the maximum relative displacement at the fourth floor is observed. A 12% reduction in the maximum absolute acceleration at the fourth floor is achieved. The maximum inter-storey drift ratio at the second floor is also reduced by up to 79%. The maximum total base shear is reduced by up to 8%.

2. For the Taft 40% earthquake record (0.0712g): The maximum recorded relative displacement at the fourth floor is reduced by up to 75%. A 9% reduction in the maximum absolute acceleration at the fourth floor is observed. The maximum inter-storey drift ratio at the first floor is reduced by up to 72%. A 21% reduction in the maximum total base shear is achieved.

3. For the Sylmar 10% earthquake record (0.0798g): A reduction of up to 73% in the maximum relative displacement at the fourth floor is achieved. The maximum measured absolute acceleration at the fourth floor is reduced by up to 21%. A 72%

reduction in the maximum inter-storey drift ratio at the first floor is observed. The maximum total base shear is reduced by up to 2%.

4. For the Kobe 10% earthquake record (0.0836g): The maximum relative displacement at the fourth floor is reduced by up to 72%. A 17% reduction in the maximum absolute acceleration at the fourth floor is observed. The maximum inter-storey drift ratio at the first floor is reduced by up to 75%. An 11% reduction in the maximum total base shear is achieved.

Although no significant reduction in absolute floor accelerations and total base shear is achieved by the 1-2-3-4 control law, the reductions in relative floor displacements and inter-storey drift ratios achieved by the control law are still significant. It must be noted that the contribution of the device friction to these response reductions is relevant due to the low intensity level of the selected earthquake records. During the seismic testing, the friction of the device was clearly present in the shake table tests whose excitation level was very low.

The reductions in seismic response achieved by the 1-2-3-4 control law are comparable to those afforded by the stiff bracing system. However, it should be noted that the stiff bracing system increases the absolute floor accelerations and base shear demand in comparison to the 1-2-3-4 control law case. Therefore, the 1-2-3-4 control law should be preferred over the stiff bracing system in applications where a reduction of the floor displacements is necessary to minimise structural damage. As described before, the device with the valves closed attached to the steel tendon represents the stiff bracing system or fail-safe mode of the resettable device.

The 2-4 control law significantly reduces the absolute floor accelerations and the total base shear compared to the other control laws which typically increase the base shear demand. This result is particularly important for retrofit applications where the foundation may not have sufficient strength to satisfy the increase in structural demand (Mulligan 2007, Chase et al. 2007). In addition, the reduction in relative floor displacements achieved by the 2-4 control law exceeds the reduction achieved by the

flexible bracing system, in which the device with the valves open is attached to the steel tendon.

Although the 1-3 control law was tested for very few earthquake records, the response reductions delivered by the 1-3 control law are similar to those achieved by the valves closed case for ground motions of high excitation level. Unlike the 2-4 control law, the 1-3 control law increases the absolute floor accelerations as well as the total base shear of the structure.

The results of the shaking table tests show that the 1-2-3-4 control law greatly reduces the maximum relative floor displacements and that the 2-4 control laws significantly reduces the maximum total base shear of the one-fifth scale structure. The switching control law, referred to as the 1-2-3-4 to 2-4 control law, combines the benefits of these two control laws. For a given input ground motion, the initial large structural motion is resisted with the 1-2-3-4 control law, that reduces the maximum floor displacement effectively, while the remainder of the ground motion is resisted with the 2-4 control law, that reduces the maximum total base shear.

The response reductions achieved by the 1-2-3-4 to 2-4 control law are comparable to those delivered by the 1-2-3-4 control law, but without increasing the floor accelerations and base shear demand significantly. The switching control law was tested for the same few earthquake records utilised to investigate the performance of the 1-3 control law. However, the switching control law proved to be very effective in reducing the seismic response by combining the benefits of the two control laws over the entire length of the earthquake records studied. This outcome further emphasises the ability of the resettable device to manipulate resisting forces depending on structural demands (Mulligan 2007).

Overall, the seismic response of the one-fifth scale structure is significantly reduced by the addition of the semi-active resettable tendon. All control laws show reductions in maximum floor displacements and inter-storey drift ratios compared to the uncontrolled case for a given earthquake ground motion. The 1-2-3-4 control law and the valves closed case have a similar performance with the greatest reductions in the seismic

response. The 1-2-3-4 control law is more effective than the 1-3 and 2-4 control laws in reducing the seismic response. This result is expected as the 1-3 and the 2-4 control laws only operate over two quadrants, whereas the 1-2-3-4 control law operates over all four quadrants of the force-displacement curve. The 1-3 and 2-4 control laws store and dissipate less seismic energy, because these laws provide resisting forces for a smaller percentage of each motion cycle and therefore have shorter active strokes. The 2-4 control law shows significant reductions in both absolute floor accelerations and total base shear. The 1-2-3-4 to 2-4 control law gives comparable results to the reductions achieved by the 1-2-3-4 control law. Finally, the valves open case is advantageous over the uncontrolled case due to the resisting forces provided by the flexible bracing system and the friction in the devices.

5.7 SUMMARY

This chapter has described a series of shaking table tests performed on a four-storey model structure to assess the effectiveness of semi-active resettable devices for seismic response reduction. Two semi-active resettable devices were installed as part of the lateral bracing of the model structure to reduce the structural response. The resettable devices modified the stiffness of the structure by following a control algorithm that took into account the measured response of the model structure and the deformations of the devices. Four earthquake records at different levels of intensity were used to investigate the effect of the resettable devices on the seismic response. Different control laws were used to manipulate the hysteretic behaviour of the resettable devices.

The results of the shaking table tests showed that the addition of the resettable tendon improves the seismic performance of the model structure significantly. The 1-2-3-4 control law and the valves closed case achieved the greatest reduction in maximum floor displacements and inter-storey drift ratios. However, they increased the maximum floor accelerations and the total base shear demand, especially the valves closed case. The response reduction achieved by the 1-3 control law was comparable to that provided by the valves closed case for ground motions of high intensity level.

The 2-4 control law was very efficient at reducing the maximum floor accelerations and the total base shear. This result is of particular interest for retrofit of existing buildings where the strength of the foundation is usually limited. The 1-2-3-4 to 2-4 control law showed comparable results to the best performance achieved by the 1-2-3-4 control law. This switching control law further confirms the capability of the resettable devices to manipulate hysteretic behaviour and to adapt to changing structural demands.

The results of the seismic testing confirm that the resettable devices are effective in reducing the structural response over a wide range of earthquake excitations and demonstrate the significant potential of these devices for the seismic protection of civil engineering structures.

Chapter 6
ANALYTICAL PREDICTIONS OF THE SHAKE TABLE TEST RESULTS

6.1 INTRODUCTION

Analytical predictions are important in the study of the behaviour of structures under severe earthquake ground motions since such large motions could cause catastrophic damage to the structure. Numerical models are essential to understand the nonlinear response of energy dissipation devices and to predict the overall structural response. It is equally important to model the behaviour of these devices in order to establish design guidelines and perform comparative studies. This chapter describes the development of a numerical model to predict the behaviour of the model structure equipped with two resettable tendons during the seismic testing. Assumptions adopted for the analytical modelling of the semi-active resettable tendon are described. It is shown that the analytical simulations can reproduce the experimentally observed behaviour of the model structure closely. Analytical predictions of the experimental device response and the seismic response contribution of the steel tendon as part of a passive tendon system are also presented.

6.2 NUMERICAL MODEL OF THE RESETTABLE TENDON

A numerical model was developed for use in the RUAUMOKO computer program to simulate the behaviour of the resettable tendon used during the shaking table tests. The analytical model of the resettable tendon is shown schematically in Figure 6.1. The model has three main components. All components are modelled as only carrying forces along the axis of the members. The first component simulates the resettable device, the second component represents the steel tendon and the third component models the steel restraint element. Each of the nodes of the model has three degrees of freedom. All of

the degrees of freedom of the nodes A and D are restrained for fully fixed boundary condition. The horizontal and vertical displacements of the node B are unrestrained however the rotation of the node is restrained. The three degrees of freedom of node C are unrestrained.

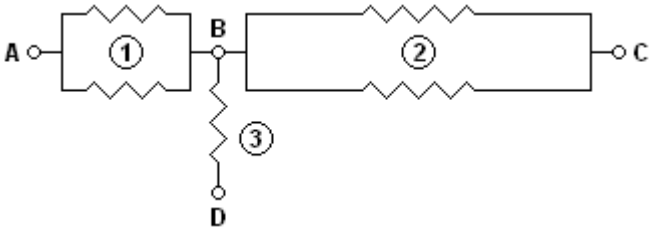

Figure 6.1 Analytical model of the resettable tendon.

6.2.1 Analytical Modelling of the Resettable Device

The semi-active resettable device was modelled by utilising two mechanical springs in parallel. One spring models the hysteretic behaviour of the device and the other spring simulates the friction of the device. The spring member available in the RUAUMOKO program and shown in Figure 4.15 is used to represent the resettable device. The spring member follows the 1-2-3-4, 1-3 and 2-4 control laws shown in Figures 3.2, 3.3 and 3.4, respectively.

As described in Chapter 3, the force developed by the device depends on the pressure of the active chamber and the change in the chamber volume depends on the displacement of the device piston (x). For a change in the volume of the chamber, the resisting force can be calculated by using Equations 3.1 and 3.2 as follows

$$p_2 = p_1\left(\frac{V_1}{V_2}\right)^{\gamma} \tag{6.1}$$

with $p_1 = p_2 = p_0$

$$F(x) = sign(\dot{x})\,p_0 A\left[\left(\frac{V_1}{V_2}\right)^{\gamma} - 1\right] \tag{6.2}$$

where p_1 and V_1 are the pressure and volume of the chamber before piston displacement, p_2 and V_2 are the pressures and volume of the chamber after piston displacement, p_0 is the initial pressure (atmospheric), A is the piston area and $\dot{x}$ is the velocity of the device piston.

For the 1-3 control law, the device force given by Equation (6.2) is equal to zero when the displacement and velocity have opposite signs. For the 2-4 control law, the force is equal to zero when the displacement and velocity have the same signs. For all control laws, the device force is set to zero on any change of direction of the displacement. A stiffness of 750 kN/m and a saturation force of 7.295 kN were utilised to model the hysteretic behaviour of the device. These values were obtained by tuning the model according to the experimental results. The following input data based on actual values of the device and working fluid (air) was utilised in the computer analyses:

a. $p_0 = 100$ kN/m^2
b. $\gamma = 1.4$
c. $A = 0.03148$ m^2
d. $L_0 = 18$ mm.

A second spring member is utilised to simulate the friction of the device. The spring member follows the elasto-plastic hysteresis rule shown in Figure 6.2. The elasto-plastic spring has a stiffness of 1000 kN/m obtained by fine tuning of the model. A friction force of 430 N based on experimental results (Mulligan 2006) was used in the analyses.

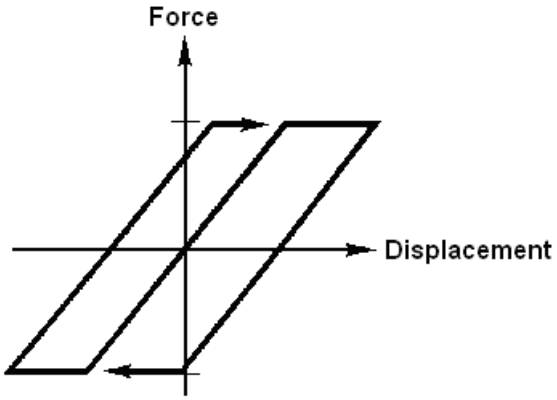

Figure 6.2 Elasto-plastic hysteresis.

The analytical model of the resettable device assumes an ideal behaviour of the device response. This includes the assumptions of instantaneous energy release and exactly symmetrical behaviour. Instantaneous energy release indicates that the response force returns to zero immediately after the device valve is opened. Symmetrical behaviour requires that the centre position of the piston is assigned perfectly.

6.2.2 Analytical Modelling of the Steel Tendon

During the seismic testing, the resettable device was attached to the lower end of a steel tendon. The steel tendon was placed along the two bays and was connected to the model structure at the third floor to transfer the control forces. Two mechanical springs in parallel are used to model the steel tendon. The assemblage tolerances and slackness of the tendon are accounted for by using one of the springs and the second spring is used to stabilise the system. Two spring members are used to model the mechanical springs.

The assemblage tolerances and the slackness of the tendon are modelled by using one of the spring members with the bi-linear with slackness hysteresis shown in Figure 6.3. This hysteresis is used to represent diagonal braced systems where yield in one direction may stretch the members leading to slackness in the bracing system. The hysteresis allows for either yield in compression in a cross-braced system or for simple elastic buckling in compression which would be more appropriate in a single-braced member (Carr 2006).

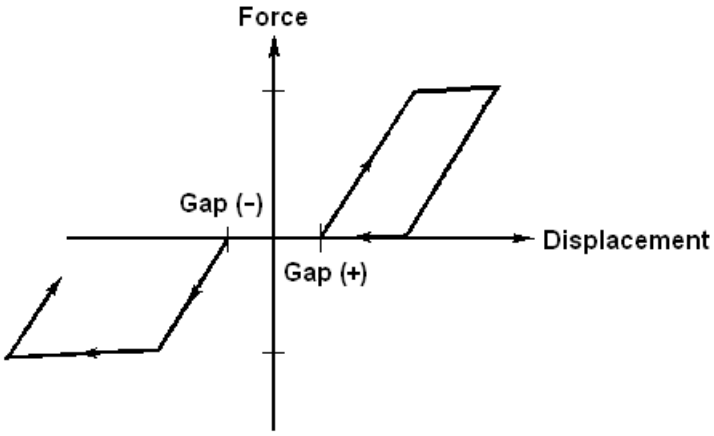

Figure 6.3 Bi-linear with slackness hysteresis.

To find the appropriate slackness value (gap length) of the steel tendon was a difficult task. Computer simulations showed that any small variation of the slackness value had a significant impact on the seismic response of the model structure. Besides, the dynamic properties of the structure were affected dramatically. It was observed that a variation of 0.01mm in the slackness value considerably modified the natural frequencies of the structure. A slackness value of 0.2 mm delivered reliable results and therefore was adopted in the analyses.

The other spring member is mainly used for numerical stabilization. The stabilization is required to provide control of the node B (Fig. 6.1), when the force in the device is zero and the steel tendon is in the gap region shown in Figure 6.3. In this case, none of the components has any stiffness leading to difficulties in solving the equation of motion at node B. The spring member follows the linear elastic hysteresis is shown schematically in Figure 6.4. The actual stiffness of the steel tendon is approximately 35,430 kN/m. In the computer simulations, 90% of this stiffness value was assigned to the spring with gap and 10% was allocated to the elastic spring.

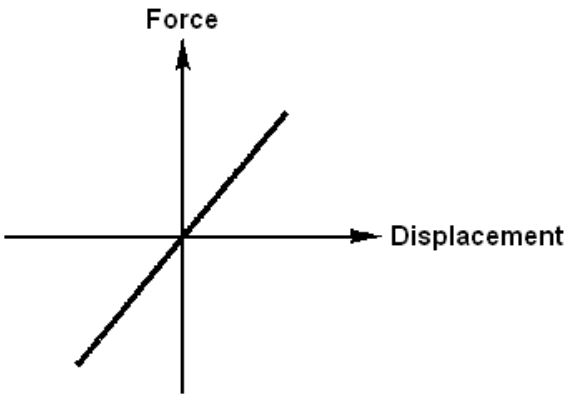

Figure 6.4 Linear elastic hysteresis.

6.2.3 Analytical Modelling of the Restraint Element

The numerical model of the resettable tendon is completed by a transversal mechanical spring. This spring prevents the movement of the other two components of the model

normal to their axes and provides stability to the entire system. An assemblage of steel plates served as the restraint element during the seismic testing. The steel plates were fixed to the shake table to provide support to the resettable device and suppress any slipping of the device and, consequently, of the steel tendon. The restraint element was modelled by using a spring member with an elastic hysteresis. Since this linear elastic spring was required to have a large stiffness, the actual stiffness (180,800 kN/m) of the assemblage of steel plates was utilised in the numerical simulations.

6.3 NUMERICAL MODEL OF THE STIFF AND FLEXIBLE BRACING SYSTEMS

The mathematical model described in the previous section was also utilised to simulate the behaviour of the rigid and flexible bracing systems during the seismic testing. The stiff bracing system corresponds to the valves closed case in which the resettable device with the valves closed is attached to the steel tendon. The flexible bracing system represents the valves open case in which the resettable device with the valves open is attached to the steel tendon.

When the valves are closed, the resettable device serves as an air spring in which the spring stiffness is provided by the bulk modulus of the air in the device cylinder. For the valves closed case, the device was modelled using a spring member with a linear elastic hysteresis. A stiffness of 400 kN/m was selected for the linear spring.

When the valves are open, the resettable device provides only a small quantity of damping due to friction, air leakage and heat loss. For the valves open case, the device was also modelled using a spring member with a linear elastic hysteresis. A spring stiffness of 30 kN/m was used for the computer simulations.

It should be noted that the stiffness value of both bracing systems was determined by tuning the analytical model with the results obtained experimentally.

6.4 COMPARISON OF THE ANALYTICAL PREDICTIONS WITH THE EXPERIMENTAL RESULTS

The analytical predictions were obtained by nonlinear computer analyses using the RUAUMOKO computer program. The numerical model was tuned to the experimental results by using the sub-program HYSTERES available in the RUAUMOKO platform. HYSTERES takes a displacement time-history and computes the associated hysteresis loop for a specified stiffness, yield strength and post-yield behaviour. The sub-program can be used to verify a particular hysteresis loop and to determine the most suitable hysteresis loop for use in a dynamic analysis by selecting the best loop parameters (Carr 2006).

6.4.1 Comparison of Displacement Time-Histories

Figures 6.5 through 6.9 show comparisons of the results predicted by the numerical model with the results of the shaking table tests. The comparisons are presented in the form of displacement time-histories at the third floor (i.e. the floor that the resettable tendon is attached to). Experimental and analytical results are shown for the 1-2-3-4, 1-3 and 2-4 control laws, and for the valves closed and valves open cases. Comparisons are presented for selected earthquake ground motions.

Overall, the analytical predictions compare well with the experimental results. It can be seen that the numerical model is able to closely reproduce the main features of the dynamic response of the one-fifth scale structure. In particular, the earthquake response predicted by the numerical model for the 1-3 control law, and the valves closed and valves open cases is in close agreement with the experimentally observed response. These results demonstrate that the analytical model developed for this research can be utilised with confidence to predict and study the behaviour of the model structure under severe earthquake ground motions.

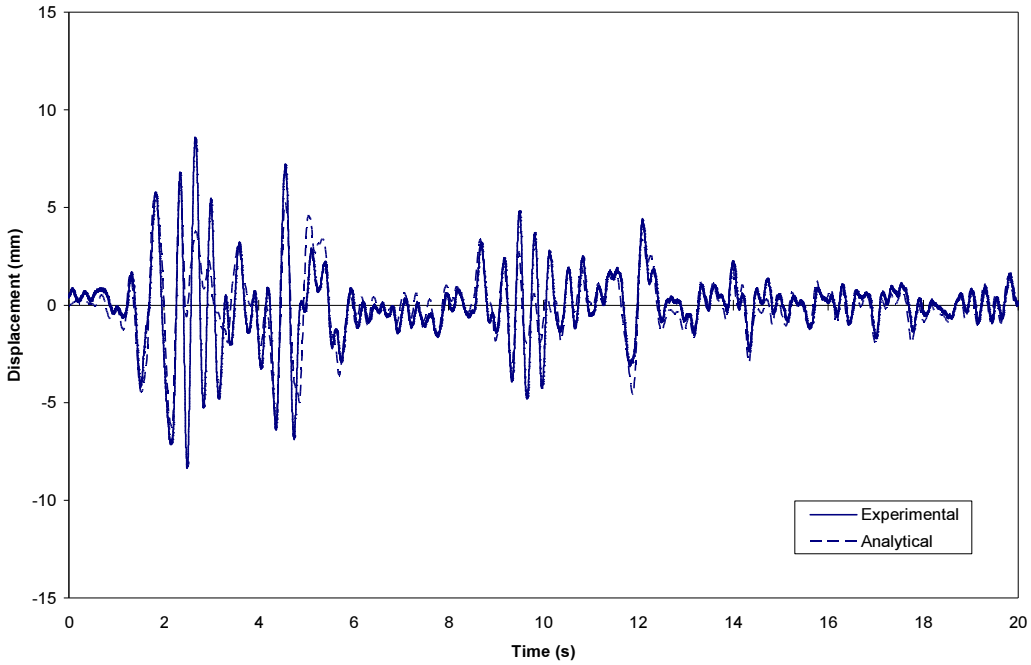

(a) El Centro 60% earthquake

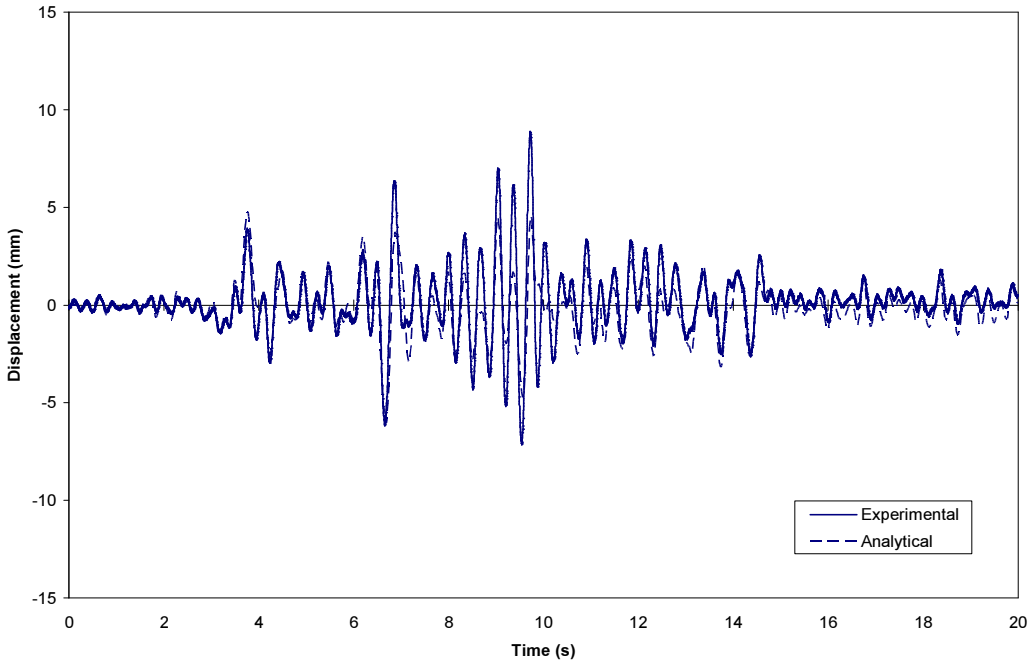

(b) Taft 80% earthquake

Figure 6.5 Comparison of the displacement time-history for the 1-2-3-4 control law.

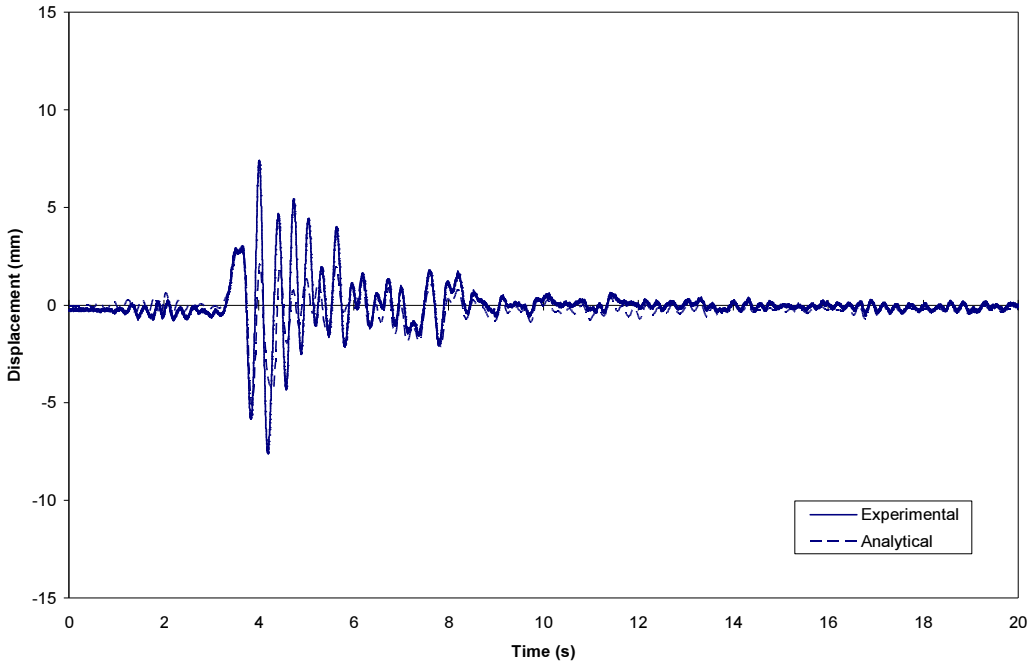

(c) Sylmar 20% earthquake

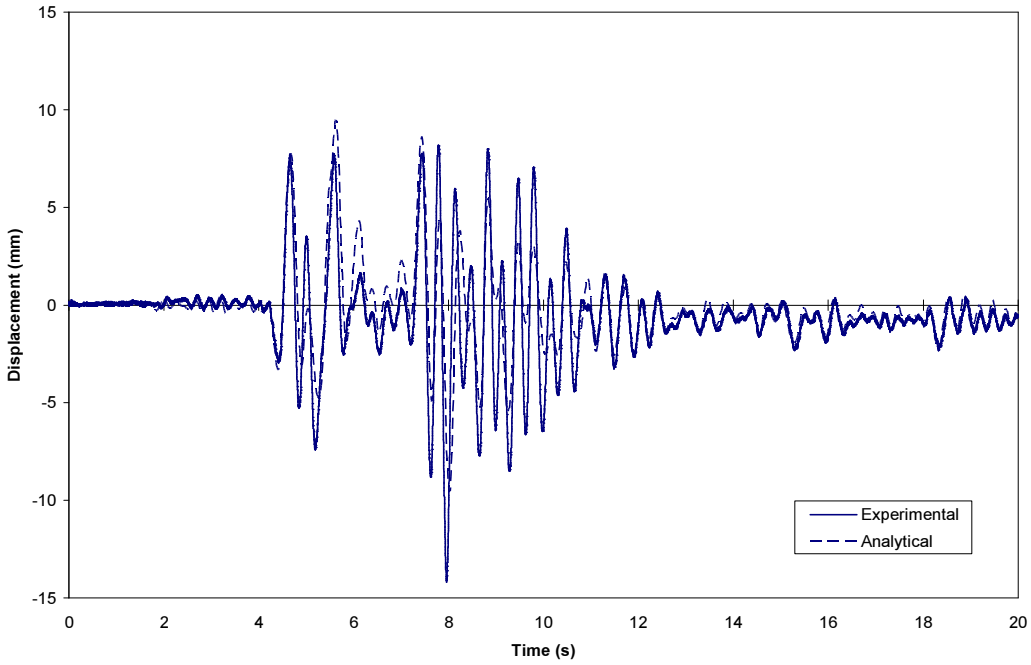

(d) Kobe 25% earthquake

Figure 6.5 (Continued).

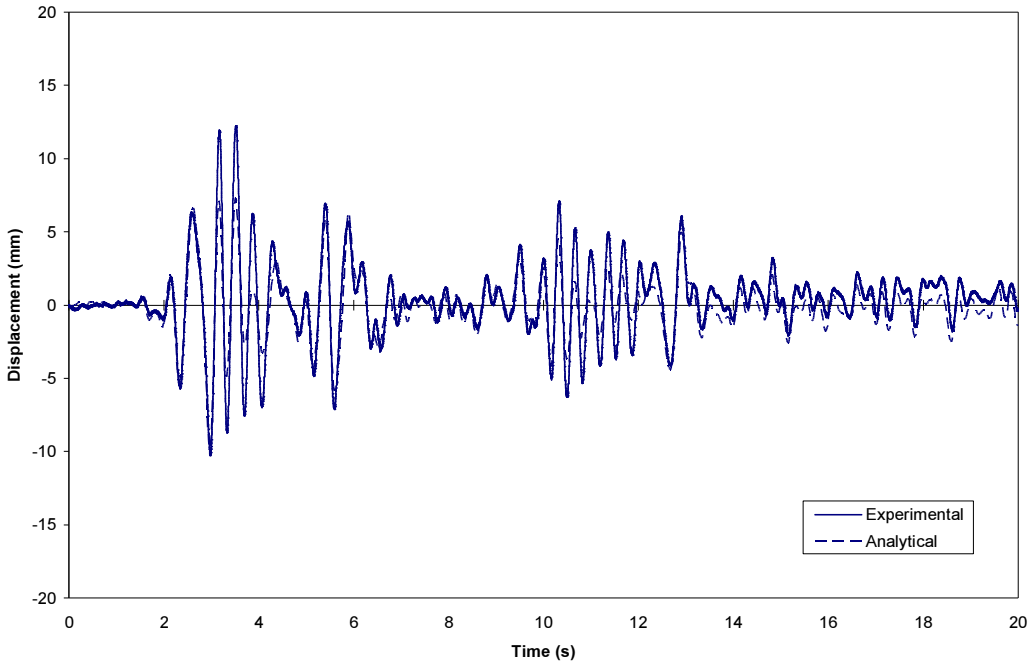

(a) El Centro 70% Modified earthquake

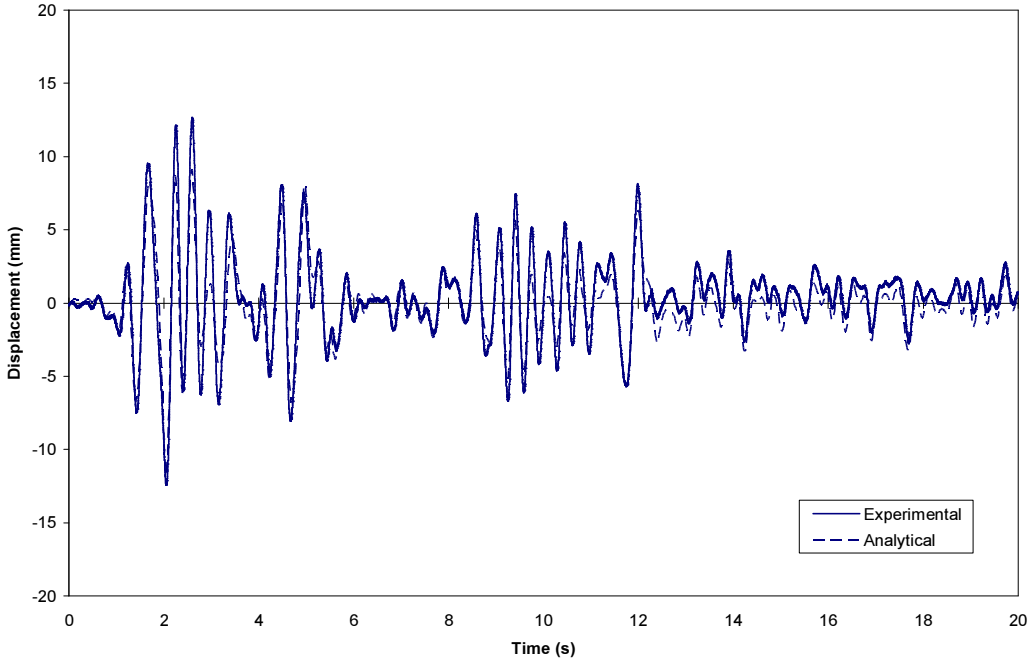

(b) El Centro 80% Modified earthquake

Figure 6.6 Comparison of the displacement time-history for the 1-3 control law.

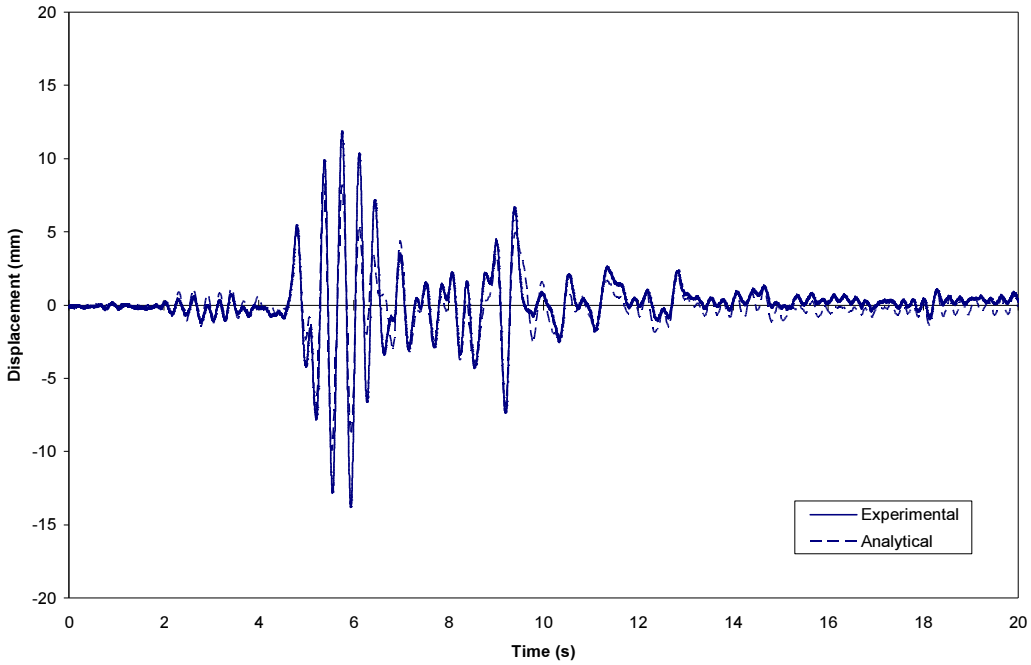

(c) Sylmar 30% Modified earthquake

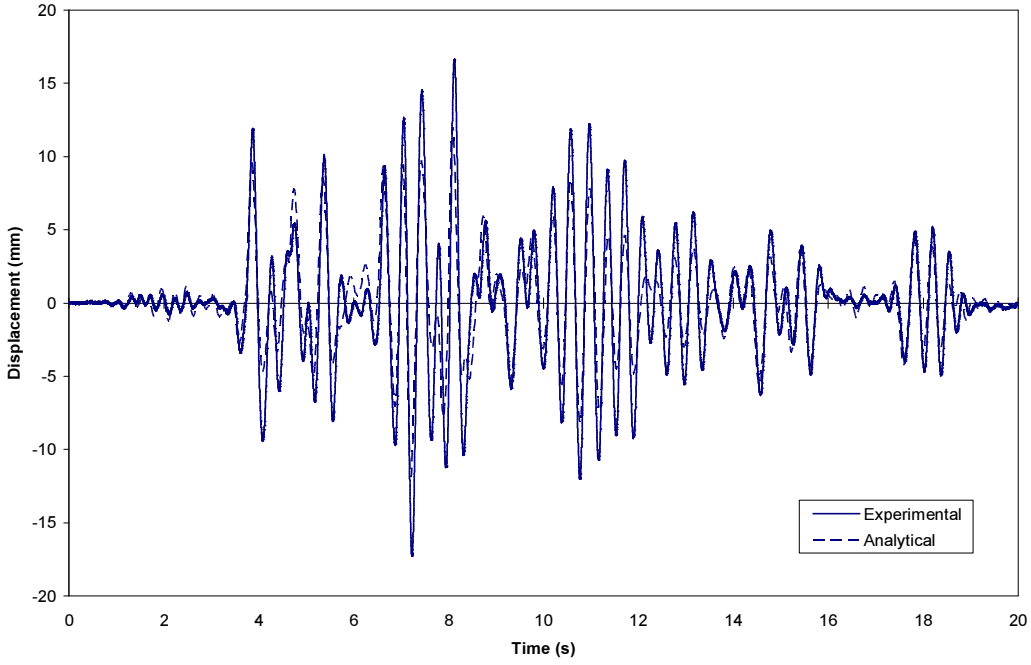

(d) Kobe 30% Modified earthquake

Figure 6.6 (Continued).

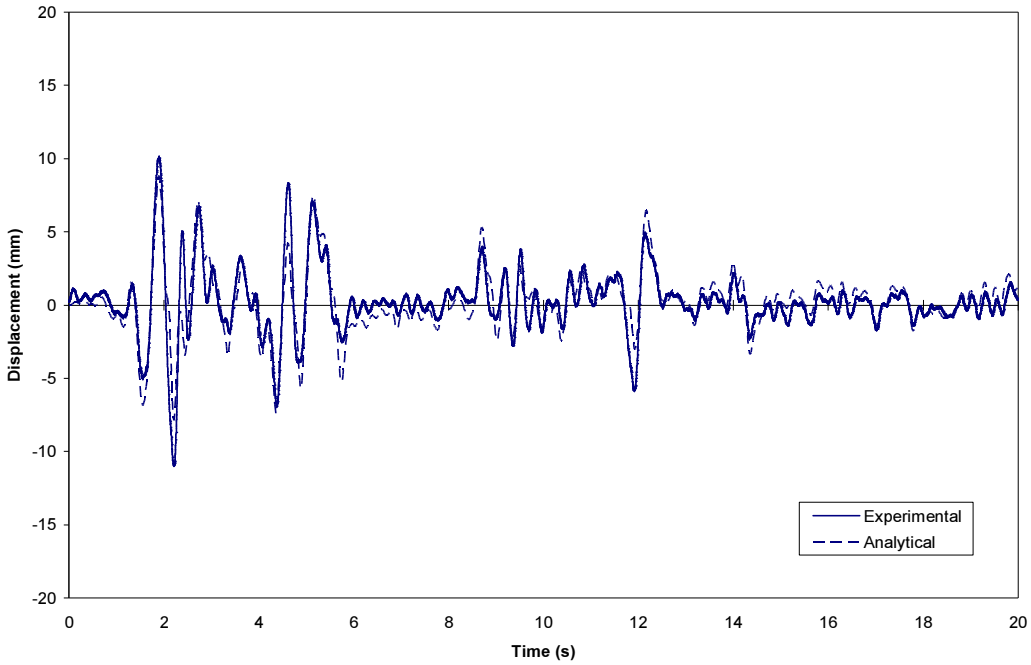

(a) El Centro 60% earthquake

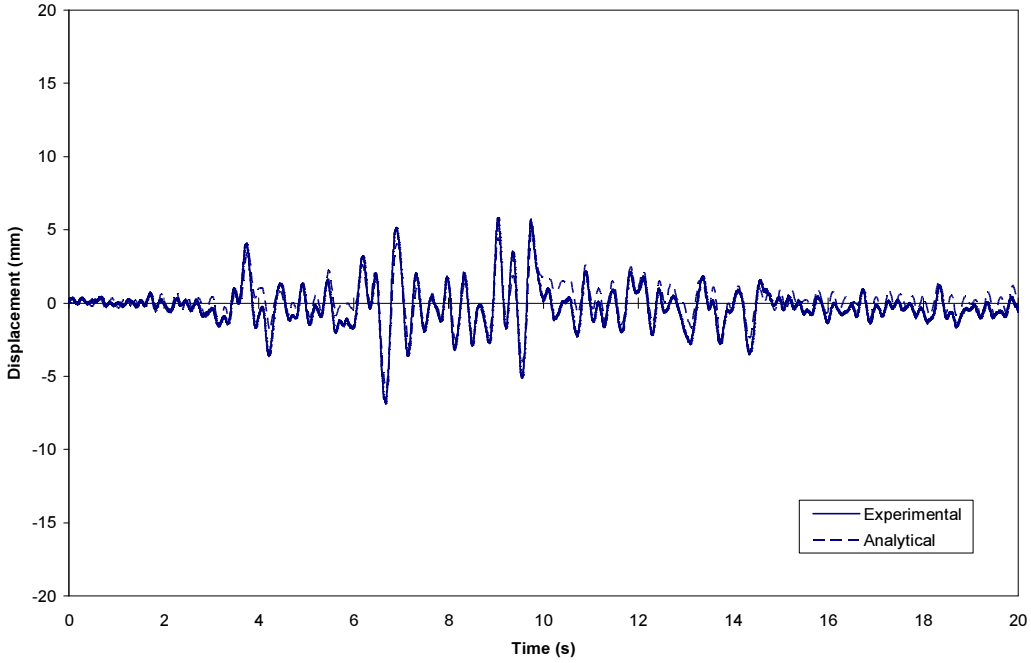

(b) Taft 80% earthquake

Figure 6.7 Comparison of the displacement time-history for the 2-4 control law.

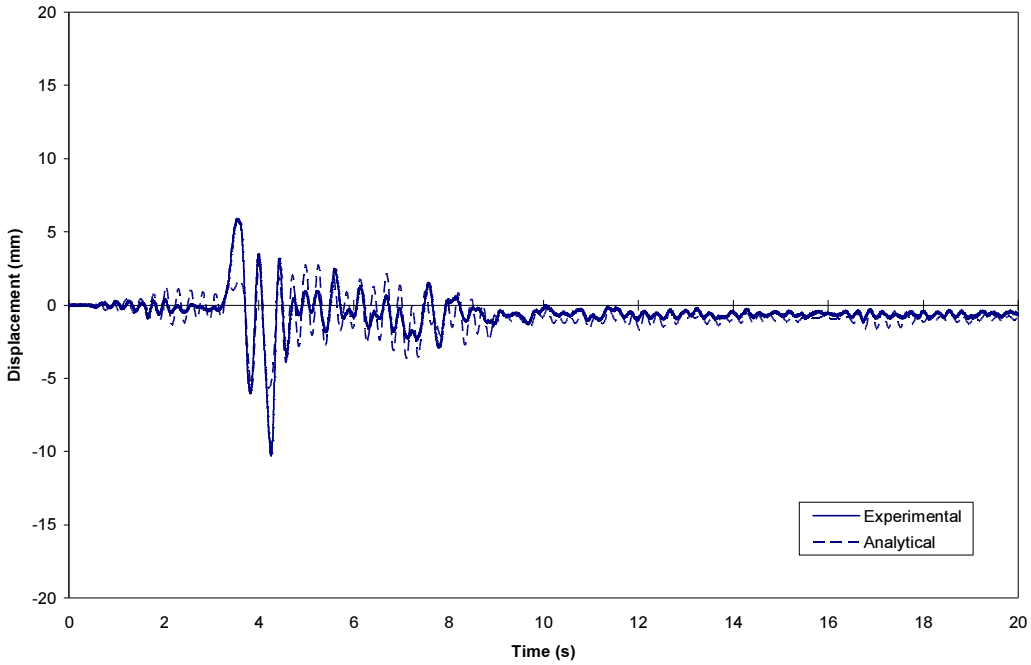

(c) Sylmar 20% earthquake

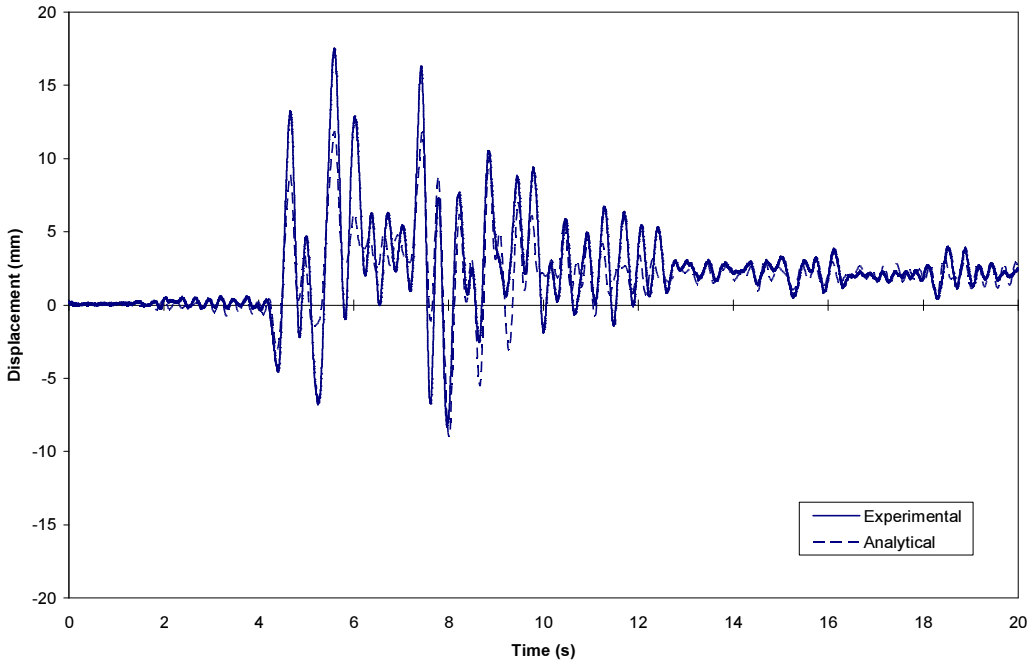

(d) Kobe 25% earthquake

Figure 6.7 (Continued).

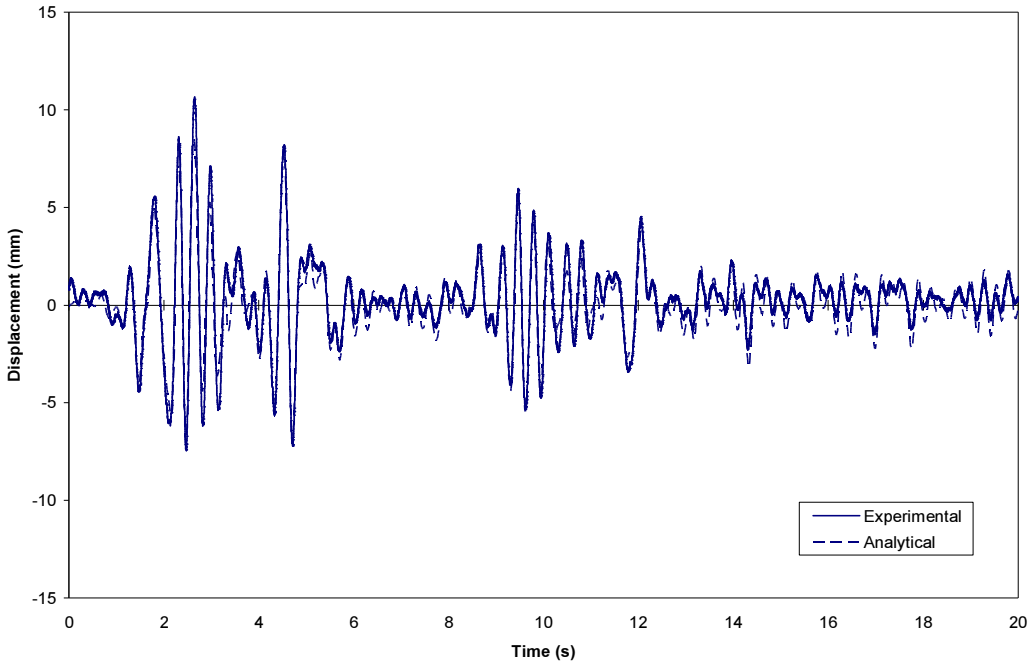

(a) El Centro 60% earthquake

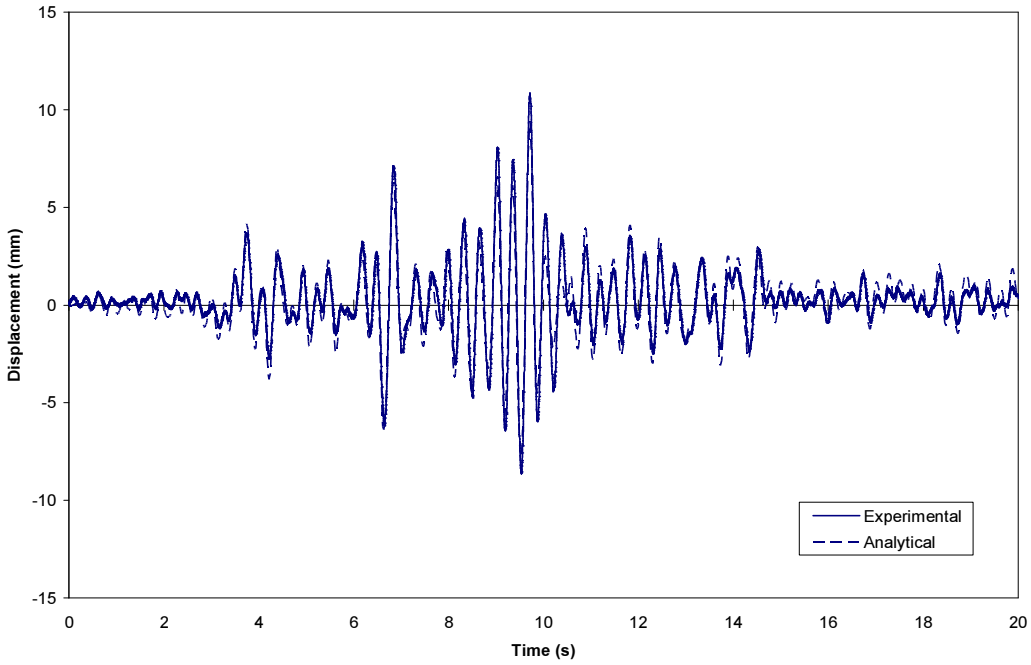

(b) Taft 80% earthquake

Figure 6.8 Comparison of the displacement time-history for the valves closed case.

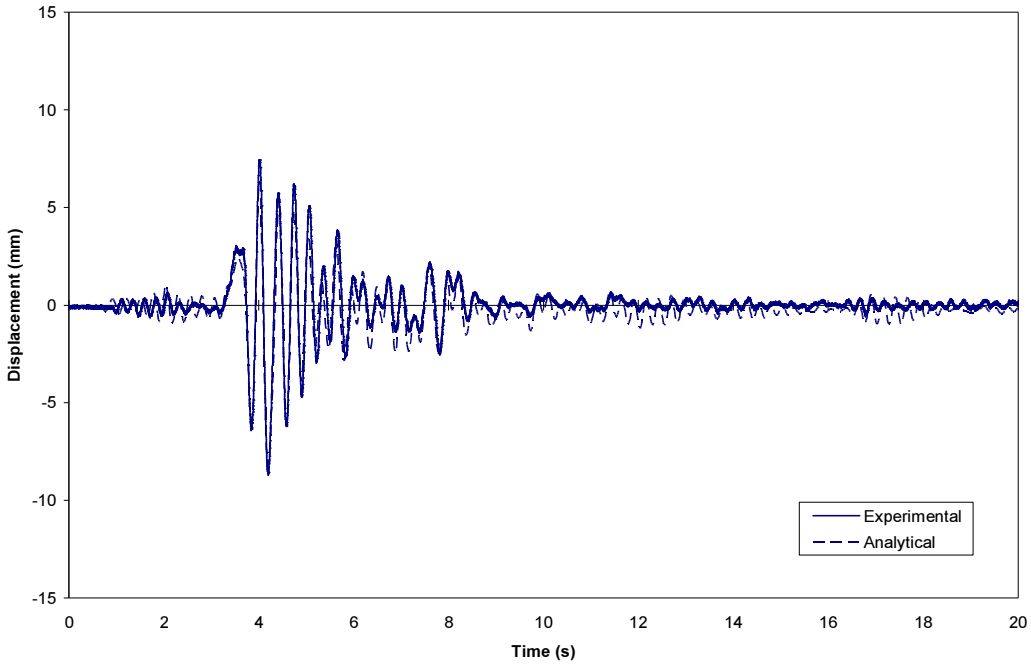

(c) Sylmar 20% earthquake

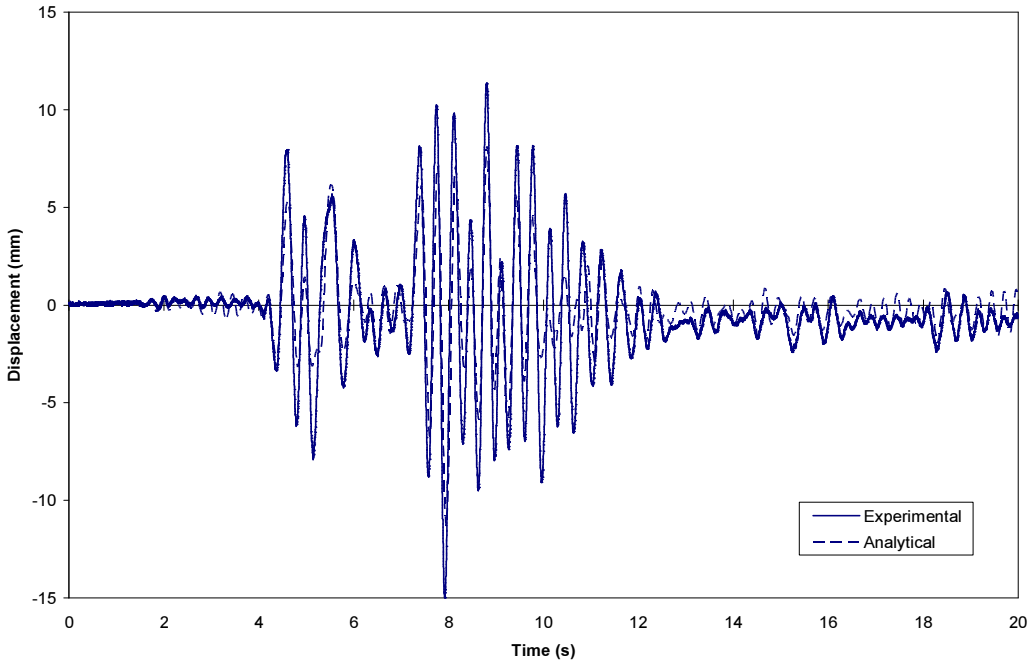

(d) Kobe 25% earthquake

Figure 6.8 (Continued).

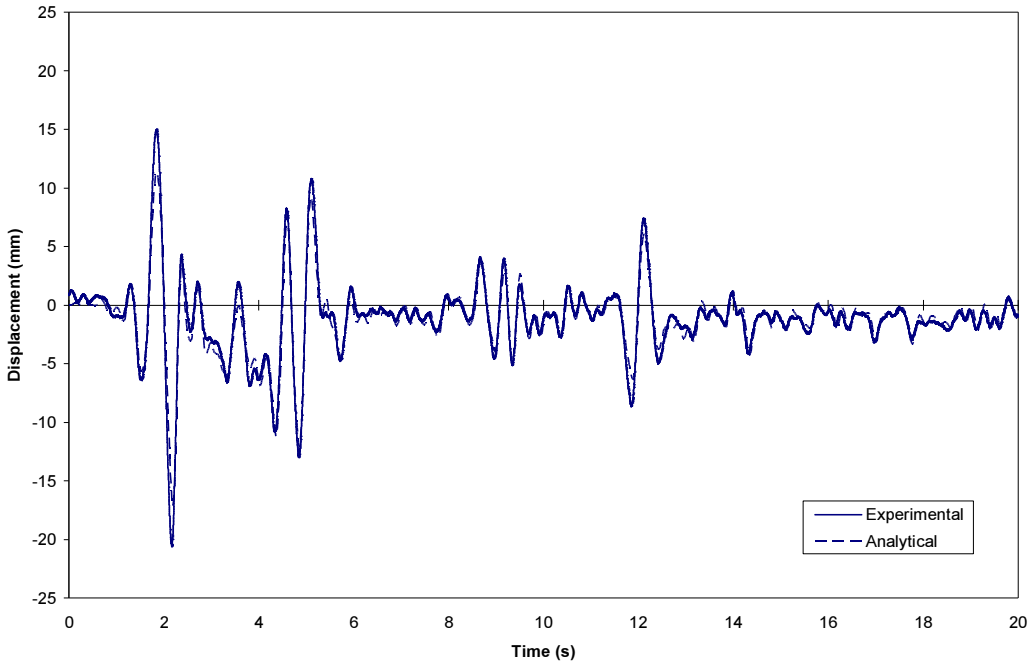

(a) El Centro 60% earthquake

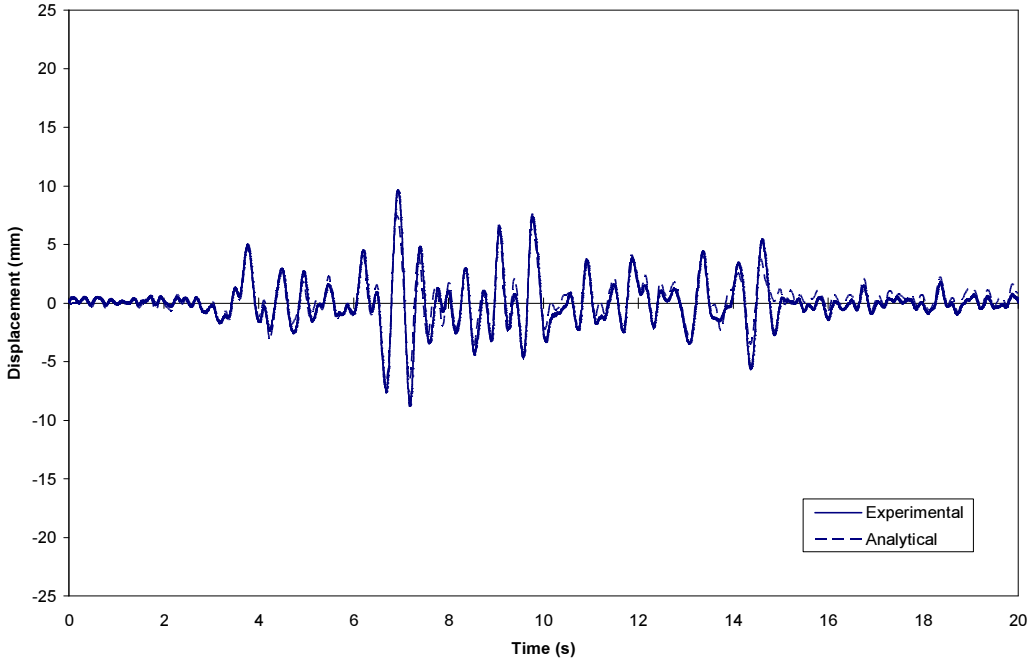

(b) Taft 80% earthquake

Figure 6.9 Comparison of the displacement time-history for the valves open case.

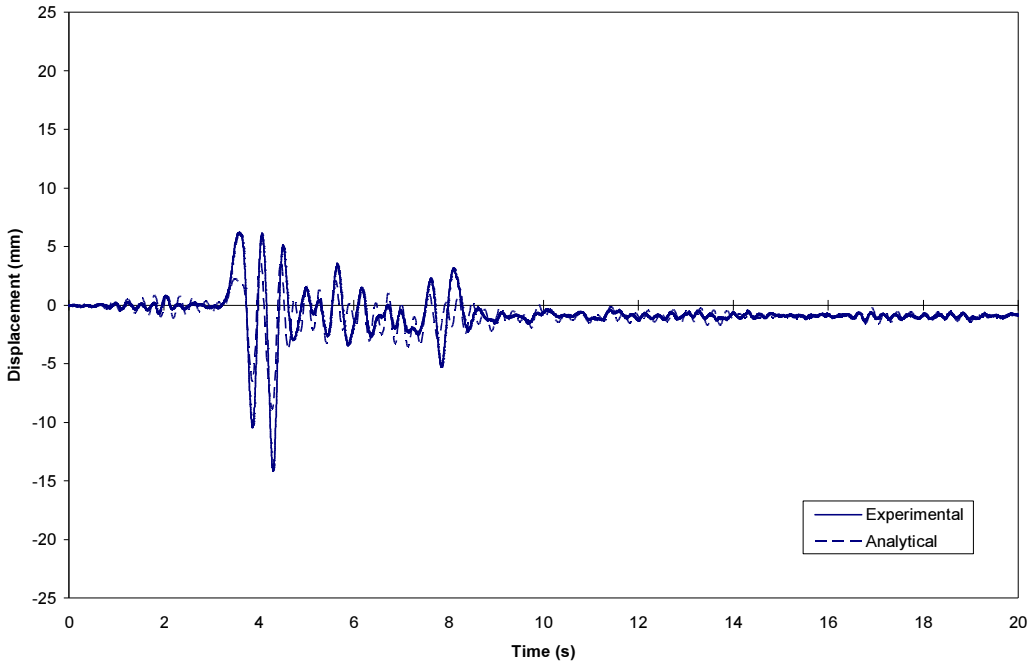

(c) Sylmar 20% earthquake

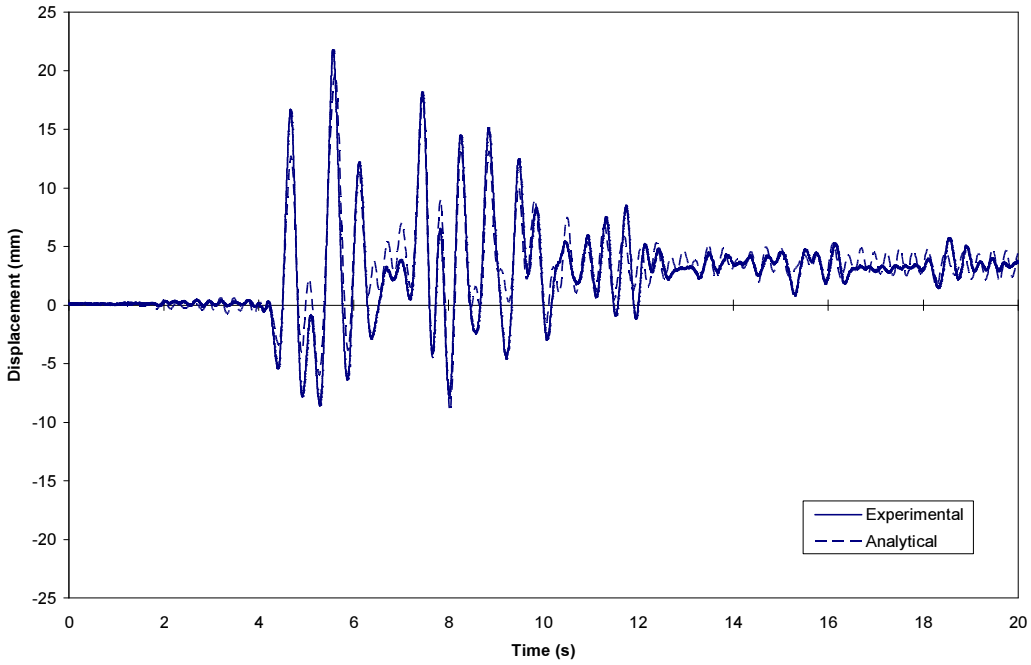

(d) Kobe 25% earthquake

Figure 6.9 (Continued).

6.4.2 Comparison of the Device Response

In this section, comparisons of analytical and experimental results are made in terms of resisting forces developed by the device against displacements of the device piston. As described in Chapter 5, a linear potentiometer was placed along the axis of the device to measure the displacements of the piston shaft with respect to the device housing. The resisting forces of the resettable device were measured by a load cell located between the device and the steel tendon. Comparisons are shown in Figures 6.10 to 6.14 for the 1-2-3-4 and 2-4 control laws, and for the valves closed and valves open cases under El Centro 60% earthquake, and for the 1-3 control law under El Centro 70% Modified earthquake. In the figures, the experimental response of the two resettable devices is compared first, the average response is then obtained from the experimental responses, and the analytically predicted response is presented at the end.

As shown in Figures 6.10 to 6.14, the experimental responses of the two resettable devices are very similar, which indicates that it may be possible to build multiple devices that will show identical dynamic behaviour and mechanical properties, when subjected to earthquake loads. Therefore, if it is required to install a resettable device on each side of the structure, no detrimental effects, such as torsion, will be introduced or amplified by small differences in the behaviour of the devices (Mulligan 2007). Floor rotation measurements taken by the fibre-optic gyroscope (FOG) described in Chapter 8 confirmed that no significant torsional effects were present during the seismic testing of the model structure.

In general, the experimentally observed response of the resettable device is similar to the response predicted by the analytical model, especially with respect to the maximum device forces and piston displacements. However, the resettable devices appear to be unable to reproduce the shape of the analytically predicted hysteresis loop. The causes of the deviation away from the ideal hysteretic behaviour of the device could not be identified properly. However, it is believed that the following factors could have had a significant impact on the resulting hysteresis loop produced by the device during the shake table tests:

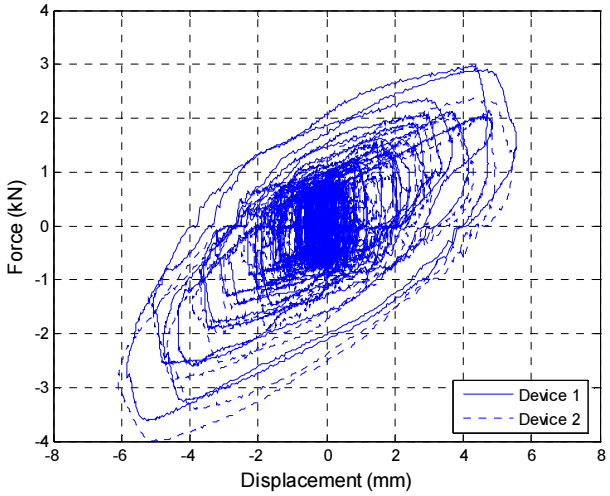

(a) Experimental response

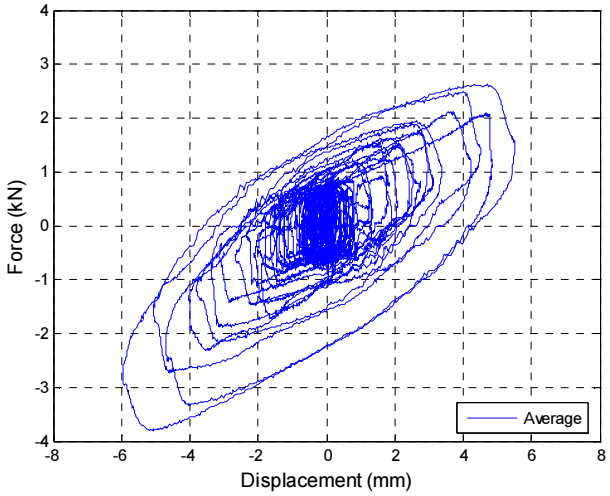

(b) Average response

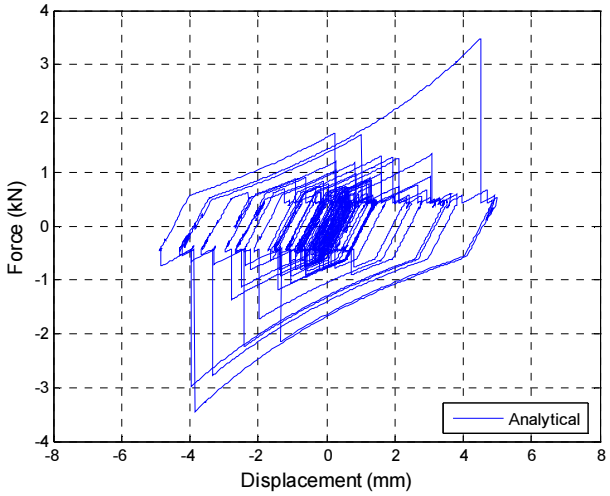

(c) Analytical response

Figure 6.10 Comparison of device response for the 1-2-3-4 control law.

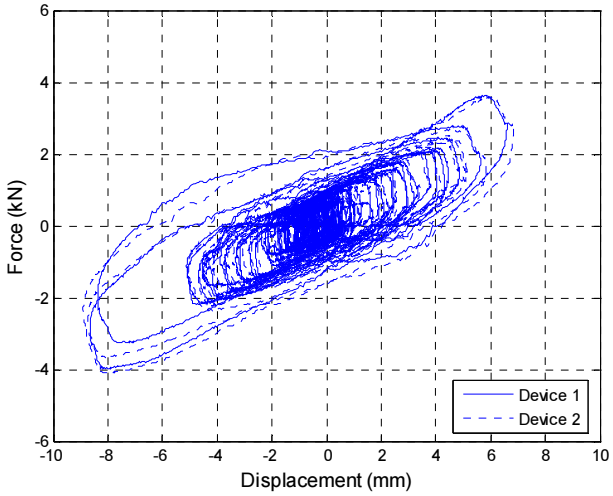

(a) Experimental response

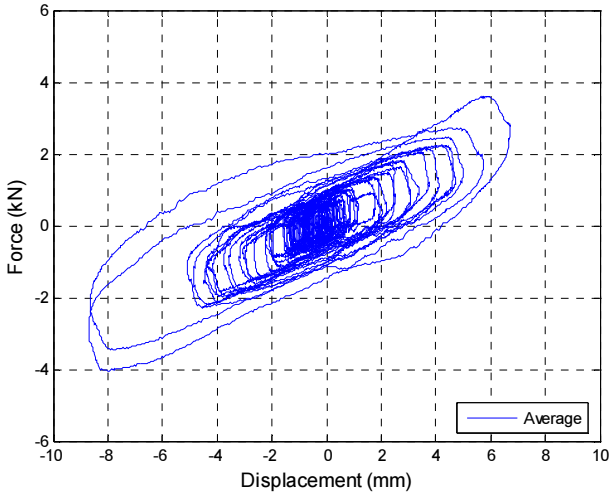

(b) Average response

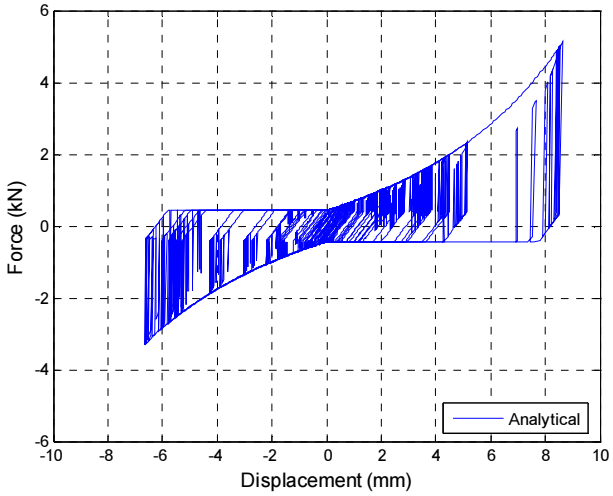

(c) Analytical response

Figure 6.11 Comparison of device response for the 1-3 control law.

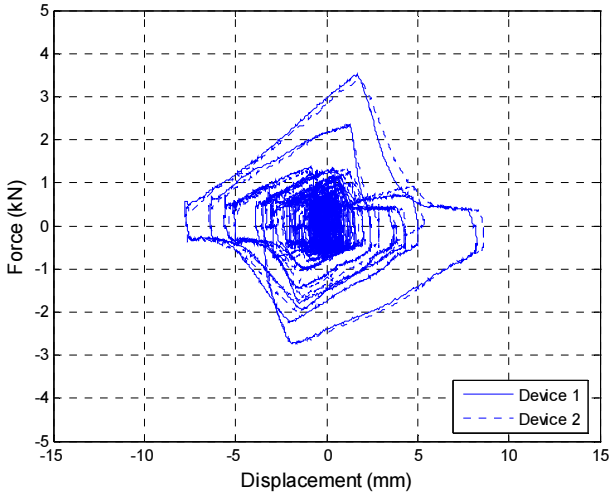

(a) Experimental response

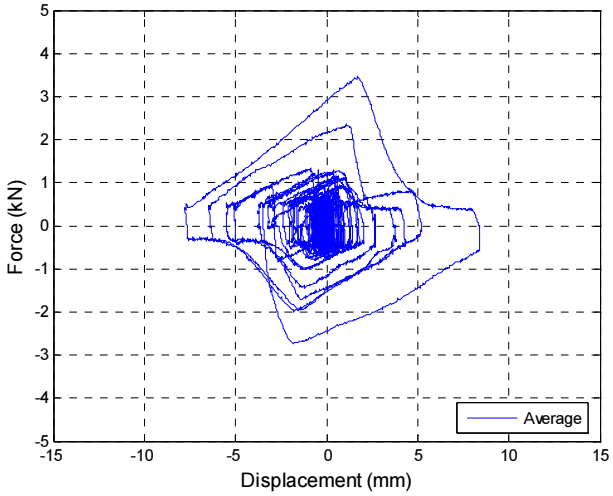

(b) Average response

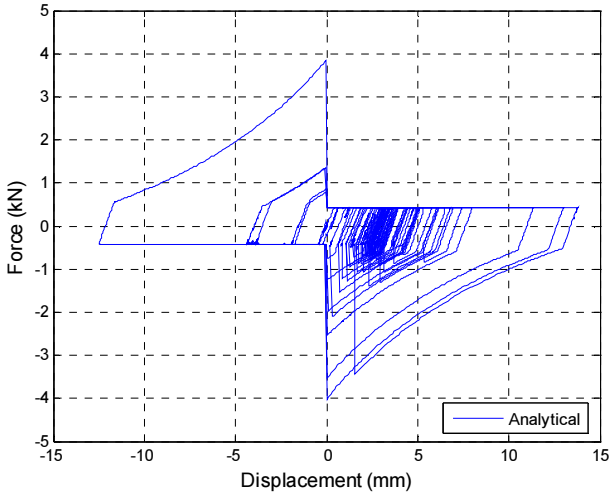

(c) Analytical response

Figure 6.12 Comparison of device response for the 2-4 control law.

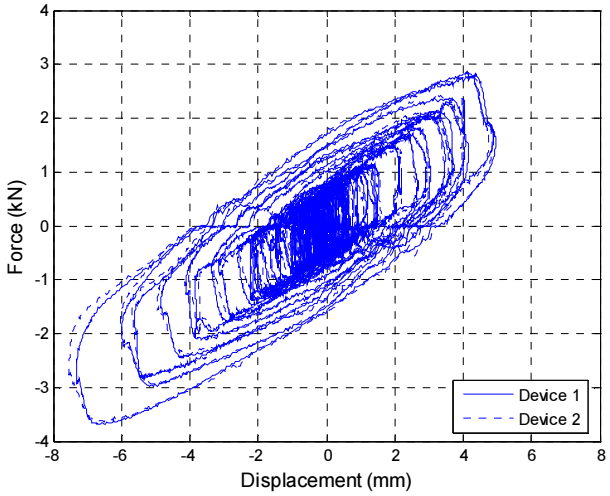

(a) Experimental response

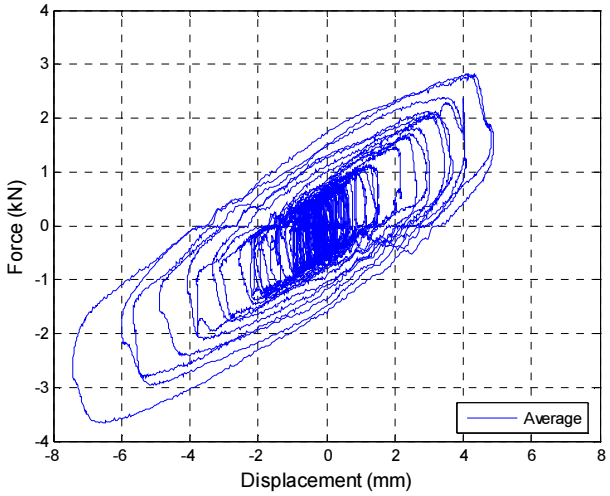

(b) Average response

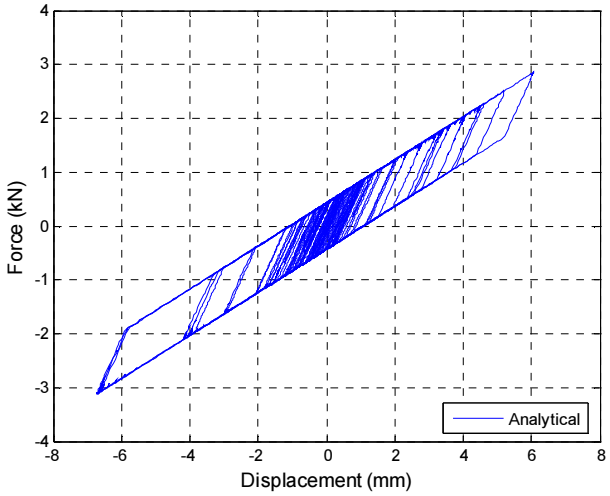

(c) Analytical response

Figure 6.13 Comparison of device response for the valves closed case.

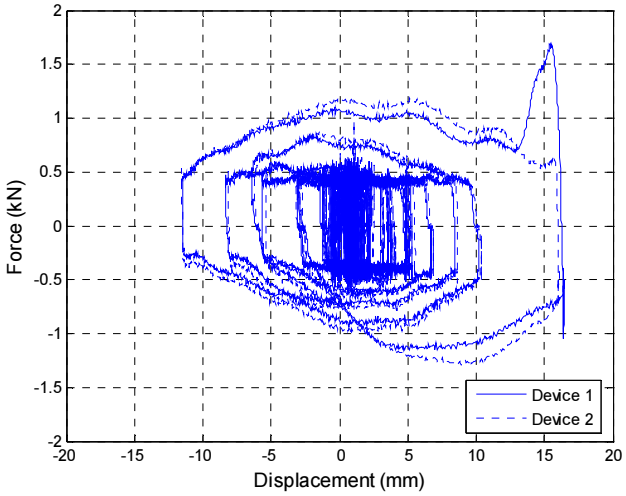

(a) Experimental response

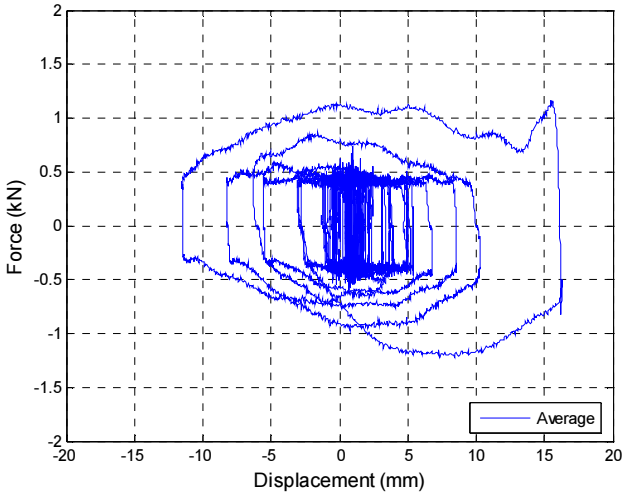

(b) Average response

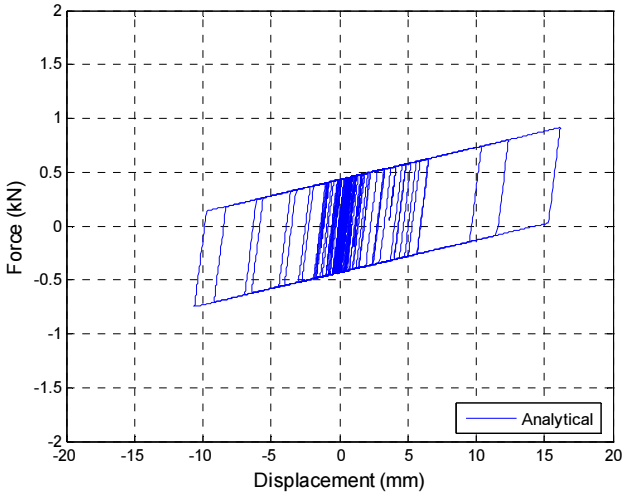

(c) Analytical response

Figure 6.14 Comparison of device response for the valves open case.

a. Friction between the piston seals and the cylinder wall of the device
b. Energy release rate and timing of the actual device valve
c. Response delay between the valve activation and the actual valve operation.

Furthermore, the convex curved shape of the experimental hysteresis loops can be attributed to viscous damping due to air flowing through the valve orifice. This effect was first observed during the characterisation testing of the device with the valves open when subjected to a high-frequency sinusoidal motion (Mulligan 2007).

6.4.3 Contribution of a Passive Tendon to Seismic Response Reduction

An analytical passive tendon is now used to investigate qualitatively the contribution of the steel tendon to the seismic response reduction of the structure during the seismic testing. As mentioned before, the steel tendon was utilised to transfer the control forces developed by the device to the structure. However, it also provided additional stiffness to the structural system.

The computational model described in Section 6.2 is used to analyse behaviour of the passive tendon that includes the steel tendon and the resettable device. The device is considered to be a linear-elastic spring with a nominal stiffness of 30 kN/m. This spring stiffness is obtained by fine tuning of the model and is based on the average dynamic properties of the stiff and flexible bracing systems described in Section 6.3. Since the device is still attached to the tendon, it is assumed that the actual performance of the steel tendon lies between the performance of the stiff and flexible bracing systems.

Figure 6.15 compares the experimental responses of the uncontrolled case and 1-2-3-4 control law with the analytical seismic response of the structure fitted with the passive tendon (steel tendon and device). In this case, the device acts as a passively controlled damper. The El Centro 40% earthquake record is selected as the input ground motion. This record intensity prevented the yielding of the uncontrolled model structure during the seismic testing.

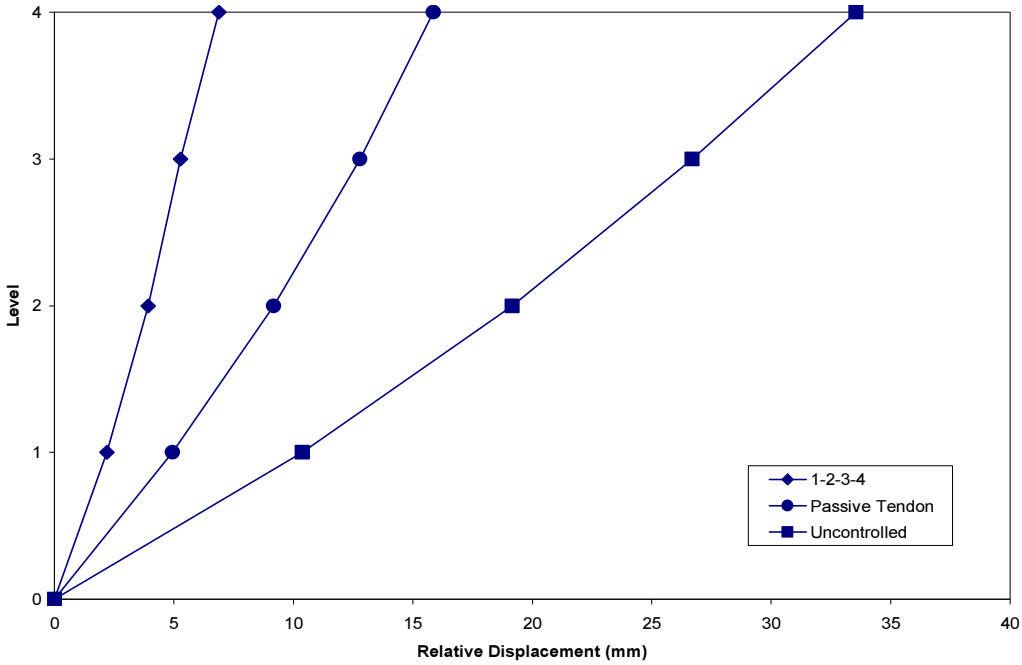

(a) Maximum relative displacements

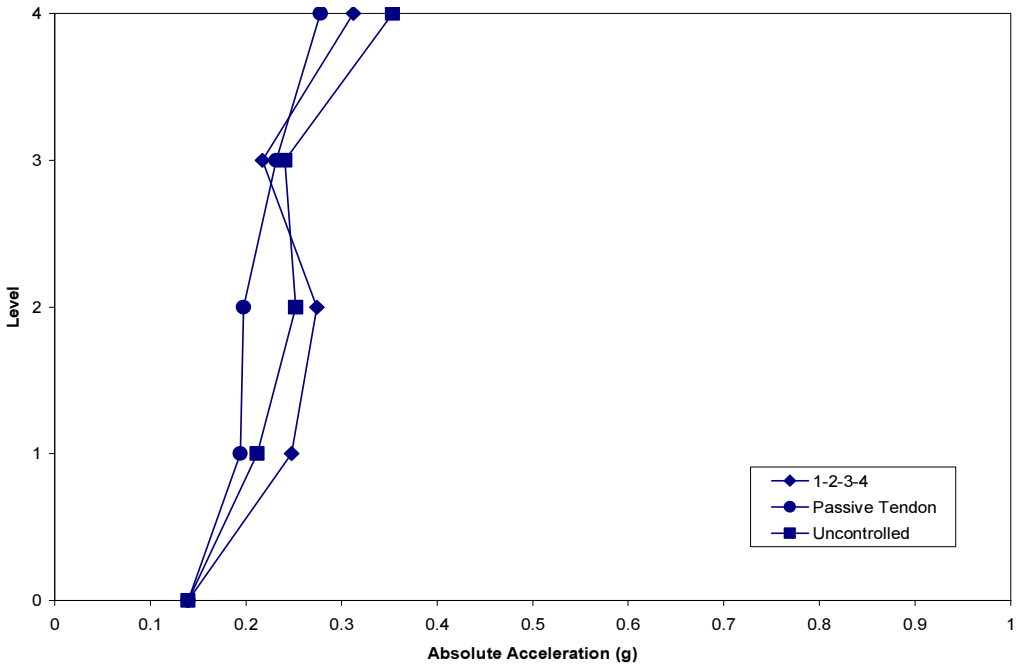

(b) Maximum absolute accelerations

Figure 6.15 Contribution of the passive tendon to the seismic response reduction.

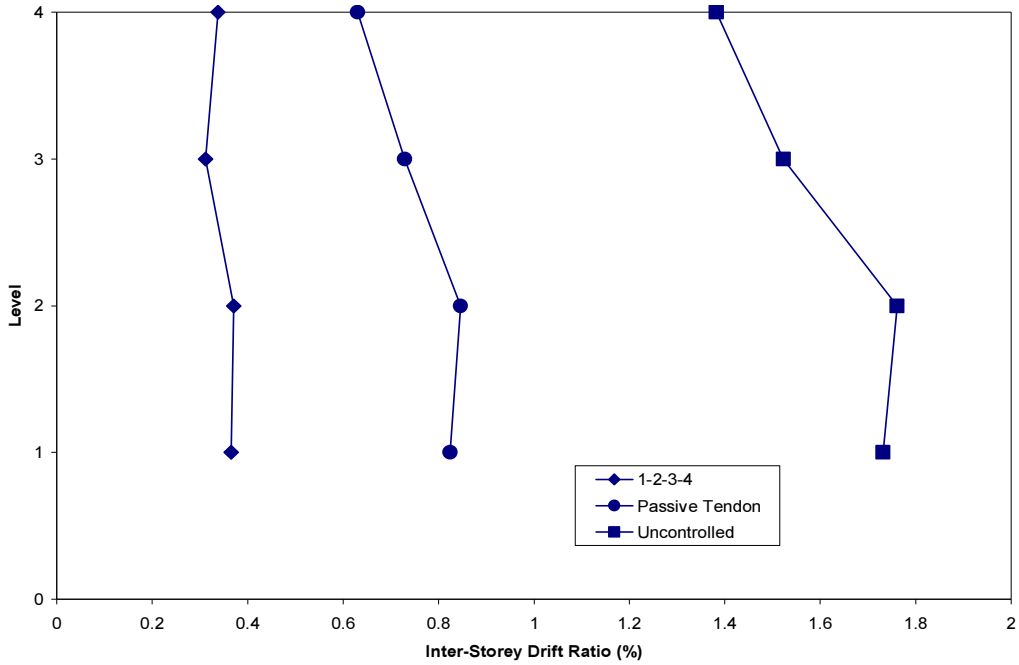

(c) Maximum inter-storey drift ratios

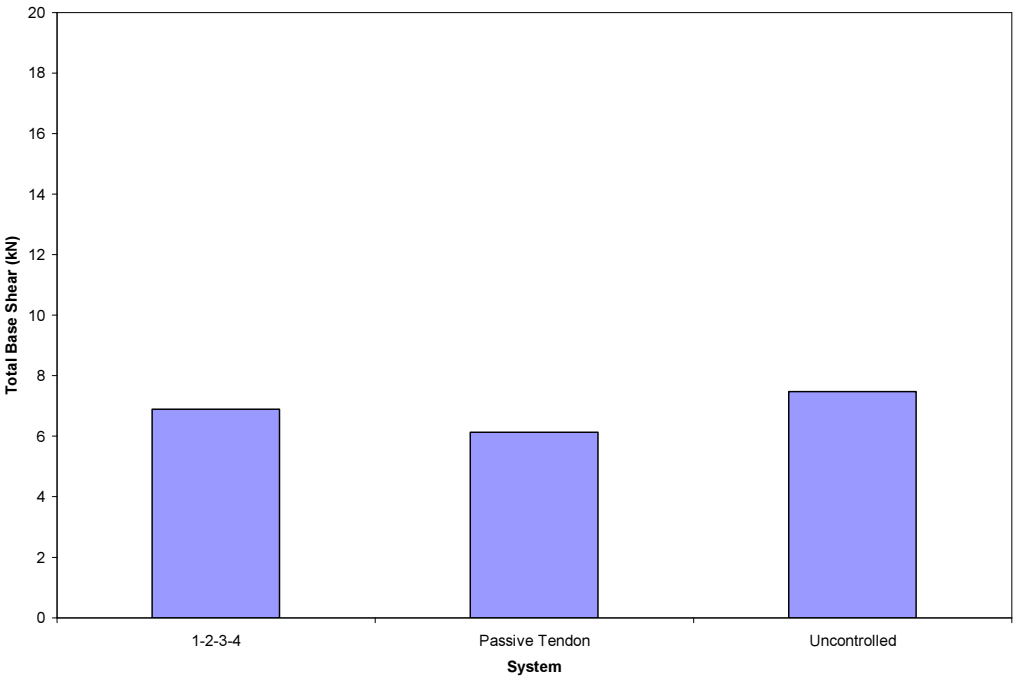

(d) Maximum total base shear

Figure 6.15 (Continued).

The comparisons show that the average contributions of the passive tendon to the reduction of the maximum relative displacements and inter-storey drift ratios are 66% and 67%, respectively. The maximum absolute accelerations are reduced by up to 14% on average and the maximum total base shear is reduced by up to 18%.

These results suggest that the contribution of the steel tendon to the seismic response reduction could have been significant during the shake table testing of the model structure. However, it is important to note that the influence of the steel tendon becomes less significant for earthquake records of higher intensity where the impact of the device friction is limited and the resisting forces developed by the resettable device are relatively large.

In addition, the effectiveness of the analytically modelled passive tendon in reducing the seismic response can be largely attributed to the contribution of the resettable device modelled as an additional spring that provides supplemental damping to the system.

6.5 ADDITIONAL COMMENTS ON THE ANALYTICAL PREDICTIONS

Overall, the numerical model developed herein is able to reproduce the seismic response of the one-fifth scale structure closely. The analytical predictions provided by the model compare well with the experimentally observed results. Section 6.4.1 shows that the responses predicted for the 1-3 control law, and the valves closed and valves open cases compare well with the experimental response of the model structure. These results indicate that the analytical model can be utilised with confidence to further study the seismic behaviour of the one-fifth scale structure.

However, it is suggested that more research work needs to be done to improve the performance of the analytical model developed in this research. Future research should include a better representation of the stiffness and friction force of the resettable device. The energy release rate and time, and any response delay of the device valves should be accounted for. The modelling of the slackness of the steel tendon is an important issue

that needs improvement. Finally, the impact of the tendon slackness on the earthquake response should be further investigated.

6.6 SUMMARY

Analytical predictions of the shake table test results have been presented in this chapter. A numerical model was developed to simulate the earthquake response of the one-fifth scale structure equipped with two semi-active resettable tendons. The model has three primary components. The first component represents the resettable device, the second component simulates the steel tendon and the third component models the steel restraint element. The three components of the model were modelled using spring members with different hysteretic behaviours. Nonlinear dynamic analyses using the RUAUMOKO computer program were performed to assess the accuracy of the mathematical model. Displacement time-histories at the third floor are used to compare the analytical and experimental results. The 1-2-3-4, 1-3 and 2-4 control laws, and the valves closed and valves open cases are compared for different earthquake ground motions. Comparisons of the analytical predictions with the experimental results indicate that the numerical model is able to simulate the seismic behaviour of the model structure well. The device response observed experimentally was also compared with analytical predictions given by the computational model. Finally, the contribution of the steel tendon to the seismic response reduction of the model structure was investigated by using a passive tendon based on the numerical model.

Chapter 7
IMPLEMENTATION OF RESETTABLE DEVICES IN STRUCTURAL BUILDING SYSTEMS

7.1 INTRODUCTION

This chapter describes various issues relevant to the implementation of semi-active resettable devices in civil engineering structures. Analytical studies are carried out to investigate the performance of a twelve-storey reinforced concrete building subjected to earthquake excitations and controlled by resettable devices. Computer simulations are performed to determine the optimal utilization of the resettable devices in the structure. The effectiveness of the devices in controlling the seismic response and their location, number, arrangement and connection to the structure are discussed. The contribution to the seismic response of the pre-stressed tendons and bracings used by the control system is investigated. The effects of variations in the control laws used to control the operation of the devices are examined. The use of a lever system and a high-pressure air source is investigated to improve the seismic performance of the resettable devices. Reductions in maximum relative displacements, absolute accelerations, inter-storey drift ratios and total base shear are presented to assess the effectiveness of the resettable devices.

7.2 CHARACTERISTICS OF THE TWELVE-STOREY BUILDING

The response quantities associated with the structure without energy dissipation devices (uncontrolled response) form the basis for the selection of the desired performance level for which the devices should be designed. Therefore, the damping ratio required to achieve the targeted response reduction relative to the uncontrolled response is of primary concern in the design of structures with energy dissipation devices. Although the design of supplemental devices for the retrofit of structures does not require additional effort beyond a regular retrofit design, there may be other issues regarding

the capacity of existing structural elements, which should be carefully evaluated during the retrofit process (Pekcan 1998).

The reinforced concrete building shown schematically in Figure 7.1 is used to analyse the seismic performance of the semi-active resettable devices. The building has twelve storeys and two horizontal bays. The moment-resisting frame structure was designed by Jury (1978) to examine the seismic load demands on columns of reinforced concrete multi-storey frames.

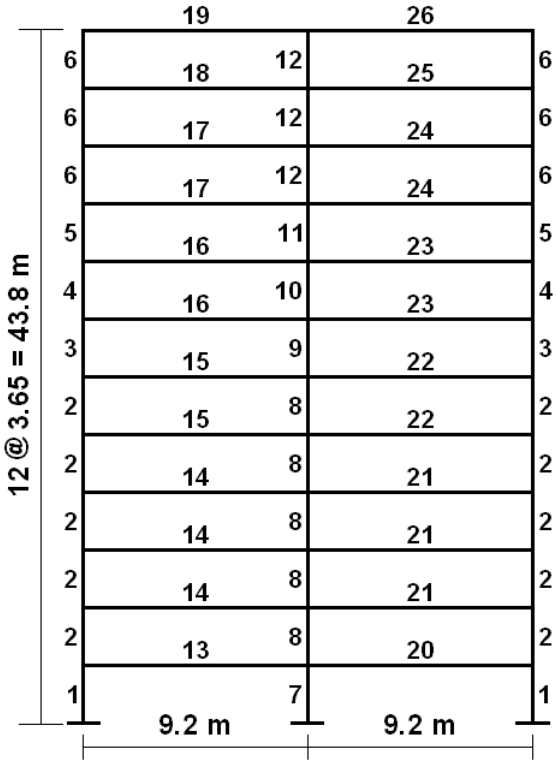

Figure 7.1 Twelve-storey reinforced concrete building.

The reinforced concrete building was designed in accordance with the provisions of the New Zealand Loadings Standards NZS 4203 and NZS 3101. The frame is considered to be a typical two-bay interior frame of a building of twelve floors. It is assumed that the frame is required to resist the component of the earthquake ground motion in the plane of the frame only. The component in the perpendicular direction is assumed to be taken by other resisting systems (e.g. shear walls). Torsional effects for the building are not

taken into account (Jury 1978). Table 7.1 outlines the section properties of the column and beam members of the twelve-storey reinforced concrete building.

Table 7.1 Section properties of the column and beam members (refer to Figure 7.1).

Type	Cross-sectional area (m^2)	Effective shear area (m^2)	Moment of inertia (m^4)
1	0.1938	0.1938	0.014550
2	0.1938	0.1938	0.014550
3	0.1750	0.1750	0.010790
4	0.1750	0.1750	0.010790
5	0.1625	0.1625	0.008582
6	0.1625	0.1625	0.008582
7	0.3200	0.3200	0.025600
8	0.3200	0.3200	0.025600
9	0.2629	0.2629	0.017270
10	0.2629	0.2629	0.017270
11	0.2278	0.2278	0.012980
12	0.2278	0.2278	0.012980
13	0.1800	0.1800	0.029520
14	0.1800	0.1800	0.029520
15	0.1800	0.1800	0.029520
16	0.1700	0.1700	0.025030
17	0.1600	0.1600	0.020860
18	0.1600	0.1600	0.020860
19	0.1600	0.1600	0.020860
20	0.1800	0.1800	0.029520
21	0.1800	0.1800	0.029520
22	0.1800	0.1800	0.029520
23	0.1700	0.1700	0.025030
24	0.1600	0.1600	0.020860
25	0.1600	0.1600	0.020860
26	0.1600	0.1600	0.020860

Table 7.2 shows the fixed-end moments and shear forces at the two ends of the beam members. Positive member moments cause tensile stresses on the bottom fibres and positive shear forces act in the local y-direction on the positive local x-face of the beam section. Tensile axial forces are positive (Carr 2006). Table 7.3 presents the positive and negative yield moments at the two ends of the beam members of the twelve-storey structure.

Table 7.2 Fixed-end moments and shear forces (refer to Figure 7.1).

Type	M1 (kNm)	M2 (kNm)	V1 (kN)	V2 (kN)
13	-180.1	-179.8	-135.8	135.8
14	-180.1	-179.8	-135.8	135.8
15	-180.1	-179.8	-135.8	135.8
16	-183.7	-182.0	-133.4	133.4
17	-184.2	-182.6	-131.1	131.1
18	-184.2	-182.6	-131.1	131.1
19	-184.2	-182.6	-131.1	131.1
20	-179.8	-180.1	-135.8	135.8
21	-179.8	-180.1	-135.8	135.8
22	-179.8	-180.1	-135.8	135.8
23	-182.0	-183.7	-133.4	133.4
24	-182.6	-184.2	-131.1	131.1
25	-182.6	-184.2	-131.1	131.1
26	-182.6	-184.2	-131.1	131.1

Table 7.3 Positive and negative yield moments (refer to Figure 7.1).

Type	M1 (kNm) (Positive)	M1 (kNm) (Negative)	M2 (kNm) (Positive)	M2 (kNm) (Negative)
13	893	-976	893	-976
14	1047	-1142	1047	-1142
15	887	-988	887	-988
16	762	-833	714	-714
17	559	-631	464	-547
18	307	-369	307	-381
19	307	-307	307	-307
20	893	-976	893	-976
21	1047	-1142	1047	-1142
22	887	-988	887	-988
23	714	-714	833	-762
24	547	-464	631	-559
25	381	-307	369	-307
26	307	-307	307	-307

A two-dimensional computer model of the reinforced concrete building was developed by Jury (1978) for the use of a computer program designed to carry out inelastic dynamic analyses. The model was later on modified to take code changes into account and implemented in the computer program RUAUMOKO. The model has 39 nodes and each node has 3 degrees of freedom. All the degrees of freedom of the base nodes are restrained for fully fixed boundary condition. To couple the degree of freedom of the horizontal displacement, the nodes of the horizontal elements are slaved at each level. This implies rigid floor slabs. A reduction in the size of the stiffness matrix and hence a large saving in computing time results from this approximation. All degrees of freedom have inertia (including the joint rotations). Rotational mass is assigned to the joints to allow for rotational inertia. Although rotational inertia will have an effect on the behaviour of a real structure during its elastic response, the effect will be minimal after beam hinging has occurred. However, the inclusion of mass for the rotational degree of freedom of a joint results in a better ordered stiffness matrix, which leads to reductions in computing time (Jury 1978).

A two-node element with rigid end-blocks is utilised to model the beam and column members of the structure. Rigid end-blocks of the beams are assumed as one half the appropriate column depths and rigid end-blocks of the columns are assumed as one half the appropriate beam depths. Rigid end-blocks, as modelled in the computer program, are unlikely to exist in actual structures. This is because of the high stresses that exist in these regions. However, the employ of rigid end-blocks in the modelling enables the formation of plastic hinges in beams and columns to occur at the faces of the adjacent transverse members (Jury 1978).

A frame type member is adopted to model all members of the concrete building. The concrete beam-column member is used to represent the behaviour of the three columns of the first storey and the one-component beam member (Giberson 1969) is adopted to model the other beam and column members. The hysteretic behaviour of the first storey columns and all beam members is modelled by using an elasto-plastic hysteresis. In contrast, a linear elastic hysteresis is adopted to model the hysteretic behaviour of the other column members of the building.

An elastic modulus of 25 GPa and a shear modulus of 10.4 GPa are adopted for all members of the concrete building. The Poisson's ratio is taken as 0.2. The shear deformation of the members is considered in the analysis by using the effective shear area of the member sections. The building has a total seismic weight of 19,188 kN. Table 7.4 shows the distribution of the seismic weight in the structure.

Table 7.4 Distribution of the seismic weight.

Level	Weight (kN)
1	1625
2	1625
3	1625
4	1625
5	1625
6	1623
7	1597
8	1595
9	1571
10	1571
11	1571
12	1535
Total	**19188**

In concordance with the original computer model developed by Jury (1978), initial stiffness Rayleigh damping is adopted herein for the computer analyses. The damping matrix based on the Rayleigh damping model utilises the stiffness of the structure at the beginning of the time-history. The computed damping matrix is constant throughout the time-history analysis and the tangent, secant and elastic damping matrices are identical. This means that the effective damping increases as the structure softens, because the Rayleigh coefficients α and β were computed for the initial natural frequencies of free vibration and some of the frequencies have now decreased (Carr 2006). As mentioned in Chapter 4, the Rayleigh damping model has shown that the level of damping in the higher modes of free vibration can be very large (Carr 1997). A value of 5% of critical damping is assumed for the first and tenth vibration modes of the structure.

The P-Delta effects are included in the analyses and the constant average acceleration method developed by Newmark (1959) is utilised to integrate the equation of dynamic equilibrium. A time step of 0.001 seconds is chosen for the nonlinear dynamic analyses.

7.3 CHARACTERISTICS OF THE CONTROL SYSTEM

As mentioned in Chapter 4, the purpose of incorporating energy dissipation devices in the design or retrofit of a structure is to reduce its seismic response. Increasing damping in a structure usually reduces the forces and deformations induced by the ground motion in structural elements. The amount of reduction varies depending on the mass, stiffness and inherent damping characteristics of the structure. It also depends on the amplitude, frequency content and duration of the earthquake ground motion. Therefore, it is not possible to design a supplemental damping system that will be equally effective for all types of structures. Each design problem should be treated on its own merits taking into consideration the following issues (Pekcan 1998):

a. The suitability of various control systems
b. The amount of damping required
c. The type of structural system
d. The characteristics of the ground motion.

It is common in the design and retrofit of structural building systems to idealise the actual multi-degree-of-freedom (MDOF) system with an equivalent single-degree-of-freedom (SDOF) system, such that the SDOF system describes the most relevant characteristics of the MDOF system. In the same way, any preliminary attempt to design a control system may be simplified to allow the designer the use of pre-defined response spectra (Pekcan 1998).

The control system proposed in this research uses rigid rods attached to the two ends of the device piston. The rigid rods transfer the control forces produced by the device to a tendon system. The tendon system consists of pre-stressed tendons that transfer the

control forces to the structure at different floor levels. The pre-stressed tendons span the two horizontal bays of the structure. A schematic of the implementation of the control system is shown in Figure 7.2.

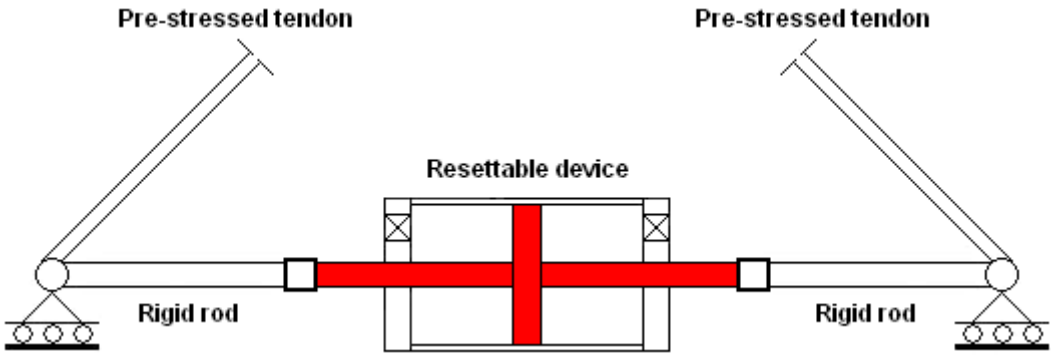

Figure 7.2 Schematic of the system implementation.

7.3.1 Description of the Resettable Device

The semi-active resettable device is modelled using the spring member available in the RUAUMOKO program. The spring member is shown schematically in Figure 4.15. The spring member follows the 1-2-3-4, 1-3 and 2-4 control laws described in Chapter 3 and shown collectively in Figure 7.3. The input parameters of the device are based on the demands of the twelve-storey reinforced concrete building. The maximum force delivered by the resettable device is set at 500 kN. Preliminary dynamic analyses indicated that the structure would have a maximum displacement of approximately 0.20 m at the twelfth floor. Consequently, a device stiffness of 2,500 kN/m was adopted in the computer analyses.

The initial pressure (i.e. atmospheric pressure) of the chamber p_0 is considered to be 100 kN/m^2. The ratio of specific heats γ for air is 1.4. The expected maximum displacement of the structure determines the length L_0 of the device chamber. Considering a safety margin of 0.05 m, a chamber length of 0.25 m is adopted. The required diameter of the device cylinder can be determined by using Equation 3.12. The device diameter D is found to be 1.686 m. The area of the piston A is then calculated as 2.232 m^2.

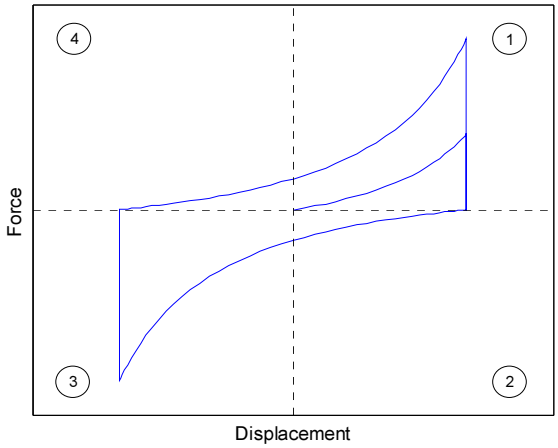

(a) 1-2-3-4 control law

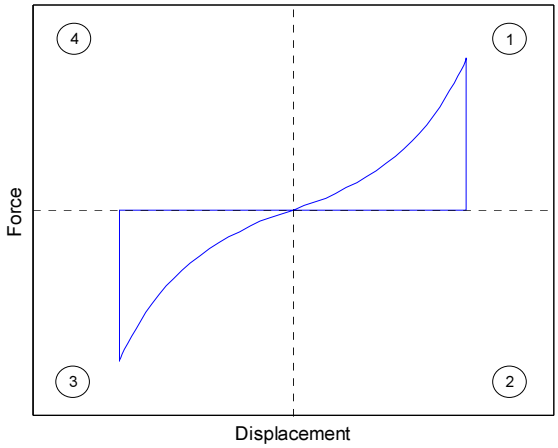

(b) 1-3 control law

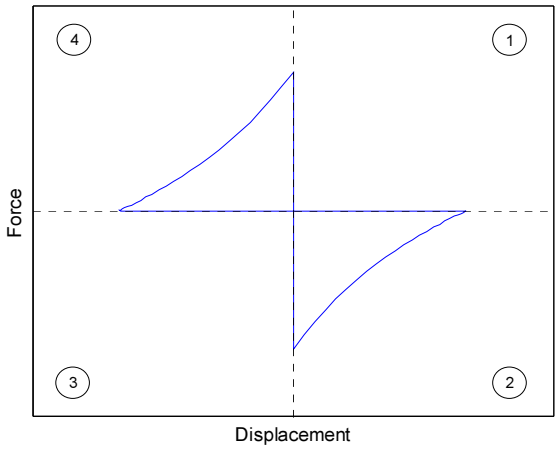

(c) 2-4 control law

Figure 7.3 Control laws.

Although the presence of the device friction was evident during the seismic testing of the one-fifth scale structure, the friction of the resettable device used in this analytical research is not taken into account. This is due to the lack of information to accurately quantify the amount of friction that will be present in full-scale resettable devices. To the author's knowledge, there are not full-scale resettable devices built or being built at the present time. Therefore, the here presented model assumes that the control force delivered by the device is due to the air being pressurised and that there is no friction between the moving parts of the device (i.e. the piston rings and the inside wall of the cylinder). However, because of the fact that two or more truss element when connected in series can cause numerical instability, a friction force of 1 kN is used to maintain the stability of the spring member that simulates the resettable device.

7.3.2 Description of the Rigid Rod

The two ends of the device piston are considered to be attached to rigid rod in order to transfer the control forces to a system of pre-stressed tendons with high axial stiffness. A spring member with a linear elastic hysteresis is used to model the rigid rod. The rigid rod is required to have a large stiffness to transfer the control forces efficiently. Hence, the stiffness of the rod is considered to be 5,000,000 kN/m. The rigid rod can move in the horizontal direction freely. The rigid rod only represents a link between the device and the pre-stressed tendons and does not add stiffness to the system.

7.3.3 Description of the Pre-stressed Tendon

The control forces delivered by the resettable device are transferred to the twelve-storey building using a pre-stressed tendon attached to the rigid rod. The tendon is modelled by using a spring member that follows the bi-linear with slackness hysteresis shown in Figure 6.3. For this particular case, no compression forces and no gaps were utilised in the analyses. It is assumed that the tendon works only in tension and can develop a maximum tension force of 500 kN. The initial pre-stress level of the tendon is set at 50

kN based on results obtained from static analyses of the twelve-storey structure. The pre-stressed tendon has a stiffness of 2,500 kN/m.

It should be noted that the tendons may be slack or pre-stressed. If slack tendons are used, only one tendon of the diametrically opposed pair will work at any given time. However, if the tendon is pre-stressed the initial stiffness is increased and the pair of tendons will continue to work together. Initial pre-stressing can significantly modify the distribution of internal forces of the structural elements. Depending on the pre-stress level, the magnitude of the induced forces due to pre-stressing may reach values that approach the capacity of the members (Pekcan 1998). Therefore, this factor may impose limitations to the level of initial pre-stress and should be carefully considered in the design and particularly in retrofit applications. However, the pre-stressed force given by a static analysis of the structure provides a good indication of the pre-stress level of the tendon during the initial stages of the design. Initial pre-stressing can also reduce the problems associated with the sudden loading of the supplemental control system, as long as there is no appreciable creep or relaxation in the system.

Research has shown that when the tension is applied in later loading cycles (e.g. when the tendons are slack due to yielding) the loading may be applied abruptly and may cause high accelerations through the height of the structure. A further concern is that the structure lacks redundancy. These disadvantages of tension-only tendon systems can be overcome by pre-stressing the supplemental damping system together with the steel tendon. Depending on the initial pre-stress level, pres-stressing can prevent the system from becoming slack (Pekcan 1998).

In addition, high strength steel tendons can efficiently provide the building with lateral strength, especially when lack of strength and stiffness are the main deficiencies of an existing building. An increase in stiffness usually means an increase in storey shear forces. However, in actual applications, the shear forces can be safely transferred to the foundation level by the pre-stressed tendons. For this purpose, the tendons can be attached to specially designed anchorages built apart from the structure. Moreover, the tendons could be stressed and then encased in fireproof ducts filled with concrete.

7.4 EARTHQUAKE RECORD AND CONTROL LAW

In the following sections, two-dimensional nonlinear time-history analyses using the computer program RUAUMOKO are performed to examine the effectiveness of the semi-active resettable devices in reducing the seismic response of the twelve-storey reinforced concrete structure.

The north-south component of the 1940 El Centro earthquake is adopted as the input ground motion in the computer analyses. However, the 1952 Taft S21W, 1994 Sylmar County and 1995 Kobe N00E earthquake records are utilised in Section 7.6.3 as well. Apart from Section 7.7, the 1-2-3-4 control law is selected to simulate the hysteretic behaviour of the resettable device.

The seismic performance of the structure is evaluated in terms of reductions in relative displacements, absolute accelerations, inter-storey drift ratios and total base shear, which includes the contribution of the pre-stressed tendons to the seismic response. The results are presented for comparison to the structure without resettable devices installed and referred to as the uncontrolled structure or system A (Fig. 7.1).

7.5 IMPACT OF THE DISTRIBUTION AND NUMBER OF DEVICES

The objective of this initial study is to investigate the effects of the distribution and number of resettable devices on the seismic response of the twelve-storey reinforced concrete building. The control forces are applied via pre-stressed tendons between the floor where the device is placed on and the respective upper floors. The tendons span the two horizontal bays. Rigid rods attached to the two piston ends are used to transfer the control forces from the device to the tendon system.

The adequate distribution of energy dissipation devices in tall buildings is essential, since a poor placement of the devices can be detrimental to the dynamic response by changing the balance of structural modes in the response (Hunt 2002). Four different

arrangements are used to assess the impact of the device distribution on the seismic response of the building, Computer simulations are carried out to investigate the effect of one, two, three and four devices distributed through the height building (Franco-Anaya et al. 2008b).

Figure 7.4 shows the systems considered for this investigation. In the system A1 the resettable device is located on the ground level of the building and the device forces are transferred via tendons between the ground level and level 12. For the system A2 one resettable device is placed on the ground level and a second device is located on level 6. In the system A3 three devices are installed on the ground level, level 4 and level 8, respectively. Four resettable devices located on the ground level, level 3, level 6 and level 9, respectively, are considered for the system A4. These four arrangements are selected primarily to determine whether it is necessary to have devices attached to each floor when controlling the seismic response of tall buildings.

It is important to note that the control force on the floor considered is in fact the force within the pre-stressed tendon. Therefore, the actual control forces applied to the structure are reduced by the cosine of the angle of the tendon.

Figure 7.5 shows the overall benefits of the different device distributions in reducing the earthquake response of the twelve-storey reinforced concrete building. The maximum response envelopes indicate that the seismic response is reduced by all of the systems. Systems A1 and A2 show a very similar performance in reducing the maximum relative displacements and inter-storey drift ratios. The maximum absolute accelerations in some levels are slightly reduced by all of the systems. All of the systems increase the maximum total base shear slightly.

It can be seen that increasing the number of devices does not improved the seismic performance of the structure. For instance, the response reductions achieved by the system A4 with four devices installed are less significant than those obtained by the system A1 that only uses one resettable device. This effect caused by actuator-actuator interaction was properly recognised by Hunt (2002).

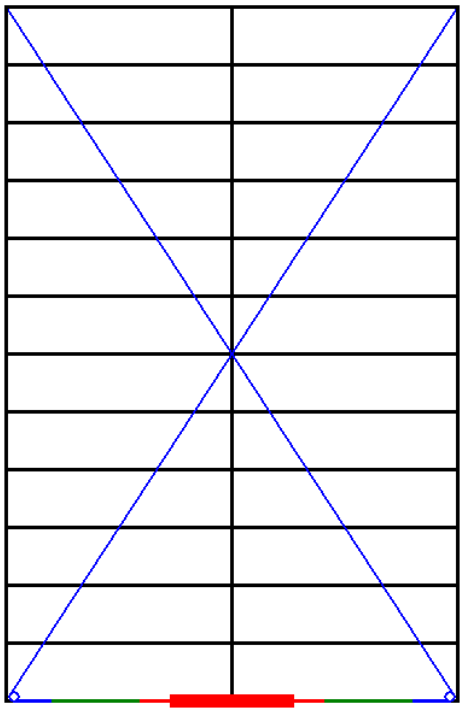

(a) System A1

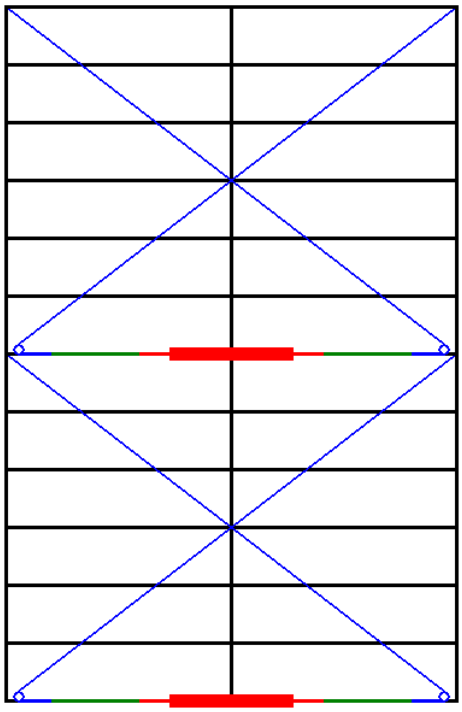

(b) System A2

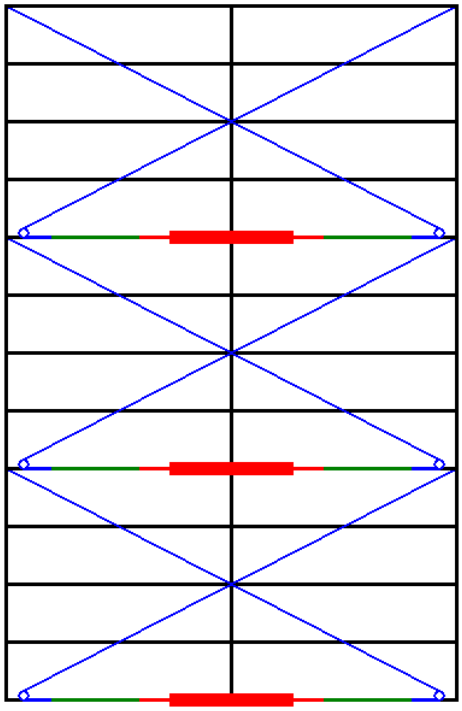

(c) System A3

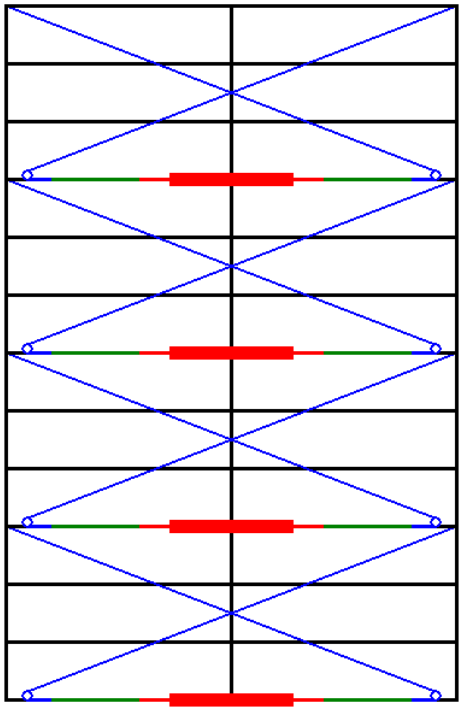

(d) System A4

Figure 7.4 Distribution of the resettable devices.

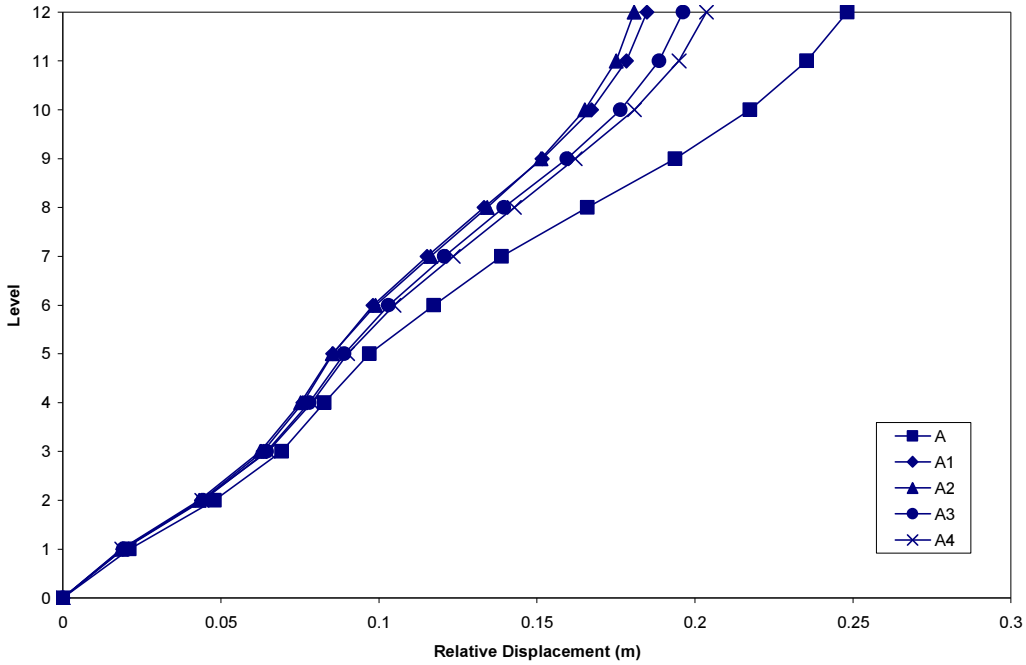

(a) Maximum relative displacements

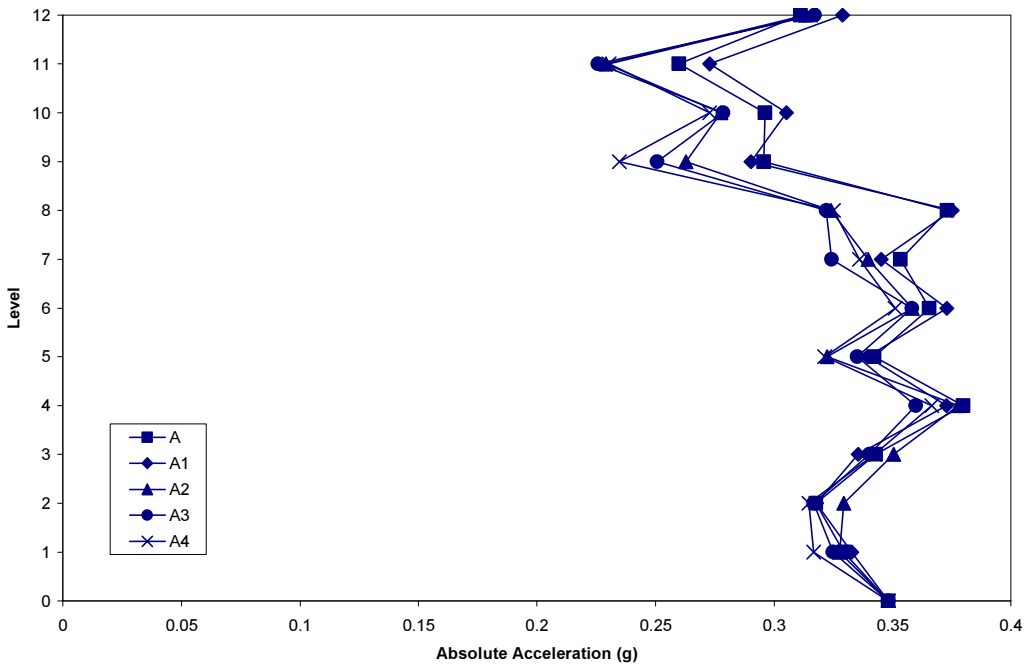

(b) Maximum absolute accelerations

Figure 7.5 Effect of the distribution and number of devices.

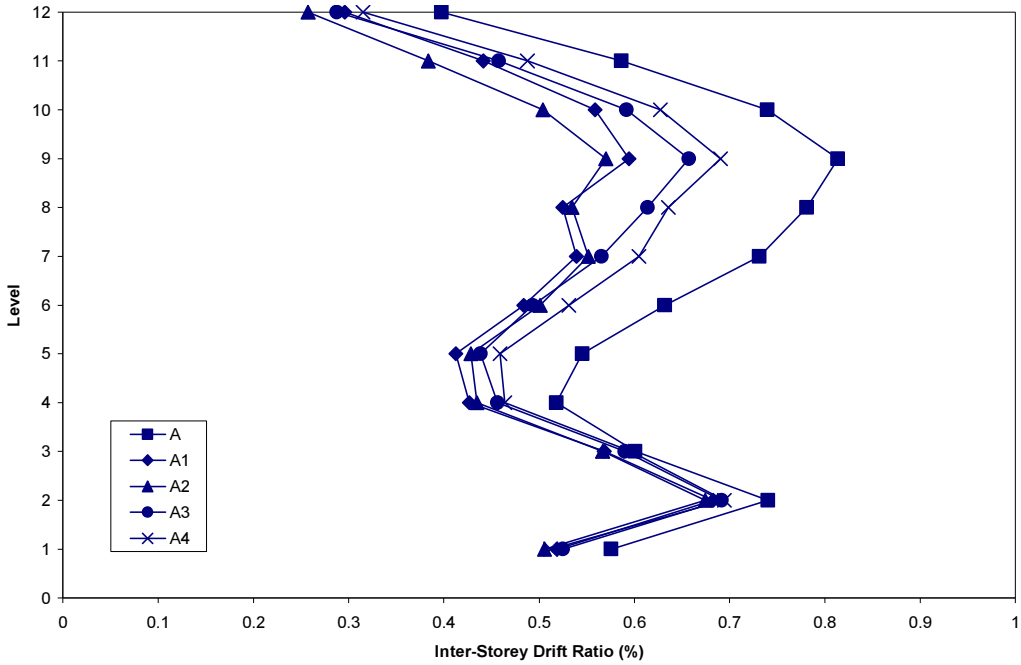

(c) Maximum inter-storey drift ratios

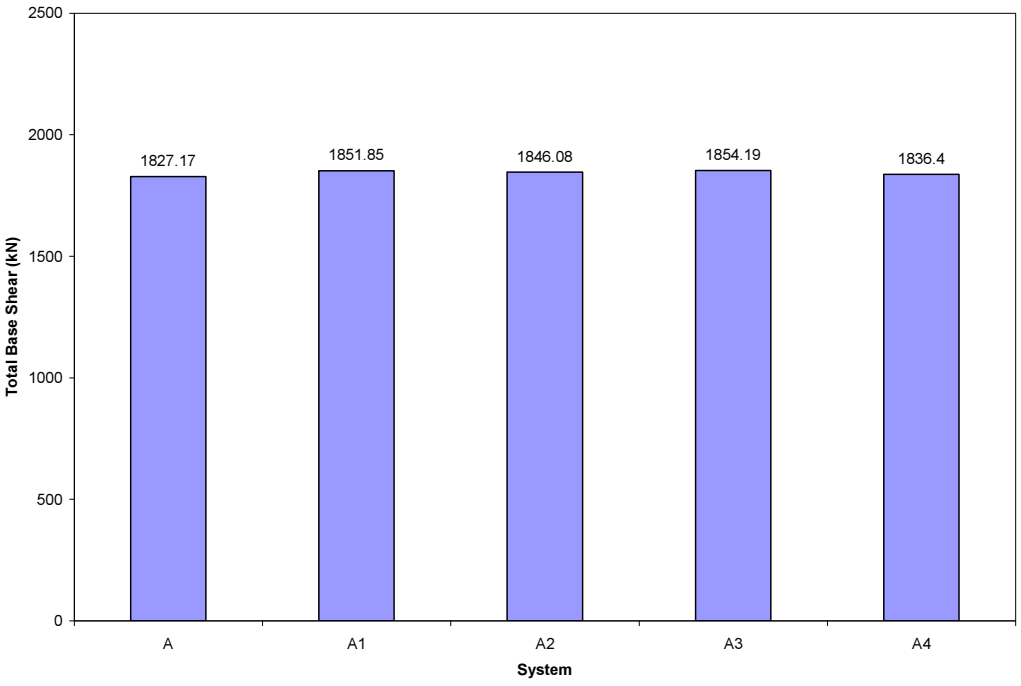

(d) Maximum total base shear

Figure 7.5 (Continued).

This effect reflects the influence of higher modes on the seismic response and requires adjustment of how the control laws are designed and implemented for tall structures. In structures with higher modal contributions, the devices placed on adjacent floors may in fact have a negative impact due to the equal and opposite reaction forces applied to the floors on which they are placed. When higher modes are present, the velocity of the floors may be slightly out of phase. Therefore, the resettable device may actually apply control forces for which the reaction forces increase the response of some of the floors while attempting to restrict others. Furthermore, with devices installed on each floor, the reaction forces can cancel out the effect of the device below and, thus, accelerate certain floors away from their equilibrium position (Chase et al. 2005c, Hunt 2002).

7.6 IMPACT OF THE TENDON CONFIGURATION

In this study, four tendon configurations are investigated to assess the effects of the resettable devices on the seismic response of the twelve storey building. These tendon configurations showed the best performance among a large number of other tendon configurations investigated. The control forces delivered by the device are applied by means of pre-stressed tendons. The pres-stressed tendons span the two bays of the building. Rigid rods are used to transfer the control forces from the device to the tendon system.

7.6.1 Seismic Response of the Tendon Configurations

The different tendon configurations examined in this research are shown in Figure 7.6. In the system A1-12 the devices are not placed between individual floors to avoid the cancelling of control forces due to higher modal contributions. Instead, one resettable device is installed on the ground level and the control forces are applied to each level of the structure by using pre-stressed tendons connected to the device piston. Reduction of the control forces due to the tendon angle is minimised by installing the tendons along the two bays of the structure. The system A1-12 is shown in Figure 7.6a. Although the

system A1-12 represents a very impractical and uneconomical solution, it removes the possibility of actuator-actuator interaction, since all response measurements and reaction forces are relative to the ground floor.

The system A1_2 shown in Figure 7.6b utilises one resettable device installed on the ground floor and has two pre-stressed tendons attached between the ground and level 12 of the building. The pre-stressed tendons span through the two horizontal bays. This system also eliminates the detrimental effects of the actuator-actuator interaction by using only one resettable device. Research has shown that supplemental damping devices installed on the ground floor are not effective in reducing the seismic response of upper storeys of the structure. On the contrary, the deformations of the upper storey tend to amplify (Pekcan 1998). However, this "whipping" effect can be reduced by using conventional bracing systems in the upper storeys or by installing a tuned mass damper (TMD) at the top of the building. The system A1_2 utilises two pre-stressed bracing systems to minimise the effects of the upper storey whipping. One bracing system is installed on the lower half and the other bracing system is placed on the upper half of the building. The bracing systems are placed along the two bays of the twelve-storey reinforced concrete structure.

It was shown in the previous section that the system A2 can reduce the maximum relative displacement and inter-storey drift efficiently by using two resettable devices. Based on this finding, the system A2_1 shown in Figure 7.6c employs two devices to control the seismic response of the moment-resisting frame structure. One of the devices is placed on the ground with pre-stressed tendons attached to the level 6. Other device is located on the level 6 and has pre-stressed tendons attached to the top of the building. In addition, a large pre-stressed bracing system installed between the ground floor and the top of the building provides additional stiffness to the structure. The bracing and tendon systems span through the entire width of the building. This system intends to avoid the use of a huge device needed to provide large control forces by having two smaller devices evenly distributed through the height of the structure instead.

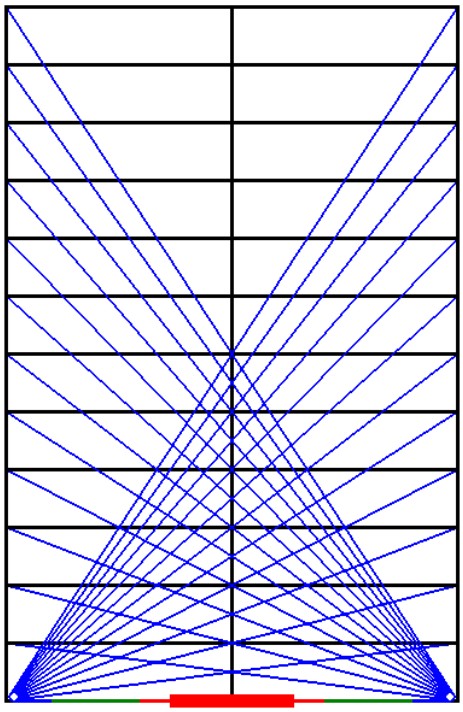

(a) System A1-12

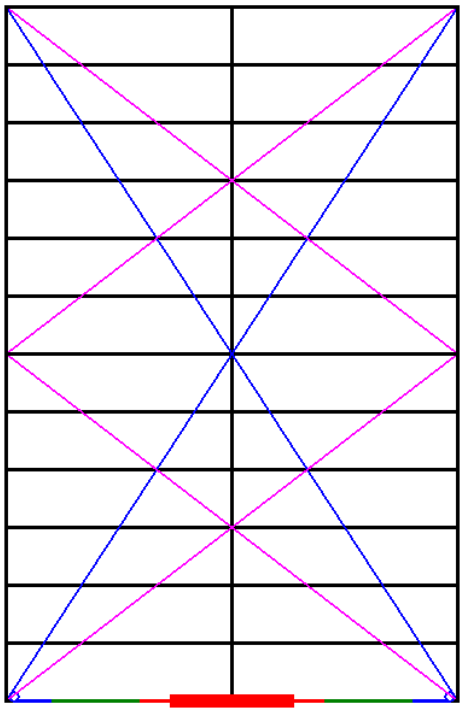

(b) System A1_2

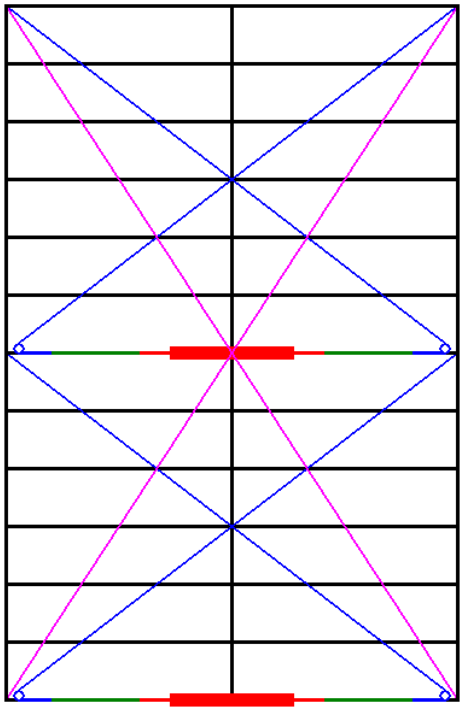

(c) System A2_1

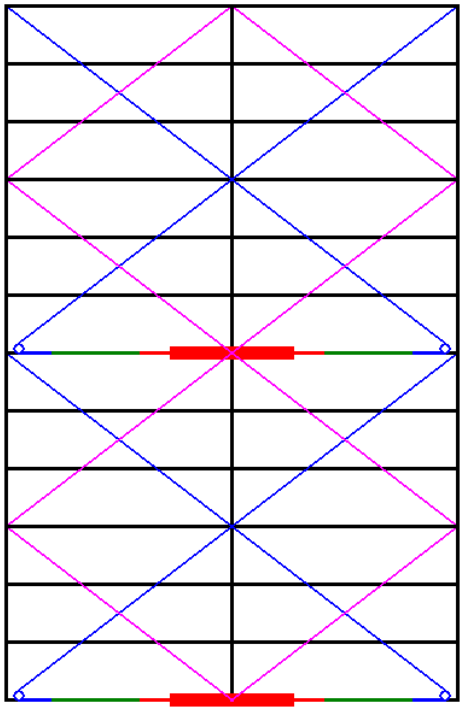

(d) System A2_3

Figure 7.6 Tendon systems for the twelve-storey building.

The system A2_3 has similar device distribution and tendon configuration to the system A2_1. However, the system A2_3 has three bracing systems distributed along the height of the building instead of having only one bracing system. A main bracing system is placed between level 3 and level 9; and two secondary bracing systems are located between the ground and level 3, and between level 9 and level 12, respectively. The objective of this configuration is to examine the effect of the number of pre-stressed bracings in the seismic response of the structure. System A2_3 is shown in Figure 7.6d.

The bracing systems of the systems A1_2, A2_1 and A2_3 are modelled by utilising a spring member. The bi-linear with slackness hysteresis is used to simulate the behaviour of the bracing. No compression forces and no gaps are used in this investigation. Like the pre-stressed tendon, the bracing system works in tension only and can develop a maximum tension force of 500 kN. The bracing element has an initial pre-stress level of 50 kN and a stiffness of 2,500 kN/m.

Figure 7.7 shows maximum response envelopes for the tendon systems obtained from the computer simulations. It can be seen that all of the considered systems reduce the seismic response of the twelve-storey frame structure. System A1-12 shows the best performance in reducing the maximum relative displacement and inter-storey drift ratios. A very similar performance is shown by systems A1_2 and A2_2 in reducing the maximum relative displacements and inter-storey drift ratios. All of the systems reduce the maximum absolute accelerations in some levels of the structure. Systems A1-12, A1_2 and A2_1 increase the maximum total base shear. System A2_3 slightly reduces the maximum total base shear.

Although the response reductions achieved by the system A1-12 are significant, the additional stiffness provided by the pre-stressed tendons greatly contributes to the improvement of the seismic response. It should be noted that the elaborate distribution and large number of the pre-stressed tendons prevent the system A1-12 from being implemented in actual multi-storey buildings.

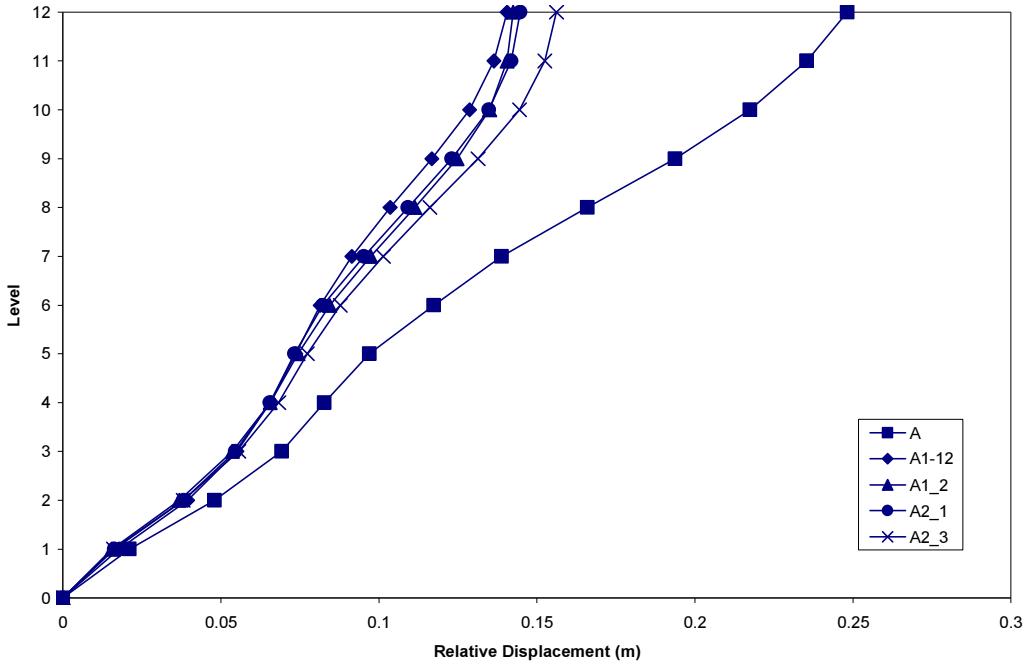

(a) Maximum relative displacements

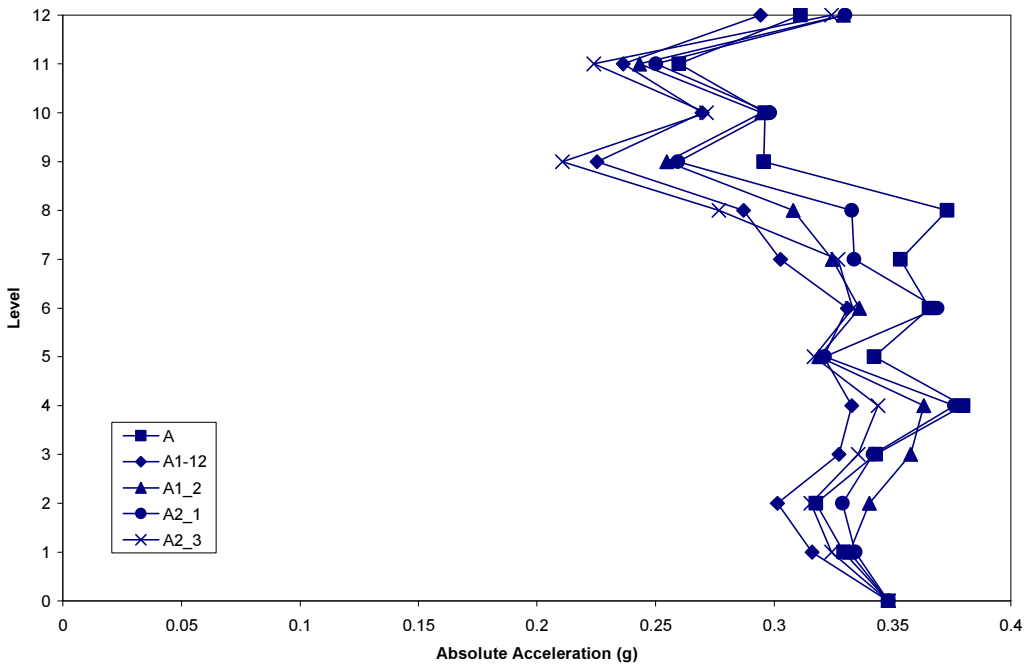

(b) Maximum absolute accelerations

Figure 7.7 Effect of the tendon configuration.

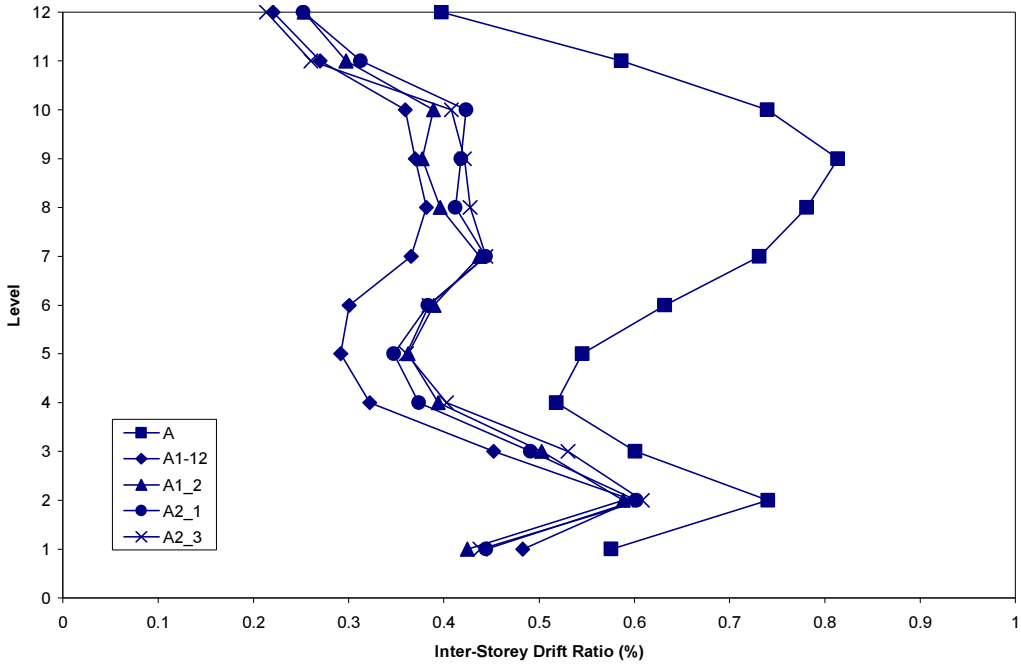

(c) Maximum inter-storey drift ratios

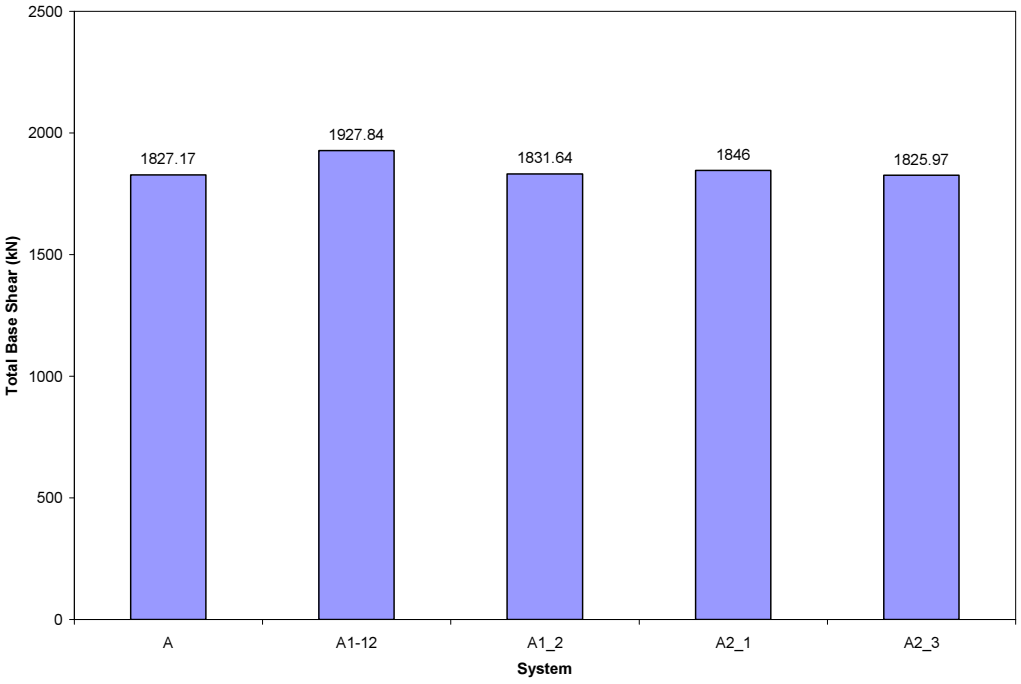

(d) Maximum total base shear

Figure 7.7 (Continued).

7.6.2 Contribution of the Pre-stressed Tendons and Bracing Systems to the Seismic Response Reduction of System A2_3

Since the pre-stressed tendons and the bracing systems provide additional stiffness and damping to the control system, it is of interest to investigate their overall contribution to the seismic response reduction of the twelve-storey reinforced concrete structure. The pre-stressed tendons are used to transfer the control forces produced by the resettable device to the structure. The bracing systems minimise the effects of the upper storey whipping and provide additional stiffness to the multi-storey structure. The system A2_B shown in Figure 7.8 is adopted to evaluate the contribution of the pre-stressed tendons and bracing systems to the seismic response reduction.

System A2_B has neither resettable devices nor rigid rods installed. The arrangement of the pre-stressed tendons and the bracing systems is similar to that of the system A2_3 shown in Figure 7.6d. The pre-stressed tendons and bracing systems are placed along the two horizontal bays of the building. Two pre-stressed tendon systems are installed along the height of the building. One pre-stressed tendon system is installed on the lower half and the other one is placed on the upper half of the building. Three bracing systems are distributed within the building's height. A main bracing system is located between level 3 and level 9; and two secondary bracing systems are placed between the ground floor and level 3, and between level 9 and level 12, respectively.

The pre-stressed tendon and the bracing of system A2_B are modelled utilising a spring member. The bi-linear with slackness hysteresis shown in Figure 6.3 is used to simulate the behaviour of the pre-stressed tendon and the bracing. No compression forces and no gaps are utilised in the computer analyses. The pre-stressed tendon and bracing work in tension only and are able to develop a maximum tension force of 500 kN. The initial pre-stress level is assumed to be equal to 50 kN. The nominal stiffness of the spring member is considered to be 2,500 kN/m. The same values were used in Section 7.6.1 for the modelling of the pre-stressed tendon and bracing of the System A2_3.

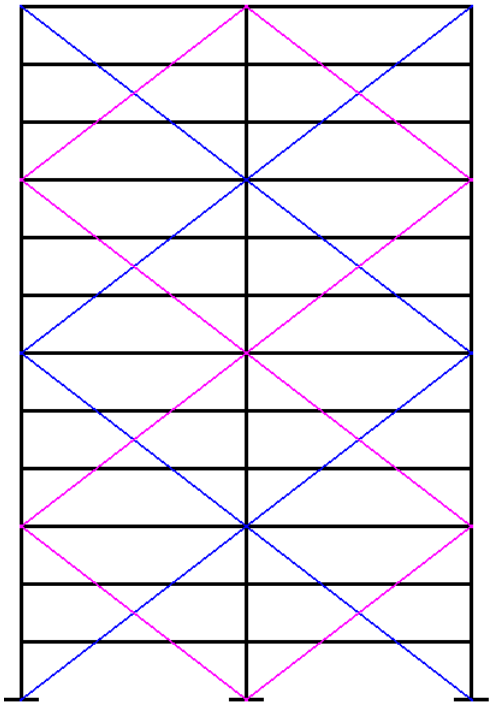

Figure 7.8 System A2_B.

Maximum response envelopes of the systems A, A2_3 and A2_B are compared in Figure 7.9 for the 1-2-3-4 control law under the north-south component of the El Centro earthquake. The comparisons show that the average contributions of the pre-stressed tendons and bracing systems to the reduction of the maximum relative displacements and inter-storey drift ratios are 43% and 61%, respectively. However, the maximum absolute accelerations are increased by up to 4% on average and the maximum total base shear is increased by up to 2%.

These results show the significant contribution of the pre-stressed tendons and bracing systems to the reduction of the seismic response, especially to the reduction of the inter-storey drifts. However, the use of the pre-stressed tendons and bracing systems without resettable devices increases the accelerations and the total base shear. In contrast, the system A2_3 with two resettable devices installed not only reduces the displacements and inter-storey drifts but also the accelerations and the total base shear. These results highlight the ability of the resettable devices combined with pre-stressed tendons and bracings to reduce the floor displacements and inert-storey drifts without increasing the floor accelerations and the base shear demand significantly.

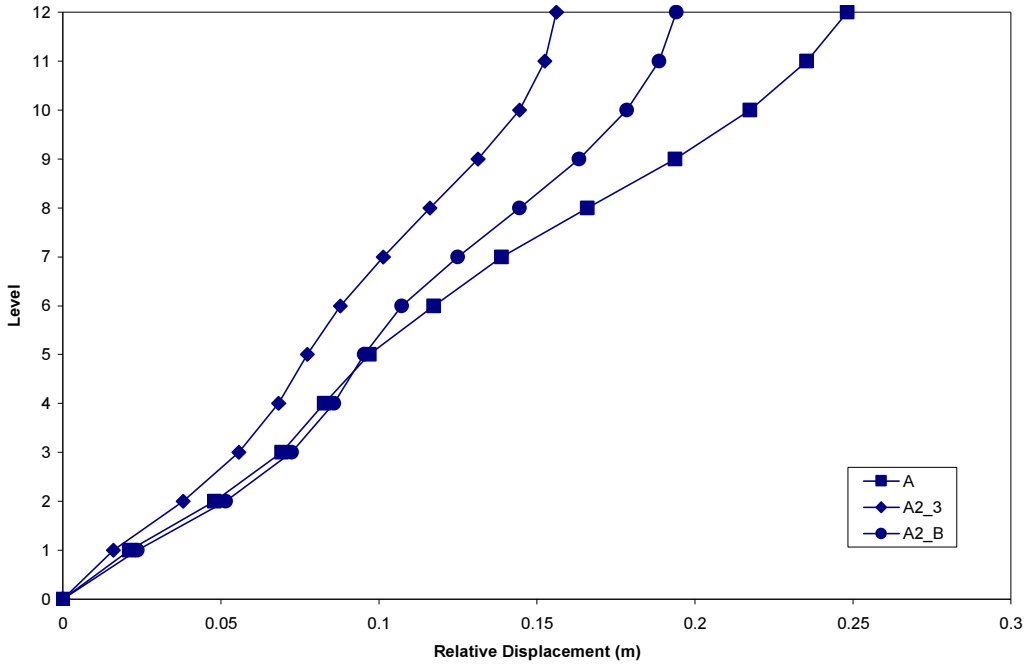

(a) Maximum relative displacements

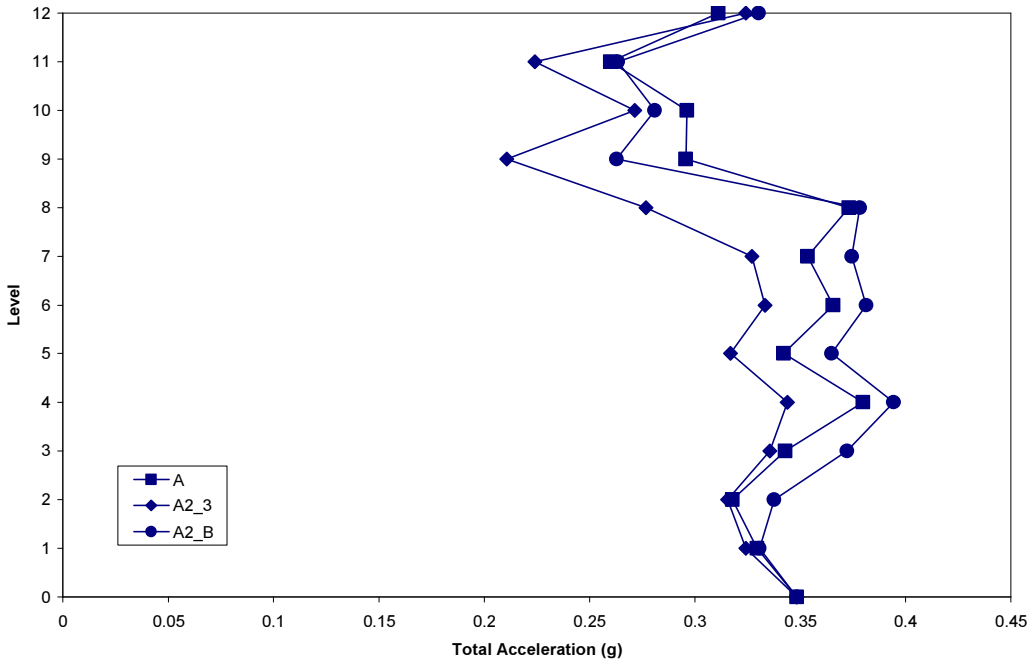

(b) Maximum absolute accelerations

Figure 7.9 Contribution of system A2_B to the seismic response reduction.

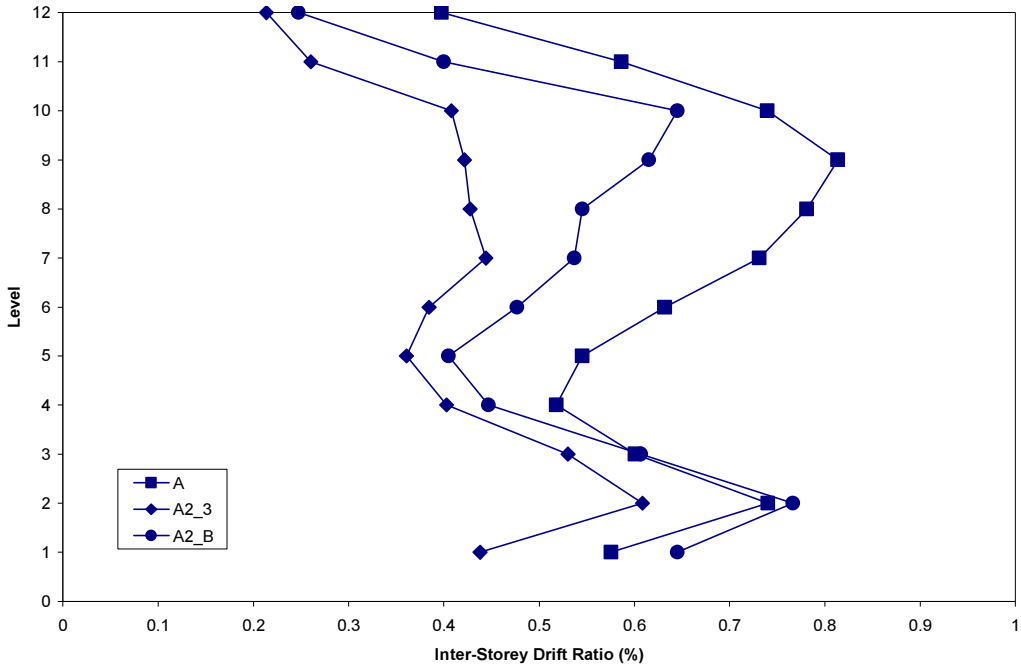

(c) Maximum inter-storey drift ratios

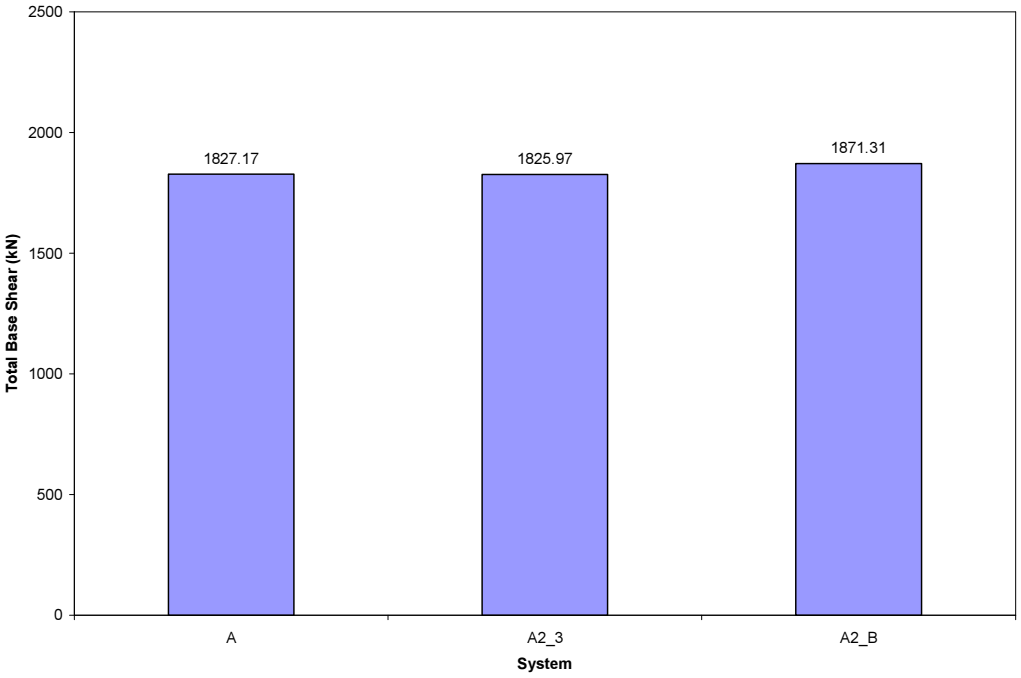

(d) Maximum total base shear

Figure 7.9 (Continued).

7.6.3 Response of System A1_2 under Different Earthquakes

The correct selection and design of the energy dissipation device are essential to ensure the reduction of the structural response under severe seismic events. However, for structures subjected to impulse-type earthquake ground motions, there are other factors that should be considered in the design. It is well known that even a slight increase in the damping value may be significantly beneficial for flexible structures with small inherent viscous damping. However, pulse-type ground motions can result in an early peak response, which can be practically impossible to control by using conventional damping systems. This behaviour is a unique feature of near-field ground motions. In general, near-field motions produce high acceleration, velocity and displacement responses over the long-period range. Under such seismic loads, excessive deformations may accumulate in the lower storeys of flexible structure, which in turn may cause structural collapse (Pekcan 1998, Yang and Agrawal 2002).

In this section, the seismic performance of the system A1_2 shown schematically in Figure 7.6b is examined for four different earthquake ground motions. This system represents an efficient and economical solution in comparison to the other tendon systems considered. The following earthquake records are used to evaluate the seismic response of system A1_2:

e. Imperial Valley, 18 May 1940 – El Centro north-south (NS) component
f. Kern County, 21 July 1952 – Taft S21W component
g. Northridge, 17 January 1994 – Sylmar County Hospital (Chan 9: 0 deg) scaled by 70% (0.5583g).
h. Kobe, 17 January 1995 – JMA Observatory N00E component.

Maximum response profiles of system A1_2 under the different earthquake records are shown in Figures 7.10 to 7.13. The 1-2-3-4 control law is used to model the hysteretic behaviour of the resettable device. The seismic response of system A1_2 is compared to the response of system A (uncontrolled structure).

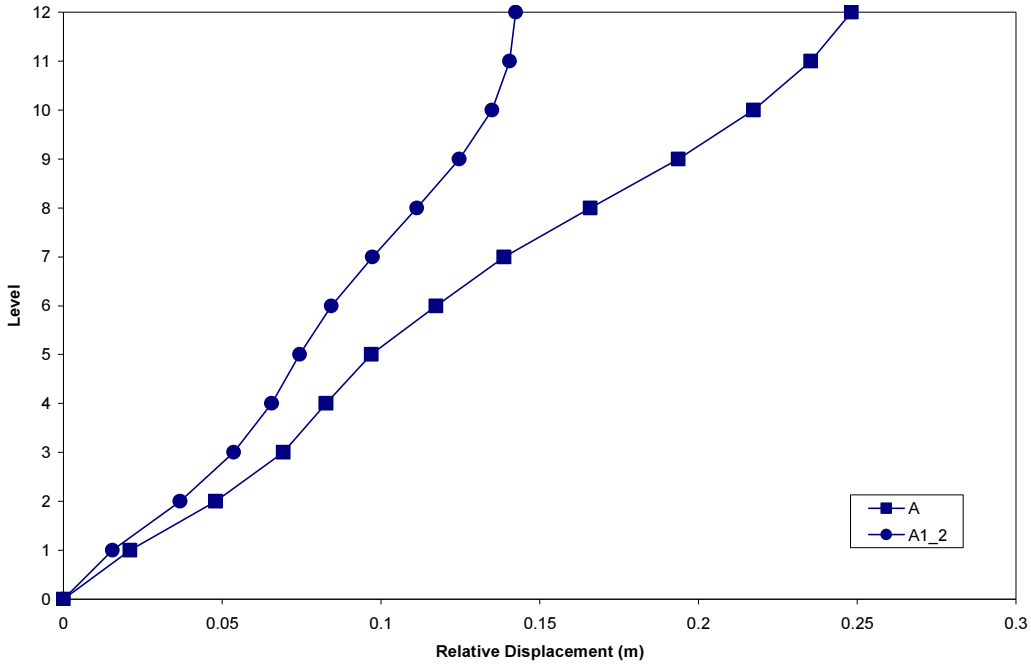

(a) Maximum relative displacements

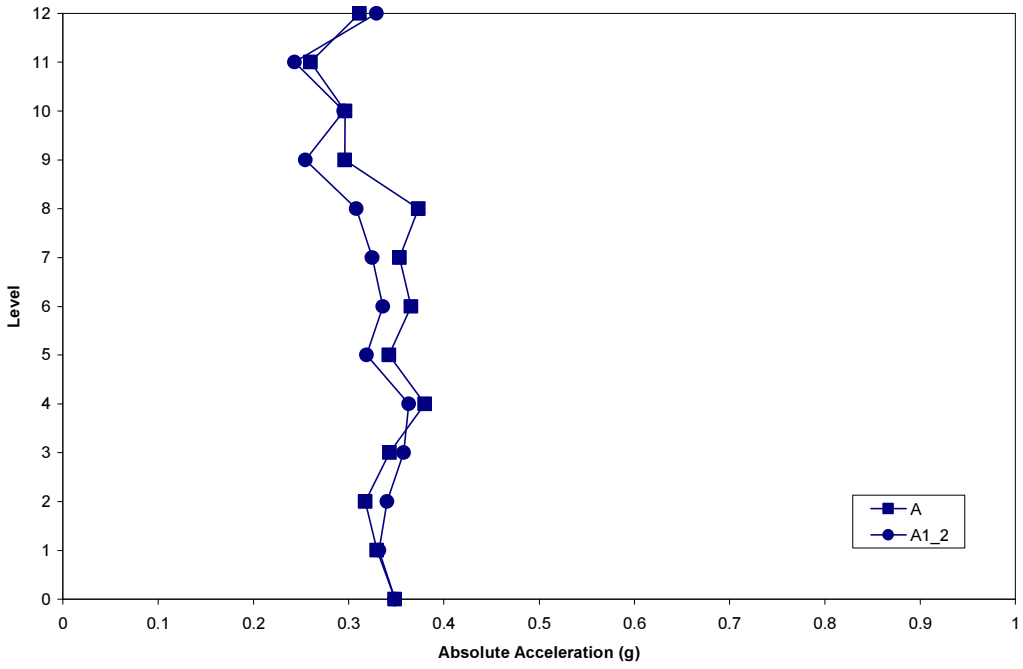

(b) Maximum absolute accelerations

Figure 7.10 Maximum response envelopes for El Centro earthquake.

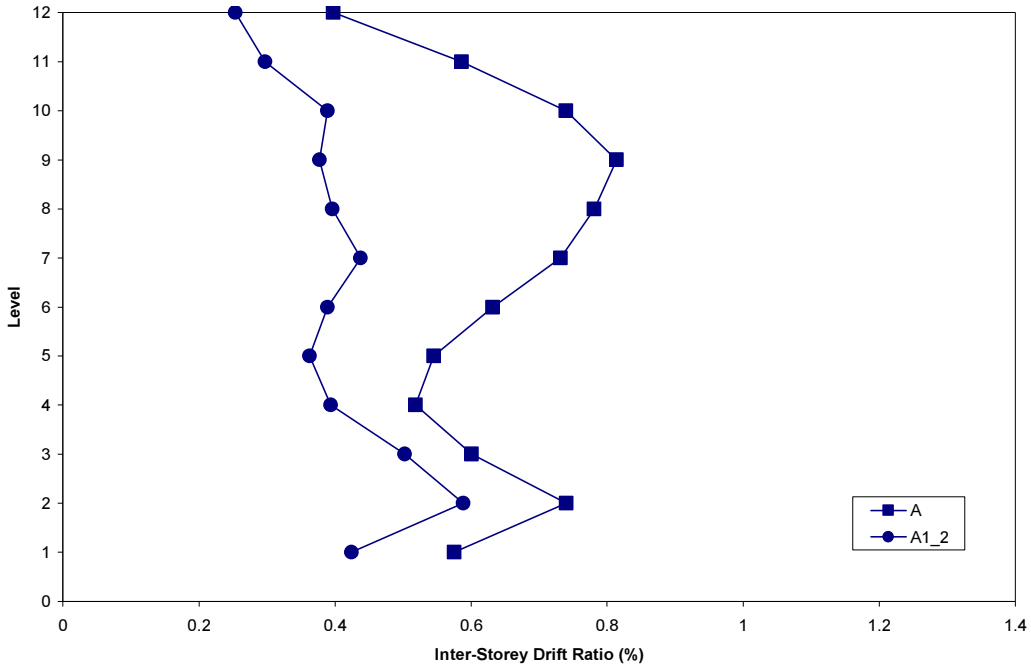

(c) Maximum inter-storey drift ratios

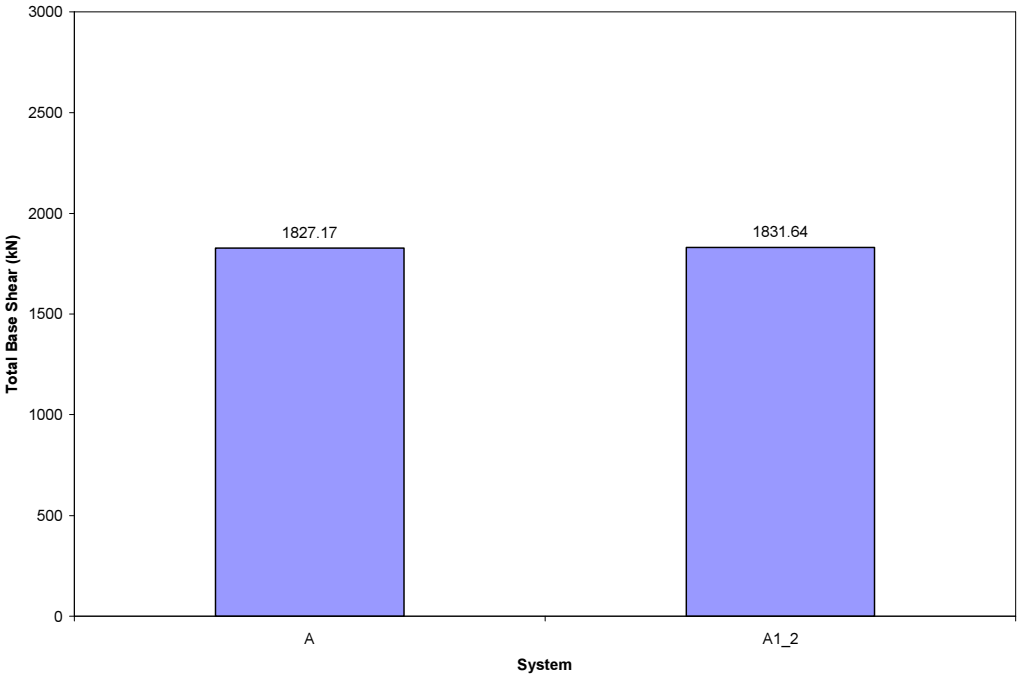

(d) Maximum total base shear

Figure 7.10 (Continued).

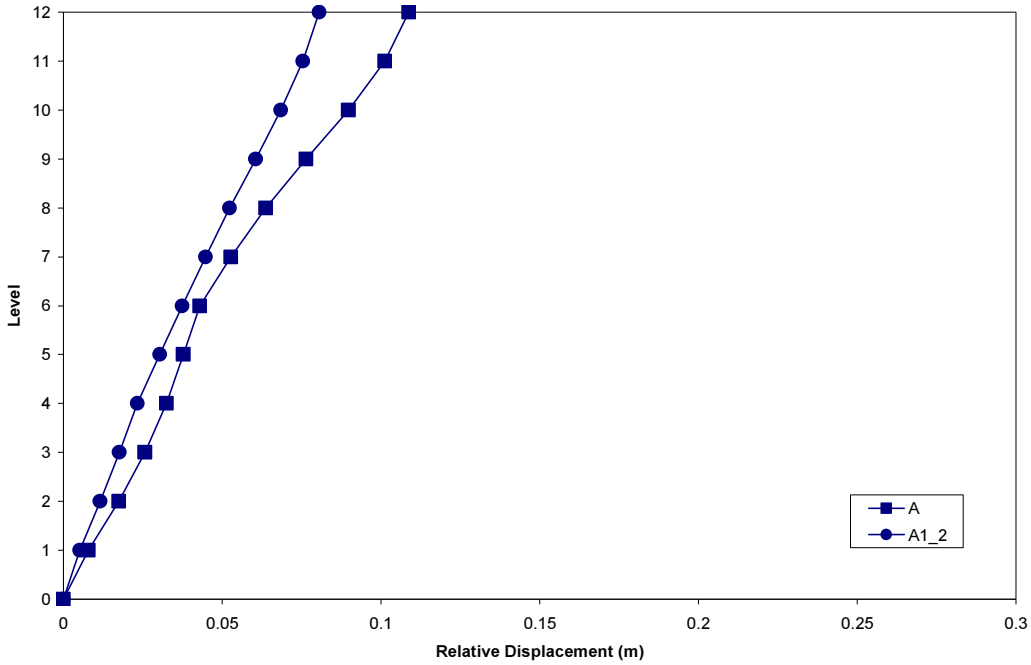

(a) Maximum relative displacements

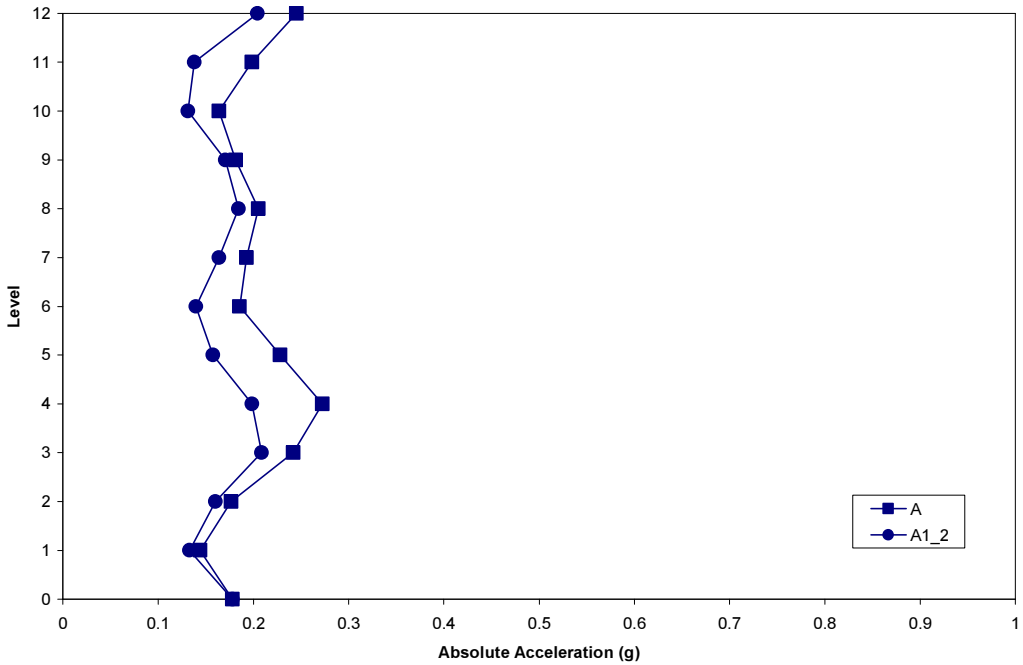

(b) Maximum absolute accelerations

Figure 7.11 Maximum response envelopes for Taft earthquake.

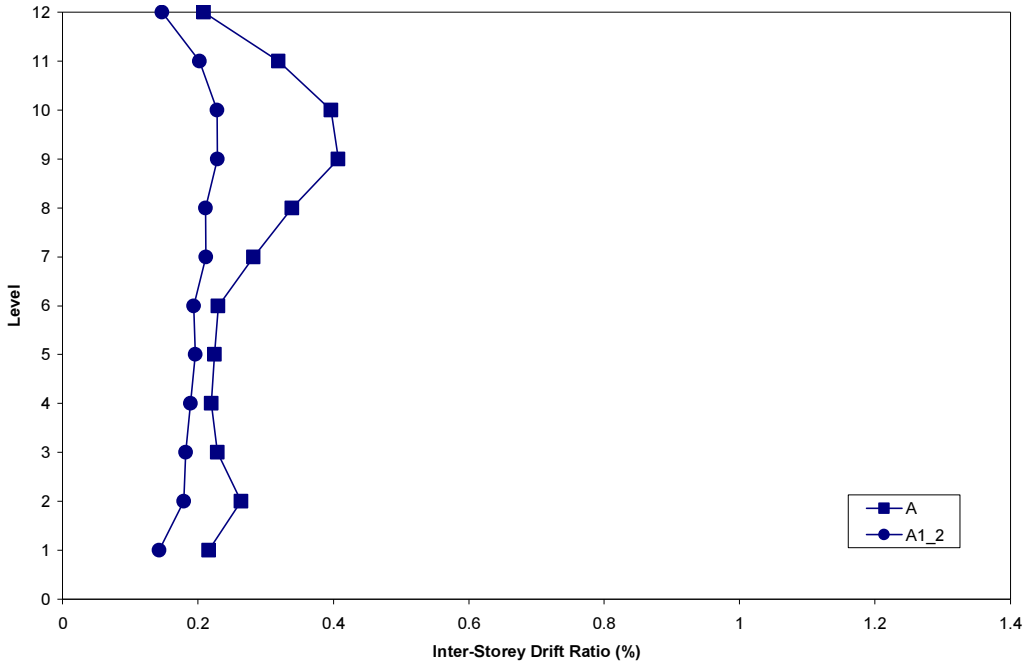

(c) Maximum inter-storey drift ratios

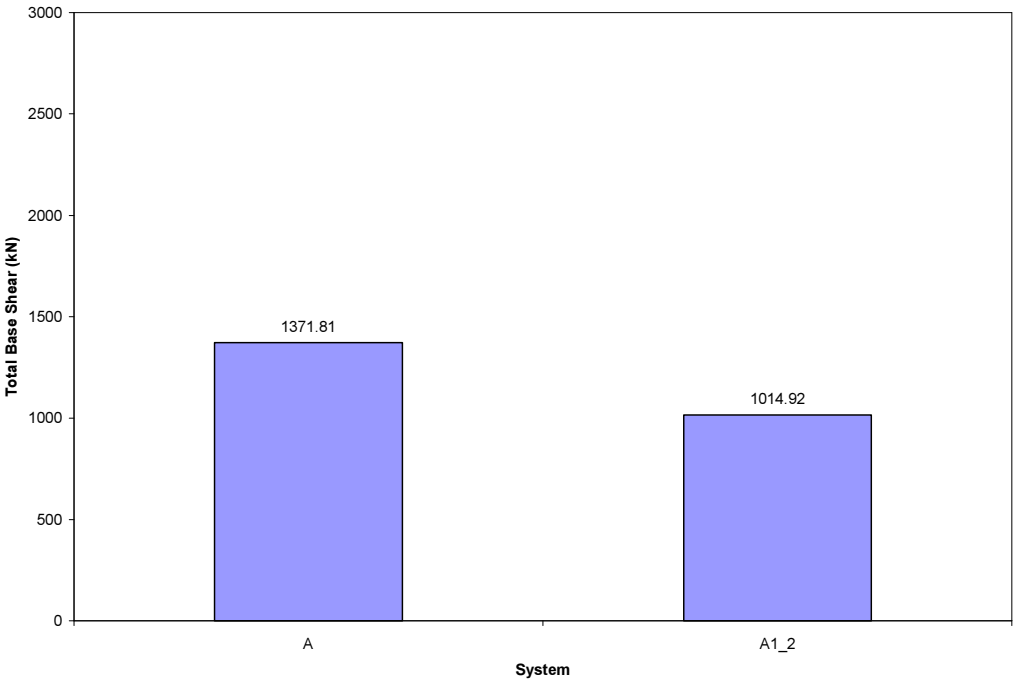

(d) Maximum total base shear

Figure 7.11 (Continued).

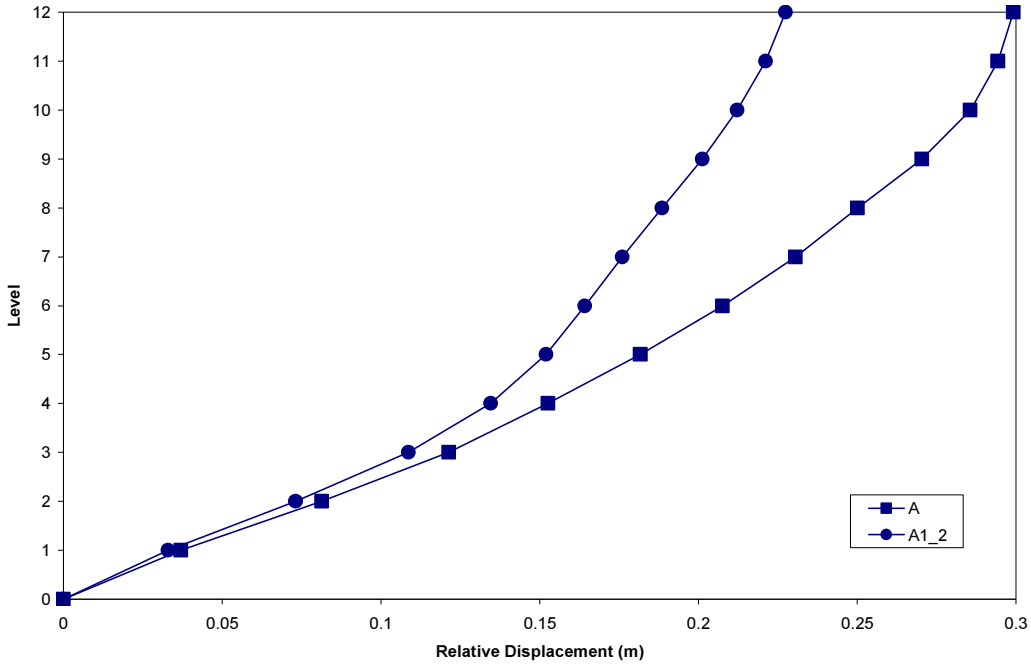

(a) Maximum relative displacements

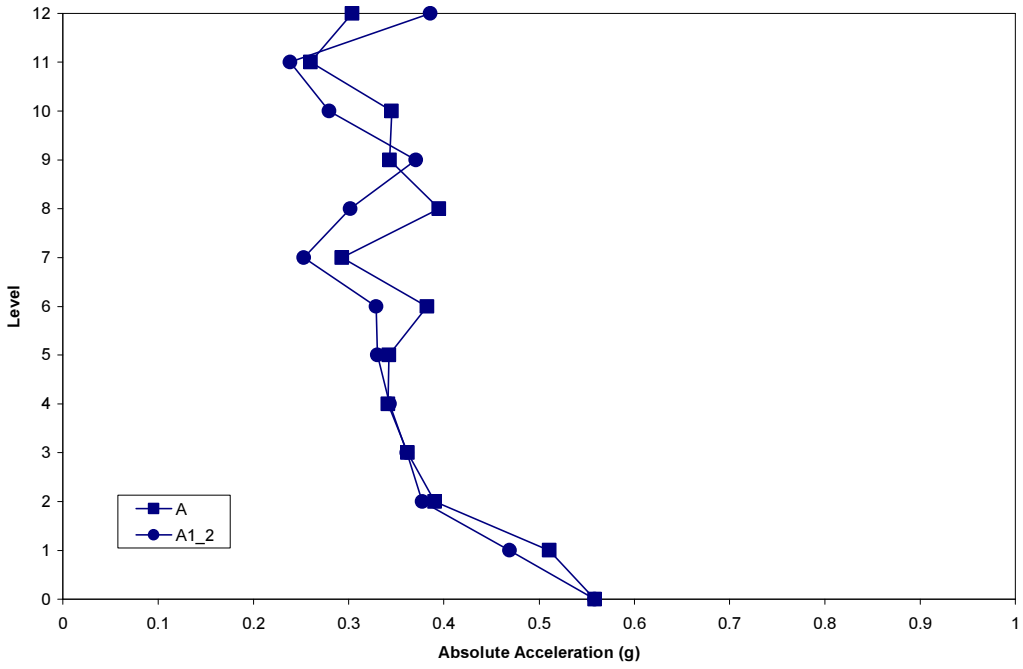

(b) Maximum absolute accelerations

Figure 7.12 Maximum response envelopes for Sylmar 70% earthquake.

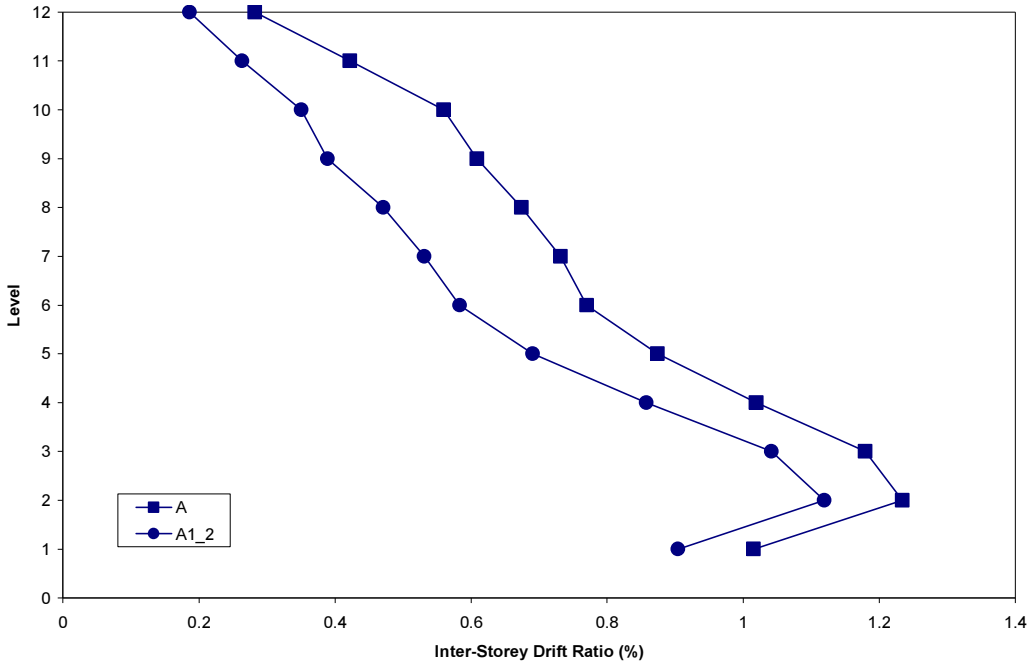

(c) Maximum inter-storey drift ratios

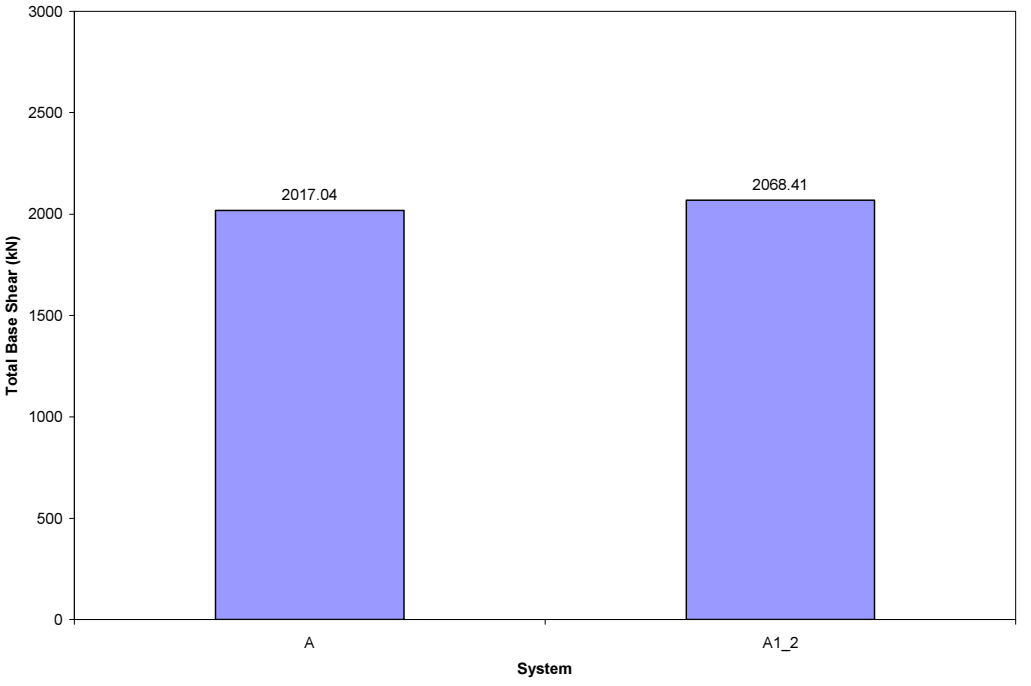

(d) Maximum total base shear

Figure 7.12 (Continued).

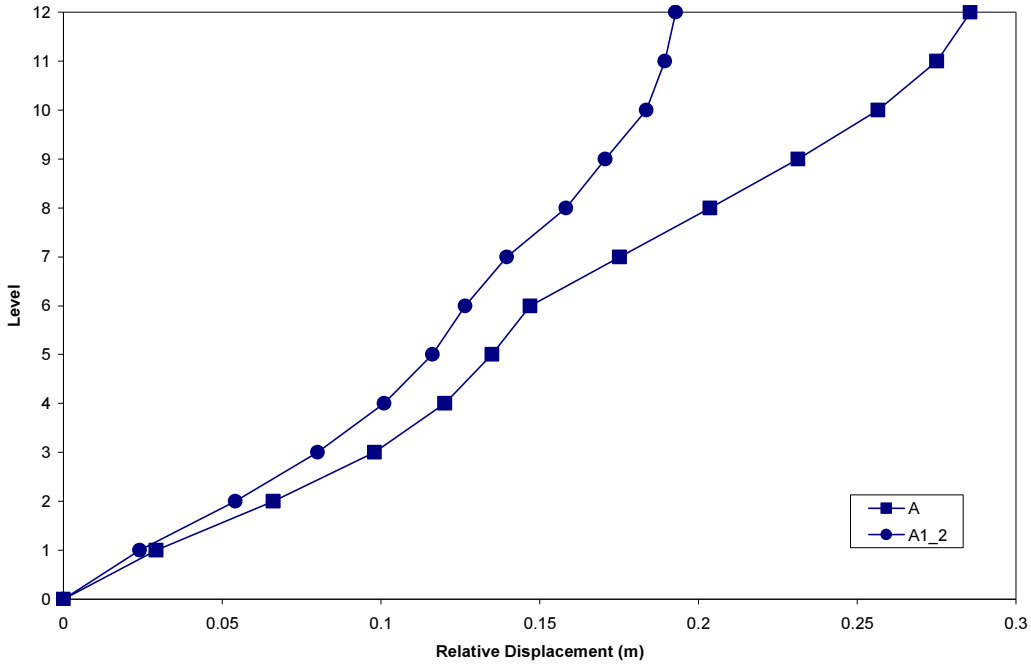

(a) Maximum relative displacements

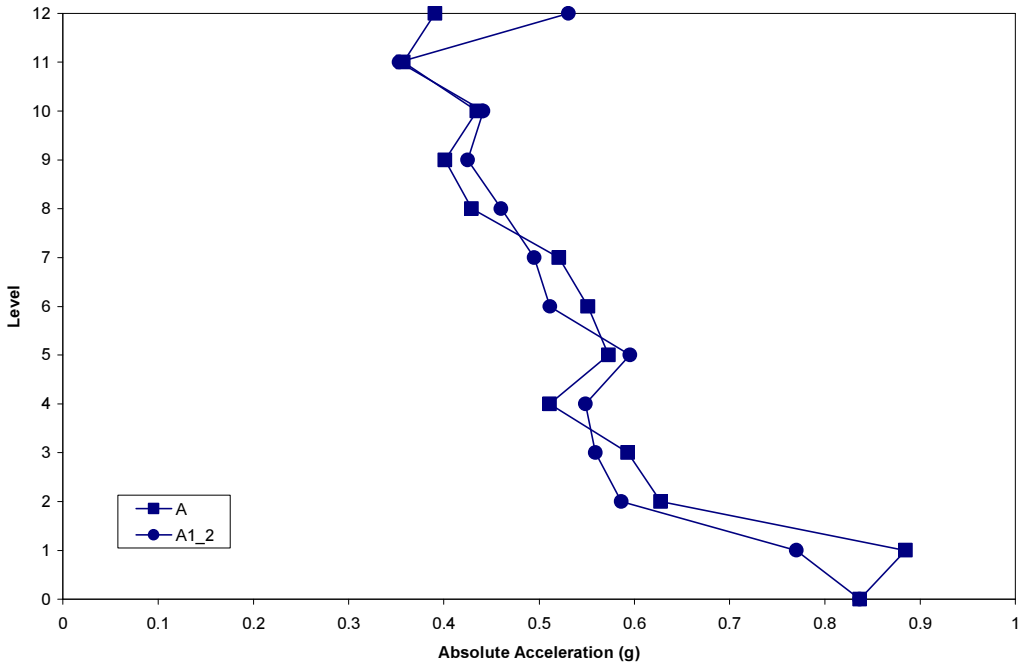

(b) Maximum absolute accelerations

Figure 7.13 Maximum response envelopes for Kobe earthquake.

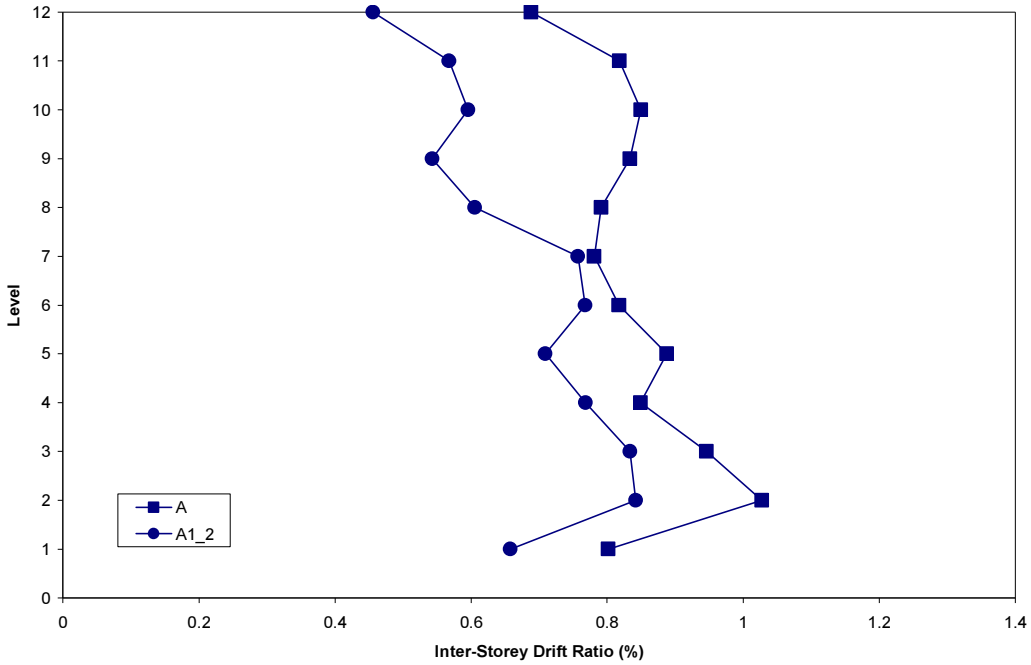

(c) Maximum inter-storey drift ratios

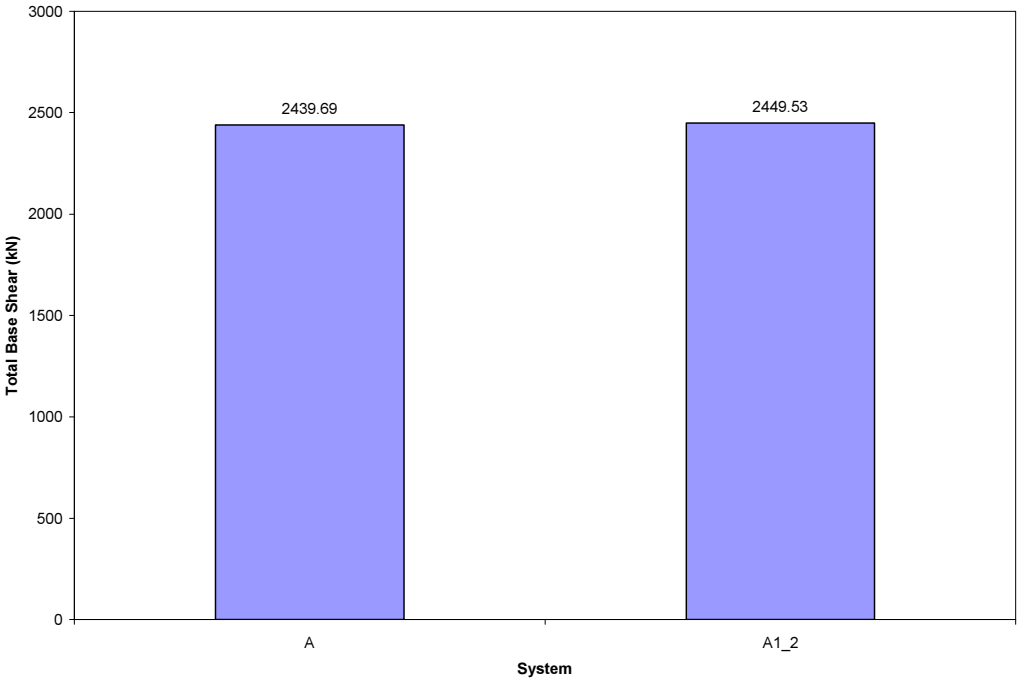

(d) Maximum total base shear

Figure 7.13 (Continued).

Figure 7.10 shows maximum response profiles for the north-south component of the 1940 El Centro earthquake record. A reduction of up to 43% in the maximum relative displacement at level 12 is observed. The maximum absolute acceleration at level 4 is reduced by up to 4%. A 54% reduction in the maximum inter-storey drift ratio at level 9 is achieved. However, the maximum total base shear is slightly increased by up to 0.2%.

Maximum response profiles are shown in Figure 7.11 for the S21W component of the 1952 Taft earthquake record. The maximum relative displacement at level 12 is reduced by up to 26%. A 27% reduction in the maximum absolute acceleration at level 4 is observed. The maximum inter-storey drift ratio at level 9 is reduced by up to 44%. A reduction of up to 26% in the maximum total base shear is achieved.

Figure 7.12 shows maximum response profiles for the Sylmar County 1994 acceleration record scaled by 70% of its actual intensity. A 24% reduction in the maximum relative displacement at level 12 is achieved. The maximum absolute acceleration at level 2 is reduced by up to 8%. A 9% reduction in the maximum inter-storey drift ratio at level 2 is observed. The maximum total base shear is increased by up to 3%.

Maximum response profiles are shown in Figure 7.13 for the N00E component of the 1995 Kobe earthquake record. The maximum relative displacement at level 12 is reduced by up to 33%. A 13% reduction in the maximum absolute acceleration at level 2 is observed. The maximum inter-storey drift ratio at level 2 is reduced by up to 18%. The maximum total base shear is slightly increased by up to 0.4%.

Figures 7.10 to 7.13 show that considerable response reductions are achieved by the system A1_2. In particular, the seismic response under the Taft earthquake is efficiently reduced by the system A1_2. These results indicate that semi-active resettable devices can effectively reduce the response of civil engineering structures over a wide range of earthquake ground motions.

7.7 IMPACT OF THE CONTROL LAW

This analytical investigation examines the effects of three different control laws on the seismic response of the twelve-storey reinforced concrete building. The system A2 shown in Figure 7.4b is adopted to analyse the performance of the control laws under seismic excitation. The 1-2-3-4, 1-3 and 2-4 control laws shown in Figure 7.3 are used to simulate the hysteretic behaviour of the resettable device.

Figure 7.14 shows maximum response profiles for the control laws and the uncontrolled structure. All control laws reduce the maximum relative displacements and inter-storey drift ratios efficiently. The maximum absolute accelerations are reduced in some levels of the structure by all of the control laws. However, the maximum total base shear is increased slightly by all control laws.

The simulation results show that the response reduction achieved by each of the control laws is very similar (Franco-Anaya et al. 2008b). The differences in response reduction delivered by all of the three control laws are not significant. This result complicates the selection of an appropriate control law to reduce the seismic response of this particular structure.

Other tendon systems were also used to investigate the impact of the three control laws. However, the results showed no significant difference in the seismic response reduction provided by the control laws. It was observed that the effect of the control laws was only noticeable by increasing the number of devices in the structure or by unrealistically increasing the stiffness of the devices.

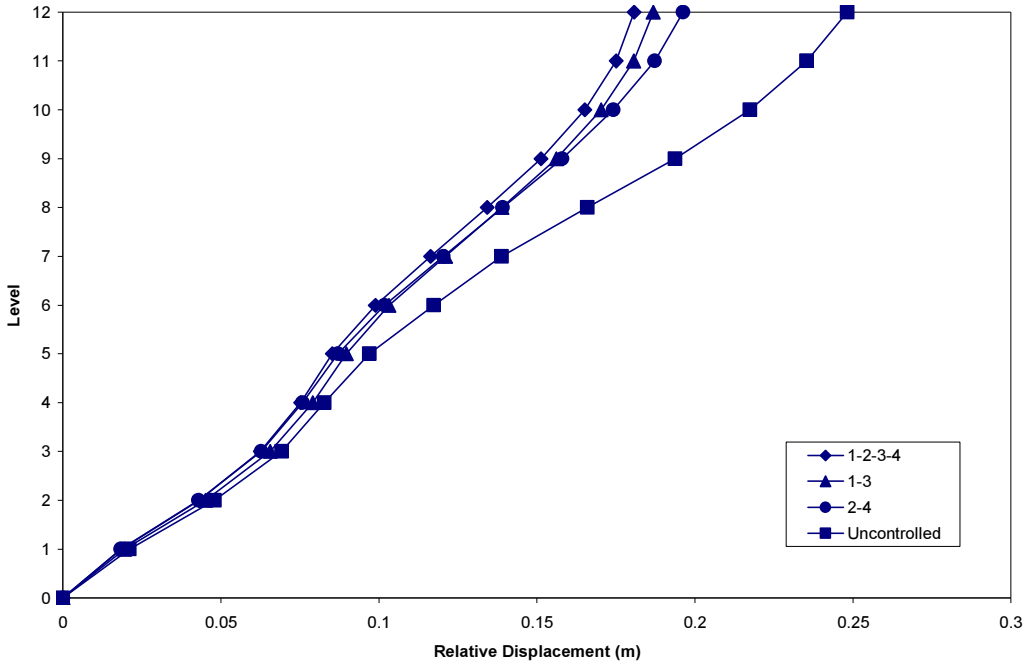

(a) Maximum relative displacements

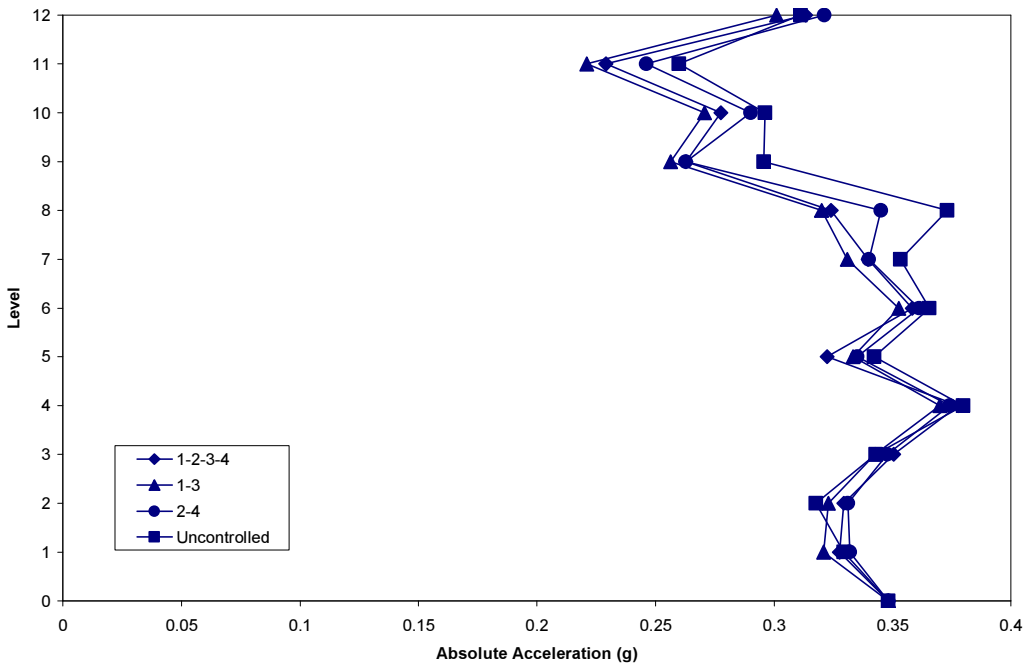

(b) Maximum absolute accelerations

Figure 7.14 Effect of the control law.

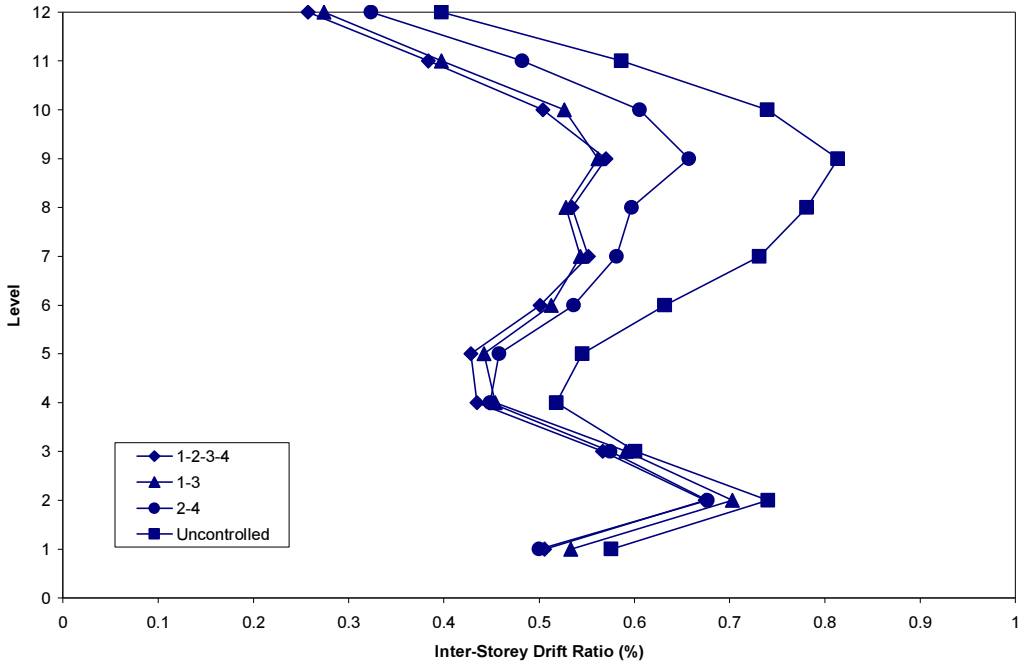

(c) Maximum inter-storey drift ratios

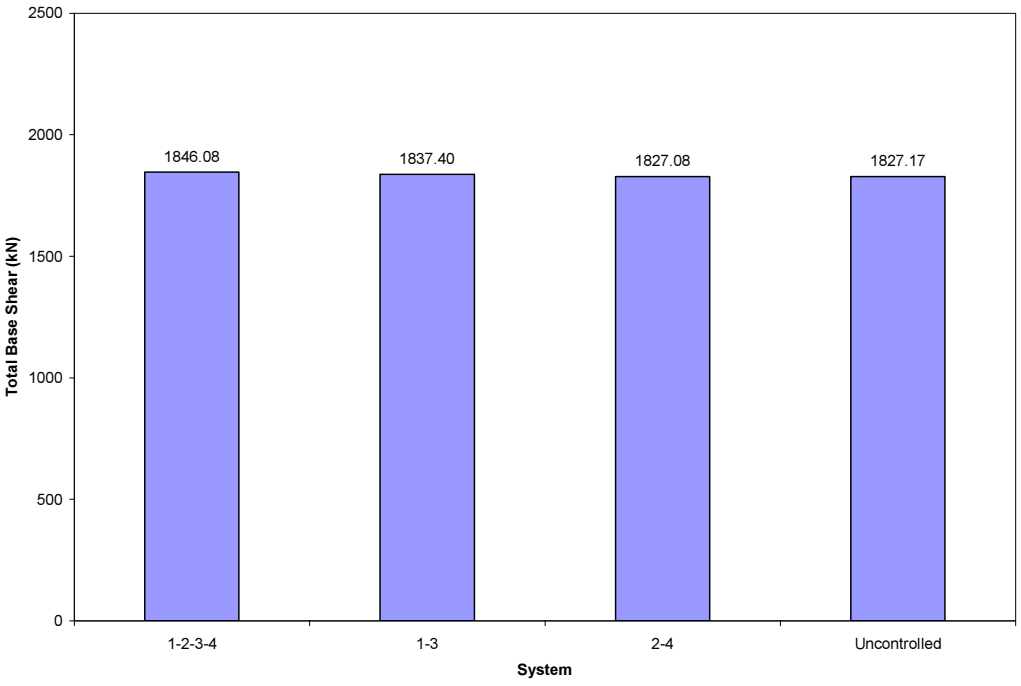

(d) Maximum total base shear

Figure 7.14 (Continued).

The effect of combining two different control laws to reduce the seismic response of the structure is now investigated. The response of the system A2 is examined for the north-south component of the 1940 El Centro ground motion. Different combinations of the 1-2-3-4, 1-3 and 2-4 control laws are utilised to control the response of the two resettable devices employed by the system A2.

Three combinations of the control laws are selected for the inelastic time-history analyses. These combinations showed the best seismic performance among all possible combinations of the three control laws. Figure 7.15 shows the maximum response envelopes for the combinations considered. The results are presented for comparison to the 1-2-3-4 control law and the uncontrolled structure.

In the combination 1-2-3-4 and 1-3, the device installed on the ground is controlled by the 1-2-3-4 control law and the response of the device placed on level 6 is based on the 1-3 control law. For the combination 2-4 and 1-2-3-4, the behaviour of the device placed on the ground level is controlled by the 2-4 control law, while the response of the device located on level 6 follows the 1-2-3-4 control law. In the combination, 2-4 and 1-3, the response of the device placed on the ground level is based on the 2-4 control law and the device installed on level 6 is controlled by the 1-3 control law.

Figure 7.15 shows that no significant improvement is made by combining the different control laws. All combinations are able to reduce the earthquake response compared to the uncontrolled case. It is observed that the combinations can achieved the same level of response reduction compared to the 1-2-3-4 case, in which the response of the two resettable devices is controlled by the 1-2-3-4 control law. These results indicated that the impact of the control law in reducing the seismic response is minimal for this particular reinforced concrete building.

The results presented in Sections 7.5, 7.6 and 7.7 suggest that an optimal solution for the implementation of resettable devices in multi-storey buildings should consider the capacity of the device, the configuration of the tendon system and the control law.

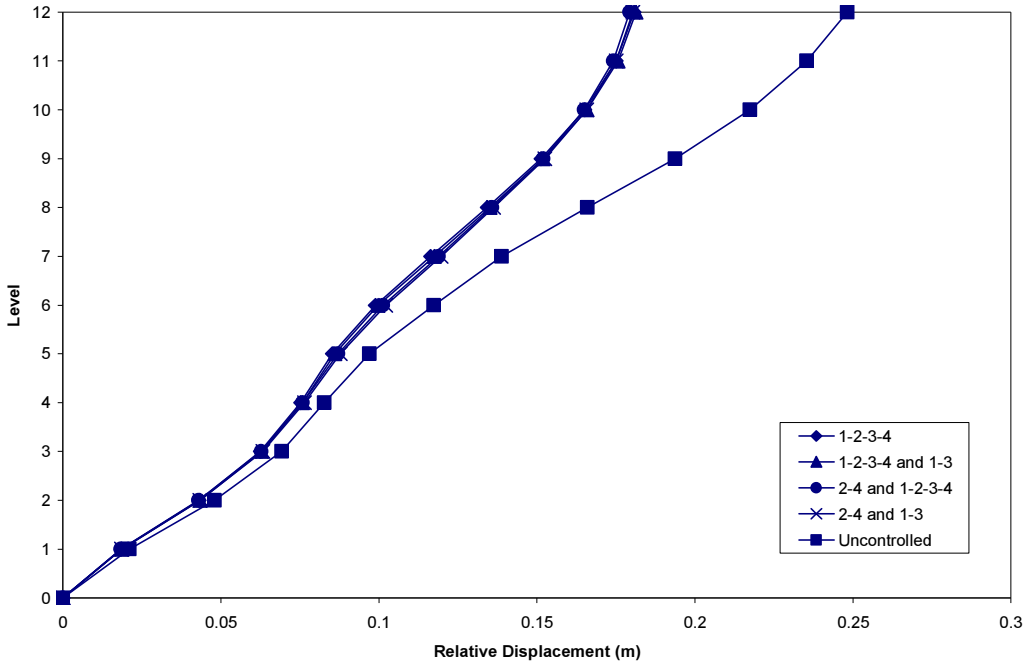

(a) Maximum relative displacements

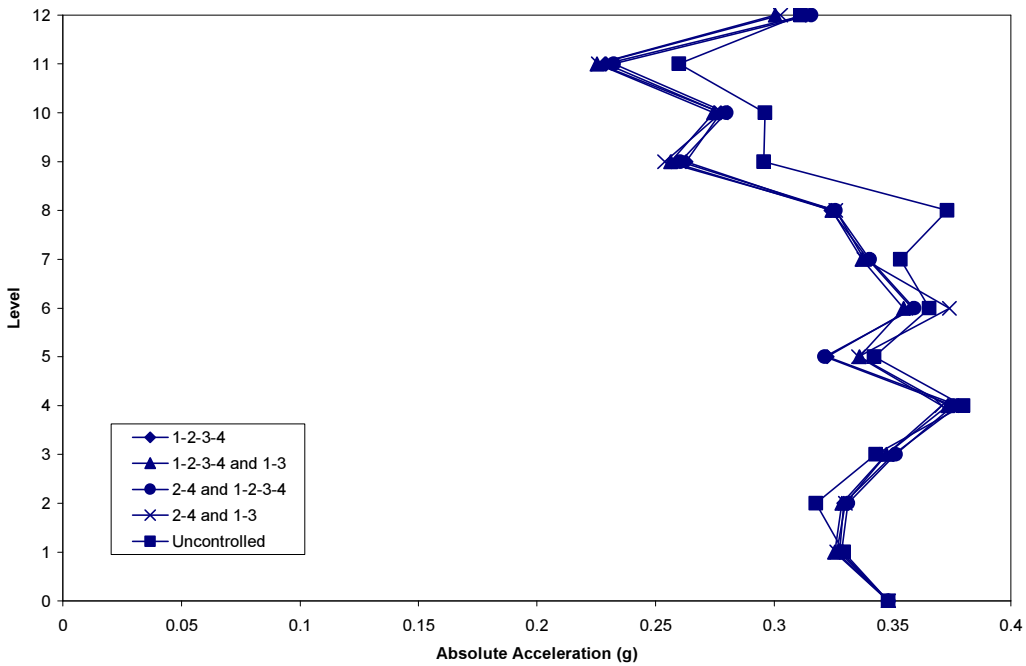

(b) Maximum absolute accelerations

Figure 7.15 Effect of combining the control laws.

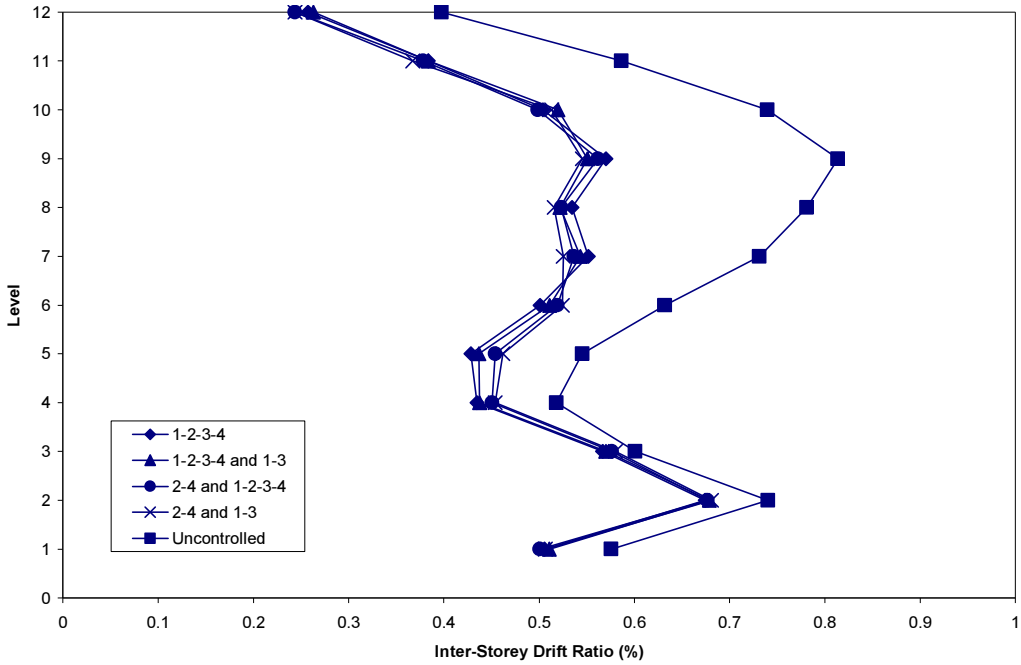

(c) Maximum inter-storey drift ratios

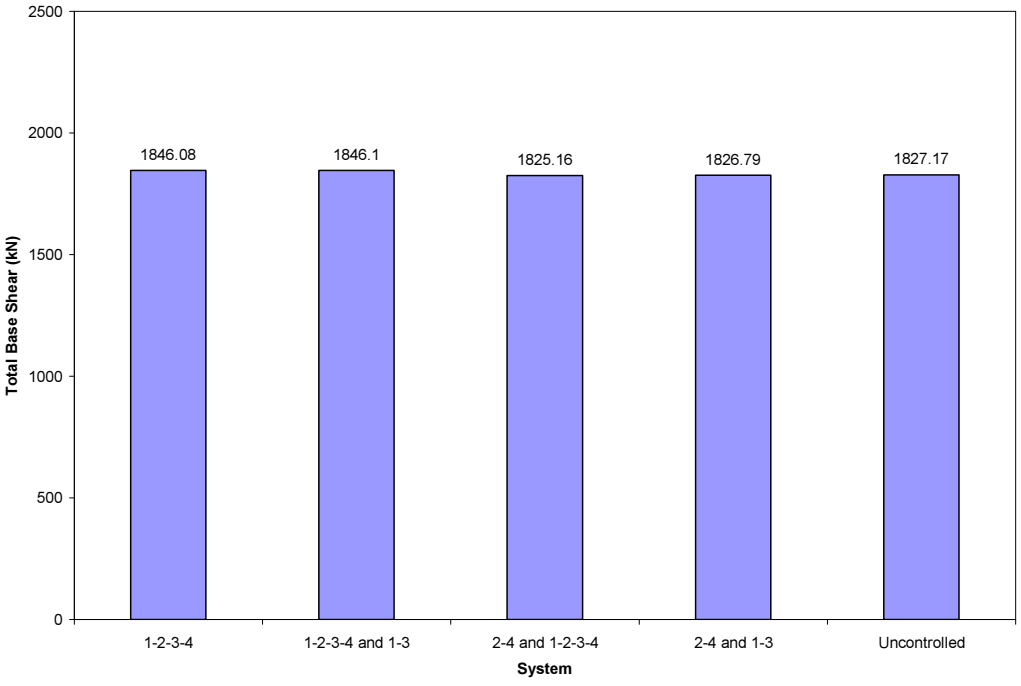

(d) Maximum total base shear

Figure 7.15 (Continued).

7.8 IMPROVING THE PERFORMANCE OF RESETTABLE DEVICES

The maximum device force is the limiting factor when using resettable devices that use air as the working fluid. In this study, two different approaches are used to improve the performance of the semi-active resettable device. The first approach considers the use of a special lever system attached to the device to increase the resisting forces delivered by the device. In the second approach, an external high-pressure air source connected to the device is used to increase the resisting forces and stiffness of the device.

7.8.1 Lever System

The lever system shown in Figure 7.16 is used to improve the performance of resettable devices under earthquake load. The lever system connects one end of the device piston to the rigid rods. The resisting forces produced by the resettable device can be amplified by manipulating the stiffness or the length of the levers of the system. Connecting the device to the lever system amplifies the piston displacements and therefore the device forces. The levers are modelled using the spring member with a linear elastic hysteresis. The spring members modelling the levers are connected in series. A normal hinge is used to connect the two spring members.

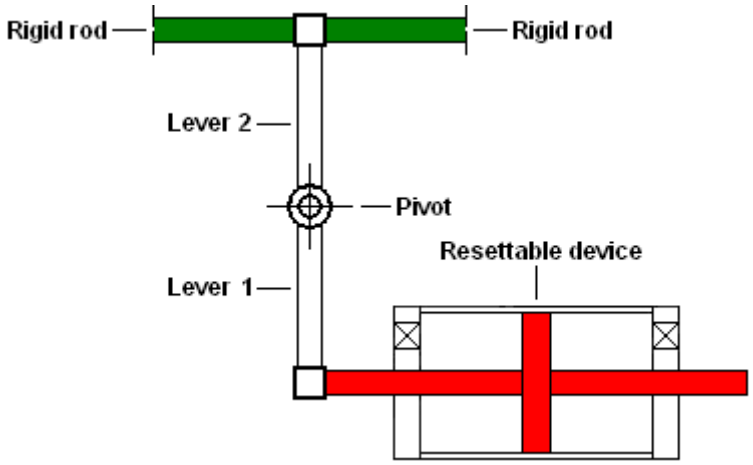

Figure 7.16 Lever system attached to the resettable device.

7.8.2 High-pressure Air Source

Resettable devices that use air as the working fluid provide modest resisting forces and stiffnesses based on the volume of the device chamber. Increasing the resisting forces in relation to the same chamber volume improves the energy dissipation capacity of the device and enables a broader range of structural applications. Larger resisting forces can be achieved by using a different working fluid, by using a pressurised gas (Leavitt et al. 2005, 2006, Yang et al. 2007) or by connecting the device to a high-pressure air source to increase the pressure of the active device chamber (Mulligan et al. 2007, Mulligan 2007). The latter approach requires only minor modification to the device design or the control methods.

The resisting force delivered by the device depends on the differential pressure between the two chambers of the device. Therefore, the larger the differential pressure the larger the resisting force produced. The base pressure is defined as the pressure in the active chamber before the air is compressed due to a change in chamber volume caused by the displacement of the piston. Increasing the base pressure in the active chamber prior to any piston motion greatly increases the differential pressure between the chambers because the opposite chamber does not have the increase in base pressure (Mulligan 2007).

The addition of the high-pressure air source may further improve the ability of the resettable device to sculpt structural hysteretic behaviour. The active chamber can be pre-pressurised or allowed to work from atmospheric pressure providing the possibility of the device having a differential response depending on the type or direction of the motion (Mulligan et al. 2007, Mulligan 2007). It should be noted that the ability to add a high-pressure air source and to utilise it for differential response is only possible due to the independent chamber design of the resettable device presented in this research.

A schematic of the high-pressure air source connected to the device is shown in Figure 7.17. For the implementation of this pre-pressurising configuration in actual structures, the high pressure can be supplied by stand alone tanks attached to the device or via a

central pressure system. Typically, there are only a few large pulses during a large seismic event. Therefore, a relatively small pressure supply can provide the device with sufficient air mass and pressure for the duration of these pulses (Mulligan 2007).

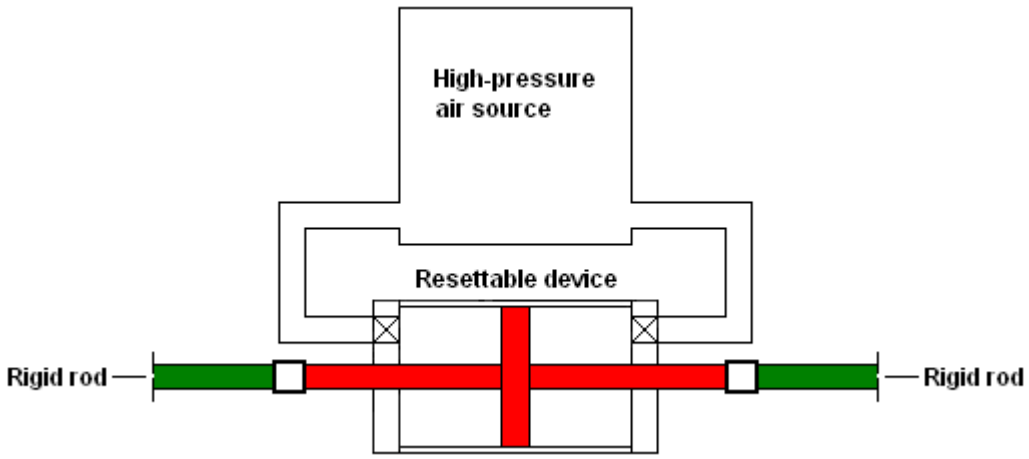

Figure 7.17 Resettable device connected to a high-pressure air source.

An approach similar to that shown in Figure 7.17 uses an additional controlled valve per chamber that generates a four-valve resettable device (Mulligan 2007). The additional valves are utilised to release the stored energy by exhausting the pressurised air to the atmosphere. The four-valve configuration enables larger differential pressures between the device chambers and consequently larger resisting forces in the device. Furthermore, the four-valve configuration allows more complex control laws to be implemented in comparison to the original two-valve configuration of the device.

7.8.3 Simulation Results

System A1_2 is selected to analyse the performance of the two approaches under the north-south component of the 1940 El Centro earthquake. Nonlinear dynamic analyses using RUAUMOKO are conducted to evaluate the performance of the approaches in reducing the seismic response of system A1_2. The 1-2-3-4 control law is utilised to simulate the hysteretic behaviour of the resettable device.

The lever system requires a large stiffness to be effective therefore a spring stiffness of 5,000,000 kN/m is adopted for use in the program RUAUMOKO. The lengths of the lever 1 and lever 2 are assumed to be 1.5 m and 0.5 m, respectively. The system A1_2 enhanced by the addition of the lever system is denoted as the system A1_2_L.

It is assumed that the resettable device is connected to an external pressure vessel that provides additional air pressure to both chambers of the device. This represents an approximation of the differential pressure approach described above. However, the addition of pressure to the device chambers can also increase the resisting forces and the stiffness of the resettable device to a certain extent. For the computer analysis, the initial atmospheric pressure and an additional 0.3 atmospheres of pressure are adopted for each of the device chambers. It is important to note that the addition of a large amount of air pressure could destabilise the system in particular during small cycle motions (Ji et al. 2007). The system A1_2 equipped with the high-pressure air source is referred to as the system A1_2_P.

Maximum response envelopes are presented in Figure 7.18. The performance of the systems A1_2_L and A1_2_P is evaluated in terms of reductions in maximum relative displacements, absolute accelerations, inter-storey drift ratios and total base shear. The simulation results are presented for comparison to the system A without any resettable device and to the system A1_2 using neither lever system nor high-pressure air source.

It can be seen in Figure 7.18 that the systems A1_2_L and A1_2_P improve the seismic response compared to the original system A1_2. Reductions in the maximum relative displacement and inter-storey drift ratio are achieved by the two enhanced systems. The maximum absolute acceleration and total base shear are also reduced especially by the system A1_2_P that utilises the high-pressure source.

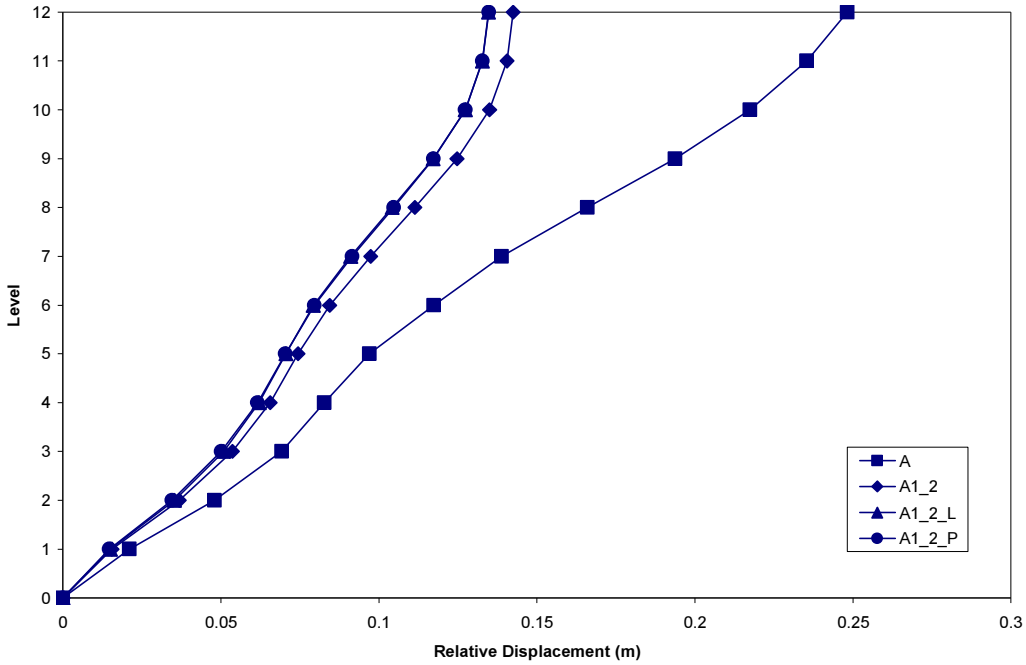

(a) Maximum relative displacements

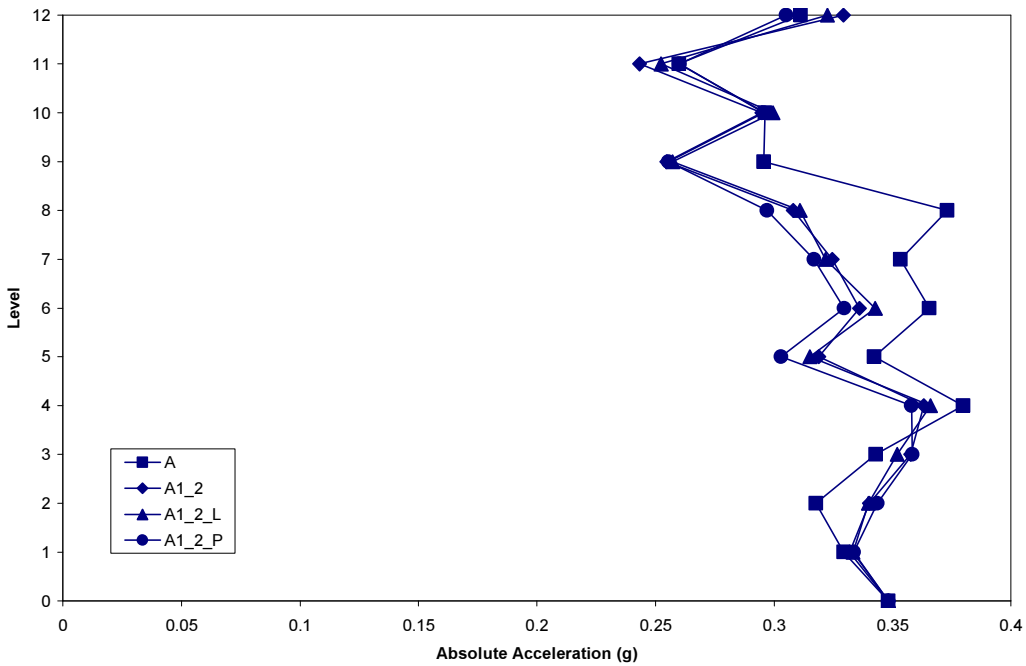

(b) Maximum absolute accelerations

Figure 7.18 Effect of improving the device force.

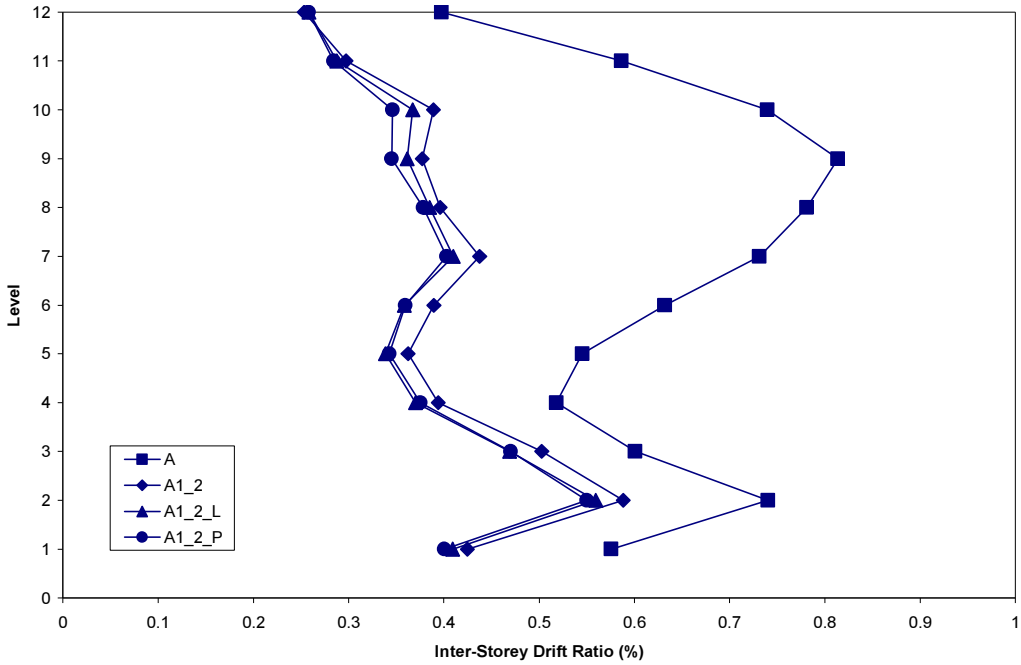

(c) Maximum inter-storey drift ratios

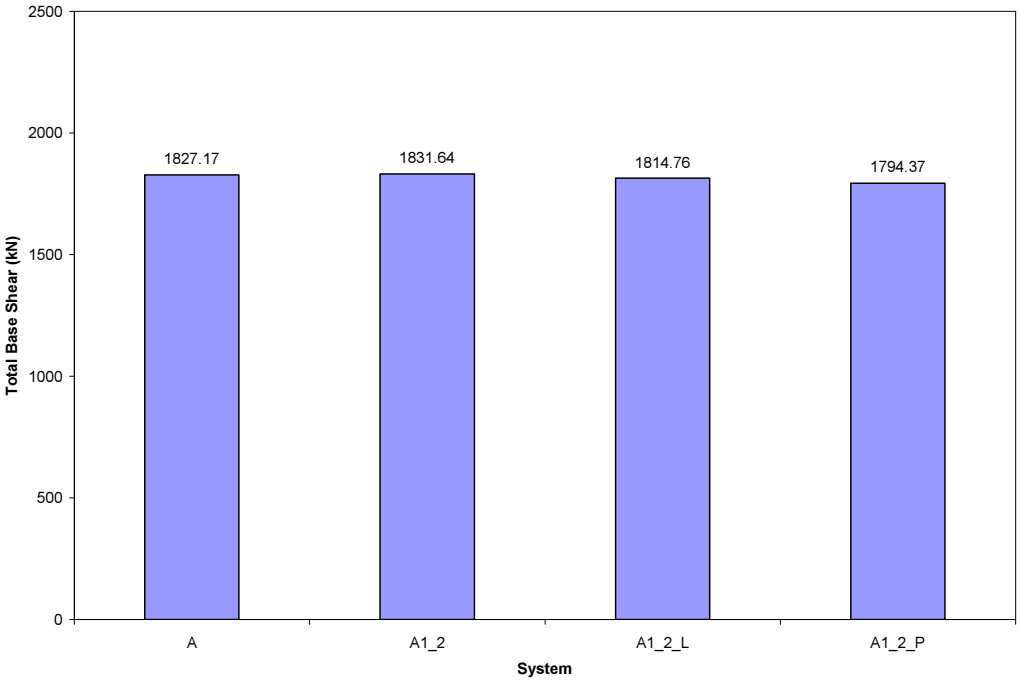

(d) Maximum total base shear

Figure 7.18 (Continued).

These analytical results demonstrate that the addition of the high-pressure air source effectively increases the resisting forces produced by the device, compared to forces produced when using the atmospheric pressure. Experimental studies show that the addition of one pressurised atmosphere to the initial pressure in the active chamber more than doubles the maximum force delivered by the device using the 2-4 control law (Mulligan et al. 2007, Mulligan 2007).

It can be concluded that the implementation of a special lever system and the addition of a high-pressure air source are an effective way to increase the maximum resisting forces delivered by resettable devices that use air as the working fluid. The implementation of the two approaches eliminates the need for increasing the original size of the device.

7.9 RECOMMENDATIONS FOR DEVICE IMPLEMENTATION

Recommendations for the implementation of resettable devices in building systems can be drawn from the studies presented in previous sections. The recommendations include the following:

- The stiffness of the resettable devices is based on the maximum force delivered by the device and on the maximum displacement experienced by the structure during severe earthquake loading. Preliminary nonlinear dynamic analyses of the structure without supplemental devices can provide an indication of the maximum structural demand expected to select the appropriate device stiffness.

- The placement of resettable devices on each storey of the building should be avoided due to the negative effects of any actuator-actuator interaction.

- The low level of the forces produced by the resettable devices is a limiting factor for devices that utilise air as the working fluid. However, the use of a high-pressure air source can be an effective means to increase the resisting forces of the resettable devices provided that the addition of air pressure does not destabilise the system.

- Other techniques such as lever-like systems may be utilised to increase the piston displacement of the resettable device and amplify the device force transmitted to the structure.

- Since resettable devices offer high response adaptability, the use of these devices together with other passive or active control techniques could improve the overall performance of the resettable devices.

- Pre-stressed tendons should be used to transfer the control forces of the resettable device to the structure. The maximum pre-stressed force given by the static analysis of the structure provides a good indication of the level of pre-stress required by the tendons.

- The use of resettable devices in combination with pre-stressed tendons and bracings should be preferred over the use of pre-stressed tendons and bracings alone to reduce the floor displacements and inter-storey drifts of multi-storey buildings. The use of pre-stressed tendons and bracings without resettable devices increases the floor accelerations and total base shear. The addition of the resettable devices enables the reduction of the structural displacements and inter-storey drifts without increasing the floor accelerations and the base shear demand significantly.

7.10 SUMMARY

This chapter has presented a description of a number of relevant aspects related to the implementation of resettable devices in structural building systems. Analytical studies were performed to investigate the performance of a twelve-storey reinforced concrete building subjected to earthquake ground motion. The seismic response of the frame structure was controlled by using various control strategies based on resettable devices. Computer simulations were performed to determine the optimal utilization of the resettable devices in the moment-resisting frame building.

The dynamic characteristics of the twelve-storey building and the control system were described. The effectiveness of the devices in reducing the earthquake response was discussed in relation to the location, number and arrangement of the devices. The seismic response contribution of the pre-stressed tendons and bracings utilised by the control system was evaluated. Different control laws were used to control the operation of the resettable devices. The effects of the control laws on the seismic response of the structure were examined. A lever system and a high-pressure air source were utilised to increase the resisting forces delivered by resettable devices that use air as the working fluid. Maximum response envelopes were used to evaluate the effectiveness of the devices in reducing the seismic response of the twelve-storey reinforced concrete building. Recommendations for the implementation of resettable devices in structural building systems are presented.

Chapter 8
FIBRE-OPTIC GYROSCOPES FOR CIVIL ENGINEERING APPLICATIONS

8.1 INTRODUCTION

The torsion effect caused by asymmetries in buildings, where the centre of stiffness differs from the centre of mass, can be evaluated by using differential measurements of accelerometers. However, the effect of the structural rotations has traditionally been neglected in studies on the seismic response of structures. This was mainly because their influence was thought to be small and there were no suitable devices available to properly measure the response of the structures to rotations. However, different types of inertial rotation sensors exploiting the Sagnac effect have now reached the necessary sensitivity to be used for the investigation of rotations in civil engineering structures.

Fibre-optic gyroscopes (FOGs) are passive interferometers where a beam of light is split in two equal parts. These parts then travel along several hundred metres of glass fibre coil around a closed circuit, one in the clockwise and the other in the anticlockwise sense. When the beam is recombined upon exiting the fibre, it shows a fringe pattern, which depends on the rate of rotation, but does not change with translation. The rotation rates measured in this way are absolute with respect to the local universe. Therefore, the measurement device does not require an external reference frame to operate.

This chapter investigates the feasibility of the use of FOGs to measure the rotation rates, rotations, displacements and inter-storey drifts of civil engineering structures. FOGs are devices that utilise the Sagnac effect to detect mechanical rotations interferometrically from optical beams. They are compact, easy to install and, unlike conventional linear potentiometers, do not require a fixed reference frame to operate. Shake table tests were performed on the four-storey one-fifth scale structure equipped with a fibre-optic gyroscope. Four different earthquake ground motions were used in this experimental

study. During the seismic testing, the FOG was first attached to one of the first floor columns and then to the third floor of the model structure. Relative displacements at the first floor and rotations at the third floor were calculated from the measurements provided by the FOG. A very good agreement was observed between the measurements obtained with the FOG and those provided by a conventional linear potentiometer. The experimental results validated the accuracy of the measurements recorded by the FOG as well as the dynamic range of the instrument. The FOG was also installed on the Sky Tower in Auckland to evaluate the displacements of the tower structure. A series of measurements were carried out on the 54th and 60th floors during three days. The measurements taken by the FOG provided a very good signal to the noise ratio of the measurement quantity.

It is important to emphasise that this chapter discusses a very important investigation on the first applications of the FOG in civil engineering. The research work presented here differs from the principal research topic reported in the thesis. However, it is included because of the importance of the FOG as an emerging sensor technology for monitoring of civil infrastructure. In addition, the laboratory testing of the FOG was carried out in conjunction with the experimental validation of the semi-active resettable devices.

8.2 MEASUREMENT OF ROTATIONS IN CIVIL ENGINEERING

In civil engineering, rotations are an important measure of the structural response. Any torsional rotation in a building will cause the translational movement of the structural members located away from the centre of rotation. As a consequence, these structural translations need to be added to the translations of the members associated with the horizontal components of the earthquake ground motion during the design process.

The rotation of the column members of building structures is measured as the inter-storey drift. The inter-storey drift is the difference in the horizontal displacement from one floor to the next and is usually divided by the inter-storey height. Typically, the inter-storey drift is expressed as a percentage of the storey height. The magnitude of the

inter-storey drift is a measure of the damage expected in the structure due to seismic excitation (Algan 1982).

The measure of torsional rotations and inter-storey drifts is reasonably easy on small-scale structural models. However, it is very difficult to measure the structural rotations on large-scale structural models and actual structures. The torsional rotations can be measured by dividing the difference in the accelerations recored by two accelerometers by the distance between the accelerometers in the direction perperdicular to the motion. The result is then integrated twice with respect to time to obtain the torsional rotations. However, the applicability of this technique is limited due to the inherent sensor drift and the small offset from zero in the absence of an input signal.

In the laboratory, the inter-storey drifts can be calculated from displacements measured by conventional potentiometers that require a fixed reference frame. However, for real structures, the inter-storey drifts can not be easily determined because there is no reference frame that may be used to measure the floor displacements. Although it is possible to set up a frame attached to the floor below in order to measure the relative displacement at the floor above, this is not a very practical solution.

Another approach is to set up a light source next to the ceiling and to direct it to a grid-like receiving device located on the floor that detects the movement of the light source. However, besides the hardware complexity of this approach, it is also vulnerable to the building deformations, amplified by the length of the light beam.

Unlike conventional linear potentiometers, FOGs do not require a fixed reference frame to operate and therefore they are much easier to use in actual applications. In the case of the differential measurements of two accelerometers mentioned before, the geometry of the measurement arrangement with respect to the centre of rotation is of significant importance for the resolution of the measurement technique. In contrast, the FOG can provide the correct angle of rotation even when the centre of rotation is a long way off from the sensor.

Furthermore, the FOG can also be used to detect and monitor damage in structures. If several FOGs are placed on each storey or on discrete locations along the height of the building, any difference in the rotation rate between the parts of the building will be an indication of energy dissipation and therefore potential structural damage.

8.3 OPTICAL GYROSCOPES

Optical gyroscopes have replaced conventional mechanical gyroscopes in commercial jetliners, booster rockets and orbiting satellites. Such devices are based on the Sagnac effect (also called the Sagnac interference), first demonstrated by the French physicist Georges Sagnac in 1913.

In Sagnac's demonstration, a beam of light was split such that a part travelled clockwise and a part anticlockwise around the same area in a rotating platform. Although both beams travelled within a closed loop, the beam travelling in the direction of rotation of the platform returned to the point of origin slightly after the beam travelling opposite to the platform's rotation. As a result, a "fringe interference" pattern (interferogram) was detected that depended on the precise rate of rotation of the turntable and the size of the area.

Sagnac interferometers are absolutely referenced to the local universe and therefore do not require an external reference frame to operate. Gyroscopes using the Sagnac effect began to appear in the late 1960s, following the invention of the laser and development of fibre optics (Britannica, Lefevre 1993).

8.3.1 Ring Laser Gyroscopes

A ring laser gyroscope is an active Sagnac interferometer in which internally generated laser beams are travelling in opposite directions around a triangular or square contour defined by highly reflecting mirrors. The mirrors are rigidly attached to a sensor block,

defining the size of the enclosed area and therefore the sensitivity of the measurement device. When the sensor is rotated around an axis perpendicular to the laser beam plane, the Sagnac effect causes a frequency shift between the two laser beams, which is strictly proportional to the rate of rotation. Superimposing both laser beams through a beam-splitter at the output of one of the mirrors generates an interferogram and makes this frequency shift accessible (Stedman 1997). Figure 8.1 shows a schematic representation of a ring laser gyroscope.

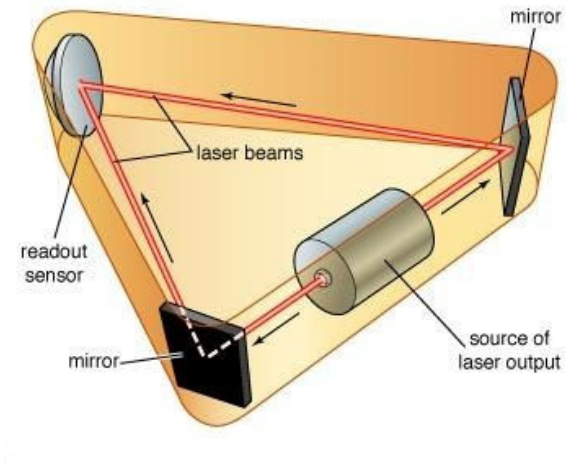

Figure 8.1 Ring laser gyroscope (Britannica).

A ring laser gyroscope can measure the absolute rotation of whatever environment it is placed on or attached to. Small ring lasers are used for navigation in aircraft, submarines and spacecraft. Large ring lasers have been utilised to measure subtle variations in the rotation rate of the earth (Schreiber et al. 2004). Large ring lasers have also successfully recorded signals of rotational ground motions induced by large earthquakes (Igel et al. 2005, Suryanto et al. 2006).

8.3.2 Fibre-optic Gyroscopes

A fibre-optic gyroscope (FOG) is a passive Sagnac interferometer employed to detect mechanical rotations such as tilts or torsions. The sensor houses a coil of about 0.5 km of optical fibre. Two beams of light travel along the fibre in opposite directions. Due to the Sagnac effect, the beam travelling against the rotation experiences a slightly shorter

path than the other beam. The resulting phase shift is a measure of the rate of rotation when the beams are recombined (Lefevre 1993).

A μFORS-1 model manufactured by LITEF (GmbH) in Germany was used in this research. The sensor has a random walk noise error level of less than 0.1 degrees per square root Hz, which becomes visible for signals of periods of approximately 50 seconds or longer. For the here presented measurements, this error source is far too small to be detected. In comparison to ring lasers a FOG is much smaller and not so delicate in operation. The FOG is approximately 100 × 80 × 25 mm in size and needs to be connected to a computer and a power supply. A photograph of the FOG is shown in Figure 8.2.

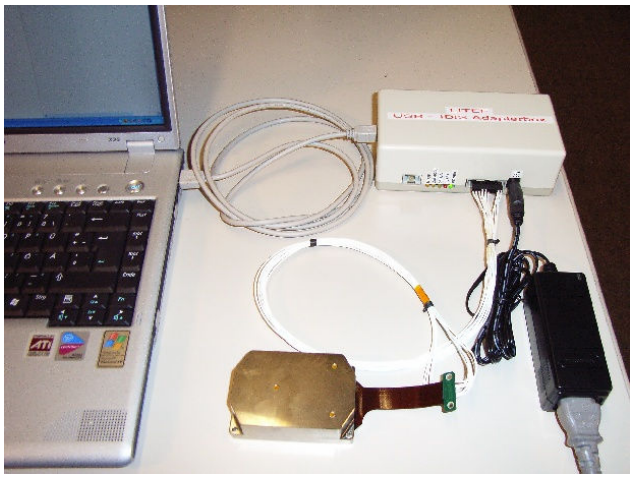

Figure 8.2 Fibre-optic gyroscope.

8.4 OPERATION AND VERIFICATION

The operation concept of the FOG is entirely based on optical signals and thus there are no mechanical moving parts inside the sensor. The FOG works efficiently over a range of excitation frequencies between 0.001 Hz and 2 kHz. Furthermore, a well defined reference to the north can be obtained from the FOG's measurements, which provides

an additional advantage of using the FOG for long term monitoring of the structural stability.

8.4.1 Operation Principle of the FOG

The operation principle of the FOG is very simple. However, the actual sensor design is highly complex in order to obtain high sensor stability and resolution. A schematic of the operation principle of the FOG is shown in Figure 8.3. A narrow spectral line-width light beam is generated by a light source (S) and passed on to a beam splitter of equal intensity. The two light beams generated are then guided around a monomode fibre coil in opposite directions. After passing through the fibre, the two beams are superimposed again by the same beam splitter and steered onto a photo-detector (D).

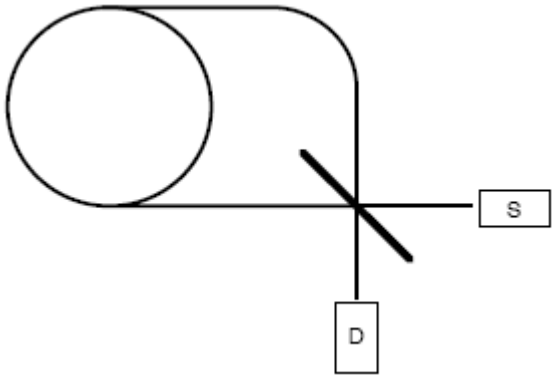

Figure 8.3 Opreration principle of the FOG.

If the entire apparatus is at rest, each of the beams travels the same distance and there is no phase difference between the two beams. However, if the FOG is rotating about the normal vector of the fibre coil, the two beams do not travel the same distance and a phase shift between the light beams is observed. Since the signals travel at the speed of light, the phase shift obtained is very small. Therefore, a modulation technique, pulsed operation and $\pi/2$-phase shifting for one sense of propagation are employed to achieve maximum sensitivity. Additionally, the sensor is operated in a closed loop configuration in order to ensure a wide dynamic range (Lefevre 1993).

8.4.2 Shake Table Measurements

Shake table tests on scaled models of structures are widely used to study their behaviour during an earthquake ground motion. The inter-storey drifts of the model structure can be precisely determined under these controlled laboratory tests. For this purpose, a rigid reference frame is mounted on the fixed laboratory floor. By using several displacement transducers attached to the reference frame it is possible to measure the displacements of the structural model along the axis of translation of the shake table. The inter-storey drifts of the model structure are then determined from the displacements measured by the transducers. Since the FOGs do not require a reference frame, they can measure the inter-storey drift as a rotation around the normal vector of the fibre coil.

In order to evaluate the suitability of fibre-optic gyroscopes for civil structures under seismic excitations, a series of shake table tests were performed on the one-fifth scale structure described in Chapter 4. A photograph of the test structure is shown in Figure 8.4. The photograph shows the five transducers used to measure the floor displacements of the four-storey model structure during the shake table tests. The linear transducers were mounted on the steel reference frame also shown in the photograph. The reference frame was fixed to the laboratory floor.

Figure 8.4 One-fifth scale structure with fixed reference frame.

The one-fifth scale structure was subjected to the following earthquake ground motions:

a. Imperial Valley, 18 May 1940 – El Centro north-south (NS) component
b. Kern County, 21 July 1952 – Taft S21W component
c. Northridge, 17 January 1994 – Sylmar County Hospital (Chan 9: 0 deg)
d. Kobe, 17 January 1995 – JMA Observatory N00E component.

The amplitude of the earthquake records was scaled in order to excite the four-storey model structure with earthquake ground motions of different intensity. Various linear potentiometers and accelerometers were used to measure the response of the model structure and the motion of the shaking table. As shown in Figure 8.5, a fibre-optic gyroscope was attached to the centre column of the first floor of the test structure to measure the rotation rates of the column.

Figure 8.5 FOG attached to the centre column.

Several shaking table tests were conducted using the above-mentioned earthquakes at various peak ground acceleration levels. In this study, response time-histories for the following ground motions are presented: El Centro 30%, Taft 40%, Sylmar 10% and Kobe 10% with corresponding peak ground accelerations of 0.10g, 0.07g, 0.08g and 0.08g, respectively. These earthquake intensities were selected to prevent inelastic deformations in the model structure during the seismic testing (Franco-Anaya et al. 2007a, 2007b).

An assessment of the accuracy of the FOG's measurements is made by comparing the measurements provided by the FOG with those delivered by a conventional linear potentiometer with a fixed reference frame (Fig. 8.4). The column's rotation is obtained by numerical integration of the rotation rate (degrees per second) measured by the FOG without an external reference frame. The floor displacement is then calculated by multiplication of the column's rotation by the height of the first floor. In the same way, the column's rotation is calculated with the inverse tangent of the displacement at the first floor, obtained by conventional potentiometers, divided by the storey height. The rotation rate is then determined by numerical differentiation of the column's rotation (Franco-Anaya et al. 2008a).

In the previous calculations, it is assumed that the centre column of the model structure is undergoing rigid rotation. The displacements caused by any other type of deformation such as beam bending or joint rotation are considered to be insignificant.

Figures 8.6 through 8.9 show a comparison in terms of rotation rates, centre column's rotations and first floor displacements measured by the FOG with those provided by a conventional potentiometer. An excellent agreement is observed between both sensors for all of the records used in the seismic testing. Small discrepancies can be observed between the displacement obtained with the transducers and the displacement computed from the rotation rate measured by the FOG at the peak values of the graphs. However, this reflects a systematic effect caused by deformations of the transducer arms under maximum strain. The breaks that might be observed in the FOG's data are the result of a software problem in the data logger of the FOG, which was identified only later on during the data analysis.

The FOG was also attached to the third floor to check torsional velocities in the model structure. However, there were only very small torsional motions detected because the structure is symmetric and the seismic excitation was applied in one direction only (Franco-Anaya et al. 2008a). Figures 8.10 through 8.13 show measurements obtained with the FOG at the third floor of the model structure for the earthquake ground motion considered.

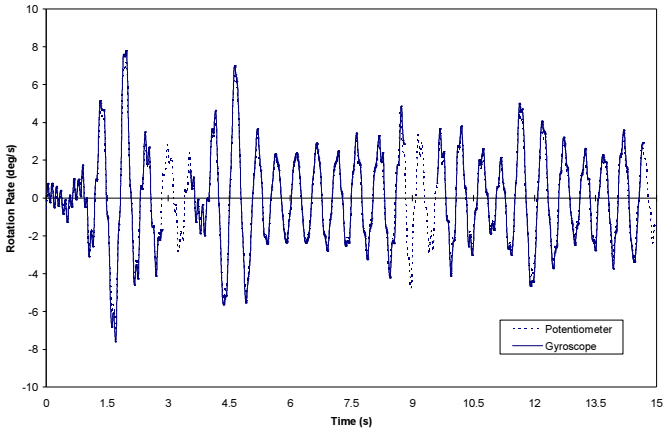

(a) Rotation rate of centre column

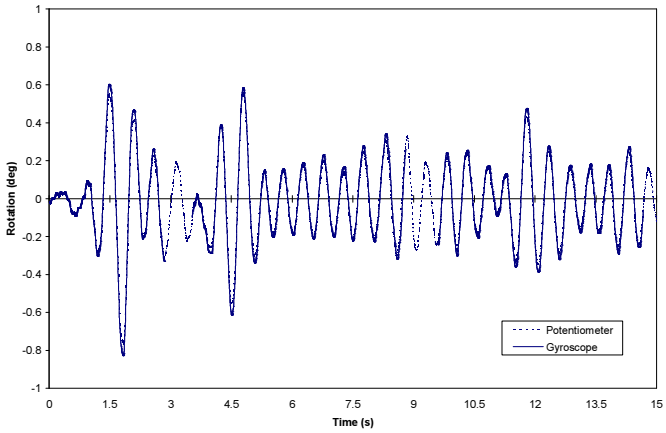

(b) Rotation of centre column

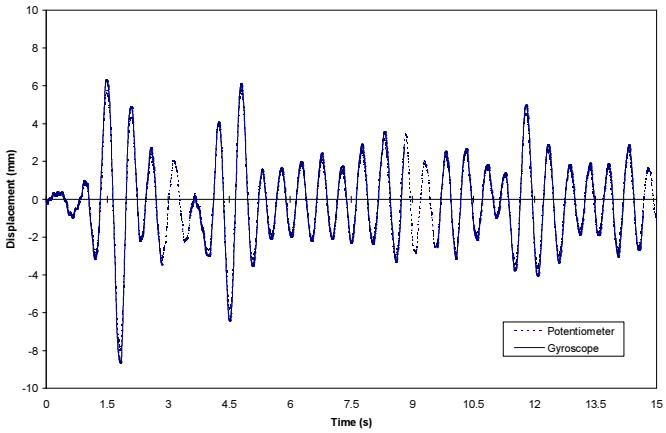

(c) Relative displacement at first floor

Figure 8.6 Measurements for El Centro 30% earthquake.

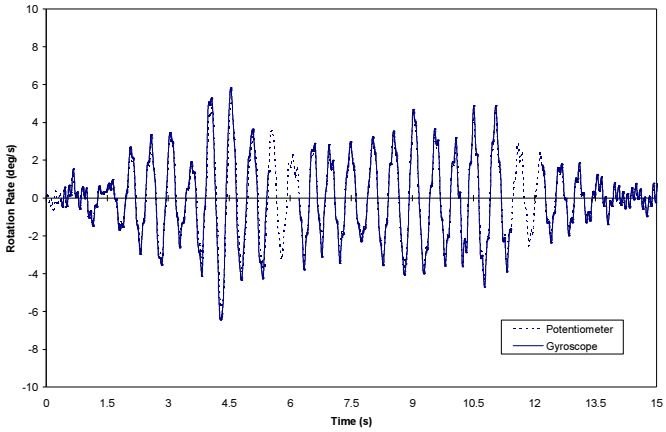

(a) Rotation rate of centre column

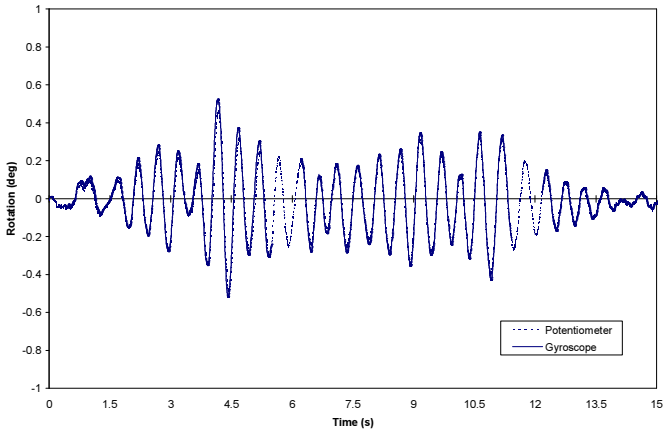

(b) Rotation of centre column

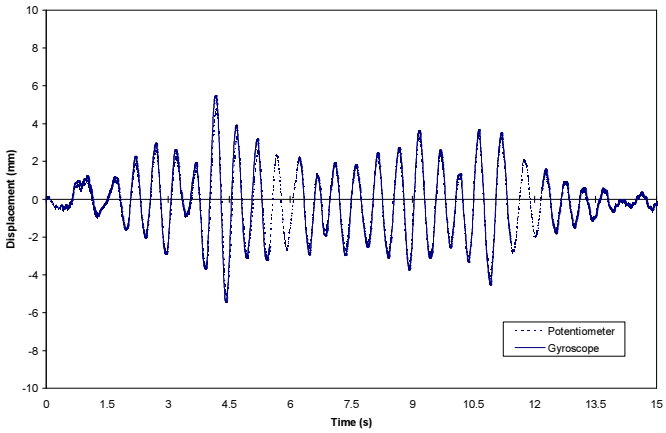

(c) Relative displacement at first floor

Figure 8.7 Measurements for Taft 40% earthquake.

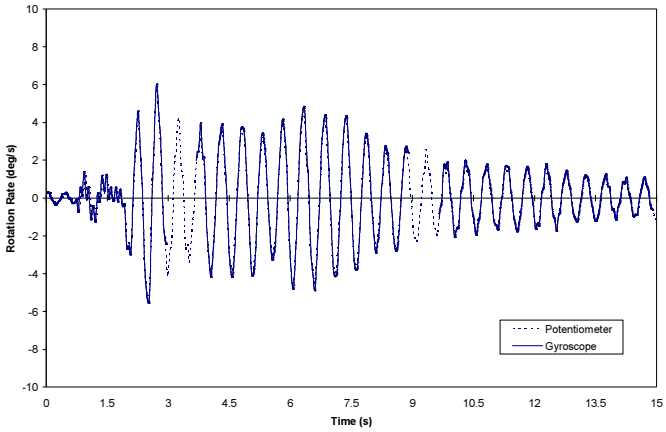

(a) Rotation rate of centre column

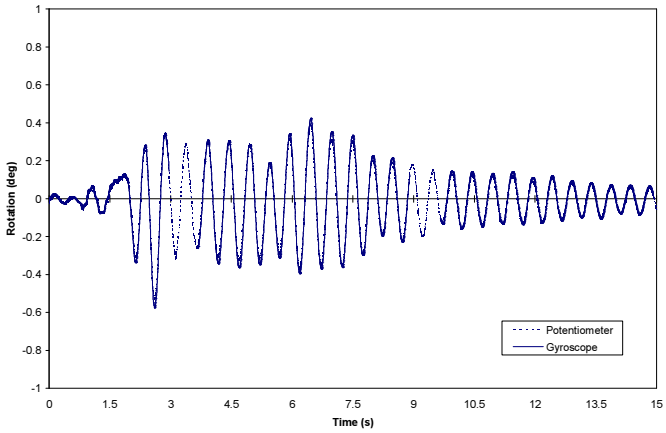

(b) Rotation of centre column

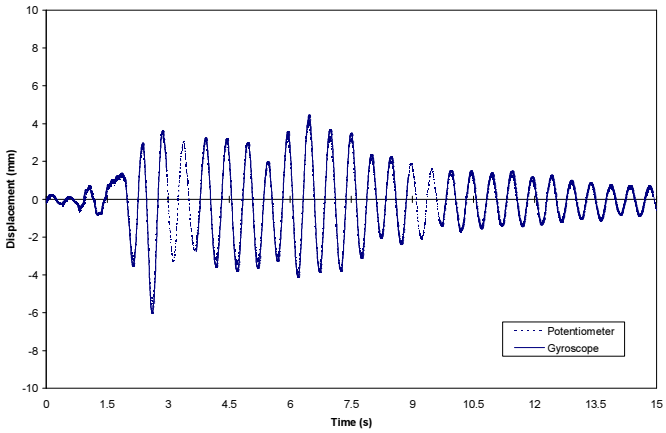

(c) Relative displacement at first floor

Figure 8.8 Measurements for Sylmar 10% earthquake.

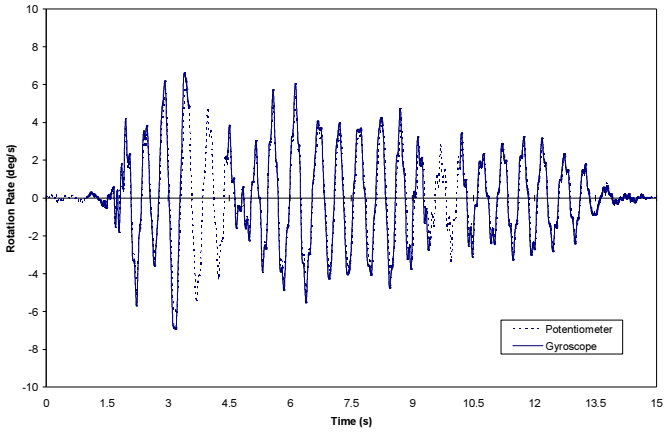

(a) Rotation rate of centre column

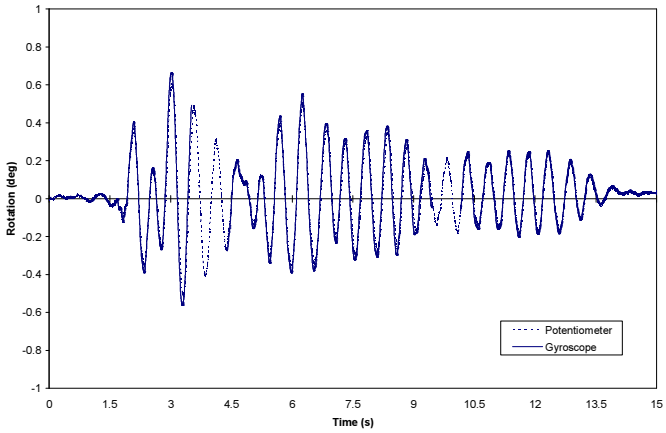

(b) Rotation of centre column

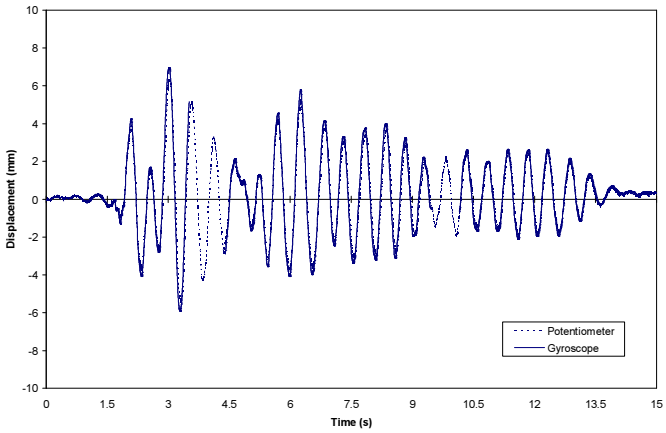

(c) Relative displacement at first floor

Figure 8.9 Measurements for Kobe 10% earthquake.

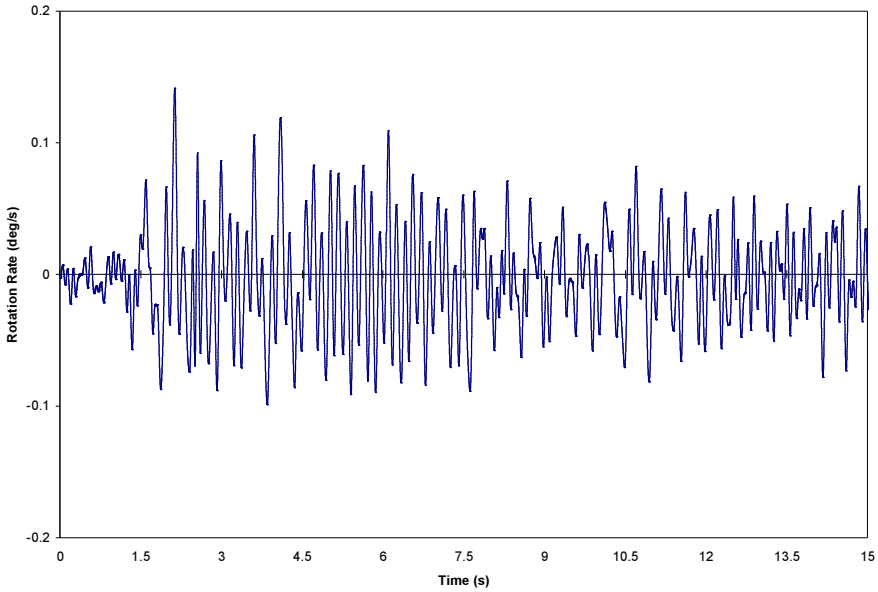

(a) Torsional rotation rate

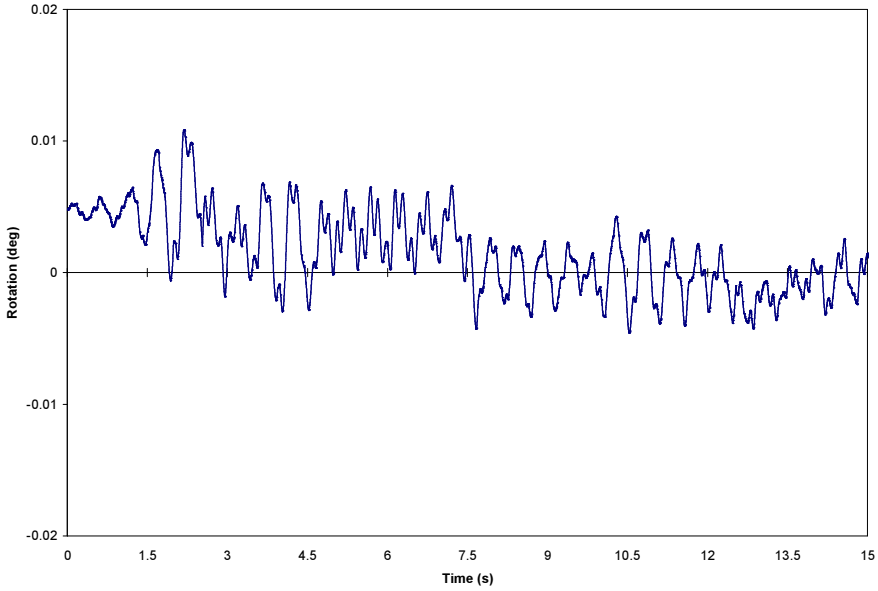

(b) Torsional rotation

Figure 8.10 Measurements at the third floor for El Centro 30% earthquake.

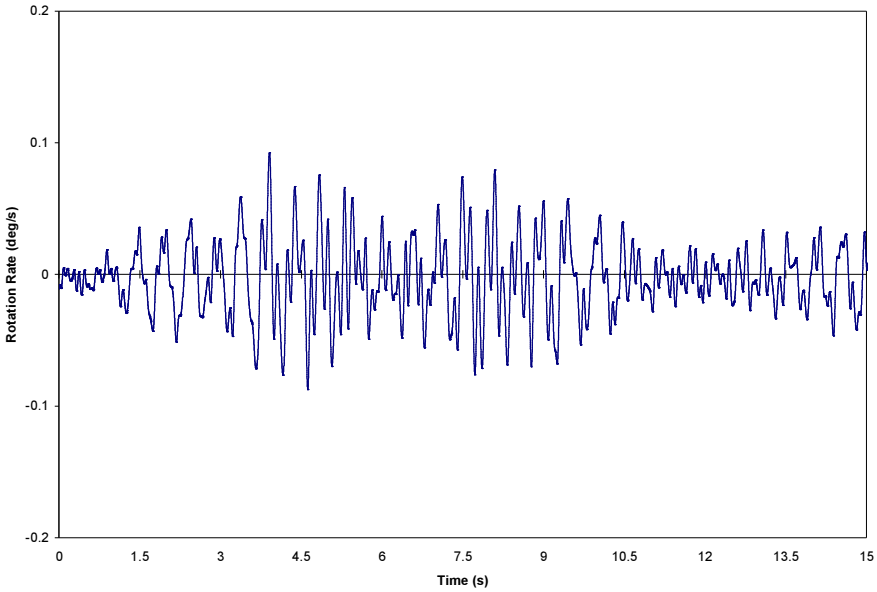

(a) Torsional rotation rate

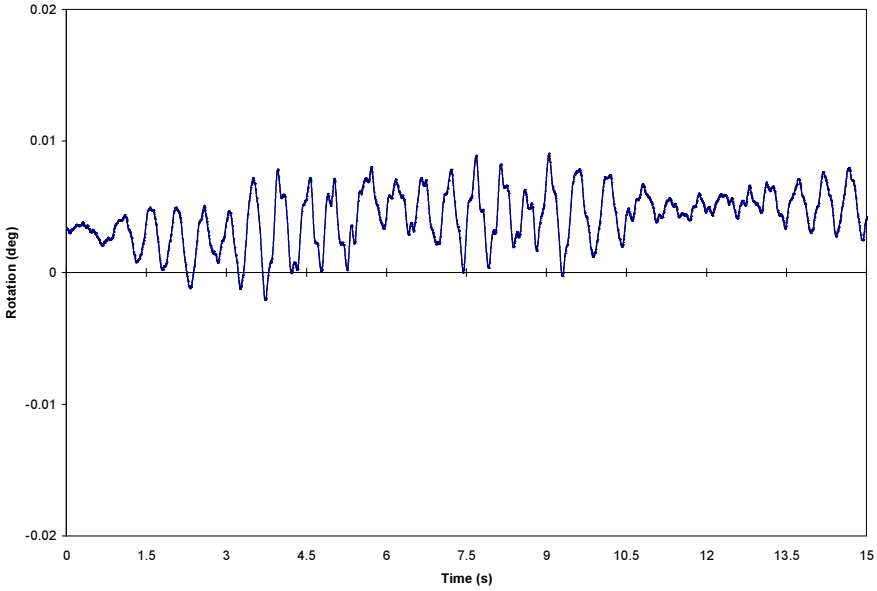

(b) Torsional rotation

Figure 8.11 Measurements at the third floor for Taft 40% earthquake.

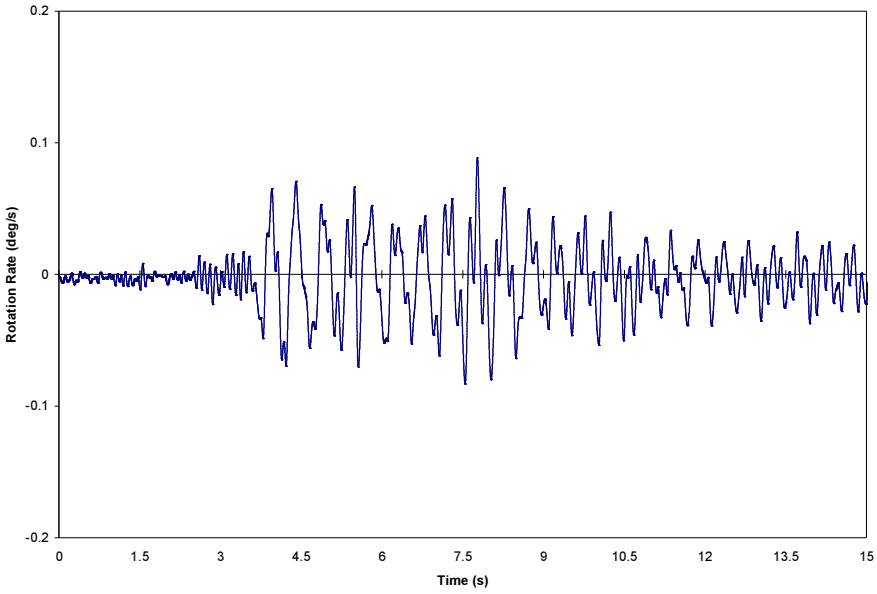

(a) Torsional rotation rate

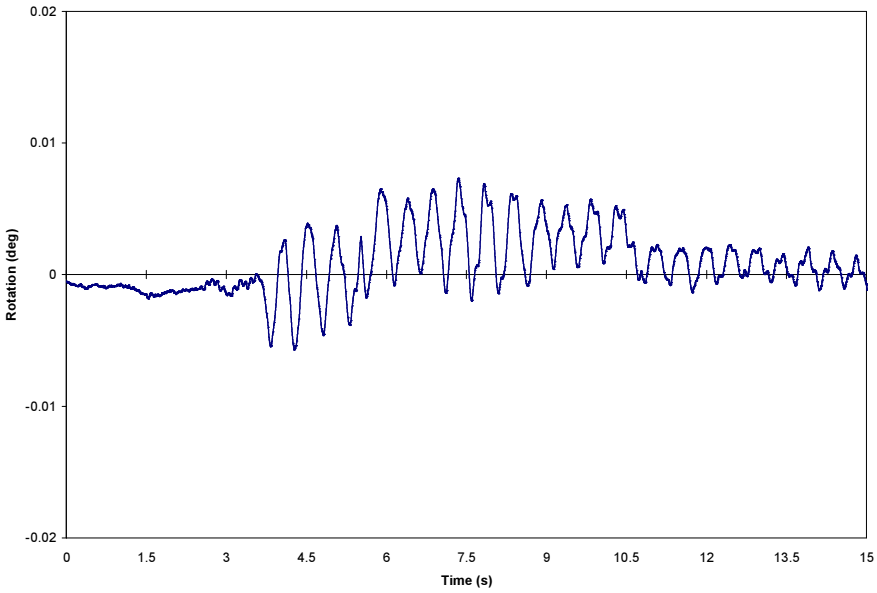

(b) Torsional rotation

Figure 8.12 Measurements at the third floor for Sylmar 10% earthquake.

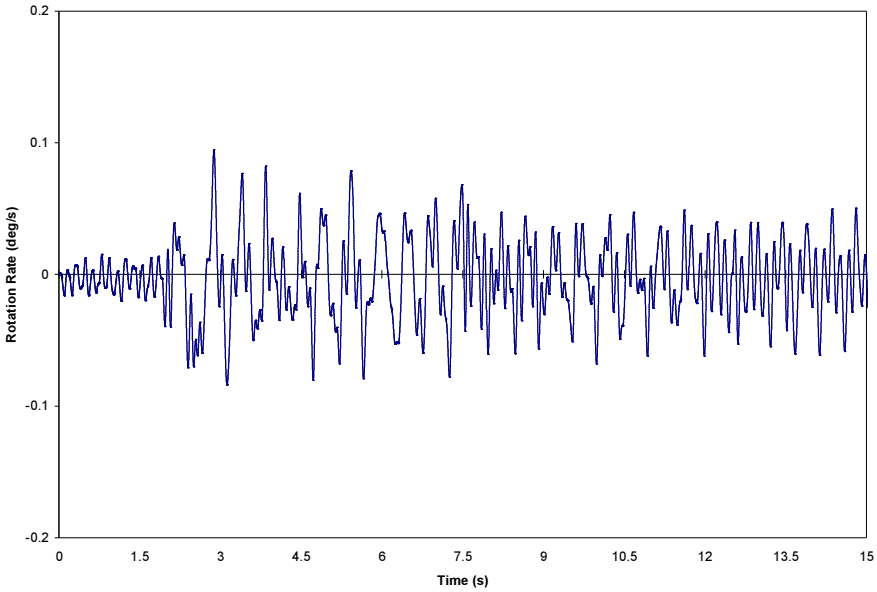

(a) Torsional rotation rate

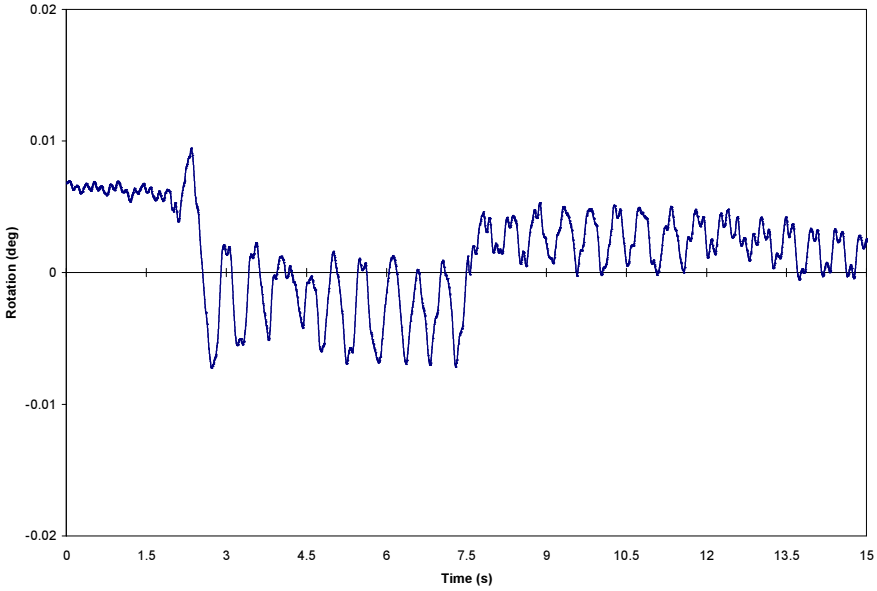

(b) Torsional rotation

Figure 8.13 Measurements at the third floor for Kobe 10% earthquake.

8.4.3 Measurements at the Sky Tower

The FOG was also used to measure the displacements of the 328 m tall Sky Tower in Auckland. Here, the device was clamped to antenna frames on the outside of the tower at level 54 and to window supports at level 60. Figure 8.14 shows a photograph of the FOG firmly attached to the structure at the 60th floor. It only took a few minutes to set up the sensor and start taking readings from the Sky Tower. The resonance frequency of the rocking motion of the Sky Tower is about 0.16 Hz which corresponds to a period of approximately 7 s.

Figure 8.14 FOG attached to the window of the Sky Tower.

During a three-day period of time, several measurement series with durations between 6 and 12 minutes were taken under calm wind conditions. Wind speeds varied between 24 km/h and 36 km/h. The computer recorded the instantaneous rotation rate measured by the FOG around the axis perpendicular to the coil of the glass fibre at one-millisecond intervals. In the orientation shown in Figure 8.14 the sensor was sensitive to the rocking motion of the structure.

Figure 8.15 shows one sample out of approximately 20 data sets obtained over the 3 days. The measured rotation rate was integrated to yield the excursion angles of the structure and then converted to a structural displacement as a high-resolution function of time. It can be seen in Figure 8.15a that the typical excursions reach a level of about 2

cm peak to peak over periods of about 7 seconds. The envelope of these excursion measurements shows the response of the Sky Tower to wind gusts. It is important to note that the measurements have a very good signal to noise ratio despite the small overall values (Franco-Anaya et al. 2008a).

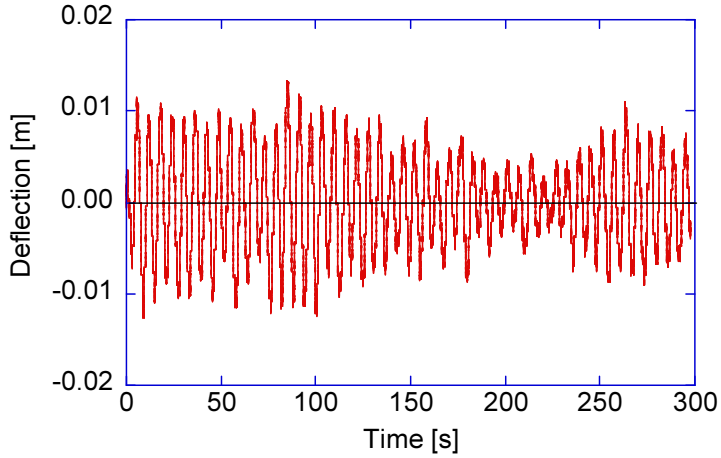

(a) Displacement time-history

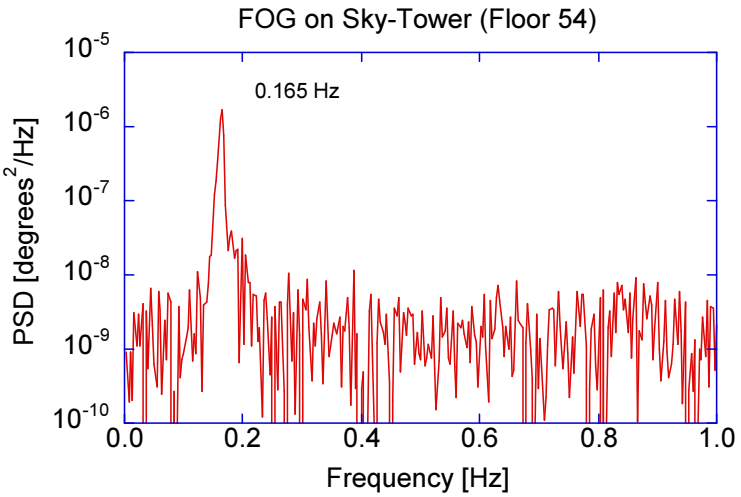

(b) Power spectrum

Figure 8.15 Measurements at level 54 of the Sky Tower.

A power spectrum was obtained from the displacement time-history at level 54 of the Sky Tower. The power spectral density (PSD) describes how the power of the signal is

distributed with frequency. A resonance frequency of 0.165 Hz that corresponds to the rocking mode of the structure can clearly be seen in Figure 8.15b.

8.5 SUMMARY

This chapter has described a novel measurement concept that utilises a fibre-optic gyroscope (FOG) as the measurement device. FOGs are devices that use the Sagnac effect to interferometrically detect mechanical rotations from optical beams. They are absolutely referenced to the local universe and therefore do not require an external reference frame to operate. Shake table measurements of the one-fifth scale structure and displacement measurements at the Sky Tower validated the suitability of these sensors for applications in civil engineering.

The FOG was attached to one of the first storey columns of the model structure during the seismic testing. Four earthquake records at different levels of intensity were used to investigate the accuracy of the measurements recorded by the FOG. Column rotations and displacements at the first floor were calculated from the rotation rates measured by the FOG. A very good agreement was observed between the measurements obtained with the FOG and those provided by a conventional linear potentiometer. The FOG was also used to measure rotation rates (i.e. torsion) at the third floor of the model structure. However, no significant torsional motions were measured because of the symmetry of the model structure. The shake table results validated the accuracy of the measurements recorded by the FOG.

The measurement concept was also applied at the 328 m tall Sky Tower in Auckland. The Sky Tower was considered a challenging target because of the demands involved for the measurement technique. The FOG was installed on the 54th and 60th floors of the tower structure. During three days, several sets of measurements were carried out under calm wind conditions. The measurements taken by the FOG provided a very good signal to noise ratio of the measurement quantity and confirmed the suitability of the sensor for applications in actual civil engineering structures.

Chapter 9
CONCLUSIONS AND CONTRIBUTIONS OF THE RESEARCH

9.1 EXECUTIVE SUMMARY

In this research, the effect of adding structural viscous damping was examined for a single-degree-of-freedom (SDOF) system. The concept of 2-4 viscous damping was introduced. This concept involves the addition of viscous damping to the second and fourth quadrants of the force-displacement curve. Numerical simulations were used to demonstrate the validity of the concept for linear SDOF systems subjected to harmonic and seismic excitations. Time-history analyses and response spectra for SDOF systems were presented to assess the effect of adding 2-4 viscous damping. Although this topic is an aside to the main direction of the thesis, it shows the important benefits of adding viscous damping to certain portions of the dynamic hysteresis loop and introduces the concepts that are discussed subsequently in the thesis. The approach can be extended to study the effects of adding viscous damping to all quadrants and to the first and third quadrants of the force-displacement diagram, referred to as the 1-2-3-4 and 1-3 viscous damping, respectively. Since the 2-4 viscous damping can reduce the structural response but without increasing the loads on the foundation of the structure, it was chosen to be investigated here.

In recent years, semi-active resettable devices have been considered for applications in earthquake engineering. These devices offer several advantages in comparison to other semi-active control devices. Resettable devices manipulate the stiffness properties of the structure and are capable of producing large resisting forces. The basic design of the device is feasible for pneumatic and hydraulic implementations and employs relatively simple mechanisms and control logic. The device offers a great deal of reliability due to its reliance on standard hydraulic or pneumatic concepts, in particular when compared to devices that employ more mechanically and dynamically complicated smart materials

such as electro-rheological and magneto-rheological fluids. Resettable devices rely on very low power consumption and are subjected to a set of decentralised control logic.

A newly developed semi-active resettable device for the seismic protection of civil engineering structures was proposed. Unlike conventional devices, this device has a novel two-chambered design that eliminates the need to rapidly dissipate seismic energy between the two chambers. The two-chambered design employs each side of the device piston independently. This approach treats each piston side as an independent chamber with its own valve and control. The independent chamber design allows a wider variety of control laws to be imposed, as each valve can be operated independently, allowing independent control of the pressure on each side of the piston. The device also offers the opportunity to sculpt structural hysteretic behaviour due to the possibility to control the device valve and reset times actively. The device uses air as the working fluid for simplicity and to make use of the surrounding atmosphere as the fluid reservoir.

Analytical studies were carried out to evaluate the seismic performance of the resettable devices. A tendon element with an ideal (linear) resettable hysteresis was adopted as the energy dissipation device to reduce the seismic response of a four-storey one-fifth scale structure. Several tendon configurations under different earthquake ground motions were used to evaluate the effectiveness of the resettable tendon. Nonlinear time-history analyses were carried out to determine the optimal configuration of the semi-active resettable tendon in the structure. The seismic performance of the model structure was evaluated in terms of reductions in relative displacements, absolute accelerations, inter-storey drift ratios and total base shear.

A series of shake table tests were performed on the one-fifth scale structure to assess the effectiveness of the resettable devices in reducing the seismic response of structures. Two semi-active resettable devices were installed as part of the lateral bracing of the model structure to reduce the structural response. The dynamic characteristics of the structure and resettable devices were investigated. Four earthquake records at different levels of intensity were used to investigate the effect of the addition of the devices on the seismic response. During the seismic testing, the devices modified the stiffness of

the structure by following a control algorithm that took into account the measured responses of the model structure and the devices. Different control laws were used to manipulate the hysteretic behaviour of the resettable devices.

A numerical model was developed to simulate the seismic response of the semi-active resettable tendon used during the shake table tests. The mathematical model has three primary components. The first component represents the resettable device, the second component simulates the steel tendon and the third component models the steel restraint element. The three components of the model were modelled using spring members with different hysteretic behaviours. Inelastic dynamic analyses utilising the RUAUMOKO computer program were performed to assess the accuracy of the computational model.

Analytical studies were conducted to investigate the performance of a twelve-storey reinforced concrete building subjected to earthquake excitations and controlled by resettable devices. Computer simulations were performed to determine the optimal utilization of the resettable devices in the structure. The effectiveness of the devices in reducing the seismic response was discussed in relation to the number and distribution of the devices. Various tendon configurations were used to transfer the control forces to the frame building. The impact of different control laws on the seismic response of the structure was examined. The use of a lever system and a high-pressure air source was investigated to improve the seismic performance of the resettable devices. A number of recommendations are given for the implementation of resettable devices in structural buildings systems.

Fibre-optic gyroscopes (FOGs) are passive interferometers where a beam of light is split in two equal parts. These parts then travel along several hundred metres of glass fibre coil around a closed circuit, one in the clockwise and the other in the anticlockwise sense. When the beam is recombined upon exiting the fibre, it shows a fringe pattern, which depends on the rate of rotation, but does not change with translation. The rotation rates measured in this way are absolute with respect to the local universe. Consequently, the measurement device does not require a reference frame to operate.

Finally, a new measurement concept that employs fibre-optic gyroscopes was proposed to measure the rotation rates, rotations, displacements and inter-storey drifts of civil engineering structures. FOGs are compact, easy to install and, unlike conventional potentiometers, do not require a fixed reference frame to operate. Shake table tests were performed on the four-storey one-fifth scale structure equipped with a fibre-optic gyroscope. Relative displacements at the first floor and rotations at the third floor were calculated from the measurements provided by the FOG. The FOG was also used to measure the displacements of the 328 m tall Sky Tower in Auckland. The FOG was installed on the 54th and 60th floors of the tower structure. During three days, numerous sets of measurements were recorded under calm wind conditions. This research differs from the main research topic covered in the thesis. However, it is included here due to the importance of the FOG as an emerging measurement concept in civil engineering. Moreover, the experimental validation of the FOG was conducted in conjunction with the seismic testing of the one-fifth scale structure.

9.2 CONCLUSIONS OF THE RESEARCH

Important conclusions and observations of the research reported in this doctoral thesis are listed below:

- Simulation results presented in Chapter 2 indicated that the addition of 2-4 viscous damping was beneficial for reducing the harmonic and seismic response of a wide range of SDOF systems. The 2-4 viscous damping has the potential to reduce the response of the structure without increasing the loads on the foundation.

- The optimal configuration of the linear resettable tendon described in Chapter 4 follows the load-balancing concept widely utilised in the design of pre-stressed concrete elements. Analytical investigations showed that the system B1-3 based on the optimal tendon configuration significantly reduces the relative displacements, inter-storey drift ratios and total base shear. The linear resettable tendon consists of a tendon member with a linear resettable hysteresis.

- The shake table test results reported in Chapter 5 confirmed the effectiveness of the semi-active resettable devices to reduce the seismic response of the model structure and demonstrated the significant potential of the devices for the seismic protection of civil engineering structures. The conclusions related to the shake table testing of the model structure are given in what follows.

  The reductions in floor displacements and inter-storey drifts achieved by the 1-2-3-4 control law are comparable to those afforded by the valves closed case (stiff bracing system). However, the valves closed case increases the floor accelerations and base shear demand in comparison to the 1-2-3-4 control law. In consequence, the 1-2-3-4 control law should be preferred over the valves closed case for applications in new or existing structures where reductions in floor displacements are necessary to avoid structural damage.

  The 2-4 control law reduces the absolute floor accelerations and the total base shear compared to the other control laws. Therefore, the 2-4 control law could be used for the retrofit of existing structures where reducing the shear demand at the foundation is preferable over expensive and complicated foundation strengthening.

  For ground motions of high level of excitation, the response reductions delivered by the 1-3 control law are similar to those achieved by the valves closed case. However, the 1-3 control law does not increase the floor accelerations and the total base shear as much as the valves closed case.

  The switching control law or 1-2-3-4 to 2-4 control law reduces the seismic response efficiently by combining the benefits of the 1-2-3-4 and 2-4 control laws over the entire length of the earthquake record.

  The valves open case delivers larger seismic response reductions than those of the uncontrolled case because of the resisting forces provided by the flexible bracing system and the friction in the devices.

- Comparisons of analytical predictions with experimental results indicated that the numerical model developed in Chapter 6 was able to reproduce the experimental behaviour of the devices and the resettable tendon used during the shake table tests of the one-fifth scale structure.

- A semi-active control system is proposed in Chapter 7 for reducing the earthquake response of a twelve-storey reinforced concrete building. The control system uses a resettable device, rigid rods and pre-stressed tendons. The conclusions based on analytical studies of the control system include the following:

  Increasing the number of resettable devices in the structure does not reduce the seismic response. On the contrary, the response of the structure is amplified. This effect is caused by actuator-actuator interaction and reflects the influence of higher modes on the seismic response of tall structures.

  The use of pre-stressed tendons and bracings without resettable devices increases the floor accelerations and the total base shear of the structure. In contrast, the use of resettable devices combined with pre-stressed tendons and bracings reduces the floor displacements and inter-storey drifts without increasing the floor accelerations and the base shear demand significantly.

  The reduction of the seismic response achieved by the 1-2-3-4, 1-3 and 2-4 control laws is very similar for this particular structure. The difference in response reduction delivered by the three control laws is not significant. Different combinations of the control laws do not lead to further improvement of the response reduction. However, all control laws and their combinations reduce the seismic response effectively.

  The previous conclusions may indicate that an optimal solution for the future implementation of resettable devices in multi-storey structures should include the device capacity, tendon configuration or control architecture and control law.

A lever system placed between the structure and the device and a high-pressure air source connected to the device can be used to improve the seismic performance of the resettable devices. Both approaches efficiently increase the maximum resisting forces delivered by resettable devices that use air as the working fluid. Furthermore, the use of any of the approaches eliminates the need for increasing the original size of the device.

- The results of the shake table tests and the in-situ testing presented in Chapter 8 validated the suitability of the fibre-optic gyroscope (FOG) to measure structural rotations in civil engineering. Comparison of displacement measurements obtained during the shake table tests of the model structure confirmed the accuracy of the measurements recorded by the FOG and the dynamic range of the sensor. The measurements taken by the FOG at the Sky-Tower provided a very good signal to the noise ratio of the measurement quantity.

9.3 CONTRIBUTIONS OF THE RESEARCH

It is considered important to identify the material that is new in this research and makes a unique contribution to the fields of earthquake engineering and structural control. The main contributions of this research include the following:

- The concept of the 2-4 viscous damping is introduced to reduce the harmonic and seismic response of single-degree-of-freedom (SDOF) systems. Linear time-history analyses and response spectra for a wide range of SDOF systems are presented to assess the effect of adding 2-4 viscous damping.

- A computational model is developed to study the performance of a linear resettable tendon in reducing the seismic response of structures. Nonlinear dynamic analyses are performed on a four-storey model structure equipped with the resettable tendon. The effects on the earthquake response resulting from the addition of the resettable tendon are examined.

- A newly developed semi-active resettable device is proposed to reduce the seismic response of civil engineering structures. Shake table tests are performed on a one-fifth scale structure equipped with two prototype resettable devices. The shake table tests represent the first large-scale application of these resettable devices in civil engineering. The tests also validate the ability of the devices to sculpt or re-shape structural hysteretic behaviour for the first time. The results of the shake table tests are presented and interpreted.

- A mathematical model is developed to predict the behaviour of the resettable device used during the shake table tests. Inelastic time-history analyses are performed to examine the effectiveness of the model. Comparisons of analytical predictions with experimental results are presented to evaluate the accuracy of the numerical model.

- Tendon arrangements and strategies based on semi-active resettable devices are proposed to mitigate the seismic response of structural building systems. Inelastic dynamic analyses are carried out to evaluate the performance of a twelve-storey reinforced concrete building controlled by resettable devices. Relevant issues for the implementation of resettable devices in actual building systems are identified.

- A new measurement concept that uses fibre-optic gyroscopes (FOGs) is introduced to measure the rotation rates, rotations, displacements and inter-storey drifts of civil engineering structures. Different shake table measurements of the one-fifth scale structure and displacement measurements at the Sky Tower in Auckland validated the suitability of the FOGs for civil engineering applications. The shake table tests and the in-situ testing are the first civil engineering applications of the FOG.

It is important to note that although this research is mainly oriented towards earthquake engineering applications, the results here presented are certainly of interest within the general framework of strategies for dynamic response reduction and provide useful information for the use of semi-active resettable devices and fibre-optic gyroscopes in other engineering fields.

Chapter 10
FUTURE RESEARCH

The analytical and experimental studies presented in this doctoral thesis have shown that the semi-active resettable devices are an effective means of mitigating the seismic response of civil engineering structures. However, some of the findings of this research have indicated that various issues related to this novel control technique require further investigation. These issues include the following:

- In this research, the resettable devices were implemented in the form of bracing or tendon systems to reduce the seismic response of structures. However, it should be noted that any other structural configuration, in which the resettable devices are connected in series to structural elements storing elastic strain energy, may be used to demonstrate the effectiveness of the resettable devices. For example, equally valid configurations can be obtained by connecting the resettable devices to a tuned mass damper system or by inserting the devices between the foundation elements and the superstructure of a building.

- As described in Chapter 3, the here presented resettable device utilises air as the working fluid and is able to sculpt or re-shape structural hysteretic behaviour due to the possibility of controlling the device valves and reset times actively. It should be noted that the benefits provided by the independent control of the device valves could be generalised to similar viscous damping devices to enhance the hysteretic behaviour of such devices.

- The significant effect of the friction on the performance of the resettable device was observed during the shaking table tests of the one-fifth scale structure described in Chapter 5. The impact of the friction between the seals around the device piston and the cylinder wall needs to be evaluated, both qualitatively and quantitatively, for the potential implementation of the semi-active resettable devices in civil engineering structures.

- The control system and the structure do not behave as independent dynamic systems but rather interact with each other. Interaction effects also occur between the sensors and the structure. These control-structure and sensor-structure interactions were considered to be negligible in this research. However, it would be advantageous to investigate these interaction effects before the full-scale implementation of resettable devices.

- Control algorithms for the operation of the resettable devices need to be developed to include, in addition to the usual performance parameters of the structure, relevant aspects such as control-structure interaction, device and sensor dynamics, parametric uncertainties, control force limitations, valve operation and time delay.

- System integration is another important issue that requires further investigation. The controlled structure, the semi-active resettable device, the sensor responses and the control hardware and/or software must be considered as an entire system during the design process.

- Additional investigations are necessary to refine the computational model of the resettable tendon developed in Chapter 6. A closer representation of the stiffness and the friction force of the resettable device should be included in futures studies. The energy release time and any response delay of the device valves should be included in the modelling. The modelling of the tendon slackness needs to be improved and its effect on the seismic response further investigated.

- It was shown in Chapter 7 that one of the limiting factors for the implementation of the resettable devices in full-scale civil structures could be the moderate resisting forces delivered by the device in comparison to its size. Although the addition of a high-pressure air source proved to be an effective solution, further research work is required to increase the level of the resisting forces produced by resettable devices.

- The use of the resettable devices in combination with other passive or active control techniques could reduce the effects of the actuator-actuator interaction and improve

the response forces produced by the resettable device alone. However, analytical and experimental studies need to be carried out in this direction.

- Like other semi-active control devices, the resettable devices rely on very low power consumption. However, reliable and long-life power sources for the operation of the devices during severe earthquake loads need to be advanced.

- It would be very beneficial to develop maintenance strategies, self diagnostics and automated correction to ensure that all the components of the resettable device will work properly when called upon after not being in operation for extended periods of time.

- It is recommended that the design methodology of the resettable devices should be established on the basis of performance criteria that evaluate the safety and function of the structure. A primary task for future research is the development of prototype design standards or specifications that complement the existing design standards.

These kinds of issues must be addressed before the semi-active resettable devices can systematise the technology for performance design and ensure structural safety against destructive environmental loads.

REFERENCES

Algan, B. B. (1982). “Drift and damage considerations in earthquake resistant design of reinforced concrete buildings.” PhD Thesis, University of Illinois, Urbana-Champaign, Illinois.

Barroso, L. R., Chase, J. G., and Hunt, S. (2003). “Resettable smart dampers for multi-level seismic hazard mitigation of steel moment frames.” *Journal of Structural Control,* 10(1), 41-58.

Bishay-Girges, N. W. (2004). “Seismic protection of structures using passive control system.” PhD Thesis, Department of Civil Engineering, University of Canterbury, Christchurch, New Zealand.

Bobrow, J. E., Jabbari, F., and Thai, K. (1995). “An active truss element and control law for vibration suppression.” *Smart Materials and Structures,* 4(4), 264-269.

Bobrow, J. E., Jabbari, F., and Thai, K. (2000). “A new approach to shock isolation and vibration suppression using a resetable actuator.” *Journal of Dynamic Systems, Measurement, and Control,* 122(3), 570-573.

Britannica Online Encyclopedia (http://www.britannica.com/eb/topic-1033455/fibre-optic-gyroscope).

Carr, A. J. (1997). “Damping models for inelastic structures.” *Proc., 2nd Asia-Pacific Vibration Conference,* Kyongju, Korea.

Carr, A. J. (2006). “RUAUMOKO-Inelastic dynamic analysis program.” Computer Program Library, Department of Civil Engineering, University of Canterbury, Christchurch, New Zealand.

Casciati, F., Magonette, G., and Marazzi, F. (2006). *Technology of semiactive devices and applications in vibration mitigation,* John Wiley & Sons, Ltd., Chichester, England.

Chase, J. G., Mulligan, K. J., Gue, A., Mander, J. B., Alnot, T., Rodgers, G., Deam, B., Cleeve, L., and Heaton, D. (2005a). "Resetable devices with customised performance for semi-active seismic hazard mitigation of structures." *Technical Papers, NZSEE Conference 2005, Planning and engineering for performance in earthquakes,* Wairakei, New Zealand, P. Brabhaharan, ed., New Zealand Society for Earthquake Engineering Incorporated, Wellington.

Chase, J. G., Hudson, N. H., Lin, J., Elliot, R., and Sim, A. (2005b). "Nonlinear shake table identification and control for near-field earthquake testing." *Journal of Earthquake Engineering,* 9(4), 461-482.

Chase, J. G., Mulligan, K. J., Hunt, S. J., Barroso, L. R., and Deam, B. L. (2005c). "Actuator-actuator interaction and instability in decentralised control of non-linear seismically excited tall structures." *Proc., 9th International Conference on Structural Safety and Reliability,* Rome, Italy.

Chase, J. G., Mulligan, K. J., Gue, A., Alnot, T., Rodgers, G., Mander, J. B., Elliott, R., Deam, B., Cleeve, L., and Heaton, D. (2006). "Re-shaping hysteretic behaviour using semi-active resettable device dampers." *Engineering Structures,* 28(10), 1418-1429.

Chase, J. G., Mulligan, K. J., Elliott, R. B., Rodgers, G. W., Mander, J. B., Carr, A. J., and Franco-Anaya, R. (2007). "Re-shaping hysteresis: Seismic semi-active control experiments for a 1/5th scale structure." *Proc., 8th Pacific Conference on Earthquake Engineering,* Singapore.

Chey, M. H., Mander, J. B., Carr, A. J., and Chase, J. G. (2006). "Multi-storey semi-active tuned mass damper building system." *Proc., 19th Conference on the Mechanics of Structures and Materials, Progress in mechanics of structures and materials,*

Christchurch, New Zealand, P. J. Moss, and R. P. Dhakal, eds., Taylor & Francis/Balkema, Leiden, The Netherlands.

Chopra, A. K. (2001). *Dynamics of structures: Theory and applications to earthquake engineering,* 2nd Edition, Prentice-Hall, Inc., Upper Saddle River, New Jersey.

Clough, R. W., and Penzien, J. (1993). *Dynamics of structures,* 2nd Edition, McGraw-Hill, Inc., New York.

Connor, J. J., and Klink, B. S. A. (1996). *Introduction to motion based design,* Computational Mechanics Publications, Southampton, UK and Boston, USA.

Dodd, L. L., and Restrepo-Posada, J. I. (1995). "Model for predicting cyclic behavior of reinforcing steel." *Journal of Structural Engineering,* 121(3), 433-445.

Franco-Anaya, R., Carr, A. J., Mander, J. B., and Chase, J. G. (2006). "Seismic protection of a four-storey one fifth scale structure using semi-active resetable tendon elements." *Proc., 19th Conference on the Mechanics of Structures and Materials, Progress in mechanics of structures and materials,* Christchurch, New Zealand, P. J. Moss, and R. P. Dhakal, eds., Taylor & Francis/Balkema, Leiden, The Netherlands.

Franco-Anaya, R., Carr, A. J., Mander, J. B., Chase, J. G., Mulligan, K. J., and Rodgers, G. W. (2007a). "Seismic testing of a model structure with semi-active resetable devices." *Proc., NZSEE Conference 2007, Performance by design: Can we predict it?,* Palmerston North, New Zealand, G. Beattie, ed., (CD-ROM), New Zealand Society for Earthquake Engineering Incorporated, Wellington.

Franco-Anaya, R., Carr, A., and Chase, G. (2007b). "Experimental investigation on semi-active resettable devices for seismic protection of structures." *Proc., 12th Asia-Pacific Vibration Conference,* Sapporo, Japan.

Franco-Anaya, R., Carr, A. J., and Schreiber, K. U. (2008a). "Qualification of fibre-optic gyroscopes for civil engineering applications." *Proc., NZSEE Conference 2008, Engineering an earthquake resilient New Zealand,* Wairakei, New Zealand, (CD-ROM), New Zealand Society for Earthquake Engineering Incorporated, Wellington.

Franco-Anaya, R., Carr, A. J., and Chase, G. (2008b). "Semi-active resettable devices for seismic protection of civil engineering structures." *Proc., 14th World Conference on Earthquake Engineering,* Beijing, China.

Giberson, M. F. (1969). "Two nonlinear beams with definitions of ductility." *Journal of the Structural Division, ASCE,* Vol. 95, No. ST2, 137-157.

Hahn, G. D., and Sathiavageeswaran, K. R. (1992). "Effects of added-damper distribution on the seismic response of buildings." *Computers and Structures,* 43(5), 941-950.

Hanson, R. D., and Soong, T. T. (2001). *Seismic design with supplemental energy dissipation devices,* EERI monograph (MNO-8), Earthquake Engineering Research Institute, Oakland, California.

Horwich, G. (2000). "Economic lessons of the Kobe earthquake." *Economic Development and Cultural Change,* 48(3), 521-542.

Housner, G. W., Bergman, L. A., Caughey, T. K., Chassiakos, A. G., Claus, R. O., Masri, S. F., Skelton, R. E., Soong, T. T., Spencer, B. F., and Yao, J. T. P. (1997). "Structural control: Past, present, and future." *Journal of Engineering Mechanics,* 123(9), 897-971.

Hrovat, D., Barak, P., and Rabins, M. (1983). "Semi-active versus passive or active tuned mass dampers for structural control." *Journal of Engineering Mechanics,* 109(3), 691-705.

Humar, J. L. (2002). *Dynamics of structures,* 2nd Edition, A. A. Balkema Publishers, Lisse, The Netherlands.

Hunt, S. J. (2002). "Semi-active smart-dampers and resetable actuators for multi-level seismic hazard mitigation of steel moment resisting frames." ME Thesis, Department of Mechanical Engineering, University of Canterbury, Christchurch, New Zealand.

Hunt, S. J., Chase, J. G., and Barroso, L. R. (2002). "The impact of time varying equilibrium location in the semi-active control of non-linear seismically excited structures." *Proc., 7th International Conference on Control, Automation, Robotics and Vision,* Singapore.

Igel, H., Schreiber, U., Flaws, A., Schuberth, B., Velikoseltsev, A. and Cochard, A. (2005). "Rotational motions induced by the M8.1 Tokachi-oki earthquake, September 25, 2003." *Geophysical Research Letters*, Vol. 32, L08309.

Jabbari, F., and Bobrow, J. E. (2002). "Vibration suppression with resettable device." *Journal of Engineering Mechanics,* 128(9), 916-924.

Ji, H., Badel, A., Qiu, J., Lefeuvre, E., Richard, C., and Guyomar, D. (2007). "Piezoelectric vibration damping by an enhanced semi-passive method." *Proc., 12th Asia-Pacific Vibration Conference,* Sapporo, Japan

Jury, R. D. (1978). "Seismic load demands on columns of reinforced concrete multi-storey frames." ME Thesis, Department of Civil Engineering, University of Canterbury, Christchurch, New Zealand.

Kao, G. C. (1998). "Design and shaking table tests of a four-storey miniature structure built with replaceable plastic hinges." ME Thesis, Department of Civil Engineering, University of Canterbury, Christchurch, New Zealand.

Karnopp, D., Crosby, M. J., and Harwood, R. A. (1974). "Vibration control using semi-active force generators." *Journal of Engineering for Industry,* 96(2), 619-626.

Leavitt, J., Jabbari, F., and Bobrow, J. E. (2005). "Optimal control and performance of variable stiffness devices for structural control." *Proc., 2005 American Control Conference,* Portland, Oregon.

Leavitt, J., Bobrow, J. E., Jabbari, F., and Yang, J. N. (2006). "Application of a high-pressure gas semi-active resettable damper to the benchmark smart base-isolated building." *Structural Control and Health Monitoring,* 13(2-3), 748-757.

Lefevre, H. C. (1993). *The Fiber-Optic Gyroscope*. Artech House Incorporated, ISBN-13: 978-0890065372.

Lin, T. Y. (1963). *Design of prestressed concrete structures,* 2nd Edition, Wiley, New York.

Lin, X. (1999). "Analysis and design of building structures with supplemental lead dampers under earthquake and wind loads." PhD Thesis, Department of Civil Engineering, University of Canterbury, Christchurch, New Zealand.

Mulligan, K. J., Chase, J. G., Gue, A., Alnot, T., Rodgers, G., Mander, J. B., Elliott, R., Deam, B., Cleeve, L., and Heaton, D. (2005). "Large scale resetable devices for multi-level seismic hazard mitigation of structures." *Proc., 9th International Conference on Structural Safety and Reliability,* Rome, Italy.

Mulligan, K. J. (2006). Personal communication.

Mulligan, K. J., Chase, J. G., Mander, J. B., and Elliot, R. (2007). "Semi-active resetable actuators incorporating a high pressure air source." *Proc., NZSEE Conference 2007, Performance by design: Can we predict it?,* Palmerston North, New Zealand, G.

Beattie, ed., (CD-ROM), New Zealand Society for Earthquake Engineering Incorporated, Wellington.

Mulligan, K. (2007). “Experimental and analytical studies of semi-active and passive structural control of buildings.” PhD Thesis, Department of Mechanical Engineering, University of Canterbury, Christchurch, New Zealand.

Newmark, N. M. (1959). “A method of computation for structural dynamics.” *Journal of the Engineering Mechanics Division, ASCE,* Vol. 85, No. EM3, 67-94.

Nishitani, A., and Inoue, Y. (2001). “Overview of the application of active/semiactive control to building structures in Japan.” *Earthquake Engineering and Structural Dynamics,* 30(11), 1565-1574.

Pekcan, G. (1998). “Design of seismic energy dissipation systems for reinforced concrete and steel structures.” PhD Thesis, State University of New York at Buffalo, Buffalo, New York.

Pekcan, G., Mander, J. B., and Chen, S. S. (2000). “Balancing lateral loads using tendon-based supplemental damping system.” *Journal of Structural Engineering,* 126(8), 896-905.

Rodgers, G. W., Mander, J. B., Chase, J. G., Mulligan, K. J., Deam, B. L., and Carr, A. (2007). “Re-shaping hysteretic behaviour-Spectral analysis and design equations for semi-active structures.” *Earthquake Engineering and Structural Dynamics,* 36(1), 77-100.

Rodriguez, M., Restrepo, J. I., and Carr, A. J. (2000). “Earthquake resistant precast concrete buildings: Floor accelerations in buildings.” *Research Report 2000-6,* Department of Civil Engineering, University of Canterbury, Christchurch, New Zealand.

Rodríguez, M. E., Restrepo, J. I., and Blandón, J. J. (2006). "Shaking table tests of a four-story miniature steel building-Model validation." *Earthquake Spectra,* 22(3), 755-780.

Rosser, J. B. (1967). "A Runge-Kutta for all seasons." *SIAM Review,* 9(3), 417-452.

Schreiber, K. U., Velikoseltsev, A., Stedman, G. E., Hurst, R. B., and Klügel, T. (2004). "Large ring laser gyros as high resolution sensors for applications in geoscience." *Proceedings of the 11th St. Petersburg International Conference on Integrated Navigation Systems*, 326-331.

Serino, G., Occhiuzzi, A., and Georgakis, C. (2001). "Experimental study and perspectives of semi-active oleodynamic devices for seismic protection of structures." *Experimental investigations on semi-active and passive systems for seismic risk mitigation,* CAFEEL-ECOEST2/ICONS Report No. 7, Franchioni, G., ed., Laboratório Nacional de Engenharia Civil, Lisboa, Portugal.

Singh, M. P., and Moreschi, L. M. (2002). "Optimal placement of dampers for passive response control." *Earthquake Engineering and Structural Dynamics,* 31(4), 955-976.

Soong, T. T. (1990). *Active structural control: Theory and practice,* Longman, Scientific & Technical, Longman Group UK Limited, Essex, England.

Soong, T. T., and Spencer, B. F., Jr. (2002). "Supplemental energy dissipation: State-of-the-art and state-of-the-practice." *Engineering Structures,* 24(3), 243-259.

Spencer, B. F., Jr., and Sain, M. K. (1997). "Controlling buildings: A new frontier in feedback." *IEEE Control Systems Magazine,* 17(6), 19-35.

Spencer, B. F., Jr., and Nagarajaiah, S. (2003). "State of the art of structural control." *Journal of Structural Engineering,* 129(7), 845-856.

Stedman, G. E. (1997). “Ring-laser tests of fundamental physics and geophysics.” *Reports on Progress in Physics,* 60(6), 615-688.

Suryanto, W., Igel, H., Wassermann, J., Cochard, A., Schuberth, B., Vollmer, D., Scherbaum, F., Schreiber, U., and Velikoseltsev, A. (2006). “First comparison of array-derived rotational ground motions with direct ring laser measurements.” *Bulletin of the Seismological Society of America,* 96(6), 2059-2071.

Symans, M. D., and Constantinou, M. C. (1997). “Seismic testing of a building structure with a semi-active fluid damper control system.” *Earthquake Engineering and Structural Dynamics,* 26(7), 759-777.

Symans, M. D., and Constantinou, M. C. (1999). “Semi-active control systems for seismic protection of structures: A state-of-the-art review.” *Engineering Structures,* 21(6), 469-487.

Wilson, E. L., and Penzien, J. (1972). “Evaluation of orthogonal damping matrices.” *International Journal for Numerical Methods in Engineering,* 4(1), 5-10.

Yang, J. N., Kim, J. H., and Agrawal, A. K. (2000). “Resetting semiactive stiffness damper for seismic response control.” *Journal of Structural Engineering,* 126(12), 1427-1433.

Yang, J. N., and Agrawal, A. K. (2002). “Semi-active hybrid control systems for nonlinear buildings against near-field earthquakes.” *Engineering Structures,* 24(3), 271-280.

Yang, J. N., Bobrow, J., Jabbari, F., Leavitt, J., Cheng, C. P., and Lin, P. Y. (2007). “Full-scale experimental verification of resetable semi-active stiffness dampers.” *Earthquake Engineering and Structural Dynamics,* 36(9), 1255-1273.

Yao, J. T. P. (1972). “Concept of structural control.” *Journal of the Structural Division, ASCE,* Vol. 98, No. ST7, 1567-1574.

Appendix A
COMPARISON OF RESPONSE SPECTRA

Response spectra obtained with the sub-program SPECTRA of the computer program RUAUMOKO are used to verify the response spectra provided by the MATLAB-based code developed to analyse the effect of adding viscous damping to SDOF systems and described in Chapter 2. The sub-program SPECTRA is designed to compute and plot the response spectra for an input earthquake accelerogram. This sub-program computes the spectral displacement (SD), spectral velocity (SV), pseudo spectral velocity (PSV), spectral acceleration (SA) and pseudo spectral acceleration (PSA). The sub-program also produces energy spectra (Carr 2006).

Figures A.1 to A.4 show comparisons of response spectra for the following earthquake ground motions:

a. Imperial Valley, 18 May 1940 – El Centro north-south (NS) component
b. Kern County, 21 July 1952 – Taft S21W component
c. Northridge, 17 January 1994 – Sylmar County Hospital (Chan 9: 0 deg)
d. Kobe, 17 January 1995 – JMA Observatory N00E component.

The fraction of critical damping is assumed to be 5%, which is a widely utilised value for civil engineering structures. It can be seen that the response spectra obtained by the MATLAB-based code match very well with the response spectra provided by the sub-program SPECTRA for all of the earthquakes investigated.

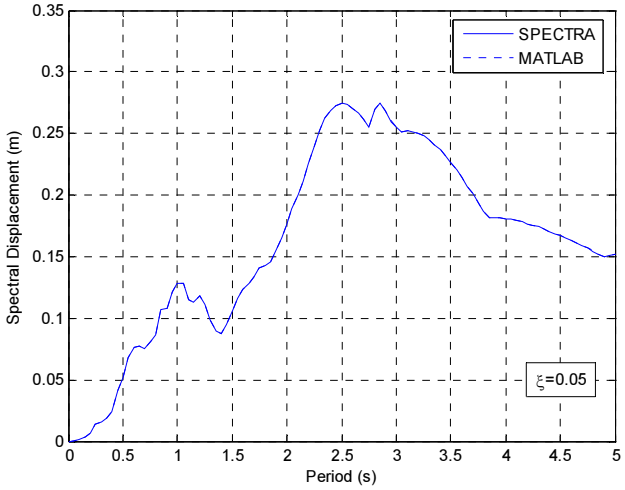

(a) Displacement response spectrum

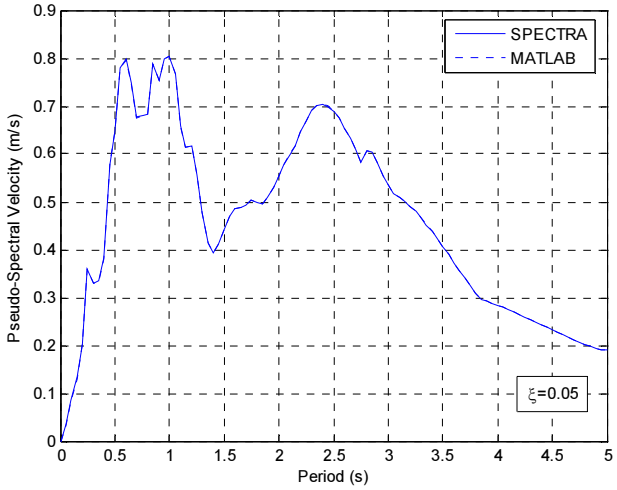

(b) Pseudo-velocity response spectrum

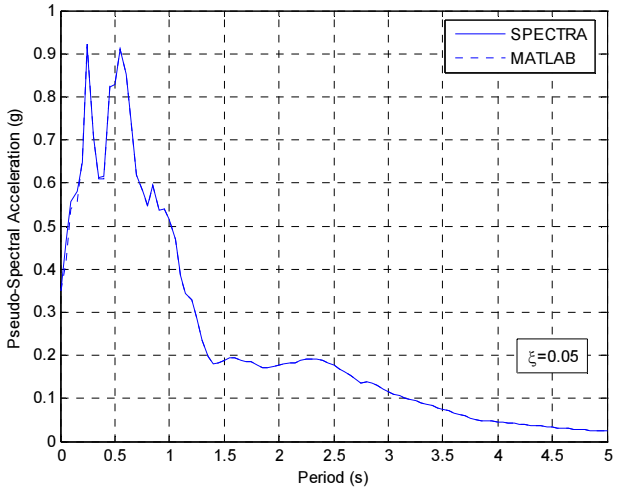

(c) Pseudo-acceleration response spectrum

Figure A.1 Comparison of response spectra for El Centro earthquake.

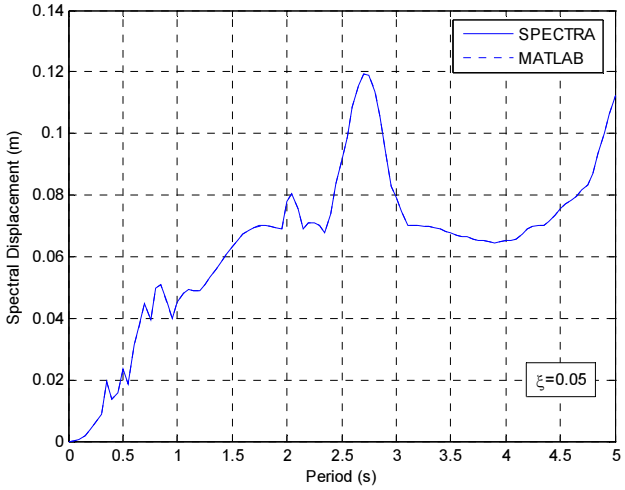

(a) Displacement response spectrum

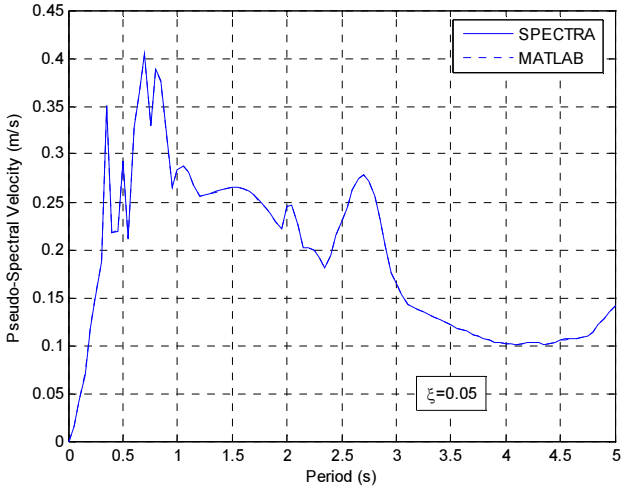

(b) Pseudo-velocity response spectrum

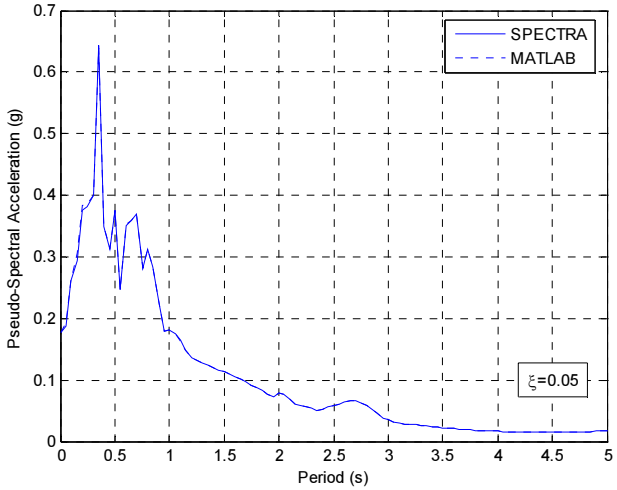

(c) Pseudo-acceleration response spectrum

Figure A.2 Comparison of response spectra for Taft earthquake.

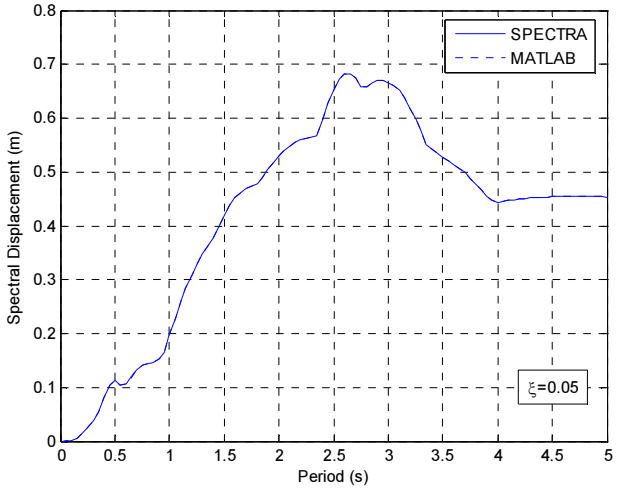

(a) Displacement response spectrum

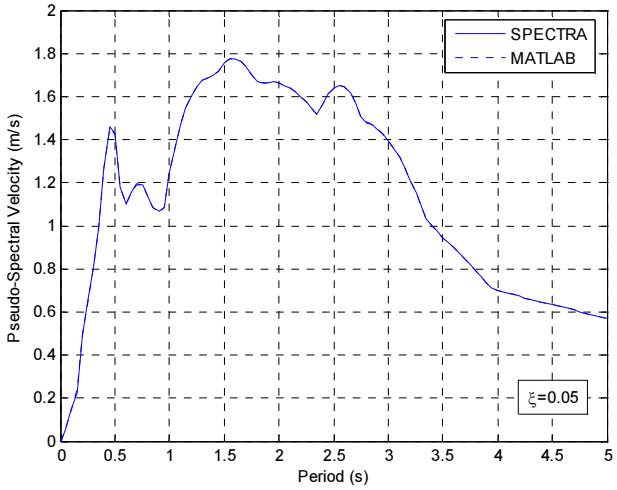

(b) Pseudo-velocity response spectrum

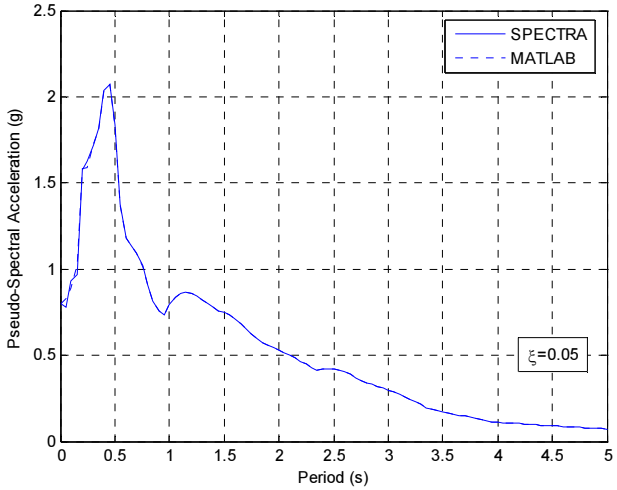

(c) Pseudo-acceleration response spectrum

Figure A.3 Comparison of response spectra for Sylmar earthquake.

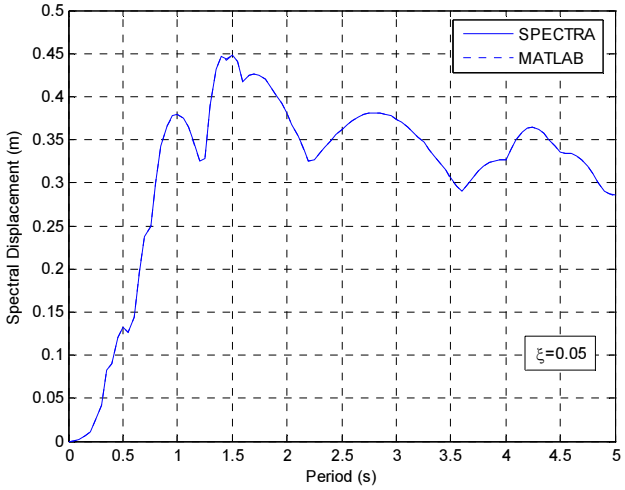

(a) Displacement response spectrum

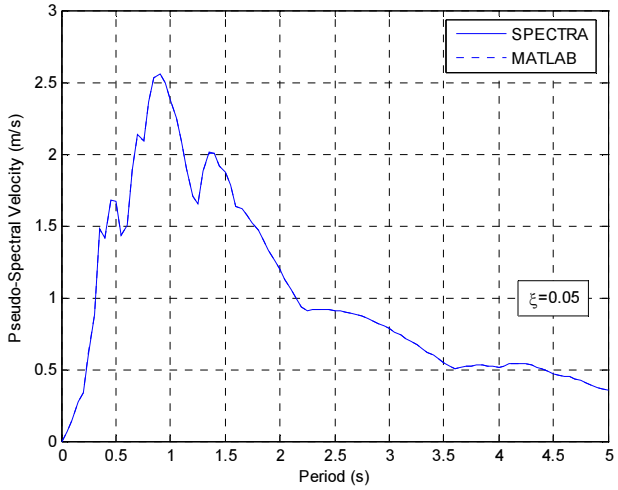

(b) Pseudo-velocity response spectrum

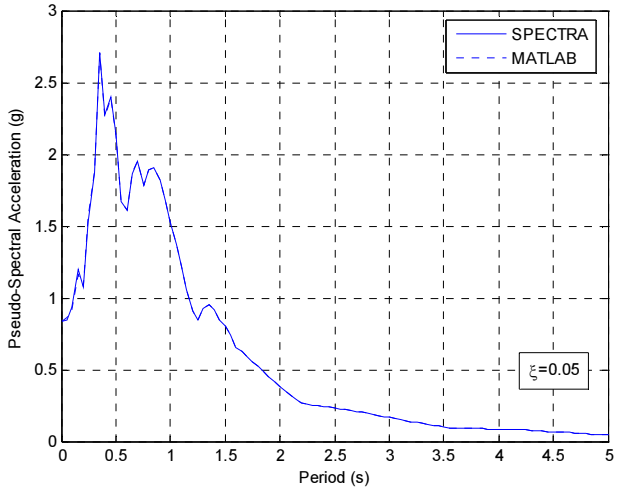

(c) Pseudo-acceleration response spectrum

Figure A.4 Comparison of response spectra for Kobe earthquake.

Appendix B
RESPONSE OF THE A-SYSTEMS AND B-SYSTEMS UNDER DIFFERENT EARTHQUAKES

Figures B.1 to B.6 show maximum response envelopes for the A-Systems and the B-Systems described in Chapter 4. The analytical results are presented for the following scaled earthquake records:

a. Kern County, 21 July 1952 – Taft S21W component scaled by 90% (0.1602g)
b. Northridge, 17 January 1994 – Sylmar County Hospital (Chan 9: 0 deg) scaled by 20% (0.1595g)
c. Kobe, 17 January 1995 – JMA Observatory N00E component scaled by 20% (0.1673g).

The seismic performance of the systems is evaluated in terms of reductions in relative displacements, absolute accelerations, inter-storey drift ratios and total base shear.

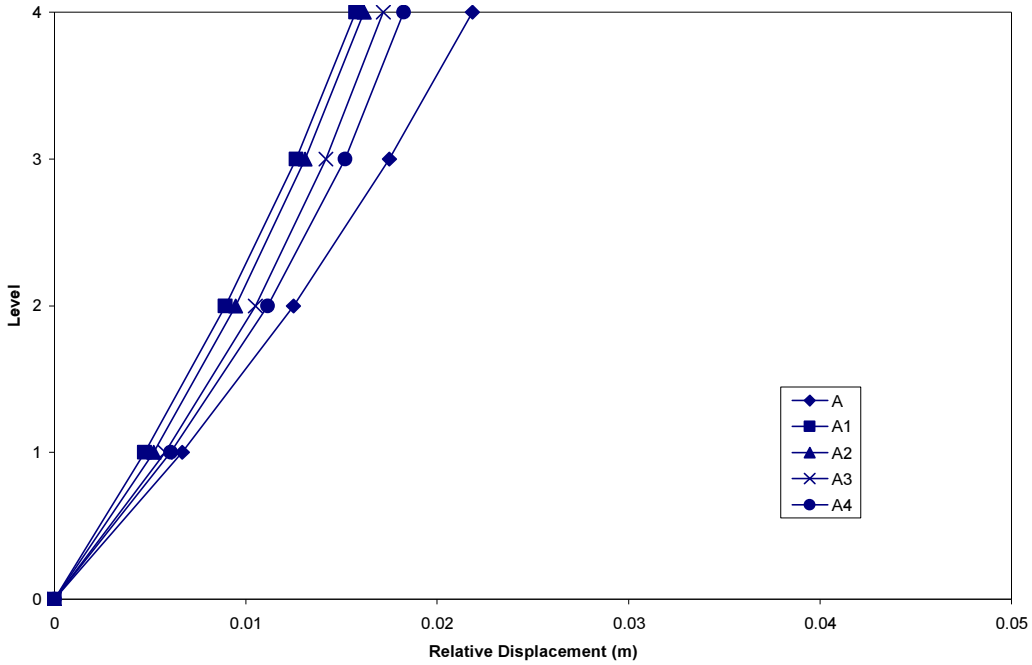

(a) Maximum relative displacements

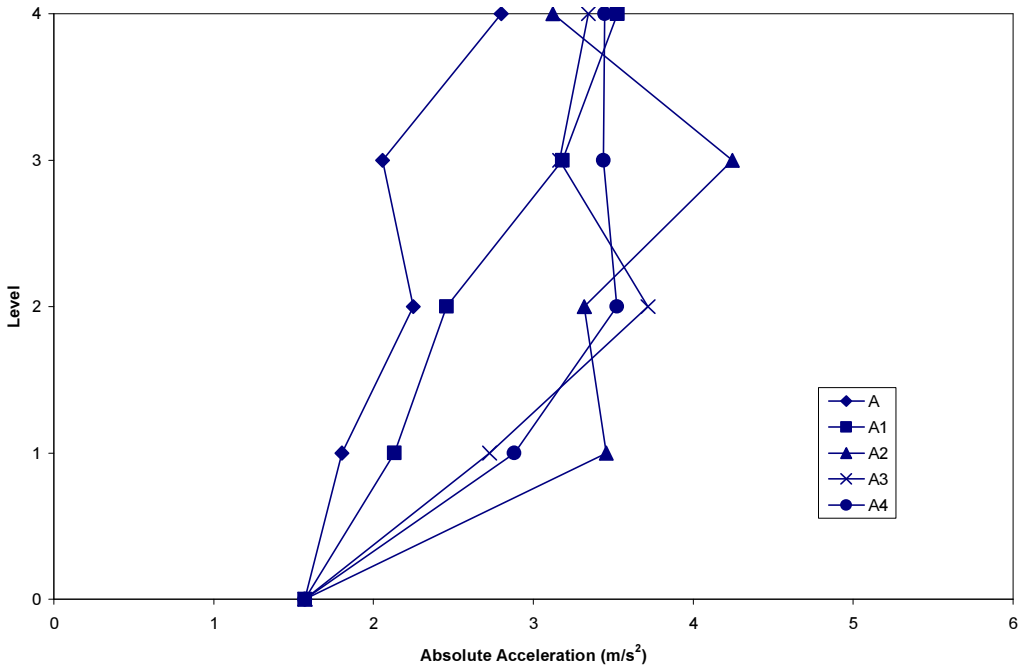

(b) Maximum absolute accelerations

Figure B.1 Maximum response envelopes of A-Systems for Taft 90% earthquake.

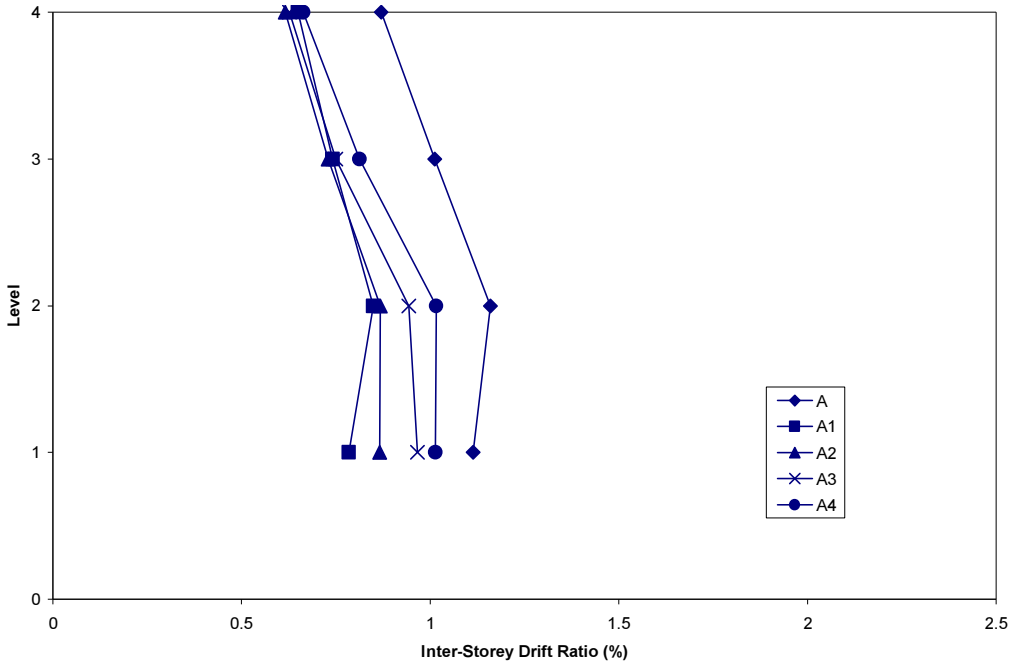

(c) Maximum inter-storey drift ratios

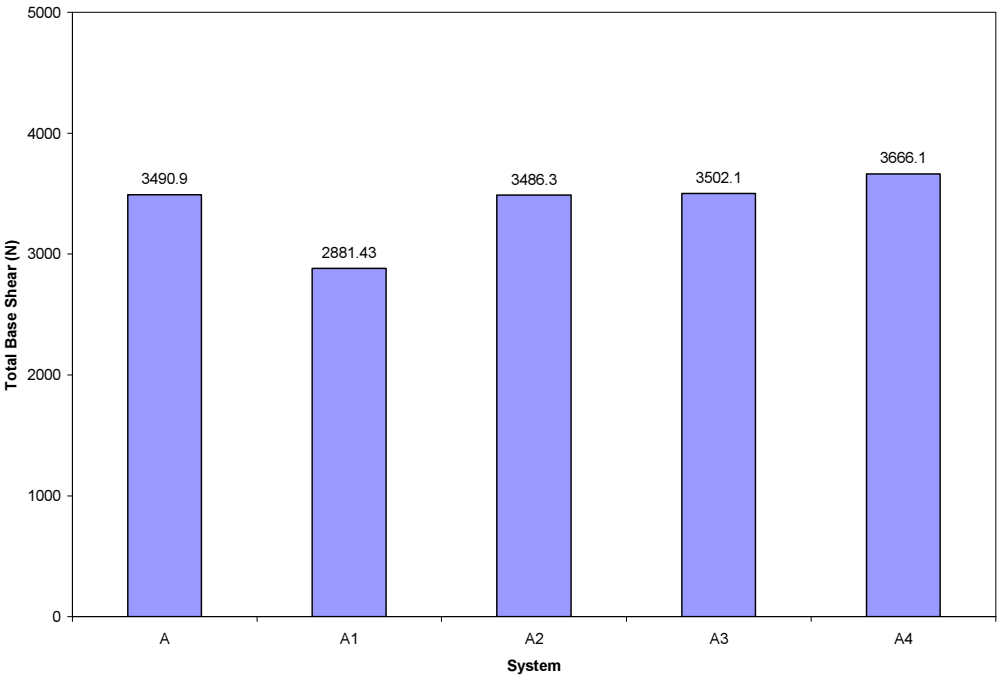

(d) Maximum total base shear

Figure B.1 (Continued).

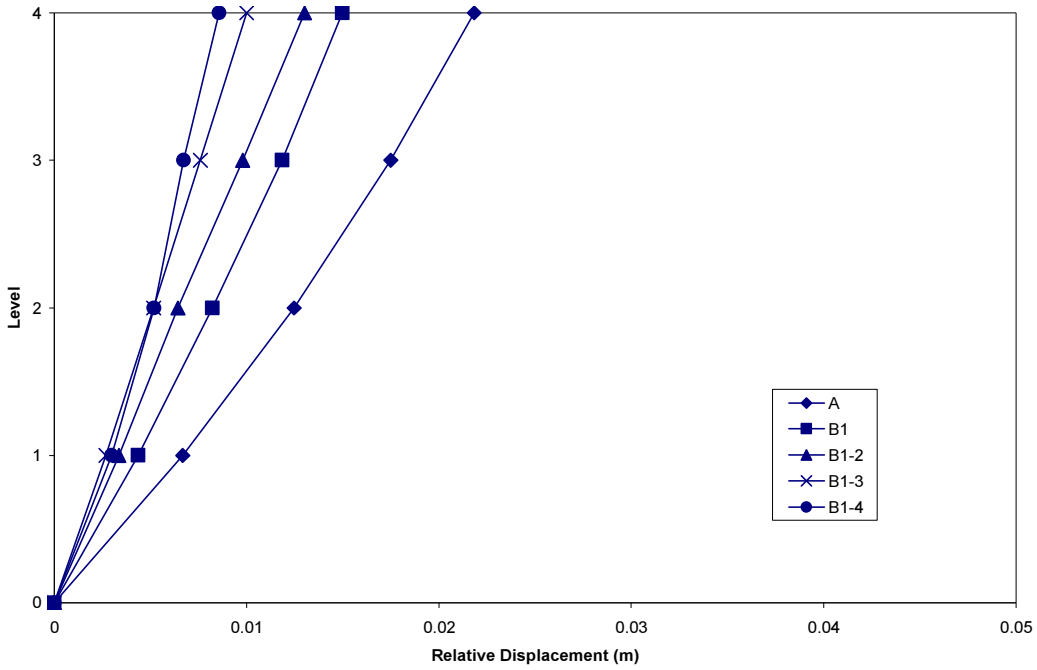

(a) Maximum relative displacements

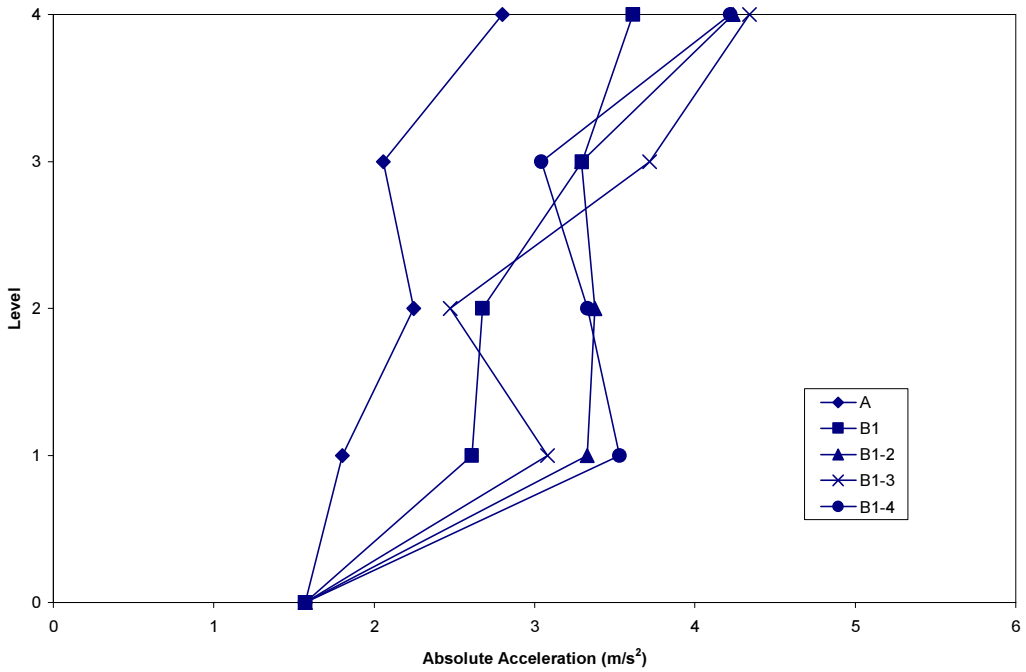

(b) Maximum absolute accelerations

Figure B.2 Maximum response envelopes of B-Systems for Taft 90% earthquake.

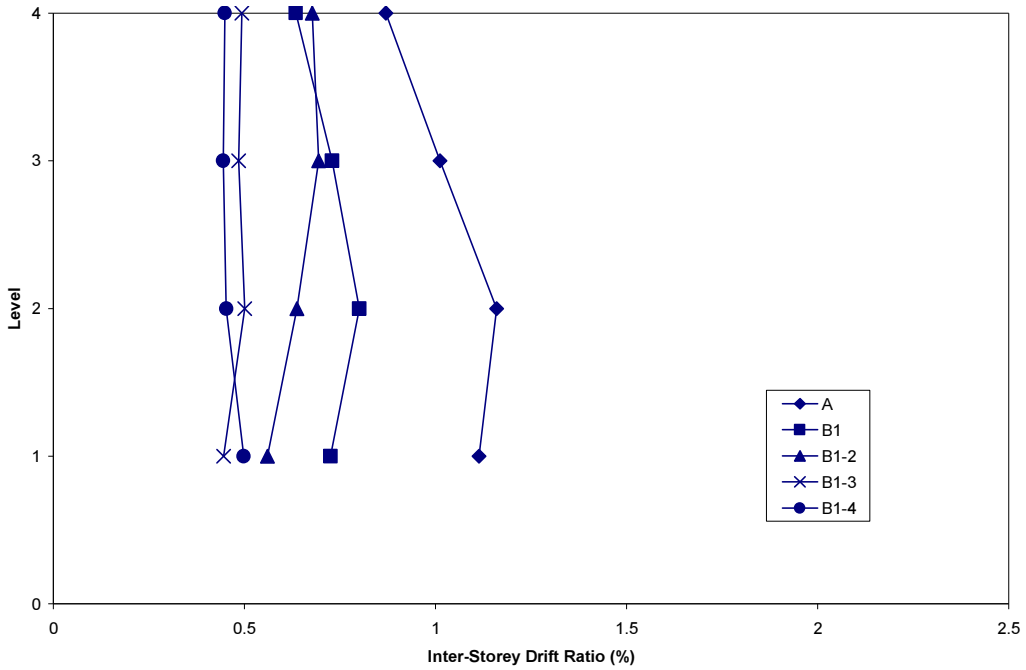

(c) Maximum inter-storey drift ratios

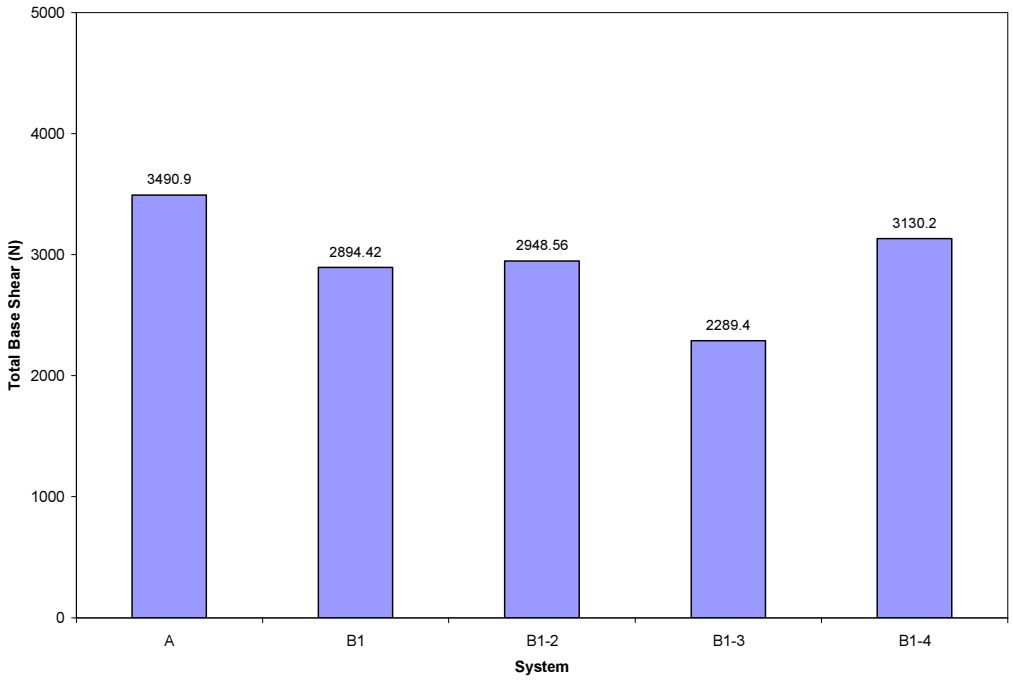

(d) Maximum total base shear

Figure B.2 (Continued).

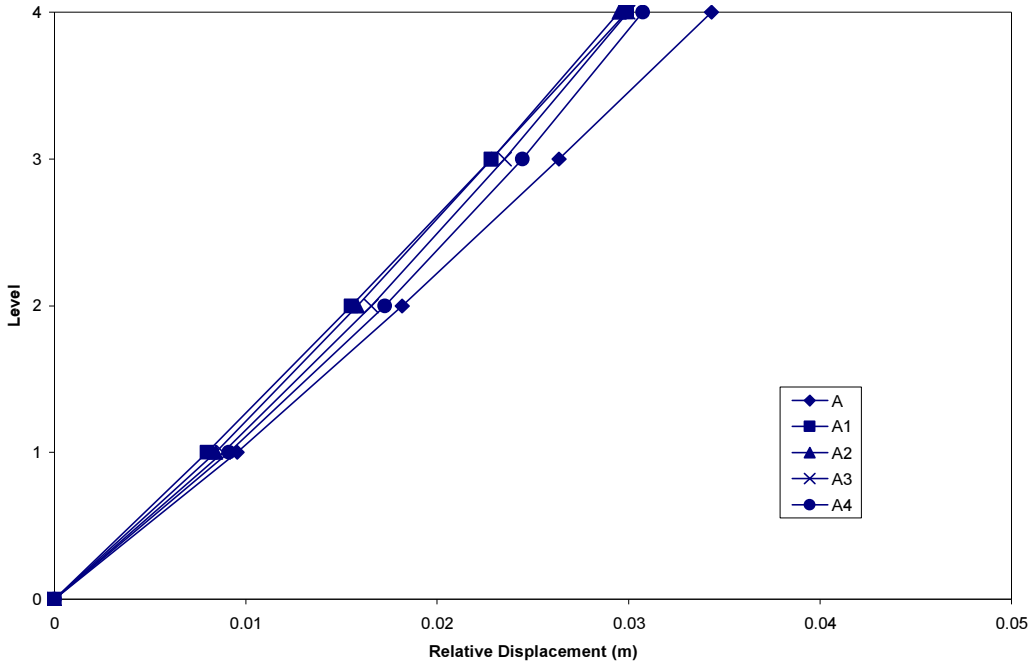

(a) Maximum relative displacements

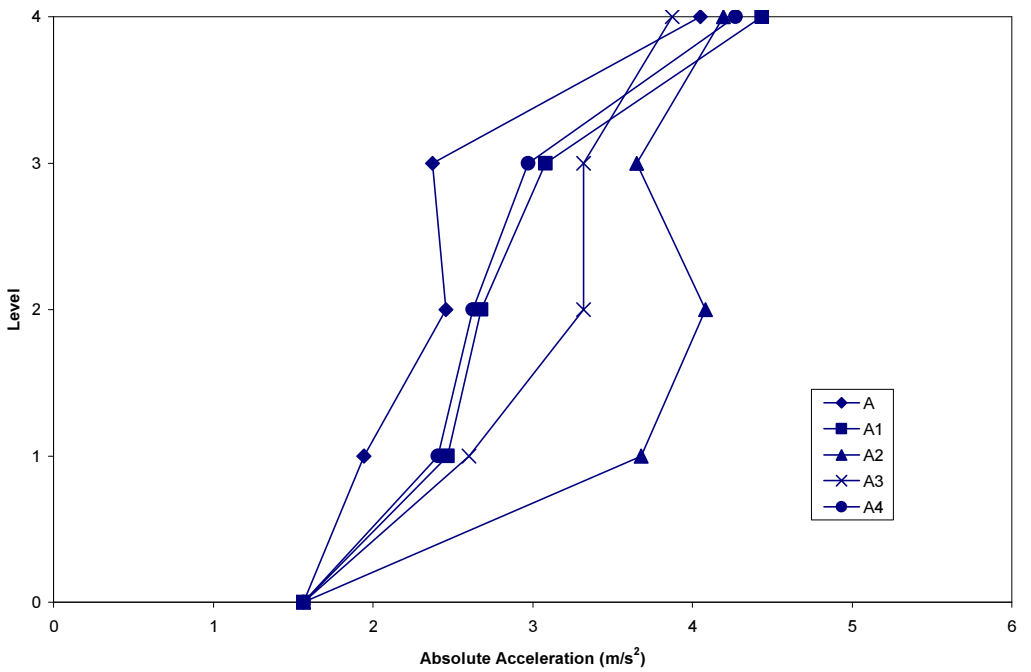

(b) Maximum absolute accelerations

Figure B.3 Maximum response envelopes of A-Systems for Sylmar 20% earthquake.

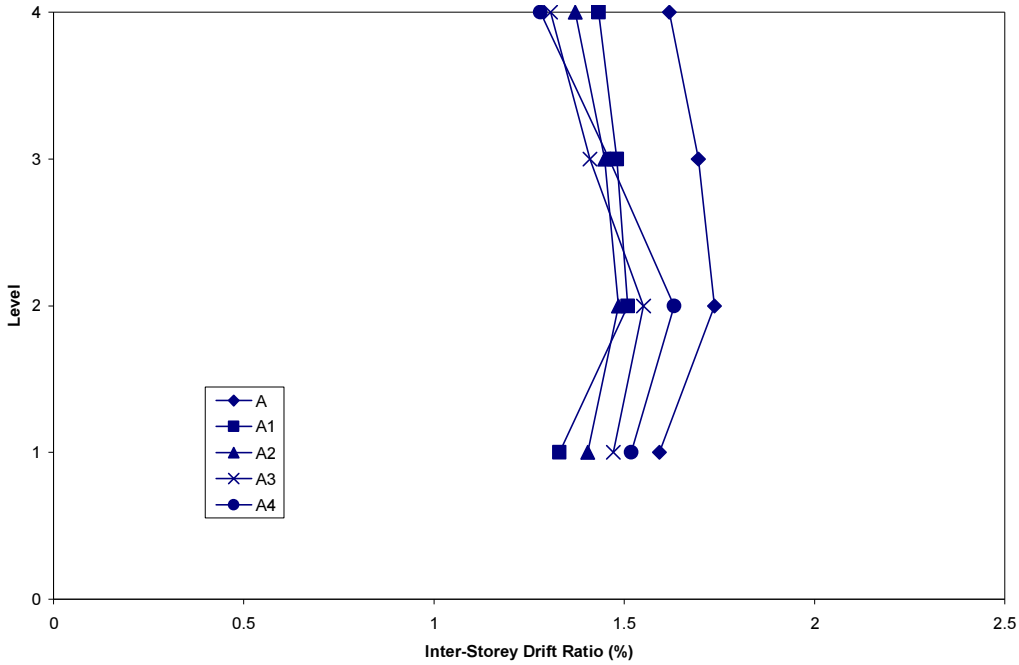

(c) Maximum inter-storey drift ratios

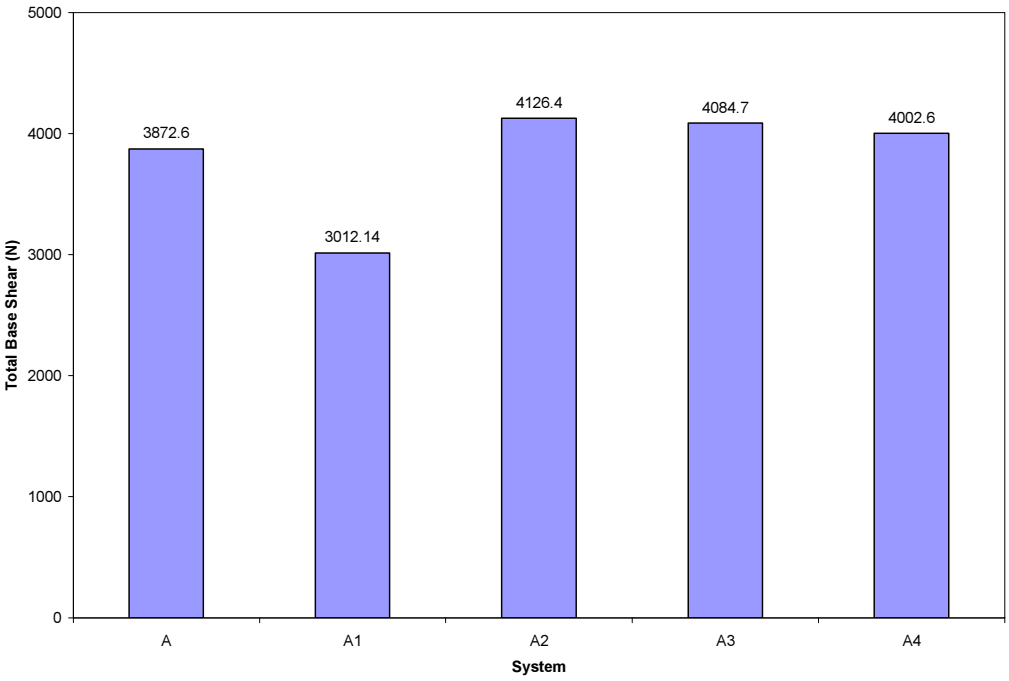

(d) Maximum total base shear

Figure B.3 (Continued).

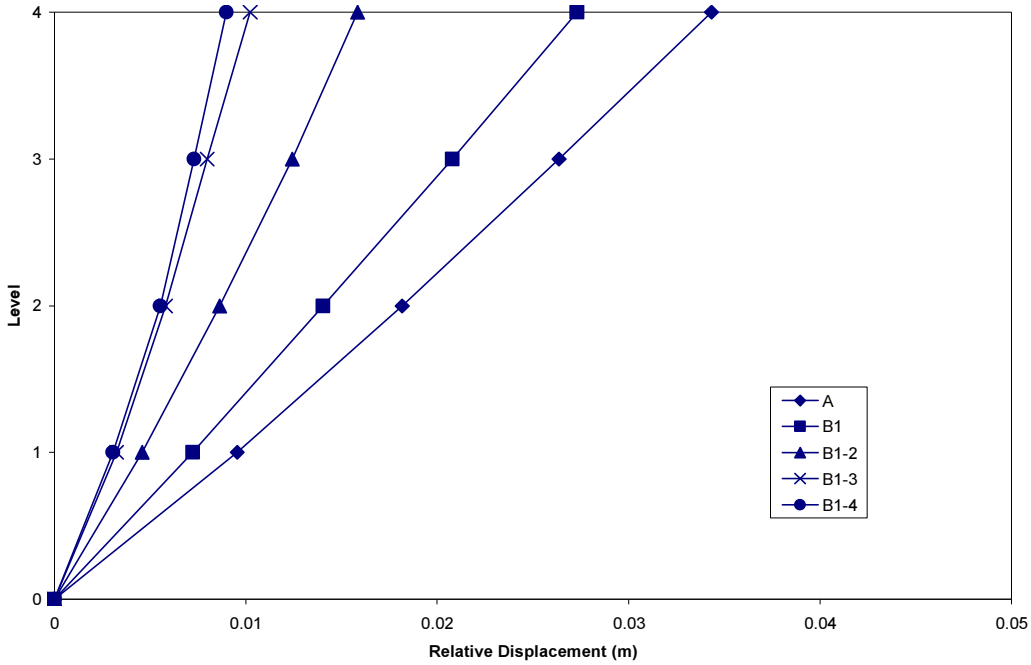

(a) Maximum relative displacements

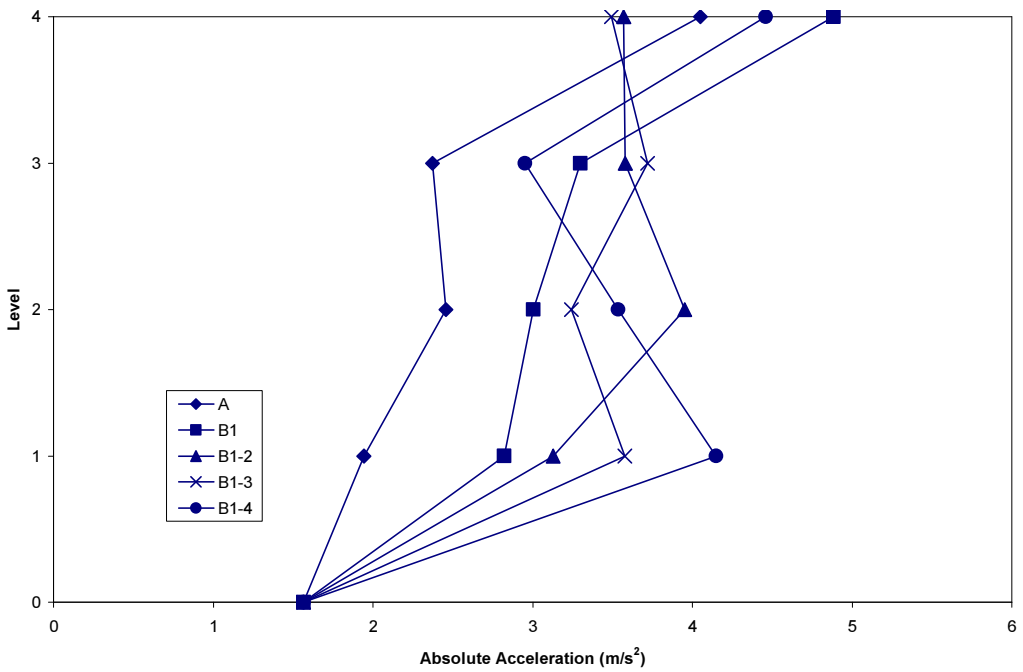

(b) Maximum absolute accelerations

Figure B.4 Maximum response envelopes of B-Systems for Sylmar 20% earthquake.

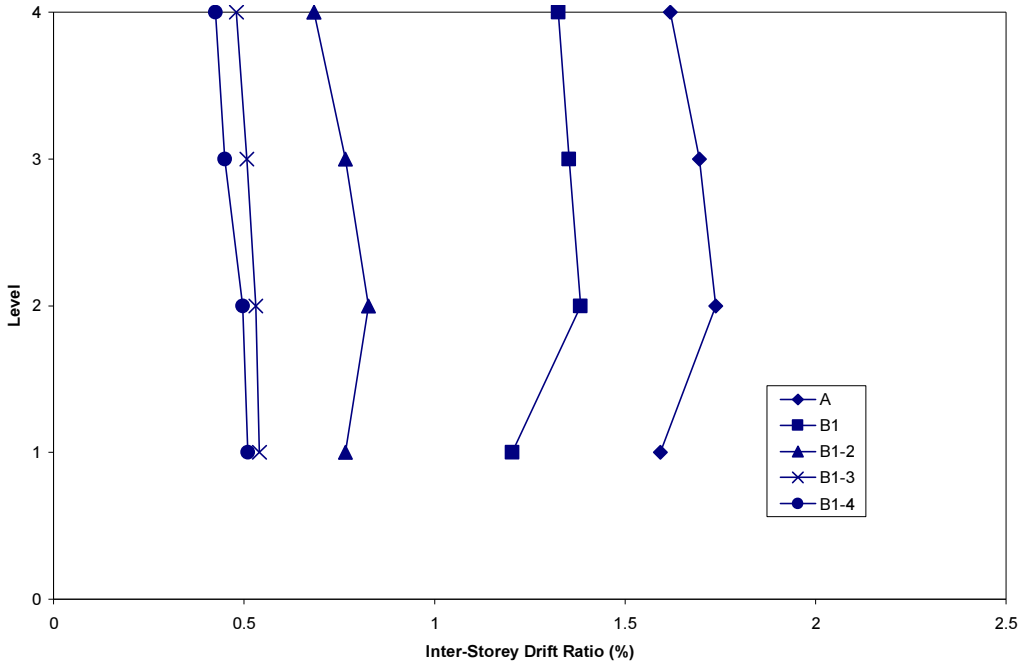

(c) Maximum inter-storey drift ratios

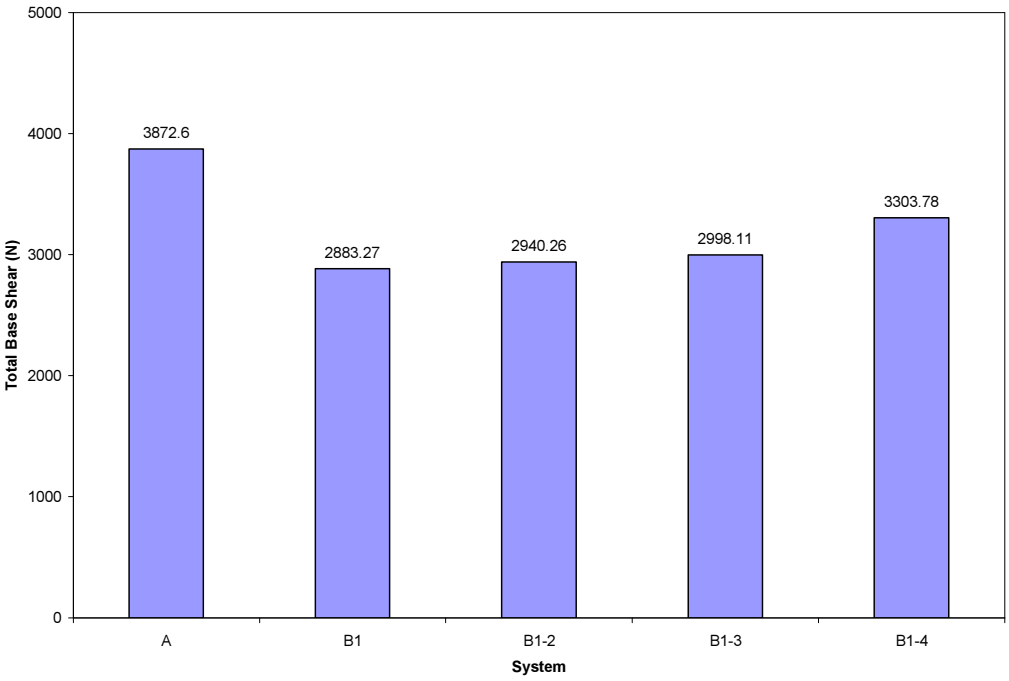

(d) Maximum total base shear

Figure B.4 (Continued).

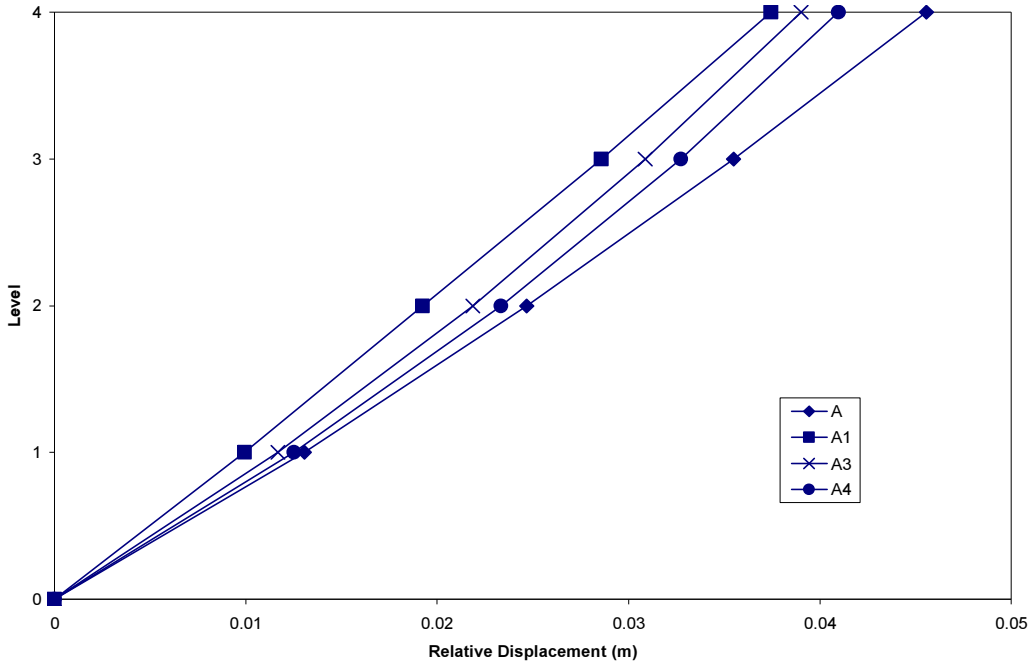

(a) Maximum relative displacements

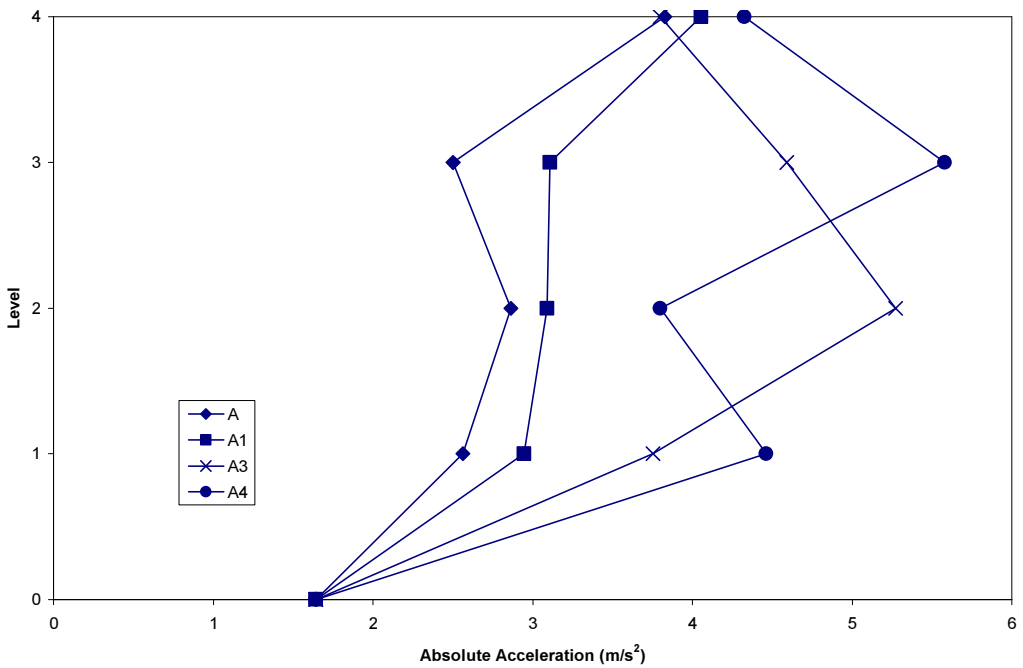

(b) Maximum absolute accelerations

Figure B.5 Maximum response envelopes of A-Systems for Kobe 20% earthquake (System A2 collapses under this earthquake ground motion).

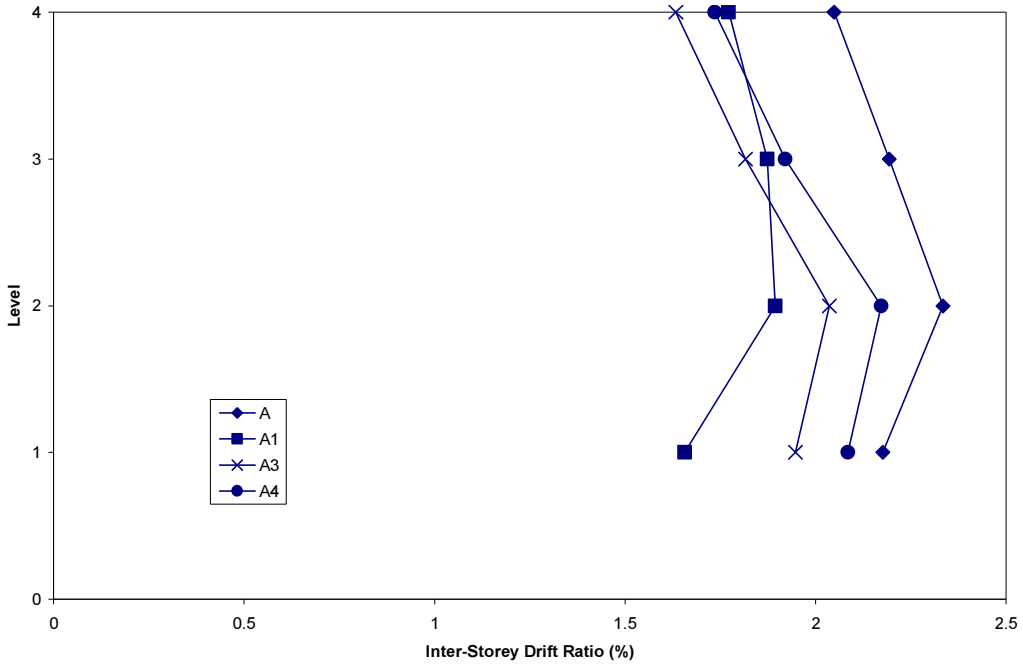

(c) Maximum inter-storey drift ratios

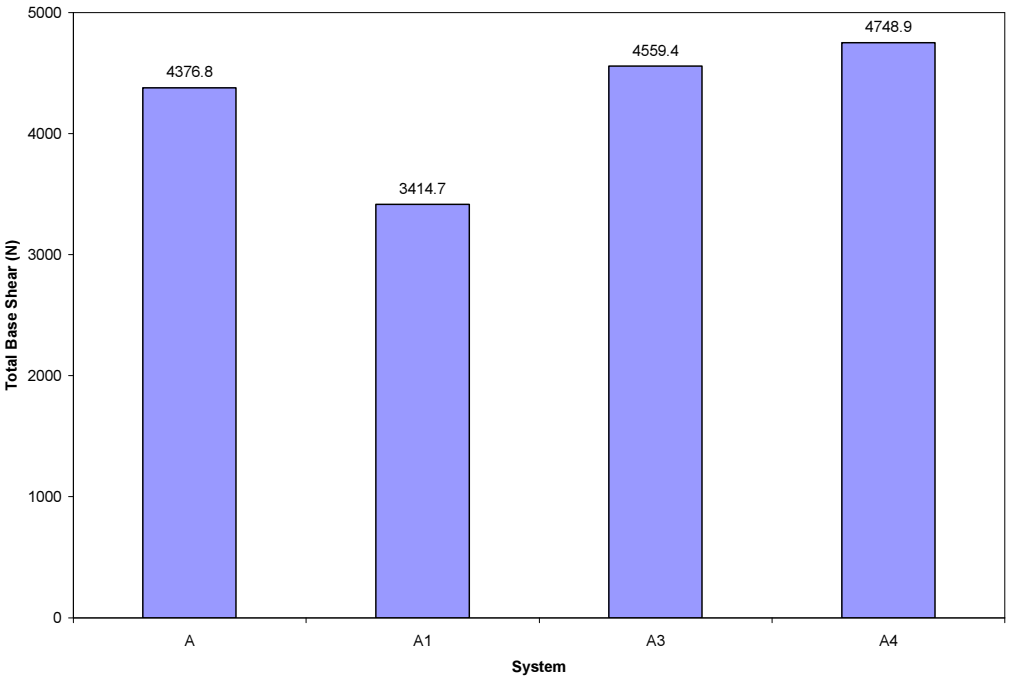

(d) Maximum total base shear

Figure B.5 (Continued).

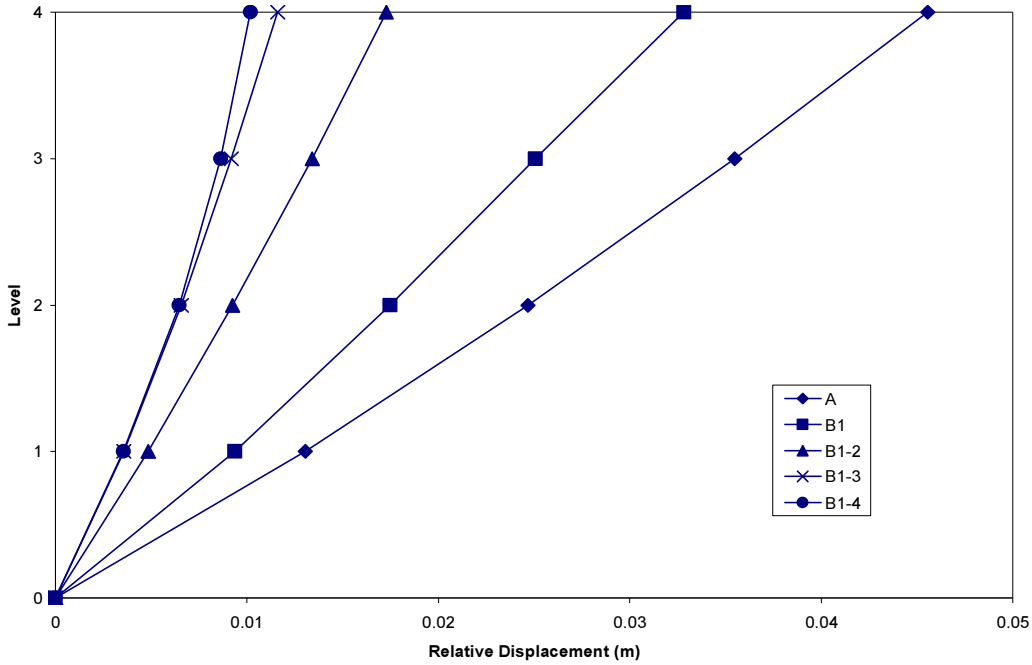

(a) Maximum relative displacements

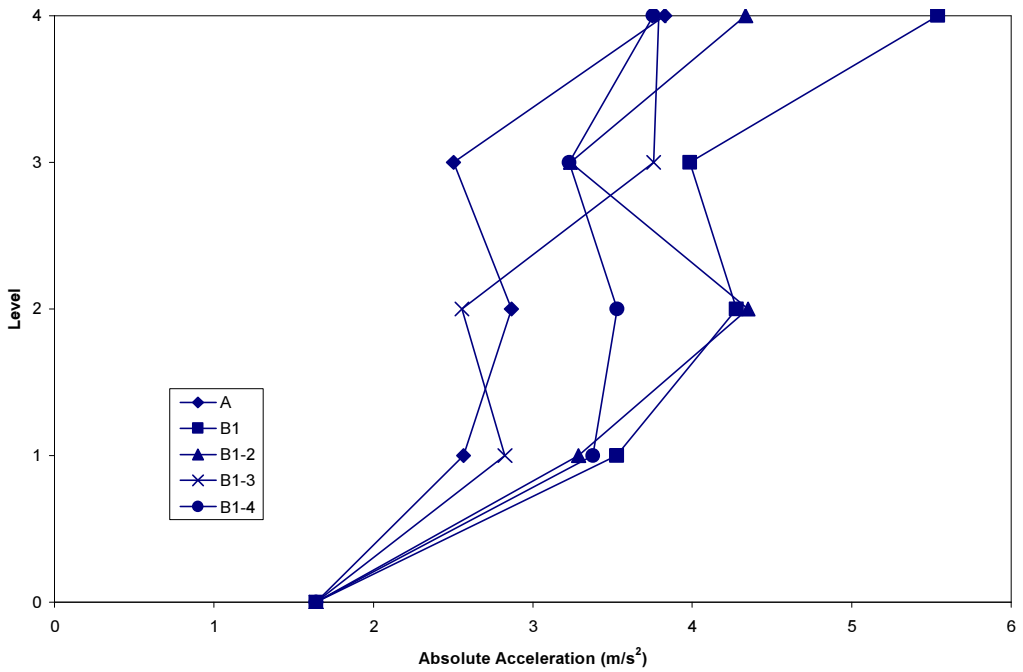

(b) Maximum absolute accelerations

Figure B.6 Maximum response envelopes of B-Systems for Kobe 20% earthquake.

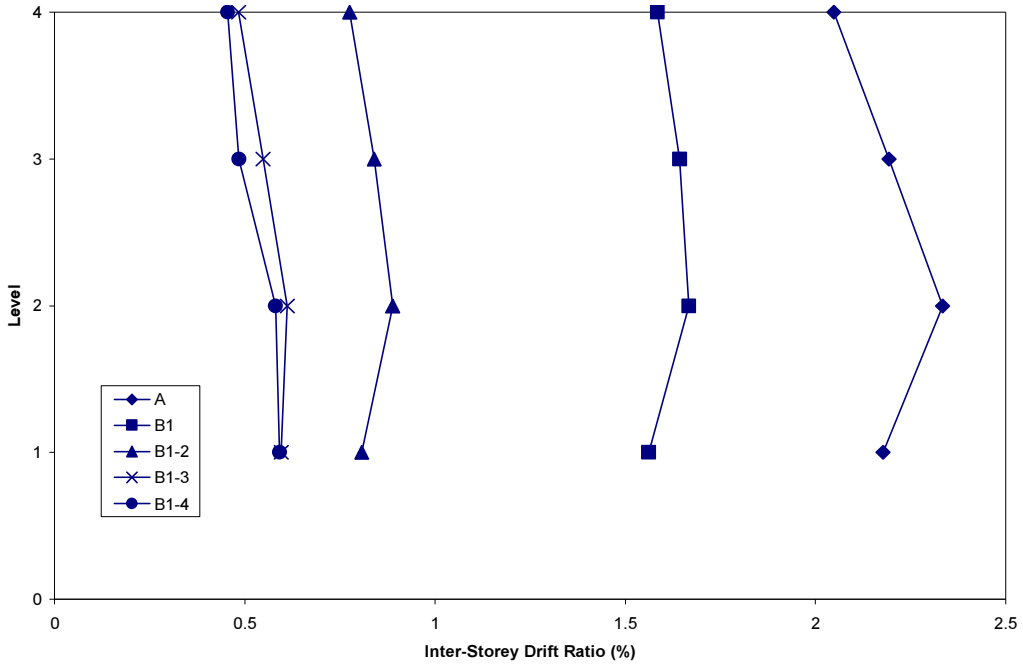

(c) Maximum inter-storey drift ratios

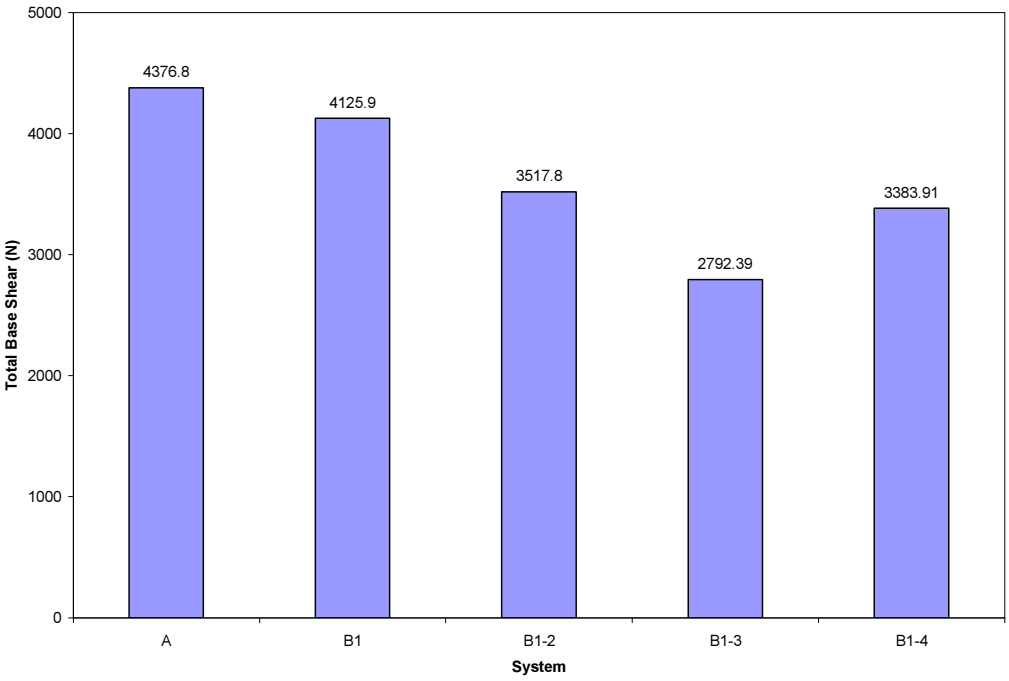

(d) Maximum total base shear

Figure B.6 (Continued).

Appendix C

MEASUREMENT OF DISPLACEMENTS AND RECORD MODIFICATION

Appendix C contains information that supports the research work presented in Chapter 5 of this thesis. The appendix is divided into the following sections:

C.1 Verification of the Displacement Measurements

C.2 Modification of the Earthquake Records.

C.1 VERIFICATION OF THE DISPLACEMENT MEASUREMENTS

During the experimental testing, the absolute displacements were measured by linear potentiometers placed at the mid-height of the storeys, because the end blocks of the columns would rotate due to bending of the longitudinal beams. These displacement measurements are considered to be accurate enough, because the column and beam members are relatively stiff and the rotations occur only at the end blocks (Kao 1998, Bishay-Girges 2004). The absolute displacement at each floor level was calculated by linearly interpolating the displacement measured above and below the corresponding floor level. The absolute displacement at the fourth floor was directly measured by a linear potentiometer. Relative floor displacements were obtained by subtracting the absolute displacement of the shaking table to the absolute floor displacements.

The accuracy of the floor displacements obtained with the numerical interpolation was verified by comparison with the double integration of the accelerometer data for each floor and by direct displacement measurements at the third floor. A comparison of the calculated and the measured displacement at the third floor is shown in Figure C.1.1 for selected earthquake records. An excellent agreement can be observed between the two measurement approaches for the uncontrolled structure.

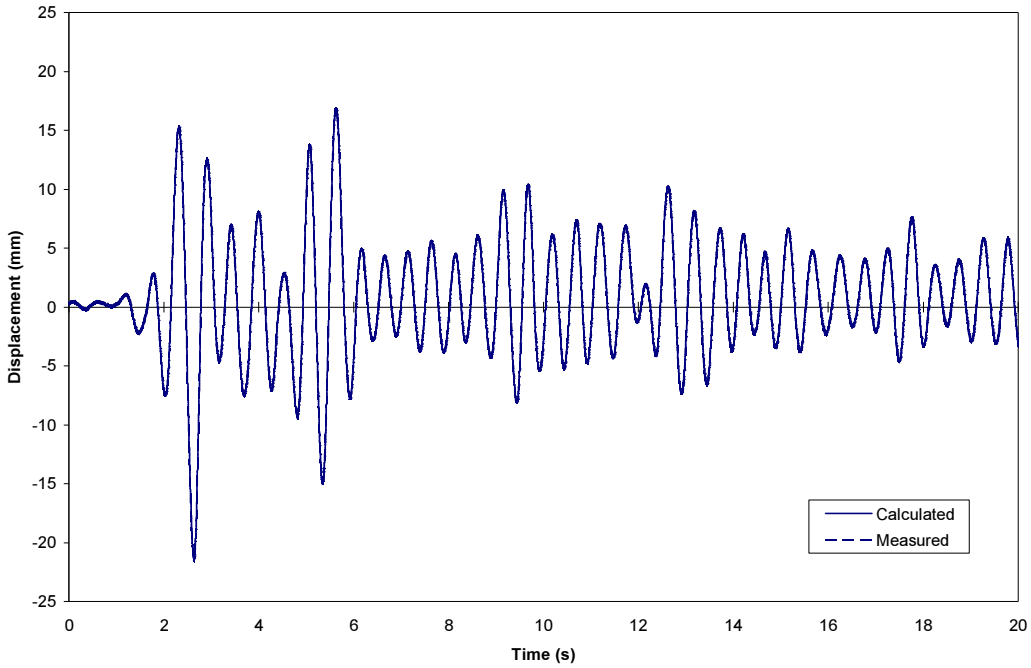

(a) El Centro 30% earthquake

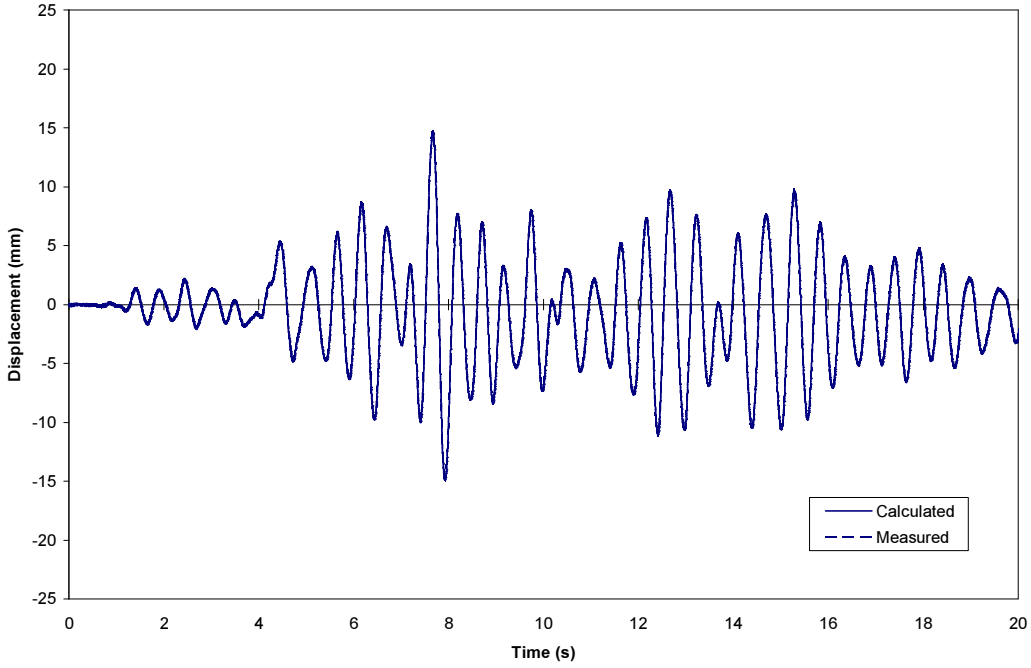

(b) Taft 60% earthquake

Figure C.1.1 Displacement comparison at third floor for the uncontrolled case.

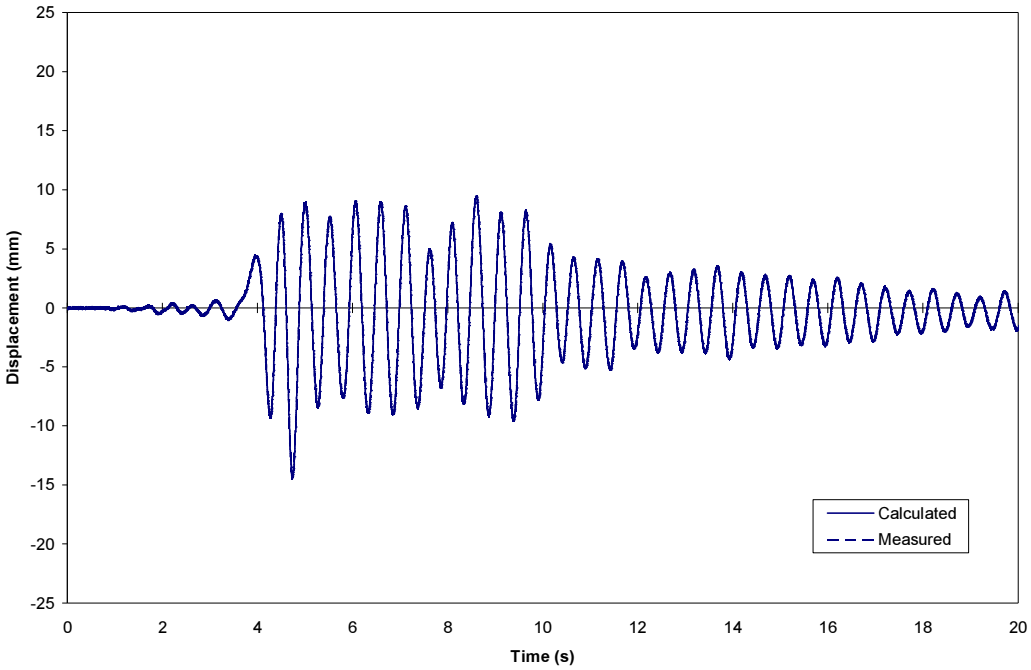

(c) Sylmar 10% earthquake

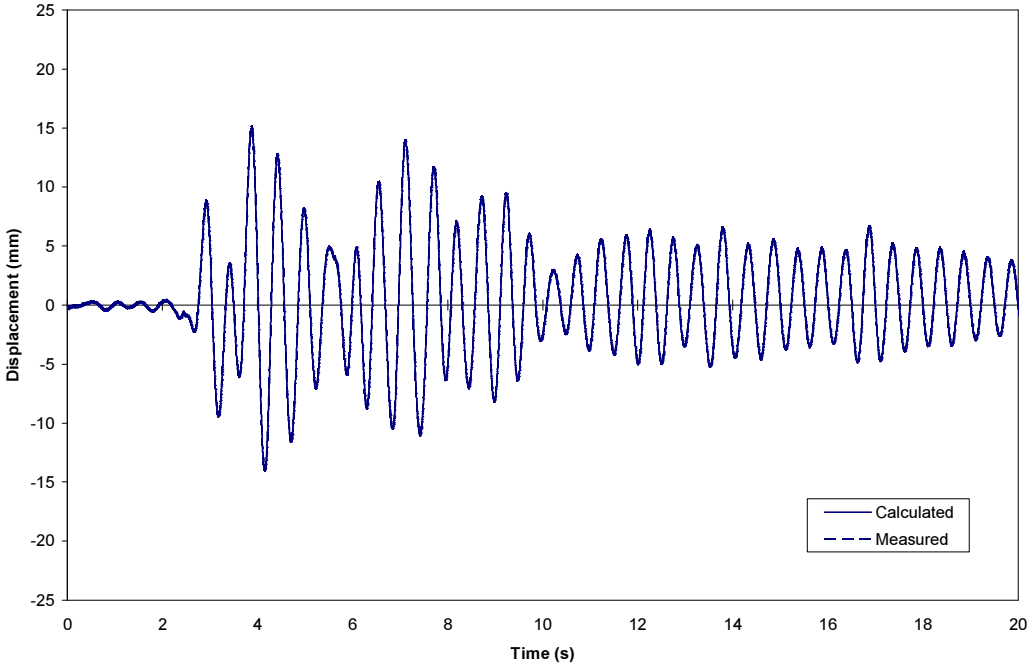

(d) Kobe 10% earthquake

Figure C.1.1 (Continued).

C.2 MODIFICATION OF THE EARTHQUAKE RECORDS

The simulation of earthquakes for seismic testing requires an accurate reproduction of the acceleration records. It is also essential to understand the dynamics of the shaking table system used to reproduce the earthquakes. Typically, a shaking table consists of a table capable of moving in one direction on linear bearings actuated by current driven servo-valves. The servo-valves are controlled by displacement feedback and designed to ensure that the table tracks a desired reference input motion.

Large shaking table systems can have trouble by accurately tracking near-field seismic inputs due to actuation limitations or poor control design for these inputs. The response of the shaking table to near-field ground motions can include large acceleration spikes up to twice the magnitude of the input acceleration record. This problem is caused by the binding of the table on the linear bearings, due to moment loads induced from the shaking table-structure interaction, as well as variable friction and velocity saturation (Chase et al. 2005b).

Due to velocity saturation of the servo-valves, the unidirectional shaking table used in this research was unable to accurately track certain far-field and near-field earthquake ground motions. Thus, the acceleration record of these ground motions was modified in such a way that velocity saturation was avoided. The objective of the adopted approach was to retain most of the characteristics of the original acceleration record including the peak ground acceleration. The record modification should also ensure that unexpected acceleration spikes did not occur while also achieving optimal tracking o the reference input motion (Chase et al. 2005b, Mulligan 2007).

Figures C.2.1 through C.2.6 show a comparison of the ground motion components and response spectra for the original and modified earthquake records. The original record of the Taft earthquake was not modified for the seismic testing. However, its ground motion components and response spectra are shown in Figures C.2.7 and C.2.8 for completeness.

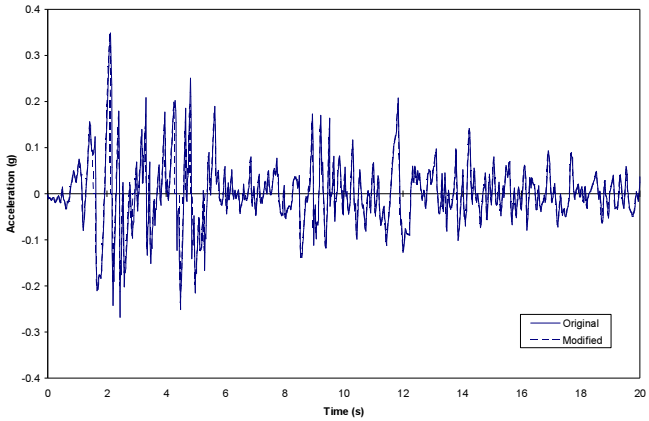

(a) Ground acceleration

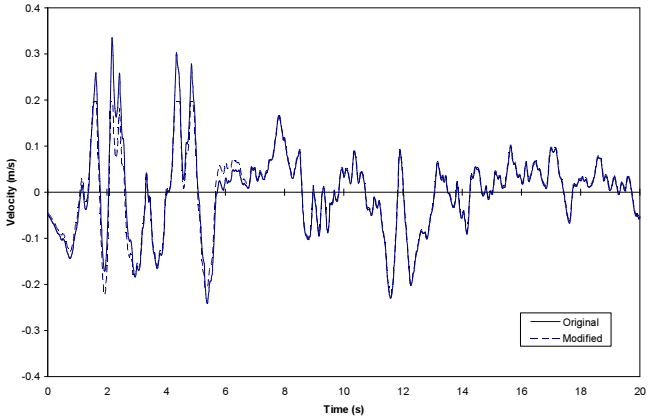

(b) Ground velocity

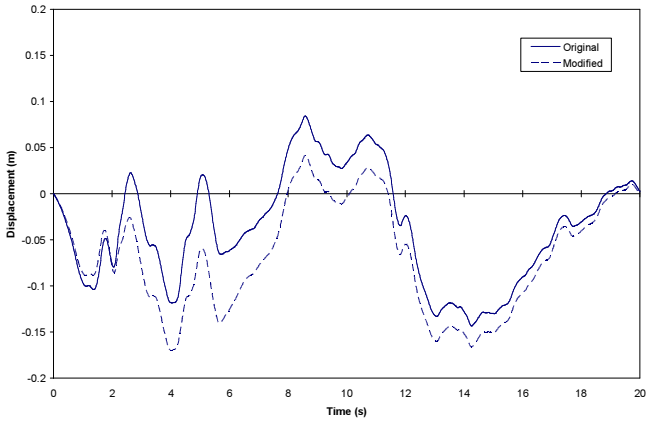

(c) Ground displacement

Figure C.2.1 Comparison of ground motion components for El Centro earthquake.

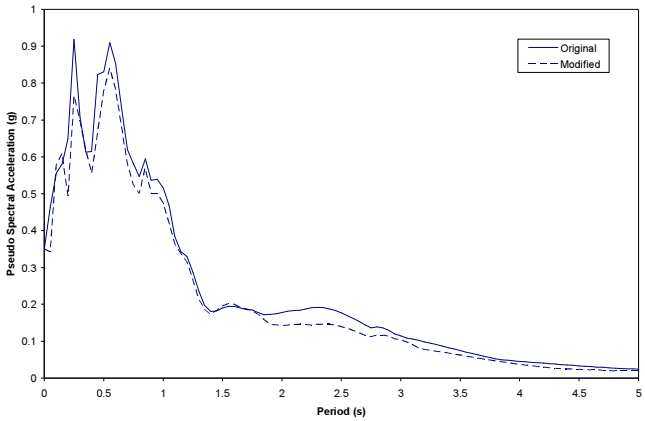

(a) Pseudo spectral acceleration

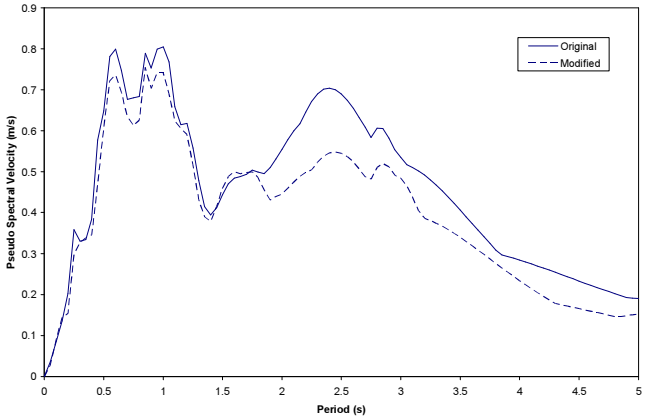

(b) Pseudo spectral velocity

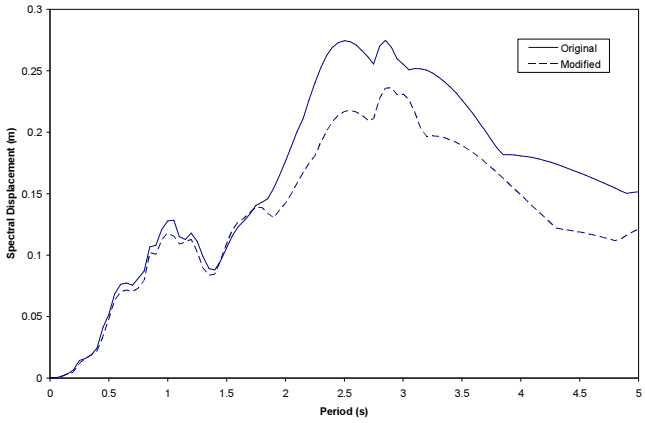

(c) Spectral displacement

Figure C.2.2 Comparison of response spectra for El Centro earthquake ($\zeta = 5\%$).

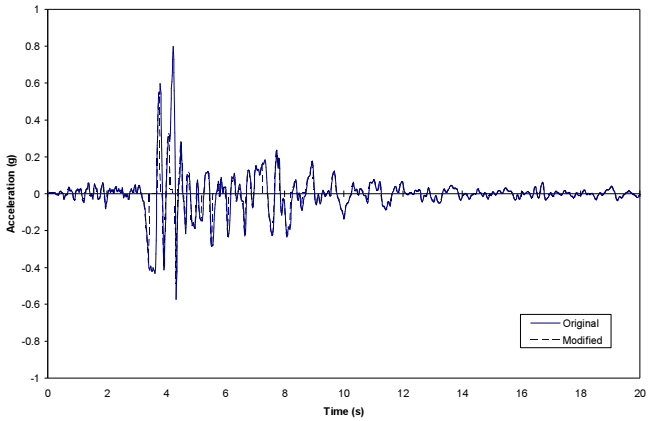

(a) Ground acceleration

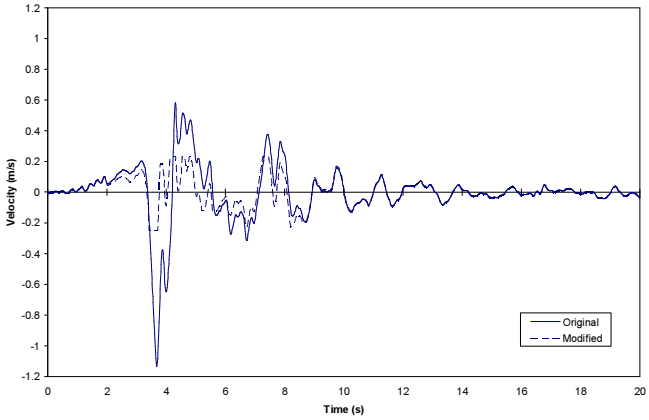

(b) Ground velocity

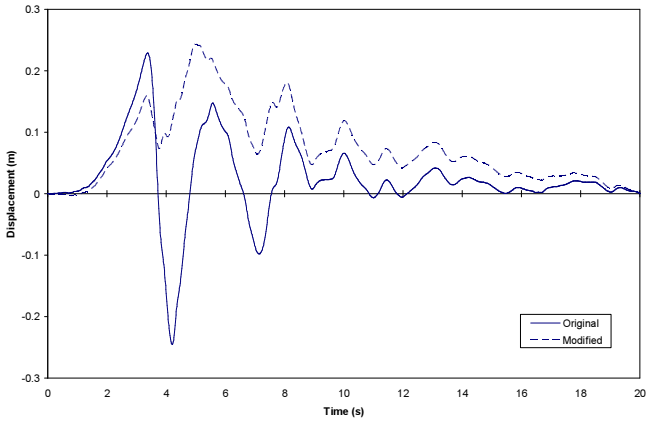

(c) Ground displacement

Figure C.2.3 Comparison of ground motion components for Sylmar earthquake.

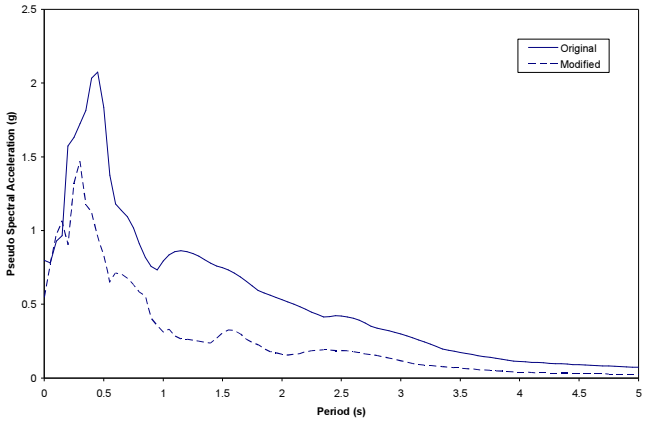

(a) Pseudo spectral acceleration

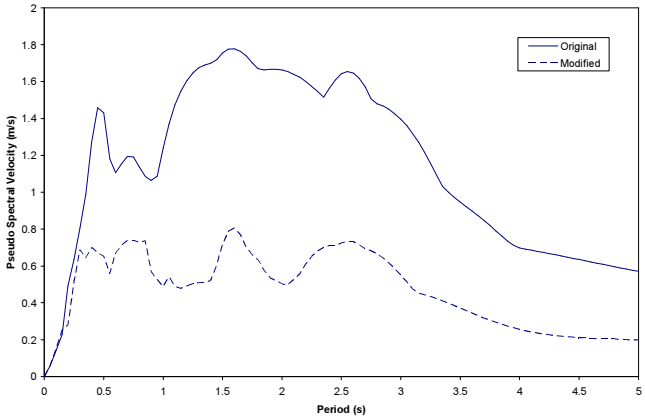

(b) Pseudo spectral velocity

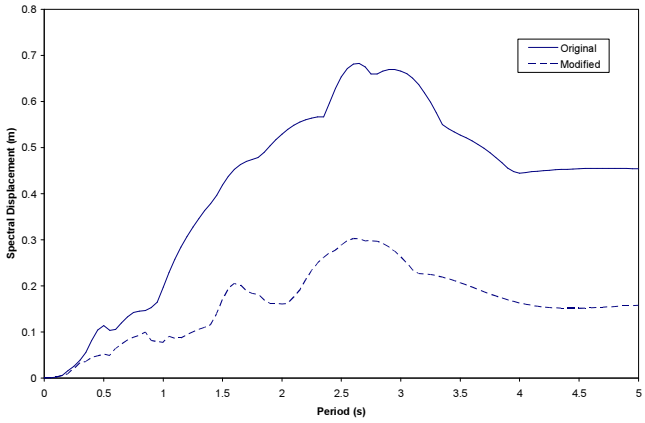

(c) Spectral displacement

Figure C.2.4 Comparison of response spectra for Sylmar earthquake ($\xi = 5\%$).

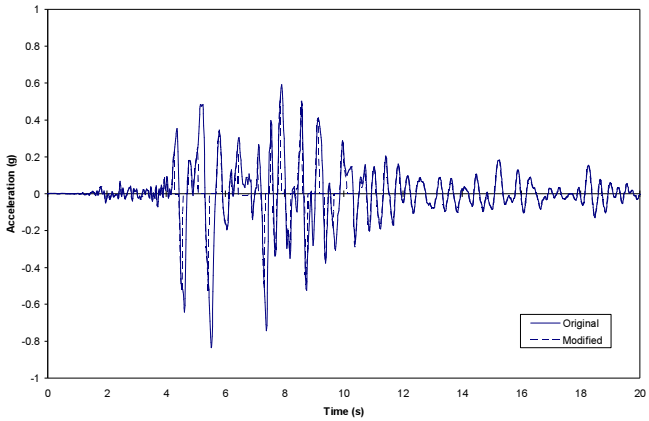

(a) Ground acceleration

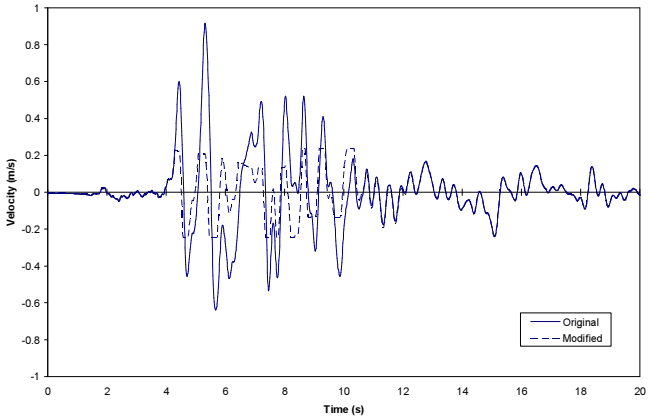

(b) Ground velocity

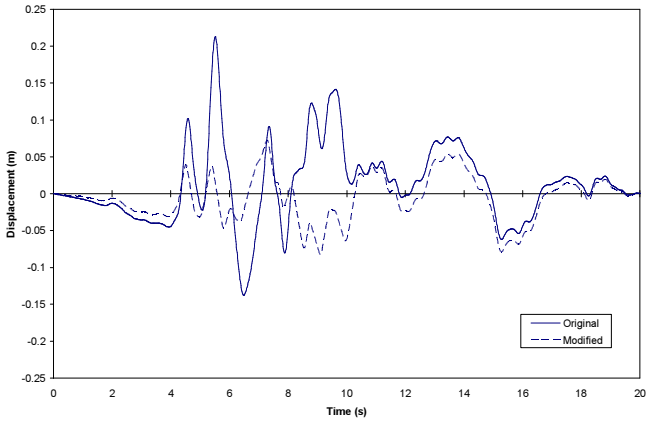

(c) Ground displacement

Figure C.2.5 Comparison of ground motion components for Kobe earthquake.

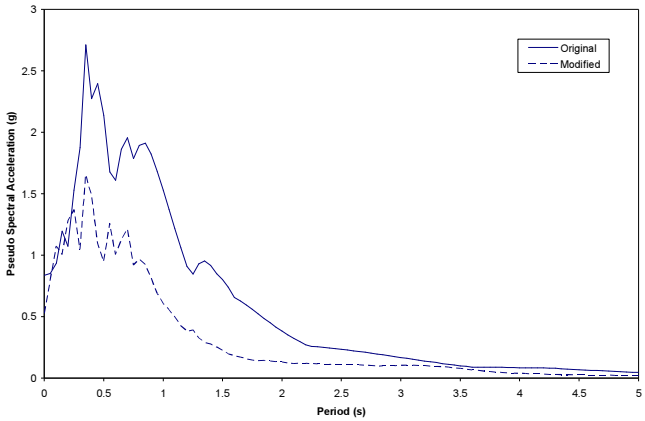

(a) Pseudo spectral acceleration

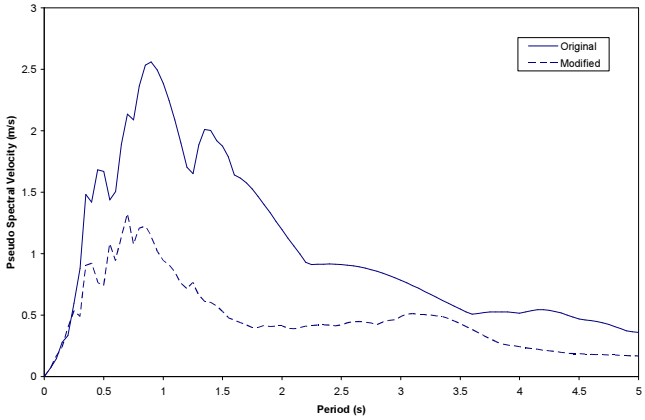

(b) Pseudo spectral velocity

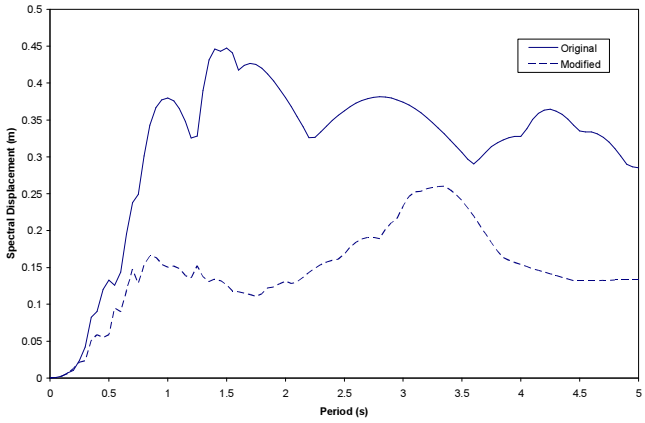

(c) Spectral displacement

Figure C.2.6 Comparison of response spectra for Kobe earthquake ($\zeta = 5\%$).

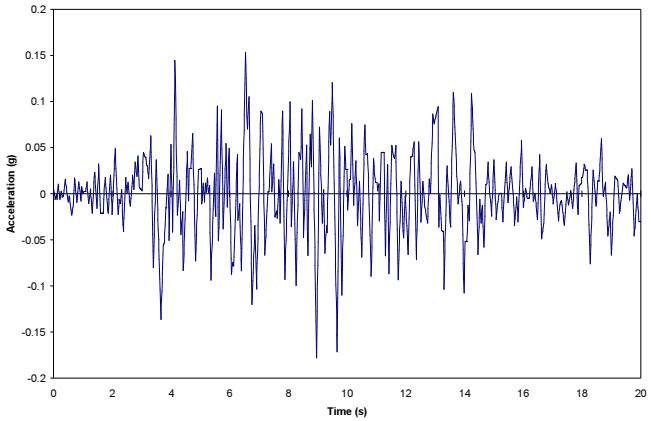

(a) Ground acceleration

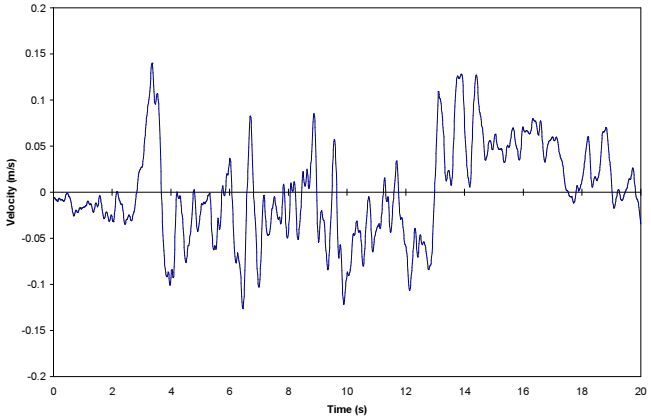

(b) Ground velocity

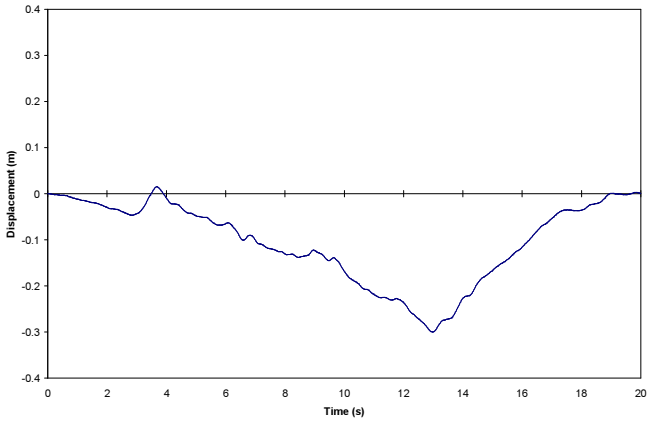

(c) Ground displacement

Figure C.2.7 Ground motion components of Taft earthquake.

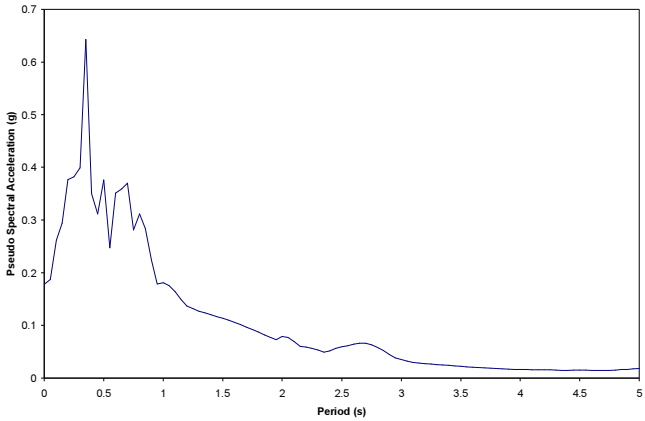

(a) Pseudo spectral acceleration

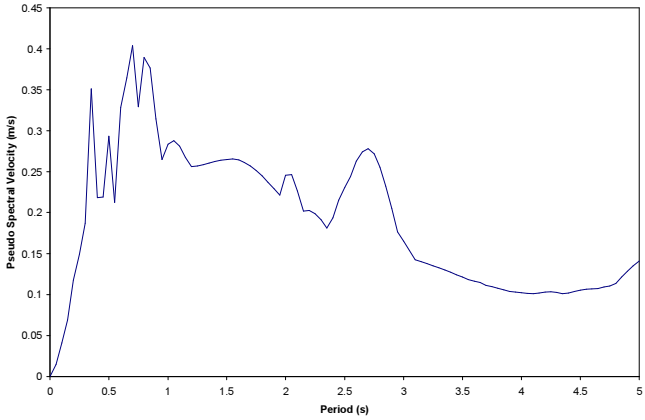

(b) Pseudo spectral velocity

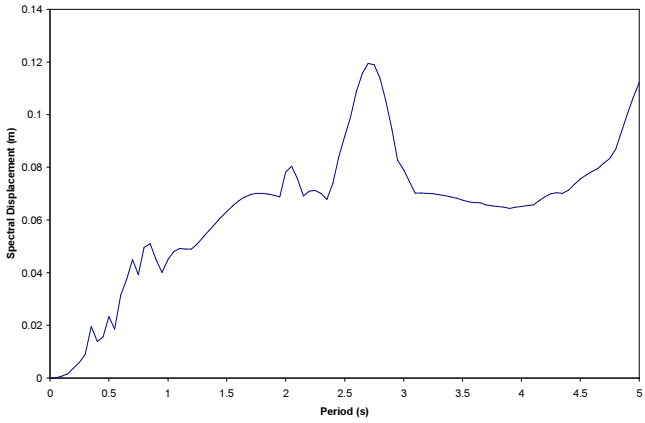

(c) Spectral displacement

Figure C.2.8 Response spectra for Taft earthquake ($\xi = 5\%$).

Appendix D
EXPERIMENTAL RESULTS

Appendix D shows the results of the shaking table test performed on the one-fifth scale structure. Maximum response envelopes of relative floor displacements, absolute floor accelerations, inter-storey drift ratios and total base shear are presented for all input ground motions used during the seismic testing. The value of total base shear includes the contribution of the semi-active resettable tendon consisting of the device and steel tendon. The appendix is divided into the following sections:

D.1 Maximum Response Envelopes for El Centro earthquake
D.2 Maximum Response Envelopes for Taft earthquake
D.3 Maximum Response Envelopes for Sylmar earthquake
D.4 Maximum Response Envelopes for Kobe earthquake.

D.1 MAXIMUM RESPONSE ENVELOPES FOR EL CENTRO EARTHQUAKE

Maximum response envelopes are presented for the following scaled earthquake records with corresponding peak ground accelerations:

1. El Centro 10% (0.0348g)
2. El Centro 20% (0.0697g)
3. El Centro 30% (0.1045g)
4. El Centro 40% (0.1393g)
5. El Centro 50% (0.1742g)
6. El Centro 60% (0.2091g)
7. El Centro 70% Modified (0.2451g)
8. El Centro 80% Modified (0.2800g)
9. El Centro 90% Modified (0.3150g)
10. El Centro 100% Modified (0.3500g).

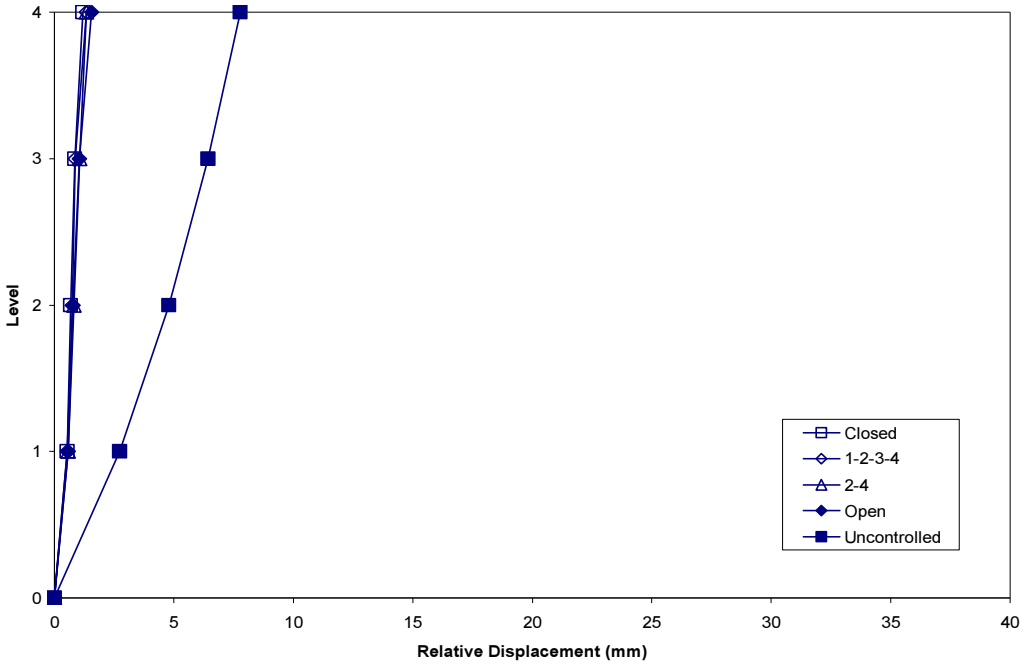

(a) Maximum relative displacements

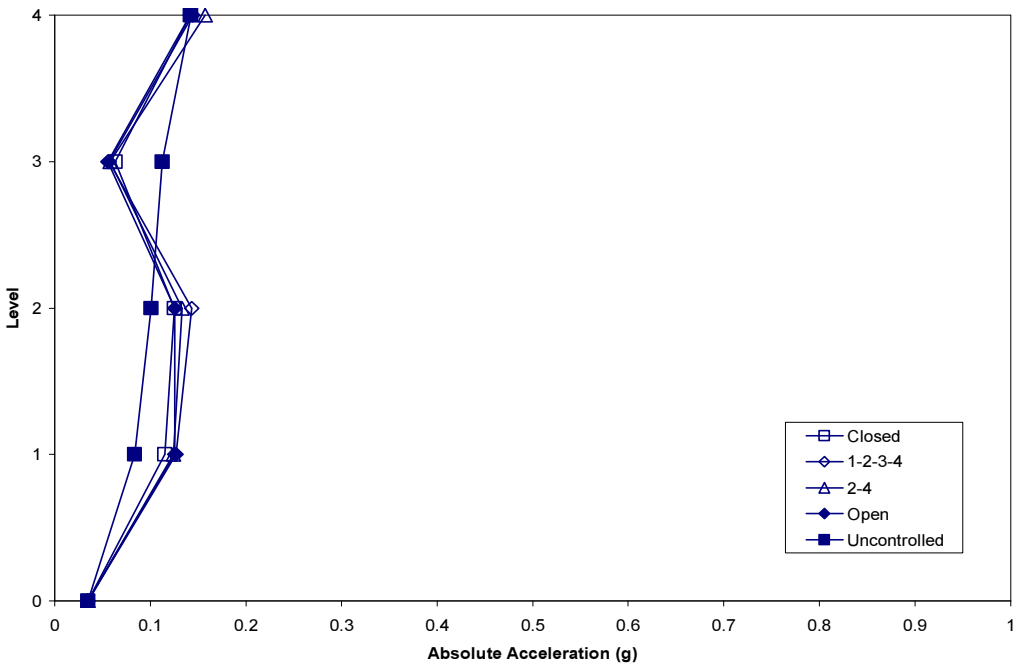

(b) Maximum absolute accelerations

Figure D.1.1 Maximum response envelopes for El Centro 10% earthquake.

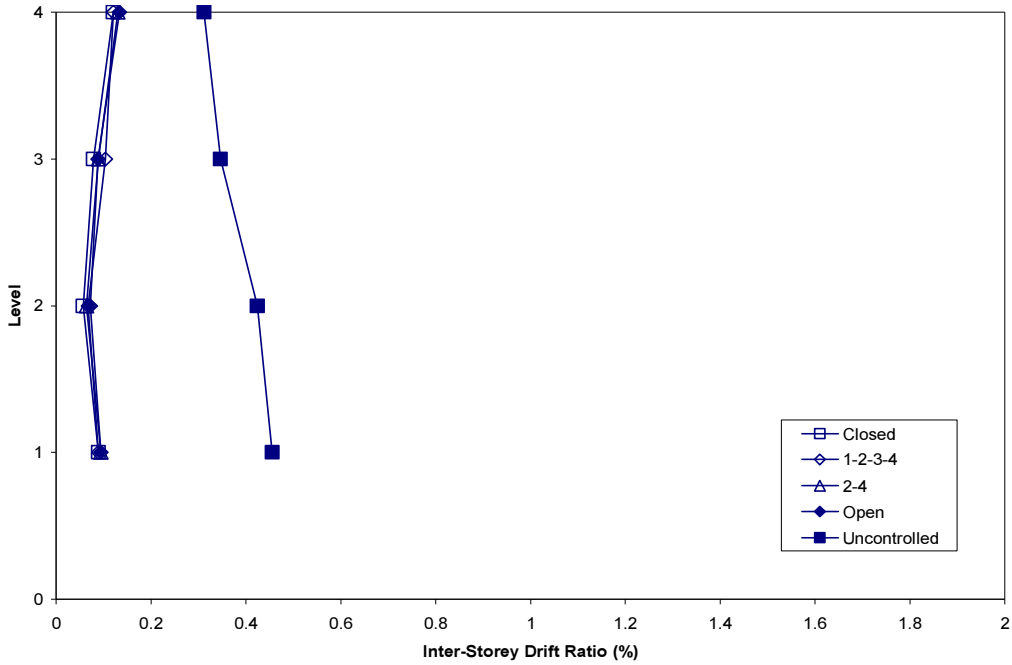

(c) Maximum inter-storey drift ratios

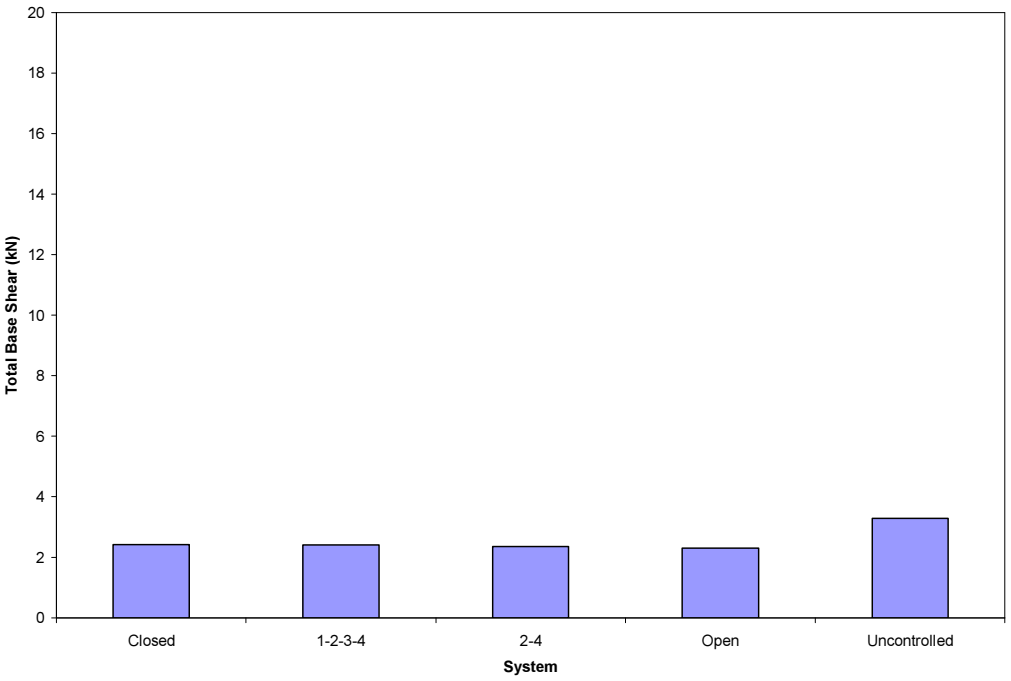

(d) Maximum total base shear

Figure D.1.1 (Continued).

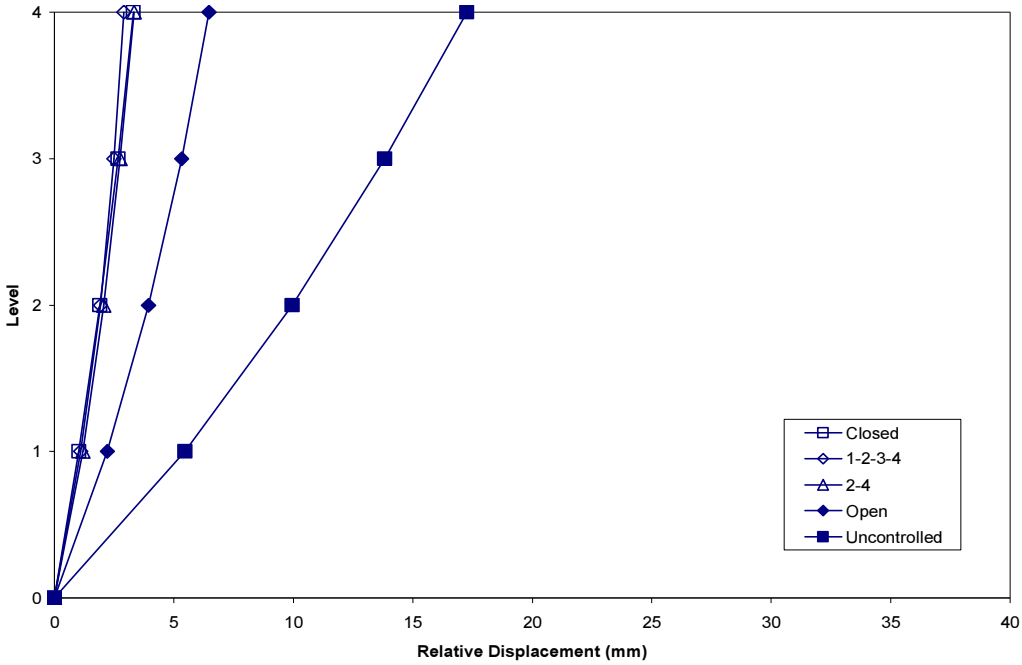

(a) Maximum relative displacements

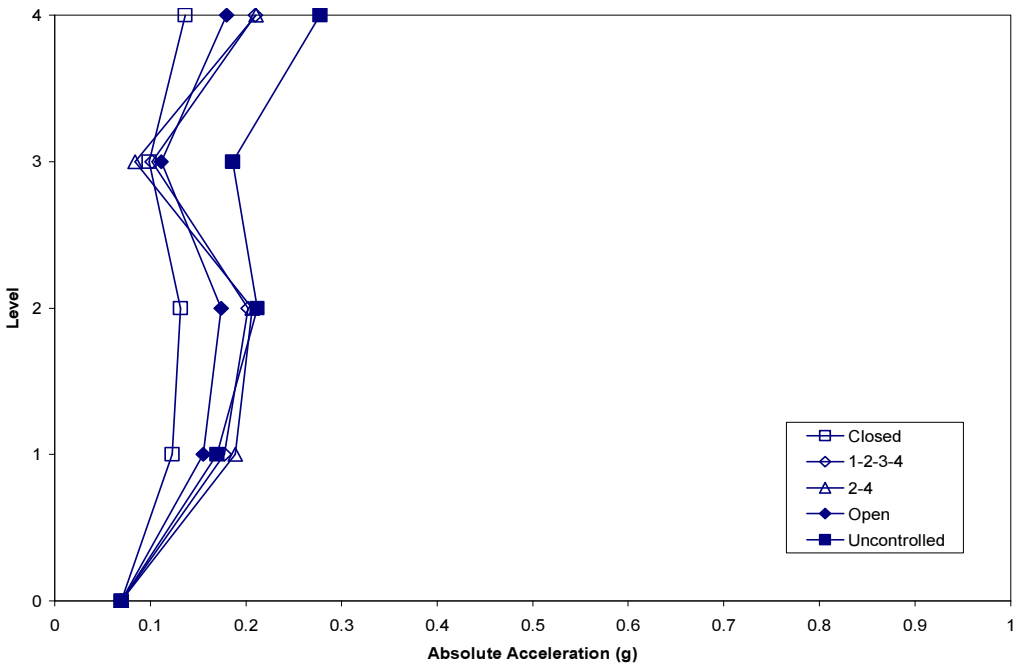

(b) Maximum absolute accelerations

Figure D.1.2 Maximum response envelopes for El Centro 20% earthquake.

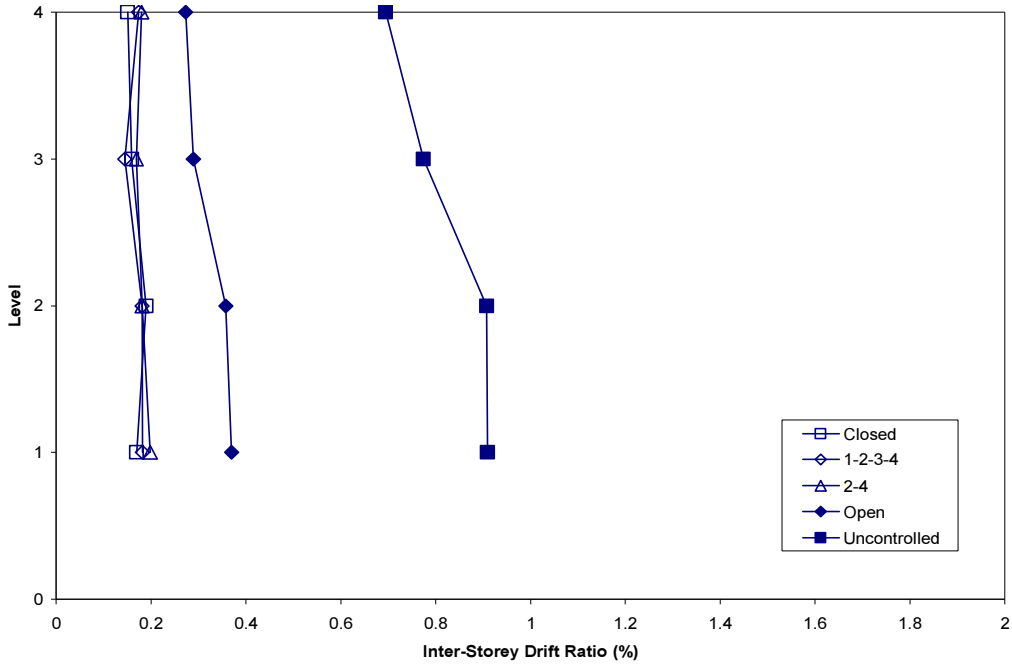

(c) Maximum inter-storey drift ratios

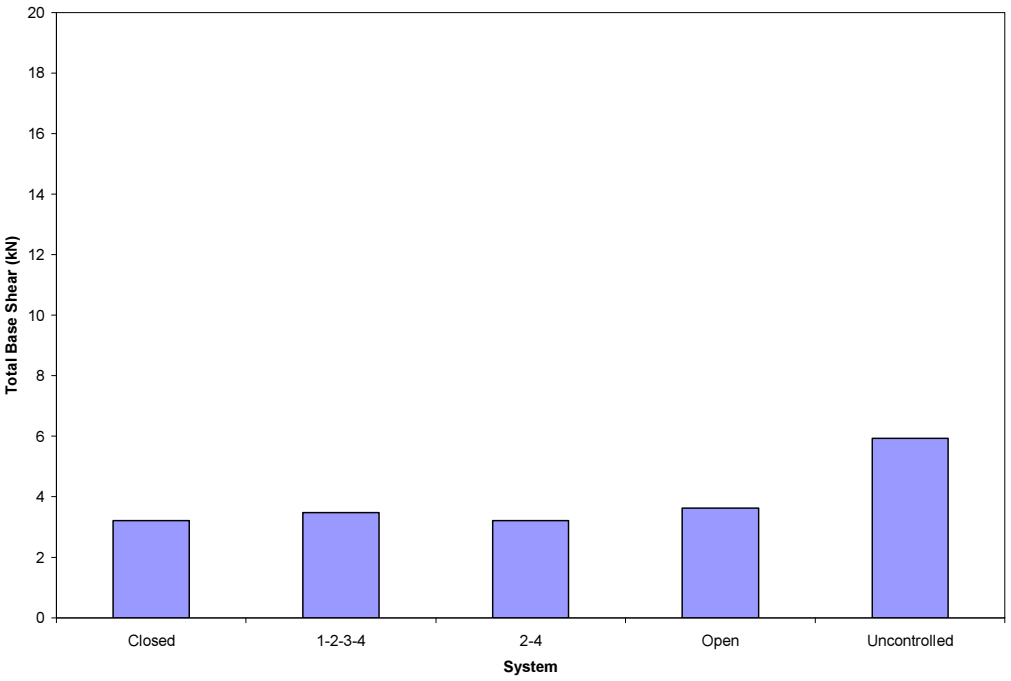

(d) Maximum total base shear

Figure D.1.2 (Continued).

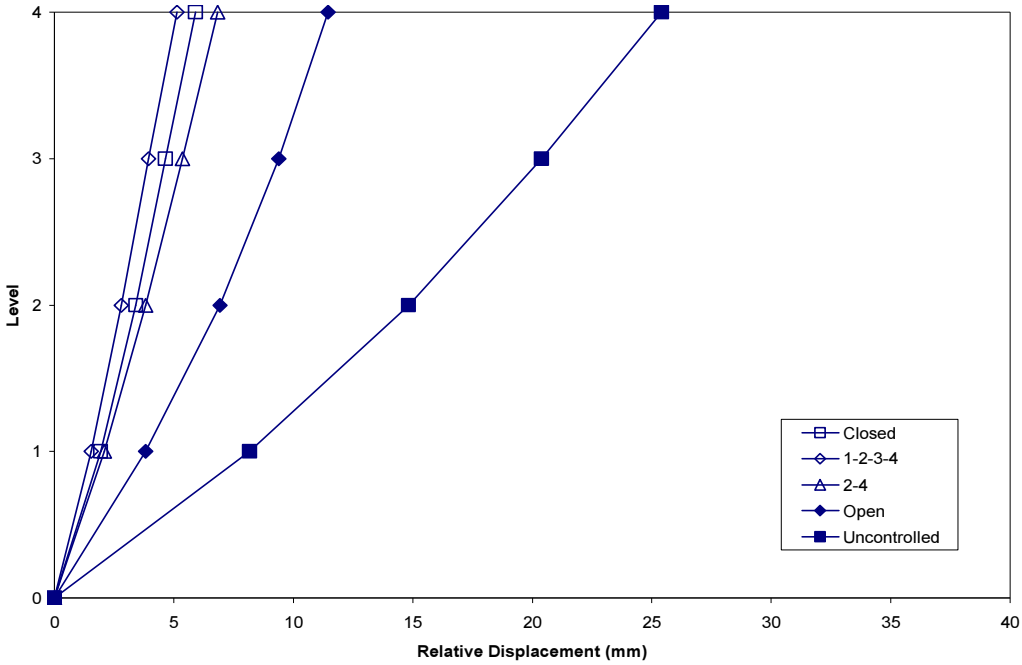

(a) Maximum relative displacements

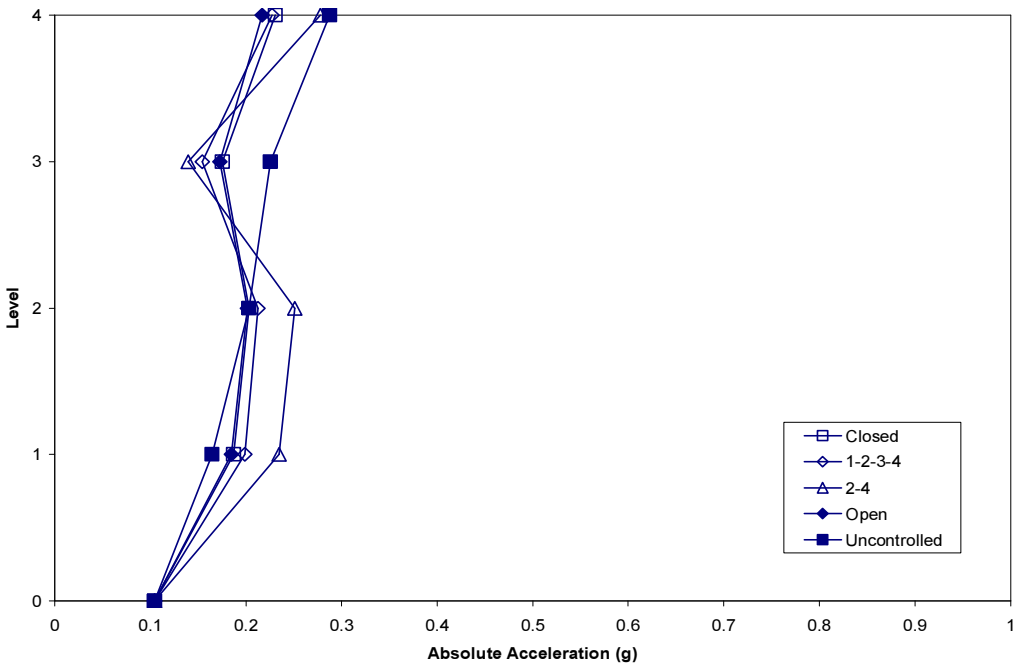

(b) Maximum absolute accelerations

Figure D.1.3 Maximum response envelopes for El Centro 30% earthquake.

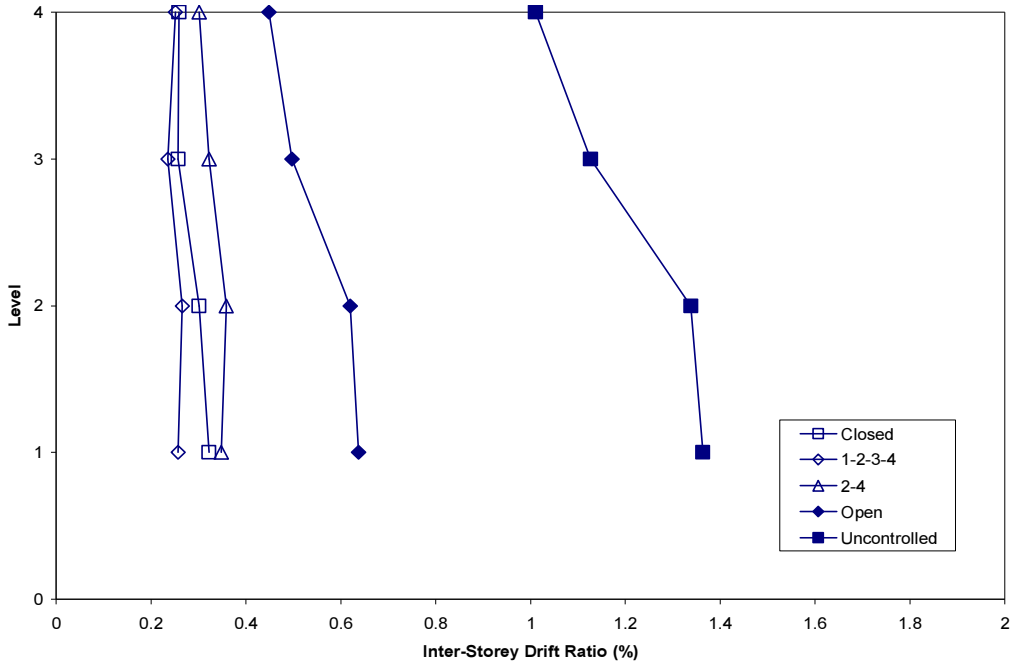

(c) Maximum inter-storey drift ratios

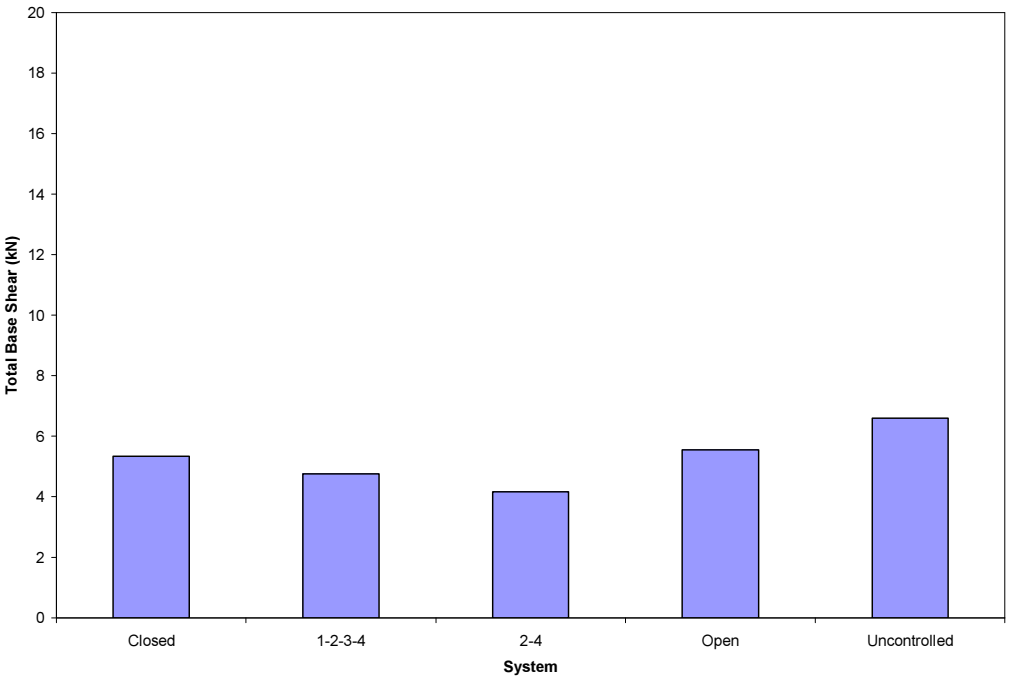

(d) Maximum total base shear

Figure D.1.3 (Continued).

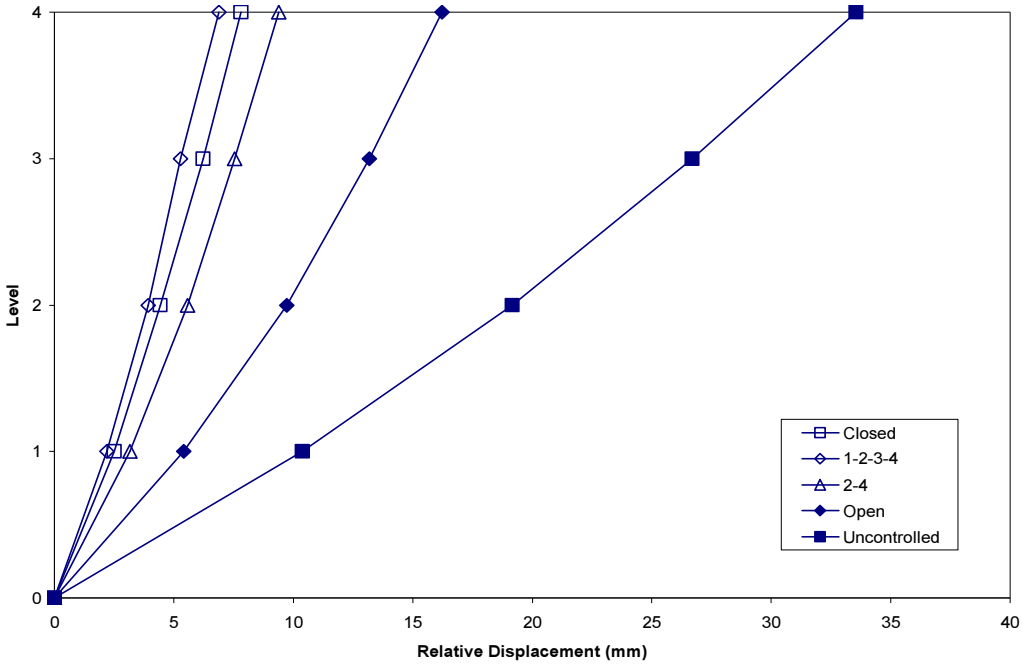

(a) Maximum relative displacements

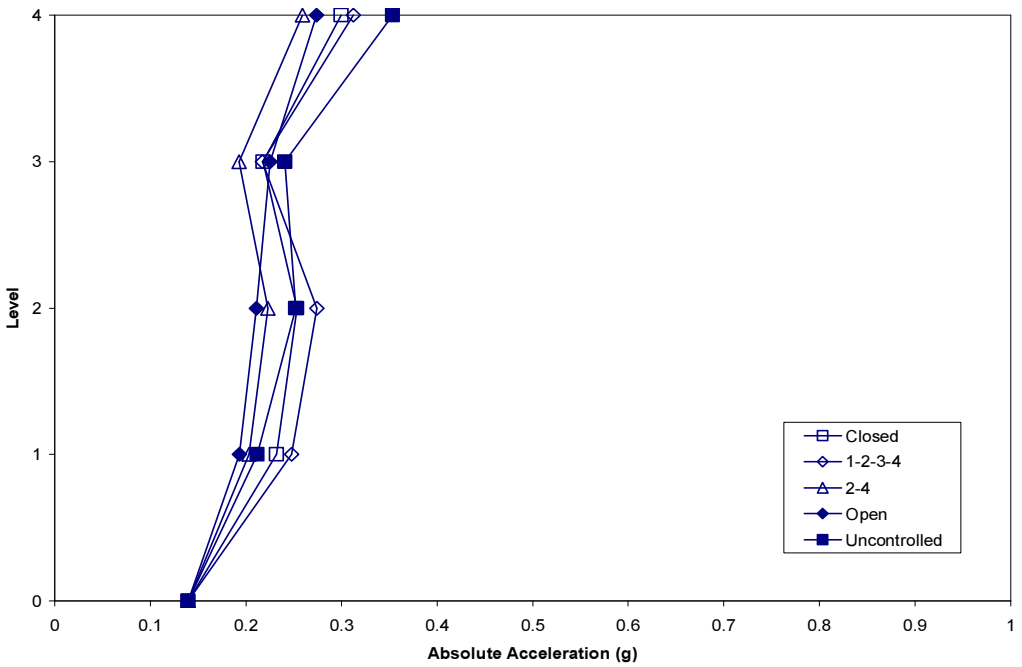

(b) Maximum absolute accelerations

Figure D.1.4 Maximum response envelopes for El Centro 40% earthquake.

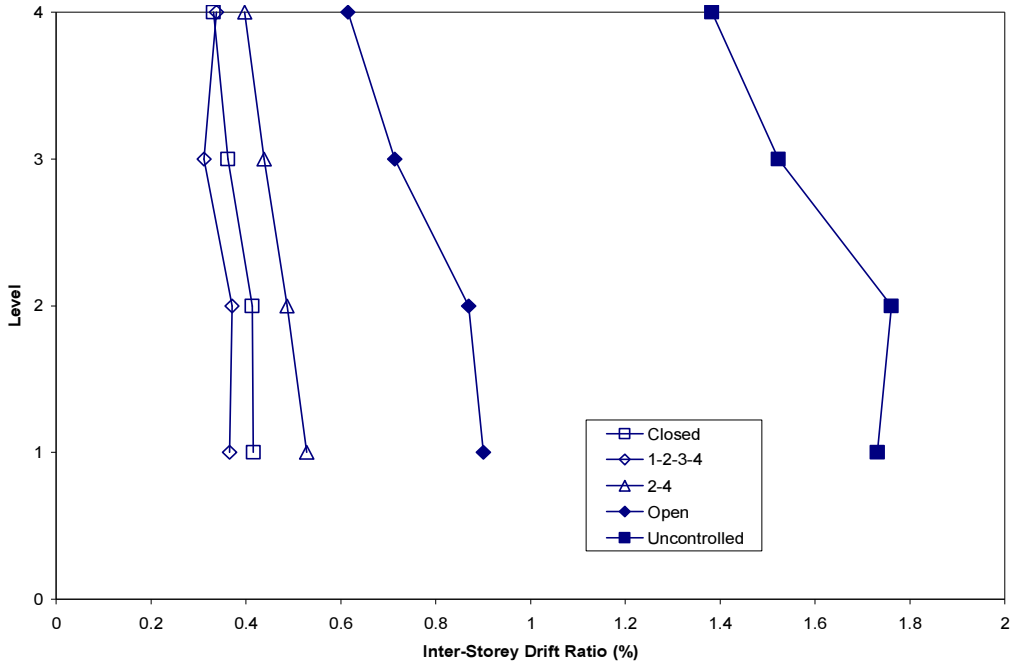

(c) Maximum inter-storey drift ratios

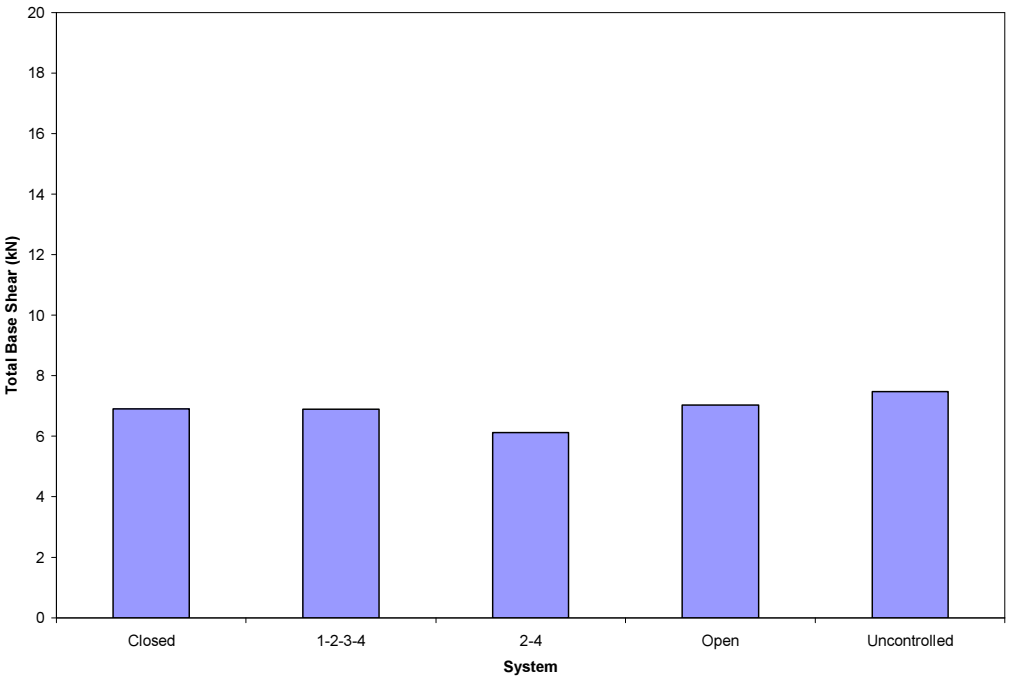

(d) Maximum total base shear

Figure D.1.4 (Continued).

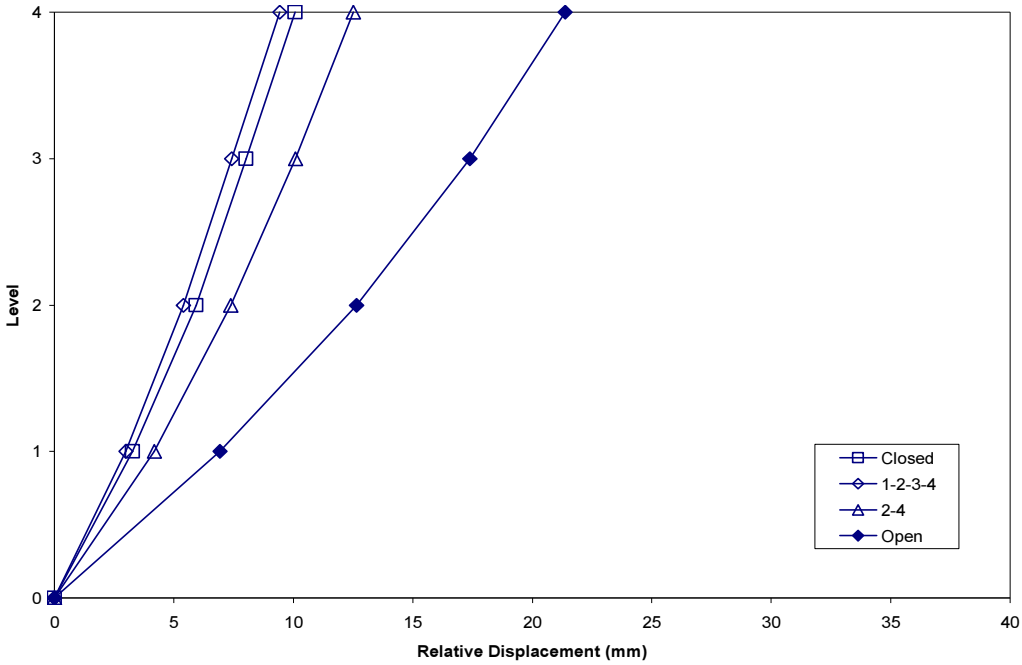

(a) Maximum relative displacements

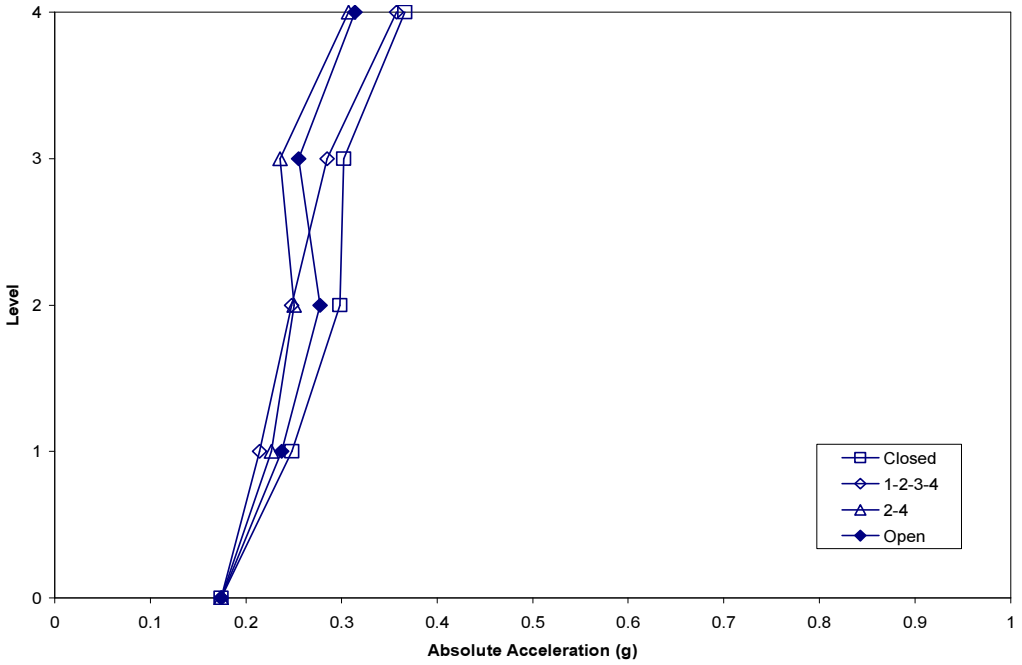

(b) Maximum absolute accelerations

Figure D.1.5 Maximum response envelopes for El Centro 50% earthquake.

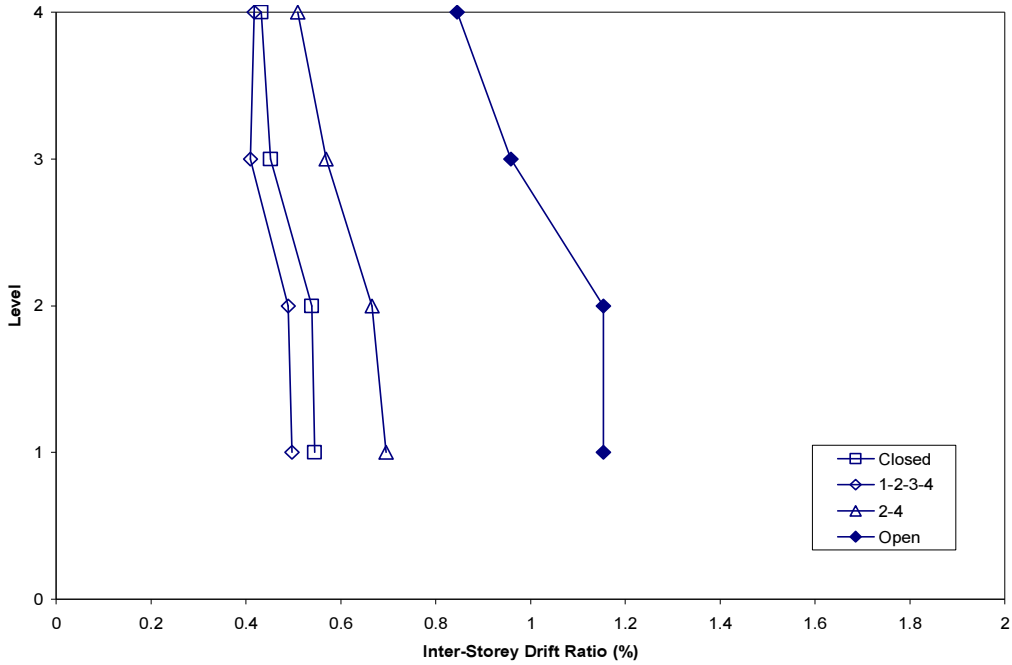

(c) Maximum inter-storey drift ratios

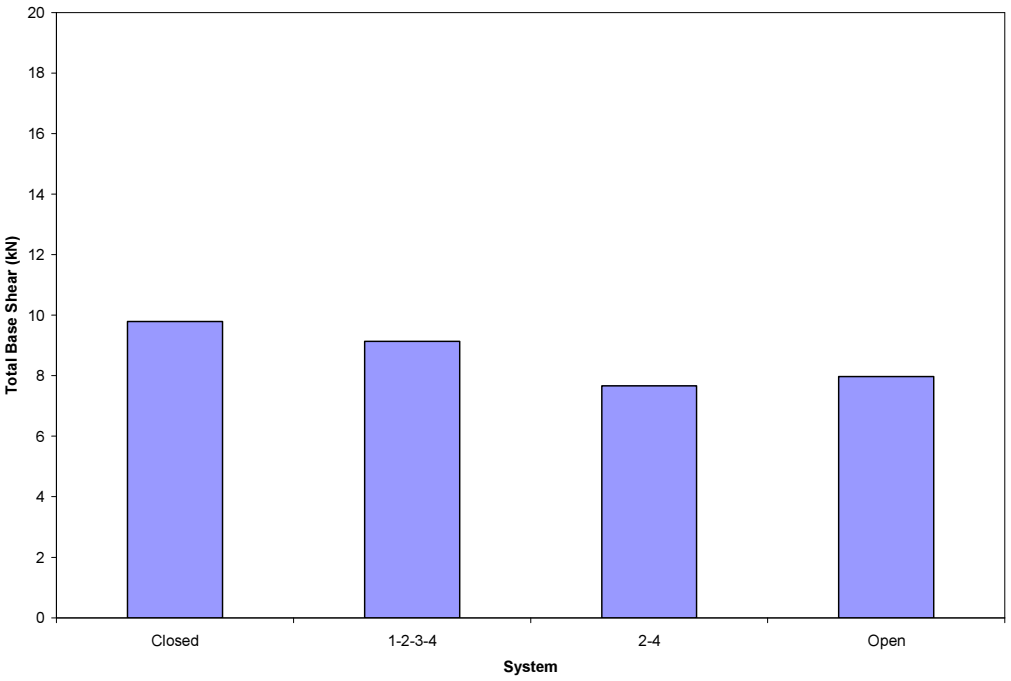

(d) Maximum total base shear

Figure D.1.5 (Continued).

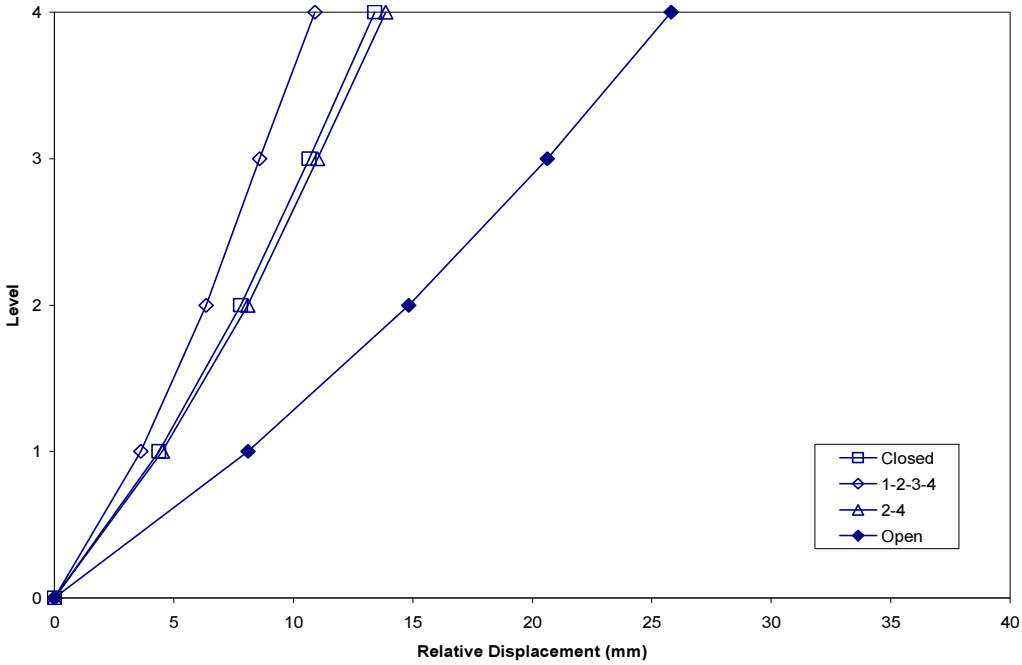

(a) Maximum relative displacements

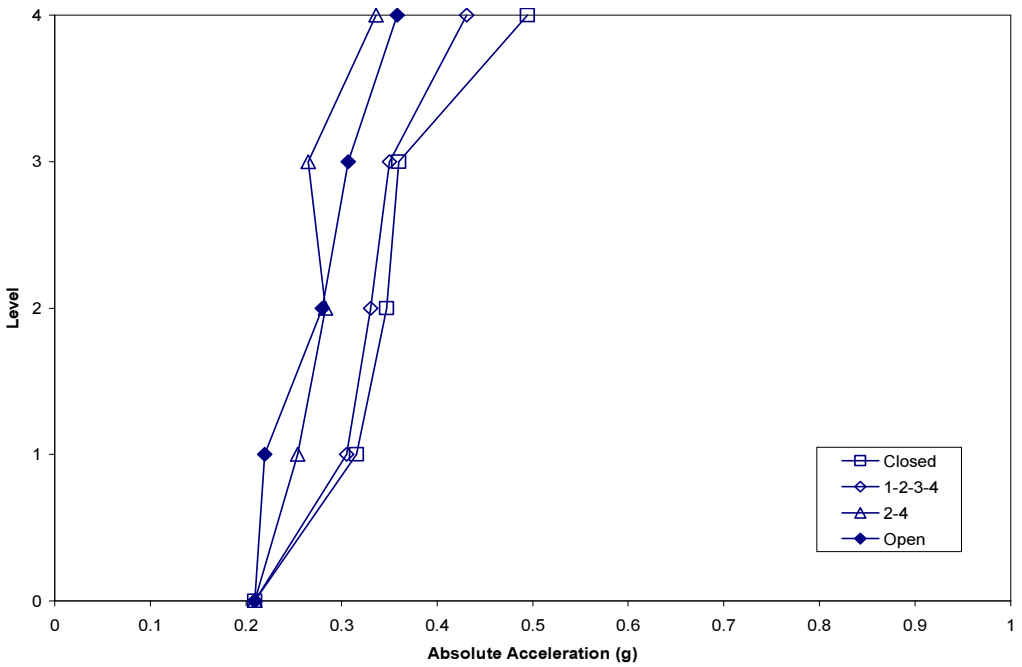

(b) Maximum absolute accelerations

Figure D.1.6 Maximum response envelopes for El Centro 60% earthquake.

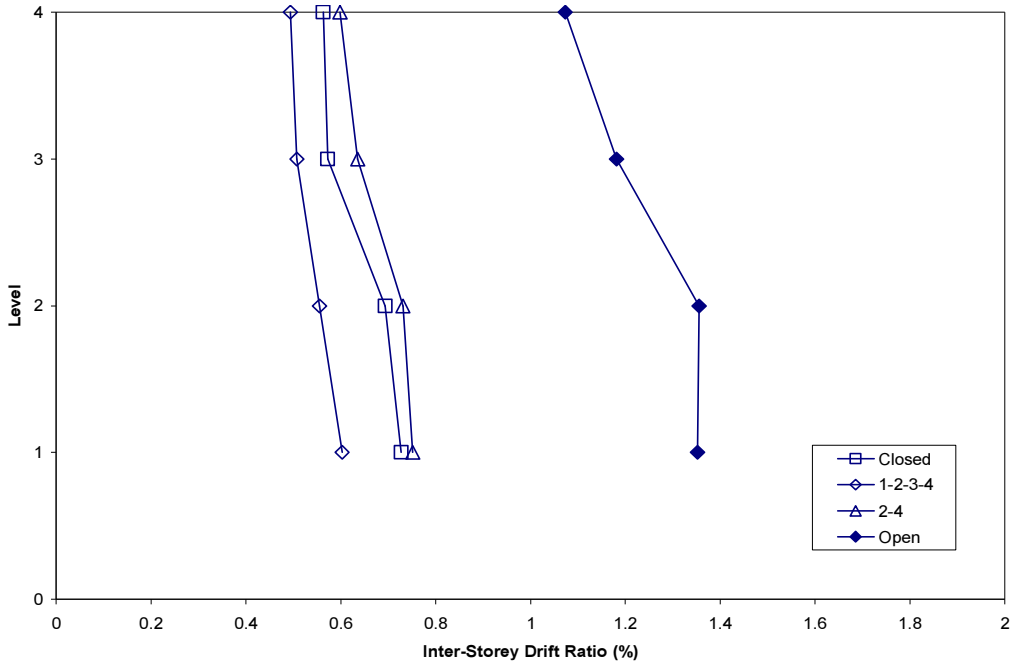

(c) Maximum inter-storey drift ratios

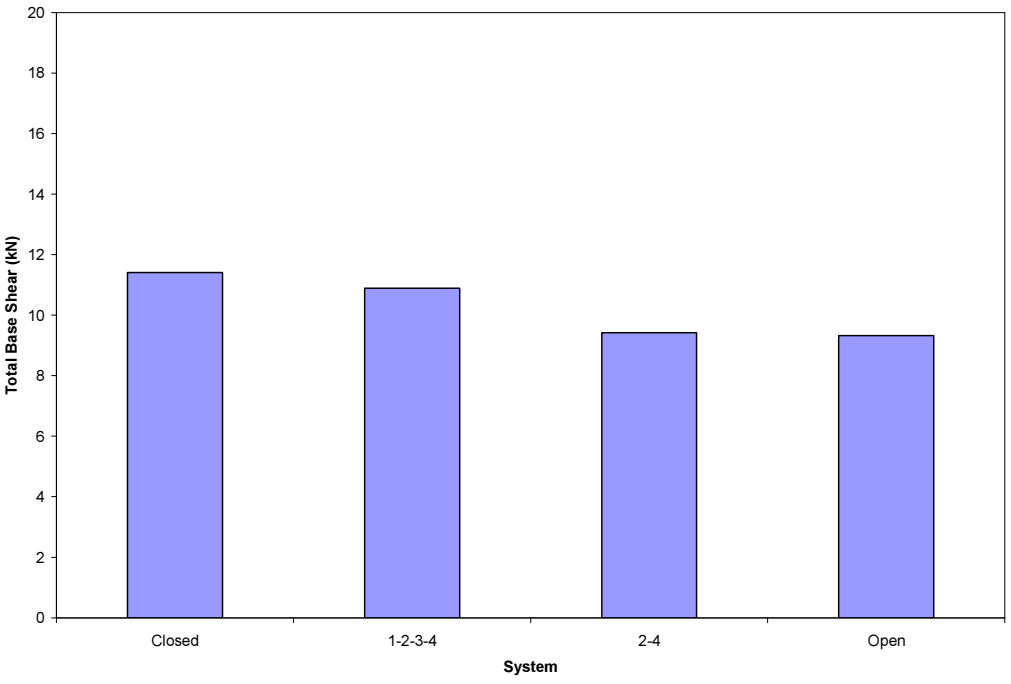

(d) Maximum total base shear

Figure D.1.6 (Continued).

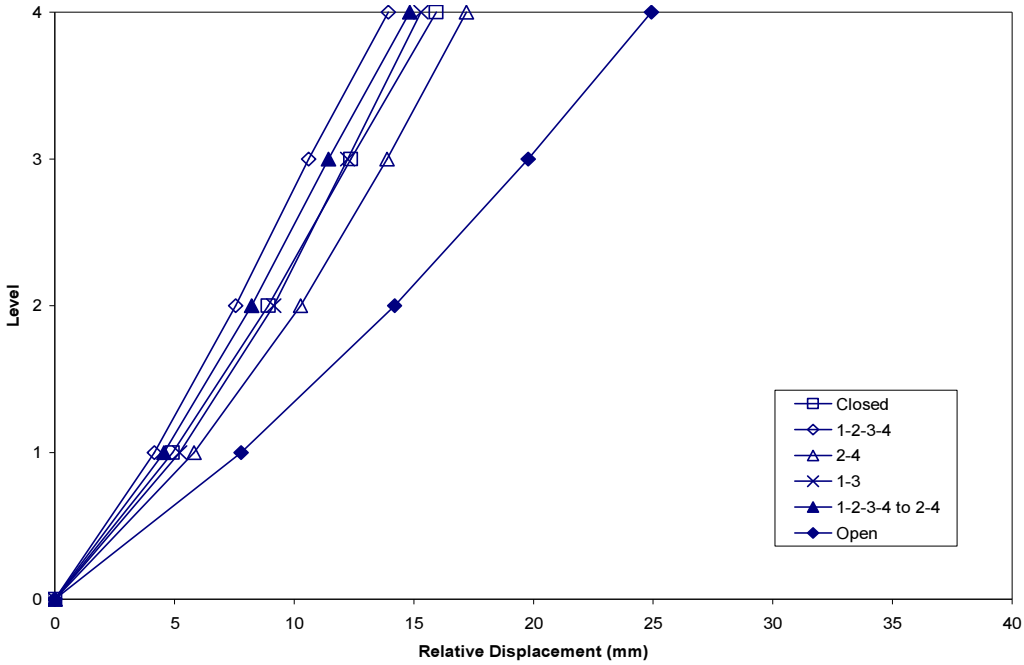

(a) Maximum relative displacements

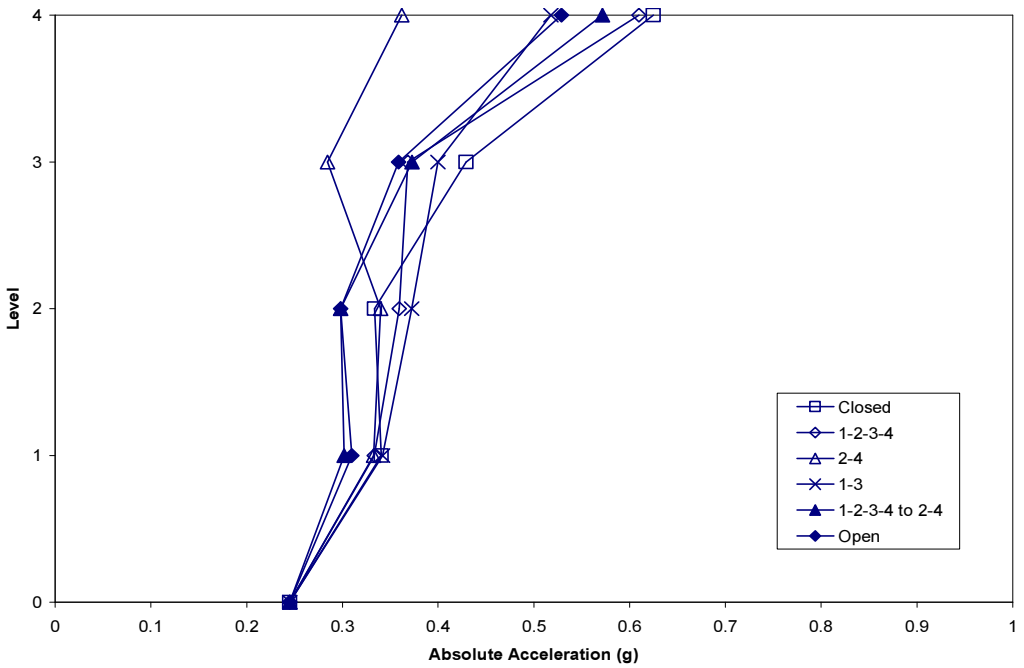

(b) Maximum absolute accelerations

Figure D.1.7 Maximum response envelopes for El Centro 70% Modified earthquake.

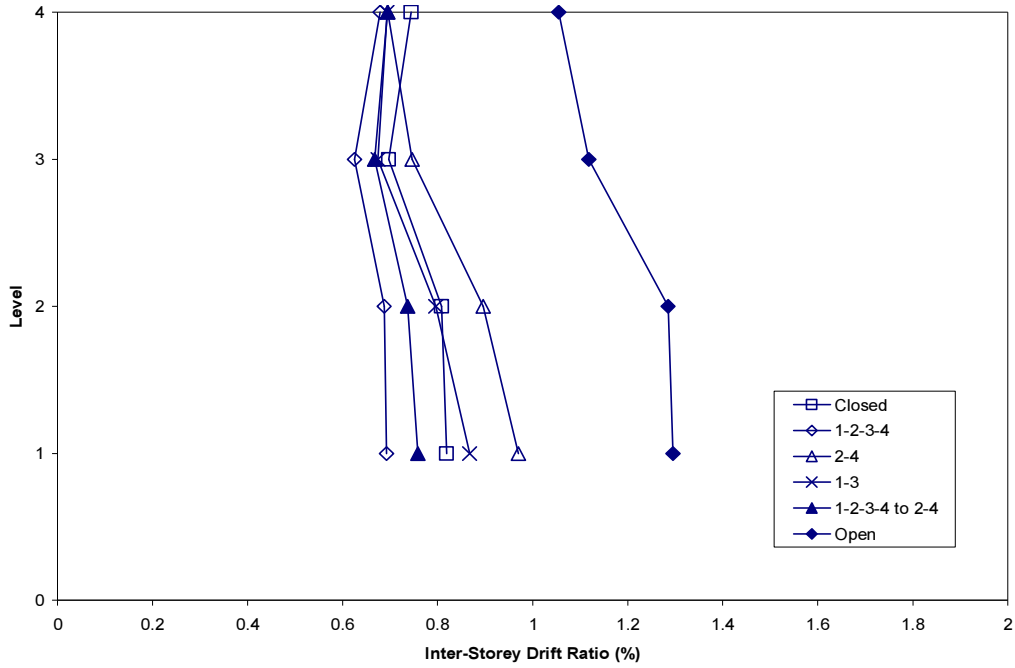

(c) Maximum inter-storey drift ratios

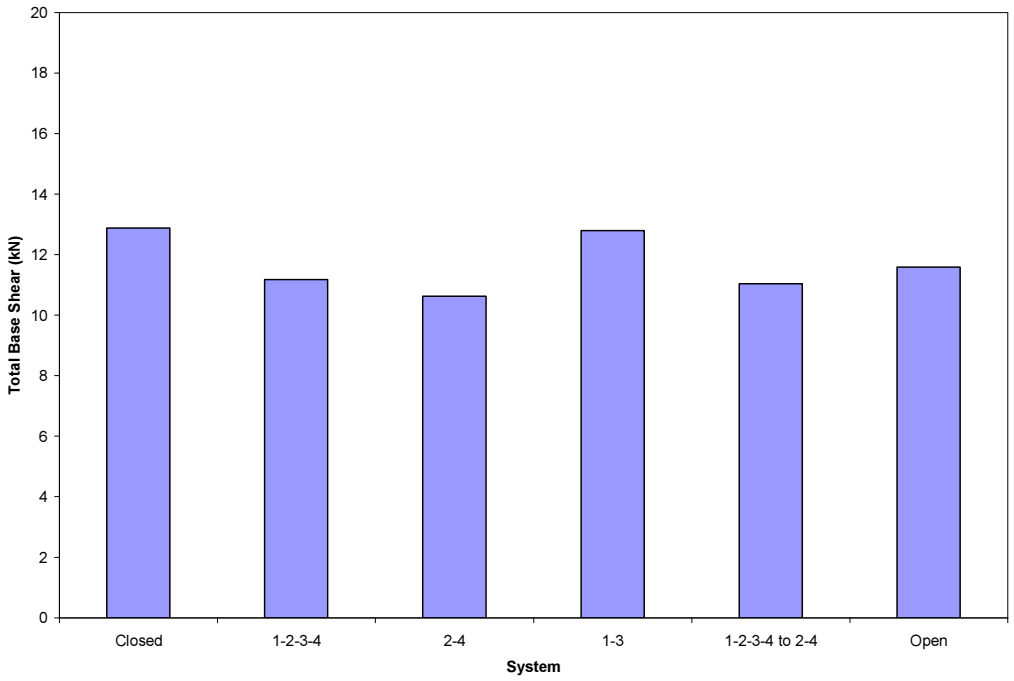

(d) Maximum total base shear

Figure D.1.7 (Continued).

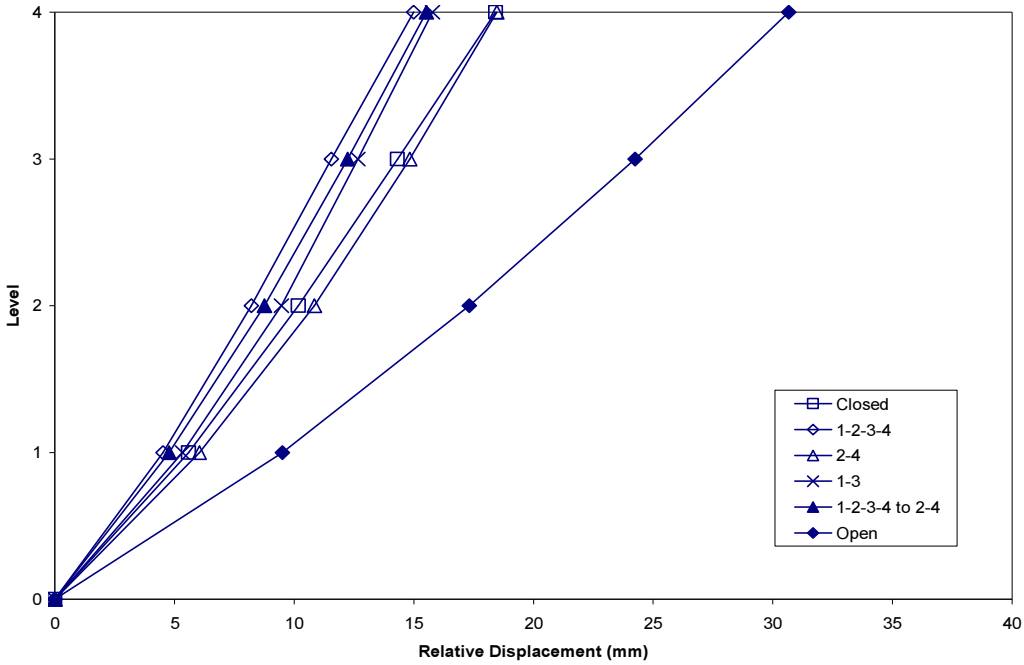

(a) Maximum relative displacements

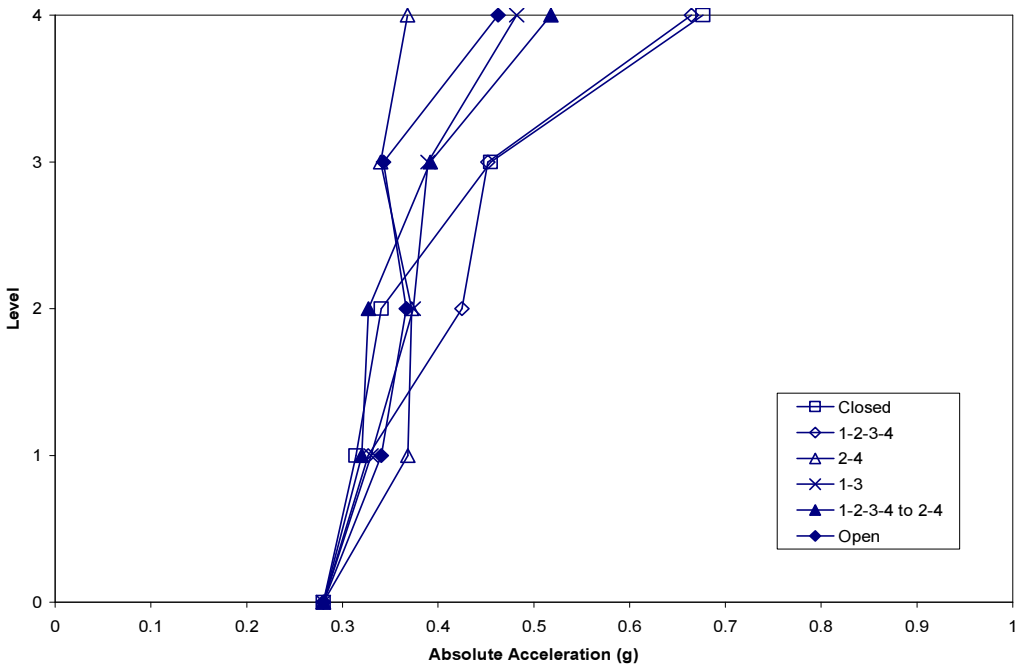

(b) Maximum absolute accelerations

Figure D.1.8 Maximum response envelopes for El Centro 80% Modified earthquake.

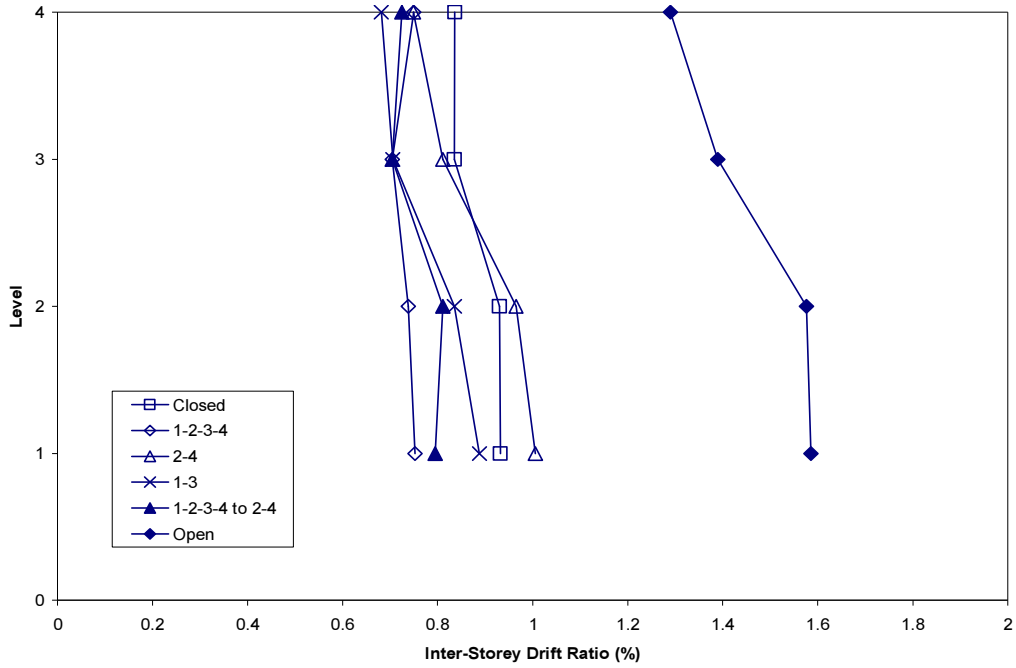

(c) Maximum inter-storey drift ratios

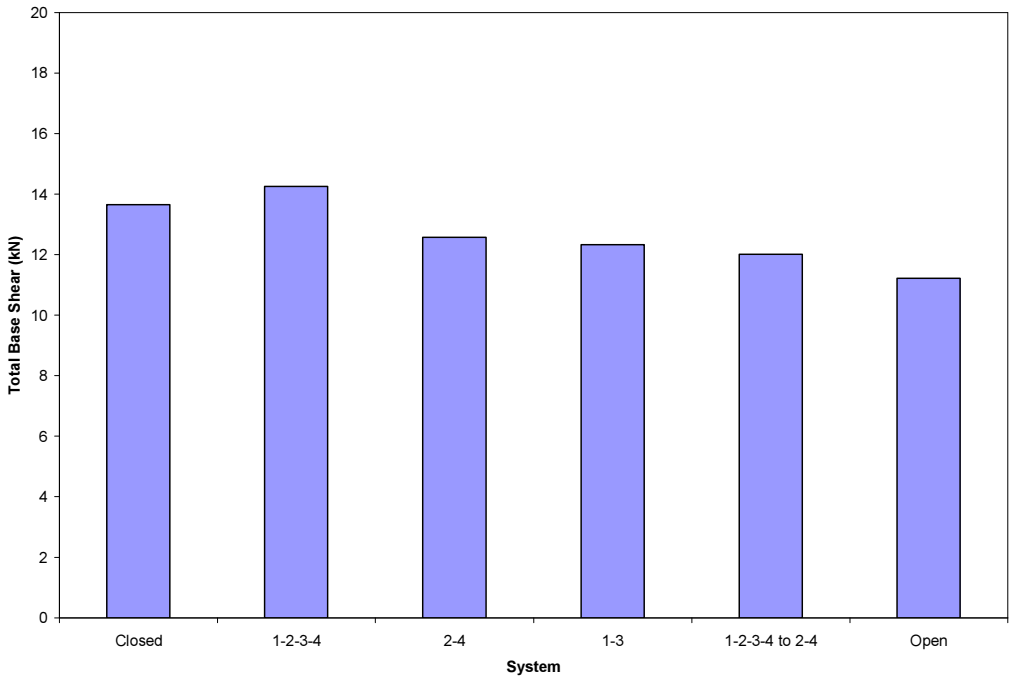

(d) Maximum total base shear

Figure D.1.8 (Continued).

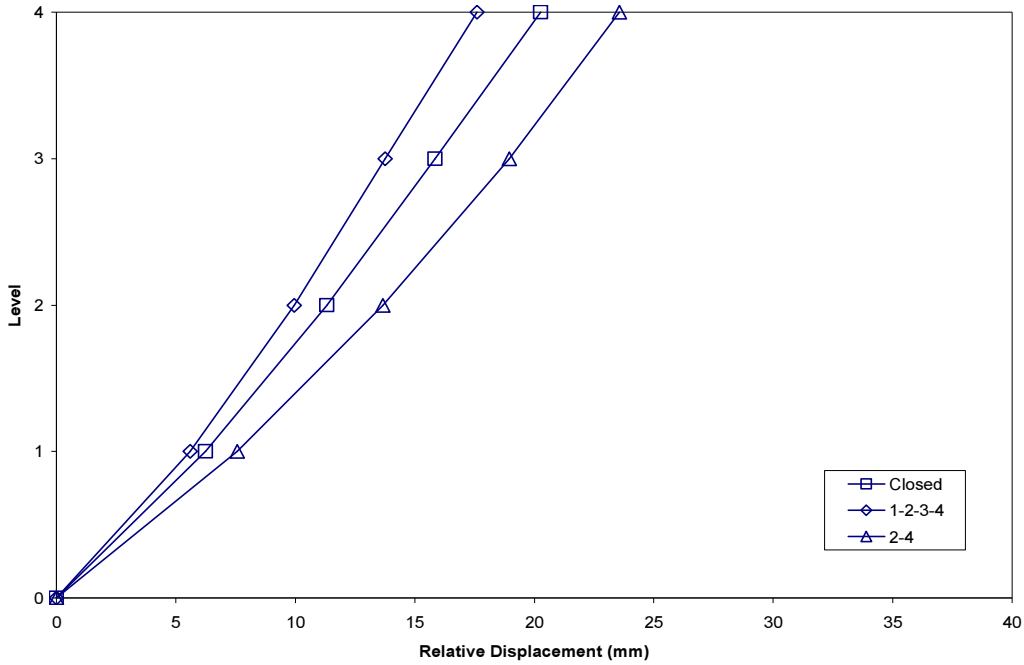

(a) Maximum relative displacements

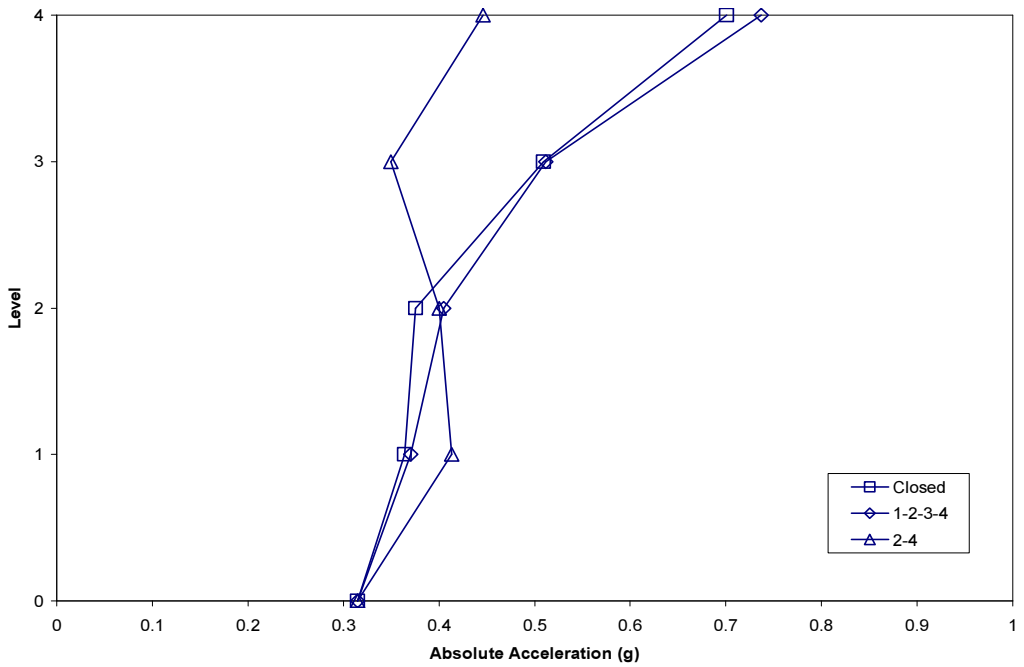

(b) Maximum absolute accelerations

Figure D.1.9 Maximum response envelopes for El Centro 90% Modified earthquake.

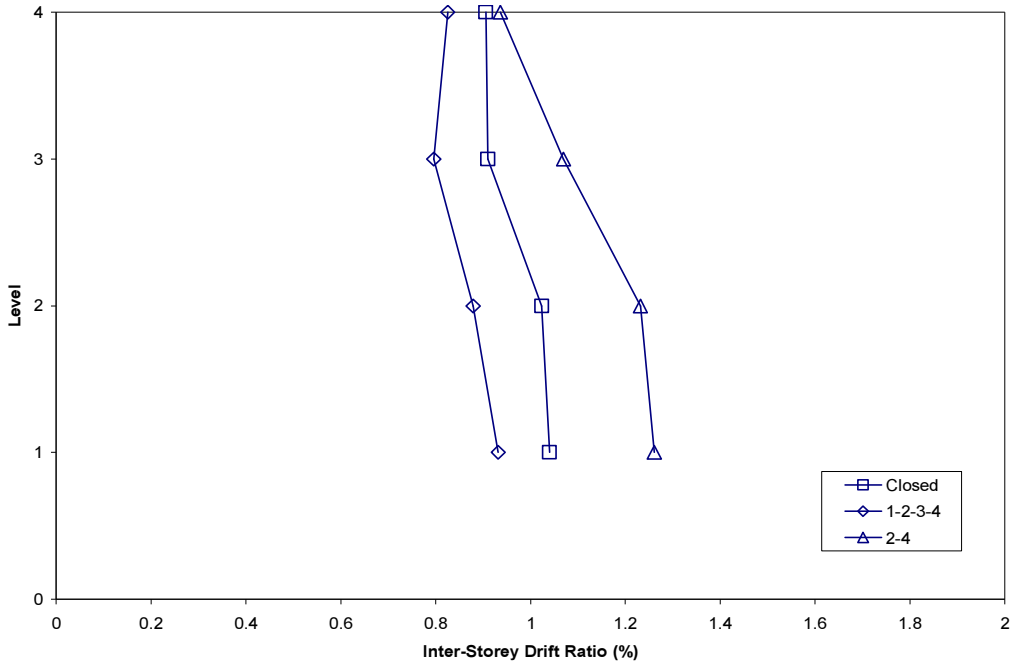

(c) Maximum inter-storey drift ratios

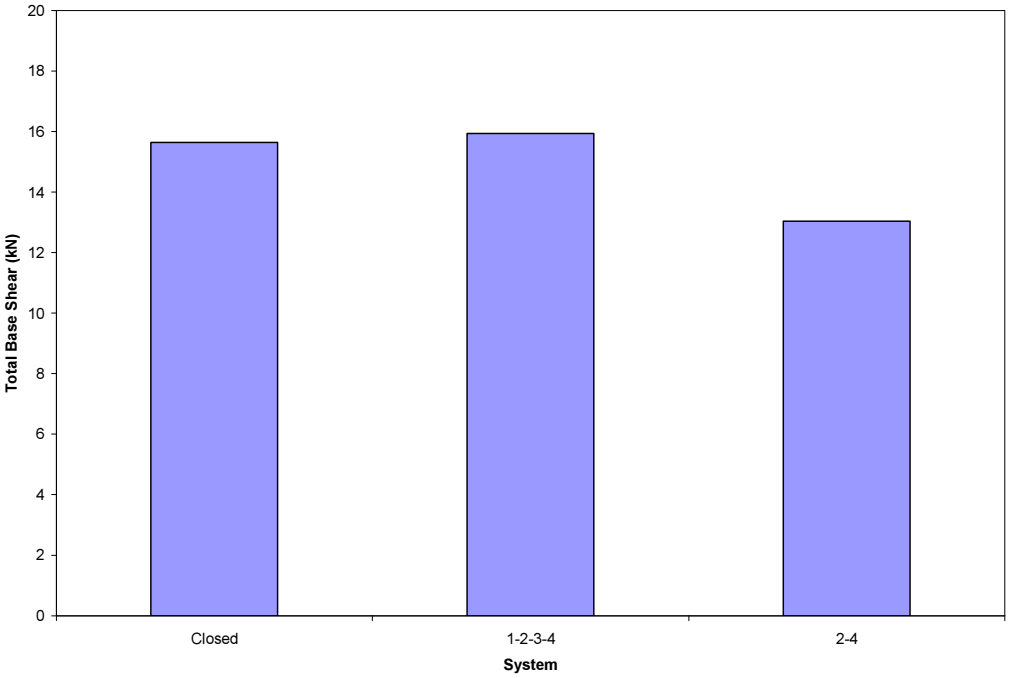

(d) Maximum total base shear

Figure D.1.9 (Continued).

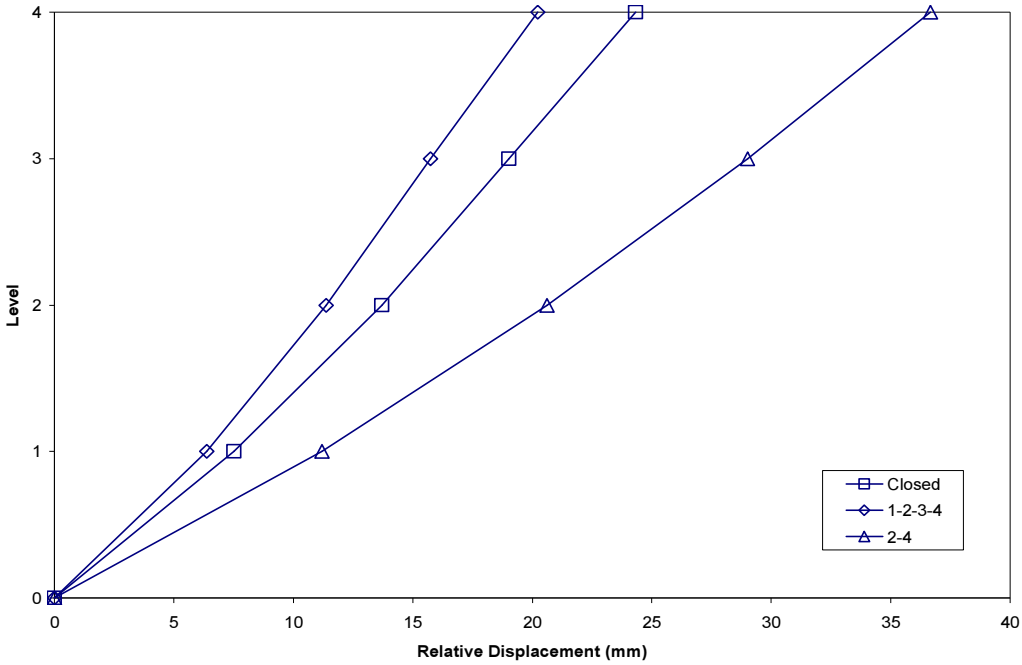

(a) Maximum relative displacements

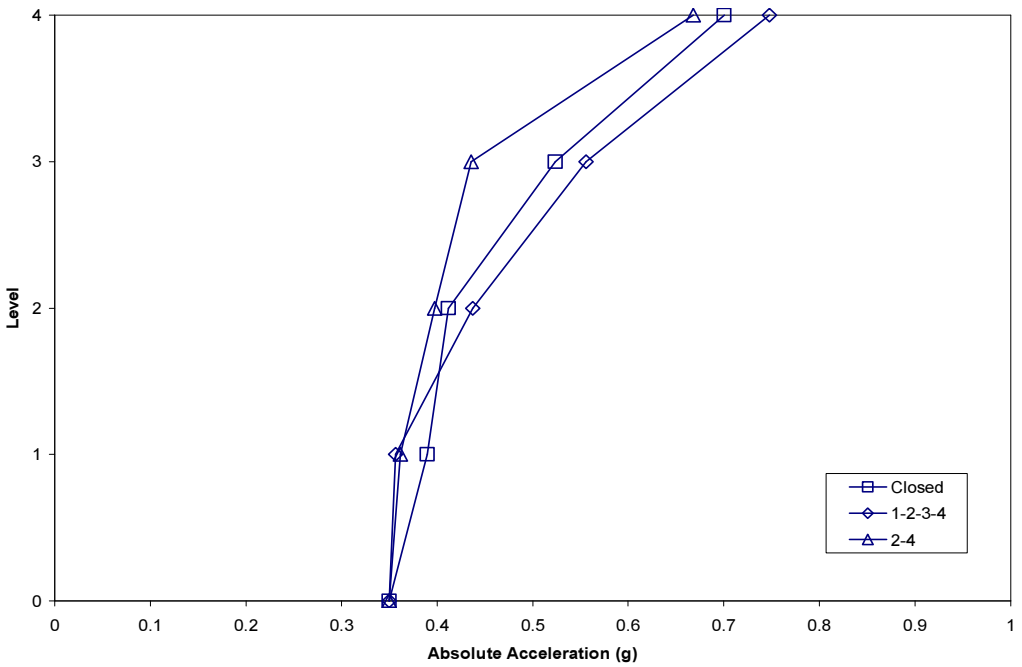

(b) Maximum absolute accelerations

Figure D.1.10 Maximum response envelopes for El Centro 100% Modified earthquake.

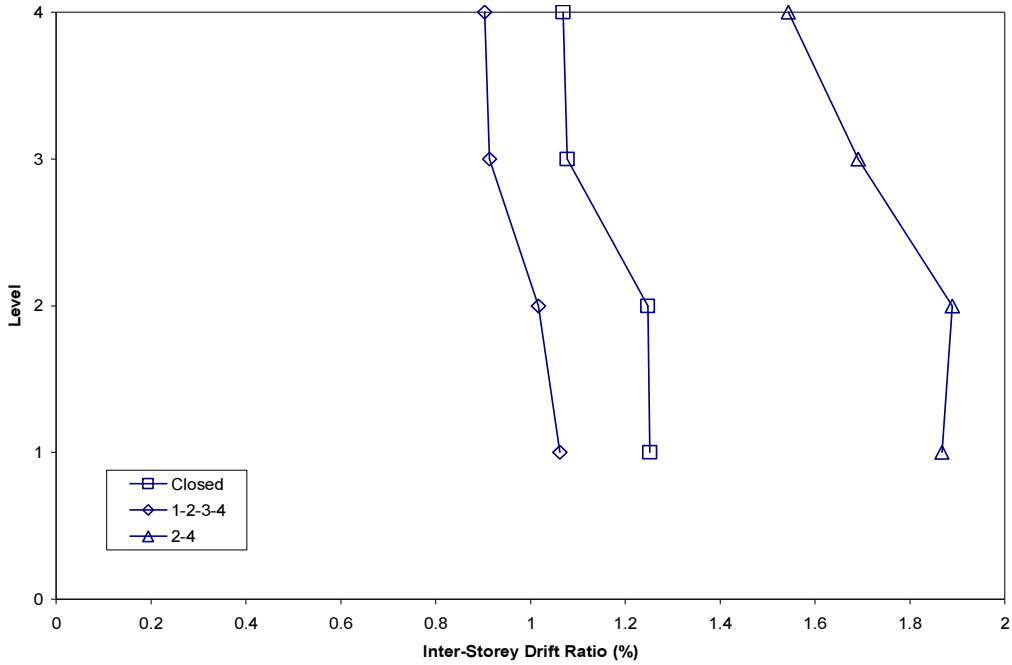

(c) Maximum inter-storey drift ratios

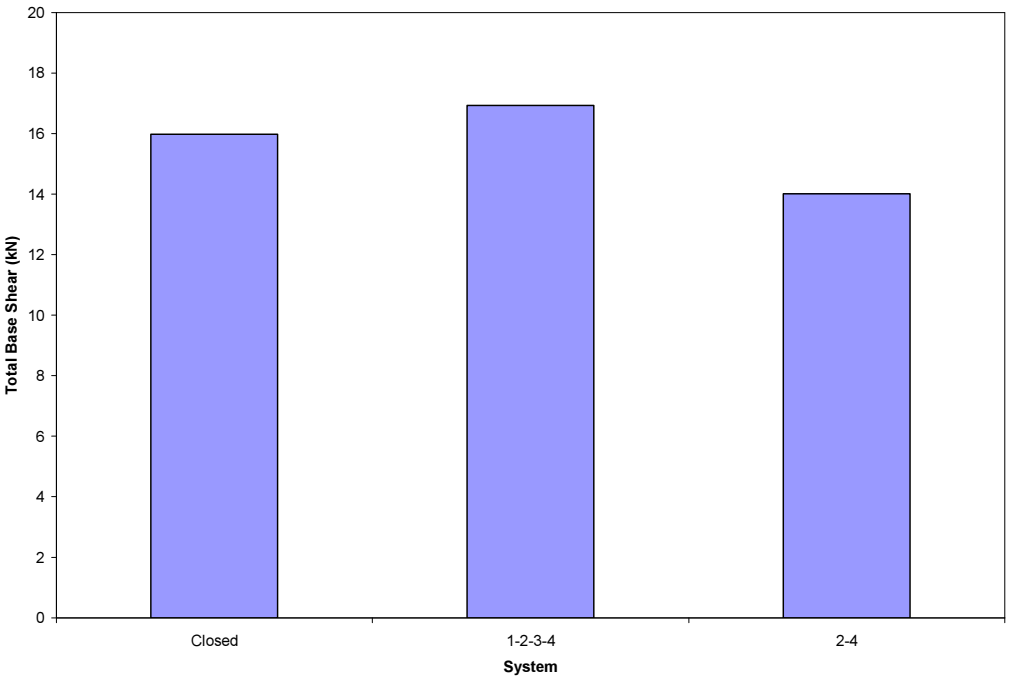

(d) Maximum total base shear

Figure D.1.10 (Continued).

D.2 MAXIMUM RESPONSE ENVELOPES FOR TAFT EARTHQUAKE

Maximum response envelopes are presented for the following scaled earthquake records with corresponding peak ground accelerations:

1. Taft 20% (0.0356g)
2. Taft 40% (0.0712g)
3. Taft 60% (0.1068g)
4. Taft 80% (0.1424g).

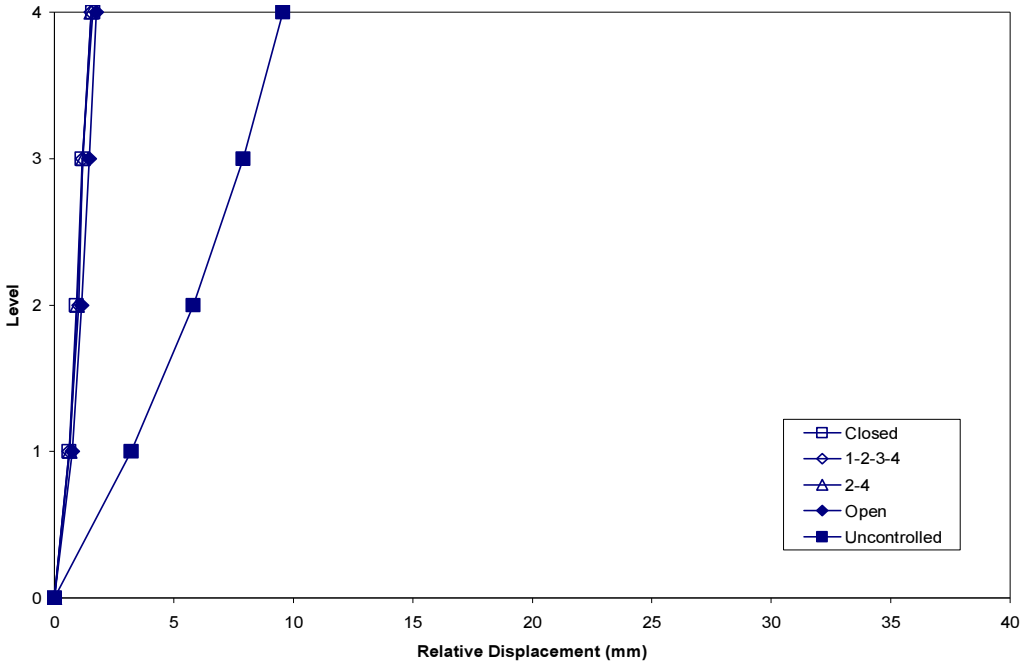

(a) Maximum relative displacements

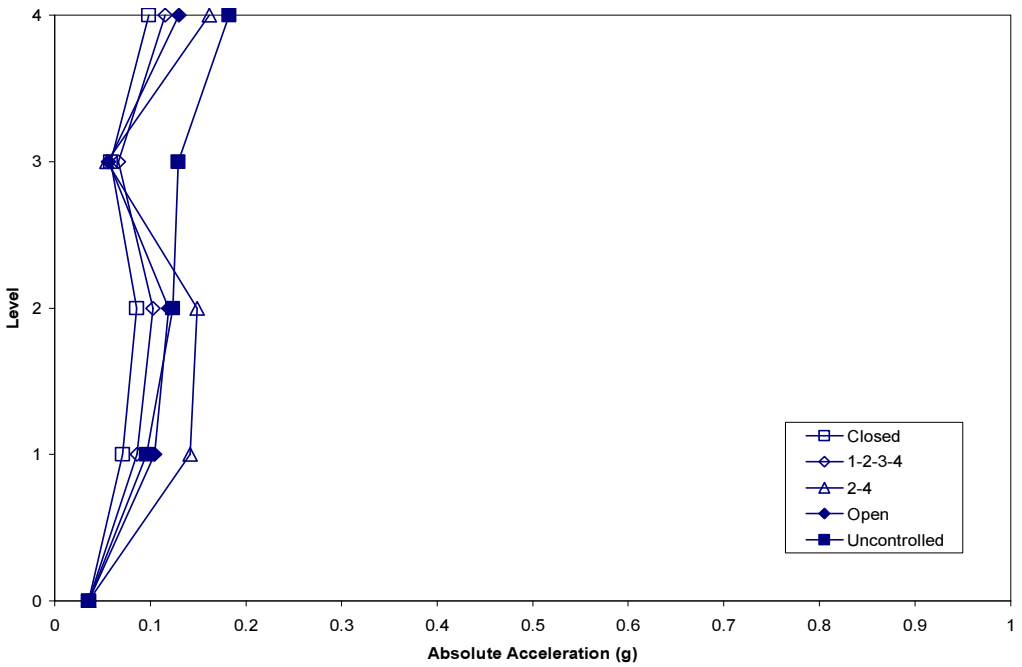

(b) Maximum absolute accelerations

Figure D.2.1 Maximum response envelopes for Taft 20% earthquake.

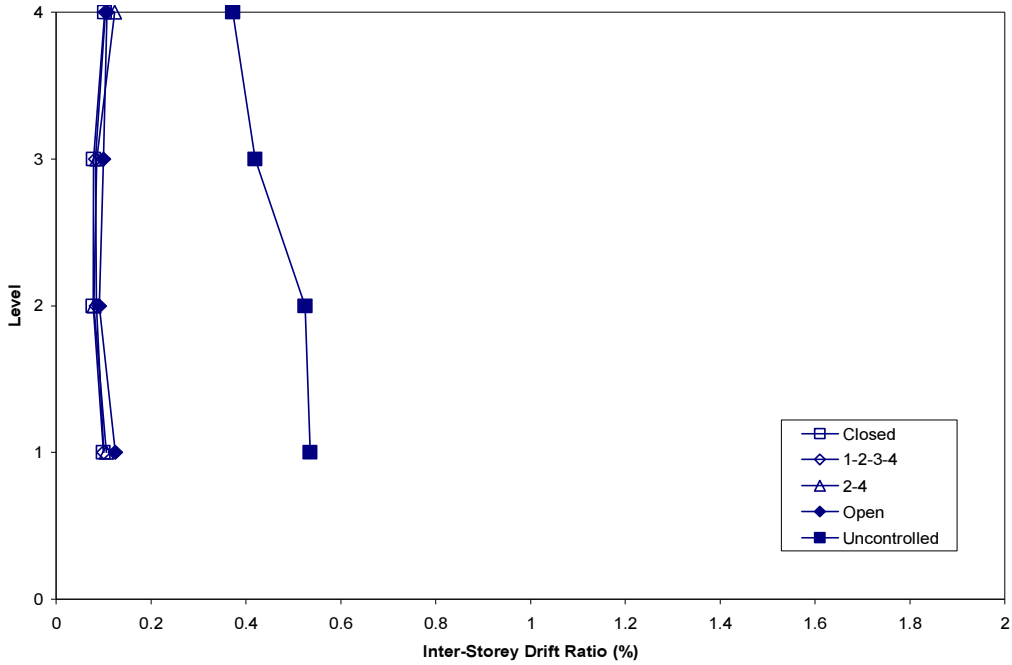

(c) Maximum inter-storey drift ratios

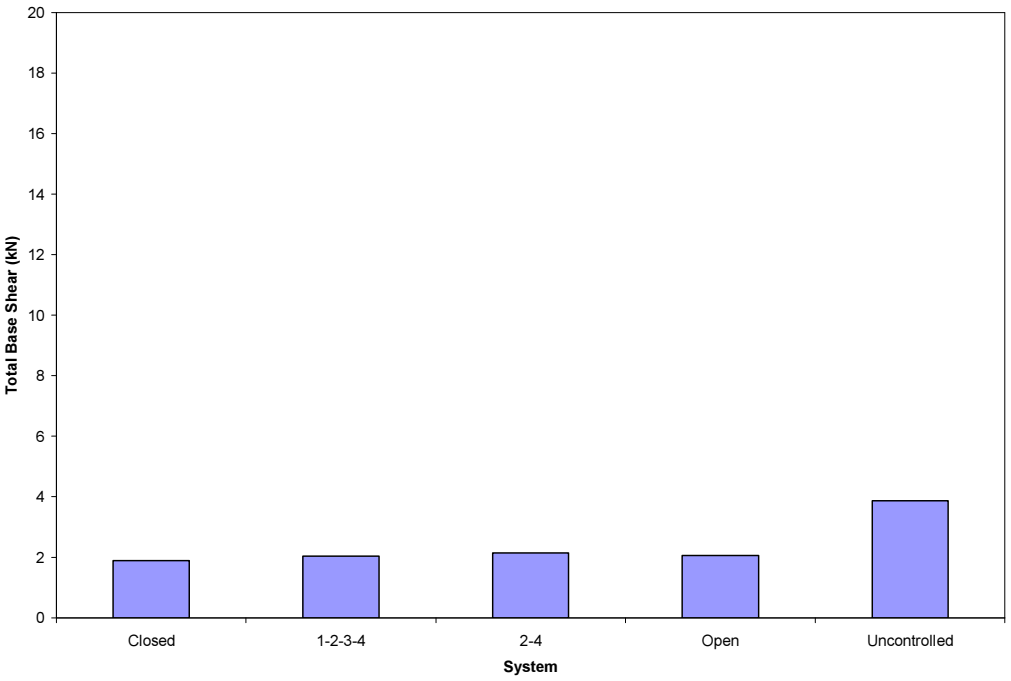

(d) Maximum total base shear

Figure D.2.1 (Continued).

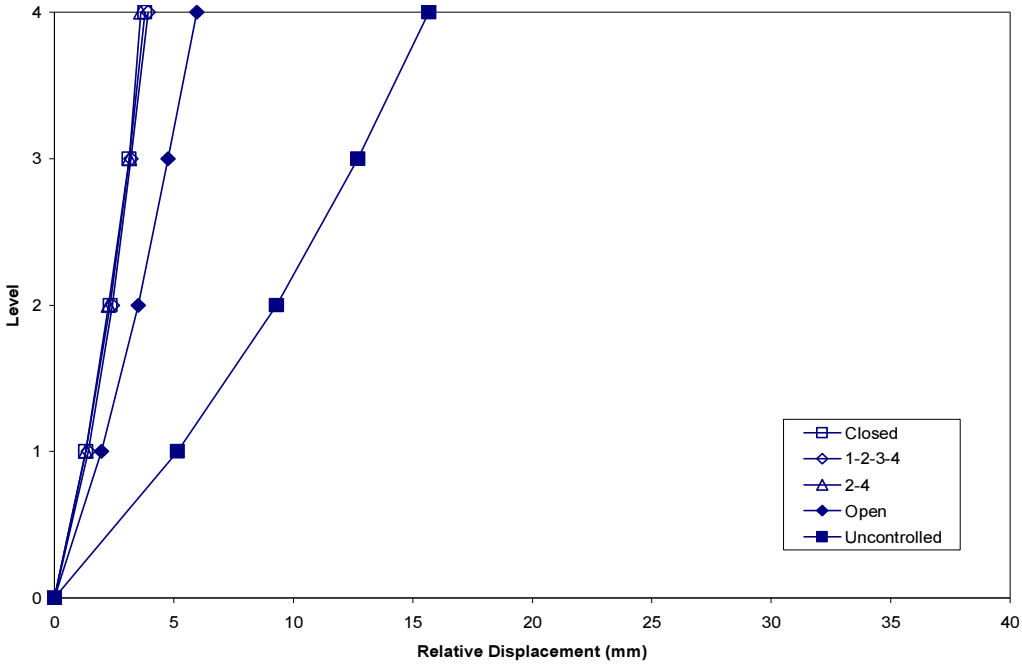

(a) Maximum relative displacements

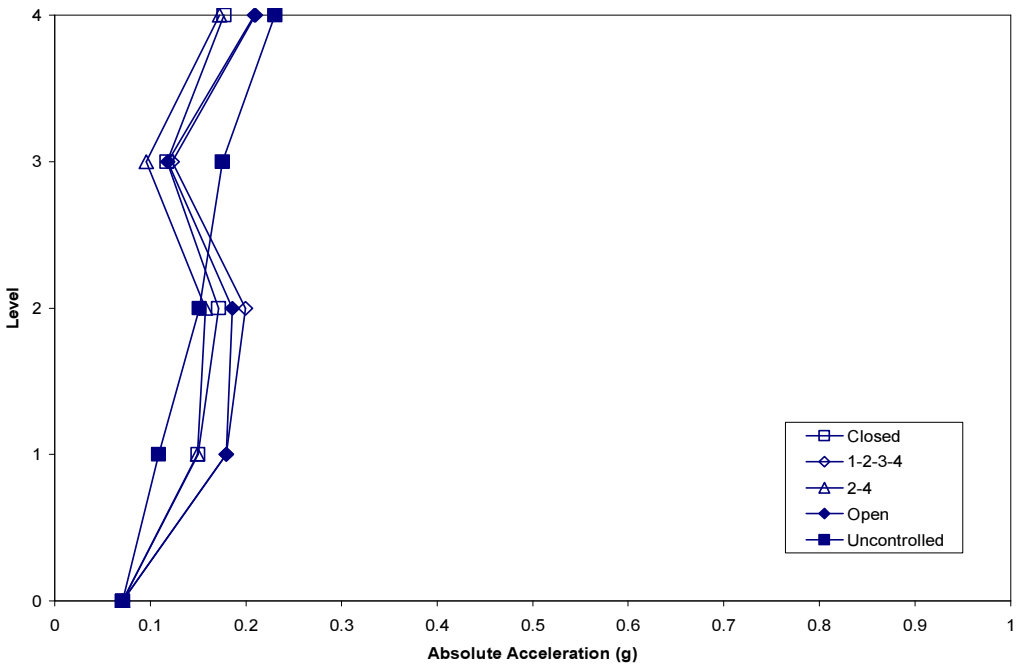

(b) Maximum absolute accelerations

Figure D.2.2 Maximum response envelopes for Taft 40% earthquake.

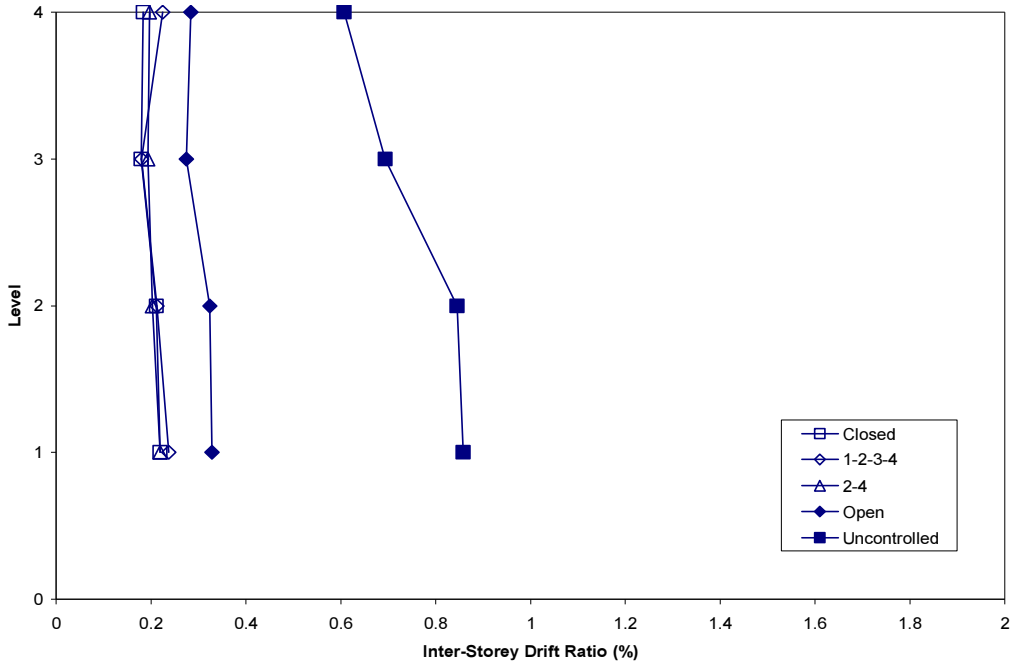

(c) Maximum inter-storey drift ratios

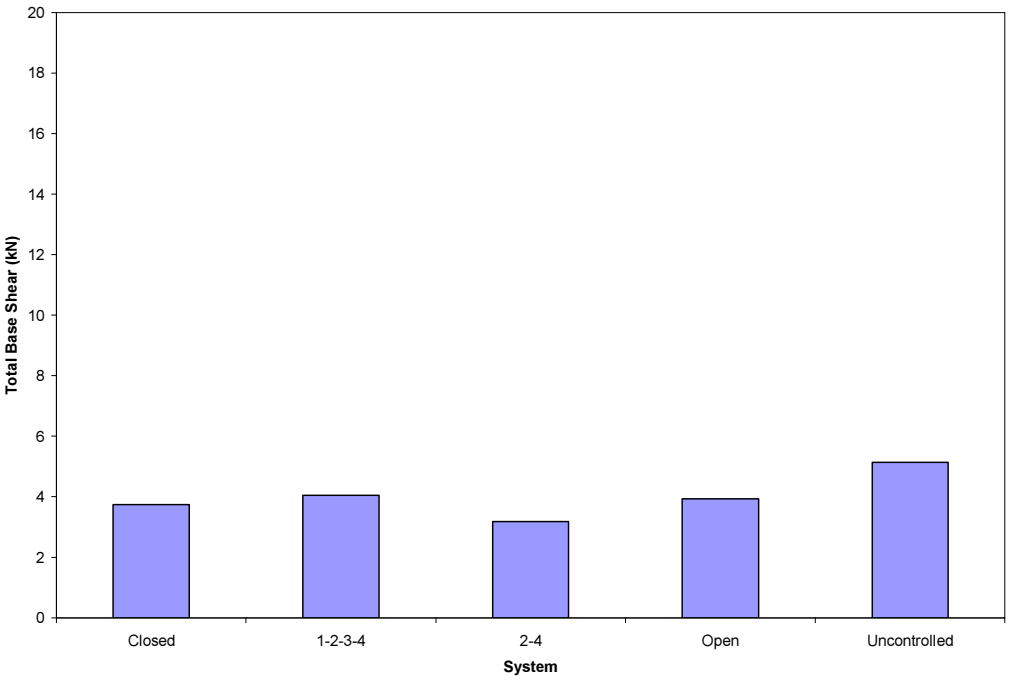

(d) Maximum total base shear

Figure D.2.2 (Continued).

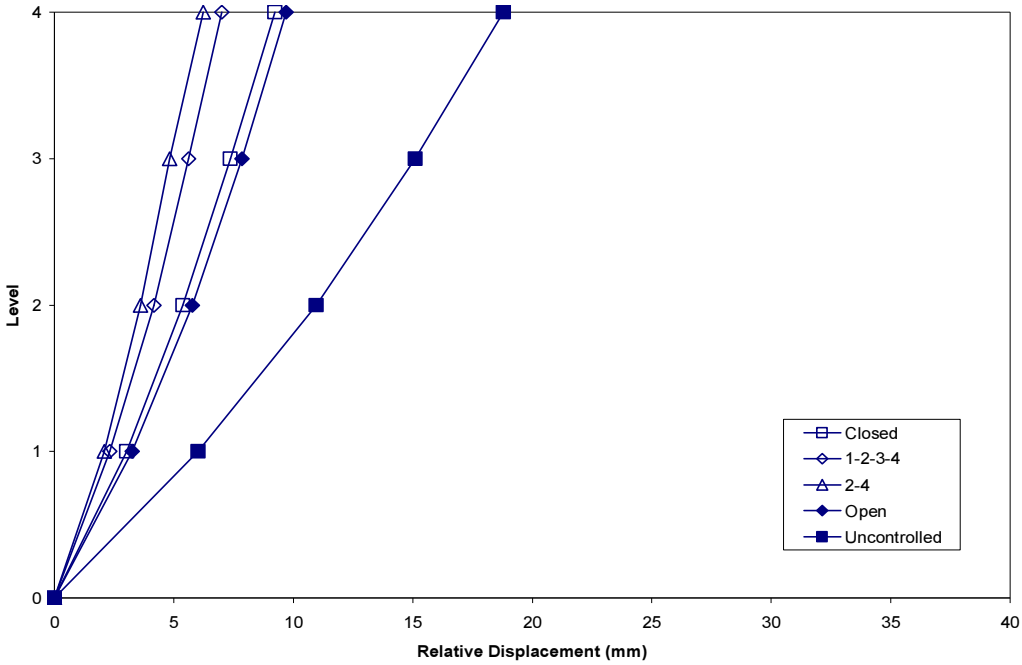

(a) Maximum relative displacements

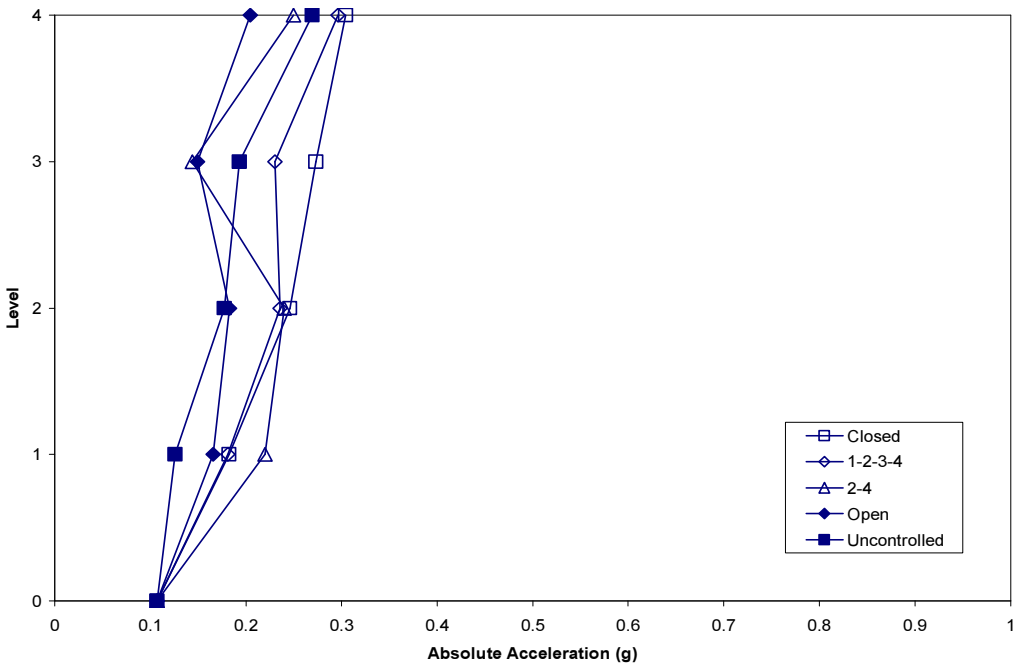

(b) Maximum absolute accelerations

Figure D.2.3 Maximum response envelopes for Taft 60% earthquake.

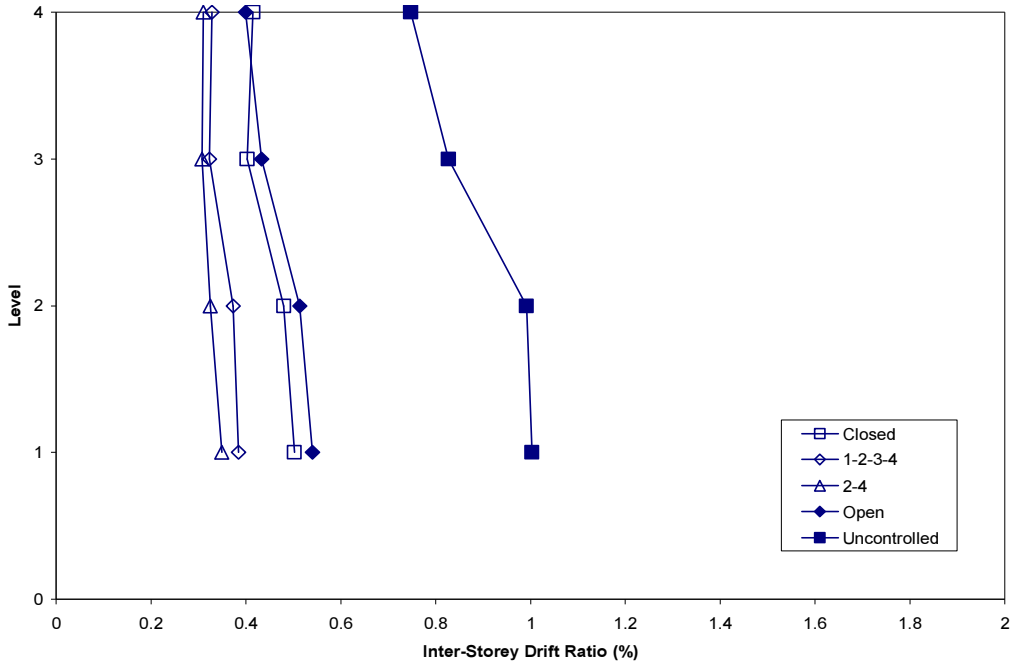

(c) Maximum inter-storey drift ratios

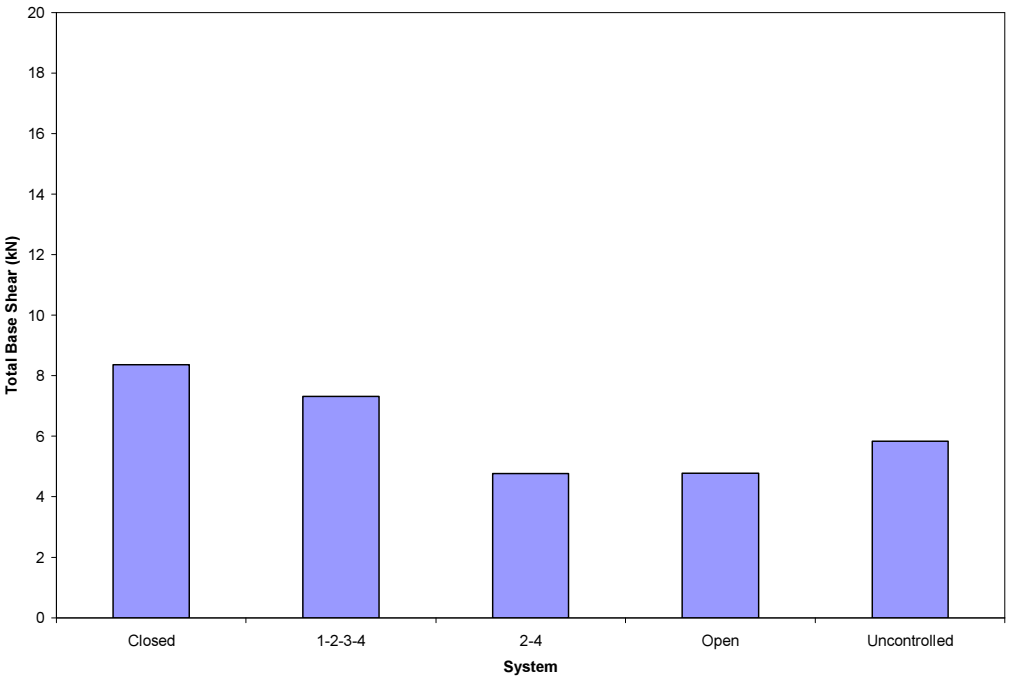

(d) Maximum total base shear

Figure D.2.3 (Continued).

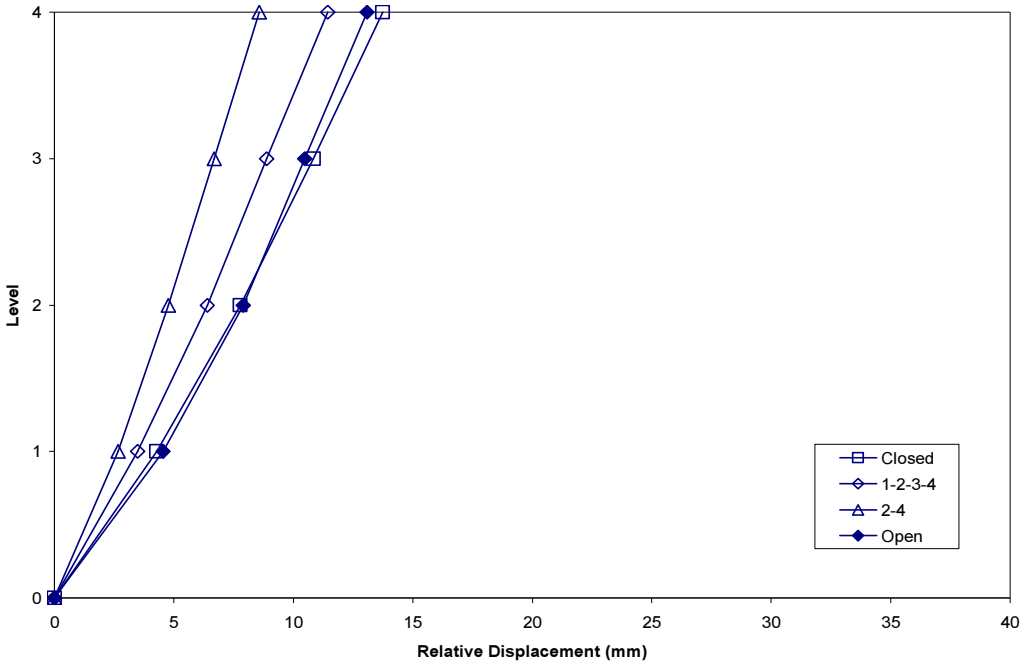

(a) Maximum relative displacements

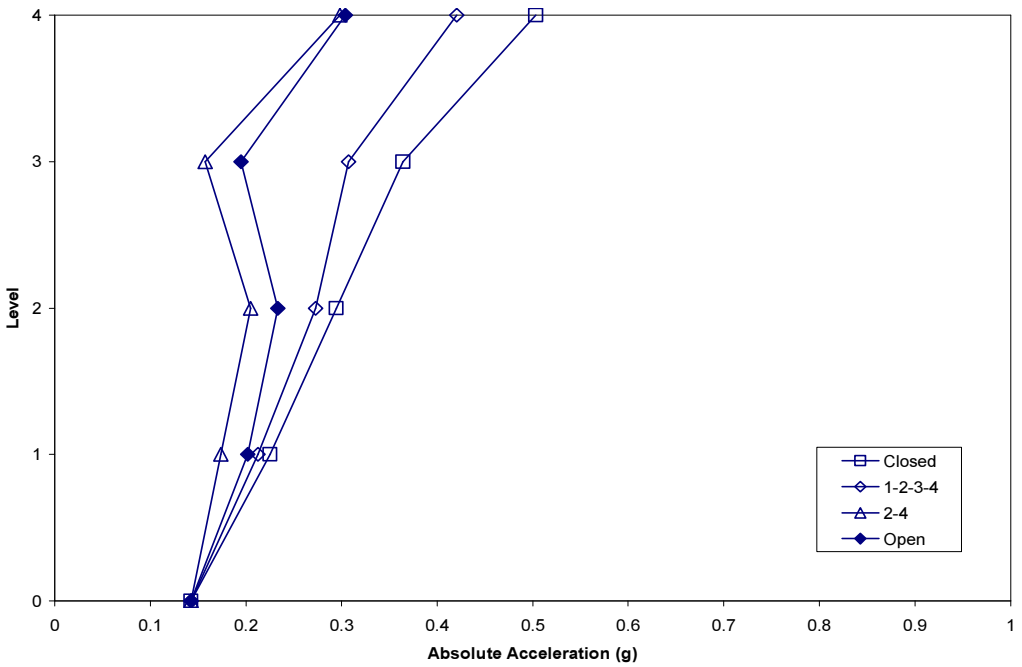

(b) Maximum absolute accelerations

Figure D.2.4 Maximum response envelopes for Taft 80% earthquake.

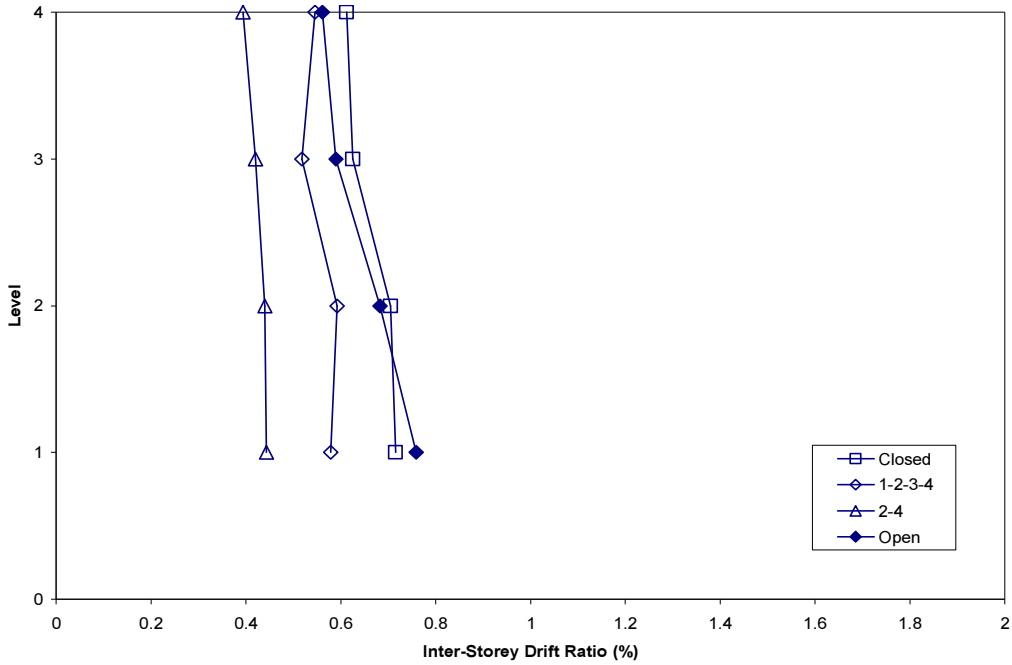

(c) Maximum inter-storey drift ratios

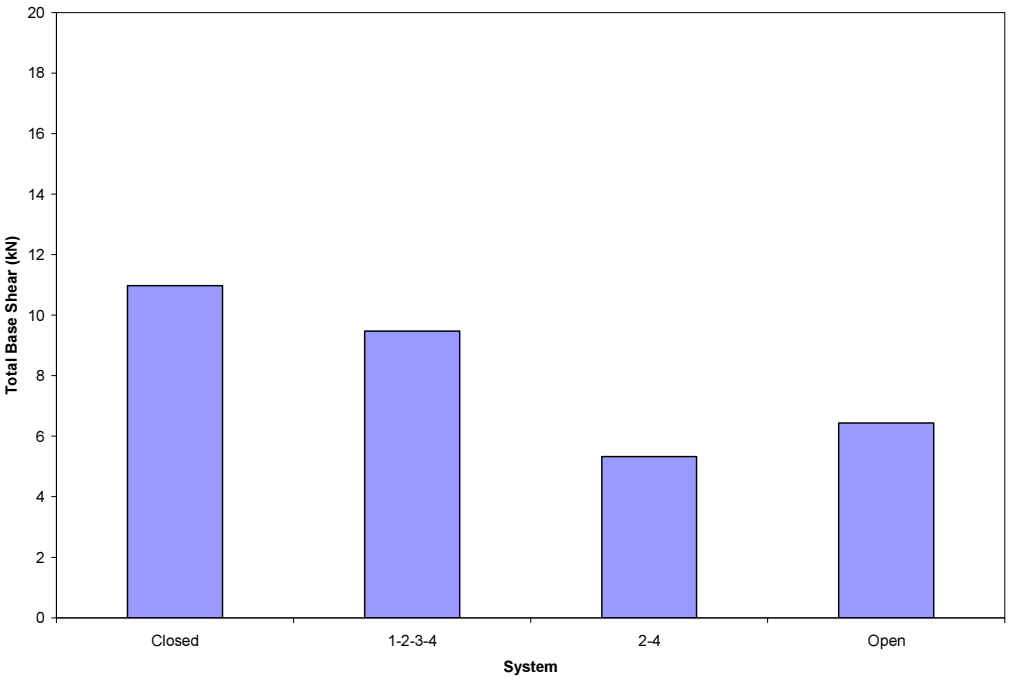

(d) Maximum total base shear

Figure D.2.4 (Continued).

D.3 MAXIMUM RESPONSE ENVELOPES FOR SYLMAR EARTHQUAKE

Maximum response envelopes are presented for the following scaled earthquake records with corresponding peak ground accelerations:

1. Sylmar 5% (0.0399g)
2. Sylmar 10% (0.0798g)
3. Sylmar 15% (0.1196g)
4. Sylmar 20% (0.1595g)
5. Sylmar 25% Modified (0.1369g)
6. Sylmar 30% Modified (0.1643g).

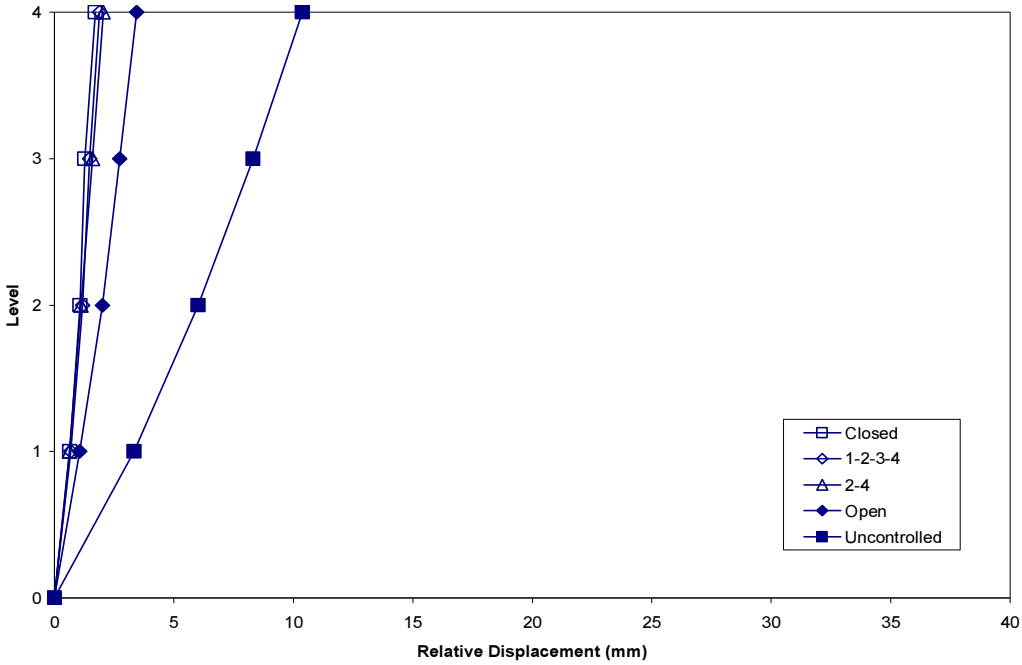

(a) Maximum relative displacements

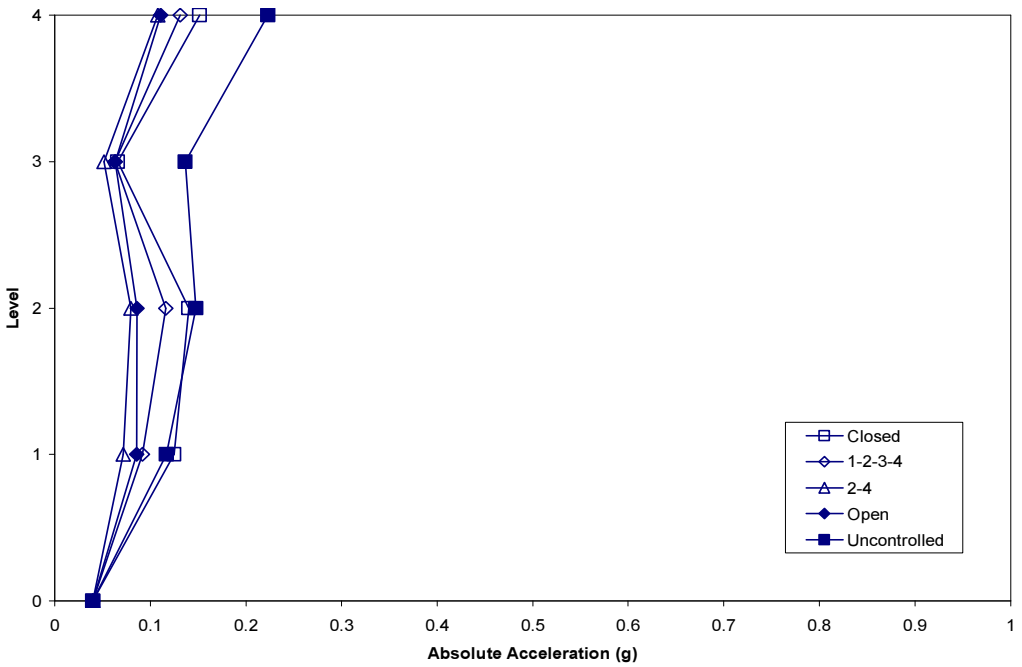

(b) Maximum absolute accelerations

Figure D.3.1 Maximum response envelopes for Sylmar 5% earthquake.

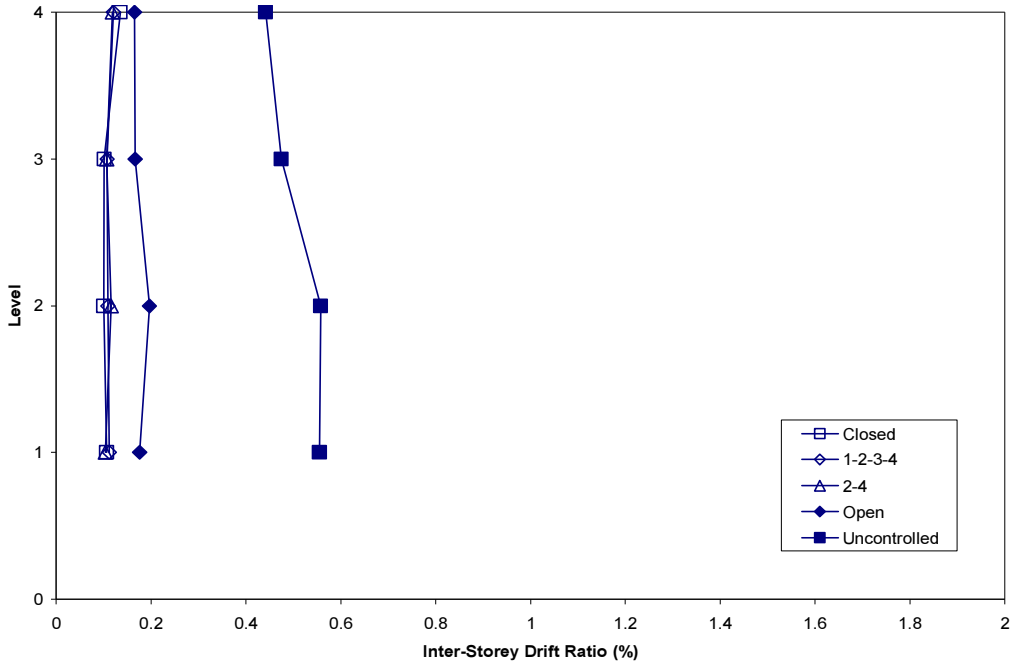

(c) Maximum inter-storey drift ratios

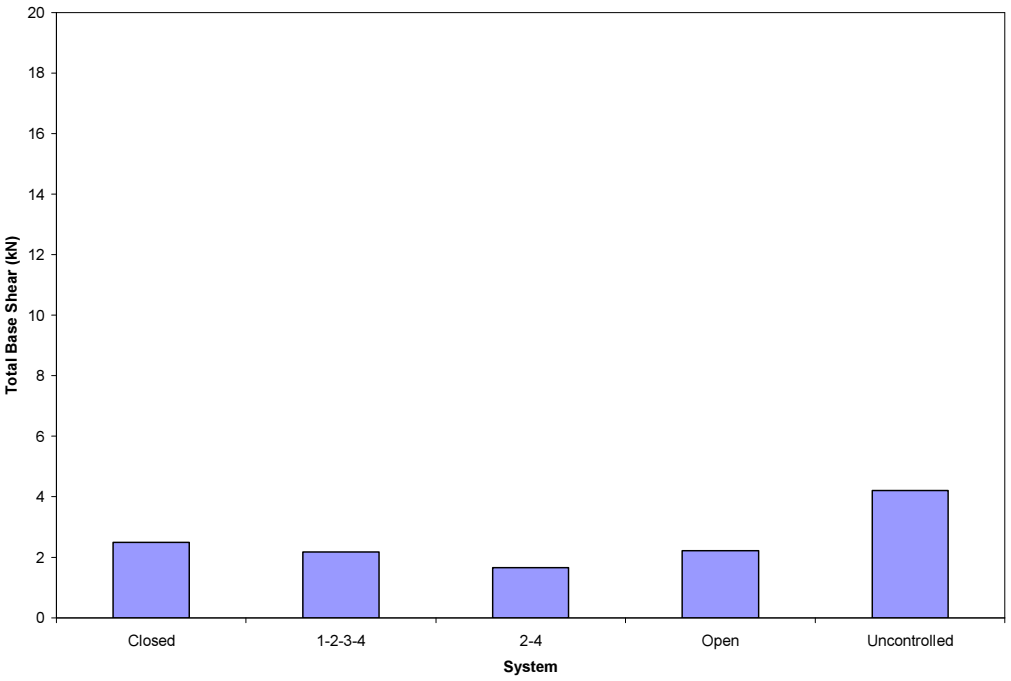

(d) Maximum total base shear

Figure D.3.1 (Continued).

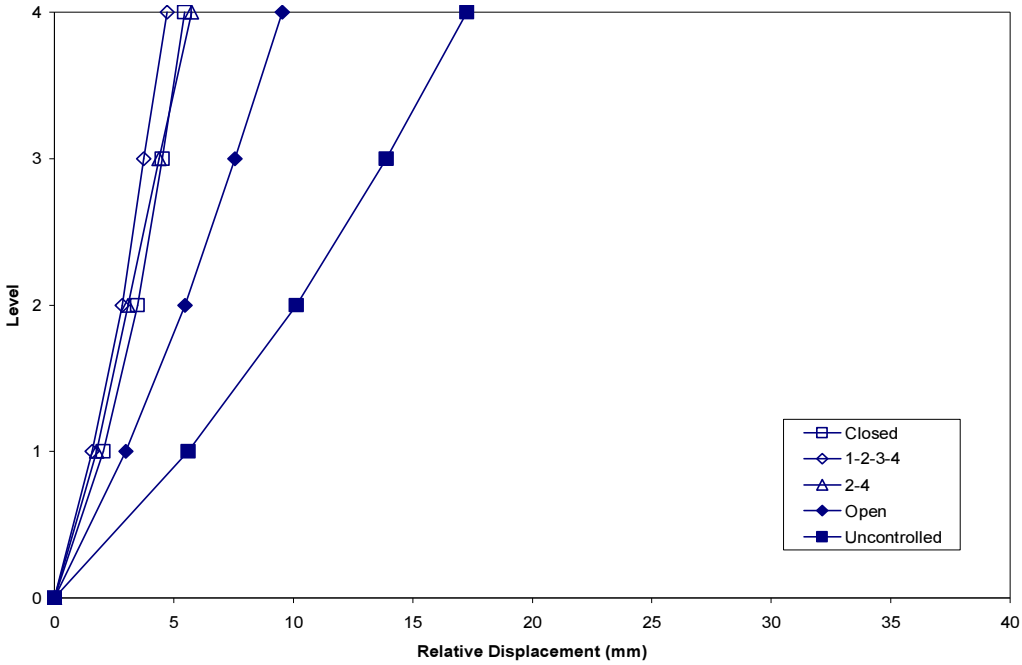

(a) Maximum relative displacements

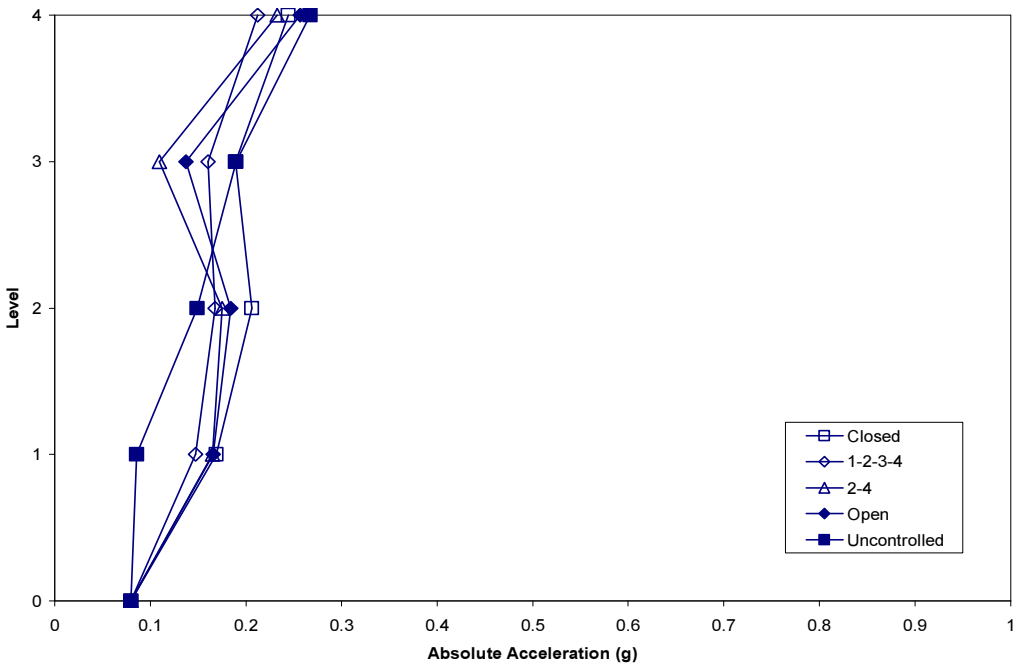

(b) Maximum absolute accelerations

Figure D.3.2 Maximum response envelopes for Sylmar 10% earthquake.

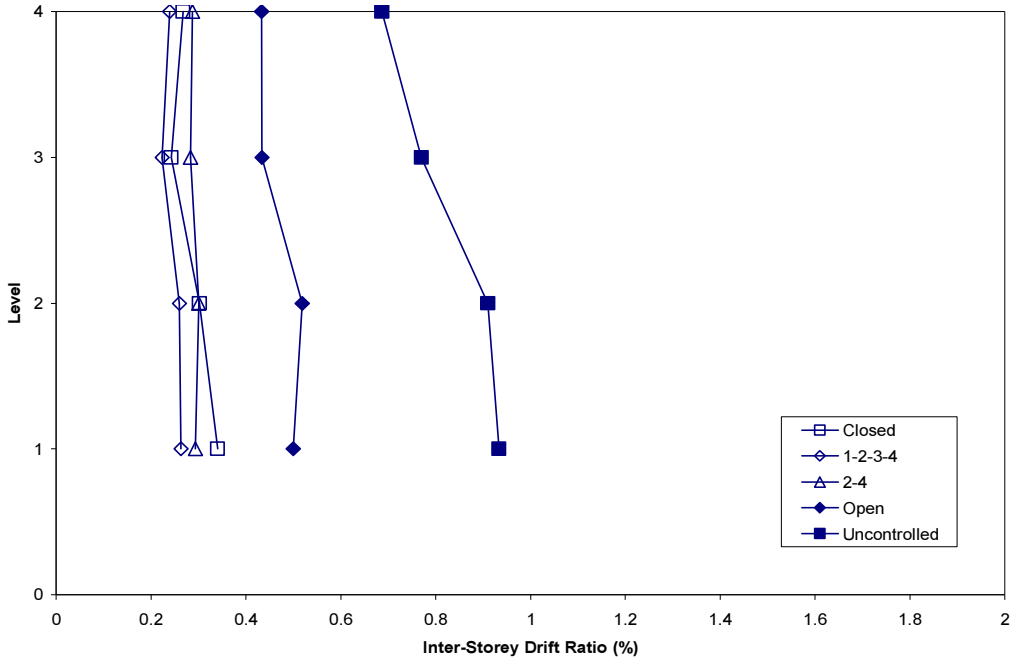

(c) Maximum inter-storey drift ratios

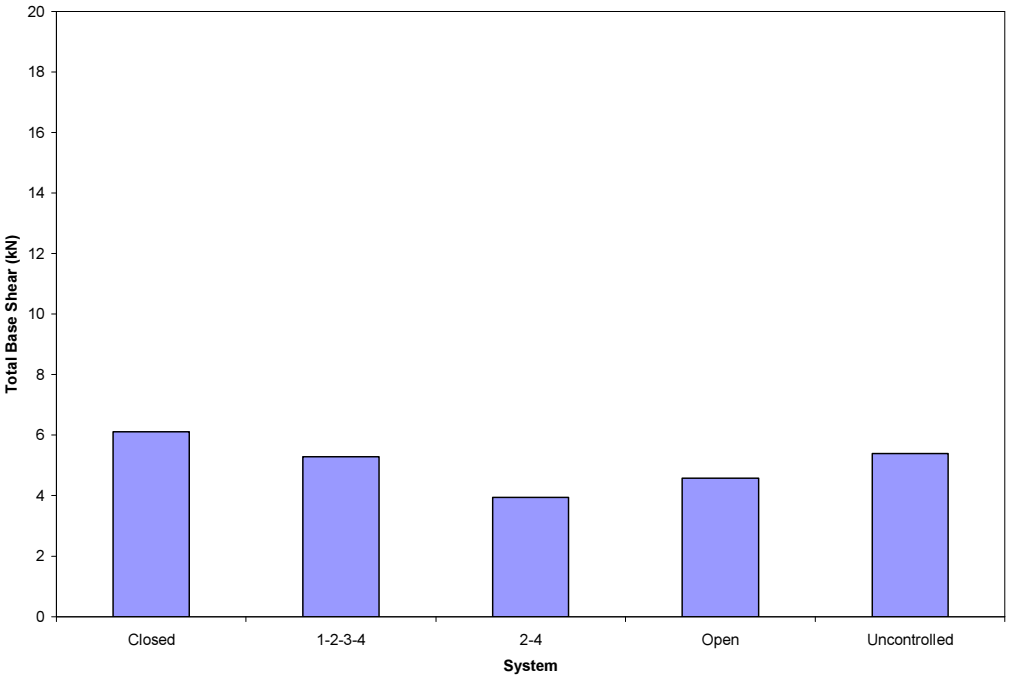

(d) Maximum total base shear

Figure D.3.2 (Continued).

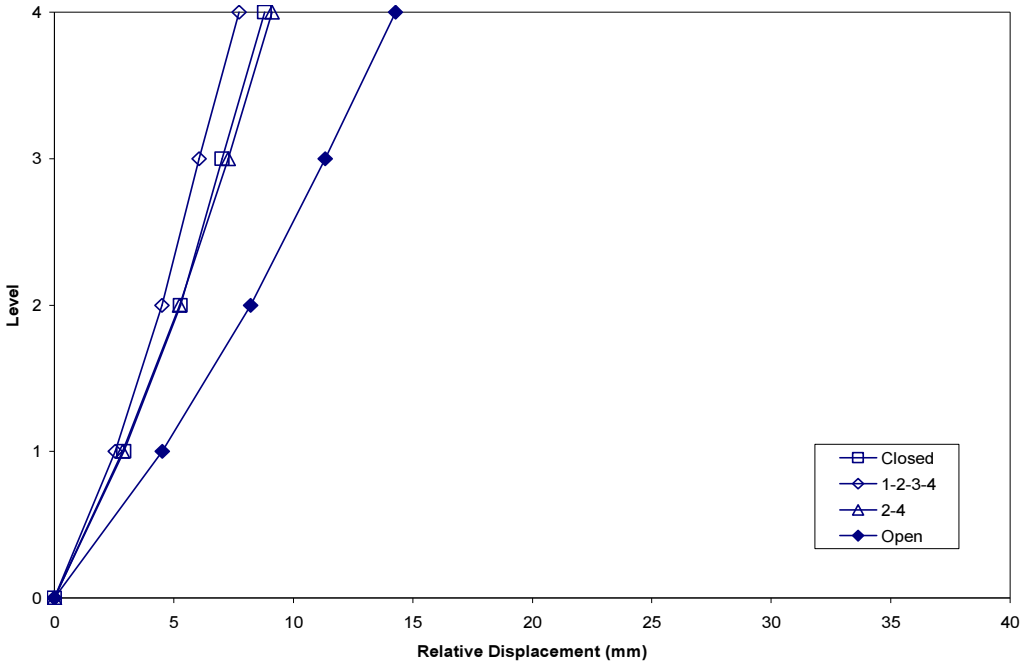

(a) Maximum relative displacements

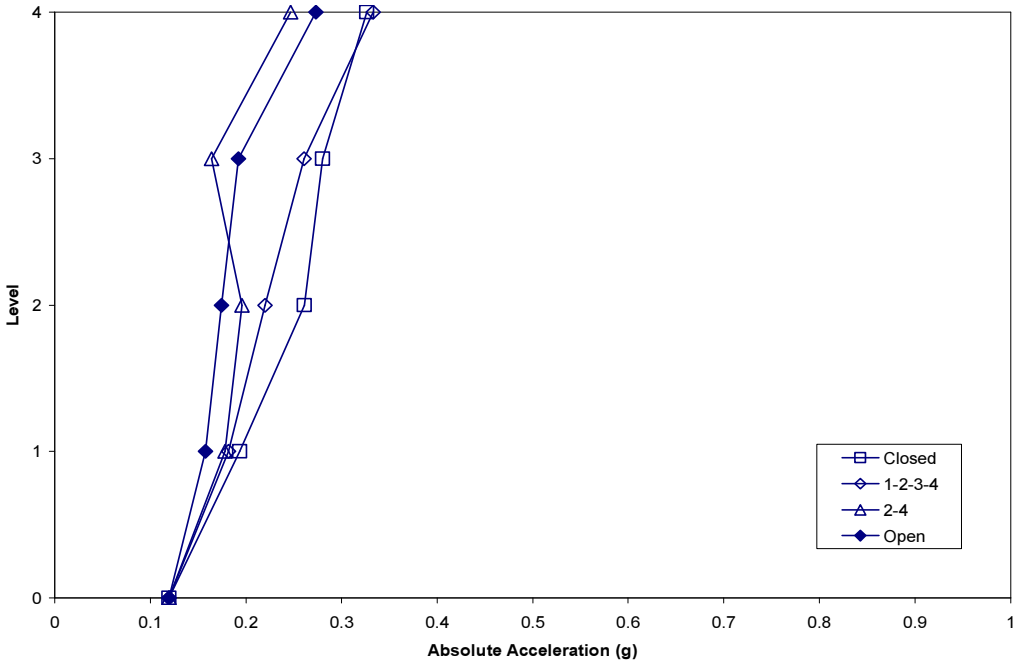

(b) Maximum absolute accelerations

Figure D.3.3 Maximum response envelopes for Sylmar 15% earthquake.

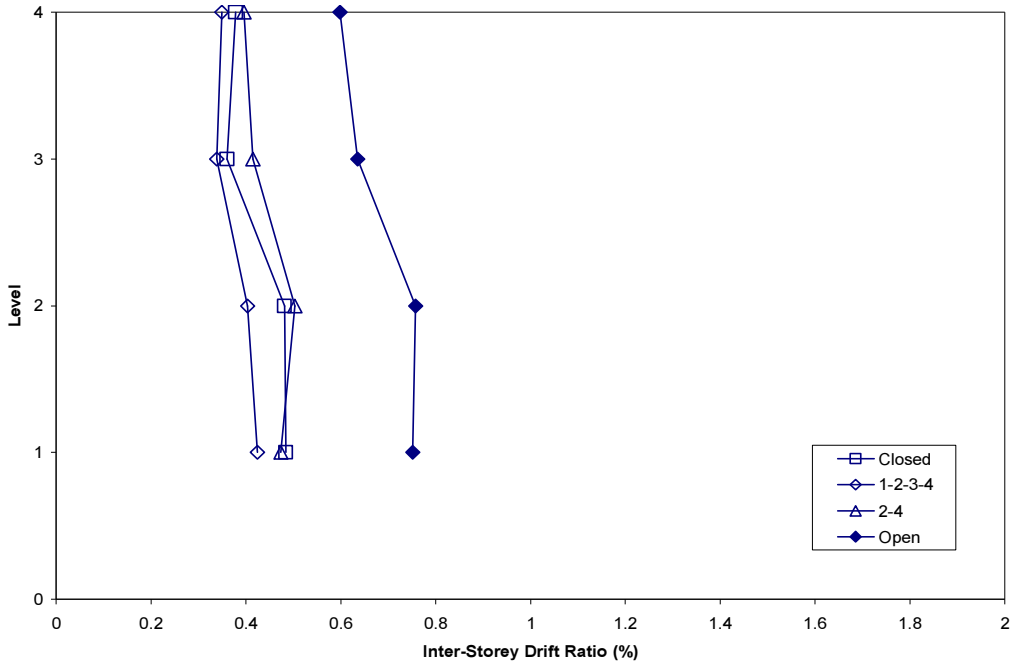

(c) Maximum inter-storey drift ratios

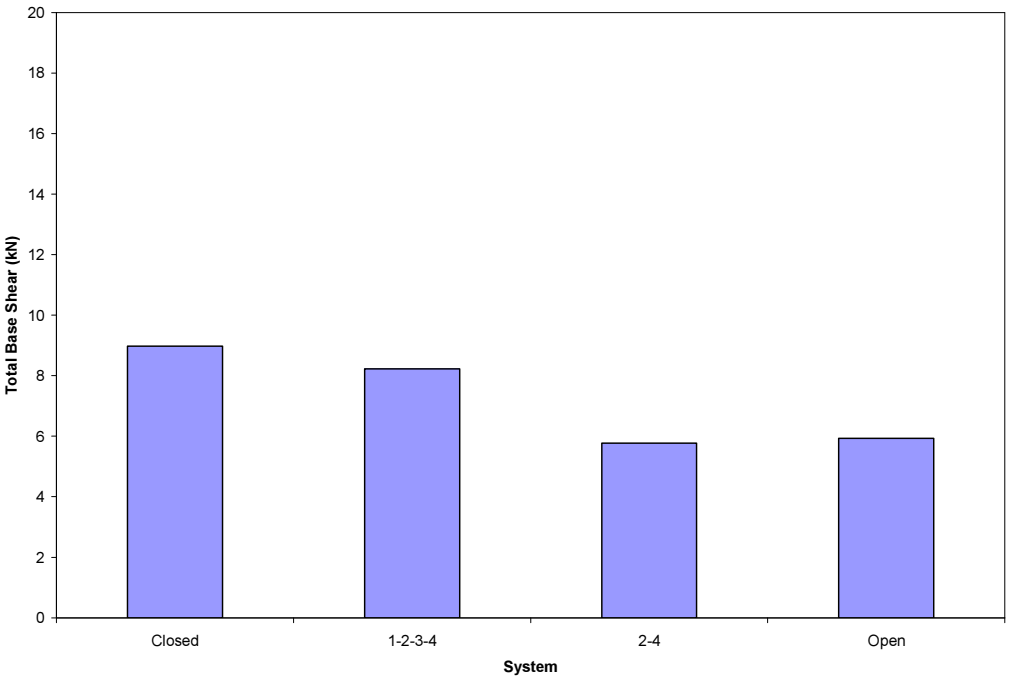

(d) Maximum total base shear

Figure D.3.3 (Continued).

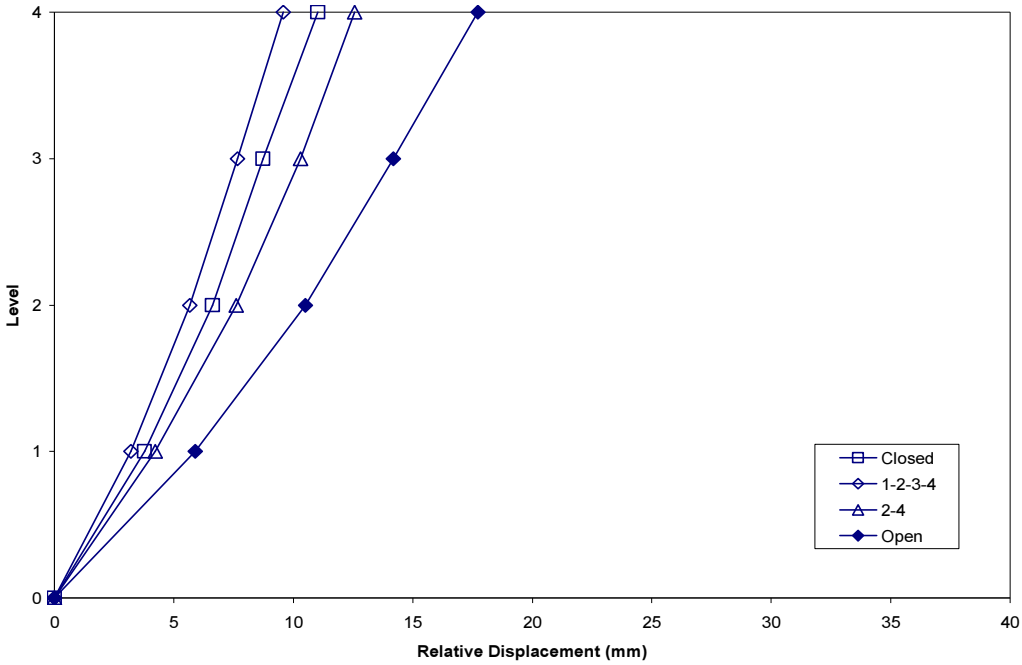

(a) Maximum relative displacements

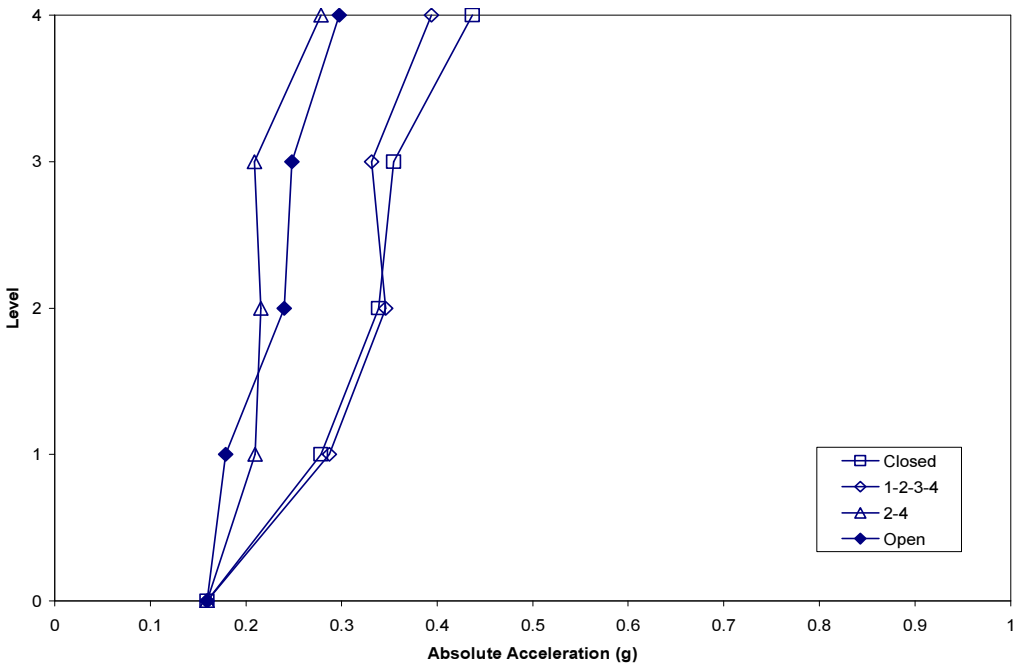

(b) Maximum absolute accelerations

Figure D.3.4 Maximum response envelopes for Sylmar 20% earthquake.

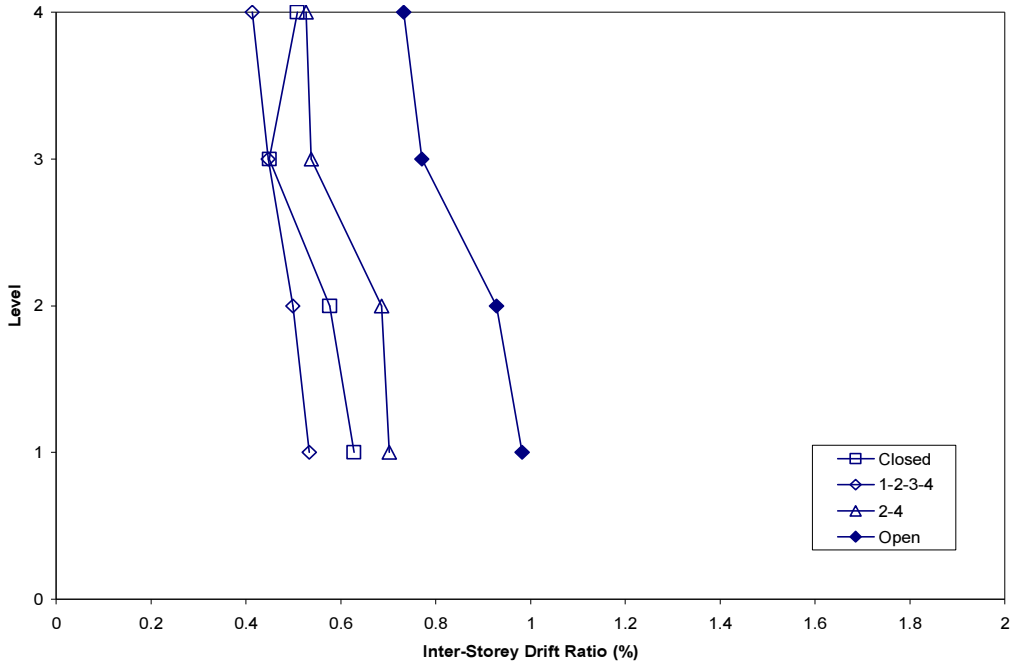

(c) Maximum inter-storey drift ratios

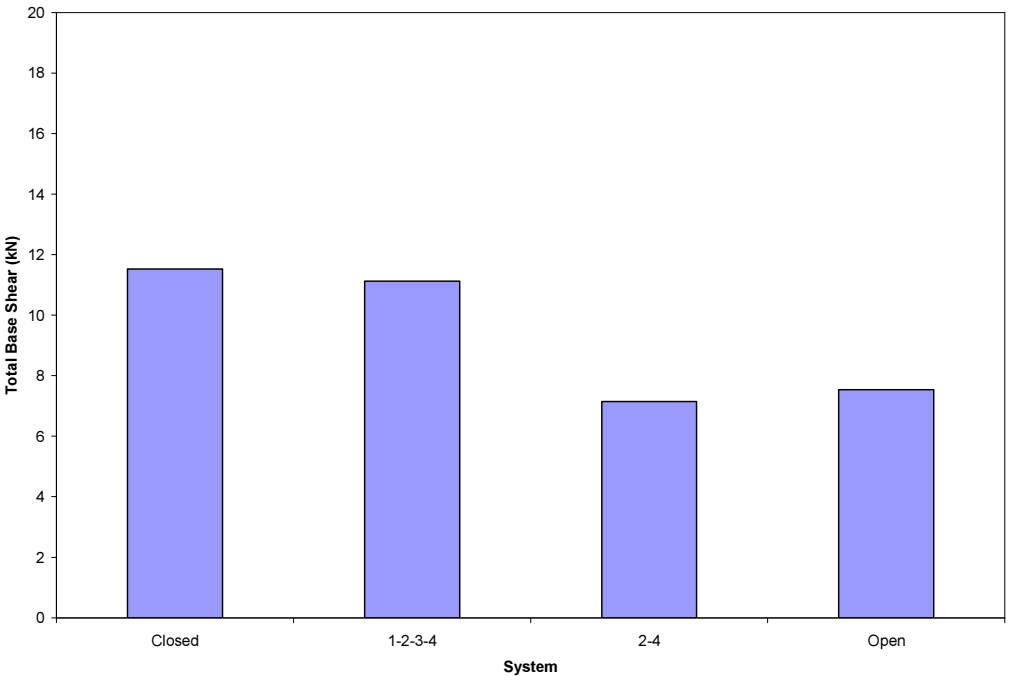

(d) Maximum total base shear

Figure D.3.4 (Continued).

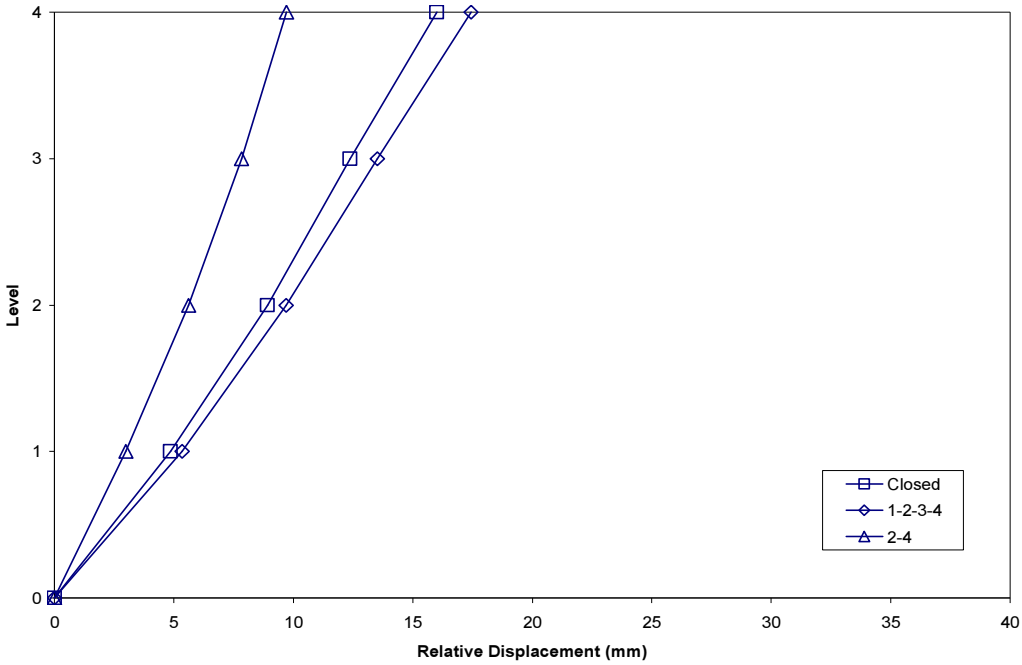

(a) Maximum relative displacements

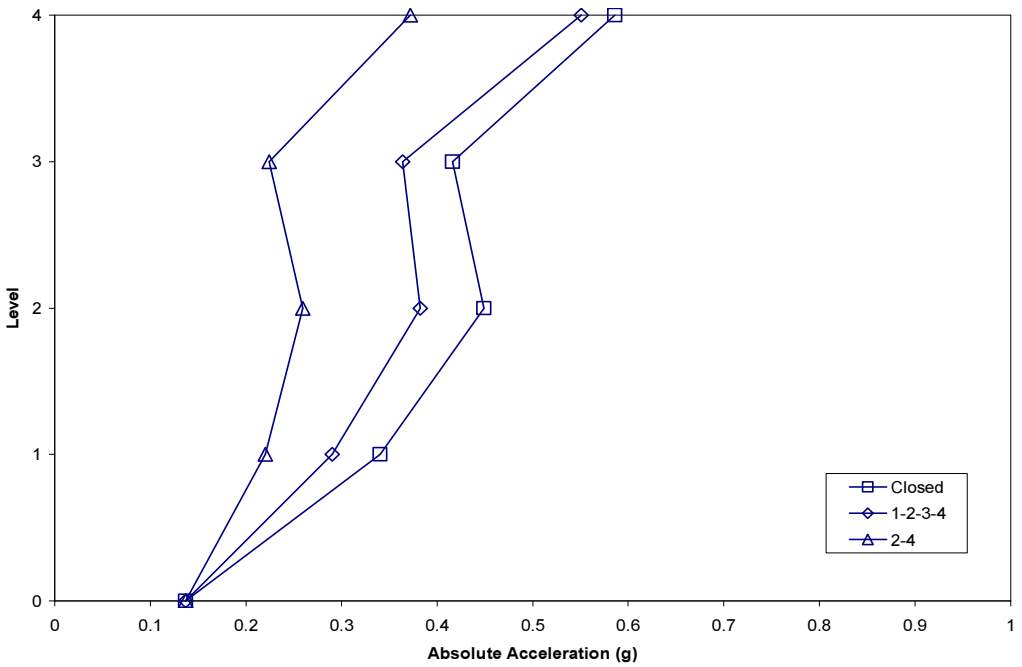

(b) Maximum absolute accelerations

Figure D.3.5 Maximum response envelopes for Sylmar 25% Modified earthquake.

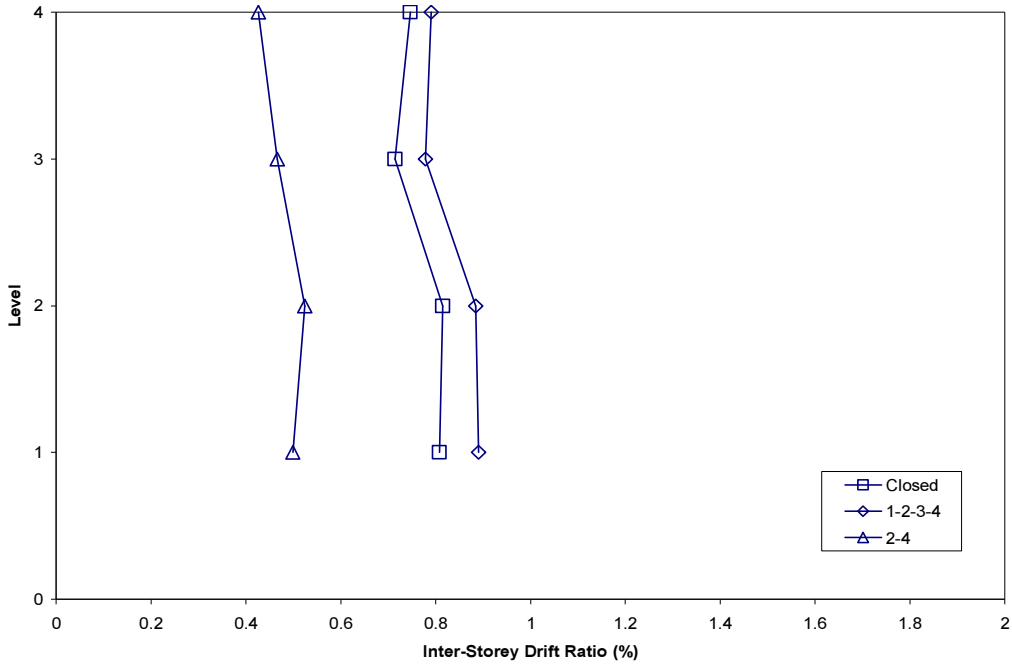

(c) Maximum inter-storey drift ratios

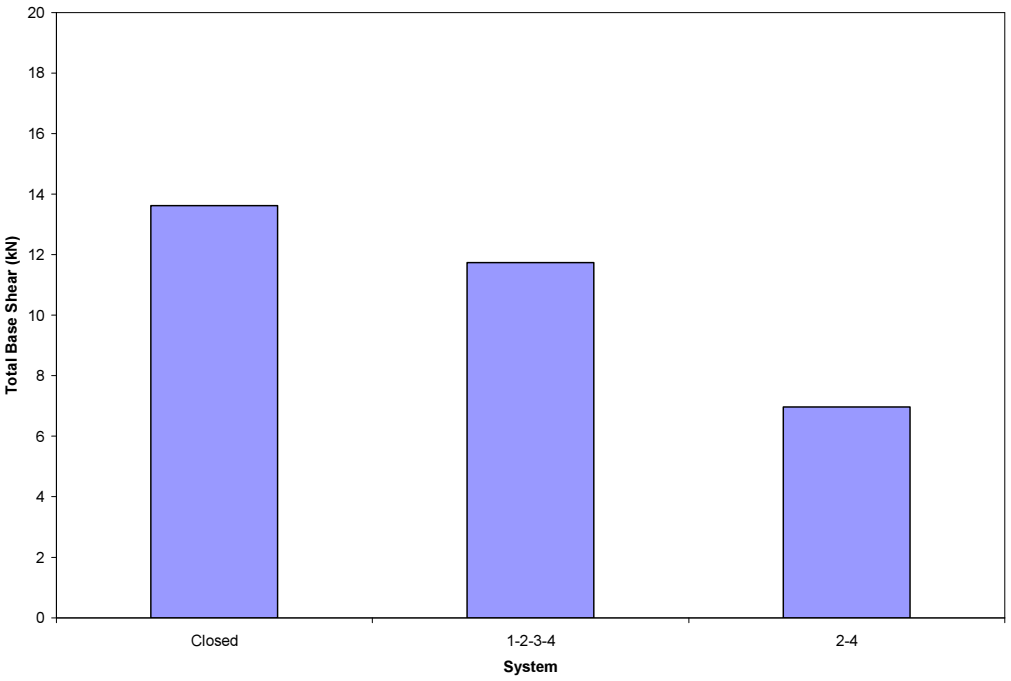

(d) Maximum total base shear

Figure D.3.5 (Continued).

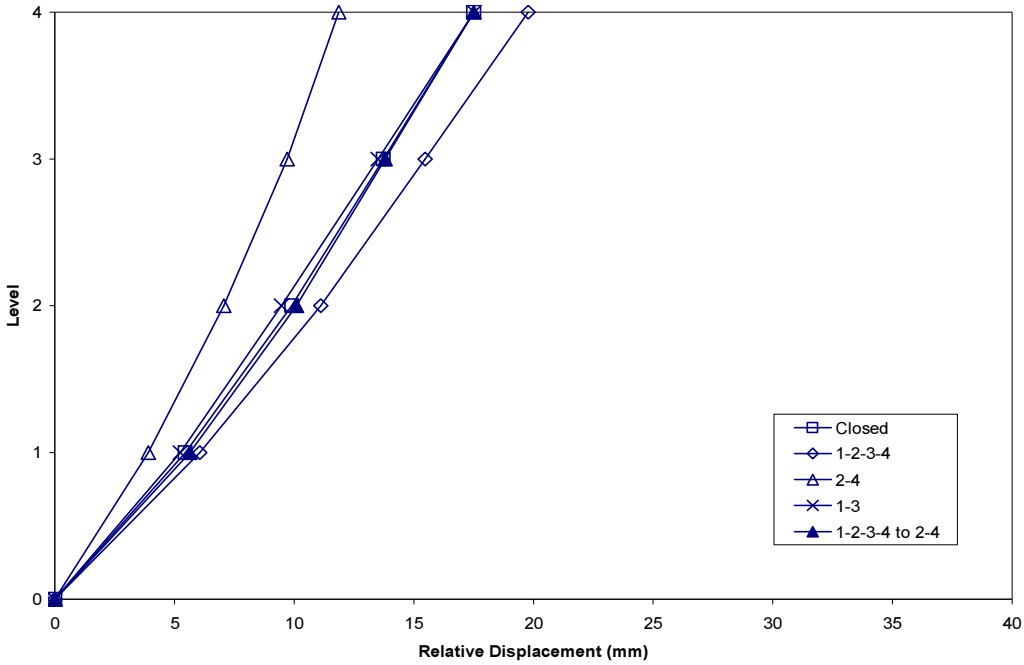

(a) Maximum relative displacements

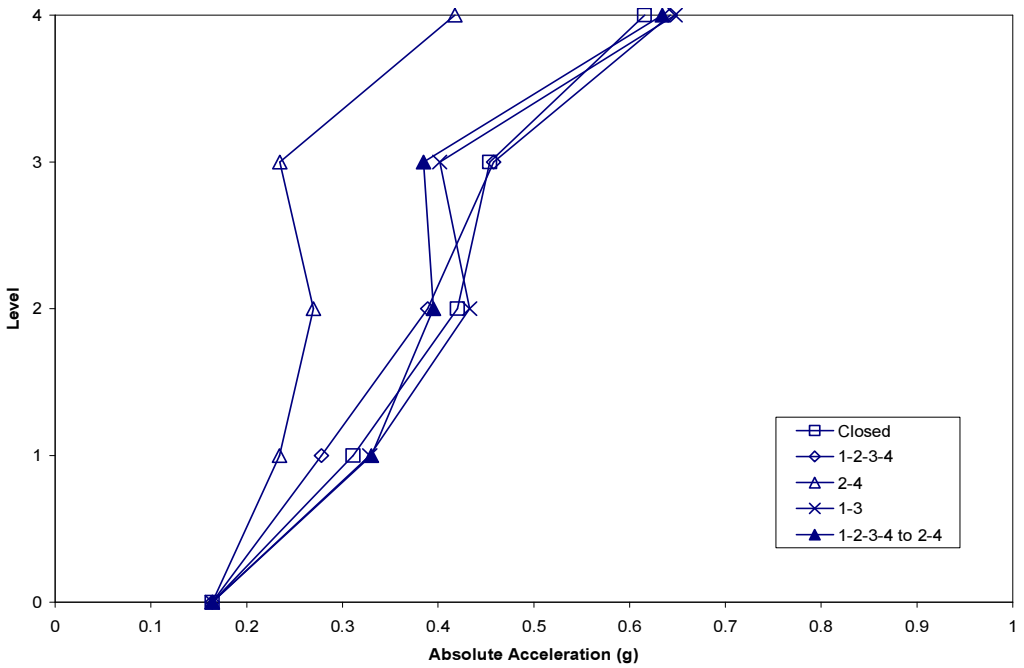

(b) Maximum absolute accelerations

Figure D.3.6 Maximum response envelopes for Sylmar 30% Modified earthquake.

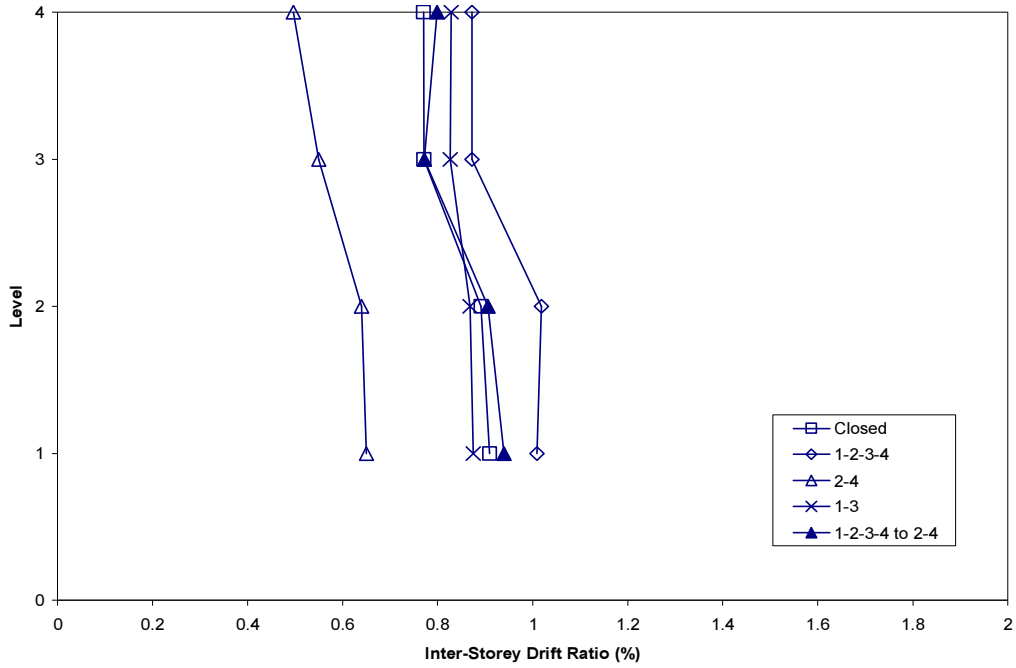

(c) Maximum inter-storey drift ratios

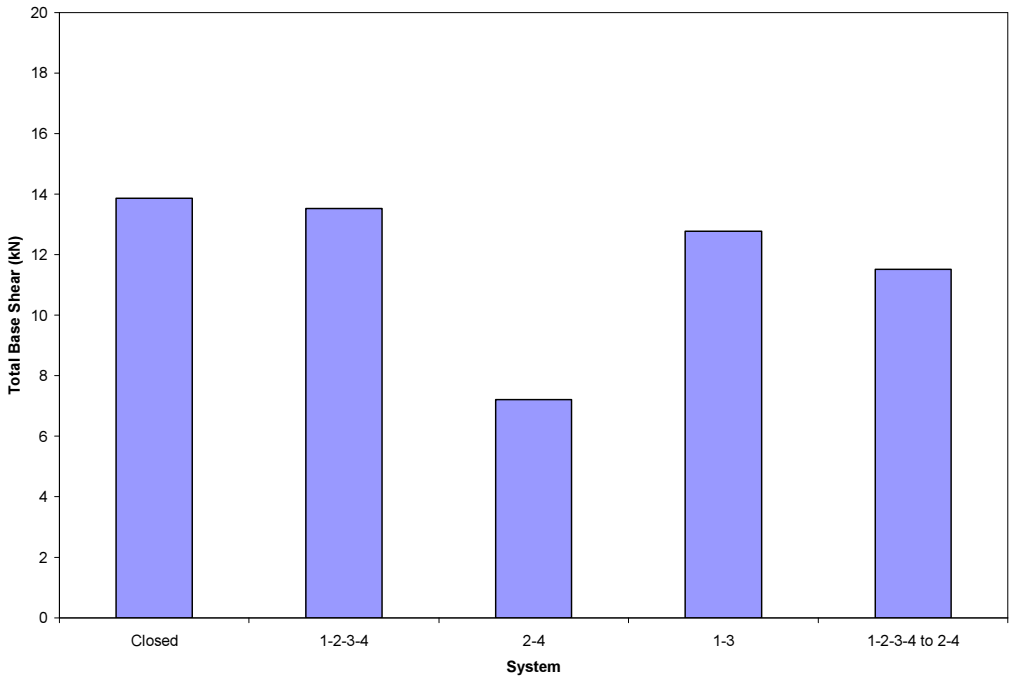

(d) Maximum total base shear

Figure D.3.6 (Continued).

D.4 MAXIMUM RESPONSE ENVELOPES FOR KOBE EARTHQUAKE

Maximum response envelopes are presented for the following scaled earthquake records with corresponding peak ground accelerations:

1. Kobe 5% (0.0418g)
2. Kobe 10% (0.0836g)
3. Kobe 15% (0.1255g)
4. Kobe 20% (0.1673g)
5. Kobe 25% (0.2091g)
6. Kobe 30% Modified (0.1583g)
7. Kobe 35% Modified (0.1847g).

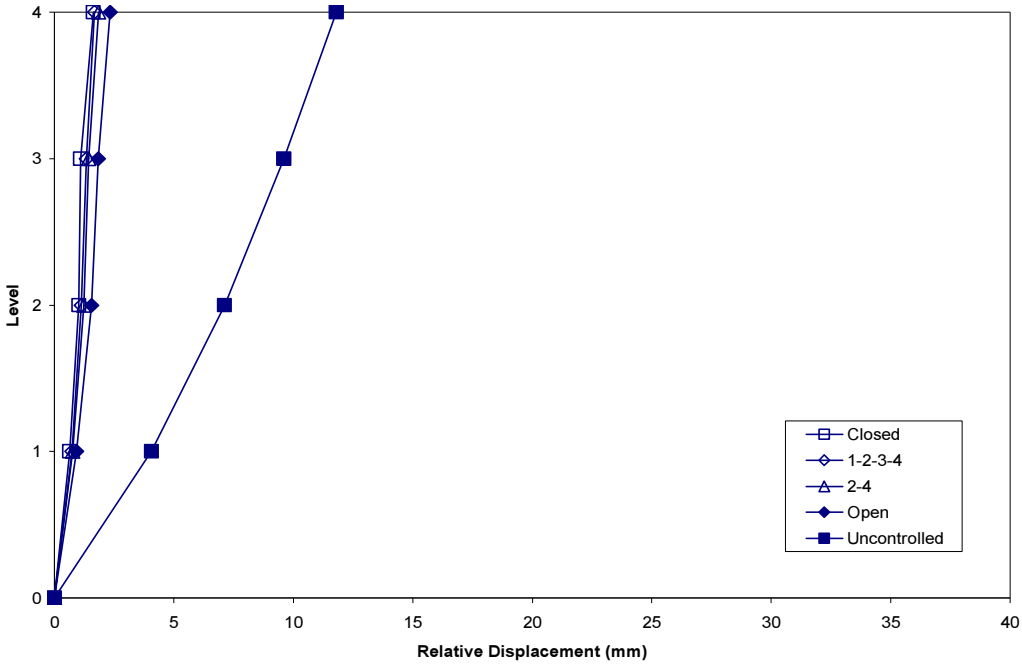

(a) Maximum relative displacements

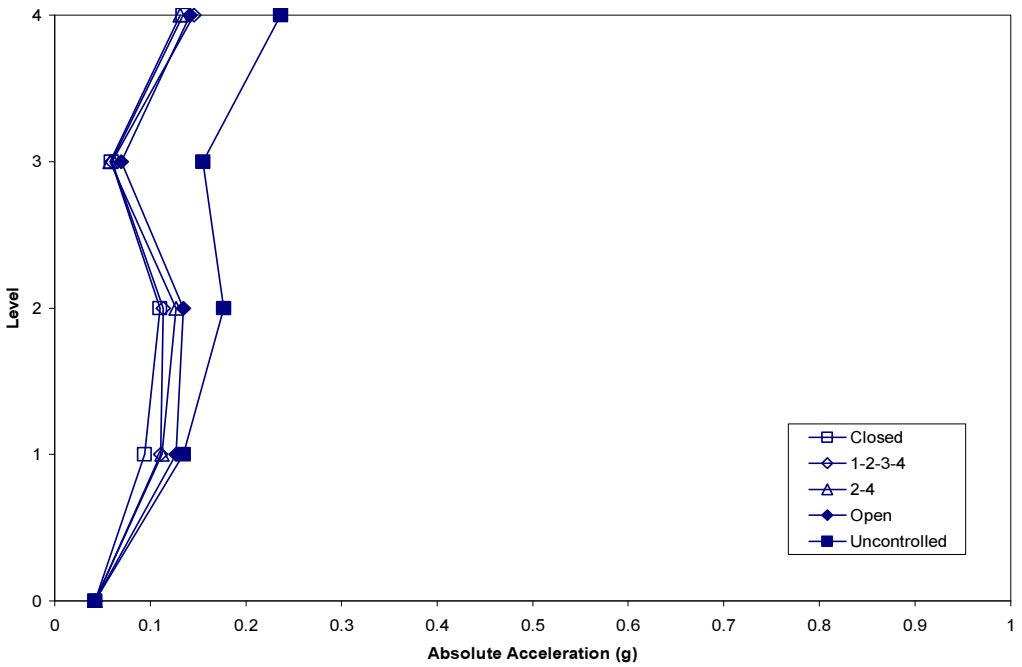

(b) Maximum absolute accelerations

Figure D.4.1 Maximum response envelopes for Kobe 5% earthquake.

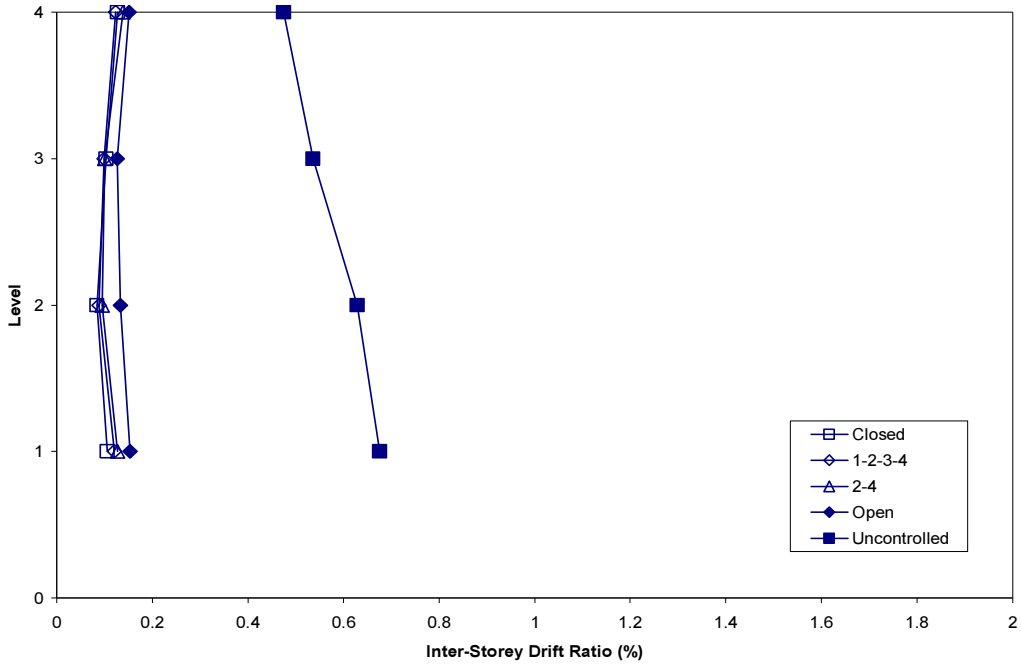

(c) Maximum inter-storey drift ratios

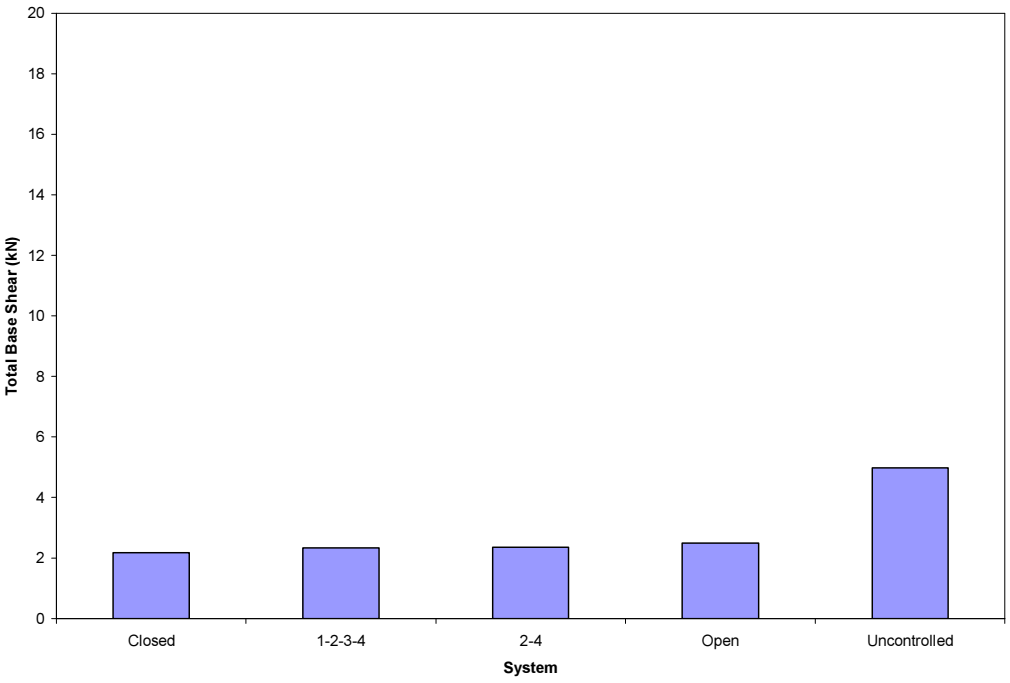

(d) Maximum total base shear

Figure D.4.1 (Continued).

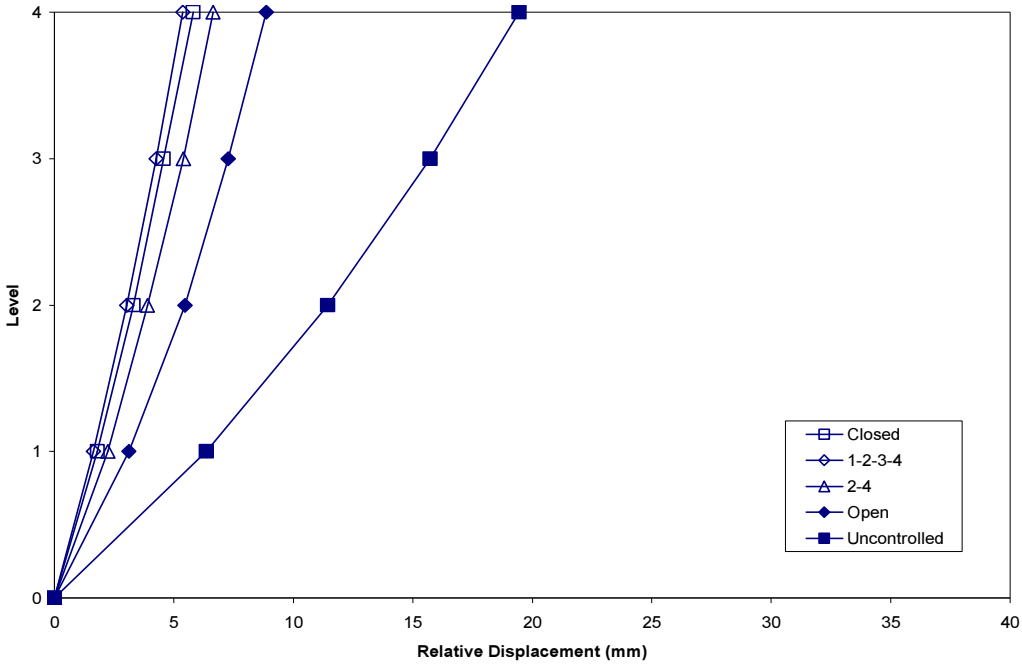

(a) Maximum relative displacements

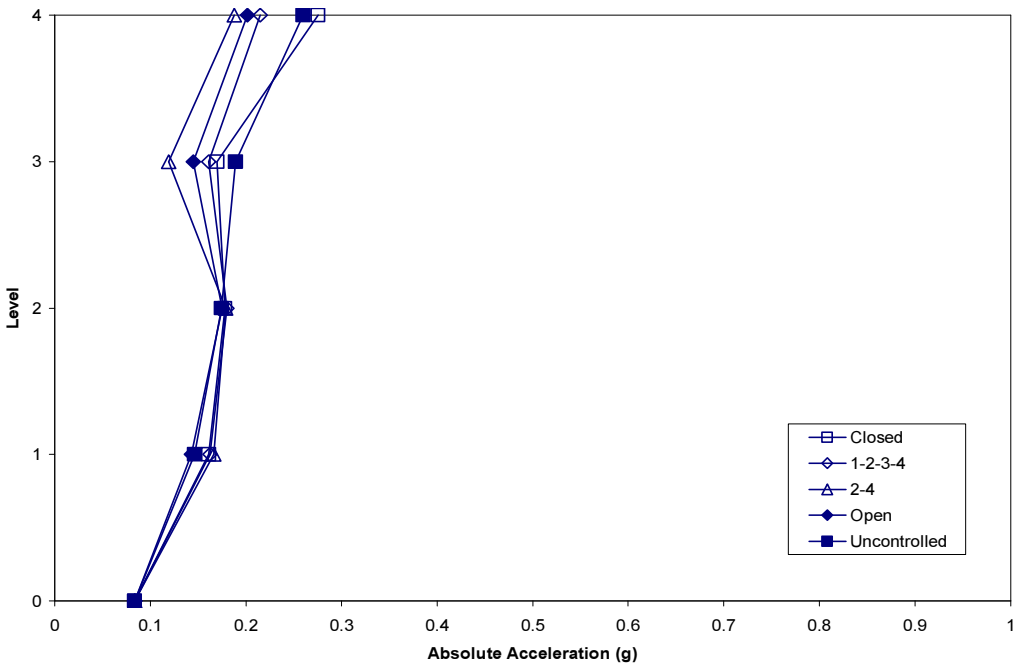

(b) Maximum absolute accelerations

Figure D.4.2 Maximum response envelopes for Kobe 10% earthquake.

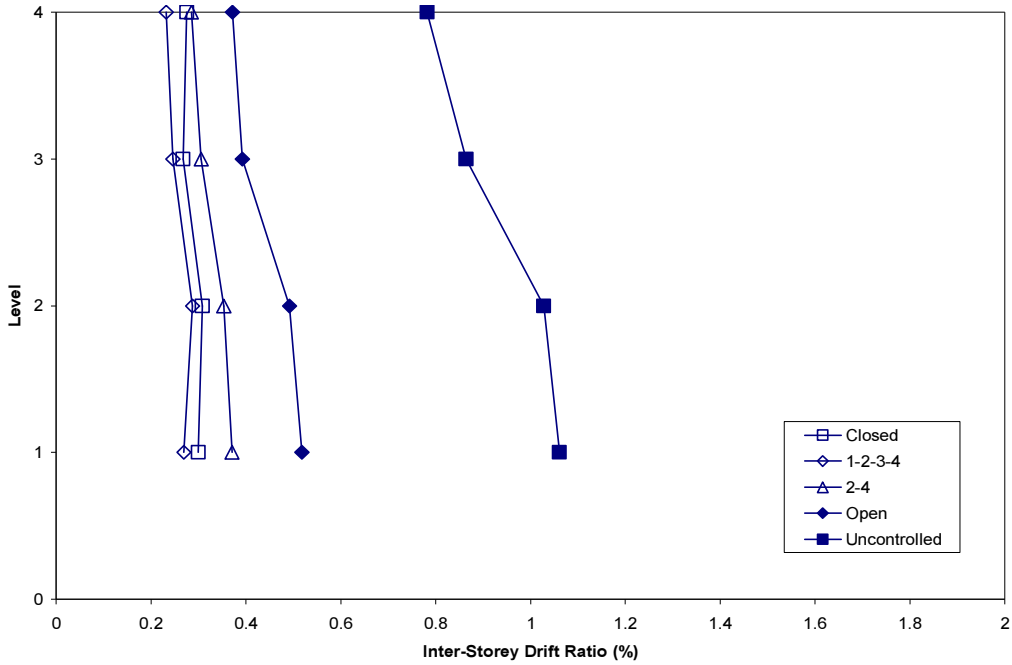

(c) Maximum inter-storey drift ratios

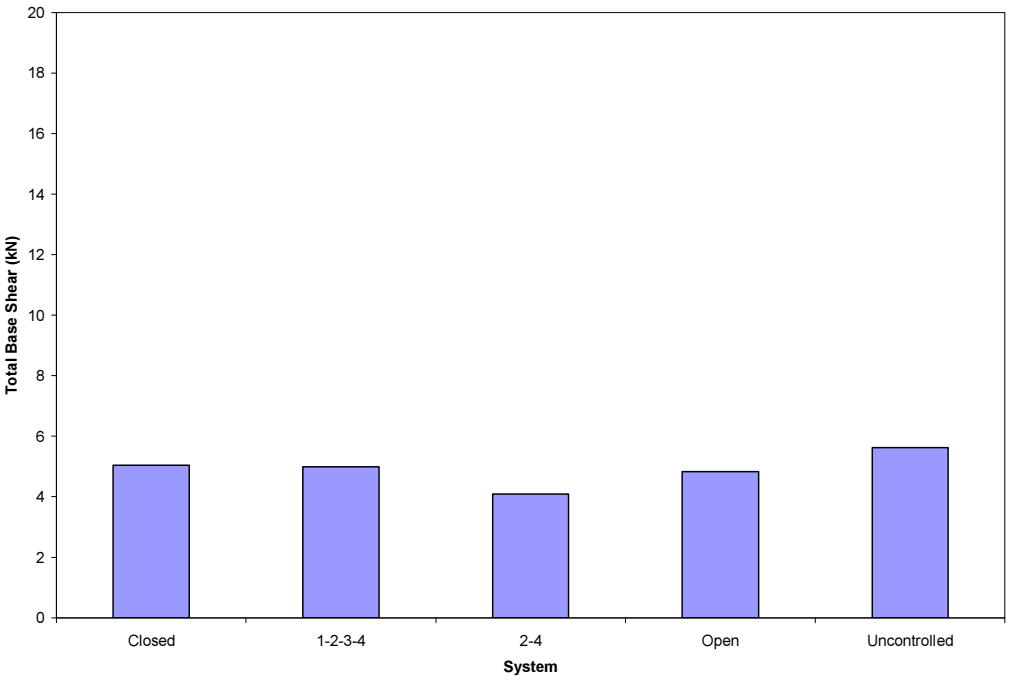

(d) Maximum total base shear

Figure D.4.2 (Continued).

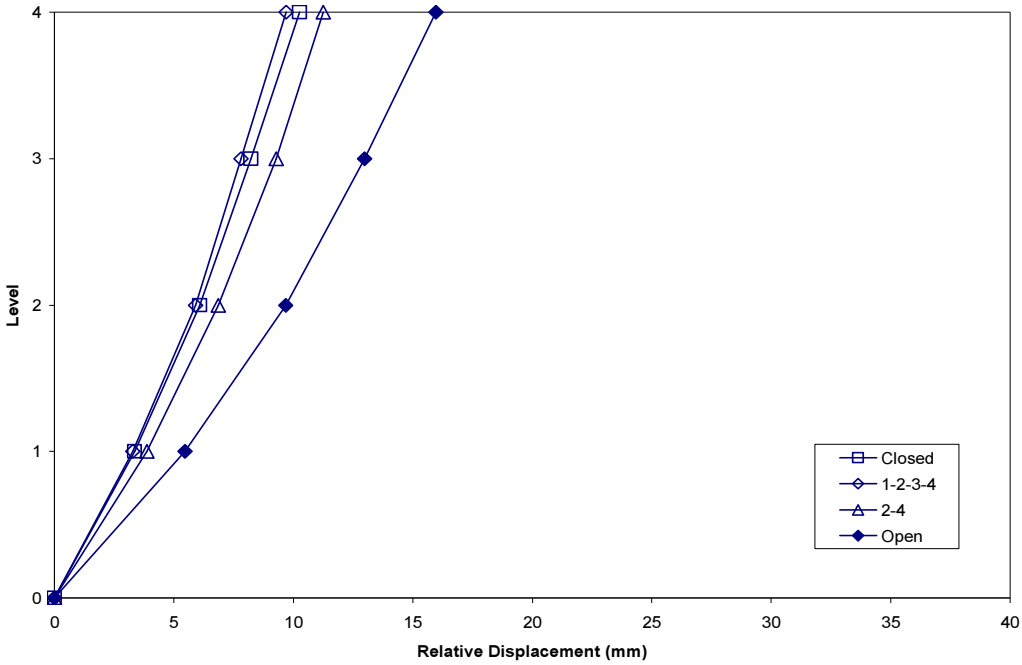

(a) Maximum relative displacements

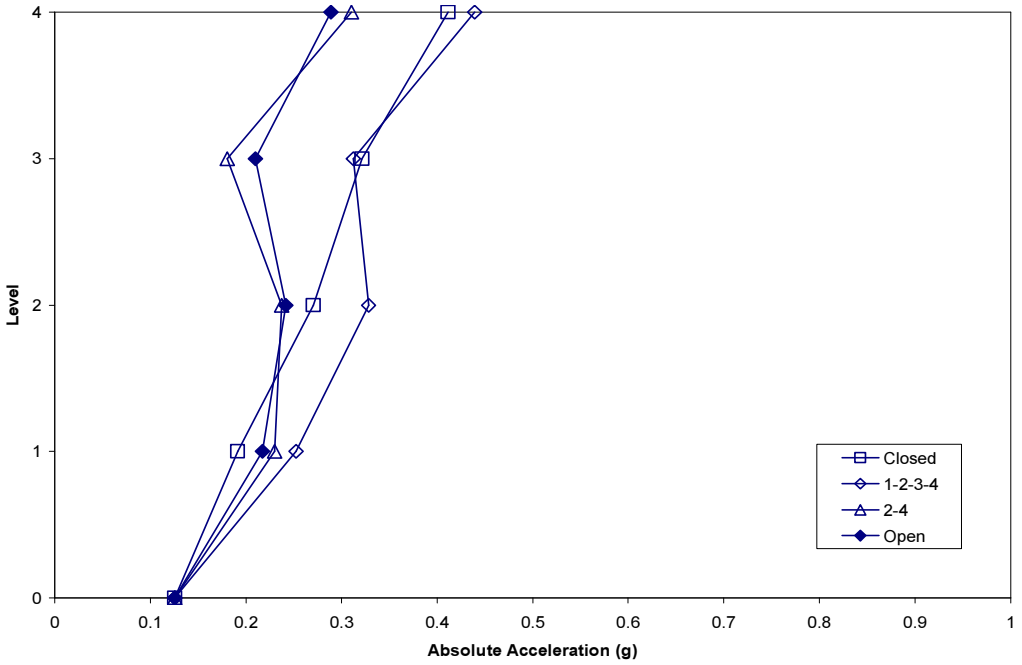

(b) Maximum absolute accelerations

Figure D.4.3 Maximum response envelopes for Kobe 15% earthquake.

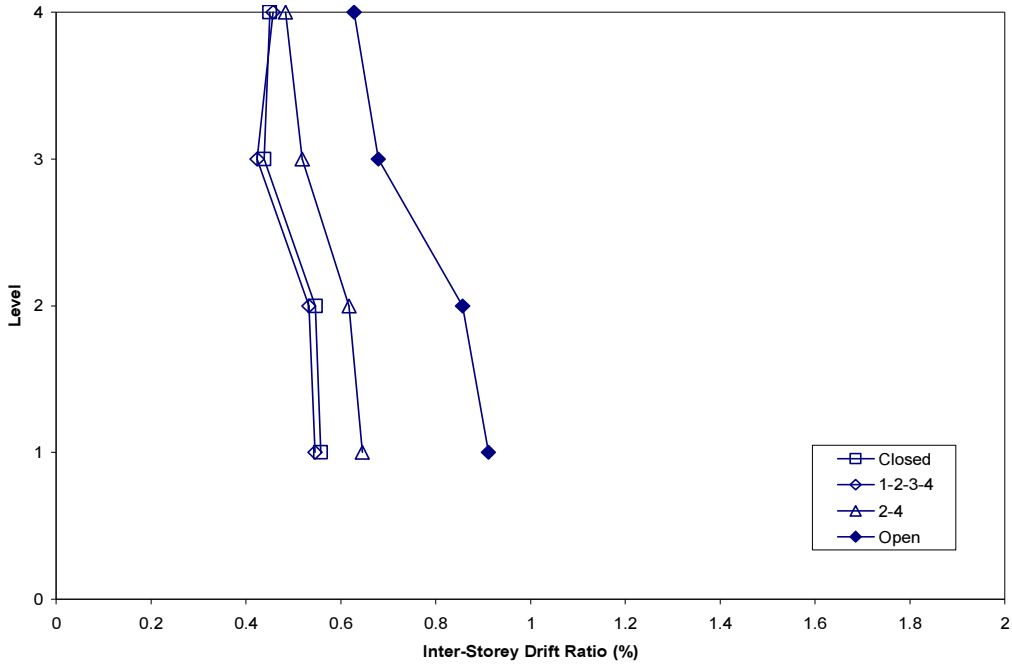

(c) Maximum inter-storey drift ratios

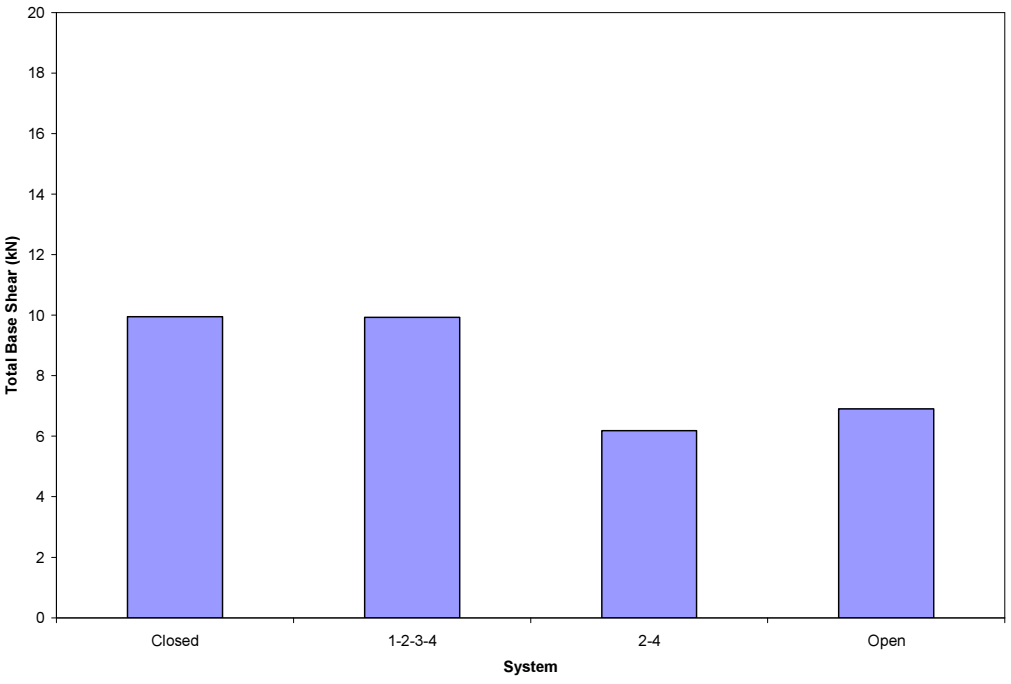

(d) Maximum total base shear

Figure D.4.3 (Continued).

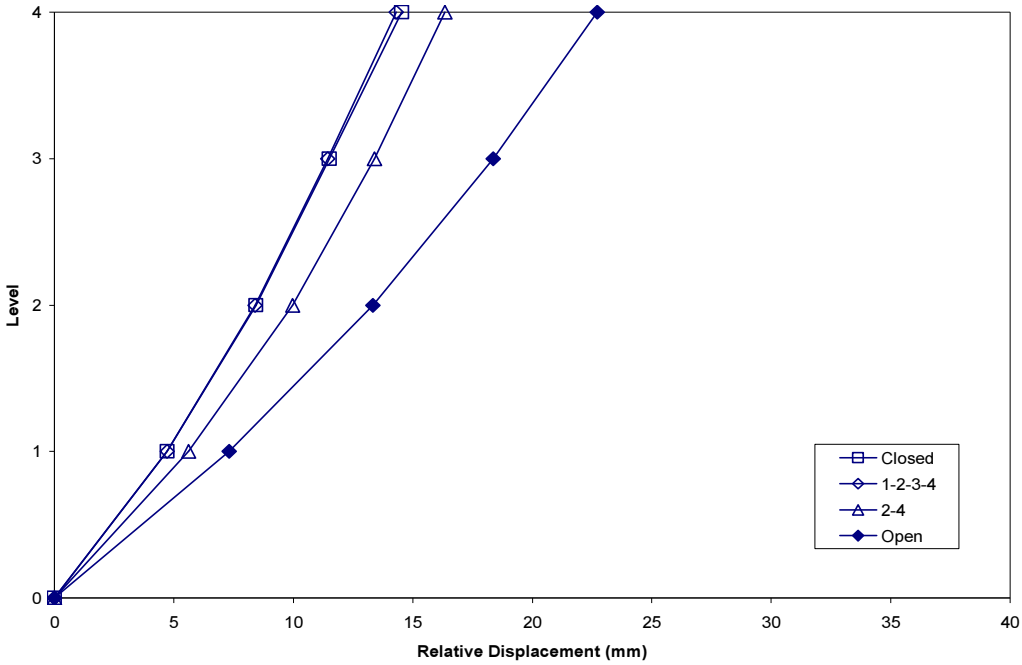

(a) Maximum relative displacements

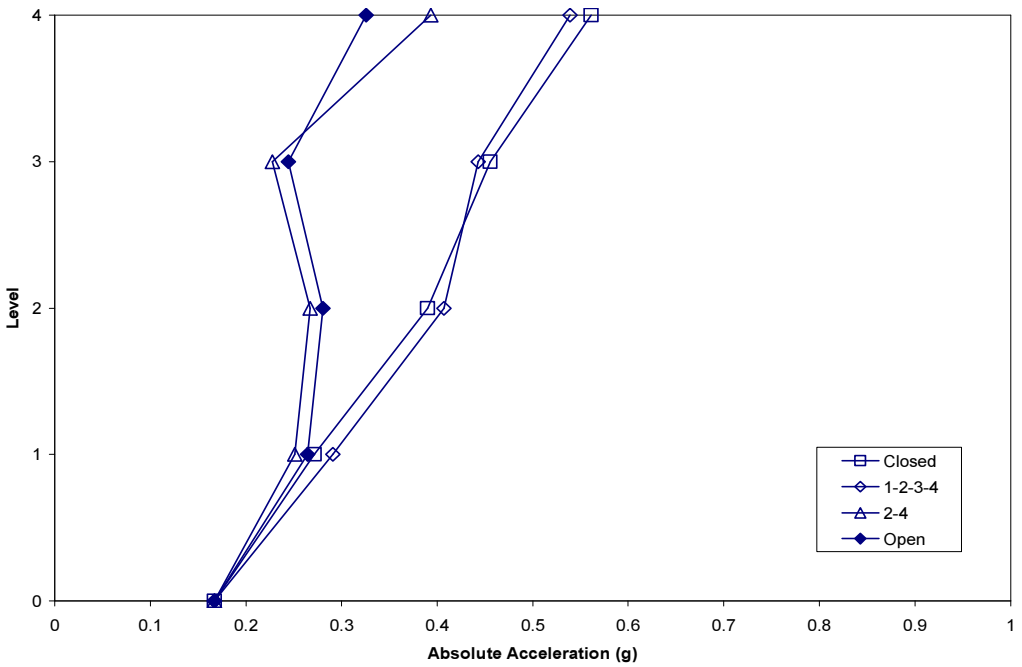

(b) Maximum absolute accelerations

Figure D.4.4 Maximum response envelopes for Kobe 20% earthquake.

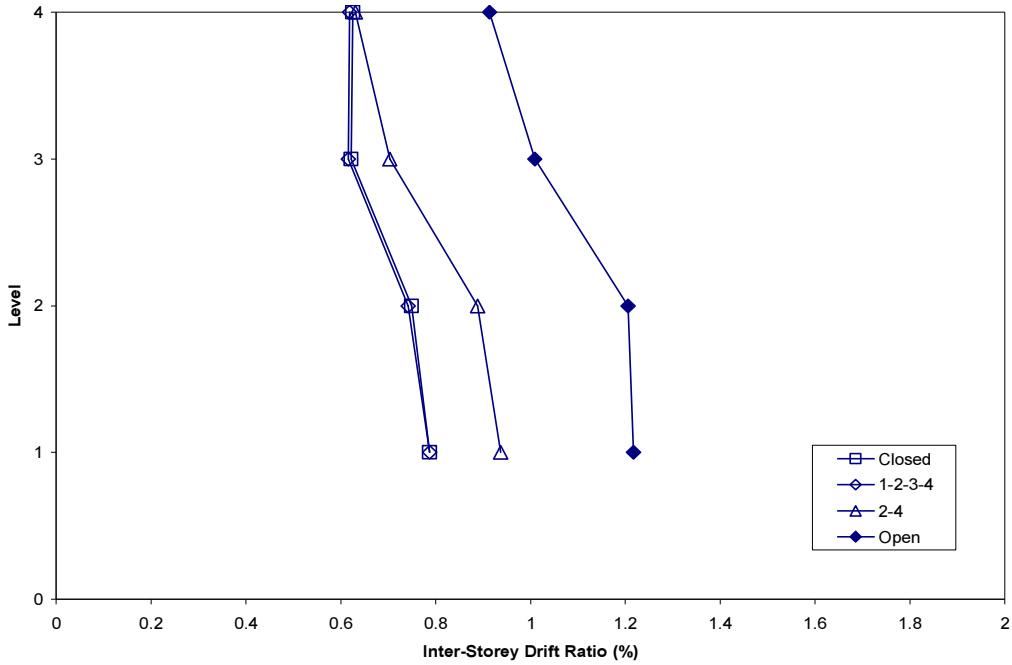

(c) Maximum inter-storey drift ratios

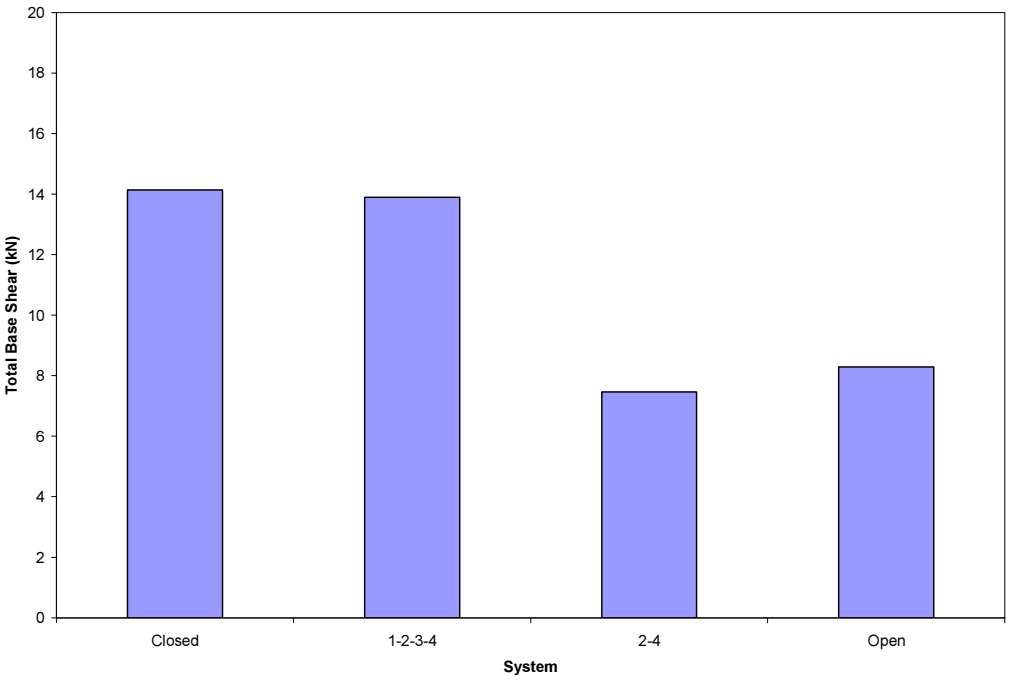

(d) Maximum total base shear

Figure D.4.4 (Continued).

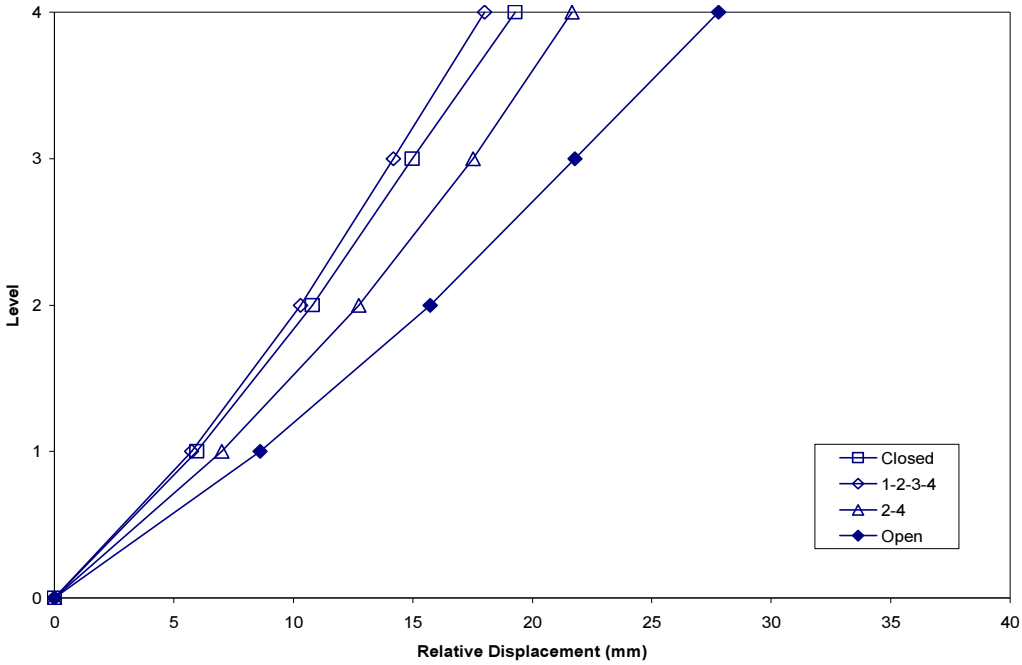

(a) Maximum relative displacements

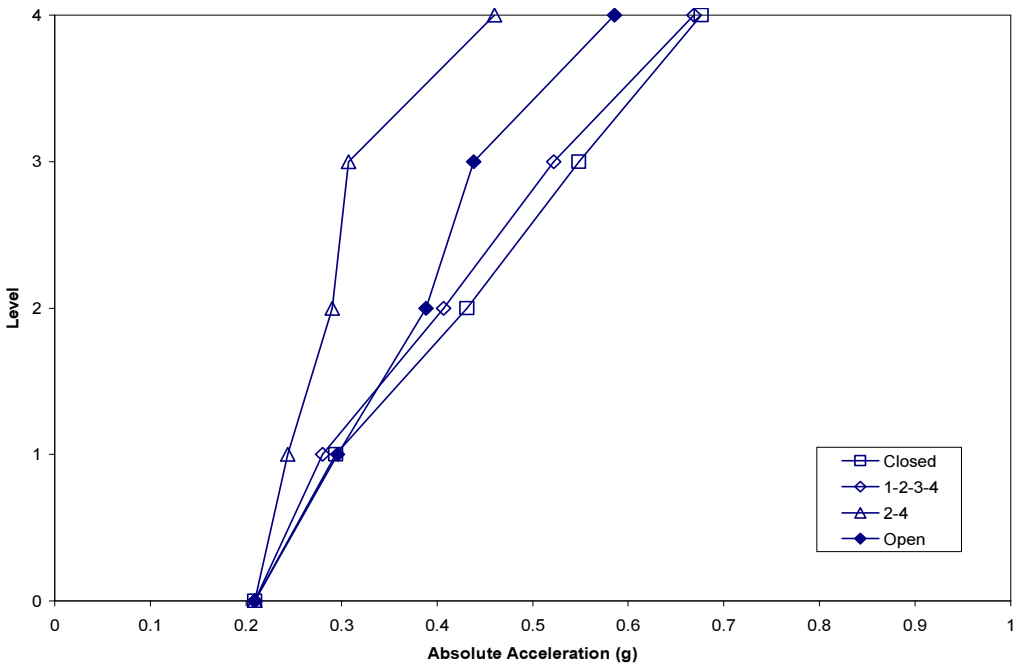

(b) Maximum absolute accelerations

Figure D.4.5 Maximum response envelopes for Kobe 25% earthquake.

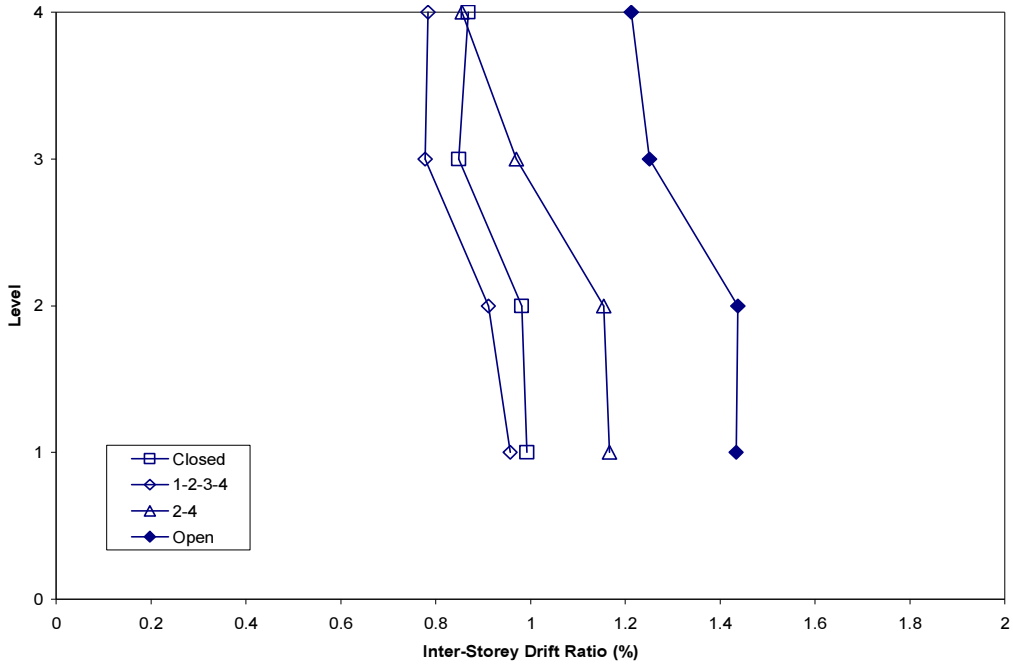

(c) Maximum inter-storey drift ratios

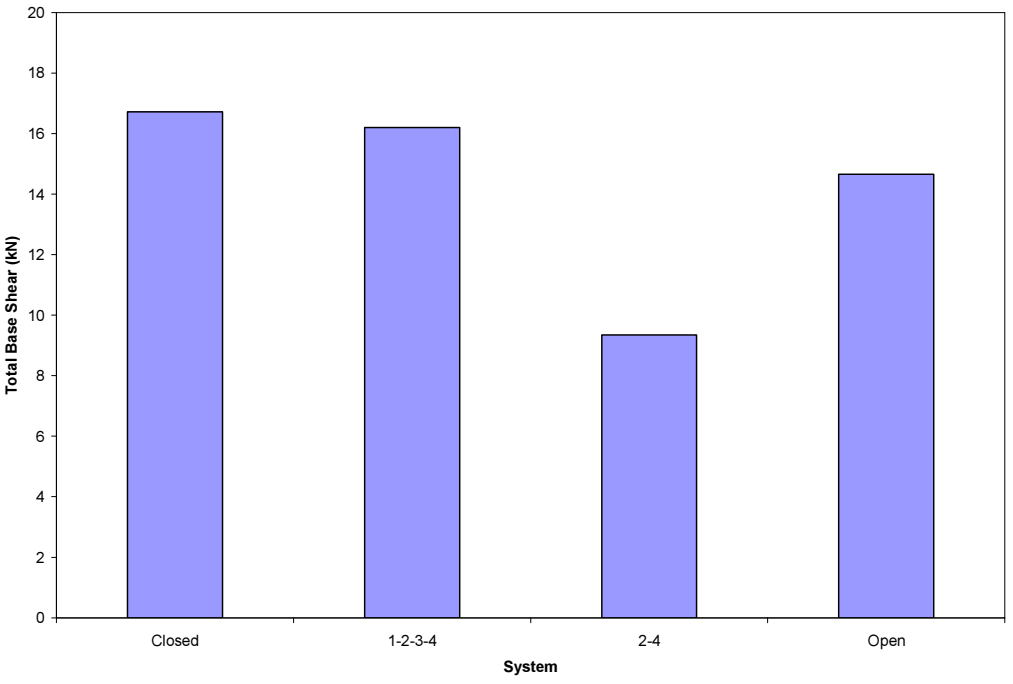

(d) Maximum total base shear

Figure D.4.5 (Continued).

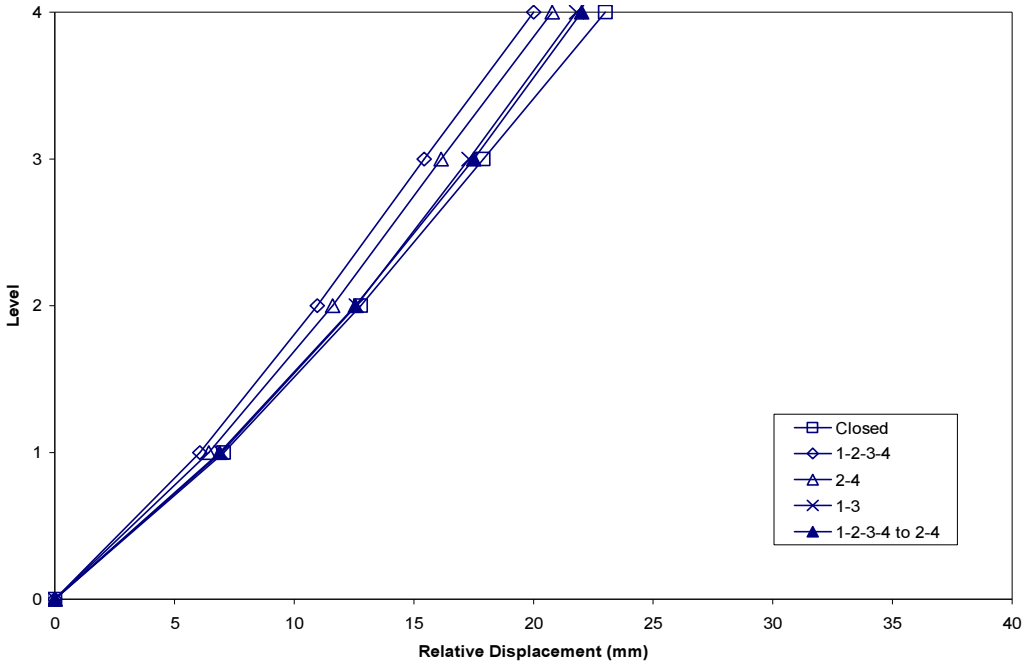

(a) Maximum relative displacements

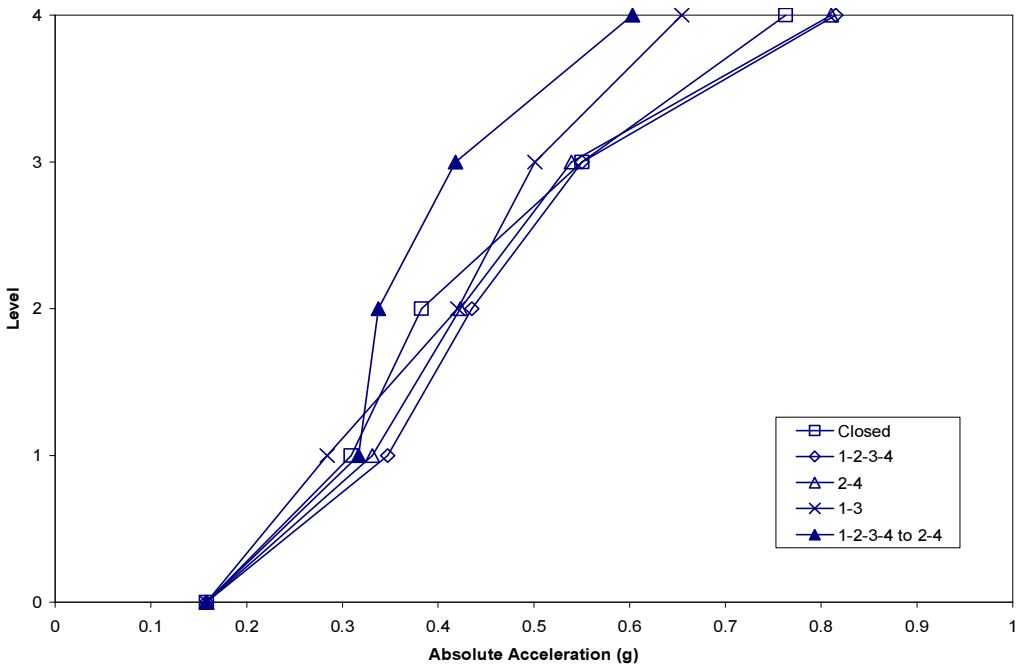

(b) Maximum absolute accelerations

Figure D.4.6 Maximum response envelopes for Kobe 30% Modified earthquake.

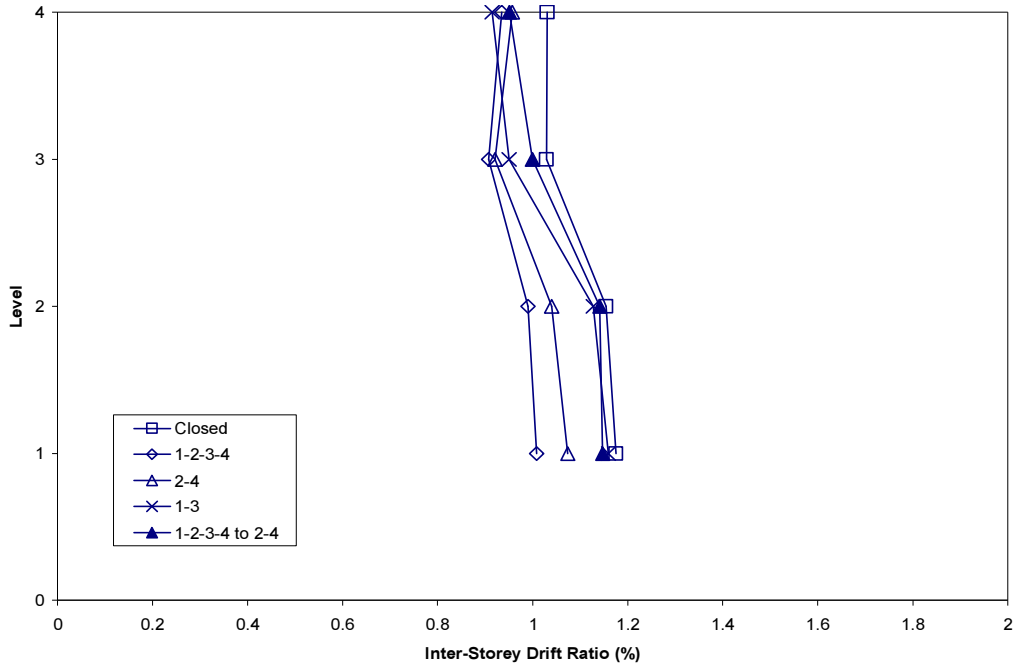

(c) Maximum inter-storey drift ratios

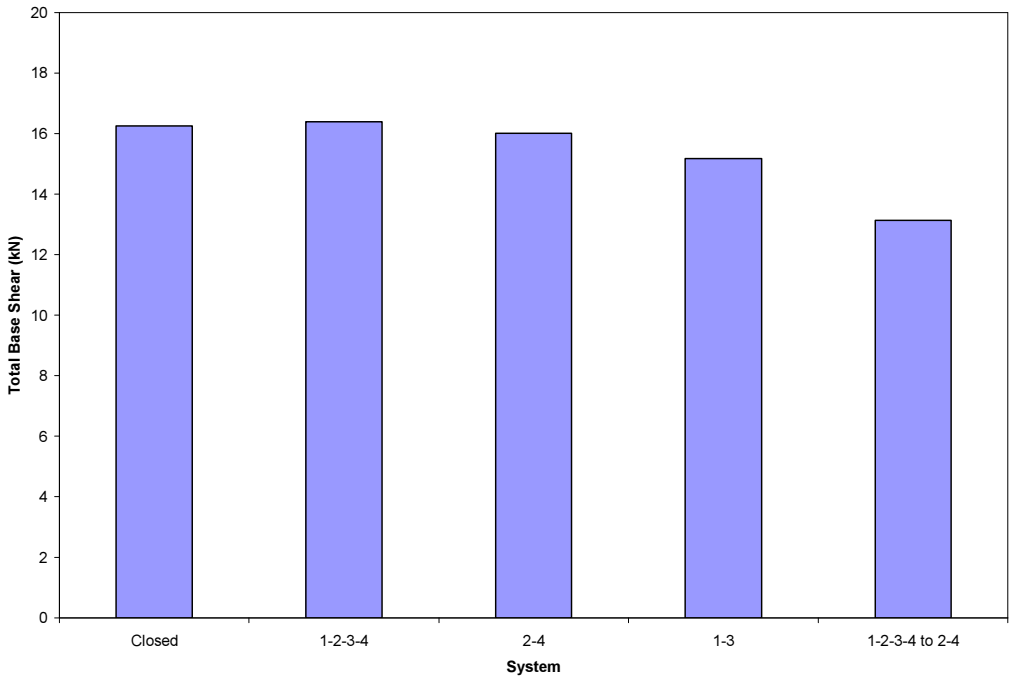

(d) Maximum total base shear

Figure D.4.6 (Continued).

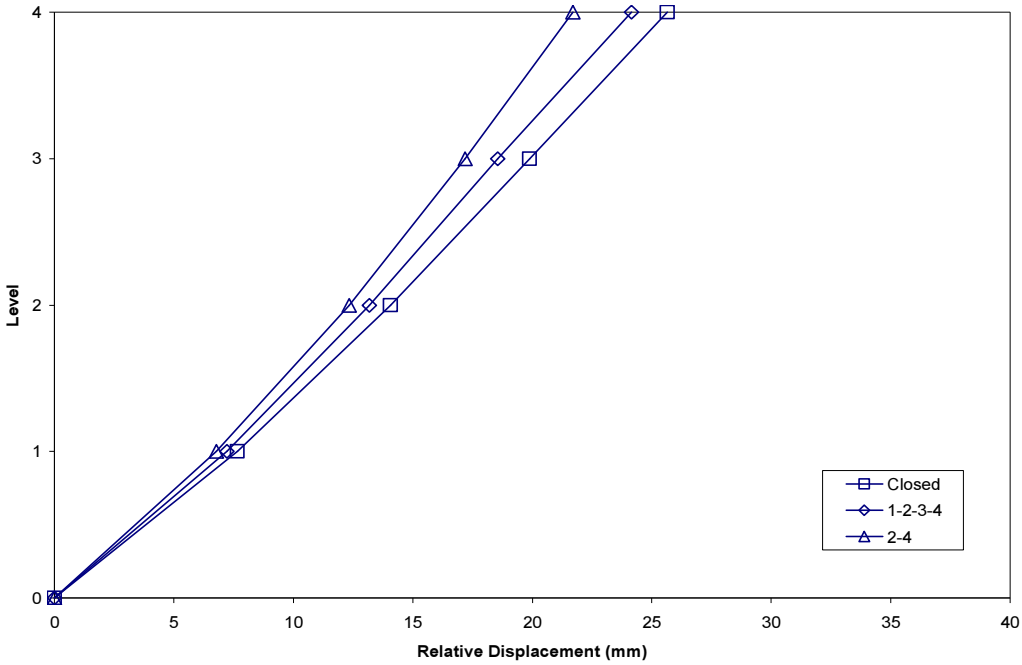

(a) Maximum relative displacements

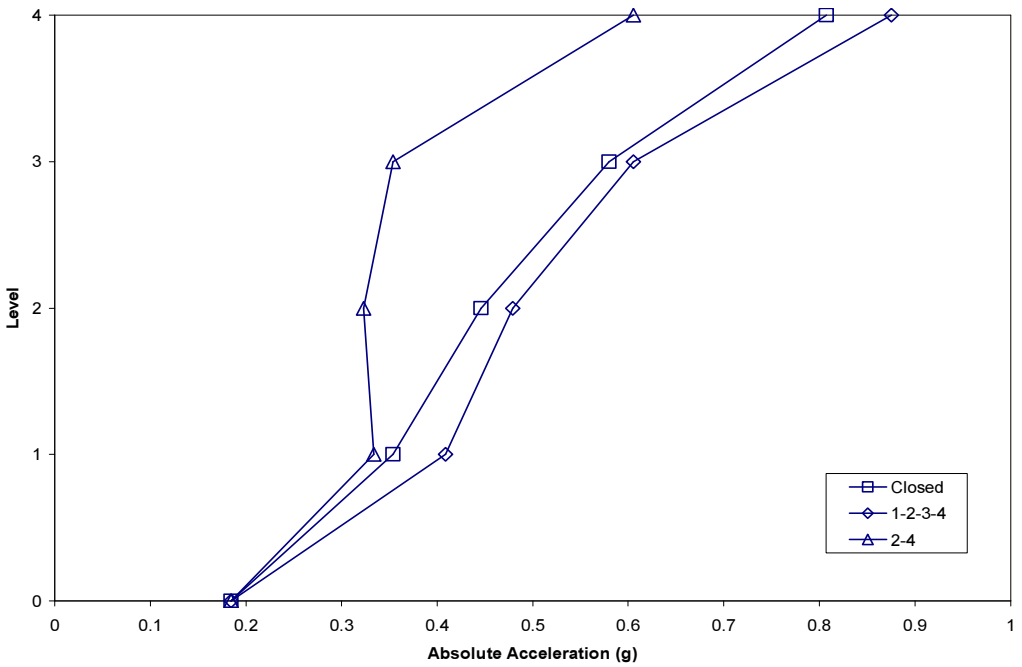

(b) Maximum absolute accelerations

Figure D.4.7 Maximum response envelopes for Kobe 35% Modified earthquake.

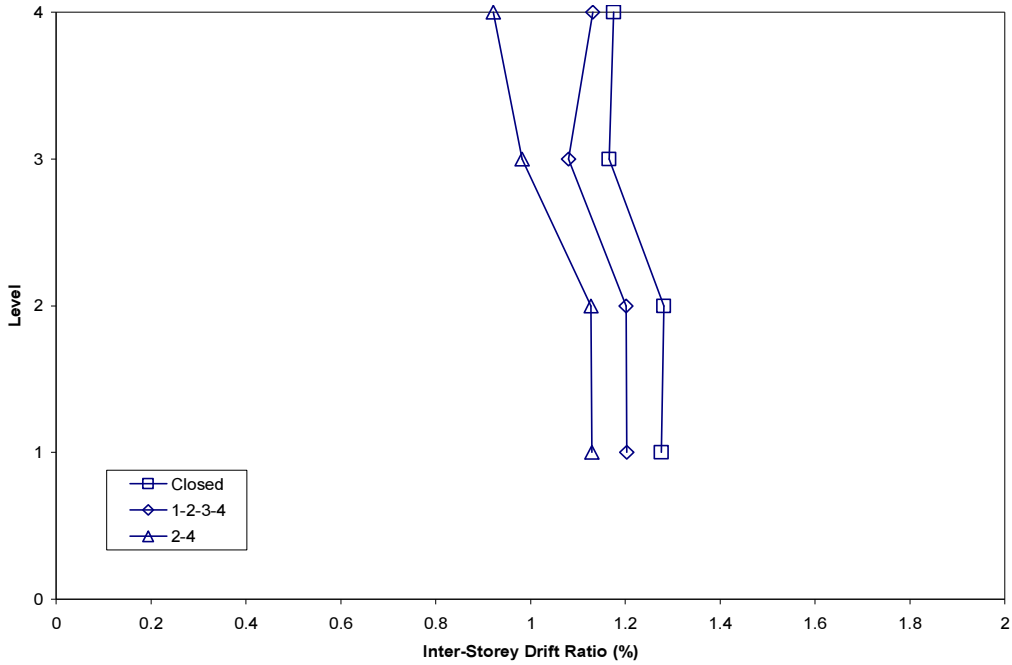

(c) Maximum inter-storey drift ratios

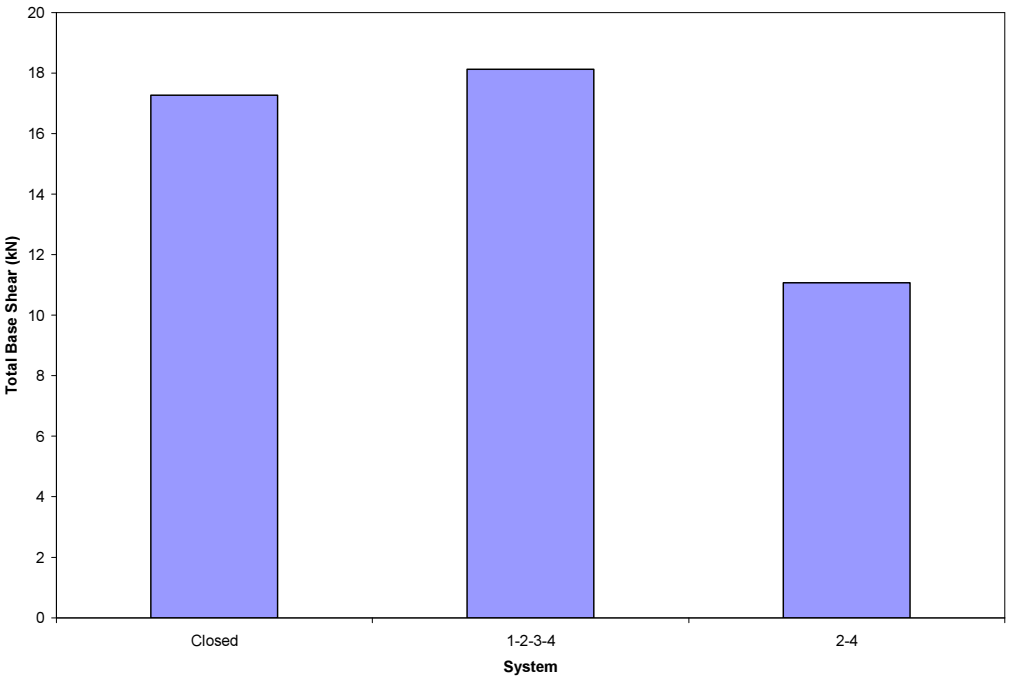

(d) Maximum total base shear

Figure D.4.7 (Continued).